THE
PHYSICAL REVIEW

A journal of experimental and theoretical physics established by E. L. Nichols in 1893

SECOND SERIES, VOL. 78, NO. 6 JUNE 15, 1950

Beta-Spectra of Gaseous A^{41} and O^{15}*

HAROLD BROWN AND VICTOR PEREZ-MENDEZ
Pupin Physics Laboratories, Columbia University, New York, New York
(Received November 21, 1949)

A magnetic semicircular focusing spectrometer with a radius of curvature of 13.6 cm has been constructed and adapted for the measurement of the β-ray spectra of emitters in gaseous phase.

The radioactive gases were produced by deuteron bombardment of gaseous samples in a cyclotron using special probes.

A^{41} (109 min.) produced by the $A^{40}(d, p)$ reaction showed a spectrum of maximum energy (1.245 ± 0.005) Mev and an allowed spectrum shape down to at least 200 kev.

The half-life of O^{15}, produced by the $N^{14}(d, n)$ reaction, was determined to be (118.0 ± 0.6) sec. The end point of its positrons was (1.638 ± 0.005) Mev. The Fermi plot departed from linearity at 300 kev, but this effect may be of experimental origin.

I. INTRODUCTION

OVER a period of fifteen years a vast quantity of experimental data concerning β-ray spectra has been accumulated, most of it misleading in greater or lesser degree. In recent months, however, the use of very thin sources[1–3] has tended to put the Fermi theory of allowed transitions[4–7] on firmer ground than previously, and the discovery and analysis of spectra of various forbidden shapes[8–10] has given strong confirmation of the Gamow-Teller[5] modification as regards forbidden transitions. However, several discrepancies have still to be clarified.

Two classes of emitters have not hitherto been thoroughly investigated. These are (a) rare gas emitters and (b) short-lived activities (a few minutes or less). The two categories overlap to some extent. The former includes such isotopes as A^{41}, Ne^{23}, and He^{6}; the latter includes most of the well-known Wigner series of "super-allowed transitions," those in which the nuclear wave functions are so alike before and after the transition that the matrix element involved is nearly equal to unity. Most of the "mirror image" nuclei are the emitters and products of this series.

The experiments described here measure the half-lives and β-spectra of two examples from these groups from about 250 kev to 4.5 Mev with gaseous sources. In the case of the short-lived emitters, use of a gas facilitates a rapid change of the source, and by monitoring the activity of the flow the necessity of accounting for the decay of the source is removed. The window necessary to keep the gas in the source chamber distorts the spectra below 250 kev. However, by confining the investigation to spectra of end-point energy greater than 1 Mev, not only can the end points be obtained but a decision can be reached on whether the spectra are of the allowed shape or not ($\frac{3}{4}$ of the spectrum is sufficient for this purpose). Previously, short-lived β-spectra measurements using a β-spectrometer have included continuous β-spectra of N^{13} (10-min. half-life)[11] and line spectra of Al^{28} (3 min.).[12] An entirely different method, involving the bombardment of sources already in the spectrometer, was recently used by Hornyak *et al.*,[13] to measure the very high energy

* Supported in part by the AEC.
[1] R. D. Albert and C. S. Wu, Phys. Rev. **74**, 847 (1948).
[2] C. S. Wu and R. D. Albert, Phys. Rev. **75**, 315 (1949).
[3] L. Feldman and C. S. Wu, Phys. Rev. **76**, 697 (1949).
[4] E. Fermi, Zeits. f. Physik **88**, 161 (1934).
[5] G. Gamow and E. Teller, Phys. Rev. **49**, 895 (1936).
[6] E. J. Konopinski and G. E. Uhlenbeck, Phys. Rev. **60**, 308 (1941).
[7] E. P. Wigner, Phys. Rev. **56**, 519 (1939).
[8] Slack, Braden, and Shull, Phys. Rev. **75**, 1965 (1949).
[9] L. M. Langer and H. C. Price Jr., Phys. Rev. **76**, 641 (1949).
[10] C. S. Wu and L. Feldman, Phys. Rev. **76**, 693, 696, 698 (1949).
[11] Cook, Langer, Price, and Sampson, Phys. Rev. **74**, 502 (1948).
[12] Benes, Hedgran, and Hole, Arkiv. f. Mat. Astro. Fys, **35a**, No. 12 (1948).
[13] Hornyak, Dougherty, and Lauritsen, Phys. Rev. **74**, 1727 (1948).

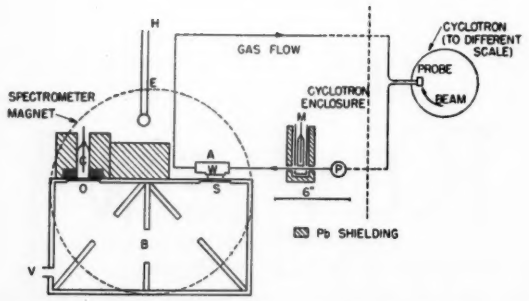

FIG. 1. Schematic diagram of the spectrometer and the pumping system for radioactive gases. *A* is the source chamber and W the thin cellophane window. *S* is the entrance slit, *O* the exit slit, and *B* the central defining baffle. *V* is the exhaust outlet and *C* the spectrometer counter, *H* the shaft and *E* the rotating coil of the spinner. *M* is the monitor counter, and *P* the circulating pump.

spectra (about 12 Mev) of the very short-lived activities of B^{12} (0.022 sec.) and Li^8 (0.8 sec.). Cloud-chamber measurements of short-lived spectra were made over ten years ago[14] but were subject to large scattering errors.

II. APPARATUS

The spectrometer was of the 180° semicircular focusing type patterned after the design of Lawson and Tyler.[15,16] The magnetic field was obtained by using an electromagnet of 4-in. core diameter to which pole tips 16 in. in diameter and 1 in. thick were attached. The maximum obtainable field in the useful region was 1500 gauss, constant to about 0.1 percent. Current was supplied by a voltage stabilized generator which was constant to better than $\frac{1}{2}$ percent. The measurement of the magnetic field was obtained by balancing the rectified a.c. signal generated in a rotating coil in the magnetic field against a standard voltage. The field is inversely proportional to R_s, the resistance on a voltage divider. Measurements showed that the change in magnetic field never exceeded 0.2 percent in 20 minutes.

The vacuum envelope for the spectrometer, a rectangular parallelepiped 2 in.×8 in.×16 in., (Fig. 1) is of brass with aluminum cover plates. The brass surfaces are everywhere covered by polystyrene strips $\frac{1}{4}$ in. thick. These are designed to reduce the scattering, as the backscattering coefficients† are roughly Cu≃0.30, Al≃0.10, polystyrene≃0.03. The spectrometer chamber was machined near the source fitting (*S*) so as to increase the distance from the (polystyrene-lined) brass of the spectrometer wall to the source position which can be taken either as the solid source, where used, or the first slit (which acts as a virtual source in the case of gaseous emitters).

Two sets of baffles are employed in this spectrometer; one limits the beam height to $\frac{3}{4}$ in. and the other limits the angular spread. The baffle plates are constructed in sandwich form. The side facing the beam is made of $\frac{1}{4}$-in. polystyrene, to reduce scattering; the other side is made of $\frac{1}{8}$-in. brass, which is sufficient to stop 4.5-Mev betas. The edges of both halves were beveled to the most advantageous angles. The exit and entrance slits are 2.0 cm high and either 0.5 or 1.0 cm wide. For spectra whose end points are less than 2 Mev, a 0.15-cm thickness of brass is used for entrance and exit slits; for those greater than 2 Mev, a 0.30-cm thickness is used.

The pressure in the spectrometer is always less than 1μ of Hg which is equivalent to a weight per unit area (over a 45-cm electron path length) of 0.06μ g/cm².

The counters used were of the thin end-window type, using mica windows of thickness 1.4 mg/cm². Corrections for variation in counting efficiency with electron energy, and for counting losses due to deadtime, were negligible.

The correction for absorption and scattering in the counter window was made by finding the numbers of electrons of various energies (from a P^{32} source) counted with various thicknesses of mica interposed before the counter window. Using the relation $N=N_0e^{-kw}$ for the number of electrons transmitted, the correction curve shown in Fig. 2 was obtained.

III. THE SOURCE CHAMBER

The novel feature of this spectrometer is the incorporation of a source chamber which allows the spectrum of the activity to be investigated when the substance is in the gaseous phase.

A. Construction

The source chamber, shown in Fig. 3, consists of a 0.5-mm sheet of aluminum welded to a $\frac{1}{8}$-in. aluminum top and semicircular sides. A thin window is attached by rubber gaskets and the tube is sealed into the spectrometer by the usual gasket-compression arrangement.

Brass tubing is attached to the sides of the chamber for the purpose of introducing the gas. The monitor (Section IV) is attached to the system along the line through which the gas flows into the source chamber.

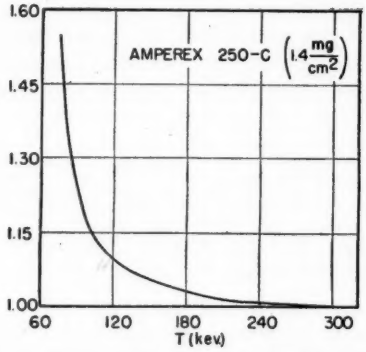

FIG. 2. Window transmission correction for the counter used.

[14] Fowler, Delsasso, and Lauritsen, Phys. Rev. **49**, 561 (1936).
[15] J. L. Lawson and A. W. Tyler, Rev. Sci. Inst. **11**, 6 (1940).
[16] A. K. Saha, Ind. J. Phys. **19**, 97 (1945).
† These are rough values obtained from measurements in this laboratory for saturation back-scattering.

B. Instrumental Scattering

The reliability of the results obtained is limited by the scattering of β-particles which may take place either in the source chamber or in the spectrometer.

From geometrical consideration of Fig. 3a, b it can be seen that we may neglect the single scattering into the effective beam from all surfaces except a narrow section of the aluminum backing, the edges of the entrance slit, and the thin window which isolates the radioactive gas. Since the scattering coefficient of all surfaces involved is 10 percent or less, double scattering can be neglected as a source of error in the spectrum.

The scattering from the thin aluminum backing has been estimated[17] from the solid angles involved and the reflection coefficient, which has an upper limit of 0.2 at 200 kev.[18] The ratio of the number back-scattered and passing through the slit to those passing through without scattering is approximately 0.2 percent (calculated on the basis of straight line trajectories) for a typical point P in the middle of the source volume which contribute to the beam. For those electrons emitted very near the backing a larger fraction of those entering the beam will have been scattered into it, but these form only a small fraction of the total emitted; those electrons emitted near the window will have virtually no chance of being reflected into the beam from the backing. The average ratio over the entire volume for such scattering is less than 1 percent.

The scattering from the first slit is similar to that of the other baffles; both scattering and partial penetration of electrons through the edges occur. Since this slit is the closest to the source, its effect will be the greatest.

Using an average distance of 3.0 cm from the source point to the slit, not more than 0.1–0.2 percent of the β-particles which emerge in the detectable beam should be scattered from the first slit. In view of the possibility of large small-angle scattering, however, this estimate was checked experimentally when the A^{41} spectrum was taken. In this case spectra were taken with both the 0.3 and 0.15-cm thickness slits, and found to agree down to about 200 kev, indicating that the first slit has a negligible effect on the spectra above 200 kev.

The distortion of the β-ray spectra by the window separating the source from the spectrometer is best evaluated with the aid of the data of White and Millington,[19] who found that a thin film in front of a monoenergetic beam of electrons produces an energy distribution whose maximum occurs near $T_0-\Delta T$, where T_0 is the initial energy and ΔT is some average energy loss (given by the range-energy curve), and, furthermore, that the breadth (full width at half-maximum) of the distribution is also of the order of ΔT, or $\Delta(H\rho)$ in momentum units. For sufficiently large values of ΔT the low energy tail of the distribution becomes extremely pronounced.

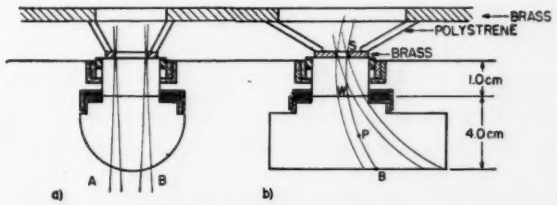

FIG. 3. (*a*) Detail drawing of source chamber, side section. *A* and *B* are the limiting β-ray trajectories which enter the spectrometer counter without scattering. (*b*) Detail drawing of source chamber, front section. The limiting detectable trajectories are shown. Point *B* is a point on the backing, *P* is a source point, W a point on the window, and *S* at the slit.

To determine the effect of the thin window on the source chamber, the ratio $\Delta(H\rho)/H\rho$, as well as the average energy loss ΔT, has been calculated as a function of the electron energy. Table I gives the quantities involved, with ΔT and $\Delta(H\rho)/H\rho$ calculated for a window 2.5 mg/cm^2.

The two effects (shift and spread of energies) can be estimated from this table. The shift at very high energies is nearly constant, and must be considered in evaluating the end point from the observed spectra. With decreasing energy the shift increases; the important quantity is this increase, which tends to distort the spectrum. Actually one should add to the measured energy obtained from the reading on the spinner the value ΔT before plotting the curves. This correction, however, would be negligible above about 200 kev (for 2.5 mg/cm^2 window); so the procedure followed has been to plot the data as obtained, and subsequently to add ΔT at high energy to get the end point. It is also in the region of about 250 kev that the straggling becomes comparable with the resolution width. One would then expect that the large area under the low energy tail would cause a rise in the observed number of the β-rays at those energies. Above the 250-kev region the window effects can therefore be neglected.

C. Resolution and Intensity

Graphical determinations have been made of the solid angle subtended by the entire slit system (including the entrance slit) at various points in the source volume, as a function of the radius of curvature. For 1.0-cm entrance and exit slits, the results are shown (Fig. 4) for two points. Curve *A* represents $T(\rho)$ for a source point 2.0 cm below and 0.2 cm to the right of the center of the exit slit (this corresponding to a point near the top of the source); curve *B* represents that for a source point 6.0 cm below and 0.5 cm to the right (near the backing). These and many other such curves show that the expected mean radius of curvature is 13.5 to 13.6 cm; that a point in the source near the slit has $T_{max}\simeq 0.25$ percent (for 1.0-cm slit); a distant one

[17] Bethe, Rose, and Smith, Proc. Am. Phil. Soc. **78**, 573 (1938).
[18] Rutherford, Chadwick, and Ellis, *Radiations from Radioactive Substances*, (Cambridge University Press, London, 1930) pp. 411–444.
[19] P. White and G. Millington, Proc. Roy. Soc. **A120**, 701 (1928).

TABLE I. Energy loss and straggling of electrons.

T(Mev)	4.0	0.8	0.4	0.3	0.25	0.20	0.15
ΔT(kev)	4.5	4.5	7.0	8.5	9.0	10.0	11.0
$\Delta(H\rho)/H\rho$ in %	0.1	0.4	1.0	1.3	1.7	2.9	4.2

has $T_{max}\simeq 0.16$ percent. These correspond to angles in the median plane of about 30° and 18°. For 0.5-cm slits these angles (and transmissions) are divided by about 2. The resolutions observed on the transmission curves are 3.5 to 4.0 percent for wide (1.0 cm) and about one-half of that for the narrow (0.5 cm) slits. Since the transmission curves corresponding to various points in the source are displaced relative to each other, over-all figures for the resolutions might be put at 5.0 and 2.5 percent respectively.

The relative transmissions for the solid and gaseous cases can be obtained from Fig. 3b. If the difference in length of the curved paths passing through different points of the slit is neglected, the effective volume contributing to the electron beam passing through an element dS of area on the slit is approximately LdS where L is this length.

The important thing to notice about the beam from the gaseous source emerging from the entrance slit is that it has the same angular distribution as the beam from the solid source actually entering the chamber. Since the emergent beams over the useful solid angle are the same in intensity distribution for the two cases, the approximate intensity and resolution for the gaseous sources can be ascertained by employing solid sources instead.

To summarize the conclusions drawn, we have for a gaseous source using 0.5-cm slits:

$T_m\simeq 0.001$, $\delta\simeq 0.02$ and the active volume $2.0\times 4\times 0.5=4$ cm³.

With 1.0-cm slits, $T_m\simeq 0.002$, $\delta\simeq 0.04$ and $V_a\simeq 8$ cm³.

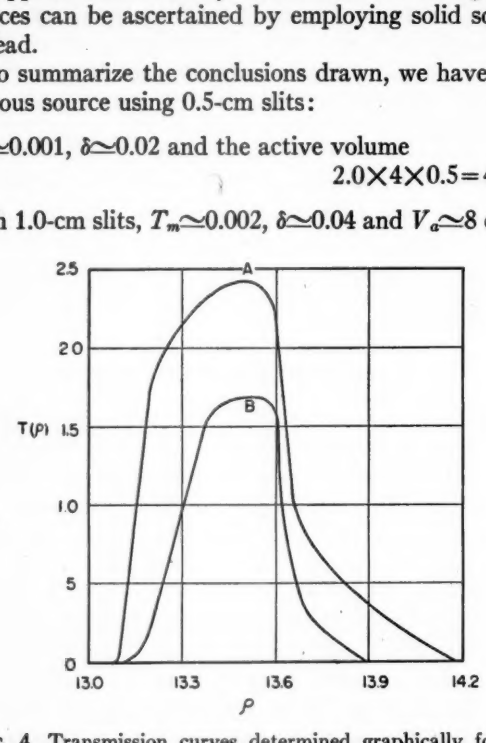

FIG. 4. Transmission curves determined graphically for two points in the source chamber. $T(\rho)$ is the fraction of the total solid angle subtended by the exit slit at the source point. ρ is the radius of the curvature (in cm) of the β-ray trajectory.

The average counting rate over a spectrum is given (for an approximately triangular resolution curve) by $nT_m\delta V_a$, where n is the number of disintegrations per second per cm³ in the "active volume" of the source.

IV. THE MONITOR AND GAS PROBE

To take account of the decay of the source and its variation in intensity as the bombarding cyclotron beam varies, an end-window geiger counter (Fig. 1) was placed along the gas pumping line about 8 cm from the source chamber. To avoid having the particles from the gas line travel in curved paths before being counted by the monitor counter, the entire system is magnetically shielded. Since positrons originating in the source chamber could travel in curved paths and produce γ-rays which might be counted by the monitor, the magnetic shield is surrounded by a $\frac{7}{8}$-in. thick lead shield. Changing the magnetic field in the spectrometer has no effect on the counting rate of the monitor so long as the source strength remains the same, indicating that the shielding is successful in making the count of the monitor directly proportional to the source strength. Without the shielding the monitor count changes by as much as a factor of two as the magnetic field varies.

The gas probe[20] consists of a water-cooled solid copper head with holes for gas flow. The bombardment chamber is covered with a copper window 1 mil thick. Deuteron beams of average current up to about 25μ amp. were used; of this about 15μ amp. hits the window and passes through the length (about 5 cm) of the bombardment chamber.

The gas to be bombarded is pumped through and, along with the gaseous products of deuteron-induced reactions, out of the probe. The tube carrying it passes out of the cyclotron enclosure (through the shielding) past the monitor counter and enters the source chamber of the spectrometer. The flow rate is high enough (several hundred cm³/sec.) so that the concentration of radioactive gas is effectively the same near the monitor and in the source chamber. Figure 1 shows the pumping system used with the gas probe.

V. SOLID SOURCES

The instrument was calibrated with the photoelectrons from annihilation radiation. Figure 5 shows the curve of intensity *vs.* the spinner reading for a thick lead foil (50 mg/cm²). Using both thick and thin radiators,[21,22] the value obtained for $1/R_{s0}$ corresponding to the known $H\rho$ of 2615 gauss-cm (or energy of $mc^2-E_{Pb,K}=422.5$ kev) is 4.20×10^{-4} mho.

Thus $H\rho=2615\times(2380/R_s)$ gauss-cm so that we have a conversion formula to give the momentum in

[20] H. Brown and V. Perez-Mendez, Phys. Rev. **75**, 1286 (1949).
[21] Jensen, Laslett, and Pratt, Phys. Rev. **75**, 458 (1949).
[22] Hornyak, Lauritsen, and Rasmussen, Phys. Rev. **76**, 731 (1949).

gauss-cm corresponding to a given reading on the voltage divider at balance.

The radius of curvature obtained from the value of $H\rho$ for a given voltage divider setting (immediately above) and the magnetic field for that same setting (obtained from the comparison with the G. E. Fluxmeter) is $\rho = 13.62$ cm. This is quite close to the geometrically predicted value for the maximum of the $T(\rho)$ curve (about 13.6).

To check this calibration the internal conversion electrons from the 185-kev γ-ray[23,24] of In^{114} were investigated, and found to agree with the locations observed on the Columbia solenoidal spectrometer[25] (1465 and 1580 gauss-cm). The resolution, using a 0.5-cm wide solid source and a detector slit of equal width, was about 3 percent.

In order to check the over-all performance of the spectrometer, the spectrum[26] of P^{32} was measured, using a number of thin samples. The spectrum obtained gave a Fermi plot linear approximately down to 200 kev, with an end point at 3.39 mc^2. The agreement with the results of previous investigations leads us to conclude that this semicircular-focusing spectrometer gives reliable information on the number of β-rays of various energies emitted from the vicinity of the source.

VI. RESULTS

A. Argon 41

The first gas whose spectrum was investigated was A^{41}. It was produced in the gas probe by deuteron bombardment of spectroscopically pure argon (which is 99.6 percent A^{40}). The A^{41} is produced by a (d, p) reaction, the beam consisting of 15 to 25μ amps. of 8-Mev deuterons, and the bombardment was for 45 to 70 minutes in various cases. The probe was arranged so that the cyclotron beam fell on the window by attaching the probe to the pumping system and bombarding nitrogen, which produces a short-lived activity (2-min. O^{15}). The probe was then filled with argon and sealed off. Following the bombardment, the argon was transferred by expansion to an evacuated flask and from there to the previously evacuated source chamber which fits into the spectrometer. Because of the long half-life, continuous pumping is not necessary. The pressure of the argon in the source chamber was about 10 cm Hg so that its equivalent thickness is 0.8 mg/cm^2. The window thickness was 2.0 mg/cm^2.

In evaluating the data taken from the spectrometer and monitor counters, the background can be divided into two parts. The first is the (constant) part due to cosmic radiation, emission from the counter walls, etc. This is subtracted from the raw counting rates of both spectrometer and monitor counters to get the number of counts due to the activity under investigation. However, there is a second background which also must be subtracted. This fraction depends on the amount of activity in the source chamber; it consists of counts produced by γ-rays (of nuclear type and also from annihilation of positrons) or the photo-electrons and Compton electrons produced by them which register in the spectrometer counter. The counter was shielded from the direct γ-radiation by the lead shielding inside and outside the vacuum envelope, but the secondary electrons produced in various parts of the spectrometer, and particularly near the exit slit, have some probability of being detected. These portions are near the counter, so that the secondary electrons should not be too much affected by the magnetic field. Compton and photo-electrons produced in the exit slit which have enough energy to pass through the rest of the slit and register in the counter have a very small cross section for production. Calculation indicates, for instance, that if N positrons are incident on the entire slit, about $0.2\,N$ pass through the rectangular hole in it, and less than $0.005\,N$ Compton and photo-electrons produced by the annihilation of the positrons are counted—thus an additional fraction of $2\frac{1}{2}$ percent is introduced. This second background thus consists mainly of secondary electrons produced in the parts of the spectrometer near the exit slit, and of stray radiations from the sample under investigation.

Experiments have shown that in the energy region outside of the spectrum (for both directions of H) the ratio of this "background" to the monitor count is a constant. The same result is also obtained by covering the detector slit with the sliding gate. This ratio was

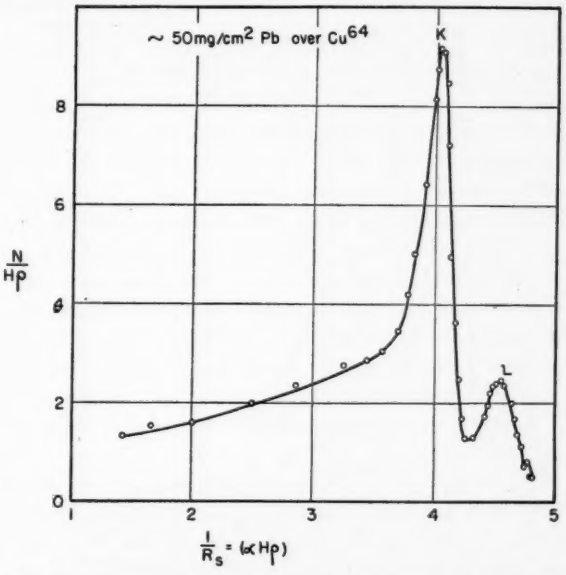

FIG. 5. Spectrum of the photo-electrons ejected from a thick lead radiator by the annihilation radiation of Cu^{64}. R_s is the reading on the potentiometer in ohms ($\times 10^4$). $1/R_s$ is proportional to the electron momentum. N is in arbitrary units, and $N/H\rho$ is the number of electrons per unit momentum range. Background has been subtracted.

[23] J. L. Lawson and J. M. Cork, Phys. Rev. **57**, 982 (1940).
[24] P. W. Levy, Plutonium Project Report, MonP-250, p. 26 (1947).
[25] Wu, Albert, and Feldman (private communication).
[26] K. Siegbahn, Phys. Rev. **70**, 127 (1946).

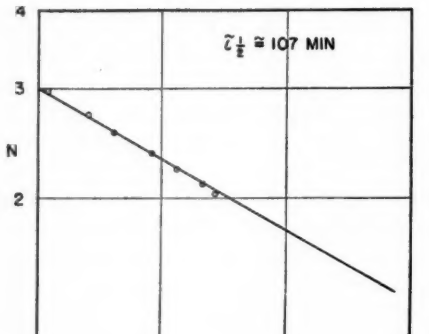

FIG. 6. Decay curve of A^{41}, taken simultaneously with the spectrum. N is in arbitrary units, T is the time in minutes. Only a few of the experimental points are shown.

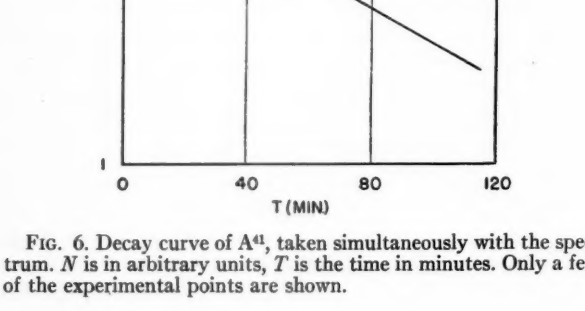

FIG. 7. Fermi plot of the A^{41} β-spectrum. ϵ is the electron energy (rest+kinetic) in units of mc^2. N is the number of electrons per unit momentum range, and f the Fermi function $\eta^2 F(Z, \epsilon)$. $(N/f)^{\frac{1}{2}}$ is in arbitrary units. The resolution is shown. Where the statistical error is greater than the size of the open circles, it is shown by the vertical lines.

therefore subtracted from the ratio of spectrometer counts to monitor counts in identical time intervals (following subtraction of the constant background) in order to obtain the true spectrum of the sample being investigated.

The spectrum of A^{41} was previously investigated in a cloud chamber by Kurie, Richardson, and Paxton.[27] They obtained, using the Konopinski-Uhlenbeck plot extrapolation, an end point of 1.5 Mev. Bleuler *et al.*,[28] using a coincidence-absorption method, concluded that the spectrum was complex, consisting of a 1.18-Mev negative electron group in cascade with a 1.3-Mev γ-ray 99.3 percent of the time, and a 2.55-Mev β-ray 0.7 percent of the time. They obtained a 109.4-min. half-life.

The decay curve taken by the monitor simultaneously with the measurement of the spectrum is shown in Fig. 6, and indicates a half-life of 107±3 min., in adequate agreement with the more accurate half-life of Bleuler *et al.* The spectrum, corrected for counter window absorption, but uncorrected for finite resolution at the high energy tail, is shown in Fig. 7. The Fermi plot is a straight line down to about 160 kev, indicating that the spectrum is of the allowed shape. Correcting for finite resolution on the tail of the spectrum brings those points practically into the straight line. The discrepancy, which does not greatly exceed experimental error, might be due to the very small fraction of high energy betas in the second group. These would not be detectable, because of the very low intensity, except perhaps near the end point of the low energy group. No internal conversion of the γ-ray is found; this is to be expected in view of its high energy. The extrapolated end point from the data uncorrected for source window absorption is 1240 kev; correcting for this absorption (5 kev at high energies) gives 1245±5 kev. This agrees satisfactorily with the value of Bleuler, Boltmann, and Zünti which is 1180±50 kev. The value calculated for ft, using $Z=19$ (residual nucleus), $\epsilon_0=1245$ kev and 109.4 min. for t, is 1.26×10^5 sec., which puts the transition $A^{41}\rightarrow K^{41}+e^-$ into the "allowed" (forbidden only by the difference in symmetry of the nuclear wave functions) class for medium nuclei.

B. Oxygen 15

The O^{15} spectrum was first investigated in a cloud chamber by Fowler, Delsasso, and Lauritsen[14] who found that O^{15} emitted positrons with an end point of 1.7 Mev, using the K−U extrapolation. A recent

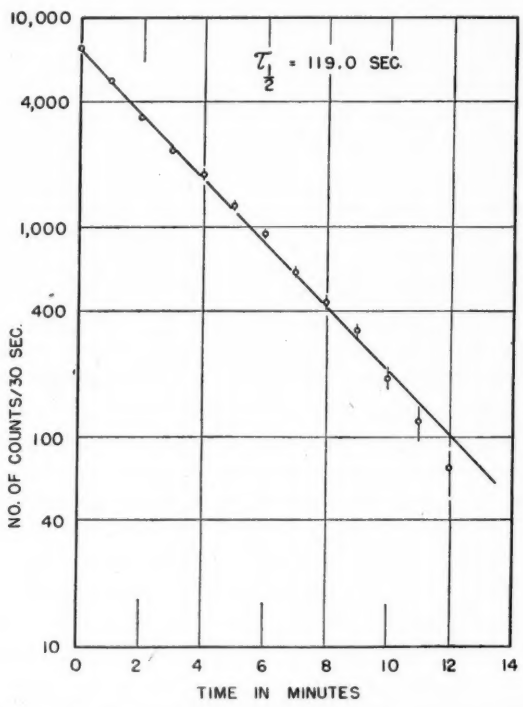

FIG. 8. Decay curve of O^{15}. Each point represents the number of counts over a 30-sec. period, corrected for background and counter deadtime.

[27] Kurie, Richardson, and Paxton, Phys. Rev. **49**, 368 (1936).
[28] Bleuler, Boltmann and Zünti, Helv. Phys. Acta **19**, 419 (1946); **20**, 195 (1947).

measurement using absorption in aluminum, by Sherr, Meuther, and White,[29] gave an end point of 1.68 Mev.

Using nitrogen gas continuously circulated, O^{15} was produced by the N^{14} (d, n) reaction. The deuteron beam passing through the bombardment chamber was about 20μ amp. For accurate measurement of the half-life a cylindrical disintegration chamber of copper, with a 1-cm hole covered with Cu foil, was substituted for the source chamber. By taking counts over 30-sec. intervals out of every minute, decay curves showing the half-lives were obtained. A sample decay curve, corrected for counter background and deadtime, is shown in Fig. 8. The half-life of O^{15} as obtained from a series of eight decay curves, is 118.0 ± 0.6 sec., which is somewhat lower than previous values.[30] The linearity of the logarithmic plot of the decay curves indicates that only one activity is present, as would be expected on the basis of the isotopic abundance and relative cross sections involved in the competing reactions, the most important of which (N^{14} (d, p)) produces inactive N^{15}.

The spectrum was taken by the method previously described. Figure 9 shows the Fermi plot obtained from it. It gives an end point (corrected for source-window absorption at high energies) of 1.683 ± 0.005 Mev, which agrees with the cloud-chamber and absorption measurement results within their experimental errors. The graph shown is the result of four runs, normalized to the same value in the intermediate energy region (500 to 800 Mev).

The Fermi plot is essentially linear down to an energy of about 300 kev. Some slight curvature away from the axis might be inferred, but its departure from a straight line, if any, is very small and could be attributed to source thickness, which has the effect of giving the observed spectrum a more positive curvature.

Below 300 kev the Fermi plot deviates sharply from linearity, showing an excess of positrons experimentally. This is probably due to the combined effect of source thickness and source window thickness. Since the pressure in the source chamber is 25 cm Hg, the equivalent thickness of the gas is 1 mg/cm²; the window thickness was about 2.6 mg/cm². The effect of source thickness plus the straggling of β-particles in the window could combine to make the O^{15} curve deviate from the theoretical allowed shape at a higher energy than the A^{41}, as is the case. Taking the window thickness plus half the source thickness as an approximate value to compare with the White-Millington data gives 2.3 mg/cm² for A^{41} and 3.2 for O^{15}. $\Delta(H\rho)/H\rho$ due to thickness becomes equal to the spectrometer resolution half-width (3 percent) for 160 and 260 kev respectively. These are near the observed points of deviation.

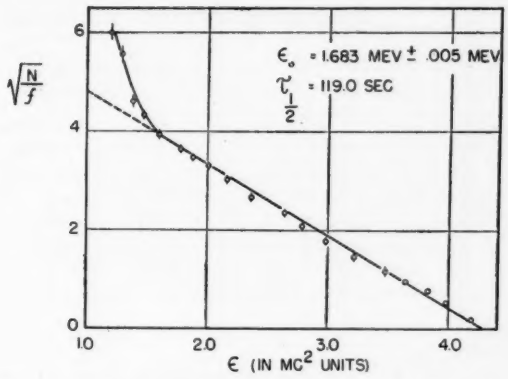

FIG. 9. Fermi plot of the O^{15} β-spectrum (positrons).

The curve for O^{15} thus indicates an allowed spectrum, though the possibility of a compound spectrum is not completely excluded. This is what is expected from such a "mirror image" transition of the Wigner series. The ft value calculated from $\epsilon_0=1.683$ Mev, $t_{\frac{1}{2}}=118.0$ sec. and $Z=7$, is 3910 sec., which is of the same order as the other emitters in group OA (light emitters of the allowed class). The mass difference between O^{15} and N^{15} is $\epsilon_0+2mc^2=2.705$ Mev. Since N^{15} has a measured mass of 15.00489 amu, the mass of O^{15} is 15.00780 amu.

ACKNOWLEDGMENTS

We should like to express our gratitude to Professor W. W. Havens, Jr., who suggested the problem, and to Professors J. R. Dunning, L. J. Rainwater, and E. T. Booth, and Dr. C. S. Wu for their constant advice and encouragement. Thanks are also due to Miss Miriam Levin and the cyclotron crew for their continued willing assistance.

We should also like to thank the United States AEC, which aided materially in the performance of this research.

[29] Sherr, Meuther, and White, Phys. Rev. **75**, 282 (1949).
[30] W. Bothe and W. Gentner, Zeits. f. Physik **112**, 45 (1939).

Deuteron-Proton Scattering Using Photographic Techniques*†

F. A. RODGERS,‡ H. A. LEITER,¶ AND P. G. KRUGER
Physics Department, University of Illinois, Urbana, Illinois
(Received November 7, 1949)

The differential scattering cross section for 9.94±0.08-Mev deuterons scattered by protons has been determined with nuclear track emulsions as detectors. The deuterons were obtained from the cyclotron while the target consisted of hydrogen gas at a pressure of approximately 5 cm of mercury.

The photographic plates were arranged so that they recorded simultaneously at all laboratory angles from 12.5° to 65°. Approximately 5000 proton tracks at each of 12 angles in this range were counted. Geometrical, slit scattering, and slit penetration corrections have been made to the number of tracks counted.

I. INTRODUCTION

EXPERIMENTS on the scattering of protons by deuterons have been reported by Tuve, Heydenburg, and Hafstad[1] in which the incident protons had energies up to 830 kev and by Taschek[2] at much lower energies. Primakoff[3] and Ochial[4] have attempted a theoretical analysis of the results obtained by Tuve, Heydenburg, and Hafstad. Their conclusions were that the experimental work showed anomalies which they could not explain. Sherr, Blair, Kratz, Bailey, and Taschek[5] have recently reported results in the energy range from 0.825 to 3.49 Mev which show a rather uniform decrease in cross section with increasing energy. Furthermore, their results in the neighborhood of 830 kev did not show the anomalies obtained by Tuve, Heydenburg, and Hafstad.

All the workers mentioned above used electrical detection methods and scattered protons by deuterons, probably because of the simplification this afforded in the analysis of the data. In the present work photographic detection methods were used to measure the scattering of deuterons by protons. This choice of bombarding particle was made for convenience in analysis.

The use of photographic plates in scattering experiments has several very definite advantages over other common methods of detection. The plates are continuously sensitive in contrast to the small sensitive time of cloud chambers. They also can be used to register simultaneously over a large range of scattering angles while maintaining angular definition. This is in sharp contrast to the restrictions on electrical detection methods. Finally, the extreme simplicity of the photographic plate as a detection unit would alone be a strong point in its favor.

The main disadvantage associated with photographic plates arises in the analysis of the data. The analysis can be very tedious in those uses where different nuclei have to be distinguished, the energy has to be determined, or the angle has to be measured for each particle. However, the present experiment was arranged so that none of the above information had to be determined from measurements on the track. Instead, all that was required was a determination of the number of proton tracks registered at a given angle.

Chadwick, May, Pickavance, and Powell[6] reported preliminary results from a chamber designed for scattering of light nuclei from a gas target which used one plate to record all data from 10° to 170° in the laboratory system. They gave an excellent summary of the advantages derived from photographic plates and of the problems peculiar to their use. More recently, Dearnley, Oxley, and Perry[7] have used photographic plates to determine the absolute cross section for proton-proton scattering in which they used rectangular defining slits and registered data from 10° to 45° in the laboratory system.

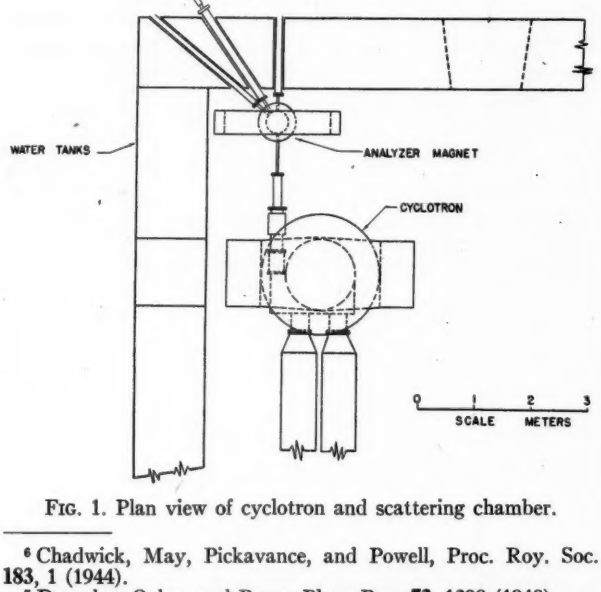

FIG. 1. Plan view of cyclotron and scattering chamber.

* Submitted in partial fulfillment of the requirements for the Ph.D. by F. A. Rodgers.
† This work has been supported jointly by the ONR and AEC.
‡ Now at the University of Wisconsin, Madison, Wisconsin.
¶ Now with the Westinghouse Laboratories, Pittsburgh, Pennsylvania.
[1] Tuve, Heydenburg, and Hafstad, Phys. Rev. **50**, 806 (1936).
[2] R. F. Taschek, Phys. Rev. **61**, 13 (1942).
[3] H. Primakoff, Phys. Rev. **52**, 1000 (1937).
[4] K. Ochial, Phys. Rev. **52**, 1221 (1937).
[5] Sherr, Blair, Kratz, Bailey, and Taschek, Phys. Rev. **72**, 662 (1947).
[6] Chadwick, May, Pickavance, and Powell, Proc. Roy. Soc. **183**, 1 (1944).
[7] Dearnley, Oxley, and Perry, Phys. Rev. **73**, 1290 (1948).

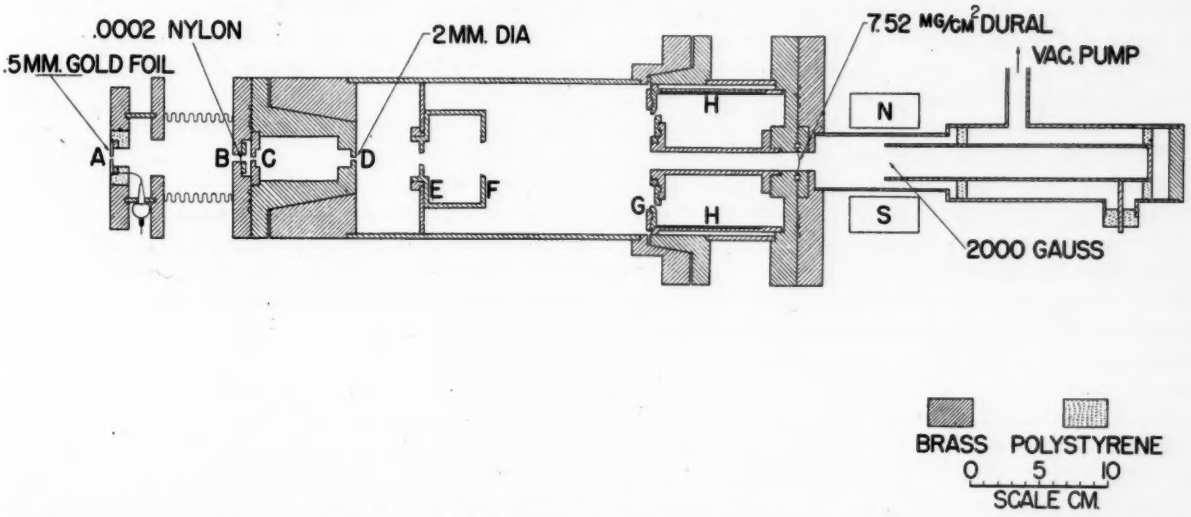

FIG. 2. Cross section of the scattering chamber and Faraday cage. A. Gold foil slit for stopping down the deuteron beam. B. Nylon foil separating cyclotron vacuum from scattering chamber. C, D. Two-mm collimating slits. E, F. Antiscattering baffles. G. Annular slit. H. Photographic plate tangent to inside circumference of cylinder.

II. SCATTERING APPARATUS

The scattering chamber was located in front of the 37° exit tube of the University of Illinois cyclotron as shown in Fig. 1. The deuteron beam from the cyclotron passed down the exit tube, through the magnetic analyser, and out the exit tube which passes through the water tanks surrounding the cyclotron. Figure 2 shows the details of the scattering chamber. The deuteron beam was stopped down to a diameter of 4 mm by a gold foil located 4 in. in front of the first collimating slit of the scattering chamber. The gold foil was insulated so that the current to it could be registered and this current served as a monitor during the experimental runs.

The two collimating slits (C and D) were each 2 mm in diameter and spaced 3 in. apart. They were carried in a ground brass cone to facilitate removal and also to guarantee exact positioning upon replacement. The divergence of the beam after collimation was found by placing a photographic plate at the back of the scattering chamber and allowing the beam to strike it for an instant. This method gave a half-angle divergence of approximately 11 min. The small value is largely due to the distance between the cyclotron and the scattering chamber. It was increased to approximately 17 min. by the presence of hydrogen at a pressure of approximately 5 cm of mercury in the scattering chamber and a 0.2-mil Nylon foil $\frac{1}{4}$ in. in front of the first collimating slit which separated the hydrogen gas in the scattering chamber from the high vacuum of the cyclotron and exit tube.

The detection of the scattered particles occurred in the "camera" which held an annular defining slit and the photographic plate holder. All but 120° of the annular slit was open so that six photographic plates could be exposed at the same time, thus using about 180° of the azimuthal angle. The annular slit and camera were so designed that all laboratory scattering angles from 12.5° to 65° could be recorded simultaneously. In order to obtain this advantage the slits had to be designed so that some particles could penetrate through the edges of the slit. This effect will be considered later.

The camera, like the collimating slit holder, was sealed on to the scattering chamber by means of a ground brass cone. A black cloth covered the camera and flange when the camera was removed to the dark room. The undeflected particles passed down the inner tube of the camera, through the 7.5-mg/cm² aluminum foil at the back of the camera, and into the Faraday cage.

The six photographic plates were supported on a brass cylinder so that the plane of the emulsion and the long edge of the plate were parallel to the unscattered deuteron beam. Three-by-one-inch Ilford nuclear track plates, Type C-2, with an emulsion thickness of 50μ were used. The position of a track on the plate and the position of the plate relative to the annular slit determined the angle of scattering, eliminating the necessity of measuring the angle of each track.

To prevent any deuterons which might scatter off the last collimating slit from reaching the photographic plate, antiscattering baffles were included (see Fig. 2). These were designed so that the last collimating slit could see neither the annular slit nor the walls of the chamber beyond the antiscattering baffles.

III. AUXILIARY APPARATUS

The undeflected deuterons were collected in a Faraday cage and the charge collected, integrated by a low current Q-meter. This apparatus as well as the method of calibrating the Q-meter is described else-

where.[8] An error of one percent has been ascribed to the value of the resistance and an error of one percent to calibration voltage. This gives a value of 1.4 percent error[9] in the charge measurement.

The scattering chamber was evacuated by means of a 10-liter per sec. oil diffusion pump backed by a mechanical fore pump. Without photographic plates in the chamber the pressure could be reduced to about 7×10^{-6} mm of mercury as measured by an ionization gauge. With plates in the camera the pressure could be reduced to less than 5×10^{-5} mm of mercury after 24 hr. After closing off the scattering chamber from the pumps a rate of rise occurred of about 1.5×10^{-4} mm of mercury per min.

The hydrogen was admitted to the system through a heated palladium tube. Both the palladium tube and the diffusion pump were separated from the scattering chamber by liquid air traps to reduce the chance of contamination. The pressure of the hydrogen in the chamber was measured by means of an oil manometer, the difference in height being measured by a cathetometer. The oil manometer was constructed of $\frac{1}{2}$-in. inside diameter glass tubing and filled with Octoil-*S*. The density of Octoil-*S*, which has been outgassed, has been measured[10] to be

$$0.9104[1-0.000733(t-25)]\ \text{g/cm}^3\pm0.05\ \text{percent},$$

where t is the temperature of the oil in degrees centigrade. This is in good agreement with the manufacturer's value of 0.9103 g/cm³. The vapor pressure of Octoil-*S* has been given by the manufacturer as 7×10^{-9} mm of mercury. The "closed" side of the manometer was pumped continuously by the oil diffusion pump associated with the scattering chamber. The temperature was measured by a thermometer placed with the bulb inside the chamber near the scattering volume and the stem outside the chamber.

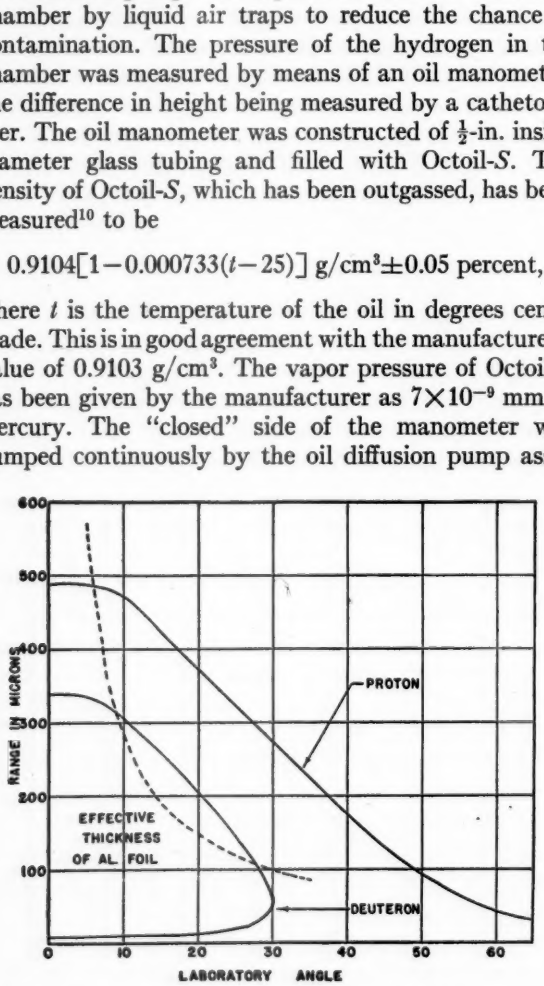

FIG. 3. Range of recoil protons and scattered deuterons in Ilford C-2 emulsion. The differences between the dashed line and the solid lines give the residual range of the particles in the emulsion when 19 mg/cm² aluminum foil is placed over the emulsion.

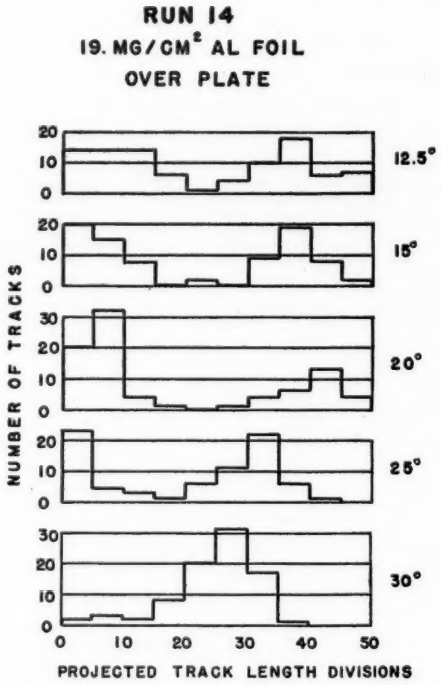

FIG. 4. Histograms of track lengths as seen projected on the eyepiece scale of the microscope.

The photographic plates were studied under a binocular microscope using bright field illumination and a magnification of about 260 times. The plates were held in a plate holder designed so that the means of positioning the plates were the same as in the camera plate holder. This was necessary since the edges of the photographic plate were not even and thus the edges of the plate holder had to serve as reference lines.

IV. EXPERIMENTAL PROCEDURE

A preliminary consideration of deuteron-proton scattering based on conservation of energy and momentum showed that the range of the scattered and recoil particles in the emulsion, as a function of laboratory angle, is as shown in Fig. 3. This shows that above 30° only proton recoils occur while below 30° three groups of particles occur—(1) recoil protons, (2) low energy scattered deuterons corresponding to large scattering angles in the center-of-mass system, and (3) high energy scattered deuterons corresponding to small scattering angles in the center-of-mass system.

All three low angle groups could be allowed to register on the photographic plate, but in this case even if 100μ-thick emulsions were used the distinction between proton and deuteron tracks would require a careful examination of each of the tracks.

By a fortunate combination of geometry and the range relation shown in Fig. 3, it was possible to place

[8] R. E. Meagher, Phys. Rev. 78, 667 (1950).
[9] See footnote 13 of reference 8.
[10] Measured by E. J. Zimmerman.

a 19.0-mg/cm² aluminum foil over that part of the plate which registered deuterons, reducing the length of the registered tracks to a point where the differentiation between proton and deuteron tracks was easy. This was due to the fact that the deuteron tracks were only about 25 percent as long as the proton tracks when the 19.0-mg/cm³ foil was in place rather than 80 percent as long. Another advantage in using the aluminum foil was that a smaller fraction of the particles which penetrated the slit edge were allowed to register on the plate at those angles at which the penetration factor otherwise would have been the largest.

The effect of the aluminum foil is shown by histograms, given in Fig. 4, of the track lengths observed at various angles. The scattering in the aluminum foil and the emulsion broaden the peak somewhat, but the proton group remains well defined.

An experimental run was started by loading the camera and placing the camera, Faraday cage, and Q-meter in position. The systems were allowed to pump down for approximately 24 hr., the last 6 hr. with liquid air on the traps, in order to get rid of the water vapor from the photographic plates. After the pressure had dropped below 5×10^{-5} mm of mercury in the scattering chamber, the Q-meter was calibrated. The scattering chamber was then closed off and filled with hydrogen. After filling, the system was allowed to stand for 10 min. to come to equilibrium and then the pressure and temperature of the hydrogen were read. The plates were then exposed by passing a deuteron beam of about 10^{-9} amp. through the scattering chamber for about one-half hour. This was sufficient to give approximately 2500 tracks at each experimental point. After the exposure, the pressure and temperature of the hydrogen were re-measured and the Q-meter re-calibrated. The hydrogen pressure increased about 0.2 percent during the run do to the change in liquid air level in the traps. This change was linear with time and therefore the average pressure during the run was used in the calculations.

The camera was then removed to the dark room and the photographic plates were developed for 15 min. in Kodak D-19, diluted four to one, and fixed for 45 min.

In addition to two runs as described, a vacuum scattering run was made to determine the effectiveness of the scattering baffles. This run was similar in every way to the regular run except that after closing off the scattering chamber from the pumps a time equal to that required to fill with hydrogen was allowed to elapse before the beam was turned on.

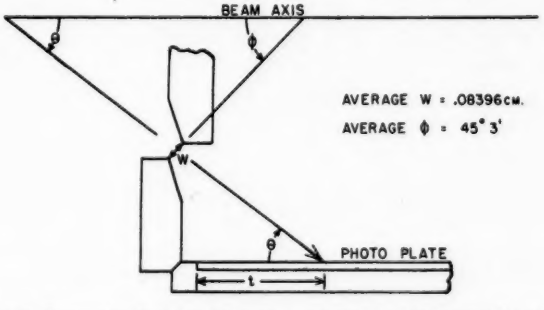

FIG. 5. Geometry for the distance, t, along the photographic plate corresponding to a scattering angle, θ.

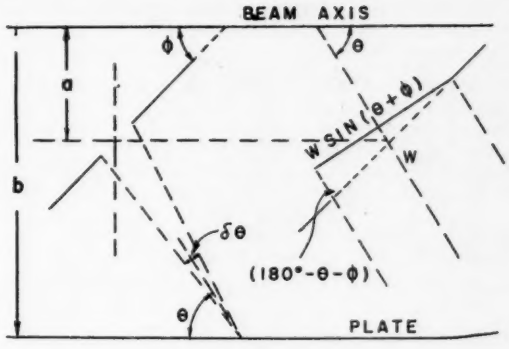

$$\delta\theta = \frac{W \sin(\theta+\phi) \sin\theta}{(b-a)}$$

FIG. 6. Geometry for calculating $\delta\theta$. $\delta\theta$ is defined as the angle subtended by the annular slit at the swath on the photographic plate.

V. CONSTANTS OF THE APPARATUS

The laboratory cross section is given as a function of the laboratory angle, θ, by

$$\sigma_{\text{lab}}(\theta) = N(\theta)/n_i n_t \mathfrak{L}(\theta)\delta\Omega, \tag{1}$$

where $N(\theta)$ = number of proton tracks counted, n_i = number of incident deuterons, n_t = number of target hydrogen atoms per cm³, $\mathfrak{L}(\theta)$ = beam length effective at the angle θ, and $\delta\Omega$ = solid angle recorded at the angle θ.

The geometrics from which θ and $\delta\theta$ were determined are shown in Figs. 5 and 6, respectively. Since a given swath on the photographic plate records over an angle increment, $\delta\theta$, equal to the polar angle subtended by the annular slit at that swath, this angle, $\delta\theta$, is the polar angle contribution to the expression for $\delta\Omega$.

At each angle in this interval,

$$(\theta_0-\delta\theta/2)<\theta<(\theta_0+\delta\theta/2),$$

the effective length of the beam is just equal to the swath width since the photographic plate is parallel to the beam. This effective length is obtained by extending a line from each side of the swath inclined at an angle, θ, to the beam until they intersect the beam. In some cases more than one swath was used in order to obtain a sufficient number of tracks. In these cases the swaths were taken immediately adjacent to each other. Thus in these cases

$$\mathfrak{L}(\theta) = S \cdot w, \tag{2}$$

where S is the number of swaths per plate and w is the swath width.

The quantities which are functions of the angle are

TABLE I. Constants of the experiment.

Swath width, $w=0.01869\pm0.00005$ cm
Slit width, $W=0.08396\pm0.00008$ cm
Slit angle, $\phi=45°\ 3'\pm12'$
Plate radius, $b=4.780\pm0.005$ cm
Slit radius, $a=3.173\pm0.002$ cm
Axial distance from slit to swath $=(t+0.2396)\pm0.004$ cm
Swath length, $h=1.000\pm0.004$ cm, or $=1.500\pm0.004$ cm
Energy of deuterons $=9.94\pm0.08$ Mev
Acc. due to gravity, $g=980.139$ cm/sec.^{2}

given as

$$\theta=\tan^{-1}(b-a)/(t+0.2396\text{ cm}), \tag{3}$$

$$\delta\theta=W\sin(\theta+\phi)\sin\theta/(b-a), \tag{4}$$

$$\delta\beta=2\text{ (No. of plates) }\tan^{-1}\text{ (swath length/2b)}, \tag{5}$$

and since there are six plates,

$$\delta\beta=12\tan^{-1}(h/2b), \tag{6}$$

where $h=$swath length. Thus

$$\sigma_{\text{lab}}(\theta)=(b-a)N(\theta)/n_i n_t SwW\sin(\theta+\phi)\sin^2\theta\delta\beta.$$

The conversion to the center-of-mass cross section is given by

$$\sigma_{\text{C.M.}}(\alpha)=\sigma_{\text{lab}}(\theta)d\Omega_\theta/d\Omega_\alpha. \tag{7}$$

The scattering angle in the center-of-mass system will be defined in the present work as the angle through which the particles are deflected. With this convention there is no ambiguity concerning which particle is the incident particle in the laboratory system.

By use of this convention the relation between the recoil angle, θ, of the proton in the laboratory system and the corresponding center-of-mass angle, α, is given by

$$\alpha=(180°-2\theta), \tag{8}$$

while

$$d\Omega_\alpha/d\Omega_\theta=\sin\alpha d\alpha/\sin\theta d\theta=4\cos\theta. \tag{9}$$

Table I summarizes the measurements of the required dimensions of the apparatus.

The swath width was defined by the ends of a scale in one eyepiece of the binocular microscope as the plate passed under the objective. In counting the tracks, the point at which a particle entered the emulsion was taken as the defining position of the track. The swath width on the photographic plate, as defined by the eyepiece scale, was determined by direct measurement on an optical comparator.

W and ϕ were determined by measurements made on an optical nodal slide. This instrument was well adapted for these measurements since the slit system could be clamped in the nodal slide and then readily turned so that the axis of the slit system made any angle up to 60° with respect to the axis of the microscope. The projected openings of the slit at 45° and 60° to the axis of the slit holder were measured at 12 positions around the slit, and from these data both W and ϕ were determined from geometrical considerations.

The average deviation from the mean value of W of individual values was 0.3 percent, but any individual reading and therefore the average value of W was accurate to 0.1 percent. ϕ on the average varied by 39′ from the mean while the average was considered accurate to 12′.

The energy of the beam was determined[11] by a method involving a differential ionization chamber similar to that described by Dearnley, Oxley, and Perry[7]. This gave an energy for the deuteron beam of 10.00 ± 0.07 Mev. This had to be corrected for the 0.2-mil Nylon foil which was equivalent to 0.5 cm air or 0.04 Mev and the energy loss due to the hydrogen gas to the 45° scattering volume of 0.016 Mev. This, then, gives an energy of 9.94 ± 0.08 Mev at the center of the scattering volume. The extra 0.01 Mev in the uncertainty is to take account of the variation in energy from one scattering volume to another.

The angular definition in this experiment has two contributions. The larger contribution is given by Eq. (4). The smaller contribution is given by the angle subtended by the swath width at the annular slit. The half-angle width contributed by these two effects ran from about 1° to 2° at scattering angles of 12.5° and 55°, respectively.

Two experimental runs were made to obtain approximately a total of 5000 tracks at each angle. The data were taken in two runs in order to keep down the density of tracks for ease in counting.

The hydrogen pressure, temperature and Q-meter constants are functions of the run and are given in Table II for each of the two runs.

VI. CORRECTIONS

In order to allow simultaneous registration at many polar angles the annular slit must be designed in such

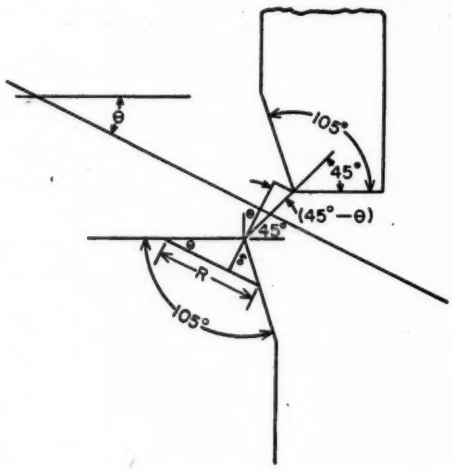

FIG. 7. Geometry for determining the penetration factor for the annular slit.

[11] Determined by C. J. Taylor.

Table II. Constants of the runs.

	Run 14	Run 16
H_2 pressure	75.00±0.02 cm of oil	75.43±0.02 cm of oil
H_2 temperature	25.7±1°C	22.8±1°C
Oil temperature	23.1±1°C	20.5±1°C
Oil density	0.9117 g/cm³±0.1%	0.9134 g/cm³±0.1%
Q-meter counts	12,160	12,161
Coulombs/count	1.028×10^{-10}±2%	1.031×10^{-10}±2%
Coulombs	1.250×10^{-6}±2%	1.254×10^{-6}±2%
n_i	7.80×10^{18}±2%	7.83×10^{18}±2%
n_t	3.249×10^{18}±0.35%	3.306×10^{18}±0.35%

a way that particles can, to a certain extent, penetrate through the edges of the slit. This results in an effective widening of the slits over the optical width. Those particles which penetrate through the edges of the slit also give shorter tracks in the emulsion than those which go through the open slit, an effect that produces a short-track tail on the track length spectrum. The fraction of the total number of tracks recorded at any angle which are due to particles which have penetrated the slit can be determined from the geometry of Fig. 7 as

$$\frac{N_p}{N_0}=\frac{2R\sin(\theta)\sin(75°-\theta)}{W\cos(45°-\theta)\sin75°}, \tag{10}$$

where N_p is the number of penetration particles, N_0 is the number of particles passing through the open slit, and R is the penetration thickness corresponding to the minimum track length accepted in the counting. R is determined by both the integral stopping power of the emulsion and the stopping power of the brass. The integral stopping power for the emulsion was determined from the length of the tracks at various angles and the known energy in the proton-proton experiment.[8] These were compared with the stopping power curves as given by Lattes, Fowler, and Cuer[12,13] for protons in Ilford emulsions with which they agreed to within five percent. The range in mg/cm² for the brass was determined using the range curves for copper given by Aron.[14] The penetration factors which have been calculated from Eq. (10) are given in Table III. The limits on the corrections are based on the probable errors in the stopping power of the Ilford emulsions and the statistics of the penetration counts.

An attempt was made to verify experimentally these calculated penetration factors without too much success. Theoretically a set of slits could be constructed in which the edges of the slits just touched. Then a run with these slits would give just the penetration tracks and the correction could be made experimentally. Actually, a set of "closed" slits of this type could not be constructed which were accurate enough to give any significant results. At some points around the annular slit, the slit would be slightly open and at other points slightly overlapping.

[12] Lattes, Fowler, and Cuer, Nature **159**, 301 (1947).
[13] Lattes, Fowler, and Cuer, Proc. Phys. Soc. London **59**, 895 (1947).
[14] *Handbook of Radioactivity and Tracer Methodology* (1948), Air Force Technical Report No. 5669, p. 183.

Table III. Slit penetration correction and target length at laboratory scattering angles.

θ in degrees	$\mathfrak{L}(\theta)$ in cm	N_p/N_0 in percent
12.5	4.0	1.3±0.4
15	3.0	2.5±0.5
20	3.0	3.8±0.5
25	2.0	4.6±0.7
30	1.5	5.4±0.8
35	1.5	4.2±0.7
40	1.5	6.9±0.6
45	1.0	4.9±0.5
50	1.0	3.4±0.3
55	1.0	2.3±0.2
60	1.0	1.2±0.1
65	1.0	0.5±0.1

The photographic plates were found to be not accurately parallel to the deuteron beam. This effect was such as to make small corrections in b, the radial distance of the plate from the beam, and in the average angle, θ. The discrepancy in b, from that given in Table I, varied linearly from −0.019 cm at the high angle end of the plate to +0.015 cm at the low angle end of the plate. This correction amounted to 0.35 percent in the worst case.

Another correction on b occurs because of the use of straight swaths on the photographic plate. The intersection of the plane of the photographic plate with the cone of constant polar scattering angle is a parabola. Thus the swath should be parabolic rather than straight. The average value of b along a given swath is greater than the value at the center of the swath by one-third

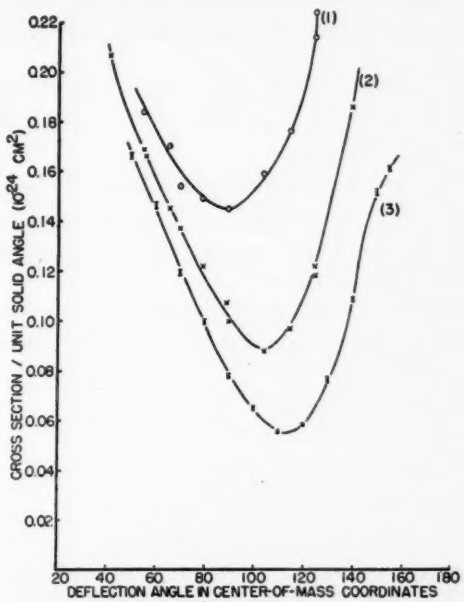

FIG. 8. Deuteron-proton center-of-mass differential cross sections. (1) 1.5-Mev protons incident on deuterium. Sherr *et al.* (2) 3.0-Mev protons incident on deuterium. Sherr *et al.* (3) 9.94-Mev deuterons incident on hydrogen. Present data.

TABLE IV. Scattering cross sections.

No. counts	θ_{lab}	$\sigma_{lab} \times 10^{24}$ cm^2	$\theta_{C.M.}$	$\sigma_{C.M.} \times 10^{24}$ cm^2	$(N)^{\frac{1}{2}}/N$
5620	12.5°	0.603	155	0.1543	1.3 percent
6426	15	0.577	150	0.1494	1.3
8271	20	0.404	140	0.1075	1.1
6000	25	0.274	130	0.0757	1.3
4679	30	0.197	120	0.0569	1.5
5668	35	0.178	110	0.0545	1.3
8058	40	0.195	100	0.0635	1.1
7098	45	0.216	90	0.0763	1.2
9524	50	0.251	80	0.0978	1.0
5599	55	0.267	70	0.1165	1.3
6458	60	0.284	60	0.1422	1.2
6568	65	0.273	50	0.1614	1.2

the difference in the value of b between the center and the end of the swath since the difference is proportional to the square of the distance from the center of the swath. This correction amounted to 1.22 percent in the worst case.

Finally, a correction is provided by the vacuum run. This will include the effects of slit scattering, contamination scattering and proton recoils from neutron background. The majority of the proton recoils were eliminated from the counting by visual inspection since most of them started in the body of the emulsion and not at the surface. The same criteria employed on the gas scattering runs were used in counting the tracks on the vacuum run. The vacuum background was largest at 30° where it was 0.4 percent. The majority of this must be due to recoil protons which started either in the surface or so near it that the difference could not be detected. The reason for believing this is that in the case of proton-proton scattering with this apparatus where both contamination scattering and slit scattering should be worse, the vacuum run background is negligible at all but the smallest angles.

The corrections mentioned resulted in a net correction of about seven percent at 40° where the net correction was largest.

VII. EXPERIMENTAL RESULTS

Two experimental runs were made in order to simplify the counting and to provide a method of checking for gross errors.

The results are tabulated in Table IV and plotted in Fig. 8. Run 16 was not counted above 50° since over 5000 tracks were obtained at each of these angles on run 14. All cross sections presented have been corrected as described in the previous section.

The percentage errors given with the cross sections in Table IV are those associated with statistics while the errors due to other sources are given below. The individual contributions to the errors are given with the measured quantities in Tables I–III. In addition to these there is the human error in counting. The counting was done by three observers, and it was found after an initial practice period that the three observers agreed within 0.5 percent on the proton-proton scattering experiment.[8] Because of increased difficulty in counting the deuteron-proton data, the estimated error due to this source has been increased to one percent.

Charge measurement, 1.4 percent. Human factor, 1.0 percent. $(b-a)$, 0.4 percent. Swath length, 0.4 percent. Swath width, 0.3 percent. H_2 temperature, 0.3 percent. Oil density, 0.1 percent. Slit width, 0.1 percent. Slit angle, ϕ, 0.1 percent. Penetration factor, 0.8 percent. Position on the plate, t, 0.4 percent.

The last three errors vary with angle. The values given are the largest and occur at 12.5°, 30°, and 40°, respectively. If we assume these largest errors in the last three above values and 1.3 percent average error for the statistical errors in σ (Table IV) we find the average net probable error for $\sigma_{C.M.}$ is 1.7 percent. This probable error would apply to the relative value of $\sigma_{C.M.}$ and to the absolute values except for footnote 9. If we take this into consideration, more probable values for the cross sections in Table IV would be obtained by increasing those given by 1.3 percent.

A statistical analysis of the data from Run 14 in which comparisons were made between the six photographic plates showed that in 35 percent of the cases the number of counts at a given angle varied by more than $\sqrt{N}$ from the average at that angle. A similar analysis for Run 16 gave 21 percent.

VIII. ACKNOWLEDGMENT

The authors wish to express their thanks to Professor R. E. Meagher for his cooperation throughout the experiment and help in making many of the measurements and to Professor G. F. Tape for the many helpful discussions of the problems associated with this experiment.

The Angular Distribution of Protons from the D—D Reaction at 10 Mev*

H. A. LEITER,† F. A. RODGERS,¶ AND P. G. KRUGER
Physics Department, University of Illinois, Urbana, Illinois
(Received November 7, 1949)

The gas-filled scattering chamber has been applied to the study of the distribution in angle of the protons from the D—D reaction with 9.94±0.08-Mev deuterons from the cyclotron. Photographic plates were used as detectors. The other charged particles produced in the reaction and from scattering processes were prevented from reaching the emulsion by covering the photographic plates with a 53.2-mg/cm² aluminum foil. Differential cross sections were determined at 10° intervals from 15° to 65° in the laboratory system. Background runs were made to determine the correction necessary because of the flux of neutrons in the chamber. Additional corrections were made for the penetration of the protons through the edges of the defining slit and for geometrical errors. The total cross section for the production of protons was calculated to be 7.3×10^{-26} cm².

I. INTRODUCTION

THE nuclear reactions

$$H^2+H^2\rightarrow H^3+H^1+Q_1 \quad (1)$$

$$\rightarrow He^3+n^1+Q_2 \quad (2)$$

have been known for many years and have been the subject of many papers.[1] The angular distribution of the disintegration products has been extensively studied[2] also.

It is the purpose of this paper to report on the angular distribution of the protons in reaction (1) when the energy of the incident deuteron is 10 Mev. A preliminary report[3] has been given earlier.

II. EXPERIMENTAL PROCEDURE

The apparatus used in this experiment was that used for measurements on deuteron-proton scattering[4] and proton-proton scattering[5] in this laboratory and has been described in detail in those papers.

A preliminary analysis[6] of the two reactions and the elastic scattering of deuterons by deuterons based on the energy and momentum conservation laws yielded the results shown in Fig. 1 for the ranges of the charged particles in the emulsion. The calculations assumed $Q_1=3.98$ Mev, for reaction 1, $Q_2=3.25$ for reaction 2, $E=10$ Mev, and a stopping power of 2000 for protons in the emulsion. Also shown in Fig. 1 is a curve giving the equivalent range in an 8-mil aluminum foil. It is seen that this thickness of foil is sufficient to stop the nuclei H^3 and He^3 and elastically scattered deuterons, while the protons would have enough energy to penetrate the foil and register in the emulsion. The neutrons from the reaction and those produced in other (d, n) processes would cause recoil protons to be produced in

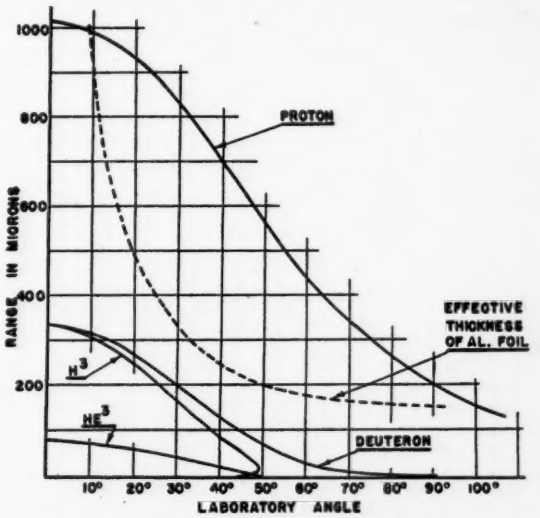

FIG. 1. Ranges of charged particles emitted in the D-D reaction and deuterons scattered by deuterons in Ilford C-2 emulsion. Dashed lines show effect of 8-mil aluminum foil covering emulsion.

* This work has been supported jointly by the ONR and the AEC.

† Submitted in partial fulfillment of the requirements for the Ph.D. at the University of Illinois. Now at Westinghouse Research Laboratories, East Pittsburgh, Pennsylvania.

¶ Now at the University of Wisconsin, Madison, Wisconsin.

[1] Oliphant, Harteck, and Rutherford, Proc. Roy. Soc. **A144**, 692 (1934); R. Ladenburg and M. H. Kanner, Phys. Rev. **52**, 911 (1937); R. B. Roberts, Phys. Rev. **51**, 810 (1937); Amaldi, Hafstad, and Tuve, Phys. Rev. **51**, 896 (1937); L. I. Schiff, Phys. Rev. **51**, 783 (1937); R. B. Myers, Phys. Rev. **54**, 361 (1938); Haxby, Allen, and Williams, Phys. Rev. **55**, 140 (1939).

[2] P. I. Dee, Nature **133**, 564 (1934); Kempton, Brown, and Maasdorp, Proc. Roy. Soc. **A157**, 386 (1936); H. Neuert, Physik. Zeits. **38**, 122 (1937); Huntoon, Ellett, Bayley, and Van Allen, Phys. Rev. **58**, 97 (1940); Manning, Huntoon, Myers, and Young, Phys. Rev. **61**, 371 (1942); Bennett, Mandeville, and Richards, Phys. Rev. **69**, 418 (1946); Bretscher, French, and Seidl, Phys. Rev. **73**, 815 (1948); E. J. Konopinski and E. Teller, Phys. Rev. **73**, 822 (1948); Blair, Freier, Lampi, Sleator, and Williams, Phys. Rev. **74**, 1599 (1948); Rosen, Tallmadge, and Williams, Phys. Rev. **75**, 1632 (1949).

[3] Leiter, Meagher, Rodgers, and Kruger, Phys. Rev. **76**, 167(A) (1949).

[4] Rodgers, Leiter and Kruger, Phys. Rev., **78**, 656 (1950).

[5] R. E. Meagher, Phys. Rev. **78**, 667 (1950).

[6] Treatments of the mechanics involved in nuclear reactions may be found in M. S. Livingston and H. A. Bethe, Rev. Mod. Phys. **9**, 276 (1937); C. E. Mandeville, J. Frank. Inst. **244**, 385 (1947); L. I. Schiff, *Quantum Mechanics* (McGraw-Hill Book Company, Inc., New York, 1949), 96; A. O. Hanson and R. F. Taschek, Preliminary Report No. 4, Nuclear Science Series, National Research Council.

the emulsion while the high energy neutrons might also produce deuteron recoils of sufficient energy to penetrate the foil. These effects would have to be determined by background runs in which the protons would be prevented from reaching the emulsion.

The procedure followed for the experimental runs was identical with that described in reference 4. For the final data two runs and two background runs were made, exposing six plates in each run. One background run was made with a hollow brass tube (of a thickness sufficient to stop the protons) extending from the plate holder to the front of the chamber, while the second run was made with a brass plate covering the annular defining slit.

III. CALCULATIONS

The differential cross section in the laboratory system for the reaction can be expressed by the equation

$$\sigma(\theta)=\frac{\text{No. of protons per unit solid angle}}{\text{No. of incident deuterons}}\cdot\frac{1}{\text{No. of target nuclei per cm}^2}. \quad (3)$$

For convenience the factor giving the number of target nuclei per cm^2 is split into two parts: the number of atoms per cm^3, which may be easily calculated from the measured temperature and pressure of the gas in the chamber, and the effective length of the beam from which the protons can reach the photographic plate, which may be calculated from the geometry involved.[7] Thus, the above equation becomes

$$\sigma(\theta)=N_0(\theta)/n_i n_t L(\theta)\delta\Omega, \quad (4)$$

where $\sigma(\theta)$ is the laboratory cross section per unit solid angle, $N_0(\theta)$ is the number of protons projected into a solid angle at an angle θ with respect to the deuteron beam, n_i is the number of incident deuterons in the beam, n_t is the number of target nuclei per cm^3, and $L(\theta)$ is the effective target thickness.

The quantities $\delta\Omega$ and $L(\theta)$ depend on the geometry of the camera and the area in which the tracks are counted. From Fig. 2 the solid angle $\delta\Omega$ for a rectangular swath of width w across one of the plates at a radius b from the beam axis is seen to be

$$\theta\Omega=\frac{w\gamma\sin^3\theta}{b}, \quad (5)$$

where γ is the angle at the axis subtended by the length of the swath. From Fig. 3 the effective target thickness is

$$L(\theta)=\frac{W\sin(\theta+\phi)}{\sin\theta}\cdot\frac{b}{b-a}, \quad (6)$$

where W is the optical width of the slit, ϕ is the angle of inclination of W with respect to the beam axis, b is the radial distance from the axis to the photographic plate, and a is the radial distance from the axis to the center of the slit. A small correction is necessary for the finite width of the swath.

To find the cross section in the center-of-mass system use is made of the definition

$$\sigma_{\text{C.M.}}(\alpha)d\Omega_\alpha=\sigma_{\text{lab}}(\theta)d\Omega_\theta \quad (7)$$

where α is the angle of emission of the proton in the center-of-mass system. The ratio of the solid angles may be calculated from

$$g(\alpha,\theta)=d\Omega_\theta/d\Omega_\alpha=\sin\theta d\theta/\sin\alpha d\alpha \quad (8)$$

which can be put into the form

$$g(\alpha,\theta)=\cos(\alpha-\theta)\sin^2\theta/\sin^2\alpha \quad (9)$$

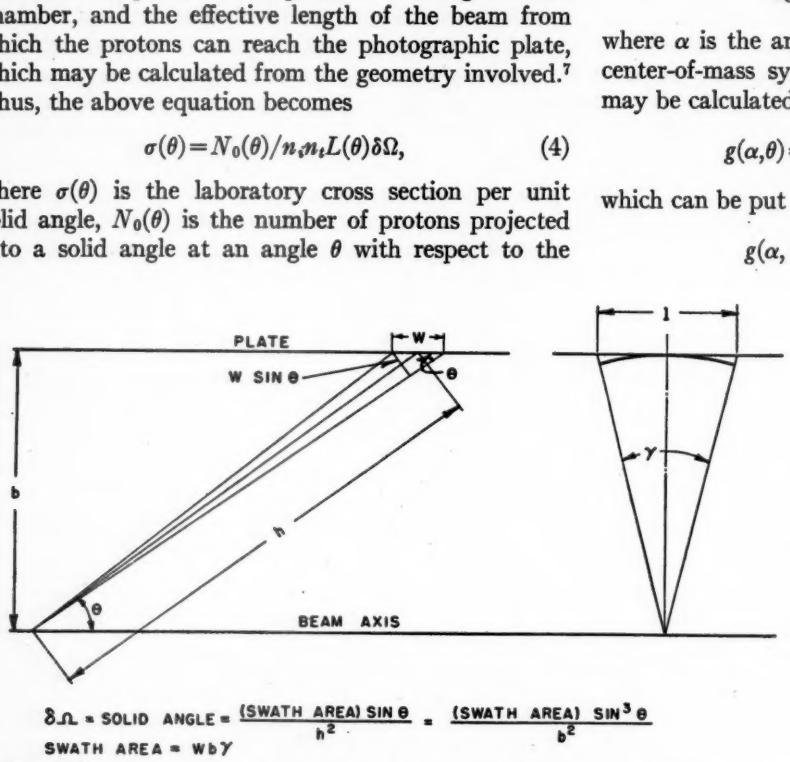

FIG. 2. Geometry for the calculation of the solid angle defined by the swath area in which tracks are counted.

[7] The viewpoint adopted here differs slightly from that in reference 4 with respect to the factor $\theta\delta L(\theta)$, following more closely that of Herb, Kerst, Parkinson, and Plain, Phys. Rev. 55, 998 (1939).

TABLE I. Constants of the runs.

	Run A	Run B
D_2 pressure	74.79±0.02 cm of oil	76.54±0.02 cm of oil
D_2 temperature	24.0±1°C	25.9±1°C
Oil temperature	23.0±1°C	24.1±1°C
Oil density	0.9118 g/cm³±0.1%	0.9110 g/cm³±0.1%
Q-meter counts	192,003	136,929
Coulombs/count	$1.036\times10^{-10}\pm2\%$	$1.032\times10^{-10}\pm2\%$
Coulombs	$1.989\times10^{-5}\pm2\%$	$1.413\times10^{-5}\pm2\%$
n_i	$1.242\times10^{14}\pm2\%$	$0.882\times10^{14}\pm2\%$
n_t (for 99.5% D_2)	$3.243\times10^{18}\pm0.4\%$ atoms/cm³	$3.294\times10^{18}\pm0.4\%$ atoms/cm³

by making use of the relations

$\sin(\alpha-\theta)=$vel. of center of mass/vel. of proton in center-of-mass system)$\sin\theta$ and

$$v_{C.M.}/v_{p,C.M.}=(E/3(E+2Q_1))^{\frac{1}{2}} \qquad (11)$$

where E is the energy of the incident deuteron in the laboratory system. Thus the cross section in the center-of-mass system is obtained by multiplying the laboratory cross section by $g(\alpha, \theta)$.

IV. EXPERIMENTAL DATA

The run constants for the two experimental runs are given in Table I. The geometrical constants associated with the apparatus are given in Table I of reference 4.

V. CORRECTIONS

Because of the high energy of the protons from the reaction the correction due to protons which penetrate the edges of the defining slit should be considerable. Following the procedure outlined in reference 4 [see Fig. 7 and Eq. (10) of that paper], the ratio of the penetration tracks to the open slit tracks was calculated. This was done by applying the integral stopping power curves for the emulsion[5] to the minimum range of track accepted in counting to find the energy of the proton entering the emulsion. A similar calculation involving the stopping power of the aluminum foil[8] gave the energy of the proton entering the foil. This energy was converted into range in copper[9] and compared with the range in copper that a proton passing through the open slit would have. The difference in these two ranges gave a value for the penetration thickness R from which the correction was then calculated. The results of this calculation are given in Table II. It is seen that the maximum value of the correction is about 11 percent, the values decreasing toward larger and smaller angles as would be expected from the shape of the slit edges. The limits on the corrections are based on the probable errors in the stopping powers of the emulsion, aluminum foil, copper, energy of the particles, and statistics of the penetration counts.

A second large correction in this experiment is necessary as a result of the flux of neutrons in the chamber. These neutrons can produce recoil protons in the emulsion which are hard to separate from good tracks because the finite depth of focus of the microscope would not allow the observer to tell at a glance whether the track started in the surface of the emulsion or just below the surface. In addition, the high energy neutrons could impart sufficient energy to a deuteron to cause it to penetrate the aluminum foil covering the plates. These could not of course be distinguished from the good tracks.

[8] J. H. Smith, Phys. Rev. **71**, 32 (1947).
[9] *Handbook of Radioactivity and Tracer Methodology* (1948), Air Force Technical Report No. 5669, p. 183.

TABLE II. Penetration and background corrections.

θ	N_p/N_0 in percent	Background correction in percent
15°	3.2±0.6	0.9±0.1
20°	7.0±0.8	1.8±0.1
25°	10.1±0.9	2.8±0.2
30°	11.5±0.9	3.5±0.3
35°	11.4±0.9	4.1±0.3
40°	11.0±0.9	4.1±0.3
45°	9.7±0.9	3.8±0.2
50°	7.9±0.6	3.2±0.2
55°	6.2±0.5	6.3±0.4
60°	4.3±0.2	6.7±0.4
65°	2.7±0.1	7.9±0.4

On comparing the results of the two background runs it was found that the first run with a long tube projecting to the front of the chamber gave on the average 0.5 percent more tracks than the second run which was made with a plate over the slit. The two runs were combined, account taken of the difference, normalized to run A, and a smooth curve drawn from which the correction values were taken. These values are given in Table II.

It is seen that there is a sudden jump in the correction value at 55°. This is the result of the change in criterion of minimum acceptable track length to quite small values at 55°, 60°, and 65°. Here the tracks were so short because of the high angle of incidence that it was much more difficult to observe the direction of the tracks. This increase in the number of short tracks made the correction quite large. Consequently, the authors do not feel that too much significance should be attached to the shape of the cross-section curve at these angles. In view of this effect it is advisable whenever possible to design the camera so that reasonably long tracks may be obtained.

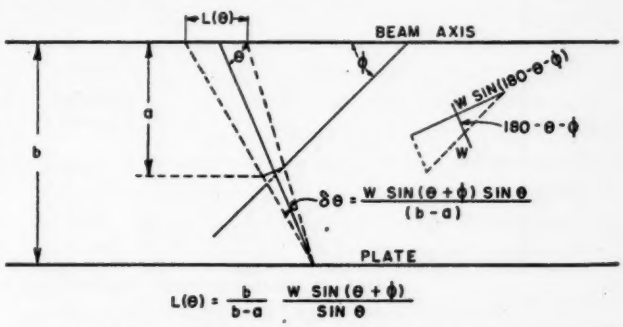

FIG. 3. Geometry for the calculation of the effective target length $L(\theta)$. Effect of finite swath width is not shown.

TABLE III. Values of cross sections.

θlab	Total No. of uncorrected tracks	$\sigma(\theta)$lab	$\alpha_{C.M.}$	$\sigma(\alpha)_{C.M.}$[a]	Probable error
15°	4845	3.24×10^{-26} cm²	21.5°	1.62	1.9 percent
20°	7211	1.90	28.5	0.968	1.8
25°	6252	0.867	35.5	0.452	2.0
30°	3584	0.511	42.4	0.274	2.2
35°	4327	0.464	49.4	0.258	2.1
40°	4392	0.573	56.1	0.331	2.1
45°	4683	0.664	62.8	0.400	2.1
50°	5896	0.723	69.4	0.458	1.9
55°	4290	0.687	75.8	0.460	2.0
60°	3961	0.644	81.9	0.458	2.0
65°	3148	0.588	88.0	0.446	2.1

[a] See footnote 13 in reference 5.

Other small corrections of less than one percent at all angles were necessary because of the lack of parallelism of the plate with the beam, and because rectangular instead of parabolic swaths were used (see reference 4).

The angular resolution varied from about 1° at $\theta=12.5°$ to about 2° for $\theta=65°$.

VI. EXPERIMENTAL RESULTS

The results of the two experimental runs are given in Table III. The total uncorrected number of tracks is given for each angle. The cross sections given have been corrected as described above. These values have been plotted in Fig. 4 with the results obtained by the Minnesota group at 3.5 Mev for comparison.[10]

The probable errors for each angle are given in Table III. These include the statistical error in the net number of tracks after subtracting the background tracks and the penetration tracks. Other errors are the same as those listed in reference 4, except for the human error which has been increased to 1.6 percent and the penetration error which has been treated separately for each angle according to the data given in Table II. The human error was increased to 1.6 percent because it was found that the neutron background tracks made accurate counting more difficult than for the previous work. This was deduced from the number of tracks counted on several different swaths by three different observers. The error in the deuteron energy (±0.08 Mev), 0.8 percent has not been included in the values in Table III. The determination of the deuteron energy is discussed in reference 4.

A possible source of uncertainty in this experiment is the contamination of the gas in the chamber or in the beam. For the latter, the presence of 5-Mev protons would be the only possibility since molecular hydrogen could be accelerated along with the deuterons but would break up on going through the Nylon foil. This would affect the Q-meter readings, giving too large a value for the number of incident deuterons. Contaminates in the chamber would be a different matter. If the energies of the various particles from the reaction and from the scattering of 10-Mev deuterons and 5-Mev protons from

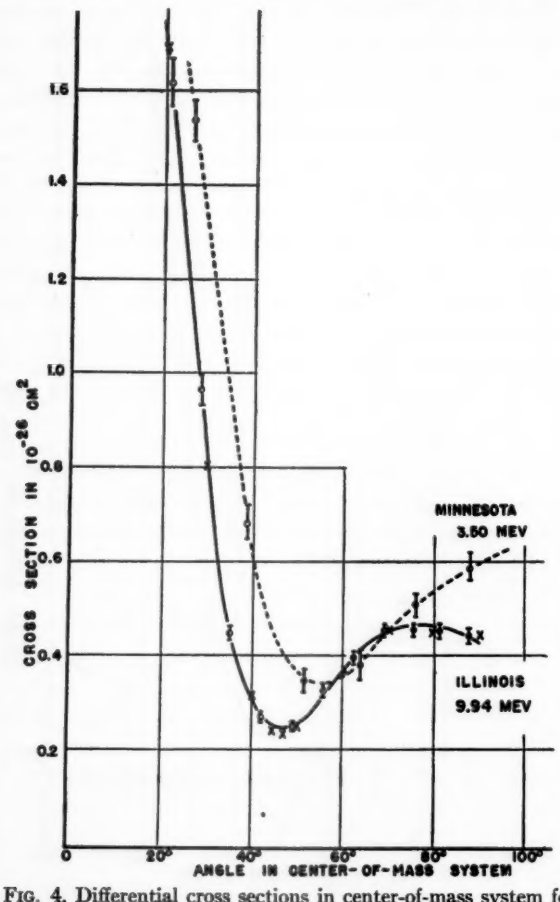

FIG. 4. Differential cross sections in center-of-mass system for the production of protons from D-D. Dashed curve shows results obtained by Blair *et al.* (reference 10). Crosses indicate fit to series with coefficients given in Table IV.

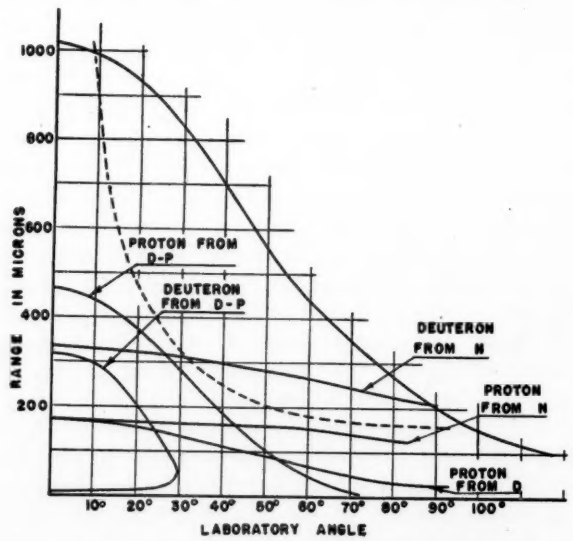

FIG. 5. Effect of contaminants. Curves show ranges in emulsion of 10-Mev deuterons and 5-Mev protons scattered from hydrogen, deuterium, and nitrogen. Upper solid line gives range of proton from D-D and dashed line is equivalent thickness of 8-mil aluminum foil.

[10] Blair, Freier, Lampi, Sleator, and Williams, Phys. Rev. 74, 1599 (1948).

possible contaminates are converted into ranges in the emulsion and plotted as a function of angle, the effect of the aluminum foil is apparent. Figure 5 shows such a plot. From this it may be seen that the only particles with sufficient energy to penetrate the foil would be deuterons scattered from some heavy nucleus such as carbon, nitrogen, or oxygen. However, the low rate of rise of pressure in the closed-off system combined with $p-p$ scattering[9] data which showed no appreciable scattering from such heavy nuclei would seem to indicate that contamination was quite small. This same plot also shows that the amount of hydrogen contamination of the deuterium is not important as far as its contribution to scattered protons is concerned, but of course must be known in order to calculate the correct number of target nuclei per cm³.

According to theoretical predictions, the cross section of the center-of-mass system should obey an expression of the form $\sigma(\alpha)=A+B\cos^2\alpha+\cos^4\alpha+\cdots$. Attempts to fit the experimental data with terms up to $\cos^6\alpha$ were unsuccessful; however, a reasonable fit was obtained with $\cos^8\alpha$ terms. These coefficients are given in Table IV. A different set would be obtained if slightly different behavior were assumed about the 90° region.

The total cross section for the production of protons

TABLE IV. Coefficients for fit of data to the series.

$\sigma(\alpha)=A+B\cos^2\alpha+C\cos^4\alpha+D\cos^6\alpha+E\cos^8\alpha$

$A=+0.442\times10^{-26}$ cm²
$B=+0.708\times10^{-26}$ cm²
$C=-5.238\times10^{-26}$ cm²
$D=+5.122\times10^{-26}$ cm²
$E=+1.942\times10^{-26}$ cm²

was obtained from the above values by computing the sum

$$\sigma_T=4\pi\sum_{\alpha=0}^{\alpha=90}\sigma(\alpha)\sin\alpha\Delta\alpha$$

for $\Delta\alpha$ taken in 10° steps. The value so obtained was $\sigma_T=7.3\times10^{-26}$ cm².

VII. ACKNOWLEDGMENT

The authors wish to express their thanks to Professors G. F. Tape and A. O. Hanson for the many helpful discussions of the problems associated with this experiment; to Professor R. E. Meagher for his cooperation throughout the experiment and help in making many of the measurements; and to the cyclotron staff for their assistance in carrying out the numerous tasks connected with the construction and operation of the equipment.

PHYSICAL REVIEW VOLUME 78, NUMBER 6 JUNE 15, 1950

Proton-Proton Scattering at 5 Mev

R. E. MEAGHER
Department of Physics, University of Illinois, Urbana, Illinois*
(Received November 7, 1949)

The differential cross section for the scattering of protons by protons has been measured at an energy of 4.96±0.08 Mev, at angles from 12.5° to 55° in the laboratory system. The scattering medium was hydrogen gas at a pressure of approximately 5 cm of Hg. The scattered or recoil protons were detected by nuclear track photographic plates. Approximately 10,000 proton tracks were counted at each angle of observation. An estimate indicates the error of each individual cross section to be about two percent. Because the observations at each angle are made simultaneously, the relative accuracy from one angle to another is smaller and amounts to about 1.3 percent.

I. INTRODUCTION

THE scattering of protons by protons has been studied at a number of energies between 0.5 and 4.2 Mev[1-4] and at 7, 8, 10, and 14.5 Mev.[5-8] This experiment provides data at 5 Mev with hydrogen gas as the scattering medium and photographic plates for the detection of scattered protons in much the same way as the scattering experiment which was done at 7 Mev by Dearnley, Oxley, and Perry.[5] However, the details of the slit system differ from those reported by them. The photographic method of detection was selected because it provided a convenient method of rejecting background counts, otherwise troublesome in electrical systems, and because it permitted the recording of a large amount of data in a relatively short cyclotron operating time.

The scattering chamber described by Rodgers, Leiter and Kruger[9] was used to carry out this experiment.

* Assisted by the Joint Program of the ONR and AEC.

[1] Tuve, Heydenburg, and Hafstad, Phys. Rev. **50**, 806 (1936); Hafstad, Heydenburg, and Tuve, Phys. Rev. **53**, 239 (1938); Heydenburg, Hafstad, and Tuve, Phys. Rev. **56**, 1078 (1939).

[2] Herb, Kerst, Parkinson, and Plain, Phys. Rev. **55**, 998 (1939).

[3] Blair, Freier, Lampi, Sleator, and Williams, Phys. Rev. **74**, 553 (1948).

[4] A. N. May and C. F. Powell, Proc. Roy. Soc. **A190**, 170 (1947).

[5] Dearnley, Oxley, and Perry, Phys. Rev. **73**, 1290 (1948).

[6] R. R. Wilson and E. C. Creutz, Phys. Rev. **71**, 339 (1947).

[7] R. R. Wilson, Phys. Rev. **71**, 384 (1947).

[8] Wilson, Lofgren, Richardson, Wright, and Shankland, Phys. Rev. **71**, 560 (1947); **72**, 1131 (1947).

[9] Rodgers, Leiter, and Kruger, Phys. Rev. **78**, 656 (1950).

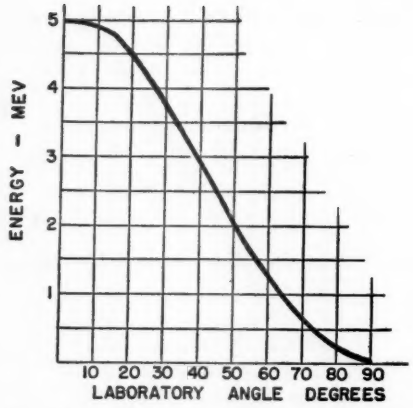

FIG. 1. Energy of scattered protons *vs.* laboratory scattering angle.

The incident beam of protons required for this experiment was obtained by accelerating singly charged molecular hydrogen ions (H_2^+).

II. SLIT SYSTEM

The equations relating the constants of the apparatus to the differential cross section are given elsewhere,[10] while the numerical values of the slit constants are given in reference 9.

In this experiment the length of the swath, either 1 cm or 1.5 cm, and the number of swaths counted for each observed angle of scattering were adjusted so that the number of tracks counted was between 5000 and 6000 per exposure per angle. A total of about 10,000 tracks were counted in two exposures for each angle. These exposures were called Run 8 and Run 10 and the final equations giving the cross section as a function of angle for these exposures are:

Run 8

$$\sigma_{\text{lab}} = (\text{counts per 1-cm swath}) \times (1.205^4 \times 10^{-4})/\sin^2\theta \sin(\theta+\phi) \text{ barns.}$$

Run 10

$$\sigma_{\text{lab}} = (\text{counts per 1-cm swath}) \times (1.239^4 \times 10^{-4})/\sin^2\theta \sin(\theta+\phi) \text{ barns,}$$

where a barn is 10^{-24} cm^2.

The penetration correction has been discussed for this apparatus in reference 9. In this experiment the fractional increase in slit width is 0.03, 0.03, 0.04, 0.03, 0.03, 0.02, 0.02, 0.01, 0.01, and 0.01, for laboratory angles of 12.5°, 15°, 20°, 25°, 30°, 35°, 40°, 45°, 50°, and 55°, respectively.

A simple experiment was carried out with slits which were approximately just closed to verify the correctness of the slit penetration correction. Within statistical errors the calculated corrections were verified.

A run was carried out which indicated that the slit scattering in this experiment amounted to approximately 0.2 percent of a normal run at 15° and about 0.02 percent of a normal run at 45°. Corrections corresponding to these figures were used in obtaining the final cross sections.

The angular resolution varied from about ±1° at 12.5° to ±2° at 55°.

[10] Leiter, Rodgers, and Kruger, Phys. Rev. **78**, 663 (1950).

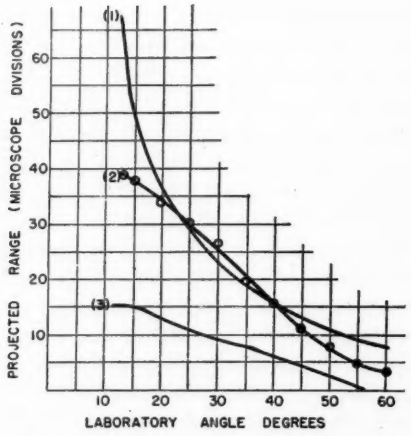

FIG. 2. (1) The projected range available *vs.* angle for an emulsion thickness of 50μ. (2) The observed maximum projected range of protons *vs.* angle. In the region between 25° and 38° a large fraction of the protons would actually hit the glass backing of the photographic plate. (3) The minimum projected range considered acceptable in counting tracks.

III. DETECTION OF PROTONS

Just as in references 9 and 10, the plates were designated C-2 and manufactured by the Ilford Company. The energy of the protons as a function of angle which the plates must register is easily calculated from the equations for conservation of energy and momentum. A graph of proton energy as a function of angle is given in Fig. 1.

The Counting of Proton Tracks

In observing the proton tracks at a given angle, the projected length varies from one track to another. The expected length of a track can be plotted and is shown in Fig. 2 as curve (2). Any given track may appear longer than that shown by a small amount because the proton may be scattered so that it makes a smaller angle with the plate than an unscattered proton. Any given track may be shorter than the curve (2) because of angular scattering, because it hits the glass backing (between 24° and 38°), because it has penetrated the slit, or because it results from some undesirable reaction unrelated to p–p scattering. Most of the tracks do fall into one large group. This can be seen by a range analysis as shown in Fig. 3.

It is not desirable to count the very short tracks because they do not represent p–p scattering (unless they penetrate the slit edge). On the other hand, relatively small amounts of scattering in angle can considerably reduce the projected range. It is, therefore, necessary to count tracks considerably shorter than the

normal length. The criterion selected for counting was such that the minimum length had to be greater than 40 percent of the normal length [Fig. 2, curve (3)].

The counting was carried out by three persons.[11] After an initial practice period it was found that any two observers agreed on the number of tracks in a given swath to better than 0.5 percent. No observer was consistently high or low. An individual observer can usually repeat his own count of a given swath to somewhat better than 0.5 percent.

IV. MEASUREMENT OF PROTON BEAM CURRENT

Proton Beam and Faraday Cage

The beam used in this experiment was obtained by accelerating molecular hydrogen ions (H_2^+). This has the advantage that the resonance and focusing conditions are substantially the same as for deuterons for which the cyclotron had been adjusted. The two protons in such an ion are, of course, bound by only a few volts so that there should be no appreciable effect on the scattering or the measurement of current since the beam must pass through a Nylon foil and a dural foil, each of which absorbs energy.

In order to show that the use of H_2^+ ions did not affect the beam current measurement, a simple experiment was performed by noting the size of the current received at the Faraday cage with and without the presence of the Nylon and aluminum foils. This experiment indicated that the current received at the Faraday cage was larger by the factor 2.03 ± 0.03 than when no foils were present. In the measurements made of proton current no error has been listed due to this cause.

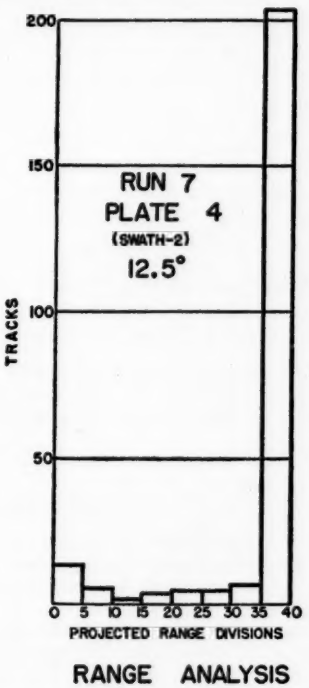

FIG. 3. A typical histogram of the tracks observed with a normal slit.

[11] H. A. Leiter, F. A. Rodgers, and the author.

TABLE I.

Faraday cage volts with respect to ground	Main cyclotron target beam current in μa	Faraday cage beam current in amp. No magnet	Magnet
+45	14±1	6×10^{-11}	10.0×10^{-11}
0	14±1	10×10^{-11}	10.1×10^{-11}
−45	14±1	15×10^{-11}	10.0×10^{-11}

An appreciable number of secondary electrons are associated with any surface struck by the beam. A permanent magnet with a field of about 2000 oersteds was placed so that its field was perpendicular to the beam at the entrance to the Faraday cage to prevent these electrons from invalidating the readings. Again a simple experiment was performed to check this. An arrangement was made to change the potential of the Faraday cage with respect to ground (the outside vacuum-tight shell) and at the same time to read current. The current at the main cyclotron target was held as constant as possible. If secondary electrons were causing any current to be registered then the accelerating voltage (45 v) would tend to change the measured value of the beam. The results are shown in Table I. Although the readings were taken rapidly so that adjustments could not drift very much, the experiment cannot be considered precise. Nevertheless, it is clear that any secondary electron effect (or leakage due to gas ionization current) must be fairly small. In measurements the effect was assumed to be negligible.

The pressure in the Faraday cage during runs was 2×10^{-5} mm of Hg as measured on an ion gauge.

Charge Measurement

An electronic circuit, briefly referred to in this paper as a "Q-meter," was used to integrate over time the current passing to the Faraday cage. Its operation was fundamentally very simple: The current from the proton beam caused a condenser of 33 $\mu\mu$f to charge up in the positive direction with respect to ground. When the potential on the condenser changed by 3 v the electronic circuit automatically shorted the condenser back to its starting potential and a total charge of about 10^{-10} coulomb was registered as a count. The process was repeated indefinitely and the number of counts was observed by a suitable scalar and register circuit.

Because the currents measured were of the order of 10^{-9} amp. electrometer type tubes were used in the input to the circuit.

The condenser of 33 $\mu\mu$f was made up mainly of the capacity of the Faraday cage to ground and to a less extent of the connecting lead wires and the electrometer tubes. Except for the actual input circuit to which the Faraday cage was connected, the circuit was a.c. coupled so that changes of d.c. potential associated with electrometer tubes could not affect the calibration. It was therefore the change in voltage of three volts

TABLE II. Run constants.

	Accepted	Closed slit run	Accepted
Run No.	8	9	10
Date of run (1948)	Nov. 18	Nov. 22	Nov. 23
Faraday cage pressure (10^{-5} mm Hg)	1.5	2.5	2
Vacuum in chamber (10^{-5} mm Hg)	5	2.0	4
Rate of rise (10^{-4} mm Hg per min.)	1.25	0.5	1.6
Beginning pressure cm of oil	75.920	74.39	73.040
Beginning temperature of oil in °C	23.7	22.6	21.5
Beginning temperature of H_2 in °C	25.0	24.8	22.9
Final pressure cm of oil	76.405	75.110	73.742
Final temperature of oil in °C	24.2	23.3	21.8
Final temperature of H_2 in °C	25.9	25.8	23.5
Total Q counts	19,204	19,202	19,201
Time of run in sec.	1632		2802
Acceleration of gravity = 980.14 cm/sec.[2]			

across the condenser which was held constant rather than the absolute d.c. values of the voltage across the condenser.

Calibration of the instrument was accomplished by using a high resistance and knowing the average voltage across the resistor. The voltage was read on two voltmeters, one at each end of the resistor measuring the respective potentials to ground. One of the voltmeters was of necessity a vacuum tube voltmeter. Both voltmeters were originally calibrated against a standard cell but their panel type movements permit reading the voltage to only about ± 0.5 percent.

The resistors were calibrated against a Victoreen resistor labeled 2540 megohms and calibrated by the Bureau of Standards to be 2450 megohms at 25°C and 2440 megohms at 30°C with a stated accuracy of ± 0.5 percent. The resistances calibrated were from 5000 to 100,000 megohms. A simple shielded Wheatstone bridge was set up with the calibrated resistor as standard. The detector for null was a polystyrene dielectric condenser of 0.1 μf. Time was allowed for the condenser to charge and then its potential was noted by the size and polarity of the signal as observed in an oscilloscope when the condenser was discharged through a 10-megohm resistor. Since this method is subject to some systematic errors a considerable error must be assigned to this measurement, especially for resistors higher than 5000 megohms. An error of one percent has been assigned to this. Considering these three errors to be 0.5, 0.5 and, one percent and combining them,[12] one obtains 1.22 percent as the error in charge measurement.

The calibrations for run 8 and run 10 made immediately preceding the runs is shown in Fig. 4.[13]

It may be noted that at low currents the "Q-meter" calibration constant increased but the instrument was generally used considerably above this region. It may be noted that the shape of the calibration curve had changed from run 8 to run 10. No explanation of this can be given though it is not reasonable that the shape should change. Accordingly, a sort of average line has been drawn for both calibrations and an error of perhaps 0.5 percent must be considered in ability to repeat measurements. This brings the combined error for charge measurement up to ± 1.32 percent.

There was some evidence that violent arcs of the cyclotron power oscillator affected the Q-meter by the insertion of extra counts. On a single such arc-back as many as 20 counts were noted. Out of a normal 19,200 counts for a run this is seen to be a possible 0.1 percent per arc-back. However, "violent" arc-backs were eliminated by operating the power oscillator on a lower step but some smaller arcs almost always occur during a run of 30 min. In trying to simulate the effect during a calibration the effect was small compared to 0.5 percent.

V. MEASUREMENT OF PROTON ENERGY

The measurement of proton energy was made by a simple range measurement. With the chamber evacuated and the Faraday cage assembly removed, the beam passed through a single dural foil about 0.001 in. thick. The maximum range of the protons was then noted on a fluorescent screen while the analyzer current was close to 28.8 amp. which was the normal value of the analyzer current during the runs. The measurements made were: "maximum" range in air = 30.4 ± 0.5 cm, atmospheric pressure = 74.79 cm of Hg, temperature = 20°C.

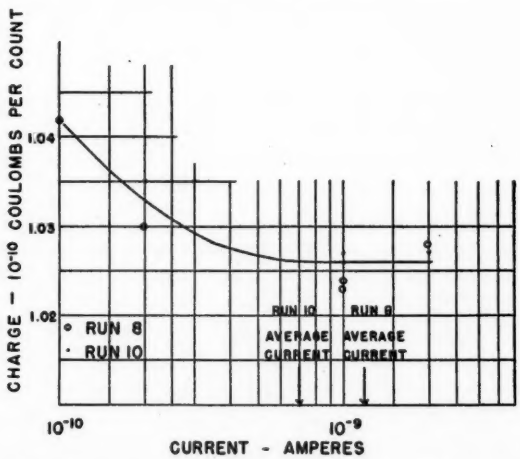

FIG. 4. Calibration of the Q-meter circuit made immediately preceding run 8 and run 10. Check points are shown taken at 10^{-9} amp. immediately following each run.

[12] R. T. Birge, Am. Phys. T. 7, 352 (1939).

[13] A second method of calibration of the Q-meter was developed by G. F. Tape and J. G. Cottingham after the completion of the experiment. The charge required for calibration was supplied (through one of the calibration resistors) by a standard condenser. The amount of the charge was determined by the measurement of a potential difference (measured with a potentiometer and standard cell with a vacuum tube circuit as detector) and a standard capacitance calibrated by the Bureau of Standards. A comparison of the two methods, resistor and capacitor, showed a difference of 1.3 percent, the capacitor method giving the lower value of coulombs per count. It is believed that the capacitor method is the more accurate of the two. Consequently, the quoted cross sections may be too low by 1.3 percent in absolute value.

TABLE III. Results of runs 8 and 10.

θ	Run 8 Number of 1-cm swaths per run	Run 8 Total counts	Run 8 σ_{lab} (uncorrected) barns	Run 10 Total counts	Run 10 σ_{lab} (uncorrected) barns	σ_{lab} average (barns)	σ_{lab} corrected for slit penetration (barns)	σ_{lab} corrected for vacuum run (barns)	$\sigma_{C.M.}$ (barns)
12.5°	36	5763	0.4881	5474	0.4767	0.4824	0.4686	0.4679	0.1198
15	27	5150	0.3960	4780	0.3780	0.3870	0.3750	0.3741	0.0968
20	18	5747	0.3629	5455	0.3541	0.3585	0.3465	0.3463	0.0921
25	12	5864	0.3509	5625	0.3461	0.3485	0.3370	0.3369	0.0929
30	9	6196	0.3435	6033	0.3440	0.3438	0.3334	0.3333	0.0962
35	6	5265	0.3264	5285	0.3369	0.3317	0.3242	0.3241	0.0989
37.5				5750	0.3232	0.3232	0.3163	0.3163	0.0997
40	6	6537	0.3190	6064	0.3043	0.3117	0.3054	0.3054	0.0997
40.5				6301	0.3095	0.3095	0.3034	0.3034	0.0998
45	1183	7102	0.2852	6988	0.2888	0.2870	0.2834	0.2833	0.1002
50				7512	0.2655	0.2655	0.2628	0.2628	0.1022
55				7304	0.2284	0.2284	0.2267	0.2267	0.0988

TABLE IV. Other corrections and final cross sections.

θ	Number of swaths counted per plate	Length of swath cm	$\frac{\Delta b \sin 2\theta}{2(b-a)} \frac{180}{\pi}$	% per degree correction	% correction due to angle	% correction due to $(b-a)$	% correction due to b	All Table IV corrections in percent	$\sigma_{C.M.}$ from Table III (barns)	$\sigma_{C.M.}$ after all corrections (barns)
12.5°	4	1.5	−0.147	+4.76	−0.70	+1.14	+0.80	+1.24	0.1198	0.1213
15	3	1.5	−0.115	+5.71	−0.65	+0.81	+0.54	+0.70	0.0968	0.0975
20	2	1.5	−0.067	+9.00	−0.60	+0.37	+0.25	+0.02	0.0921	0.0922
25	2	1.0	+0.0069	+7.88	+0.05	−0.03	−0.02	0	0.0929	0.0929
30	1	1.5	+0.022	+5.71	+0.13	−0.09	−0.06	−0.02	0.0962	0.0962
35	1	1.0	+0.097	+4.25	+0.41	−0.34	−0.23	−0.16	0.0989	0.0988
37.5	1	1.0						−0.27	0.0997	0.0994
40	1	1.0	+0.129	+2.82	+0.36	−0.45	−0.30	−0.39	0.0997	0.0993
40.5	1	1.0						−0.41	0.0998	0.0993
45	1	1.0	+0.156	+1.90	+0.30	−0.53	−0.36	−0.59	0.1002	0.0996
50	1	1.0	+0.173	0	0	−0.62	−0.42	−1.04	0.1022	0.0992
55	1	1.0	+0.180	−1.23	−0.22	−0.67	−0.45	−1.34	0.0988	0.0975

Correcting the maximum range to an atmosphere of 76 cm of Hg and 15°C one gets 29.4±0.5 cm as the maximum range. Since the mean range is about 2.7 percent less than the maximum range observed in this way,[14] the mean range is 28.6±0.5 cm. This gives an energy of 4.53±0.05 Mev. To this energy must be added the energy lost in passing through the dural foil.

From Smith[15] the figure of 8.2 mg/cm² of Al is found equivalent to 0.5 Mev of protons between 4.5 Mev and 5.0 Mev. From Aron[16] 2.00 mg/cm² of Cu is equivalent to 1 cm of air for 5.0-Mev proton, or since about 5.6 cm of air is equivalent to 0.5 Mev of protons then 2×5.6=11.2 mg/cm² of Cu is equivalent to 0.5 Mev of protons.

Since dural is approximately 95 percent aluminum and five percent copper, then 8.2×0.95+11.2×0.05 =8.35 mg/cm² of dural is equivalent to 0.5 Mev of protons. Two samples of dural foil from the same sheet as the piece used at the entrance to the Faraday cage gave 7.50 mg/cm² and 7.55 mg/cm². Taking the average, one gets for the foil thickness (7.525/8.35)×0.5=0.45 Mev. The error in this figure is a little difficult to assess.

The energy of the beam in the scattering chamber without hydrogen was then 4.98±0.05 Mev. The beam passed through about 20 cm of hydrogen gas at a

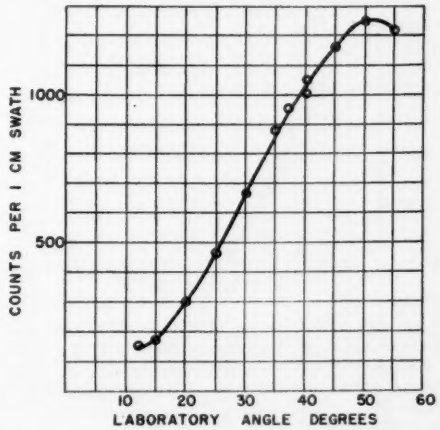

FIG. 5. The density of tracks in counts per swath area 1 cm ×0.01869 cm taken from the results of both run 8 and run 10.

[14] In an experiment which was carried out at a later date on a 10-Mev deuteron beam measuring the ionization current as a function of range Mr. C. J. Taylor has found that the mean range is about 2.7 percent less than the "maximum" range which probably would be observed by using a fluorescent screen. This same experiment would give the energy of the proton beam in the scattering chamber to be 4.93±0.05 Mev if the proton beam were assumed to have half of the energy of the deuteron beam.

[15] J. H. Smith, Phys. Rev. 71, 32 (1947).

[16] *Handbook of Radioactivity and Tracer Methodology* (1948), Air Force Technical Report No. 5669, p. 183.

pressure of 5 cm of Hg before it reached the center of scattering volume during a normal experiment. This reduced the energy to about 4.96±0.05 Mev.

An additional uncertainty in energy was introduced by the fact that the analyzer was adjusted during a run in such a way as to keep the beam in the Faraday cage a maximum. The analyzer current was thus not strictly a constant and its variation may have been due to iron hysteresis or beam energy or a combination of the two. The average variation during a run did not amount to more than ±0.2 amp. The normal current was 28.8 amp. Since the field H is proportional to the current at the low values of induction used, and the energy is proportional to the square of the field, the energy uncertainty corresponding to ±0.2 ampere is about ±1.4 percent.

Combining these errors one obtains the energy as 4.96±0.08 Mev.

VI. SCATTERING RUNS

Procedure

The filling of the main scattering chamber with hydrogen has been discussed in reference 9. Similarly, the procedure carried out in taking the data was the same. The important constants associated with the three runs from which the data were analyzed are given in Table II.

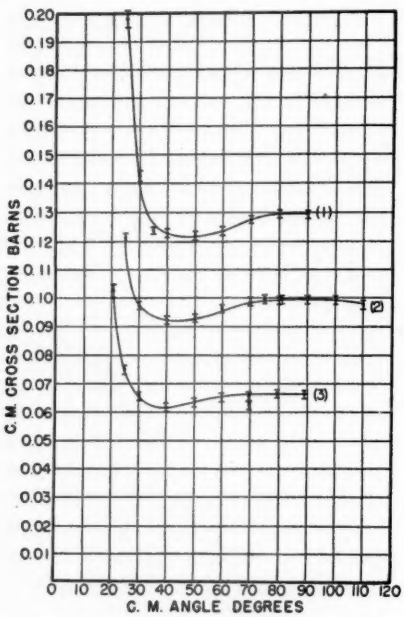

FIG. 6. Cross section *vs.* angle. (2) 4.96±0.08 Mev from Table IV; for comparison with the results published at other energies (1) shows 3.53±0.02 Mev from Blair, Freier, Lampi, Sleator, and Williams (reference 3) and (3) shows 7.03±0.06 Mev from Dearnley, Oxley, and Perry (reference 5). The errors drawn for (1) are the uncertainties listed by the authors in reproducing the cross sections from week to week, while those drawn in (2) and (3) are the relative errors from one angle to another.

Results

The results of runs 8 and 10 are shown in Tables II–IV.

A simple statistical analysis has been made of run 10. It shows that the number of counts N on 39 percent of the points on each plate deviate by more than $(N)^{\frac{1}{2}}$ with respect to the average N for the corresponding angle on all plates. Also, totaling all the counts on each plate shows that two out of the six plates deviate by more than $(N)^{\frac{1}{2}}$ from the average for all six plates.

The total number of tracks counted at each 5° angle is somewhat over 10,000 except at 50° and 55°. The total number of tracks recorded for these data is 120,175.

The conversion from laboratory cross section to center-of-mass cross section is carried out by noting that $\sigma_{C.M.}=\sigma_{lab}/4\cos\theta$ where θ is the angle in the laboratory system.

Figure 5 gives the number of tracks per 1-cm swath area (0.01869 cm²) on a plate as function of angle.

Because the 40° position on run 10 gave a low cross section, counts were made at 37.5° and 40.5°.

Corrections

Measurements of the photographic plate positions indicated that the photographic plates were not parallel to the beam. The diameter ($2b$) was measured at the low angle end and the high angle end of each pair of plates. The measurements are shown in Table V.

As a consequence of this the photographic plates were 0.0147 cm farther from the beam at the low angle end than normal and 0.0193 cm closer to the beam at the high angle end than normal. This causes certain errors, which together with an error due to the fact that the photographic plates are flat instead of curved need to be considered before obtaining the final cross sections. These corrections are given in Table IV and will now be considered.

The angle θ at which each plate was counted was not the even angle listed in the tables because b was not the normal value. The radius b is in error both because the radius changes slightly with position on the plate and because the plate is flat. The first of these errors is obtained directly from the plate position error, while the second requires finding the average angle which results from using a straight swath rather than a curved swath. The error in angle $\Delta\theta$ from these two effects is

$$\Delta\theta=\frac{\Delta b\,\sin 2\theta}{2(b-a)}\,\frac{180}{\pi}\ \text{degrees}.$$

The error in angle $\Delta\theta$ together with Fig. 5 makes possible the correction in percent due to the angle error.

An error in $(b-a)$, the radial distance from the slit to the plate, is a simple geometrical error due to the error in b.

The error in b is the result of the fact that the azimuthal angle is in error. The azimuthal angle in the derivation has been taken to be $2(c/b)$ radians where c is one-half the swath length. On the other hand, the exact azimuthal angle, since the photographic plate is flat is

$$2 \arctan\frac{c}{b} = 2\left[\frac{c}{b} - \frac{c^3}{3b^3} + \cdots\right]$$

so that a correction of $-\frac{1}{3}c^2/b^2$ is necessary.

The last column of Table IV gives the final center-of-mass cross sections for each angle.[17] These are plotted in Fig. 6.

ERRORS

An attempt is made to assign errors to each quantity entering into the final cross sections. The point of view chosen will be that of the assessment of errors for a given point on an absolute basis. Clearly some of the errors could be omitted if relative errors only, for example from one angle to another, were considered. It is believed that the errors listed below are r.m.s. errors. They will be combined by taking the square root of the sum of the squares.[12] In each case in the final table the actual error of the quantity is not necessarily listed but rather its effect upon the cross section.

Tabulation of errors.—Number of counts: human counting error, 0.5 percent; statistics, 1.0 percent.

Incident beam charge (Q-meter), 1.32 percent.

[17] The S-wave phase shifts corresponding to these data are given by J. D. Jackson and J. M. Blatt, Rev. Mod. Phys. 22, 77 (1950).

TABLE V.

Plates	High angle end b	Low angle end b
1–4	4.752 cm	4.795 cm
2–5	4.775	4.797
3–6	4.757	4.795
Average	4.761	4.795

Atoms per cm³ of gas: height of oil column, 0.05 percent; temperature, 0.3 percent; oil density, 0.1 percent.

Solid angle: swath width, 0.3 percent; swath length, 0.4 percent; b (radius to plate), 0.1 percent.

Length of target: W (slit width), 0.1 percent; $(b-a)$ 0.4 percent.

Slit penetration correction, 0.5 percent; slit angle θ, 0.1 percent.

Square root of the sum of the squares of the preceding errors, 1.94 percent.

Energy, 1.7 percent.

ACKNOWLEDGMENTS

The author wishes to thank Professor P. G. Kruger who suggested to him the general field of charged particle scattering and aided with many suggestions; Dr. F. A. Rodgers who designed and followed the construction of the scattering chamber and Dr. H. A. Leiter who aided in the construction, both of whom aided in taking data; and Professor G. F. Tape who aided with many suggestions. The accurate machining necessary on some parts of the apparatus was done by Mr. D. F. Kibler and Mr. Charles Van Holland.

The author was aided by a National Research Council predoctoral fellowship.

Correlation of Geomagnetic Cosmic-Ray Effects*

H. V. NEHER
California Institute of Technology, Pasadena, California
(Received February 27, 1950)

With the experimental data collected in a B-29 airplane and given in an earlier report, an attempt is here made to correlate several of the well-known geomagnetic effects found in cosmic rays. First, evidence is presented to show that, within the uncertainties of the experimental data and the existing calculations on the behavior of charged particles in the magnetic field of the earth, there are few if any negative primary particles in the momentum range 7 to 23 Bev/Zc compared with positives. Second, under the assumption of no primary negative particles and by correlating experimental data on the latitude effect at different zenith angles with the zenith angle effect in the east-west plane at the equator, it is possible, with the help of calculations of Vallarta *et al.* at the equator, to determine curves of minimum momentum for the primaries as a function of geomagnetic latitude. It is thus possible to plot curves for intermediate latitudes where the calculations are extremely difficult and have not been carried through in detail except in certain special cases. The results are independent of any assumed momentum distribution of, or the magnitude of charge carried by the primary particles.

I. INTRODUCTION

IT has been pointed out by Biehl, Neher, and Roesch[1] that the near-quality in the east-west effect for the penetrating and non-penetrating components at the geomagnetic equator at an air pressure of 235 g/cm^{-2} argues strongly for the same kind of primary particle responsible for both. Analysis of other data taken at the above and other pressure altitudes by these authors at the geomagnetic equator gives further evidence that the same primary particles are responsible for the non-penetrating as well as the penetrating radiation found at the above atmospheric pressure. This is contrary to the conclusion reached by Johnson and Barry[2] from their balloon flights made at 20° geomagnetic north. They found it necessary to assume a mixture of primary protons with positive and negative electrons to account for their measured small east-west effect.

Several attempts to correlate the various geomagnetic effects have been made in the past. Among these may be mentioned that of Johnson.[3] At that time the experimental data were inadequate to permit arriving at definite conclusions. Jánossy[4] finds a correlation between the east-west effect at sea level and the latitude and longitude effects assuming only incident positively charged primaries, but at high altitudes the correlation using the data then existing made it necessary to assume other kinds of primaries.

In what follows an attempt is made to correlate the various geomagnetic effects by using the calculations of Vallarta *et al.* assuming that the primary cosmic rays consists only of positively charged particles. The analysis will be independent of the magnitude of the charge carried by the primary particles and hence applicable to a mixture of positively charged particles such as protons and heavier nuclei.

The experimental data on which the following results are based were published by Biehl, Neher, and Roesch [Phys. Rev. **76**, 914 (1949)]. This article will be referred to hereafter as (A).

II. MOMENTUM OF PRIMARY PARTICLES AT THE GEOMAGNETIC EQUATOR AND LONGITUDE 80°W

On the geomagnetic[4a] equator at geographic longitude 80° W two factors reduce the least momentum of the particles that can reach a given position in the sky compared with that calculated by assuming a magnetic dipole situated at the center of the earth. One of these is due to the fact that the earth's magnetic field can best be represented by a dipole situated approximately 300 km from the center of the earth. The longitude effect found at sea level by Clay[5] and independently by Millikan and Neher[6] is explained by such an eccentric dipole. The other factor affecting the minimum momentum for particles at the equator is the tilt of the earth's magnetic field. It was pointed out by the author[7] in 1935 that the surfaces of equal horizontal intensity of the earth's magnetic field are in general tilted with respect to the surfaces of equal gravitational potential along the geomagnetic equator and that this would tend to reduce the measured east-west effect in Peru and increase it in the region of Africa.

The map published by Millikan and Neher,[8] showing lines of equal cosmic-ray intensity at sea level, agrees with magnetic maps, showing lines of equal horizontal intensity, in placing Peru approximately 60° west of the region where the axis of the equivalent dipole is farthest from the surface of the earth. Using the calculations of Vallarta[9] on the longitude effect, we

* Assisted by the joint program of the ONR and the AEC.
[1] Biehl, Neher, and Roesch, Phys. Rev. **75**, 688 (1949).
[2] T. H. Johnson and J. G. Barry, Phys. Rev. **56**, 219 (1939).
[3] T. H. Johnson, J. Franklin Inst., **226**, 533 (1938).
[4] L. Jánossy, *Cosmic Rays* (Oxford at the Clarendon Press, London, 1948), pp. 308–313.
[4a] Geomagnetic latitude as here used is computed from a dipole situated at the center of the earth.
[5] Clay, van Alphen, and 't Hooft, Physica **1**, 829 (1934).
[6] R. A. Millikan and H. V. Neher, Phys. Rev. **47**, 205 (1935).
[7] H. V. Neher, Phys. Rev. **47**, 417 (1935).
[8] R. A. Millikan and H. V. Neher, Phys. Rev. **50**, 15 (1936).
[9] M. S. Vallarta, Phys. Rev. **47**, 647 (1935).

conclude that as far as eccentricity of the dipole is concerned the minimum momentum required for a particle[9a] with electric charge Z to reach the vertical at the equator at 80° W is 14.2 Bev/Zc instead of 15.0 as calculated for the symmetrical dipole.

Curves giving the tilt of the earth's magnetic field have been published by Vallarta,[10] but for present purposes it is perhaps better to scale off the distances between lines of equal horizontal intensity from available maps. We find by such means that the tilt in the region of Peru is approximately 4° as compared with 3° taken from Vallarta's curves.

To find the effect of this tilt on the minimum momentum of a particle at the equator we use the calculation on the Störmer cones.[11] Assuming, for example, that the effect of tilt in Peru is to decrease the momentum by an amount which corresponds to changing the zenith angle in the east-west plane by 4°, we find that at the vertical the corresponding change in momentum for a particle of charge Z is -0.7 Bev/Zc. The effect of tilt and eccentricity, then, is to reduce the symmetrical dipole value at the vertical from 15 to 13.5 Bev/Zc for the region of Peru. For other zenith angles in the geomagnetic east-west plane we calculate the values shown in Fig. 1.

III. EVIDENCE OF ABSENCE OF NEGATIVE PARTICLES IN PRIMARY RADIATION

Experiments of Hulsizer[12] on burst production under lead at high altitudes indicate that the relative numbers of incident electrons to total particles at geomagnetic latitude 53°N is less than 6 percent. A comparison in reference (A) of the east-west effect with the latitude effect also indicates that the number of negative primaries relative to positives is small in the momentum range 9 to 13.5 Bev/Zc. Because of the importance of this point some further discussion may be justified.

Since the latitude effect depends on the sum of the effects due to primary positive and negative particles while the east-west effect depends on their difference, a comparison of the two constitutes a means of determining their relative numbers.

In a series of experiments reported in (A), cosmic-ray telescopes were carried at 30,000 ft. pressure altitude from 64° N to the equator along longitude 80° W. These telescopes were pointed at zenith angles 45° E, 0°, and 45° W, and included measurements with no added absorber, 10 and 20 cm of lead between the counter trays. Data taken with 10 and 20 cm of lead absorber will be used since the effects of scattering are much less important than without an absorber (see reference (A)). Shown in (A) Figs. 6 and 8 are the counting rates taken as a function of geomagnetic latitude with both 10 and 20 cm of lead for a telescope pointed 45°E as well as 45°W and also at the vertical.

Let: j_{0E} = radiation remaining at 45° E at the equator. Δj_1^+ = change in radiation at 30,000 ft. pressure altitude caused by positive primaries whose momentum lies between the least allowable value at 45° toward the west and 45° toward the east at the equator. From Fig. 1 we find these two values to be 10.3 and 23.5 Bev/Zc. Δj_1^- = similar change caused by any negative particles in this momentum range.

There is some latitude, λ_1, where the momentum for positives at 45° E becomes the same as for positives at 45° W at the equator. In going to this latitude the negatives toward the west change their minimum momentum from 23.5 to 10.3 Bev/Zc, while the positives toward the east change their momentum by the same amount. The change in momentum for negative primaries at 45° E in going from the equator to latitude λ_1 is from 10.3 down to approximately 7 Bev/Zc, the exact value being unimportant at present. This is also the range in momentum of positive particles for this same latitude change at 45°W.

Let: Δj_2^+ = change in radiation caused by positives in this latter momentum range. Δj_2^- = similar change caused by negatives in this same momentum range. Then the ratio of the change from 45°W to 45° E to that remaining at the equator is

$$\rho_1 = \frac{\Delta j_1^+ - \Delta j_1^-}{j_{0E}}. \tag{1}$$

Likewise the ratio of the change in going from the equator to λ_1 as defined above for a telescope pointing

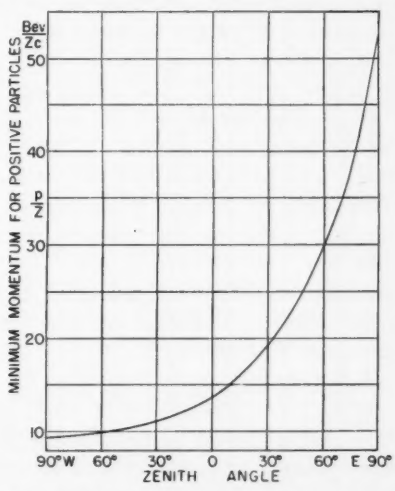

FIG. 1. Minimum momentum per unit charge for positive particles at the geomagnetic equator *vs.* zenith angle at geographic longitude 80° W. Based on calculations of Lemaitre, Vallarta *et al.* on the behavior of charged particles in the magnetic field of the earth but corrected for tilt of the magnetic field and the eccentricity of the dipole.

[9a] Expression momentum in terms of Bev/Zc, where Z is the net number of unit charges carried by the particle, gives a quantity independent of the mass and charge of the particle and the calculations based on unit charge may therefore be used. Since the heavy primary particles appear to be completely stripped of their electrons, Z for this case becomes equal to the atomic number.

[10] M. S. Vallarta, Phys. Rev. **74**, 1937 (1948).

[11] G. Lemaitre and M. S. Vallarta, Phys. Rev. **50**, 493 (1936).

[12] Robert I. Hulsizer, Phys. Rev. **76**, 164(A) (1949).

45° E to that remaining at 45° E at the equator is

$$\rho_2=\frac{\Delta j_1^+ + \Delta j_2^-}{j_{0E}}. \tag{2}$$

Further, the ratio of the change in radiation at 45° W to 45° E at latitude λ_1 to that remaining at the equator at 45° E is:

$$\rho_3=\frac{\Delta j_2^+ - \Delta j_2^-}{j_{0E}}. \tag{3}$$

Subtracting (1) from (2) and dividing by the sum of (2) and (3) we get

$$\frac{\Delta j_1^- + \Delta j_2^-}{\Delta j_1^+ + \Delta j_2^+}=\left(\frac{\Delta j^-}{\Delta j^+}\right)_{7-23}=\frac{\rho_2-\rho_1}{\rho_2+\rho_3}. \tag{4}$$

This gives the ratio of the intensity due to negative primaries in the momentum range 7 to 23 Bev/Zc to that due to positives in the same momentum range in terms of the experimental quantities, ρ. If $\rho_2=\rho_1$, then the contribution measured would be zero. The problem cannot be solved accurately since the calculations on the minimum momentum at intermediate latitudes have not been carried through. The value of ρ_2 (and ρ_3) will depend on the particular latitude at which the minimum momentum for positives at 45° E becomes equal to that at the equator at 45° W. If we choose the lower curve E_1, published by Vallarta,[10] we find this latitude to be 29.3° N. For the average of 10 and 20 cm of lead we find from reference (A) Figs. 6 and 8, $\rho_1=0.33\pm0.02$, $\rho_2=0.27\pm0.08$, $\rho_3=0.22\pm0.03$, where the uncertainties are estimated from the statistics of the counting rates and the individual values for 10 and 20 cm of lead absorber. The chief error lies in the value of ρ_2 which is the relative increase in the counting rate in going from the equator to 29.3° N for the telescope pointing 45° E. For the case of 10 cm of lead the latitude where the cosmic-ray intensity at 45° E becomes equal to that at 45° W at the equator is 28.3° N while the similar latitude for 20 cm of lead is 34.0° N. The reason for this discrepancy is not known and we have taken the average of the data for 10 and 20 cm of lead as representing the best estimate that can be made at the present time.

Using the above experimental values of ρ we find, for the ratio of negative particles to positives in the momentum range 7 to 23 Bev/Zc,

$$(\Delta j^-/\Delta j^+)_{7-23}=-0.12\pm0.15.$$

It is obvious that to be physically significant this ratio must be positive or zero. We shall in what follows assume that all of the primary particles are positively charged. The consistency of the results will be added justification for this assumption.

The procedure to be followed is to take the calculations of Vallarta *et al.* in the east-west plane at the equator as correct (Fig. 1) and then to correlate the measurements in this east-west plane with measurements as a function of some other parameter such as latitude, longitude, or azimuth. We shall use the average of the data with 10 and 20 cm of lead absorber although the accuracy is not as good as with no absorber. The justification for using the lead data is that it was shown in reference (A) that when the telescopes with lead absorber were pointed at an angle to the vertical, the counting rate was the same as when pointed at the vertical provided (a) the intervening mass of air was the same and (b) the primary radiation incident on the top of the atmosphere was the same.

IV. CORRELATION OF LATITUDE EFFECT AND ZENITH ANGLE EFFECT WITH THE CALCULATIONS OF VALLARTA *et al.*

Lemaitre and Vallarta[11] have given the boundaries to the cones for certain minimum momenta of the primary particles at the equator. The particular boundary that passes through the vertical in a north-south direction bends toward the west for increasing zenith angle. An application of Liouville's theorem implies that the primary radiation is constant at all zenith angles along this boundary. Using a lead absorber it was shown in reference (A) that the intensity measured was independent of the zenith angle and depended only on the mass of intervening air for the same incident radiation on the top of the atmosphere. We thus imply from this and from Liouville's theorem that if at two locations where the mass of intervening air is the same and the same intensity is measured, then the incident primary radiation is the same. Thus if at a certain latitude, longitude, air pressure, azimuth angle, and zenith angle a certain intensity of particles is measured that can penetrate the lead absorber, then, if the same intensity is measured at some other latitude, longitude, air pressure, azimuth angle, and zenith angle for the same mass of intervening air, the primary radiation incident

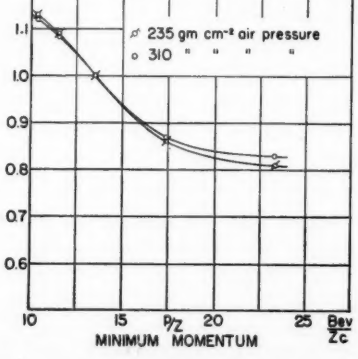

FIG. 2. Experimental values of the ratio of cosmic-ray intensity measured in the east-west plane at the geomagnetic equator to that in a direction of constant momentum through the same mass of air, *vs.* the least allowable momentum for that particular direction. See reference (A) [Phys. Rev. **76**, 914 (1949)] for experimental data.

on the top of the atmosphere is the same. This is again under the assumption that all the incident particles have the same sign of electric charge.

The zenith angle effect, as plotted in Fig. 26 of (A) is for a telescope pointed in the direction of this constant momentum boundary at the equator and hence for primary particles of the same minimum momentum as for the vertical. The ratio of the values for the same zenith angle taken in the east-west plane to those in this constant momentum direction is then different from unity only because of the different primary momentum range included. In Fig. 2 this ratio is plotted, not as a function of zenith angle, but of the least allowable momentum for the particular direction as obtained from Fig. 1. The data are for the average of 10 and 20 cm of lead taken at the atmospheric pressures of 235 and 310 g/cm^{-2}. The values at 310 g/cm^{-2} are computed from data, some of which have not been heretofore published.

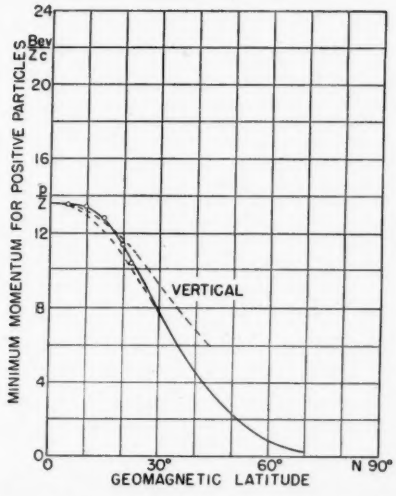

FIG. 3. Assuming only positive primaries a comparison of zenith angle effect given in Fig. 2 with the measured latitude effect at the vertical permits an experimental determination of the minimum momentum *vs.* geomagnetic latitude for the vertical direction.

We note that the asymmetry shown by the points at the greater atmospheric pressure is slightly less than that at greater altitudes as was pointed out in reference (A).

Assuming only positive primary particles, we must therefore expect the same relative increase in the latitude effect at the vertical as we go away from the equator (see reference (A), Fig. 6) as is shown in Fig. 2 when the momentum range covered is the same. We thus have sufficient information to solve parametrically for the minimum momentum of the primary particles *vs.* geomagnetic latitude. This has been done as shown in Fig. 3 down to a momentum of 10.3 Bev/*Zc* or a latitude of 22.5° N and has not been carried farther because of the increasing importance of atmospheric absorption.

Plotted in the same figure are the two limiting curves

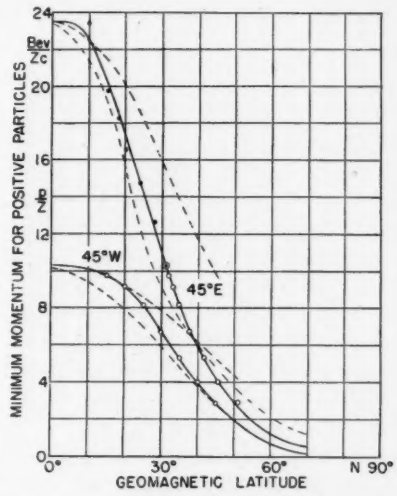

FIG. 4. Further comparison of the data given in Fig. 2 with the latitude effect at 45 E and 45° W permits an experimental determination of the minimum momentum *vs.* geomagnetic latitude for these two zenith angles.

given in a recent summary by Vallarta.[10] These are plotted on a momentum basis and are corrected for tilt of the earth's magnetic field and for the eccentricity of the dipole. The upper broken curve gives the calculated momentum a particle must have in the vertical direction at the geomagnetic latitude given by the abscissa, above which all momenta are allowed by the earth's magnetic field. The lower broken curve gives the least momentum a particle must have in order to penetrate the earth's magnetic field in a vertical direction at the geomagnetic latitude given by the abscissa.

The experimental curve has been extended to higher latitudes by gradually dropping down to the lower curve of Vallarta according to his instructions.

The next comparison we shall make with the calculations of Vallarta *et al.* is using the latitude effect at 45° as given in reference (A), Fig. 6 or 8. We have already used values at 29.3° N and the equator to correlate with the zenith angle values at 45° W and 45° E at the equator to gain some information as to the number of negative primaries compared with positives. We shall now use the intermediate values for intermediate latitudes.

Again, using the average values for 10 and 20 cm of lead absorber, we find that starting at 31° N and going toward the equator at 45° E covers the same momentum range as starting at 45° W at the equator and sweeping across the sky in the vertical plane to 45° E. Solving parametrically the two experimental curves of counting rate *vs.* geomagnetic latitude (reference (A) Fig. 6 or 8) and counting rate *vs.* momentum (Fig. 2) we arrive at the results given by the dots in Fig. 4 for minimum momentum *vs.* geomagnetic latitude.

To carry the comparison of the experimental results with calculations to higher latitudes we note from the lead curves of (A) Figs. 6 and 8 that, beginning with 0°

TABLE I. Pairs of latitudes at which the intensity at 45°W becomes equal to that at 45°E. Average for 10 and 20 cm of lead.

0 and 31.0°N	30 and 37.5°N
15 and 31.5°N	35 and 41.5°N
20 and 33.0°N	40 and 45.5°N
25 and 34.2°N	45 and 51.0°N

and 31° geomagnetic latitude where the intensity at 45° W becomes equal to that at 45° E respectively, there is a latitude where toward the west the intensity is the same as at another latitude toward the east. This means that the minimum momentum must be the same in the two cases. In Table I, pairs of latitudes are given at which these intensities become equal for the average of 10 and 20 cm of lead absorber.

These pairs of points have been plotted in Fig. 4 and shown by the circles. In plotting these we start first with the previous point at 31° N and extend the 45° E curve in such a manner that the corresponding points lying on the 45° W curve gradually drop down to the lower of the two extreme curves (shown dashed) given by Vallarta.[10]

We have thus experimentally determined in Figs. 3 and 4 the relation between minimum momentum for entrance and geomagnetic latitude at zenith angles 45° W, 0°, and 45° E. This is particularly important at intermediate latitudes where the calculations are exceedingly tedious.

It should be remarked that these curves have been strictly determined only along longitude 80° W and are not applicable to other longitudes. It will be noticed that all the experimental curves tend to lie above the upper curve given by Vallarta at low latitudes. This may be due to the peculiar variation of the earth's magnetic field along longitude 80° W.

V. CORRELATION OF AZIMUTHAL EFFECT WITH ZENITH ANGLE EFFECT AT THE EQUATOR

Lemaitre and Vallarta[11] have given curves showing the azimuthal variation of minimum momentum at several latitudes and zenith angles. We have already used their calculations for the boundary to the main cone at the equator that passes through the vertical to find the zenith angle dependence for particles of the same momenta.

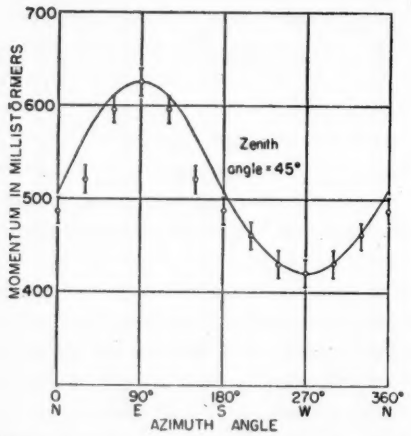

FIG. 5. Comparison of the measured azimuthal effect at zenith angle 45° with the data given in Fig. 2 permits a determination of the minimum momentum *vs.* azimuth angle.

A detailed comparison can be made at other azimuth angles by using the experimental values given in Fig. 2 with the curves shown in (A) Figs. 17 or 19. Again we solve the two curves parametrically and find the relation between minimum momentum as a function of azimuth angle. The comparison of these results with the calculations of Lemaitre and Vallarta is shown in Fig. 5 where we have used only the data with lead and zenith angle 45°. Suitable corrections to the ordinate of the calculated curve have been made to allow for eccentricity of the earth's dipole and tilt of the magnetic field as discussed earlier.

It is apparent that with due regard to the experimental errors involved there is satisfactory agreement between the calculations and the experimental values.

The data may be presented in another way as shown in Fig. 6. Here the latitude effects at the vertical and at 45° E have been plotted as a function of minimum momentum, the latter taken from Figs. 3 and 4. The smoothed experimental data are taken from (A) Fig. 8. Plotted also in Fig. 6 are the data, shown by circles, taken at definite azimuths at the equator with the same absorber. In this latter case we use the calculations of Lemaitre and Vallarta for the dependence of momentum on azimuth.[11] The broken curve is the boundary to the limits of the momentum range covered for any given zenith angle at this altitude. That part of the broken curve to the left of the dotted vertical line corresponds to the telescope pointing toward the west while that to the right of the vertical line corresponds to easterly directions.

The $22\frac{1}{2}$° curve lies below the vertical curve because of the slightly greater atmospheric depth. The agreement between the variation in azimuth at 45° zenith angle with the latitude effect at 45° E, as discussed above, is clearly brought out in Fig. 6.

It is again clear that the close agreement between the latitude and azimuthal curves where the momentum ranges overlap is further substantiation for the assumed absence of negative particles in the primary radiation in the momentum ranges involved.

VI. CORRELATION OF LATITUDE, ZENITH ANGLE AND LONGITUDE EFFECTS

An analysis similar to that carried out at the beginning of this paper gives for the minimum momentum allowable at the vertical in India, 17.0 Bev/Zc after corrections for tilt of the earth's magnetic field and eccentricity of the dipole are taken into account.

Now it was shown in reference (A) that when 10 or 20 cm of lead absorber were used there was a good correlation between the intensity measured at an angle to the vertical and that measured at the vertical provided

(1) the mass of intervening air was the same and (2) the momentum range covered was the same. This agreement is apparently due to the compensating effects of scattering and decay.

From Fig. 6 we may find the longitude effect at certain particular atmospheric depths. At 310×sec.22.5° = 335 g/cm^{-2} atmospheric depth we would expect a 13 percent decrease in intensity in going from Peru to India along the geomagnetic equator, where the change in minimum momentum is from 13.5 to 17.0 Bev/*Zc*. Now the latitude effect in the total radiation as compared with that in the penetrating was shown in (A) to be approximately equal. We would therefore expect the total radiation to have a longitude effect of 13 percent also at about 330 g/cm^{-2} air pressure. It is difficult to compare this with experimental data since similar flights have not been made in Peru and India. There is also the question of variations with time unless the flights are made simultaneously. However the figure of 13 percent is certainly not in conflict with existing experimental data taken at Bangalore and Pishawar,[13] India, and at Acapulco, Mexico,[14] using counter telescopes.

From the lower curve in Fig. 6 we find for the longitude effect at 310×sec. 67.5° = 810 g/cm^{-2} atmospheric pressure a value of 5 percent. The value found *at sea level* or 1030 g/cm^{-2} in the world survey of Millikan and Neher[15] was 4 percent.

It is of interest to compare the latitued effect at 310 g/cm^{-2} air pressure with that found at sea level. Using the data of (A) Fig. 5 for 10 cm of lead absorber at the higher altitude and that given by Millikan and Neher[15] at sea level along the same longitude (80° W) we find the values given in Table II for the ratios between the latitude effects at the two elevations for certain increments in latitude. A slight extrapolation leads us to expect a longitude effect about 4 times as large at 30,000 ft. as at sea level or a decrease of 16 percent in

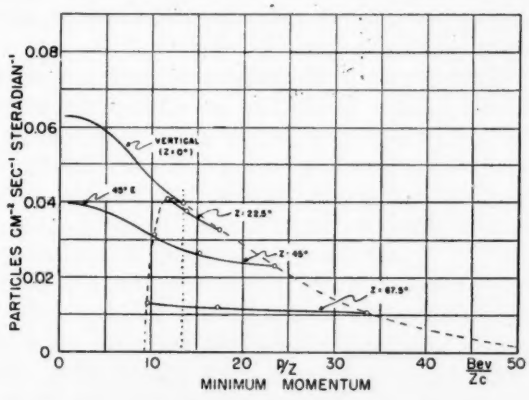

FIG. 6. Plotting intensity *vs.* minimum momentum as given by Fig. 3, 4, and 5 permits a comparison of the latitude effect with the azimuthal effect at the geomagnetic equator.

[13] H. V. Neher and W. H. Pickering, Phys. Rev. **61**, 407 (1942).
[14] Millikan, Neher, and Pickering, Phys. Rev. **63**, 234 (1943).
[15] R. A. Millikan and H. V. Neher, Phys. Rev. **50**, 15 (1936).

TABLE II. Latitude effect at 30,000 ft. (310 g/cm^{-2} air pressure) relative to that at sea level along 80°W longitude. 10 cm lead absorber. Sea level values taken with ionization chamber shielded with 10 cm of lead. 30,000 ft. data taken with counter telescope pointing at the vertical with 10 cm of lead absorber between trays of counters.

	Percent increase		
	Sea level	30,000 feet	Ratio
0–20°N	1.5	9.1	6.0
20–25	1.8	7.3	4.1
25–30	2.0	6.3	3.2
30–35	2.0	9.9	4.9
35–40	1.8	6.2	3.4
40–50	1.0	5.7	5.7

going from Peru to India along the geomagnetic equator. This is in agreement with the value taken from Fig. 6.

To give a more complete picture, Fig. 7 is included which gives the azimuthal data taken with 10 cm of lead absorber in the counter telescope at the two different elevations over Peru. Each curve gives the intensity for given masses of intervening air as a function of minimum momentum of the primary particles.

Also from Fig. 7 the absorption in the atmosphere of the radiation that can penetrate 10 cm of lead due to primaries of a certain minimum momentum may be determined by taking the intersections with vertical lines. Thus the intersections of the curves with the dotted line at 13.5 Bev/*Zc* should fall on the intensity *vs.* air pressure curve in the vertical direction in Peru taken with 10 cm of lead. Comparison with curve *B* of reference (A) Fig. 21 shows this to be true.

VII. SUMMARY

The calculations of Vallarta *et al.* on the paths of charged particles in the magnetic field of the earth have shown the general behavior to be expected in the several geomagnetic effects found in cosmic rays. By using experimental data taken on a B-29 flight to Peru it has been possible (1) to say that, within the limits of the uncertainties in the experimental data and in the

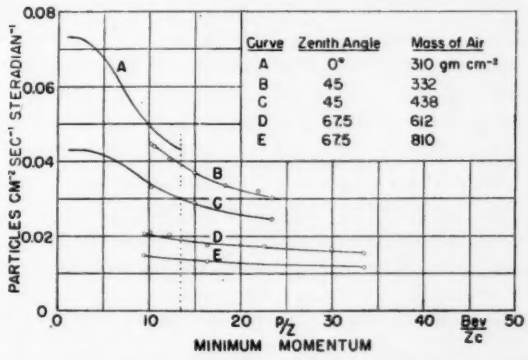

FIG. 7. Using a 10 cm lead absorber the intensity through various masses of air is given as a function of minimum momentum.

calculations of Vallarta *et al.* on the behavior of charged particles in the magnetic field of the earth, there are few if any negative primary particles in the momentum range 7 to 23 Bev/Zc compared with the positives, and (2) to find experimentally the minimum momentum for entrance for positive primaries as a function of geomagnetic latitude. This is particularly important at intermediate latitudes where the calculations become extremely difficult and have not been carried through in detail except in particular cases. The experimental determination of these curves is independent of the assumed nature of the primaries (except that they carry a positive charge), the way in which they or their secondaries are absorbed in the atmosphere or their momentum distribution at the top of the atmosphere.

Using the experimental data on the latitude, azimuthal and longitude effects in conjunction with the calculations of Vallarta *et al.*, it has been found possible to correlate all these phenomena. We may therefore say at the present time that within the experimental uncertainties all of these geomagnetic effects fit into a consistent picture.

It is again a pleasure to acknowledge the assistance given by the ONR and to the U. S. Air Forces in providing the facilities and airplane that made possible collecting the data used in this analysis.

PHYSICAL REVIEW VOLUME 78, NUMBER 6 JUNE 15, 1950

Energy Transfer to Nucleons in Cosmic-Ray Stars at 95,000 Feet*

H. L. BRADT AND M. F. KAPLON
University of Rochester, Rochester, New York

(Received February 10, 1950)

The size-frequency distribution of cosmic-ray stars produced in photographic emulsions exposed at 95,000-feet altitude and the energies associated with the non-relativistic prongs of these stars have been determined. A distribution function for the excitation energy of stars with more than 8 prongs is derived.

NUCLEAR disruption ("stars") produced by cosmic rays in photographic emulsions exposed at balloon altitudes are frequently associated with the emission of relativistic singly charged and neutral particles, the majority of which are presumably mesons.[1,2] It is to be expected that all nuclear interactions of cosmic-ray primaries will lead to an excitation of the residual nucleus which gives rise to the low energy evaporation and knock-on star fragments.

At balloon altitudes stars with twenty and more non-relativistic prongs, corresponding to excitation energies of the order of one Bev, are observed not too infrequently. The mechanism by means of which such large excitation energies can be transferred from an incident nucleon to the nucleons of the target is not obvious. By elastic collisions alone a fast nucleon can transfer to a silver nucleus not much more than about 200 Mev.

S. A. Wouthuysen[3] has calculated the probability $p(E)dE$ of an "excitation energy" (including all nucleons with energies less than about 30 to 40 Mev and all heavier fragments) in the interval between E and $E+dE$ for Ag-nuclei bombarded by primary protons, assuming an effective collision cross section equal to about 80 percent of the geometrical cross section. In these calculations nucleon-nucleon collisions are considered to be completely inelastic (leading to meson production) for energies >600 Mev and completely elastic for energies <600 Mev. The assumption of complete inelasticity certainly exaggerates the energy transfer due to the secondary nucleons produced by an energetic incident primary. On the other hand, the mesons are assumed to leave the nucleus without contributing at all to the excitation energy. Whether this assumption is justified or not depends on the nuclear interaction cross section of fast π-mesons, for which no reliable data are as yet available. The result is shown in curve 1 of Fig. 1.

In order to allow a comparison with the actual excitation energy distribution of stars produced by cosmic-ray primaries, we have determined the total energy (kinetic+binding) associated with the "black prongs" ($K/K_{\min}>7$, corresponding to $E_P<40$ Mev) of stars in Ilford C_2 and Eastman NTB3 emulsions, exposed at 95,000-feet altitude at 51°N geomagnetic latitude (curve 1 of Fig. 2). We find that some 30 percent of the black prongs are due to α-particles, at least some 10 percent to deuterons, 3 to 4 percent to H^3 and some 5 percent to fragments heavier than He. The number and energy of neutrons is assumed to be 1.3 times the number and energy of the protons. Since it actually may be quite appreciably larger,[4] the excitation

* This work was assisted by the joint program of the ONR and the AEC.

[1] U. Camerini *et al.* Phil. Mag. **40**, 1073 (1949).

[2] Kaplon, Peters, and Bradt, Helv. Phys. Acta **23**, 24 (1950).

[3] S. A. Wouthuysen (to be published).

[4] H. A. Bethe, Echo Lake Conference on Cosmic Rays (June, 1949).

energies derived on this assumption should be considered to be lower limits.

The integral size-frequency distribution of stars (uncorrected for ascent of the balloon and descent of the parachute[5] as a function of the number $N=N_b$ of black tracks is given in curve 2 of Fig. 3. This curve together with curve 1 of Fig. 2 yields the empirical "excitation energy" distribution function (represented in curve 2 of Fig. 1) for stars with $N_b>8$ prongs, which are due to the Ag and Br nuclei of the emulsion.

The analysis does not include σ-stars or stars produced by primaries with $Z\geqslant 6$. The majority of the larger stars may be assumed to be produced by cosmic-ray primaries. At 95,000-feet altitude the primary radiation contains at least some 13 percent alpha-particles.[6] Therefore at least about 20 percent of all the stars produced by primaries at this altitude are produced by α-particles.

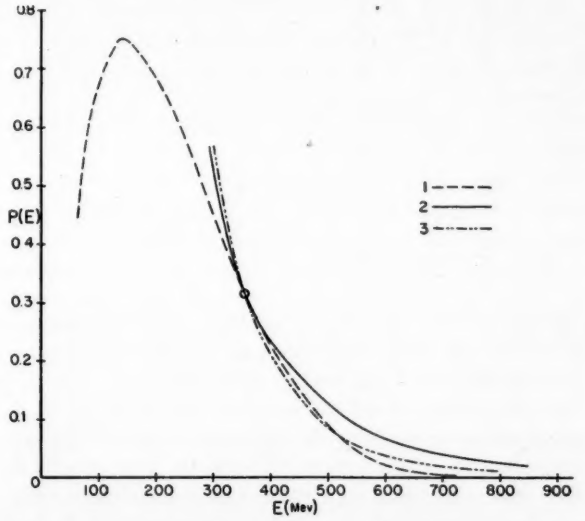

FIG. 1. Distribution function of the excitation energy of stars. Curve 1: theoretical curve of S. A. Wouthuysen. Curve 2: balloon data for stars with more than 8 black prongs. Curve 3: mountain altitude data of R. H. Brown *et al.*, for stars containing at least one minimum ionization track.

Up to about 500 Mev the empirical curve 2 decreases with energy roughly as the calculated curve 1, but shows a high energy tail extending beyond 1 Bev. A large fraction of the very energetic stars of the "tail" are certainly due to primary α-particles.

The comparison with similar curves relating to stars observed at mountain altitude, to where the primary α-particles do not penetrate, is of interest: Curve 3 of Fig. 1 shows the excitation probability for stars associated with at least one minimum ionization track, as derived from the data of R. H. Brown *et al.* obtained at Jungfraujoch.[7] The curve is somewhat steeper at moderate energies and the high energy tail is much less pronounced.

The curves of Fig. 1 indicate that with some not too unreasonable, though greatly idealized assumptions,[3] the observed excitation energy distribution above about 300 Mev can be approximately accounted for without assuming any direct excitation energy transfer to the nucleus from the mesons created, except probably for the very largest stars.

The "excitation energy" is only a fraction of the total energy associated with non-relativistic particles ($\beta=v/c<0.7$) in the large stars.[7] Figure 4 shows the numbers N_g of "grey tracks" ($1.6<K/K_{\min}<7$) per star with N_b black tracks plotted *vs.* the number of black tracks and curve 1 of Fig. 3 the relative number of stars with equal or more than $N=N_h$ heavy tracks, based on an analysis of some 1000 stars. Curve 2 of Fig. 2 shows the total energy associated with the heavy tracks $N_h=N_g+N_b$ as function of the number $N=N_h$ of heavy tracks, assuming that all grey tracks are due to protons. (Curve 3 gives the corresponding result of R. H. Brown *et al.*[7] for mountain altitude.) The relation is only slightly changed if a significant fraction of the grey tracks are mesons, provided that the total energy

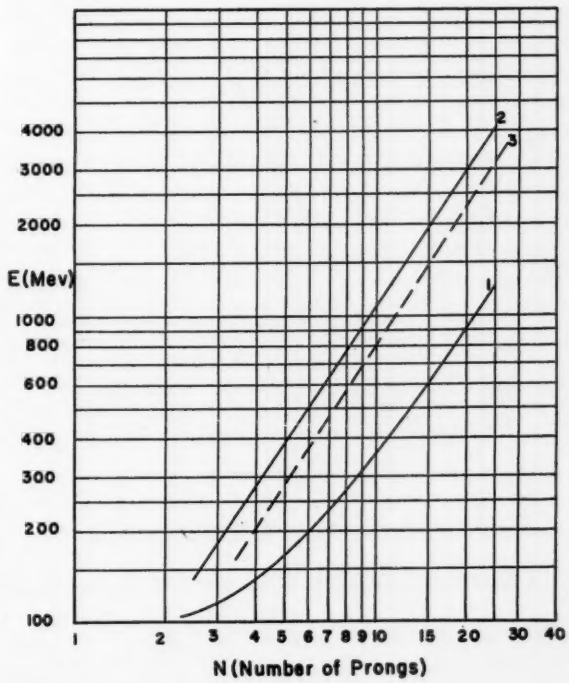

FIG. 2. Energy of stars as a function of the number of prongs. Curve 1: "excitation energy" (including all nucleons with $E<40$ Mev and heavier fragments) as function of the number of black prongs. Curve 2: energy associated with non-relativistic prongs ($\beta<0.7$) as function of the number of heavy (black plus grey) prongs. Curve 3: mountain altitude data of R. H. Brown *et al.*

[5] Freier, Ney, and Oppenheimer, Phys. Rev. **75**, 1451 (1949). For stars with >8 prongs, the correction is negligibly small.

[6] H. L. Bradt and B. Peters, Phys. Rev. **77**, 54 (1950); M. A. Pomerantz, Phys. Rev. **76**, 165 (1949).

[7] R. H. Brown *et al.*, Phil. Mag. **40**, 862 (1949). The classification of prongs follows approximately the nomenclature of these authors.

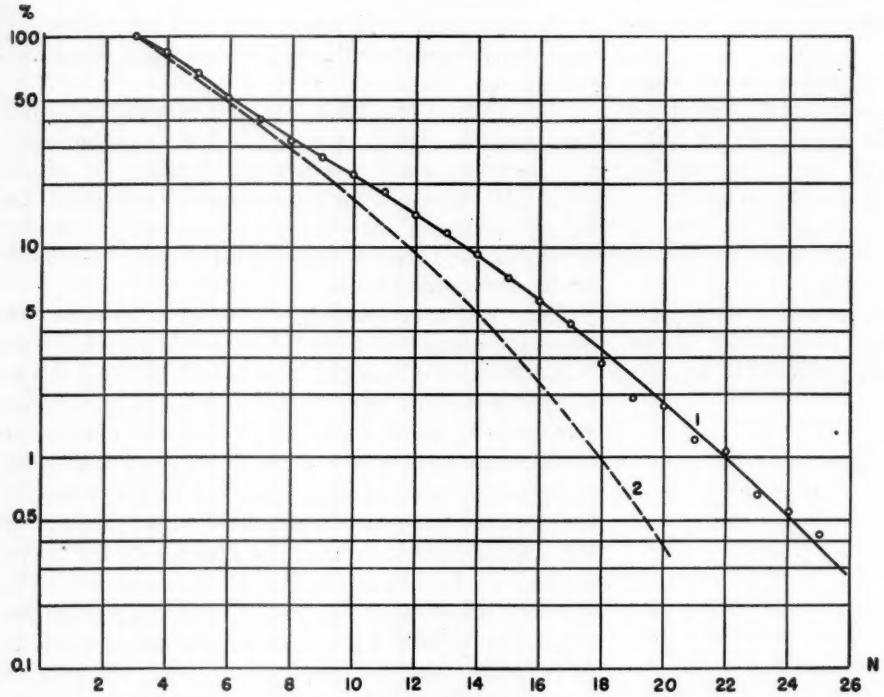

FIG. 3. Integral size frequency distribution of stars. Curve 1: frequency of stars with equal or more than N heavy prongs. Curve 2: frequency of stars with equal or more than N black prongs.

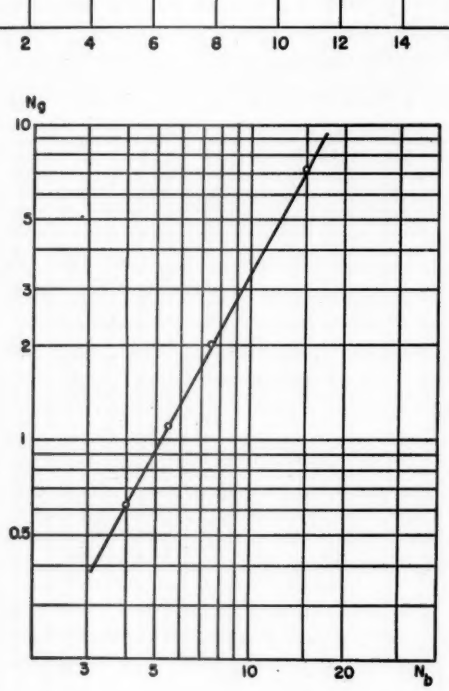

FIG. 4. Number of grey prongs N_g per star with N_b black prongs.

plotted in curve 2 of Fig. 2 includes the rest energy of these mesons and that there is an equal number of neutral mesons. (The energy is decreased by not more than 20 percent if all tracks with $1.6<K/K_{\min}<4$ are assumed to be mesons.) If we assume that all the stars with $N_b \geqslant 10$ black prongs (E greater than about 1.6 Bev) are produced by primary protons and α-particles, we deduce from their absolute frequency $S(N_b \geqslant 10) = 255$ stars/cm^3 day (17 percent of the total of 1500 stars/cm^3 day) and the primary flux data[6] a cross section

$$\sigma(N_b \geqslant 10) = 0.15 \cdot 10^{-24} \text{ cm}^2$$

per Ag, Br nucleus (average) in agreement with Freier, Ney and Oppenheimer.[5]

An upper limit for the total cross section for an energy transfer in excess of about 150 Mev by primaries to the nucleons of Ag, Br nuclei can be obtained if we assume that at least $\frac{1}{3}$ of the corrected number of stars with 3 to 6 prongs are due to C, N, O nuclei of the gelatine. We obtain $\sigma_{\text{tot}} = 1.0 \cdot 10^{-24}$ cm^2, equal to about 70 percent of the average geometrical cross section of the Ag, Br nuclei.

Disintegration of Nuclei by π^--Mesons*

W. B. CHESTON AND L. J. B. GOLDFARB
University of Rochester, Rochester, New York
(Received February 11, 1950)

Investigations of nuclear disintegrations induced by π^--meson absorption in nuclear emulsions, exposed to the π^--meson beam of the 130-in. Rochester cyclotron, have been carried out. The energy spectrum of the protons emitted from the absorptions shows two distinct processes occurring: (a) evaporation of nucleons from an excited nucleus and (b) emission of knock-on protons, brought about by the interaction of a π^--meson with a multi-particle structure in the nucleus. Of the mesons ending in the emulsion, 10 ± 2 percent give rise to protons with energies $\geqslant 30$ Mev. Strong evidence is presented for the boson character of the π^--meson.

I. INTRODUCTION

THE disintegration of atomic nuclei by the absorption of π^--mesons can be investigated by the use of nuclear emulsions. Some work in this direction has been carried out by D. H. Perkins[1] using cosmic-ray mesons. Unfortunately, because of the small mass difference between μ- and π-mesons, it is difficult to distinguish between them unless the lengths of track in the emulsion are considerable. A more satisfactory source of slow π^--mesons is a large cyclotron. It is a simple procedure to screen out the π^+-mesons and to arrange the magnetic channel so that very few μ^--mesons (which are the disintegration products of the π^--mesons produced in the cyclotron target) will reach the emulsion.

Kodak NTB-3 emulsions were exposed to the π^--meson beam of the 130-in. Rochester cyclotron by Dr. S. W. Barnes. A systematic survey was made of 429 mesons ending in one particularly favorable pellicle of 250 microns thickness. A star-size distribution, a proton energy spectrum and information concerning the nuclear recoils associated with the meson absorption were obtained.

II. EXPERIMENTAL DETAILS

Nuclear emulsions can be calibrated by determining the relationship between grain densities of the tracks of singly charged particles and the specific energy loss of these particles. The latter quantity can be found from a knowledge of the residual ranges of the charged particles in the emulsion. The grain density as a function of residual range for 15 meson tracks of residual range greater than 1000 microns was obtained. This yielded a calibration for the emulsion for protons whose energy is less than 50 Mev. The calibration curve was then extrapolated to higher energies and was spot-checked in this region by the grain densities of several meson tracks of very large residual range. Several protons of known residual range were used to check the calibration in the 30–40 Mev region. The energy of the protons emitted as disintegration products of the nuclei was determined by their specific energy loss and/or residual range.

III. STAR-SIZE DISTRIBUTION

Table I shows the star-size distribution. The data are classified according to three interpretations as to the nature of tracks less than 6 microns in length: (a) All tracks between 0 and 6 microns in length classified as recoils (one star was found containing two tracks both less than 6 microns in length; in this case only one of these tracks was considered to be a recoil); (b) all tracks between 0 and 6 microns considered as prongs for all stars; (c) all tracks between 0 and 6 microns considered as prongs for all stars except those in which these tracks are the only ones (in these cases they are considered to be "recoils"). The authors consider the last interpretation to be closest to the truth; the reasons for this and its significance are presented below. Table I also contains a star-size distribution obtained by Adelman and Jones[2] at Berkeley, which is based on 512 meson events. Their data have been classified according to interpretation (c) listed above. (It should be noted that the Berkeley group uses 5 microns as the upper limit for recoil lengths; however, this should not affect the comparison between results.)

Table II shows the star-size distribution for those stars containing protons whose energy is greater than

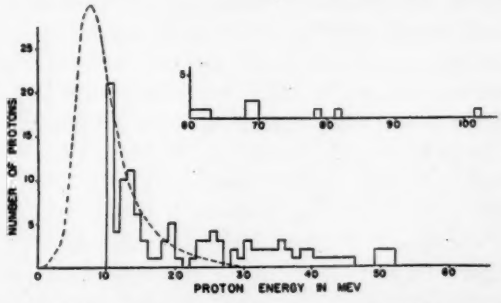

FIG. 1. Histogram representing energy distribution above 10 Mev of protons emitted as disintegration products of nuclei which have absorbed π^--mesons. The dashed curve represents energy distribution of protons evaporated from Ag nucleus of nuclear temperature between 2.5–3 Mev.

* This work was assisted by the joint program of the ONR and the AEC.

[1] D. H. Perkins, Phil. Mag. 40, 601 (1949).

[2] Private communication.

TABLE I. Star-size distribution of π^--meson induced stars.

Number of prongs	0	1	2	3	4	5
Number of stars[a]	151	100	71	69	30	8
Percent of total	35.2	23.3	16.5	16.1	7.0	1.9
Number of recoils	70±10	43	20	8	—	—
Number of stars[b]	81±10	127±10	94	81	38	8
Percent of total	18.9±2.3	29.6±2.3	21.9	18.9	8.8	1.9
Number of stars[c]	151	57	94	81	38	8
Percent of total	35.2	13.3	21.9	18.9	8.8	1.9
Percent of total[d]	30.5	17.8	26.9	15.2	7.8	1.8

[a] Tracks with lengths between 0 and 6 microns are considered as recoils.
[b] Tracks with lengths between 0 and 6 microns are considered as prongs.
[c] Tracks with lengths between 0 and 6 microns and which are the only visible tracks emanating from the absorption are considered as recoils; all others are considered as prongs.
[d] Berkeley data based on 512 stars; interpretation (c) applied, but with 5 microns as upper limit to recoil length.

30 Mev. These high energy protons are listed as prongs while, as above, the tracks less than 6 microns in length are considered first as recoils and then as prongs. (In this case, criterion (b) coincides with (c).)

IV. HIGH ENERGY PROTONS

Figure 1 is the energy spectrum of the protons of energy $\geqslant 10$ Mev emitted as disintegration products of the nuclei. This, together with the spectrum below 10 Mev, indicates two qualitative features: a spectrum which corresponds to the evaporation of particles from a nucleus of a given nuclear temperature and, in addition, a high energy ($\geqslant 30$ Mev) "tail." This "tail" gives an indication of the mechanism of interaction of the π^--meson with the nucleons in the nucleus. The dotted curve in Fig. 1 is the energy spectrum of protons evaporated from a silver nucleus of nuclear temperatuer between 2.5 and 3 Mev.[3] The theoretical curve is fitted to the experimental curve at 10 Mev. It should be noted that the evaporation spectrum predicts essentially no protons with energies above 30 Mev; it is for this reason that we have assumed that most protons above 30 Mev are high energy knock-on protons. The evaporation spectrum should not be expected to hold for the light nuclei of the emulsion. However, since most of the mesons are presumably absorbed by the heavy nuclei, the energy spectrum for all the nuclear evaporations should not essentially differ from that shown in Fig. 1.

Of the absorptions observed, 10.0±2.0 percent give rise to protons with energies $\geqslant 30$ Mev. Counting as prongs only those tracks greater than 6 microns in length, 7.9±2.0 percent of the star prongs are protons with energies $\geqslant 30$ Mev, while counting all tracks as prongs, 6.1±2.0 percent of the star prongs are protons of such energies. (The errors quoted are statistical errors.)

The absorption process has been considered by Tamor[4] as an interaction of the π^--meson with an alpha-particle-like structure and a two nucleon (proton-plus-proton or neutron-plus-proton) structure in the nucleus. The π^--absorptions in the light and heavy nuclei in the emulsion as typified by nitrogen and silver, respectively, were separately examined. According to the alpha-particle model, 12 percent of the absorptions in nitrogen and 13 percent of those in silver yield protons with energies $\geqslant 30$ Mev, while the two nucleon structure predicts that 48 and 24 percent of the absorptions in nitrogen and silver, respectively, yield high energy protons. Assuming that $\frac{2}{3}$ of the absorptions occur in the heavy elements and $\frac{1}{3}$ in the light, the two nucleon model would predict that 32 percent of the meson absorptions should give rise to protons with energies $\geqslant 30$ Mev. (It is assumed that this relative number of absorptions in light and heavy nuclei also holds for π^--mesons, although the number quoted was found for μ^--mesons; this assumption must be quite accurate.[5]) The experimental evidence favors the former hypothesis. It should be noted that Perkins observes 7±2 percent of the π^--stars (based on 120 meson events) yield fast protons (above 30 Mev). Adelman[6] has found similar results on the basis of 120 meson events.

Five of the 429 meson events observed were stars showing a visible excitation energy of approximately 100 Mev, assuming 7 Mev binding energy per particle in the nucleus. One proton track exhibited a grain density corresponding to an energy greater than 100 Mev and represents the largest visible excitation observed. In addition, three deuterons of energy between 20 and 30 Mev were observed as disintegration products. Nuclear disintegration products with such high total energy are strong evidence for the boson character of the π^--meson.[7,8]

V. RECOIL OF THE ABSORBING NUCLEUS

In an attempt to obtain information concerning the recoil of the nucleus absorbing the π^--meson, stars with one visible track emanating from the collision were examined. Figure 2 is a histogram showing the fre-

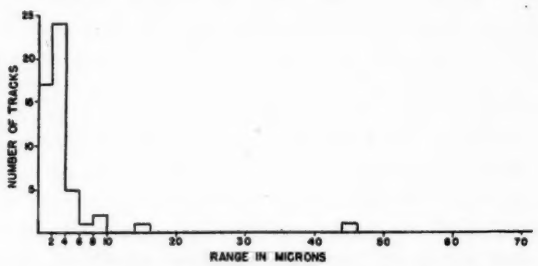

FIG. 2. Range distribution below 75 microns of tracks associated with stars showing only one visible track.

[3] Harding, Lattimore, and Perkins, Proc. Roy. Soc. **A196**, 325 (1949).

[4] S. Tamor, Phys. Rev. **77**, 412 (1950).
[5] Cosyns *et al.*, Proc. Phys. Soc. London **62**, 360A, 801 (1949).
[6] Adelman, private communication.
[7] R. E. Marshak, Phys. Rev. **75**, 700 (1949).
[8] Tiomno and Wheeler, Rev. Mod. Phys. **21**, 153 (1949).

quency of these track lengths up to 75 microns. This histogram exhibits one very striking feature: 90 percent of all tracks from one-track stars with lengths less than 75 microns are grouped in the region below 6 microns. The peak in the histogram between 2 and 4 microns may not be an actual one as the efficiency for observing tracks less than 3 microns long is low. These short tracks could be: (a) slow charged particles (e.g., protons or alpha-particles) emitted from the nucleus; (b) Rutherford scattering near the end of meson tracks; (c) recoils of the absorbing nuclei which have emitted one fast neutron as envisaged in Tamor's alpha-particle model interaction. If these tracks are slow protons or alpha-particles, it is difficult to see why there is such an abundance of track lengths below 6 microns and such a paucity between 6 and 75 microns since the energies of protons and alpha-particles whose ranges are about 6 microns in the emulsion are well below the Coulomb barriers for these particles even in a carbon nucleus. Some of these "tracks" may arise from Rutherford scattering of the meson in its last few microns. The probability for such scattering was calculated using 20 degrees as the cut-off angle for the integration since mesons which scatter through angles less than this value could not be seen in the photographic emulsion. Of those mesons which produce no disintegrations, 6 percent should show tracks between 2 and 6 microns in length if these tracks are due to Rutherford scattering of the meson. The calculation was made with a power-law dependence of range on energy in this energy region ($r = AE^x$). This probability accounts for an inappreciable fraction of the short "tracks" observed. The short "tracks" were also observed to be roughly isotropic in angular distribution, which further rules out the Rutherford scattering hypothesis with its strong angular dependence. It is therefore concluded that most of these "tracks" are in all probability recoils of the absorbing nuclei associated with the emission of high energy neutrons as is predicted by the alpha-particle model interaction.

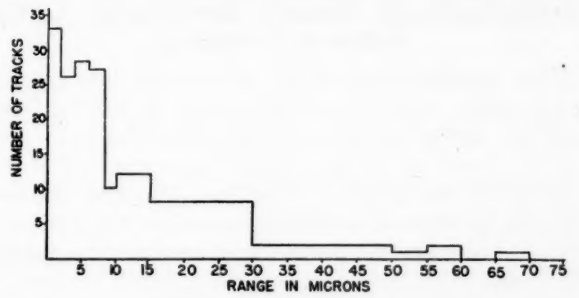

FIG. 3. Range distribution below 75 microns of tracks associated with stars showing more than one visible track.

TABLE II. Star-size distribution for stars with protons of energy $\geqslant 30$ Mev.

Number of prongs	1	2	3	4	5
Number of stars[a]	16	9	13	4	1
Percent of total	37.2	21.0	30.2	9.3	2.3
Number of stars[b]	12	11	13	6	1
Percent of total	27.9	25.6	30.2	14.0	2.3

[a] All tracks with lengths between 0 and 6 microns are considered as recoils.
[b] All tracks with lengths between 0 and 6 microns are considered as prongs.

In contrast to the data of Fig. 2, Fig. 3 gives a histogram of the lengths of tracks from stars which have more than one track. There is some evidence in the 0 to 6 micron interval of a maximum; however, it is difficult to decide what fraction of the tracks below 6 microns represents recoiling nuclei, because of the large number of tracks in the region above 6 microns.

Finally, it is worth noting that we have examined the last few microns of tracks of iron nuclei appearing in similar emulsions exposed to cosmic radiation by Drs. Bradt and Peters of this laboratory; we found that the ends of iron tracks exhibited the same visible properties as those tracks which we have interpreted as recoiling nuclei.

VI. CONCLUSIONS

The experimental evidence shows that in the process of slow π^--meson absorption by nuclei, two processes are to be considered: (1) the evaporation of nucleons from an excited nucleus; (2) the emission of energetic nucleons brought about by the interaction of the meson with some sub-structure in the nucleus. The number of events observed with high energy protons indicates that the nuclear substructure is a multi-particle one, as typified by the alpha-particle model. It is to be hoped that further work on the very short prongs, which are presumed to be nuclear recoils, will yield further evidence as to the nature of the interaction. The high visible excitation energies observed for the excited nucleus lends strong evidence for the boson character of the π^--meson.

The authors are indebted to Dr. S. W. Barnes for exposing the emulsions and to S. Tamor for many valuable discussions concerning the meson absorption mechanism. The authors also wish to express their gratitude to Dr. R. E. Marshak under whose guidance this work was undertaken.

The Disintegration of Cu^{61} *

GEORGE E. OWEN, C. SHARP COOK, AND PAUL H. OWEN
Department of Physics, Washington University, St. Louis, Missouri
(Received January 9, 1950)

By the use of very thin and uniform sources that were prepared by thermal evaporation, the positron spectrum of Cu^{61} continues to show an excess of particles in the low energy region. The presence of nuclear gamma-rays and internal conversion electrons indicates that the disintegration of Cu^{61} is complex. Magnetic spectrometer studies of the radiations from Cu^{61} have led to a tentative disintegration scheme.

I. INTRODUCTION

ACCORDING to the *ft* values,[1] the beta-disintegrations of both Cu^{61} and Cu^{64} are of the allowed type. The Fermi theory of beta-decay predicts that such an allowed transition should produce a straight-line Fermi-Kurie (F-K) plot. However, experimental results have been obtained[2,3] which seemed to indicate that the F-K plots for these two isotopes are non-linear in the low energy region. This non-linearity appeared as an excess of low energy particles, and in the case of the positrons from Cu^{61} this excess was present for all energies below 500 kev.

For the positron and negatron spectra of Cu^{64} it has been shown[4] that the deviations from the Fermi theory could be caused by an instrumental distortion. When thin sources were used in a study[5] of S^{35} and when gaseous sources were used in a study of tritium,[6] the resulting spectra were found to be in good agreement with the Fermi theory to quite low energies. Further investigations of instrumental distortions[7] have led to the conclusion that, with a properly designed chamber, the major portion of such distortions could be attributed to source thickness.

To test the dependence of the distortions on variation in source thickness, the positron distribution of Cu^{61} was selected. The fact that deviations in this spectrum occur at higher energies than in most other known allowed positron and negatron spectra seemed to favor a large dependence on source thickness.

In order that very thin and uniform sources could be prepared, an evaporator was constructed. The sources were prepared by thermal evaporation of copper from a hot tungsten filament onto a source backing.

Studies of the positron spectrum of Cu^{61} using sources prepared in this way showed the same type of deviation[8] that had previously been observed.[3] It follows that this deviation is most probably real rather than instrumental and is caused by either a complex disintegration or by some departure from the Fermi theory.

Previous coincidence studies[9] failed to disclose any nuclear gamma-rays of intensity comparable to the intensity of the annihilation quanta. This, however, does not eliminate the possibility of a complex disintegration.

A later investigation[10] of both the positrons and negatrons of Cu^{64} using sources prepared by evaporation gave spectra consistent with the Fermi theory as low as 50 kev; therefore it appears likely that the disintegration of Cu^{61} is complex. This conclusion is supported by the detection of gamma-rays in the photoelectron spectrum and internal conversion electron lines in the negatron radiations from Cu^{61}.

II. EXPERIMENTAL DETAILS

A. The Small 180° Magnetic Spectrometer (5.7 Cm Radius of Curvature)

The investigations of the continuous beta-spectra were made using a small 180° spectrometer of 5.7 cm radius.[7] Baffles are used at 30°, 90°, and 150°. The width of an internal conversion line at one-half of the maximum intensity is 1.2 percent; this was checked against the internal conversion lines of I^{131}, using sources of 42 micrograms per square centimeter average thickness.

Measurements of the magnetic field are made with a flip coil and a ballistic galvanometer. The galvanometer is calibrated against the internal conversion lines of Th(B+C) and I^{131}. To control the magnetic field current, a constant voltage d.c. generator and storage battery combination is employed. This regulator restricts variations in current to less than ± 0.5 percent. An end-window Geiger-Mueller counter is used having a zapon window for which electron transmission begins at 3 kev.

B. The Large 180° Magnetic Spectrometer (13.8 Cm Radius of Curvature)

Because of the high intensity sources which are needed for measurements of photoelectrons, a large 180°

* This work was supported by the joint program of the ONR and the AEC.

[1] E. J. Konopinski, Rev. Mod. Phys. **15**, 209 (1943).
[2] C. S. Cook and L. M. Langer, Phys. Rev. **73**, 601 (1948); J. Backus, Phys. Rev. **68**, 59 (1945); C. S. Wu and R. D. Albert, Phys. Rev. **75**, 1107 (1949).
[3] C. S. Cook and L. M. Langer, Phys. Rev. **74**, 227 (1948).
[4] G. E. Owen and H. Primakoff, Phys. Rev. **74**, 1406 (1948).
[5] R. D. Albert and C. S. Wu, Phys. Rev. **74**, 847 (1948); Price, Motz, and Langer, Phys. Rev. **77**, 744 (1950).
[6] Curran, Angus, and Cockroft, Phil. Mag. **40**, 53 (1949).
[7] G. E. Owen and C. S. Cook, Rev. Sci. Inst. **20**, 768 (1949).
[8] G. E. Owen and C. S. Cook, Phys. Rev. **76**, 1536 (1949).
[9] W. Gentner and E. Segrè, Phys. Rev. **55**, 814 (1939); Bradt, Gugelot, Huber, Medicus, Preiswerk, and Scherrer, Helv. Phys. Acta, **18**, 252 (1945).
[10] Langer, Moffat, and Price, Phys. Rev. **76**, 1725 (1949); G. E. Owen and C. S. Cook, Phys. Rev. **76**, 1726 (1949).

magnetic spectrometer,[11] having more lead shielding between source and counter than the smaller spectrometer, was employed for investigating the gamma-rays from Cu^{61}.

This instrument has a resolution of 0.6 percent for internal conversion lines, and 1.5 percent for photoelectron lines, when a 50 mg/cm² uranium radiator is used. The field current, which is regulated electronically,[12] has a variation of less than 0.05 percent.

The Geiger-Mueller counter is of the end-window type employing a zapon window whose cut-off for

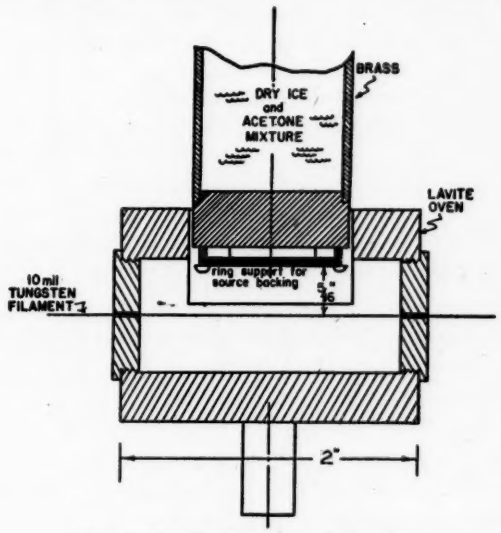

FIG. 1. Detail of the evaporator oven.

electrons is about 7 kev. To maintain a constant pressure in this counter, which has a large aperture, a pressure regulator is inserted in the filling system.[13]

C. The Photographic Spectrometer

The photographic spectrometer is of the usual 180° type and has a maximum radius of curvature of 10 cm. In order that the photographic plates and sources can be loaded and placed in position in a short time, the sources and photographic detection plates are mounted on a removable plug. This plate holder is provided with a light-tight cover which can be removed after the plug assembly is under vacuum.

The magnetic field is provided by a permanent magnet. This magnet employs two Alnico sections in order to maintain a large and stable field. The core is magnetized by means of a series of low resistance coils placed in position about the Alnico sections.

D. The Evaporator

In order to prepare sources which would be thin and uniform, an evaporator was constructed. The vacuum chamber consists of a large bell jar open at the top. A brass plate placed over this opening carries a plunger that can be removed from the chamber through an "O" ring seal.[14] The end of this plunger can be placed in a Lavite oven located on the bell jar base, and provides a means of supporting the source holder during the evaporation process. A detail of the oven is shown in Fig. 1.

The active copper is first electroplated onto a 0.01-inch diameter tungsten wire, and the wire is then placed in position in the Lavite oven. A source backing of the 0.00025-inch aluminum foil is mounted on an aluminum supporting ring and is covered by an aluminum mask. An opening in this mask allowed an exposed area of 1.0 cm×0.1 cm at the center of the backing. The foil and mask were then held 5/16 inch from the filament. A current of 5 amperes flowing for 10 seconds was observed to evaporate practically all of the copper which had been plated.

It was found advantageous to cool the backing with a dry-ice and acetone mixture which was located in the brass plunger as shown in Fig. 1. Later this procedure was modified by inserting a hollow brass sleeve, which carried the cooling mixture, into the plunger; this permitted the removal of the cold reservoir before the plunger was exposed to air and prevented the formation of ice on the source backing.

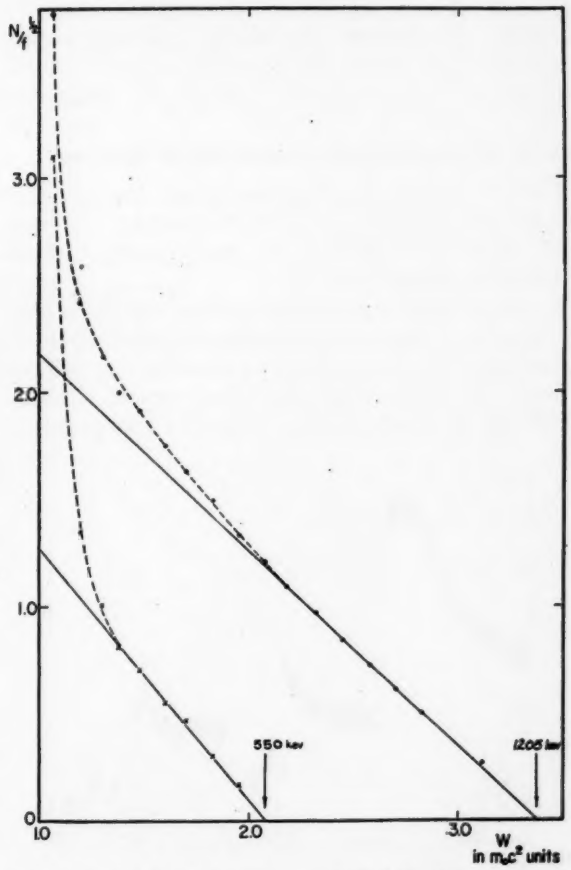

FIG. 2. F−K plot of the positrons of Cu^{61} showing the resulting F−K plot of one low energy group.

[11] F. N. D. Kurie and M. Ter-Pogossian, Phys. Rev. **74**, 677 (1948); Ter-Pogossian, Cook, Goddard, and Robinson, Phys. Rev. **76**, 909 (1949).

[12] Elmore and Sands, *Electronics, National Nuclear Energy Series* (McGraw-Hill Book Company, Inc., New York, 1949), Vol. V-1, pp. 390–393.

[13] Ter-Pogossian, Robinson, and Townsend, Rev. Sci. Inst. **20**, 289 (1949).

[14] F. N. D. Kurie, Rev. Sci. Inst. **19**, 485 (1948).

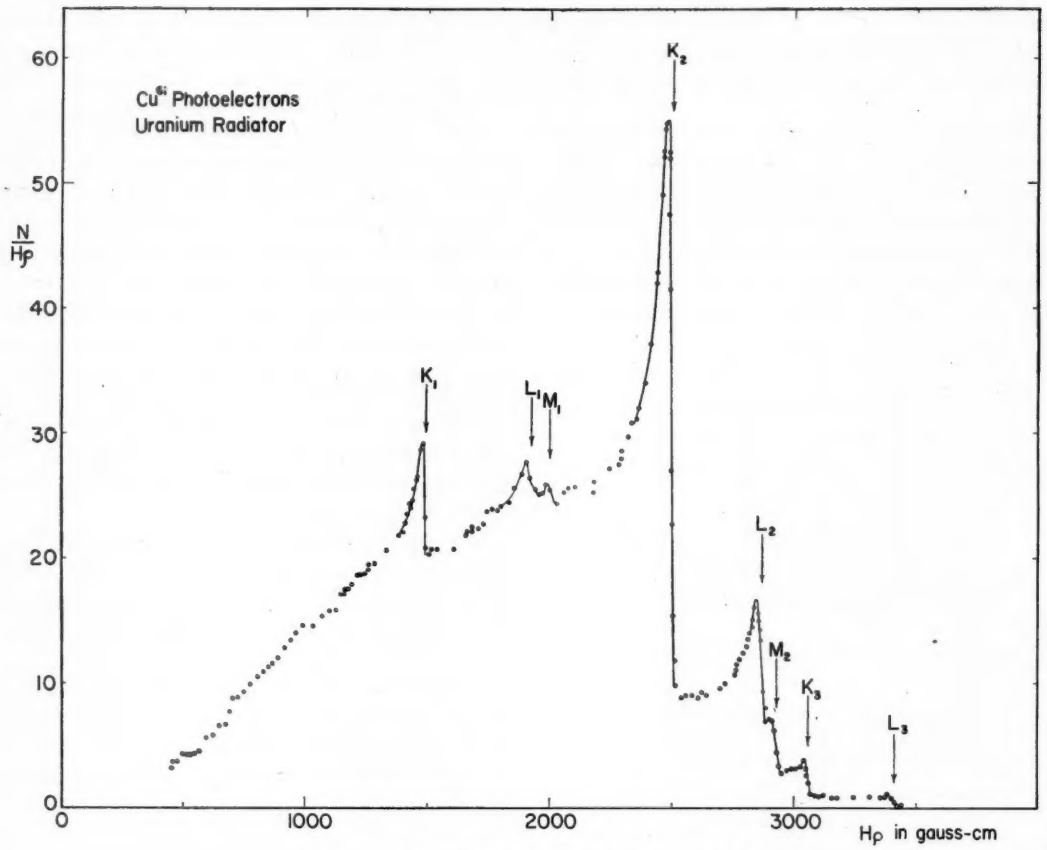

FIG. 3. Photoelectron spectrum of Cu^{61}.

E. Production and Separation of Sources

The Cu^{61} isotope was prepared carrier free by (d, n) and $(d, 2n)$ reactions on nickel. The copper was separated from the nickel by an electroplating process described by Steigman.[15]

A calculation of the equilibrium concentrations from the Nernst equation indicated that no nickel would be carried with the copper in a given electroplating process.

Since there were other short-lived copper activities formed in the bombardment, a time of approximately 2 hours was allowed for these to die out. Approximately one half-life after the initial determination of the spectrum, the positron radiations from the source were restudied, and after correction for loss of intensity because of the decay of the source, the results from both measurements were found to agree within one percent of each other.

A study[16] of the extent to which Cu^{64} will be present as an impurity in this source indicates its positron activity as being considerably less than one percent of the total positron activity of the sample.

The sources prepared by evaporation could neither be observed visually nor weighed, and were detectable only by their activity on the exposed region of the backing. Rough orders of magnitude of the thickness could be calculated from the activity present. Such calculations give a thickness of 10^{-4} microgram per sq. cm. This figure represents a lower limit to the actual thickness, because of the probable presence of small amounts of stable copper originating as an impurity in the original chemically pure nickel target. The actual thickness is probably not greater than 10^{-2} microgram per sq. cm.

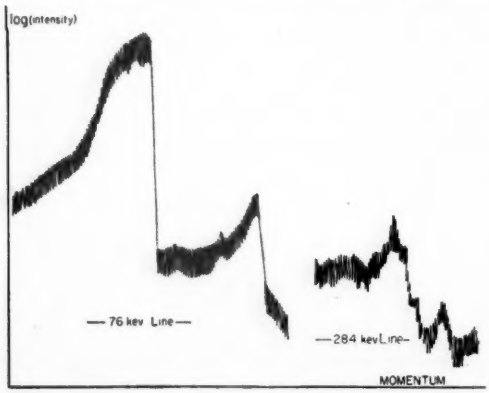

FIG. 4. Microphotometer tracing of the internal conversion lines of Cu^{61} as recorded by the photographic spectrometer.

III. RESULTS

The F-K plot of the positrons from Cu^{61}, using a source prepared by evaporation, is shown in Fig. 2. The excess of particles below 500 kev remains. Because

[15] J. Steigman, Phys. Rev. **53**, 771 (1938).

[16] C. S. Cook and C. H. Chang, Phys. Rev. **78**, 171 (1950).

it was found that sources of Cu^{64} prepared in the same manner gave agreement with the Fermi theory to energies as low as 50 kev, the evidence suggests that Cu^{61} is complex. If a second lower energy spectrum is derived by subtracting the Fermi allowed shape of the high energy spectrum from the low energy excess, an F-K plot is obtained which has a maximum energy of 550±25 kev, with a corresponding momentum distribution having an intensity of 4 percent of the total positron intensity. This second F-K plot is also shown in Fig. 2.

From consideration of the positron spectrum (and F-K plot) alone, the low energy excess in the secondary spectrum may or may not be real. It may represent a tertiary spectrum but most likely a considerable part of it represents a distortion caused by scattering from the aluminum backing.

The photoelectron spectrum resulting from the gamma-rays and annihilation radiation of Cu^{61} incident on a 50 mg/cm² uranium radiator is shown in Fig. 3. The K, L and M photoelectron lines resulting from the annihilation quanta are designated by K_2, L_2 and M_2 respectively. Additional photoelectron lines, designated by K_1, L_1, K_3 and L_3 correspond respectively to the K and L lines for two nuclear gamma-rays having energies 284±3 kev and 655±3 kev. These have also been found recently by a Swiss group.[17]

In addition, the Zürich group observed[17] an internal conversion line corresponding to a gamma-transition at 70 kev. If this transition appeared as a gamma-ray its L photoelectron line should have appeared at 49 kev (760 gauss-cm). However, no trace of such a line could be found.

A search of the negatron radiations from Cu^{61} by means of the photographic spectrometer revealed the existence of K and L internal conversion peaks corresponding to an energy approximately that reported above.[17] In addition, a very weak internal conversion line corresponding to the K radiation of the 284 kev transition was observed. Microphotometer tracings of the photographic plates which revealed these internal conversion lines are shown in Fig. 4. Intensities are on an arbitrary logarithmic scale. In order to obtain more accurate information concerning the relative intensities of these lines, they were also studied in the 6-cm radius of curvature spectrometer. The results are shown in Fig. 5. The usual background plus that caused by the negatron radiation from a small amount of Cu^{64} present in the source[16] was subtracted. The energies of the transitions in Ni^{61} as observed from the internal conversion lines are 76±2 kev and 284±3 kev.

IV. DISCUSSION AND TENTATIVE DISINTEGRATION SCHEME

In order to arrive at a disintegration scheme the comparison of the relative intensities of the several radiations from Cu^{61} is necessary. The intensity of the photoelectron lines may be compared to the total positron intensity through the annihilation radiation, whereas the internal conversion peak intensities may be compared directly with the intensity of the beta-distribution.

The comparison of areas of the photoelectron lines in

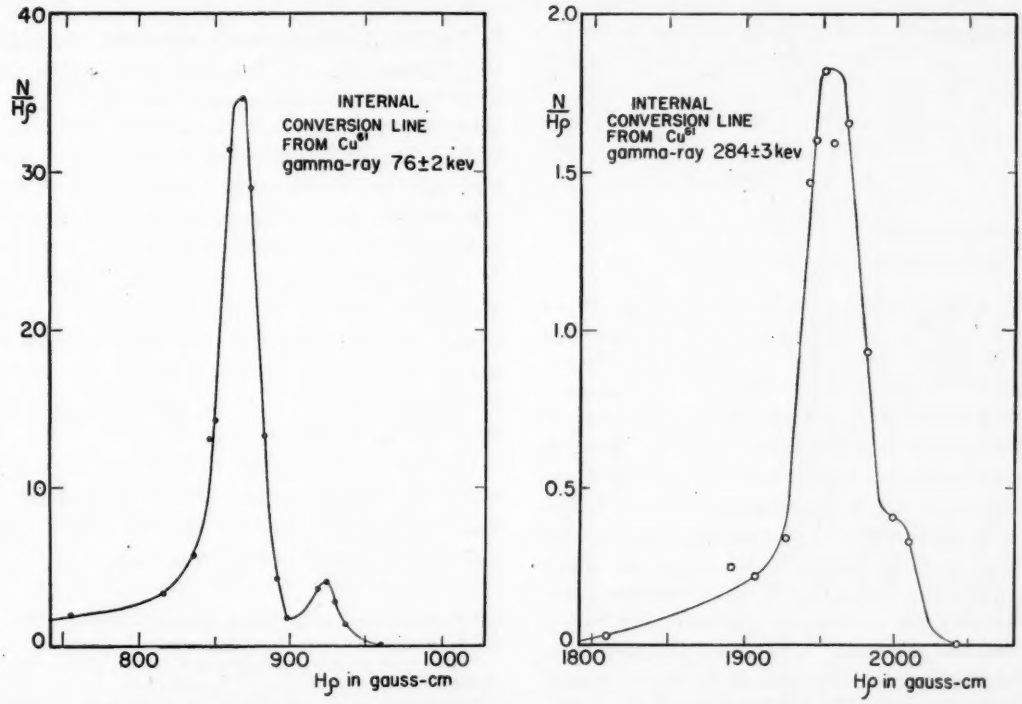

FIG. 5. Internal conversion lines of Cu^{61} as recorded by the constant radius spectrometer.

[17] Boehm, Blaser, Marmier, and Preiswerk, Phys. Rev. **77**, 295 (1950).

TABLE I. Disintegration data for Cu^{61}.

Radiation	Energy in kev	Observed intensity in % of total β^+ intensity	Calculated K/β^+ ratio	Internal conversion coefficient	Percent of total no. of disintegrations	Possible type of radiation
β_{1205}^+	1205±5	96±1	—	—	63±0.6	Allowed
K_{1205}	1205±5	—	0.29	—	18±0.15	Allowed
β_{550}^+	550±25	4.1±0.8	—	—	2.5±0.12	Allowed
K_{550}	550±25	—	~4.8	—	12.5±4	Allowed
β_{266}^+	266±13	—	—	—	0.03±0.007	Assumed Allowed
K_{266}	266±13	—	~100	—	2.3±0.8	Assumed Allowed
β_{190}^+	190±20	—	—	—	$(1.3\pm0.6)10^{-5}$	Assumed Allowed
K_{190}	190±20	—	~500	—	0.65±0.3	Assumed Allowed
γ_{284}	284±3	4.5±1	—	0.015	2.9±0.7	Electric Quadripole
γ_{76}	76±2	0.93±0.3	—	very high	0.65±0.3	?
γ_{655}	655±3	25±9	—	0	18±6	

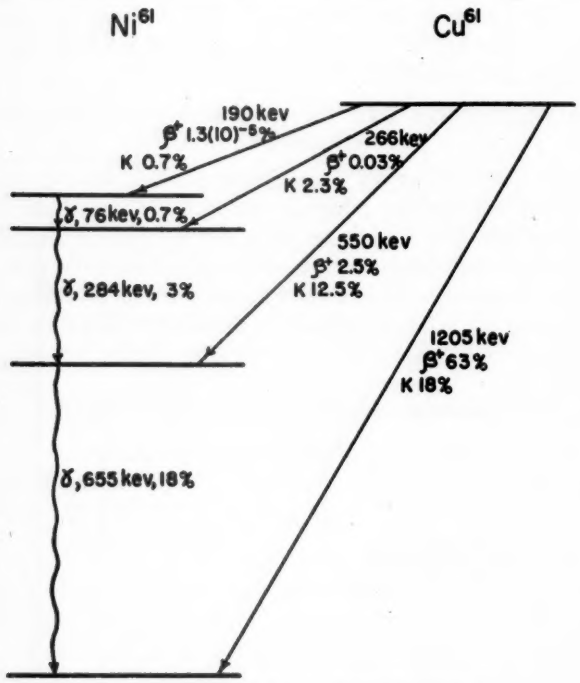

FIG. 6. Proposed decay scheme for Cu^{61}.

Fig. 3 with appropriate corrections for change in intensity as a function of energy for the photoelectric effect[18] indicates that there are approximately 25 percent as many 655 kev quanta observed as positrons. The relative percentage of 284 kev quanta with respect to positrons is even smaller, being about 4.5 percent. The internal conversion line at 284 kev is only about 0.068 percent as intense as the positron radiations. This leads to an internal conversion coefficient for the 284 gamma-transition of 0.068/4.5=0.015. Since the monochromatic radiation from the 76-kev transition was found in the internal conversion spectrum but not in the photoelectron spectrum, it has been assumed to be very highly internally converted. It is approximately one percent as intense as the positrons.

[18] W. Heitler, *The Quantum Theory of Radiation* (Oxford University Press, London, 1944), second edition, p. 124.

In addition to the positron disintegration of Cu^{61}, the K-capture transitions must also be considered. The theoretically expected (K-capture/positron) ratio for an allowed Cu^{61} transition having a maximum energy 1.205 Mev is[19] $K/\beta^+=0.29$. The corresponding expected ratio for the 550-kev transition is $K/\beta^+=4.8$.

Using this information and the intensities of the 75-kev and 284-kev gamma-transitions, one can construct the tentative disintegration scheme for Cu^{61} illustrated in Fig. 6. The experimental evidence offered does not conclusively prove the validity of this disintegration scheme. The proposed scheme is, however, consistent with all experimental evidence and is the only one which to date we have been able to construct which is consistent with this evidence.

The results of this set of experiments are summarized in Table I. It should be noted at this time that, using the evidence given in Table I as arranged in accordance with the disintegration scheme of Fig. 6, the resulting total (K-capture/positron) ratio now expected for Cu^{61} is $K_{61}/\beta_{61}^+=0.55$. This is the value found experimentally by Bouchez and Kayas[20] in their original experiments and is somewhat higher than the more recent values which have been reported.[21,22]

A radioactive isotope, Co^{61}, has been reported as decaying to Ni^{61} by negatron emission with a maximum energy of approximately 1.1 Mev.[23] Since sufficient energy is available it is possible that the disintegration scheme proposed here can be further checked through a study of the radiations from Co^{61}.

The writers would like to express their appreciation to Dr. H. Primakoff and Dr. P. S. Jastram for their many suggestions, and to Mr. M. Ter-Pogossian for assistance in the photoelectron study.

[19] E. Feenberg and G. Trigg, submitted to Rev. Mod. Phys.
[20] R. Bouchez and G. Kayas, J. de phys. et rad. **10**, 110 (1949).
[21] Huber, Ruetsche and Scherrer, Helv. Phys. Acta **22**, 375 (1949).
[22] Bouchez, de Groot, Nataf, and Tolhoek, Physica **15**, 863 (1949).
[23] G. T. Seaborg and I. Perlman, Rev. Mod. Phys. **20**, 585 (1948).

Properties of the $T^3(p,\gamma)He^4$ Reaction*

H. V. Argo, H. T. Gittings, A. Hemmendinger, G. A. Jarvis, and R. F. Taschek
Los Alamos Scientific Laboratory, Los Alamos, New Mexico

(Received March 8, 1950)

Yield and angular distribution measurements on the $T^3(p,\gamma)He^4$ reaction have been made for protons up to 2.5 Mev. The yield indicates a resonance in the He^4 nucleus at a proton energy of about 2.5 Mev, giving an excited level at 21.6 Mev. The angular yield of the gamma-rays fits an $A+B\sin^2\vartheta$ distribution very well, suggesting that the gamma-rays are due predominantly to a transition from the $^1P_1$ state to the $^1S_0$ state. An aluminum absorption curve for the secondaries produced in a lead radiator was taken, and a direct comparison made with the 17.5-Mev gamma-rays from the $Li^7(p,\gamma)Be^8$ reaction, showing that the $T^3(p,\gamma)He^4$ gamma-rays are of higher energy.

I. INTRODUCTION

DURING the last two years a rather extensive program for the study of the reactions of protons on tritium has been carried out in this laboratory. These reactions are:

$$H^1+T^3\rightarrow T^3+H^1 \quad (1)$$

$$\rightarrow He^3+n+Q_1 \quad (2)$$

$$\rightarrow He^4+\gamma+Q_2. \quad (3)$$

Since each of these three reactions has the same reacting particles, protons and tritons, and the same compound nucleus, He^4, their study has been of particular interest. Detailed reports[1,2] on reactions (1) and (2) and some preliminary results[3] on (3) have already been given. The purpose of this paper is to give a more complete account of the investigation of reaction (3).

The $T^3(p,\gamma)He^4$ reaction is of particular interest in that the gamma-ray is of higher energy than the gammas from any other observed nuclear transformation, the highest energy gamma-rays heretofore known being those of 17.5 Mev from the $Li^7(p,\gamma)Be^8$ reaction. As calculated from mass tables the value of Q_2 above is 19.8 Mev, giving a gamma-ray energy in excess of 20 Mev, depending on the incident proton energy and on the angle of observation. If the excited He^4 nucleus gives up its excitation energy with the emission of a single gamma-ray, the energy of that gamma-ray in the laboratory system and at 90° to the incident proton beam will be given by the equation

$$h\nu+\frac{(h\nu)^2}{2Mc^2}=Q_2+\frac{m_T}{m_H+m_T}E_p,$$

where M, m_H, and m_T are the masses for He^4, proton, and triton, respectively. E_p is the energy of the incident proton, and $h\nu$ is the energy of the emitted gamma-ray. For energies expressed in Mev, this equation reduces to

$$h\nu+(h\nu)^2/7452=19.8+0.7496E_p.$$

For any other angle of observation the Doppler effect must be considered, giving

$$\nu=\nu'[1+(v/c)\cos\vartheta']/(1-\beta^2)^{\frac{1}{2}}$$

where the C.M. system is primed and the laboratory system is unprimed. For such high energy gammas as these the Doppler shift is not inconsiderable, being about 300 kev when the observation is made at 0° with 1.5-Mev incident protons.

Our observations have not indicated the presence of more than one energy group, although the presence of a small amount of a low energy group would not show up in these measurements. There are some arguments that make a low energy group seem unlikely, one of which is that the presence of such a group would suggest the presence of an excited state in the compound nucleus, He^4, at some level below 20 Mev. Such states have been looked for by many observers, but so far have

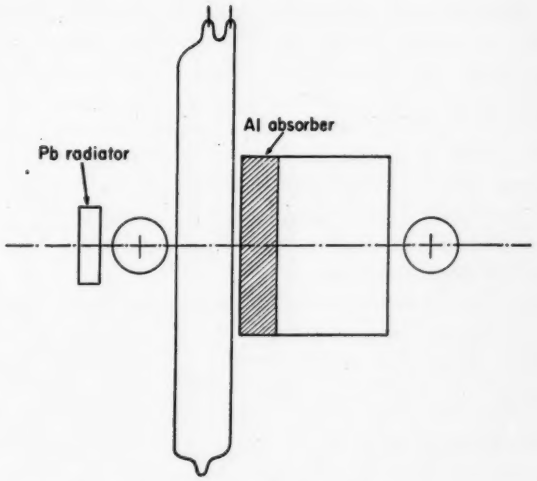

FIG. 1. Scale drawing of the triple coincidence G-M counter arrangement.

* This paper is based on work performed under Government Contract No. W-7405-eng-36 at the Los Alamos Scientific Laboratory of the University of California.

[1] Hemmendinger, Jarvis, and Taschek, Phys. Rev. **76**, 1137 (1949); Taschek, Jarvis, Hemmendinger, Everhart, and Gittings, Phys. Rev. **75**, 1361 (1949).

[2] Jarvis, Hemmendinger, Argo, and Taschek (unpublished work); Taschek, Argo, Hemmendinger, and Jarvis, Phys. Rev. **76**, 325 (1949).

[3] Argo, Gittings, Hemmendinger, Jarvis, Mayer, and Taschek, Phys. Rev. **76**, 182 (1949); R. F. Taschek, invited paper, Seattle meeting of the American Physical Society (June 27–29, 1949).

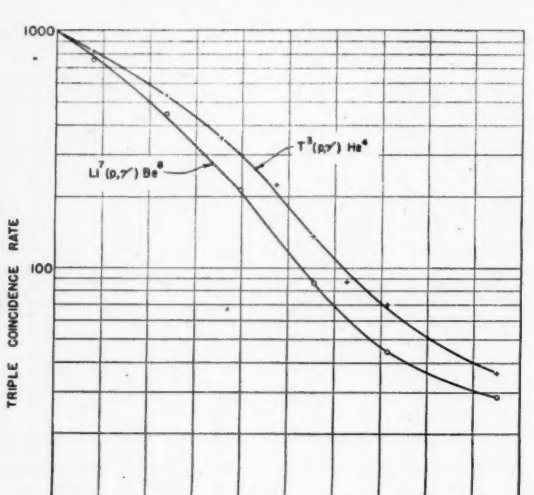

FIG. 2. Aluminum absorption curves for secondaries from Pb radiator using thick targets of Li and T^3.

never been found. However, there is good evidence from the present measurements that an excited state in He^4 does exist in the neighborhood of 21.5 Mev. A pair spectrometer capable of handling up to 30-Mev beta-particles is now under construction at this laboratory, and with this instrument it is hoped to be able to look at the energy spectrum in detail.

II. EXPERIMENTAL PROCEDURE

The Los Alamos 2.5-Mev electrostatic generator was used to produce a monoergic beam of protons. During the course of the measurements two types of tritium target were used. One was a "thick" target of tritium gas absorbed in a zirconium disk and the other a "thin" gaseous tritium target. The T^3+Zr target was of the type developed in this laboratory;[4] it has the disadvantage that while it is thick in the usual sense of being able to stop the incident protons, its yield is not the same as from a thick gaseous tritium target, but is reduced considerably by the dilution of the tritium with zirconium. A measure of the dilution was obtained by observing the neutron yields from the $T^3(p,n)He^3$ reaction for several incident proton energies and comparing these yields with those to be expected from a thick gaseous tritium target for the same proton energies.[2] The particular T^3+Zr target used had a neutron yield of about one-sixteenth that of an equivalent thick target of gaseous tritium.

The T^3+Zr target was mounted on a paddle wheel which held in addition targets of clean zirconium and lithium metals. The paddle wheel could be rotated from outside the vacuum system, making it possible to swing any one of the three targets into the path of the proton beam at will. This target was used to compare the gamma-rays from the $T^3(p,\gamma)$ reaction with those from the $Li^7(p,\gamma)$ reaction, the zirconium disk serving to determine the background. This comparison gives not only a measure of the yield but also some indication of the energy of the gamma-rays.

The proton beam was monitored with a current integrator,[5] the target being electrically insulated from the rest of the system. The beam strength was held to below one microampere to prevent overheating of the target and driving off of the tritium.

The gamma-rays were detected by observing secondary electrons with three thin-wall G-M tubes in triple coincidence, using a lead radiator 2.54 cm in diameter and 7.0 mm thick. In order to reduce the number of spurious triple counts as much as possible, the number two G-M tube was crossed with respect to numbers one and three, and various thicknesses of aluminum absorber were placed between the last two tubes as shown in Fig. 1. This whole assembly was placed inside a lead pig with walls two inches thick, which in turn was securely mounted to a large milling machine table so arranged that the pig could be rotated easily about the target as a center.

The scaler and triple coincidence circuits had a resolving time of five microseconds, making accidental triple coincidences completely negligible at even the

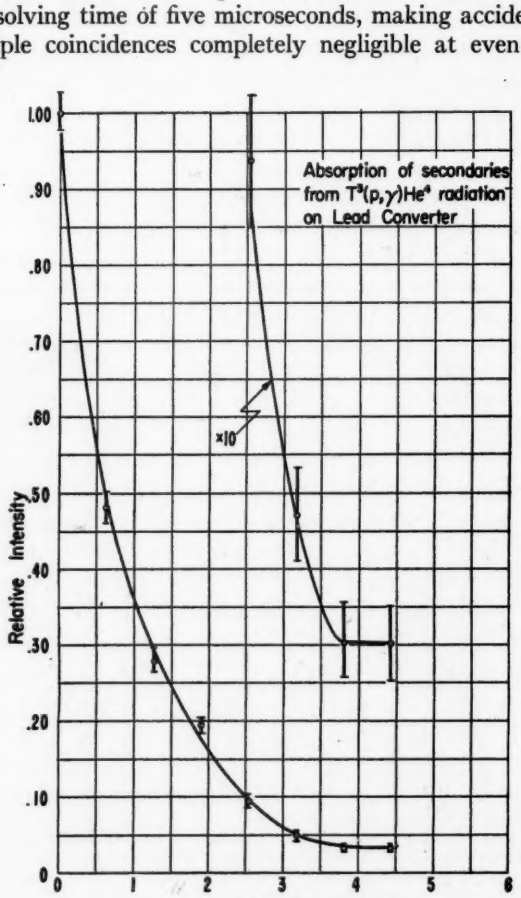

FIG. 3. Aluminum absorption curve for secondaries from Pb radiator using thin target of T^3.

[4] Graves, Rodrigues, Goldblatt, and Meyer, Rev. Sci. Inst. **20**, 579 (1949).

[5] H. T. Gittings, Rev. Sci. Inst. **20**, 325 (1949).

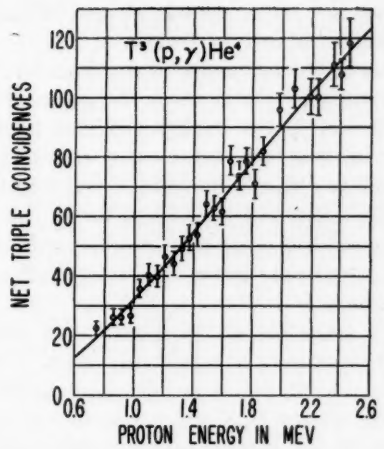

FIG. 4. Relative yield of the $T^3(p,\gamma)He^4$ reaction as a function of incident proton energy.

highest counting rates observed. The only appreciable source of background was that induced by the proton beam. At proton energies greater than 1019 kev, the threshold for the $T^3(p,n)He^3$ reaction, neutrons from this reaction produced a large background of gamma-rays within the lead pig, and individual counting rates for each of the three G-M tubes would rise markedly. However, with a one-half inch aluminum absorber between tubes number two and three the triple coincidence rate was unchanged within the statistics of our data. To show that this was so, triple coincidence rates were measured with and without a one-inch lead absorber directly in front of the radiator. One pair of measurements was made with the proton energy well above the neutron threshold, and a second pair of measurements made with the proton energy below the neutron threshold. The ratio of counting rates with and without the lead absorber was the same in each case, indicating that no appreciable fraction of the counts was due to the neutron flux above threshold.

With the lead pig oriented at 90° to the incident proton beam of 1.01-Mev energy and the lead radiator subtending a solid angle of 0.0297 steradian, the gamma-rays from the $T^3(p,\gamma)He^4$ reaction were compared directly with the 17.5-Mev gamma-rays from the $Li^7(p,\gamma)Be^8$ reaction. From Fig. 2, which shows the aluminum absorption curves for the secondaries produced by the gamma-rays, it is evident that the gamma-rays from the tritium reaction are of higher energy than those from lithium. As calculated from mass tables, the energies for these two gamma-rays are 20.6 Mev and 18.1 Mev, respectively. In the figure the triple coincidence rates for the two reactions have been normalized for zero thickness of aluminum absorber, the yield from the Zr + T^3 target being 0.117 of the yield from the thick lithium metal plate. Taking into account the dilution of the tritium by the zirconium, the concentration of the tritium, and the concentration of the lithium, the thick target yield of $Li^7(p,\gamma)$ is 1.1 times the thick target yield of $T^3(p,\gamma)$ for the incident proton energy of 1.01 Mev.

From the above information one can compare the average cross sections for the two reactions over the energy range from zero to 1.01 Mev. According to the published curves of Fowler, Lauritsen, and Lauritsen[6] the average cross section for the $Li^7(p,\gamma)$ reaction in this region is about $2.4(10)^{-28}cm^2$, giving an average cross section of $2(10)^{-28}$ cm^2 for the $T^3(p,\gamma)$ reaction.

As was pointed out, the curves in Fig. 2 are obtained from a thick target. A second aluminum absorption curve was taken in the same manner, only this time a thin tritium gas target was used. This target and method of filling have been explained in detail in the paper by Jarvis *et al.*[2] The target was filled with 20 cm Hg of tritium, giving a target thickness of about 40 kev for the 1.52-Mev incident protons. By calculation, protons of this energy will give a 20.9-Mev gamma-ray observed at 90° from the proton beam. The absorption curve obtained with this thin target has been plotted in Fig. 3.

A curve of relative yield as a function of incident proton energy was obtained using a tritium gas target of about 60-kev thickness for 1.0-Mev protons, and with the lead pig held fixed at 90°. This curve is shown in Fig. 4, the counting statistics being indicated for each point. The spread at the higher energies is considerable, due primarily to the high background, which is increas-

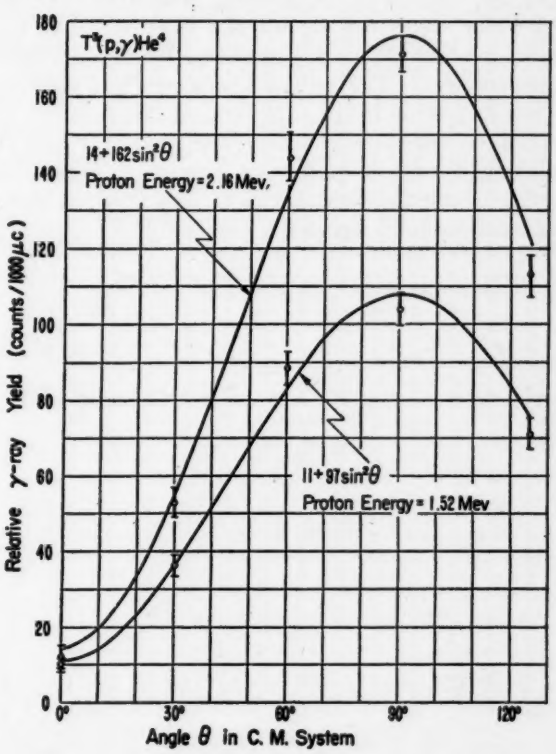

FIG. 5. Angular distribution of the gamma-rays from the $T^3(p,\gamma)He^4$ reaction.

[6] Fowler, Lauritsen, and Lauritsen, Rev. Mod. Phys. **20**, 236 (1948).

ing with energy. Backgrounds were taken for each energy point by placing H_2 in the target and running the same number of microcoulombs into the target as for a tritium run. The background was due almost entirely to (p, γ) processes in the aluminum entrance foil of the target chamber and in the walls of the target tube and chamber, and therefore was proportional to the number of microcoulombs of beam. An interesting feature of the yield curve in Fig. 4 is the rapid increase of the cross section with energy. Unfortunately, the Los Alamos electrostatic generator could produce protons of energy up to only 2.5 Mev in the target, so it was not possible to get to the high side of what appears to be a broad resonance. However, if one assumes that the curve is rising into a resonance and fits a Breit-Wigner[7] nuclear resonance curve to the data, he finds that the peak comes close to 2.5 Mev and that the half-width is about 1 Mev. For a proton energy of 2.5 Mev the energy of the emitted gamma-ray is calculated to be 21.63 Mev.

An additional indication that the compound He^4 nucleus has an excited level in this energy region comes from the recent measurements[2] in this laboratory of the $T^3(p, n)He^3$ cross section. This reaction likewise exhibits a marked rise in cross section in the neighborhood of 2.5 Mev. As with the present measurement, a higher energy could not be attained, so the high energy side of the resonance was not observed.

One of the most interesting properties of the $T^3(p, \gamma)He^4$ reaction is the angular distribution of the gamma-ray yield. This was observed for two different proton energies, 1.52 Mev and 2.16 Mev, Fig. 5 showing the results plotted in the C.M. system. There is a very pronounced angular asymmetry, the yield at 0° almost vanishing. It was of particular interest to determine whether or not the yield did go to zero at 0°, so these data were carefully repeated a number of times. As the angular resolution of the counters was 0.0297 steradian, no appreciable number of counts in the 0° direction could be due to the finite size of the detector, therefore the counts must be a real effect. To insure that the 0° counts were not just a background due to scattering from material near the target and counters, a large mass of steel was placed immediately next to the target and counters and a change looked for in the counting rate. No noticeable change was observed, indicating that scattering was giving no contribution to the counting rate.

For both cases shown in Fig. 5 the data fit an $A+B\sin^2\vartheta$ distribution reasonably well. The spread due to counting statistics is indicated on the curves. Christy[8] has shown that the apparent electric dipole distribution of the gamma-rays can be accounted for by assuming the gamma-ray is a result of a transition from the odd $^1P_1$ state to the even $^1S_0$ ground state in the He^4 nucleus. If only the $^1P_1$ state were involved a pure $(\sin^2\vartheta)$-distribution would be expected, but the fact that the yield does not vanish at 0° indicates that a small amount of another state must be present, possibly the $^3P_1$ state which would introduce a $(1+\cos^2\vartheta)$-distribution. An interesting correlation with the above arguments is provided by the yield from the $T^3(p, n)He^3$ reaction.[2] In the cosine expansions of the angular distributions in the center of mass system the coefficient of the $(\cos^2\vartheta)$-term shows evidence of a resonance. A resonance excited by p-wave protons would be expected to give resonant behavior in p-wave outgoing neutrons and thus make just the $(\cos^2\vartheta)$-term in the neutron yield show a resonant behavior.

We are indebted to Dr. Harris Mayer for assistance and advice in the early stages of this work, and we gratefully acknowledge the assistance of Mr. George Everhart in the operation of the accelerator.

[7] G. Breit and E. Wigner, Phys. Rev. 49, 519 (1936).

[8] R. F. Christy, Supplementary Paper, Seattle meeting of the American Physical Society, June 27–29, 1949; R. F. Christy (unpublished work).

A Molecular Beam Resonance Method with Separated Oscillating Fields*

NORMAN F. RAMSEY
Harvard University, Cambridge, Massachusetts
(Received February 21, 1950)

A new molecular beam resonance method using separated oscillating fields at the incident and emergent ends of the homogeneous field region is theoretically investigated in this paper. An expression is obtained for the quantum mechanical transition probability of a system between two states when the system is subjected to such separated oscillating fields. This is numerically averaged over the molecular velocity distribution and provides the theoretical shape of the resonance curves. It is found that resonances with such a technique have a theoretical half-width only 0.6 as great as those by conventional molecular beam resonance methods. In addition to producing sharper resonance minima, the new method has its resonances much less broadened by inhomogeneities of the fixed field, it makes possible resonance experiments in regions into which an oscillating field cannot be introduced, and it is more convenient and effective with short wavelength radiation.

1. INTRODUCTION

IN all previous molecular beam resonance experiments,[1–5] the oscillating fields which induce the transitions are extended approximately uniformly throughout the regions in which the energy levels of the system are investigated. This, however, is not necessarily the most advantageous method of applying the oscillating field since more useful curves for many purposes can often be obtained if the amplitude and phase of the oscillating field are varied along the path of the beam.[6] A particular arrangement that is more advantageous in many cases is one in which the oscillating field is confined to a small region at the beginning of the space in which the energy levels are being studied and to another small region at the end, there being no oscillating field in between. This case is investigated in detail theoretically in the present paper.

It is superficially surprising that information can be obtained about the energy levels of a molecule in a region of space without the radiation field inducing the transitions being extended throughout that region. However, by considering the Fourier analysis of an oscillating field on for a time τ, off for a time T, and on again for a time τ, one can see that the method of separated oscillating fields produces transitions at frequencies corresponding to the energy levels in the intermediate region in which no oscillating field exists. Alternatively this can be seen by considering certain simple examples.

The simplest special case is that of a magnetic moment associated with such a large angular momentum that the problem can be treated classically. Consider that such a magnetic moment enters a region of a fixed strong homogeneous magnetic field at the entrance and exit ends of which a weak magnetic field perpendicular to the fixed field rotates about an axis parallel to the fixed field. The rotating magnetic field then supplies a torque perpendicular to the magnetic moment which will cause the angular momentum to be reoriented with a change in the angle ϕ between the angular momentum and the fixed field. If the rotating field is not approximately of the same magnitude and direction as the Larmor precession, the angle ϕ successively increases and decreases, resulting in little net change. On the other hand, if the two rotational frequencies are approximately the same, the effects are cumulative, resulting in an appreciable change in ϕ as in the theory of the "sleeping" top or of the normal molecular beam resonance method.[1] If the angular momentum is initially parallel to the fixed field so that ϕ is equal to zero initially, it is possible to select the magnitude of the rotating field to be such that $\phi=90°$ at the end of the first oscillating region. While in the region with no oscillating field, the magnetic moment simply precesses with the Larmor frequency appropriate to the magnetic field in that region.

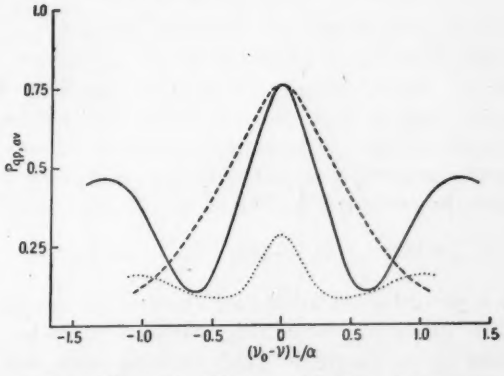

FIG. 1. Transition probability as a function of frequency near resonance. L=distance between oscillating field regions. α=most probable molecule velocity. ν=oscillator frequency. ——— New method with maximum transition probability. ····· Same with one-third the strength of oscillating field. – – – – Previous method with maximum transition probability.

* This work has been partially supported by the Joint Program of the ONR and the AEC.

[1] I. I. Rabi, Phys. Rev. **51**, 652 (1937).
[2] Rabi, Millman, Kusch, and Zacharias, Phys. Rev. **55**, 526 (1939).
[3] Kellogg, Rabi, Ramsey, and Zacharias, Phys. Rev. **56**, 728 (1939).
[4] Kusch, Millman, and Rabi, Phys. Rev. **57**, 765 (1940).
[5] H. Hughes, Phys. Rev. **72**, 614 (1947).
[6] N. F. Ramsey, Phys. Rev. **76**, 996 (1949).

When the magnetic moment enters the second oscillating field region there is again a torque acting to change ϕ. If the frequency of the rotating field is exactly the same as the mean Larmor frequency in the intermediate region there is no relative phase shift between the angular momentum and the rotating field. Consequently, if the magnitude of the second rotating field and the length of time of its application are equal to those of the first region, the second rotating field has just the same effect as the first one, i.e., increases ϕ by another 90°, making $\phi=180°$, corresponding to a complete reversal of the direction of the angular momentum. On the other hand, if the field and the Larmor frequencies are slightly different so that the relative phase angle between the rotating field vector and the precessing angular momentum is changed by 180° while the system is passing through the intermediate region, the second oscillating field has just the opposite effect to the first one, with the result that ϕ is returned to zero. If the Larmor frequency and the rotating field frequency differ by just such an amount that the relative phase shift in the intermediate region is exactly an integral multiple 360°, ϕ will again be left at 180° just as at exact resonance. However, in a molecular beam resonance experiment one can easily distinguish between exact resonance and the other cases by the fact that in the former case the condition for no change in the relative phase of the rotating field and of the precessing angular momentum is independent of the molecular velocity, whereas in the other cases the condition for an integral multiple of 360° relative phase shift is velocity dependent since a slower molecule is in the intermediate region longer and so experiences a greater shift than a faster molecule. Consequently, for the molecular beam as a whole, the reorientations are incomplete in all except the resonance cases. Therefore, one would expect a resonance curve similar to that shown in Fig. 1, in which the transition probability for a particle of spin $\frac{1}{2}$ is plotted as a function of frequency.

2. TRANSITION PROBABILITIES

Consider a molecular system which at time t_1 enters a region where it is subjected to an oscillatory perturbation which induces transitions between two molecular energy eigenstates p and q, for neither of which states there can be transitions to any other state while the system is subjected to the perturbing field. Assume the perturbation V is of such a form that

$$V_{pq}=\hbar be^{i\omega t},\quad V_{qp}=\hbar be^{-i\omega t},\quad V_{pp}=V_{qq}=0. \tag{1}$$

Such a perturbation arises, for example, if the transitions of a system containing magnetic moments are induced by a magnetic field rotating with angular velocity ω about the axis of quantization. Then if

$$\Psi(t)=C_p(t)\psi_p+C_q(t)\psi_q. \tag{2}$$

The Schrödinger time dependent equations reduce to the forms

$$\begin{aligned} ih\dot{C}_p(t)&=W_pC_p(t)+\hbar be^{i\omega t}C_q(t),\\ ih\dot{C}_q(t)&=\hbar be^{-i\omega t}C_p(t)+W_qC_q(t). \end{aligned} \tag{3}$$

If at time t_1, C_p, and C_q had the values $C_p(t_1)$ and $C_q(t_1)$ respectively, the solution of (3) at time t_1+T subject to this initial condition is

$$\begin{aligned} C_p(t_1+T)=&\{[i\cos\theta\sin\tfrac{1}{2}aT+\cos\tfrac{1}{2}aT]C_p(t_1)\\ &-[i\sin\theta\sin\tfrac{1}{2}aT\cdot\exp(i\omega t_1)]C_q(t_1)\}\\ &\cdot\exp\{i[\tfrac{1}{2}\omega-(W_p+W_q)/2\hbar]T\},\\ C_q(t_1+T)=&\{-[i\sin\theta\sin\tfrac{1}{2}aT\cdot\exp(-i\omega t_1)]C_p(t_1)\\ &+[-i\cos\theta\sin\tfrac{1}{2}aT+\cos\tfrac{1}{2}aT]C_q(t_1)\}\\ &\cdot\exp\{i[-\tfrac{1}{2}\omega-(W_p+W_q)/2\hbar]T\}, \end{aligned} \tag{4}$$

where

$$\begin{aligned} &\cos\theta=(\omega_0-\omega)/a,\quad \sin\theta=2b/a,\\ &a=[(\omega_0-\omega)^2+(2b)^2]^{\frac{1}{2}},\ \omega_0=(W_q-W_p)/\hbar. \end{aligned} \tag{5}$$

That (4) is a solution of (3) can be confirmed readily by substitution. A particular case of (4) occurs when $b=0$, in which case

$$\begin{aligned} C_p(t_1+T)&=\exp(-i(W_p/\hbar)T)C_p(t_1),\\ C_q(t_1+T)&=\exp(-i(W_q/\hbar)T)C_q(t_1). \end{aligned} \tag{6}$$

Consider a molecule on which the perturbation (1) acts while the molecule goes a distance l in time τ after which it enters a region of length L and duration T in which b is zero, after which it is again acted on by the perturbation for a time τ. To achieve greater generality, corresponding to the experimental impossibility of attaining completely uniform magnetic fields, assume that the energies of the states p and q are not constant in the intermediate region where b is zero, but that the region is divided into a number of sub-regions such that in the k'th sub-region of duration Δt_k the energies are $W_{p,k}$ and $W_{q,k}$. Then if t is taken to be zero when the first perturbation begins to act, and if

$$C_p(0)=1,\quad C_q(0)=0, \tag{7}$$

successive applications of (4) and (6) yield

$$\begin{aligned} C_p(\tau)=&[i\cos\theta\sin\tfrac{1}{2}a\tau+\cos\tfrac{1}{2}a\tau]\\ &\cdot\exp\{i[\tfrac{1}{2}\omega-(W_p+W_q)/2\hbar]\tau\}, \end{aligned} \tag{8a}$$

$$\begin{aligned} C_q(\tau)=&[-i\sin\theta\sin\tfrac{1}{2}a\tau]\\ &\cdot\exp\{i[-\tfrac{1}{2}\omega-(W_p+W_q)/2\hbar]\tau\}, \end{aligned} \tag{8b}$$

$$\begin{aligned} C_p(\tau+T)&=\Pi_k[\exp(-iW_{p,k}\Delta t_k/\hbar)]\cdot C_p(\tau)\\ &=\{\exp[-(i/\hbar)\textstyle\sum_k W_{p,k}\Delta t_k]\}\cdot C_p(\tau)\\ &=[\exp(-i\bar{W}_pT/\hbar)]\cdot C_p(\tau), \end{aligned} \tag{8c}$$

$$C_q(\tau+T)=[\exp(-i\bar{W}_qT/\hbar)]\cdot C_q(\tau), \tag{8d}$$

$$\begin{aligned} C_p(2\tau+T)=&\{[i\cos\theta\sin\tfrac{1}{2}a\tau+\cos\tfrac{1}{2}a\tau]\cdot C_p(\tau+T)\\ &-[i\sin\theta\sin\tfrac{1}{2}a\tau\cdot\exp i\omega(\tau+T)]\\ &\cdot C_q(\tau+T\}\cdot\exp\{i[\tfrac{1}{2}\omega\\ &-(W_p+W_q)/2\hbar]\tau, \end{aligned} \tag{8e}$$

$$C_q(2\tau+T)=\{-[i\sin\theta\sin\tfrac{1}{2}a\tau\cdot\exp(-i\omega(\tau+T))]\cdot C_p(\tau+T)+[-i\cos\theta\sin\tfrac{1}{2}a\tau+\cos\tfrac{1}{2}a\tau]\cdot C_q(\tau+T)\}\cdot\exp\{i[-\tfrac{1}{2}\omega-(W_p+W_q)/2\hbar]\tau\}. \quad (8f)$$

Here

$$\bar{W}_p=(1/T)\textstyle\sum_k W_{p,k}\Delta t_k=(1/L)\sum_k W_{p,k}\Delta L_k = \text{space mean value of } W_p, \quad (9)$$

with a similar interpretation for $\bar{W}_q$.

The elimination of the intermediate values of the C's from Eqs. (8a–f) yields for $C_q(2\tau+T)$,

$$C_q(2\tau+T)=2i\sin\theta[\cos\theta\sin^2\tfrac{1}{2}a\tau\sin\tfrac{1}{2}\lambda T-\tfrac{1}{2}\sin a\tau\cos\tfrac{1}{2}\lambda T]\cdot\exp\{-i[(\tfrac{1}{2}\omega+(W_p+W_q)/2\hbar)(2\tau+T)+((\bar{W}_p-W_p+\bar{W}_q-W_q)/2\hbar)T]\}, \quad (10)$$

where

$$\lambda=[(\bar{W}_q-\bar{W}_p)/\hbar]-\omega. \quad (11)$$

It follows from Eq. (10) that the probability that the system changes from state p to state q is

$$P_{p,q}=|C_q|^2=4\sin^2\theta\sin^2\tfrac{1}{2}a\tau\cdot[\cos\tfrac{1}{2}\lambda T\cos\tfrac{1}{2}a\tau-\cos\theta\sin\tfrac{1}{2}\lambda T\sin\tfrac{1}{2}a\tau]^2. \quad (12)$$

An important special case of this relation is that corresponding to a nuclear magnetic moment of spin $\frac{1}{2}$ with a gyromagnetic ratio g, in a fixed field of strength H_0, with a weak field of strength H_1 perpendicular to H_0 and rotating about H_0. In this case Eq. (12) applies with

$$\omega_0=g\mu_0H_0/\hbar,\quad \lambda=\omega_0-\omega,\qquad 2b=g\mu_0H_1/\hbar=\omega_0H_1/H_0. \quad (13)$$

These results can be extended to higher spins by the use of the Majorana formula, in the usual manner.[1,7]

3. AVERAGE OVER MOLECULAR VELOCITY DISTRIBUTIONS

For any particular dimensions of the experimental apparatus, the transition probability (12) applies to only a single molecular velocity, since the times T and τ are inversely proportional to the velocity. Hence (12) must be averaged over the distribution of molecular velocities occurring in the molecular beam. Without loss of significant generality, this averaging can be carried out most easily by performing it in but two limiting cases. One of these is for frequencies so close to resonance that $|\omega_0-\omega|$ is much less than $|2b|$, in which case Eq. (12), when integrated over the molecular velocities with the usual molecular beam weighting factor, becomes

$$\langle P_{p,q}\rangle_{Av}=2\int_0^\infty \exp(-y^2)\cdot y^3\cdot\sin^2\left(\frac{2bl}{\alpha y}\right)\cos^2\left(\frac{\lambda L}{2\alpha y}\right)dy, \quad (14)$$

where y is the molecular velocity divided by the most probable molecular velocity $\alpha=(2kT/m)^{\frac{1}{2}}$.

The other interesting limit is that for frequencies so far from exact resonance that the quantity $\lambda L/(2\alpha y)$ is sufficiently large that in averaging over the velocities the rapidly varying factor $\sin^2(\lambda L/2\alpha y)$ can be replaced by its average value of $\frac{1}{2}$, while $\sin(\lambda L/2\alpha y)$ can be replaced by its average value of zero. In this case we have

$$\langle P_{p,q}\rangle_{Av}=4\sin^2\theta\int_0^\infty \exp(-y^2)\cdot y^3\cdot\sin^2\left(\frac{al}{2\alpha y}\right)\cdot\left[1-\sin^2\theta\sin^2\left(\frac{al}{2\alpha y}\right)\right]dy. \quad (15)$$

The numerical work of evaluation of (14) and (15) can be much simplified by first reducing the expressions to sums and differences of the single integral function

$$I(\beta)=\int_0^\infty \exp(-y^2)\cdot y^3\cdot\cos(\beta/y)dy. \quad (16)$$

With this notation Eq. (14) becomes

$$\langle P_{p,q}\rangle_{Av}=\tfrac{1}{4}-\tfrac{1}{4}I\left(\frac{\lambda L+4bl}{\alpha}\right)-\tfrac{1}{4}I\left(\frac{\lambda L-4bl}{\alpha}\right)+\tfrac{1}{2}I(\lambda L/\alpha)-\tfrac{1}{2}I(4bl/\alpha), \quad (17)$$

while Eq. (15) becomes

$$\langle P_{p,q}\rangle_{Av}=\sin^2\theta\cdot(1-\tfrac{3}{4}\sin^2\theta)-\tfrac{1}{2}\sin^2 2\theta\cdot I(al/\alpha)-\tfrac{1}{2}\sin^4\theta\cdot I(al/2\alpha). \quad (18)$$

Both (17) and (18) depend on the value assumed for the experimentally arbitrary parameter $2bl/\alpha$. One

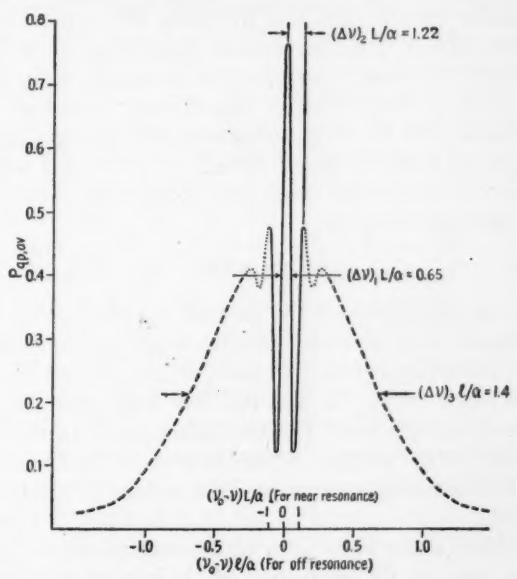

FIG. 2. Transition probability as a function of frequency. ——— Calculated near resonance. – – – – – Calculated off resonance. ····· Interpolated.

[7] E. Majorana, Nuovo Cimento **9**, 43 (1932).

TABLE I. Comparison of theoretical and experimental resonance widths.

	Theoretical value (kc)	Experimental value (kc)
$(\Delta\nu)_1$	1.16	1.2
$(\Delta\nu)_2$	2.2	2.3
$(\Delta\nu)_3$	24.0	30.0

experimental criterion that is frequently used to fix this parameter is that it is to be selected to make $\langle P_{q,p}\rangle_{Av}$ a maximum at exact resonance ($\lambda=0$). At exact resonance (14) becomes

$$\langle P_{p,q}\rangle_{Av}=2\int_0^\infty \exp(-y^2)\cdot y^3\cdot\sin^2(2bl/\alpha y)dy, \quad (19)$$

which is the same form as that to which the conventional case discussed by Torrey[8] reduces at resonance since his Eq. (7) then becomes the same as our Eq. (19) except that his β_0 is replaced by $4bl/\alpha$. Torrey shows that in his case $\langle P_{q,p}\rangle_{Av}$ is a maximum for $\beta_0=1.200\pi$. Therefore it will be a maximum in the present case for

$$2bl/\alpha=0.600\pi. \quad (20)$$

With this value the transition probability in the immediate vicinity of resonance as given in (17) has been plotted as the full line in Fig. 1 as a function of $(\nu_0-\nu)L/\alpha$, where $\nu=\omega/2\pi$. For comparative purposes, the theoretical transition probability with the conventional molecular beam resonance method as calculated by Torrey[8] is plotted with dashed lines on the same curve.

Although the relation (20) will lead to the maximum transition probability at resonance, if there is plenty of beam intensity available a sharper though weaker resonance can be obtained by using an even smaller perturbation b. This corresponds physically to the fact that with the weaker perturbation the slower molecules are relatively more effective than the fast ones and the slow molecules are in the magnetic field a longer time. This result is shown by the dotted curve of Fig. 1 which shows the theoretical transition probability with the new method and with

$$2bl/\alpha=0.200. \quad (21)$$

As an indication of the general appearance of the resonance over the entire resonance region, the transition probabilities from (17) and (18) are plotted on the same graph in Fig. 2. The full line is the part of the curve calculated from (17), the dashed line is from (18), and the dotted portion of the curve is an interpolation for the intermediate region in which neither (17) nor (18) is valid.

If $(\Delta\nu)_1$ is the half-width of the central sharp maximum, $(\Delta\nu)_2$ is the separation of the central maximum from the nearest subsidiary maximum, and $(\Delta\nu)_3$ is the width of the broad background maximum, these should have the values

$$(\Delta\nu)_1=0.64\alpha/L, \quad (\Delta\nu)_2=1.23\alpha/L, \quad (\Delta\nu)_3=1.4\alpha/l. \quad (22)$$

4. DISCUSSION

These theoretical results can be compared with the subsequent experimental observations by Kusch[9] on potassium atoms in magnetic fields of about 1.5 gauss as shown in Fig. 3. As can be seen, there is excellent qualitative agreement between the above theory and the subsequent experimental results. The asymmetry between the position of the sharp resonances and of the broad background is presumably due to the mean field in the intermediate region of the magnet being different from the values in the vicinity of the wires carrying the oscillating current, whence λ and $\omega_0-\omega$ become zero for different values of ω. In Table I the experimental and theoretical values of the quantities in (22) are compared. The theoretical values are calculated from $L=24$ cm, $l=2.5$ cm, and $\alpha=4.3\times10^4$ cm/sec. The agreement for all except $(\Delta\nu)_3$ is excellent. The 20 percent disagreement in the latter value is probably attributable to experimental variations in the strength of the field in the vicinity of the wires carrying the oscillating current. The power of the method of separated oscillating fields is well illustrated by these experimental curves. The homogeneity of the magnetic field obtainable in this experiment was such that the width of the broad maximum approximately measures the precision that could have been obtained with the earlier molecular beam resonance methods, whereas with new method provides a maximum whose width is about twenty times less.

For many applications, the molecular beam resonance method with separated oscillating fields is superior to the conventional method in a number of ways. (1) The

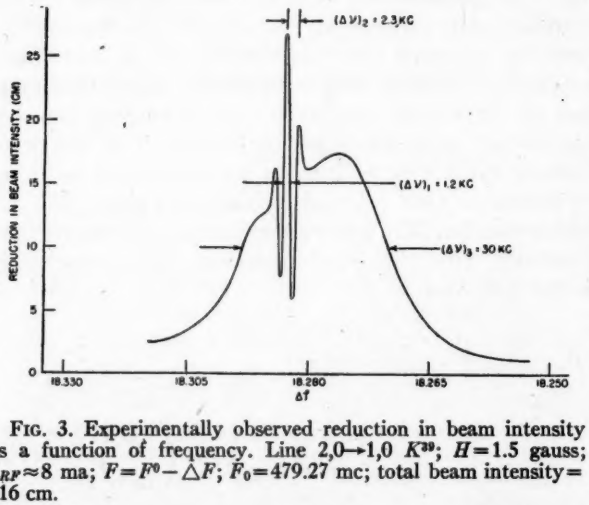

FIG. 3. Experimentally observed reduction in beam intensity as a function of frequency. Line 2,0→1,0 K^{39}; $H=1.5$ gauss; $I_{RF}\approx8$ ma; $F=F^0-\triangle F$; $F_0=479.27$ mc; total beam intensity=216 cm.

[8] H. C. Torrey, Phys. Rev. 59, 293 (1941).

[9] P. Kusch (private communication).

resonance peaks with the new method are only 0.6 as broad as the corresponding ones with conventional method and the same length of magnetic field. (2) Unlike the earlier methods, with the new method the sharpness of the peak is not reduced by non-uniformities of the constant field since from (11) and (12) above it is only the space average value of the energies which is important. The field must still be fairly uniform along the height of the beam, but this is much more easily achieved experimentally than is uniformity along the length. This advantage of the new method is particularly important and in many cases makes possible an increase in precision of a factor of twenty or more. (3) The new method is more convenient and effective at very high frequencies where the wave-length may be comparable to the length of the region in which the energy levels are investigated. (4) The new method may be applied to study energy levels of a system in a region into which an oscillating field cannot be introduced; for example, the Larmor precession frequency of neutrons can be measured while they are inside a magnetized iron block.

PHYSICAL REVIEW VOLUME 78, NUMBER 6 JUNE 15, 1950

Magnetic Shielding of Nuclei in Molecules*

NORMAN F. RAMSEY
Harvard University, Cambridge, Massachusetts
(Received March 6, 1950)

An expression is developed for the magnetic field at a nucleus resulting from the application of an external magnetic field to a polyatomic molecule which has no resultant electron orbital or spin angular momenta in the absence of the external field. The field at the nucleus is not the same as the externally applied field because of the field arising from the motion of the electrons in the molecule. The expression for the electron contribution to the magnetic field is shown to consist of two parts. The first is a simple term that is similar to the diamagnetic correction developed by Lamb for atoms. The second is a complicated one arising from second-order paramagnetism and is analogous to the term dependent on the high frequency matrix elements in the theory of molecular diamagnetism. Under certain circumstances the second-order paramagnetic term can become quite large. Since both of these terms are altered when the same nucleus is in different molecules, they at least partially and perhaps completely explain the chemical effect that has been reported by various observers in measurements of nuclear moments. For linear molecules, the second-order paramagnetic term is shown to be directly related to the experimentally measurable spin-rotational magnetic interaction constant of the molecule. This relation is particularly valuable in the important case of molecular hydrogen where it is shown that the correction for second-order paramagnetism is -0.56×10^{-6}. When this is added to the Lamb-type term as calculated by Anderson, the total magnetic shielding constant for molecular H_2 becomes 2.68×10^{-5}.

I. INTRODUCTION

IN measurements of nuclear magnetic moments, a correction must be made for the magnetic field arising from the motions of the molecular electrons which are induced by the externally applied field. For example, the application of the external magnetic field produces a diamagnetic circulation of the electrons, which in turn produces a magnetic field at the nucleus, so that the resultant field in which the nuclear Larmor frequency is measured differs from the applied field by a small but important amount. Since this shielding field is proportional to the external field it cannot be distinguished from it merely by varying the external field. Until recently the correction has been made in accordance with a theory developed by Lamb.[1] This theory is strictly applicable only to atoms since it depends on the spherical symmetry of the electric field of the nuclear electrical potential. With the precision available in nuclear moment experiments up until recently, this method of correction has been adequate even though most of the experiments have been performed with molecules instead of atoms. This has been true because the diamagnetic correction in light molecules like hydrogen is so small as to have been negligible, while in molecules with heavy nuclei the diamagnetic correction is caused chiefly by the innermost electrons and for these the problem is approximately an atomic one. However, the atomic approximation is no longer adequate in treating present experiments. The precision of experiments with light nuclei such as hydrogen has become so great (better than one part in a million) that the diamagnetic correction (27 parts in a million in H_2) is important. Furthermore, with heavier nuclei the ratios of the resonance frequencies for the same nucleus in different molecules have been measured with high precision and discrepancies have been found by various observers[2-4] that are sometimes called the chemical effect. The change in different molecular compounds of the electronic magnetic fields described in this paper will at least be an important

* This work was partially supported by the joint program of the ONR and AEC.
[1] W. Lamb, Phys. Rev. **60**, 817 (1941).
[2] W. D. Knight, Phys. Rev. **76**, 1260 (1949).
[3] W. C. Dickinson, Phys. Rev. **78**, 339 (1950).
[4] F. Bloch (private communication).

contributor to this chemical effect and may well be its complete explanation.

As with the theory of the ordinary diamagnetism and second-order paramagnetism of molecules as discussed by Van Vleck,[5] the diamagnetic shielding of a molecule differs from that of a single atom in two ways, as was pointed out by Ramsey[6] in an earlier communication. (1) The electron distribution to be used in calculating the diamagnetic correction of the Lamb[1] type is altered by the presence of the other atoms with their associated electrons in the molecule. (2) In a molecule the electrical potential is no longer spherically symmetric; hence Larmor's theorem no longer applies directly in the manner implicitly assumed in Lamb's derivation of of the atomic correction. Thus an additional term arises corresponding to second-order paramagnetism. This term is analogous to the term dependent on the orbital moments' high frequency matrix elements in the theory of molecular diamagnetism discussed by Van Vleck.[5] Physically it corresponds in part to the fact that the presence of attracting centers from several different massive nuclei prevents a simple circular diamagnetic circulation of the electrons about any one nucleus. Under certain circumstances the second-order paramagnetism terms can become quite large. General expressions for both of these terms are derived in the present paper together with a simplified method, in the case of linear molecules, for evaluating the second-order paramagnetism term from the experimentally measurable spin-rotational magnetic interaction constant. Although the magnetic field from the electrons in the molecule can in principle be either in the same direction as the externally applied field or in the opposite direction, in most cases it is in the opposite direction. Therefore, the term magnetic shielding will be used in this paper to describe the resultant of the diamagnetic and paramagnetic effects even though negative shielding is a possibility.

II. POLYATOMIC MOLECULES

Consider a polyatomic molecule in a ground state which in the absence of an external field has no resultant electron spin or electron orbital angular momentum. Most nuclear moment measurements made by any of the various nuclear resonance techniques are made with such molecules. Since the nuclei of the molecule are massive compared to the electrons, the nuclei can be treated classically to a very good approximation. In particular, in the first phases of the calculation it will be assumed that the nuclei are approximately stationary attracting centers for the electrons in an orientation specified by the subscript λ. If one wished to avoid this simplification, he could do so by following procedures analogous to those used by Van Vleck[5] in the theory of molecular magnetism. As is discussed in greater detail by Van Vleck[5] and Wick,[7] the effects of electron spin can be omitted in the subsequent discussion; except in cases of accidental degeneracies, the magnetic shielding fields from the electron spin should be of a higher order of smallness than the other contributions calculated here. This omission considerably simplifies the subsequent equations, with no change in most of the significant results. If it were desired, the methods used here could be generalized to include the electron spin explicitly.

If the magnetic shielding constant applicable to a certain nucleus in the molecule is desired, it can be obtained most easily by assuming that all other nuclei have zero magnetic moments and that the nucleus concerned has a magnetic moment of magnitude μ and of the same direction as the externally applied field, H. The energy of the molecular system in the presence of μ and H can then be calculated, and all terms whose dependence on μ and H is linear in the product μH can be collected together and called W_λ'. Let σ_λ be the desired magnetic shielding constant; i.e., if an external magnetic field of unit strength is applied, the magnetic field at the nucleus from the electron motions has a component $-\sigma_\lambda$ parallel to the applied field. If W_λ' were known, then σ_λ could be obtained from the energy relation

$$W_\lambda' = \sigma_\lambda H \mu. \tag{1}$$

Let V be the electrostatic potential energy function for the electrons, $\mathbf{A}$ be the vector potential from the nuclear magnetic moments and from the external magnetic field, $(-e)$ be the charge on the electron, and the remaining notation be that used by Van Vleck.[5] Then the Hamiltonian of the electronic system is

$$\mathcal{H} = \sum_k (1/2m)[(p_{xk}+eA_{xk}/c)^2+(p_{yk}+eA_{yk}/c)^2+(p_{zk}+eA_{zk}/c)^2]+V. \tag{2}$$

With the assumptions of the preceding paragraph and with the origin of the coordinates chosen at the nucleus for which the shielding constant is desired, one has

$$A_x = -\tfrac{1}{2}Hy-\mu y/r^3, \quad A_y=\tfrac{1}{2}Hx+\mu x/r^3, \quad A_z=0. \tag{3}$$

With these values and with the replacement of the p's by the usual differential operators, (2) becomes

$$\mathcal{H}=\mathcal{H}^{(0)}+\mathcal{H}^{(1)}+\mathcal{H}^{(2)},$$

[5] J. H. Van Vleck, *Electric and Magnetic Susceptibilities* (Oxford University Press, London, 1932).
[6] N. F. Ramsey, Phys. Rev. **77**, 567 (1950).
[7] G. C. Wick, Phys. Rev. **73**, 51 (1948).

where

$$\mathcal{H}^{(0)}=-\sum_k(\hbar^2/2m_k)\nabla_k^2+V,\quad \mathcal{H}^{(1)}=-\sum_k(H+2\mu/r_k^3)m_{zk}^0,\quad \mathcal{H}^{(2)}=(e^2/8mc^2)\sum_k(H+2\mu/r_k^3)^2(x_k^2+y_k^2),\quad (4)$$

with

$$m_{zk}^0=-(e\hbar/2mci)(x_k\partial/\partial y_k-y_k\partial/\partial x_k).\quad (5)$$

Therefore, by the usual second-order perturbation theory and with the selection of those terms of the second-order perturbation energy which are linear in the product $H\mu$, one obtains

$$\sigma_\lambda=W_\lambda'/H\mu=(e^2/2mc^2)(0\lambda|\sum_k(x_k^2+y_k^2)/r_k^3|0\lambda)-2\sum_{n\lambda'}{}'[1/(E_n-E_0)][(0\lambda|\sum_k m_{zk}^0|n\lambda')(n\lambda'|\sum_k m_{zk}^0/r_k^3|0\lambda)$$
$$+(0\lambda|\sum_k m_{zk}^0/r_k^3|n\lambda')(n\lambda'|\sum_k m_{zk}^0|0\lambda)].\quad (6)$$

For purposes of later comparison with Wick's[7] theory of rotational magnetic moments, Eq. (6) can be expressed in a somewhat different form. By virtue of the Hermitian character of m_{zk}/r_k^3, one can write

$$(n\lambda'|\sum_k m_{zk}^0/r_k^3|0\lambda)=\tfrac{1}{2}[(n\lambda'|\sum_k m_{zk}^0/r_k^3|0\lambda)+(0\lambda|\sum_k m_{zk}^0/r_k^3|n\lambda')^*]$$
$$=-(e\hbar/4mci)\sum_k\int\left[(x/r^3)\left(\psi_{n\lambda'}{}^*\frac{\partial\psi_{0\lambda}}{\partial y}-\psi_{0\lambda}\frac{\partial\psi_{n\lambda'}{}^*}{\partial y}\right)-(y/r^3)\left(\psi_{n\lambda'}{}^*\frac{\partial\psi_{0\lambda}}{\partial x}-\psi_{0\lambda}\frac{\partial\psi_{n\lambda'}{}^*}{\partial x}\right)\right]_k d\tau$$
$$=[1/(2c)]\int\sum_k(\mathbf{r}_k\times\mathbf{j}_{n\lambda'0\lambda k}/r_k^3)_z d\tau=\tfrac{1}{2}H_{n\lambda'0\lambda},\quad (7)$$

where

$$\mathbf{j}_{n\lambda'0\lambda k}=(ie\hbar/2m)(\psi_{0\lambda}{}^*\nabla_k\psi_{n\lambda'}-\psi_{n\lambda'}\nabla_k\psi_{0\lambda}{}^*).\quad (8)$$

With this and with

$$\sum_k(0\lambda|m_{zk}|n\lambda')=-(e\hbar/2mc)\sum_k(0\lambda|L_{zk}|n\lambda')=-\mu_0L_{0\lambda n\lambda'},$$

one obtains

$$\sigma_\lambda=(e^2/2mc^2)(0\lambda|\sum_k(x_k^2+y_k^2)/r_k^3|0\lambda)+\mu_0\sum_{n\lambda'}{}'[1/(E_n-E_0)][H_{0\lambda n\lambda'}L_{n\lambda'0\lambda}+L_{0\lambda n\lambda'}H_{n\lambda'0\lambda}].\quad (9)$$

In experiments with the resonance absorption and nuclear induction methods, the measurements are made with molecules of all orientations. Consequently (6) and (9) for these experiments must be averaged over all orientations of the molecule. In such an average the x, y, and z coordinates must all be equivalent. Then if Av_λ indicates an average over all orientations, one has

$$\mathrm{Av}_\lambda[\sum_\lambda(0\lambda|x_k^2/r_k^3|0\lambda)]=\tfrac{1}{3}(0|1/r_k|n),$$

so

$$\mathrm{Av}_\lambda\sigma_\lambda=(e^2/3mc^2)(0|\sum_k 1/r_k|0)-2\,\mathrm{Av}_\lambda\sum_{n\lambda'}{}'[1/(E_n-E_0]][(0\lambda|\sum_k m_{zk}^0|n\lambda')(n\lambda'|\sum_k m_{zk}^0/r_k^3|0\lambda)$$
$$+(0\lambda|\sum_k m_{zk}^0/r_k^3|n\lambda')(n\lambda'|\sum m_{zk}^0|0\lambda)],\quad (10)$$

or

$$\sigma=(e^2/3mc^2)(0|\sum_k 1/r_k|0)+\mu_0\mathrm{Av}_\lambda\sum_{m\lambda'}{}'[1/(E_n-E_0)][H_{0\lambda n\lambda'}L_{n\lambda'0\lambda}+L_{0\lambda n\lambda'}H_{n\lambda'0\lambda}].\quad (11)$$

The first term in either (10) or (11) is the same as Lamb's[1] complete expression for the diamagnetic shielding of single atoms. The second term arises from the lack of spherical symmetry of the electrical potential. The magnitude of the second term is quite comparable with that of the first. In fact, it serves to cancel off most of the contribution to the shielding by the electrons that are tightly bound to another nucleus in a distant part of the molecule. For this reason when the difficult sums in (10) or (11) cannot be evaluated an approximation to the shielding is obtained by merely evaluating the first term over just the electrons of the atom containing the nucleus; that is, by using Lamb's correction for the atom containing the nucleus. This procedure, however, would be very unsatisfactory in a molecule like H_2 where the fields of the two protons are of comparable magnitudes at most electron locations. It is also unsatisfactory in accounting for the chemical

effect[2-4] that has recently been observed in comparing the resonance frequencies of the same nucleus in different molecules. Both the first and the second terms of (10) will be altered in different molecules, and they will not necessarily be altered by exactly canceling amounts. This might be particularly true if one of the molecules had a low energy excited state for which the matrix elements in (10) did not vanish, since then $1/(E_n-E_0)$ would be large and a large second-order paramagnetism would be expected.

In (10) there is apparently a separation into two quite distinct terms of which one seems to be a simple diamagnetic term and the other a second-order paramagnetic term. However, it should be noted that these two terms are very closely related and that the separation is largely artificial. In particular, the above choice of the origin of coordinates at the nucleus where the field is desired and the selection of the arbitrary constant in the vector potential of H as in Eq. (3) make the first term in (10) correspond to a simple circular diamagnetic circulation of the electrons about the nucleus of interest. Had a different choice been made, for example, had the choice been such that the first term corresponded to a simple diamagnetic circulation of the electrons about some other point of the molecule, then both the diamagnetic term and the second-order paramagnetism term would have been altered. Of course, no physical difference can result from such a change so the two terms are necessarily altered in exactly compensating fashions. The magnitudes assigned to the physically indistinguishable diamagnetic term and second-order paramagnetic term are, however, altered. This property of (10) is closely analogous to a similar dependence of the diamagnetic and second-order paramagnetic terms of the magnetic susceptibility of a molecule on the choice of coordinate origin, even though the sum of the two terms is shown by Van Vleck[5] to be invariant to the choice of the origin.

The numerical evaluation of the summation in (10) would be extremely difficult for most molecules since the summation depends on the wave functions of the excited states of the molecule. The calculation can be somewhat simplified if one estimates somehow an average value for E_n-E_0 as was done by Van Vleck and Frank[8] in their calculation of the diagmanetism of molecular hydrogen. If ΔE is the average value of E_n-E_0, then (10) becomes

$$\sigma=(e^2/3mc^2)(0|\sum_k 1/r_k|0) -(4/\Delta E)\mathrm{Av}_\lambda[(0\lambda|\sum_{jk} m_{zj}{}^0 m_{zk}{}^0/r_k{}^3|0\lambda)]. \quad (12)$$

If

$$\mathbf{m}_k{}^0=m_{xk}{}^0\mathbf{i}+m_{yk}{}^0\mathbf{j}+m_{zk}{}^0\mathbf{k} \quad (13)$$

then taking Av_λ as in the previous averaging,

$$\sigma=(e^2/3mc^2)(0|\sum_k 1/r_k|0) -(4/3\Delta E)(0|\sum_{jk}\mathbf{m}_j{}^0\cdot\mathbf{m}_k{}^0/r_k{}^3|0). \quad (14)$$

Although this approximate form depends only on the ground state wave function, it is nevertheless very difficult to evaluate reliably since it depends on the second derivative of the wave function and is consequently very sensitive to errors in this derivative. This was clearly shown by Wick[9] who found that by taking two somewhat different wave functions in his calculations on the rotational magnetic moment of H_2 he could obtain results for a term analogous to the last one in (14) which differed from each other by more than a factor eight.

III. LINEAR MOLECULES

Although calculation of the summation in (10) would be extremely difficult for most molecules, in the case of $^1\Sigma$ linear molecules this summation can be directly related to the spin-rotational magnetic interaction constant which has been experimentally measured in certain cases. If F_λ represents the summation in (11), if for λ one writes σ when the molecule has its axis perpendicular to the field and π when the axis is parallel, and if θ is the angle between the nuclear axis and the z axis, one has

$$\mathrm{Av}_\lambda(F_\lambda)=\mathrm{Av}_\lambda(\sin^2\theta_\lambda F_\sigma+\cos^2\theta_\lambda F_\pi) =\tfrac{2}{3}F_\sigma+\tfrac{1}{3}F_\pi=\tfrac{2}{3}F_\sigma. \quad (15)$$

F_π vanishes in the above since a linear molecule is cylindrically symmetric about its axis, as a result of which $\sum_k m_{zk}{}^0$ has only diagonal matrix elements along the axis of symmetry. With (15), Eq. (11) can be written as

$$\sigma=(e^2/3mc^2)(0|\sum_k 1/r_k|0)+\tfrac{2}{3}\mu_0\sum_{n\lambda'}[1/(E_n-E_0)] \times[H_{0\sigma n\lambda'}L_{n\lambda'0\sigma}+L_{0\sigma n\lambda'}H_{n\lambda'0\sigma}]. \quad (16)$$

This result may be compared with Brooks'[9a]-Wick's[7] theories of spin-rotational magnetic interactions. Let H_r be the experimentally observed magnetic field at nucleus r due to the linear molecule rotating with an angular velocity

$$\omega=J\hbar/I, \quad (17)$$

where J is the rotational quantum number and I is the moment of inertia. Let Z_i be the charge on any nucleus of the molecule other than the one at which the shielding constant is desired, and let a_i be its distance from the desired nucleus. Then Wick's result is

$$H_r-\sum_i Z_i e\hbar J/Ia_i c=(J\hbar^2/I)\sum_{n\lambda'}[1/(E_n-E_0)] \times[H_{0\sigma n\lambda'}L_{n\lambda'0\sigma}+L_{0\sigma n\lambda'}H_{n\lambda'0\sigma}]. \quad (18)$$

[8] J. H. Van Vleck and A. Frank, Proc. Nat. Acad. Sci. **15**, 539 (1929).

[9] G. C. Wick, Zeits. f. Physik **85**, 25 (1933).

[9a] Harvey Brooks, Phys. Rev **59**, 925 (1941).

This can then be substituted into (16) and the resulting expression can be simplified by the introduction of a_0 for the Bohr radius, α for the fine structure constant, and μ_N for the nuclear magneton, $e\hbar/2Mc$, where M is the proton mass. The result, after simplification, is

$$\sigma=\frac{e^2}{3mc^2}\left(0\left|\sum_k\frac{1}{r_k}\right|0\right)-\frac{\alpha^2a_0I}{6\mu_N}\left(\sum_i\frac{2Z_i\mu_N}{Ia_i}-\frac{H_r}{JM}\right). \quad (19)$$

Although the above derivation of (19) seems to be dependent on the second order perturbation theories, both through its use of Wick's spin-rotational interaction theory and through the shielding theory of the present paper, this particular result can be obtained directly without the necessity for using either of the other derivations directly. This can most easily be done by following a procedure used in another paper by Wick[9] on rotational magnetic moments. If the molecule were rotating with angular frequency ω and in a magnetic field of just the Larmor value

$$\mathbf{H}=2mc\omega/e, \quad (20)$$

the molecule would rotate as a completely rigid body, since in a coordinate system rotating with ω the electrostatic field would be constant in time, and, by a simple extension of Larmor's theorem, the rotation of the coordinates would exactly cancel $\mathbf{H}$. Since the nuclei are at positions where the electric field is approximately zero, the rotational magnetic field at the position of the nucleus is independent of the nuclear velocity; hence to a high degree of accuracy the molecule can be considered as rotating about the nucleus at which the diamagnetic shielding is desired. Then H_r', the field at the nucleus due to the rotation in the presence of (20), is given by

$$\begin{aligned}H_r'&=-\int[\rho(\omega\times\mathbf{r})\times\mathbf{r}\cdot\omega/cr^3\omega)dv\\&\qquad-\sum_i[Z_ie(\omega\times\mathbf{a}_i)\times\mathbf{a}_i\cdot\omega/ca_i^3\omega]\\&=-(e\omega/c)(0\sigma|\sum_k(x_k^2+y_k^2)/r_k^3|0\sigma)\\&\qquad+\sum_i(Z_ie\omega/ca_i). \quad (21)\end{aligned}$$

The experimental value of H_r can be obtained from (21) by superposing a magnetic field equal and opposite to (20) to cancel it out. Therefore, one has

$$H_r=H_r'+\sigma_a2mc\omega/e. \quad (22)$$

Furthermore, just as in Eq. (15), the average over all molecular orientations gives

$$\sigma=\tfrac{2}{3}\sigma_a+\tfrac{1}{3}\sigma_\pi. \quad (23)$$

The combination of (21)–(23) with Lamb's theory for σ_π then immediately gives the desired (19).

IV. MOLECULAR HYDROGEN

The most important application of (19) is to molecular hydrogen. In this diatomic case (19) becomes

$$\sigma=\frac{e^2}{3mc^2}\left(0\left|\sum_k\frac{1}{r_k}\right|0\right)-\frac{\alpha^2a_0a^2}{6\mu_N}\left(\frac{2Z\mu_N}{a^3}-\frac{\mu'H_r}{MJ}\right) \quad (24)$$

where μ' is the reduced mass of the molecule.

The quantity $H_r\mu'/MJ$ has been experimentally measured in a molecular beam experiment by Kellogg, Rabi, Ramsey, and Zacharias[10] to be

$$H_r\mu'/MJ=(13.66\pm0.20)\text{ gauss}.$$

With this and with the current standard values for the other constants in (24),

$$\begin{aligned}\sigma&=(e^2/3mc^2)(0|\textstyle\sum_k 1/r_k|0)-(0.5291\times0.7414^2/6\\&\qquad\times137^2\times5.05)(24.62-13.66)\\&=(e^2/3mc^2)(0|\textstyle\sum_k 1/r_k|0)-(0.56\pm0.01)\times10^{-5}. \quad (25)\end{aligned}$$

Using Nordsieck's[11] wave functions, Anderson[12] has calculated the value of the first term of (25) to be $3.2_4\times10^{-5}$. On the other hand, Hylleraas and Skavlem[13] from different wave functions obtain 3.16×10^{-5}. If Anderson's value is used, σ becomes

$$\sigma=2.6_8\times10^{-5}. \quad (26)$$

This number can be contrasted to the best previous estimates for σ which were 1.8×10^{-5} and 3.24×10^{-5}. The first of these was obtained by applying Lamb's formula to a single hydrogen atom; Anderson[12] obtained the second by applying Lamb's formula directly to a hydrogen molecule.

The result (26) can be combined with Hylleraas and Skavlem's[13] value of 5.99×10^{-5} for the σ in He and with Anderson's[12] measured resonance frequency ratio in He^3 and H_2 molecules of 0.7617866 to yield a value for the ratio of the *nuclear* gyromagnetic ratios of $\gamma_{He^3}/\gamma_p=0.7617866[1+(5.99-2.68)\times10^{-5}]=0.761812$.

The shielding correction can be calculated from the simplified expression (9) only for linear molecules for which there exist spin-rotational interaction data; e.g., for molecular hydrogen. Since a number of different hydrogenous compounds are used to determine the proton resonance frequency in the various nuclear moment measurements, it is important that some one should compare with high precision the resonance frequencies in these compounds with that in molecular hydrogen. If this is done empirical values for the shielding constant of the protons in the other compounds can be obtained from the above value for H_2.

The author is grateful to Professors J. H. Van Vleck and E. M. Purcell for several stimulating discussions in the course of these calculations.

[10] Kellogg, Rabi, Ramsey, and Zacharias, Phys. Rev. **57**, 691 (1940).
[11] A. Nordsieck, Phys. Rev. **57**, 691 (1940).
[12] H. L. Anderson, Phys. Rev. **76**, 1460 (1949).
[13] E. Hylleraas and S. Skavlem (private communication).

The Low States of Li^7

R. AVERY AND C. H. BLANCHARD
Department of Physics, University of Wisconsin, Madison, Wisconsin*
(Received January 26, 1950)

An attempt is made to obtain consistency between the positive quadrupole moment of Li^7 as well as other known ground state data (spin; magnetic moment; $Be^7 \xrightarrow{K} Li^7$, Li^{7*} lifetime and branching ratio) and the assumption that the wave function belongs to an s^4p^3 configuration of nucleons. This is found to be possible with only one particular form for the spin and angular dependence of the function. This form is very different from that predicted by previous theory; in particular the D and P state probabilities are found to be 80 percent and 20 percent, respectively. It should be emphasized that the validity of the analysis depends on the accuracy of the assumptions that the quadrupole moment is positive and due only to the charge distribution of the nucleons, with no contribution arising from their interaction.

An investigation is also made of the spin of the Li^7 480-kev excited state. Previous arguments for a high spin are reviewed. Using the ground state wave function indicated, and assuming the s^4p^3 configuration also for the excited state, one can by further analysis show that an excited state of spin 5/2 or 3/2 would give fair agreement with experimental data (Be^7 K-capture data; $Li^{7*} \rightarrow Li^7 + \gamma$ lifetime). An excited state of spin 1/2, however, would give poor agreement. On the assumptions made no agreement is possible for spin greater than 5/2.

1. INTRODUCTION

THIS work was prompted by the failure of current nuclear theory to give agreement with the recently reported[1] positive value of the Li^7 electric quadrupole moment. Although it is possible that an error[2] in the interpretation of the quadrupole coupling for the molecules used in the measurement has led to an incorrect value for the quadrupole moment, this investigation proceeds on the assumption that the sign and magnitude of the quadrupole moment of Li^7 are as reported. The most widely used theory[3] of the structure of light nuclei is based on the independent particle model and simple assumptions on nuclear forces. The ground state wave function predicted by this theory for Li^7 gives a negative value for the quadrupole moment.

The first problem treated here concerns the extent to which the measured properties of the Li^7 nucleus determine the form of its wave function. No explicit assumptions on nuclear forces are made; therefore, no attempt is made to solve the dynamical problem of finding a wave function from a potential energy function. It is necessary, of course, to make some simplifying assumptions to aid in the calculations. The same approximation is used here as in reference 3: that of assuming an s^4p^3 configuration, with the four s particles (two neutrons and two protons) forming a closed s shell. This assumption is consistent with current ideas about nuclear shell structure. The aim of the investigation, then, is to establish whether or not the s^4p^3 configuration is capable of describing the Li^7 ground state and, if so, to what extent the wave function is determined by the values of the measured properties.

Because of the symmetry of the closed s shell, the nuclear properties considered here should be determined only by the p-nucleons. Consequently the calculations need involve only these particles. The choice of configuration and the value of the total angular momentum do not fix the spin and angular dependence of the wave function, since the angular momenta of the three p-nucleons can be combined to give eight linearly independent eigenfunctions of $J=3/2$. In the theory of reference 3 this arbitrariness in the spin and angular dependence of the ground state is completely eliminated by the requirement that the orbital part of the wave function be symmetric under permutations of the three p-nucleons (this property to be referred to as space-symmetry). This requirement is a consequence of the assumption that the nuclear forces are spin and charge independent and predominantly of the Majorana (space-exchange) type. Since no assumptions on nuclear forces are to be made here, the requirement of space-symmetry is ignored and thus there remains considerable freedom in the wave function.

The data to be considered are given in Table I. Odd parity is obtained by the choice of an s^4p^3 configuration. The transition probability for K-capture in Be^7 leading to the ground state of Li^7 can be treated as a property of the ground state if it is assumed that the ground state of Be^7 is identical with that of Li^7 except for interchange of neutrons and protons. This assumption has recently received rather convincing confirmation. A single excited state has been observed[4] in Be^7 at about 430 kev, in excellent correspondence with the 480-kev excited state of Li^7.

It is found possible to obtain reasonable agreement with all the data simultaneously, and the solution has the advantage of definitely singling out one spin and angular dependence for the wave function as better than any other. The wave function designated as best does not seem to have a simple interpretation, except

* This work was supported by the AEC.
[1] P. Kusch, Phys. Rev. **76**, 138 (1949).
[2] Townes, Foley, and Low, Phys. Rev. **76**, 1415 (1949).
[3] E. Feenberg and E. Wigner, Phys. Rev. **51**, 95 (1937).
[4] Brown, Chao, Fowler, and Lauritsen, Phys. Rev. **78**, 88 (1950). Johnson, Laubenstein, and Richards, Phys. Rev. **78**, 413 (1950).

that it is very different from the space-symmetric wave function given by the theory of reference 3.

The Li^7 nucleus appears to have only one low lying excited state. There has recently been considerable speculation as to the nature of this 480-kev bound level. Its spin (J^*) was long thought to be 1/2, on the assumption that the ground state and the excited state are the two members of a $^2P_{3/2,1/2}$ doublet. Support for this assignment was given by the fact that it is consistent with the theory of reference 3. The lowest lying state according to that theory is a space-symmetric ^2P, which can have total angular momentum 1/2 or 3/2. Since $J=3/2$ for the ground state, it was entirely reasonable to assume that a space-symmetric $^2P_{1/2}$ level is nearby. Since results obtained here indicate that the ground state should not be treated as a $^2P_{3/2}$ state belonging to an s^4p^3 configuration, there remains little reason to assume that the excited state is to be described as the corresponding $^2P_{1/2}$ state.

Assuming spin 3/2 for the Be^7 ground state, it is possible to assign an upper limit of 5/2 to J^* on the basis of the K-capture lifetime. Thus, only 1/2, 3/2, 5/2 are considered as possible values for J^*. The measured value of 3 for the spin of B^{10} together with the branching ratio of the reaction

$$B^{10}+\text{thermal neutron}\rightarrow\alpha+Li^7,\ Li^{7*}$$

makes the assignment of spin 1/2 to the excited state doubtful. This argument has been re-investigated and the conclusion is reached that the evidence favors, but does not insure, $J^*>3/2$.

There are two experimental data, in addition to that obtained from the $B^{10}(n,\alpha)$ reaction, which can be used to give information on the excited state: the lifetime for $Li^{7*}\rightarrow Li^7+\gamma$, and the lifetime for $Be^7\xrightarrow{K}Li^{7*}$. In each case the data specify a value for a matrix element between the excited state and the appropriate ground state. Using for the ground state wave functions of both Li^7 and Be^7 the form already found, these two data have been used to give further evidence on the value of J^*. If one assumes that the excited state belongs to the same configuration as assumed for the ground state (s^4p^3), the possibility of fitting the γ-ray and K-capture data has been investigated for each of the cases: $J^*=1/2,\ 3/2,\ 5/2$. Full consistency with the data is found to be impossible with any of these spins. The margin of disagreement for $J^*=5/2$ or 3/2, however, is not very large. $J^*=1/2$ seems to be definitely unsatisfactory.

2. THE COMPLETE SET OF FUNCTIONS FOR THE GROUND STATE

Since the closed s shell is neglected completely, a set of wave functions corresponding to a p^3 configuration is required. This set of functions is to be complete in spin and angular dependence under the restriction that two of the three particles are identical and $J=3/2$. The angular momenta of two p-nucleons can combine to form ^1S, ^3P, ^1D states. These, in turn, can combine with the p-proton to give the following eight states:

TABLE I. Data for the Li^7 ground state.

Total angular momentum (J)	3/2[a]
Magnetic moment (μ)	+3.25 n.m.[a]
Parity	Odd[b]
Quadrupole moment (Q)	+1/50 barn[c]
Half-life for $Be^7\xrightarrow{K}Li^7$ (ground states)	5.1×10^6 sec.[d]

[a] J. Mattauch and S. Fluegge, *Nuclear Physics Tables* (Interscience Publishers, Inc., New York, 1946).
[b] D. R. Inglis, Phys. Rev. **74**, 21 (1948).
[c] See reference 1.
[d] E. Segrè and C. Wiegand, Phys. Rev. **75**, 43 (1949); R. M. Williamson and H. T. Richards, Phys. Rev. **76**, 614 (1949).

$$\begin{array}{ll}(^1S,\ ^2p)^2P & (^1D,\ ^2p)^2D\\ (^1D,\ ^2p)^2P & (^3P,\ ^2p)^2D\\ (^3P,\ ^2p)^2P & (^3P,\ ^2p)^4D\\ (^3P,\ ^2p)^4P & (^3P,\ ^2p)^4S.\end{array}\qquad(1)$$

The notation is "(neutron state, proton state) combined state." $(^3P,\ ^2p)^2S$ and $(^1D,\ ^2p)^2F$ are not acceptable because they cannot give $J=3/2$. The eight functions give the required complete set.

Since no information concerning the radial behavior of the nuclear wave function is available, the following simplifying assumptions are made. The radial dependence is taken to be the same for each nucleon, and to be independent of the spin and angular dependence of the wave function. The wave function of Li^7 is thus to be approximated by a product of a factor of the form $f(r_1)f(r_2)f(r_3)$ with some linear combination of spin-angular functions.

The set of functions shown above is classified by definite neutron and proton states. Sets of functions, complete in the same sense as this set and classified differently, might be used just as well. It has been shown[5] that the symmetry under permutations of particles of a nuclear wave function may be significantly related to the nature of nuclear forces. Therefore, the following complete set,[6] in which the symmetry properties are explicitly given, is introduced:

$$\begin{array}{ll}\psi_1=^{22}P[3] & \psi_5=^{22}D[2+1]\\ \psi_2=^{22}P[2+1] & \psi_6=^{24}D[2+1]\\ \psi_3=^{24}P[2+1] & \psi_7=^{42}D[2+1]\\ \psi_4=^{42}P[2+1] & \psi_8=^{44}S[1+1+1].\end{array}\qquad(2)$$

The notation is $^{(2S+1)(2T+1)}L[\lambda_3+\lambda_2+\lambda_1]$ where $L=$ total orbital angular momentum, $S=$total spin angular momentum, $T=$total isotopic spin. The bracket symbol specifies the partition (in the standard terminology for the representations of the symmetric group[5]) to which the function belongs, and characterizes the symmetry properties of the wave function. The orbital part of ψ_1 is completely symmetric under permutations of the three p-particles and that of

[5] E. Wigner, Phys. Rev. **51**, 106 (1937).
[6] L. Rosenfeld, *Nuclear Forces* (Interscience Publishers, Inc., New York, 1949), p. 204.

ψ_8 is completely antisymmetric. ψ_1 is the wave function predicted for the Li^7 ground state by the theory of reference 3. Each of the ψ_k is understood to contain the radial dependence $f(r_1)f(r_2)f(r_3)$ where $f(r)$ is normalized. The calculations and results below are given in terms of the functions of the set (2). The relationships of these functions with those of set (1) are given in Appendix I.

3. CONDITIONS IMPOSED BY EXPERIMENTAL DATA

The wave function for the ground state of Li^7 is taken to be

$$\Psi_G=\sum_{j=1}^{8} a_j\psi_j,$$

where the a_j satisfy the normalization condition $\sum|a_j|^2=1$.

The Quadrupole Moment

The calculated value of the quadrupole moment is given by

$$Q=\sum_{j,k} a_j^* a_k Q_{jk} \tag{3}$$

where

$$Q_{jk}=(\psi_j, r_p^2(3\cos^2\theta-1)\psi_k).$$

The ψ_k are used with $M_J=J$, r_p is the distance of the proton from the center of mass of the nucleus, and θ is the angle between r_p and the z (total angular momentum) axis. The calculated values of the Q_{jk} are given in Appendix II. A basic assumption made here is that the quadrupole moment can be calculated from the charge distribution of the protons alone, with no contribution to the charge distribution resulting from the charge-exchange interaction of the various nucleons.

Difficulty arises on two counts in the comparison of the calculated value of the quadrupole moment with the measured value given in Table I. The measurement is by no means a precise one. There is also considerable uncertainty in assigning a value to the quantity $\langle r_p^2\rangle$ (the average of the square of r_p), in terms of which the calculated value is given. The value of $\langle r_p^2\rangle$ is taken to be $(e^2/mc^2)^2$, which is approximately the square of the nuclear radius as given by the formula $R=1.5A^{\frac{1}{3}}10^{-13}$ cm. The value for the quadrupole moment given by ψ_1 is of the right order of magnitude but of the wrong sign. Its cross-terms with the other ψ_k are sufficiently small that no wave function which is predominantly ψ_1 can give agreement with the sign of the measured quadrupole moment.

The Magnetic Moment

The measured value of the magnetic moment given in Table I is to be compared with the calculated value

$$\mu=\sum_{j,k} a_j^* a_k \mu_{jk},$$

where

$$\mu_{jk}=(\psi_j, m_{l\ \text{proton}}+\sum_{i=1}^{3}\mu_i\sigma_{zi}\psi_k)$$

ψ_i with $M_J=J$ are used; μ is given in nuclear magnetons when

$\mu_i=\mu_P=+2.79$ if ith particle is proton,
$\mu_i=\mu_N=-1.91$ if ith particle is neutron.

The calculated values of the μ_{jk} are given in Appendix II. The matrix elements can be evaluated exactly but the possible existence of exchange moments[7] may make the result of the calculation inaccurate.

The Be^7 K-Capture Lifetime

It is assumed that nuclear forces are charge-independent to the extent that the wave function for Be^7 may be obtained from the Li^7 wave function by merely interchanging neutrons and protons. On this assumption, the experimental data on the Be^7 K-capture can be used to give an additional condition on the Li^7 wave function. The lifetime of Be^7 against the reaction

$$Be^7+e_K \rightarrow \begin{cases} Li^{7*} & 10.7 \text{ percent} \\ Li^7 & 89.3 \text{ percent} \end{cases} \tag{4}$$

together with the branching ratio, enables one to obtain the partial lifetime of the reaction going to the ground state; this alone is of interest in the determination of the ground state function. The type of β-decay interaction assumed

$$\mathbf{I}=\sum_{i=1}^{3}\tau_{\xi i}\sigma_i, \tag{5}$$

($\tau_{\xi i}$ reverses the charge state of the ith nucleon) is, in the present treatment, consistent with either the axial vector or the tensor formulations of the theory of β-decay, and corresponds to the Gamow-Teller selection rules ($\Delta J=0, \pm1$; $0\rightarrow0$ forbidden; no parity change). The strength of the interaction is taken to be characterized by the value[8]

$$|\mathbf{I}|^2 ft_{\text{mean}}=4400, \tag{6}$$

where $|\mathbf{I}|^2$ is the absolute square of the matrix element of $\mathbf{I}$ between the two ground states. The value (6) was obtained from the $H^3\rightarrow He^3$ decay and is presumably the same for all allowed β-decay processes. The value of f is given by the K-capture relation

$$f=2\pi(\alpha Z_{\text{eff}})^3 W^2,$$

where $Z_{\text{eff}}=3.7$ for Be^7, $W=1.66=$ total energy available in units of mc^2 and $\alpha=e^2/(\hbar c)=1/137$. The experi-

[7] R. Avery and R. G. Sachs, Phys. Rev. 74, 1320 (1948).
[8] E. Wigner (private communication).

mental lifetime and (6) yield the requirement $|\mathbf{I}|^2=1.76$. The calculated value is given by

$$|\mathbf{I}|^2=(\sum_{j,k} a_j^* a_k I_{jk})^2.$$

The I_{jk} are to be found in Appendix II. Even though these matrix elements are evaluated exactly, there is considerable uncertainty in the strength of the β-interaction and even in the type of interaction to be used.

4. THE GROUND STATE WAVE FUNCTION

An investigation of the conditions on the a_j imposed by the experimental data shows that one set of values for the a_j gives reasonable agreement with all the data. No qualitatively different set gives anything like agreement. With the number of conditions to be satisfied (four: one normalization and three experimental data, Q, μ-, and β-decay) and the number of free parameters available (sixteen: the real and imaginary parts of each of the a_j) one might have expected that an excellent fit could be found with many qualitatively different choices of the a_j. Had this occurred, no unique wave function would have been determined; it would, nevertheless, have indicated consistency between the experimental data and the assumption of an s^4p^3 configuration. On the other hand, had it occurred that no fit to all the data could be found, even approximately, one might have concluded that an s^4p^3 configuration is inadequate for the description of the Li^7 nucleus.

The wave function which gives best agreement with the data is only qualitatively unique. That is, small changes of the values of the a_j in a range of general agreement with the data have only the effect of improving the agreement with one of the data at the expense of the others. The general nature of the wave function is determined, however, since the permissible variations in the a_j correspond to changes of only a few percent in the probabilities of the states involved. This spread in the values of the coefficients may be characterized by the following two wave functions:

$$\Psi_G=\tfrac{1}{4}[\psi_1-\psi_2+\psi_4+\sqrt{8}\psi_5-\sqrt{5}\psi_7] \qquad (7)$$

which gives

$$Q=0.14\langle r^2\rangle, \quad \mu=2.91 \text{ n.m.}, \quad |\mathbf{I}|^2=1.76$$

and

$$\Psi_G'=(24)^{-\frac{1}{2}}[\psi_1-\sqrt{2}\psi_2+\sqrt{2}\psi_4+\sqrt{9}\psi_5-\sqrt{9}\psi_7+\psi_8] \qquad (8)$$

which gives

$$Q=0.22\langle r^2\rangle, \quad \mu=2.70 \text{ n.m.}, \quad |\mathbf{I}|^2=1.76.$$

These are to be compared with the following values which are presumed to represent the experimental results:

$$Q=0.25\langle r^2\rangle, \quad \mu=3.25 \text{ n.m.}, \quad |\mathbf{I}|^2=1.76.$$

The differences in the values of the a_j in the two wave functions are for the most part of no interest, since significance is to be attached only to the general nature of the function and not to the *exact* values of the coefficients. However, a possible slight admixture of ψ_8 in the wave function is of interest since that function has total isotopic spin $T=3/2$ while all the other functions in both Ψ_G and Ψ_G' have $T=1/2$. (ψ_3, Ψ_6, and ψ_8 have $T=3/2$, the rest have $T=1/2$). Hence a wave function of the form (7) is consistent with the idea that T is a good quantum number, while a wave function of the form (8) is not. It is difficult to decide which of (7) and (8) gives the better agreement with experiment. The introduction of a slight admixture of ψ_8 gives a value for Q appreciably closer to the measured value, while $a_8=0$ gives the better value for μ. The measurement of Q is a very unprecise one; on the other hand, there is no good reason to expect that exchange moments are negligible in this nucleus. Thus this difficulty cannot be resolved with any certainty. It can be said, however, that the experimental data are *not inconsistent* with a wave function for which $T=1/2$, and thus suggest that T may be a good quantum number.

Since the differences between (7) and (8) are of little consequence (aside from the question of T), the simpler wave function (7) is arbitrarily selected for use in the calculations given hereafter.

An interesting result of the calculation is that the assumption of the equivalence of the Be^7 and Li^7 ground state wave functions is not essential for the determination of the form of the wave function. This form is determined uniquely by the magnetic and quadrupole moments alone.

The ground state function is very different from that given by the theory of reference 3, which is $\Psi_G=\psi_1$. The wave function (7) contains 80 percent D state and 20 percent P state, with about equal amounts of doublet and quartet spin states. The failure of L and S to be good quantum numbers may be interpreted as indicating that spin-orbit coupling cannot be neglected in any useful approximation.

It should be emphasized that the experimental fact that $Q>0$ is responsible for the inadequacy of ψ_1, in the sense that ψ_1, while giving $Q<0$, nevertheless yields entirely reasonable results for the other two data. Thus any strong deviation from simple "additivity" of individual proton charge distributions to give the nuclear quadrupole moment, such as might arise from the interaction of the nucleons, would make the value of Q calculated from (3) incorrect and thus would invalidate the results of this analysis.

Although the wave function designated as the best approximation for the Li^7 ground state is a complicated linear combination of the functions of the set (2), it might be simpler if expanded in some other, more appropriate, basis. That is, there may be good quantum numbers which have been obscured by the present choice of basic functions. The wave function is not simplified when expanded in the functions of set (1).

TABLE II. Barrier penetrabilities for $B^{10}(n,\alpha)Li^7$, Li^{7*}.

L	$E=2.3$ Mev	$E=2.8$ Mev
0	0.77	0.99
1	0.26	0.41
2	0.030	0.070
3	0.0019	0.0051

TABLE III. The ratios W^*/W necessitated by the branching ratio of (10) for the vatious possible values of compound nucleus spin and J^*.

Compound nucleus spin	J^*	L	L^*	W^*/W
5/2	1/2	1	3	2900
5/2	3/2	1	1	21
5/2	5/2	1	1	21
5/2	7/2	1	1	21
7/2	1/2	3	3	36
7/2	3/2	3	3	36
7/2	5/2	3	1	0.26
7/2	7/2	3	1	0.26

Recently published correlations[9] of the "magic numbers" of nuclear shell structure with the degeneracies given by a (jj)-coupling scheme suggest that the wave function might be simple as an expansion in characteristic functions of the individual nucleon total angular momenta (j). Each of the three p-nucleons can have $j=3/2$ or $1/2$. The set of functions, each with total angular momentum 3/2,

$$\begin{aligned}
\phi_1&=[(3/2,3/2)0,3/2] \quad & \phi_5&=[(3/2,1/2)1,1/2]\\
\phi_2&=[(3/2,3/2)2,3/2] \quad & \phi_6&=[(3/2,1/2)1,3/2]\\
\phi_3&=[(3/2,3/2)2,1/2] \quad & \phi_7&=[(3/2,1/2)2,1/2]\\
\phi_4&=[(1/2,1/2)0,3/2] \quad & \phi_8&=[(3/2,1/2)2,3/2],
\end{aligned} \tag{9}$$

using the notation

"[(individual neutron j's) total neutron j, proton j],"

is complete in the same sense as are the sets (1) and (2). These functions are given in terms of the functions of the set (2) in Appendix I. Expressed in terms of these functions, Ψ_G and Ψ_G' are,

$$\Psi_G=0.28\phi_1+0.13\phi_2+0.25\phi_3-0.27\phi_4-0.32\phi_5+0.55\phi_6+0.60\phi_8 \tag{7'}$$

$$\Psi_G'=0.18\phi_1+0.18\phi_2+0.17\phi_3-0.22\phi_4-0.45\phi_5+0.64\phi_6+0.44\phi_8. \tag{8'}$$

These differ greatly from the wave function, ϕ_1, predicted for the ground state by the spin-orbit coupling model recently suggested by Mayer.

By the assumption used above of the equivalence of the Be^7 and Li^7 ground states, the wave function (7) implies the following properties for Be^7:

$$Q(Be^7)\approx Q(Li^7)$$

$$\mu(Be^7)=-1.69 \text{ n.m.}$$

The approximate equality implied for the quadrupole moments is a detailed result and of no apparent general significance. The value given for the magnetic moment of Be^7 is found from the *measured* moment of Li^7 and the theorem[10] which relates the sum of the moments of two conjugate nuclei to the coefficients in the expansion of their mutual wave function in eigenfunctions of L and S. The coefficients for the ground state function (7) are used. If the reasonable assumption that exchange moments are equal and opposite for conjugate nuclei is valid, then the correctness of this prediction depends only on the correctness of the distribution of angular momentum between spin and orbital motion given by the wave function, regardless of exchange moment contributions.

5. THE EXCITED STATE

Recent experimental evidence suggests that the total angular momentum (J^*) of the excited state is greater than that of the ground state. This conclusion[11] is based on the determination[12] of the spin of B^{10} to be 3. Thus the compound nucleus in the reaction

$$\begin{aligned}
&\nearrow \quad Li^{7*}+\alpha+2.3 \text{ Mev (93 percent)}\\
B^{10}+\text{thermal neutron} &\\
&\searrow \quad Li^7+\alpha+2.8 \text{ Mev (7 percent)}
\end{aligned} \tag{10}$$

has spin 5/2 or 7/2. The branching ratio of the reaction is interpreted in terms of a smaller centrifugal barrier to be penetrated by the α-particle associated with Li^{7*} than by the one associated with Li^7. The corresponding smaller orbital angular momentum of the $Li^{7*}+\alpha$-system would suggest a Li^{7*} spin greater than that of Li^7.

This argument cannot be considered conclusive for the following reason.[13] The transition probability from the compound nucleus to each of the Li^7 states can be approximated as the product of a factor W, the "width without penetration," depending on the detailed nature of the nuclear wave functions involved, and a factor P, giving the penetrability of the α-particle through the barrier. The penetrabilities involved, estimated in the usual manner,[14] are listed in Table II. Very little, however, can be said about the factor W. One cannot exclude the possibility that it is very different for the two decay schemes. If it is assumed that the parity of B^{10} is even (corresponding to an s^4p^6 configuration) then the conservation of parity demands that the outgoing orbital angular momenta be limited to odd L. In Table III are listed the ratios W^*/W necessitated by the branching ratio of (10) for the various possible values of the spin of the compound nucleus and of J^*.

[9] M. G. Mayer, Phys. Rev. **75**, 1969 (1949).

[10] R. G. Sachs, Phys. Rev. **69**, 611 (1946).

[11] D. R. Inglis, Phys. Rev. **74**, 1876 (1948).

[12] Gordy, Ring, and Burg, Phys. Rev. **74**, 1191 (1948).

[13] This reinvestigation was undertaken as a result of a suggestion by Professor Fermi.

[14] H. A. Bethe, Rev. Mod. Phys. **9**, 177 (1937).

TABLE IV. Relative values of the transformation coefficients between the functions ψ and ϕ. The normalization factor is $1/(216)^{\frac{1}{2}}$.

	ϕ_1	ϕ_2	ϕ_3	ϕ_4	ϕ_5	ϕ_6	ϕ_7	ϕ_8
ψ_1	$+\sqrt{80}$	$+\sqrt{16}$	$-\sqrt{16}$	$+\sqrt{40}$	0	0	$-\sqrt{32}$	$+\sqrt{32}$
ψ_2	$+\sqrt{50}$	$+\sqrt{10}$	$+\sqrt{40}$	$+\sqrt{4}$	$+\sqrt{27}$	0	$+\sqrt{5}$	$-\sqrt{80}$
ψ_3	$+\sqrt{18}$	$-\sqrt{90}$	0	$+\sqrt{36}$	$-\sqrt{27}$	0	$+\sqrt{45}$	0
ψ_4	$-\sqrt{20}$	$-\sqrt{4}$	$+\sqrt{64}$	$+\sqrt{40}$	0	$+\sqrt{54}$	$-\sqrt{32}$	$+\sqrt{2}$
ψ_5	$+\sqrt{10}$	$+\sqrt{2}$	$+\sqrt{8}$	$-\sqrt{20}$	$+\sqrt{15}$	$+\sqrt{48}$	$+\sqrt{49}$	$+\sqrt{64}$
ψ_6	$-\sqrt{10}$	$+\sqrt{50}$	$+\sqrt{32}$	$+\sqrt{20}$	$-\sqrt{15}$	$-\sqrt{48}$	$+\sqrt{25}$	$+\sqrt{16}$
ψ_7	$-\sqrt{20}$	$-\sqrt{4}$	$-\sqrt{16}$	$+\sqrt{40}$	$+\sqrt{120}$	$-\sqrt{6}$	$+\sqrt{8}$	$+\sqrt{2}$
ψ_8	$-\sqrt{8}$	$+\sqrt{40}$	$-\sqrt{40}$	$+\sqrt{16}$	$-\sqrt{12}$	$+\sqrt{60}$	$+\sqrt{20}$	$-\sqrt{20}$

Only the smallest possible odd values for L and L^* are considered. $J^*=1/2$ cannot be excluded since a value W^*/W as high as 2900 might be expected if the wave function of the compound nucleus is approximately the product of a Li^{7*} wave function and a function describing an α-particle moving about the Li^{7*} core. Since it seems more likely on statistical grounds that the wave function of the compound nucleus does not favor such special states of aggregation, one is inclined to believe that W^*/W is of the order of unity. Then values $J^*>3/2$ are favored. If the parity of B^{10} is odd, the outgoing angular momenta are limited to even L, but the argument and the conclusion are essentially unchanged.

The interpretation of the $B^{10}(n, \alpha)$ reaction shows no preference between $J^*=5/2$ and $J^*=7/2$. The reaction (4), however, indicates that, of the two, the choice $5/2$ is far the more likely.[15] The lifetime of the reaction and the branching ratio imply that both transitions are allowed. No conventional formulation of β-decay theory permits $|\Delta J|>1$ for an allowed transition. This fact, together with the assumption that the spin of Be^7 is $3/2$, argues against $J^*=7/2$ and indicates that the only possible values of J^* are $1/2$, $3/2$, and $5/2$.

The partial lifetime[16] for Be^7 K-capture leading to Li^{7*} and the mean life[17] of Li^{7*} against γ-decay to the ground state have been used to obtain further information concerning J^*. It is assumed that the excited state can be treated as belonging to a definite configuration. To obtain agreement with the experimental data the s^4p^3 configuration (same as ground state) must be assigned to the excited state, because the β-interaction, Eq. (5), has no non-vanishing matrix elements between states belonging to different configurations.

The experimentally determined partial lifetime for K-capture fixes the matrix element of the operator (5) between the Be^7 and Li^{7*} wave function according to

$$|\mathbf{I}^*|^2=|(\mathrm{Li}^{7*}|\mathbf{I}|\mathrm{Be}^7)|^2=1.10. \tag{11}$$

Similarly the γ-ray lifetime fixes a value for the matrix element between Li^7 and Li^{7*} of some electromagnetic multipole moment of the nucleus. Since the parities of Li^7 and Li^{7*} are both taken to be odd, the γ-ray transition is due either to a magnetic dipole or to an electric quadrupole interaction. The energy available and the dimensions of the nucleus involved show[15] that the magnetic dipole transition will predominate unless accidental cancellation in nuclear matrix elements occurs. The shortness of the experimental lifetime precludes the possibility of cancellation, however, and it is therefore concluded that the γ-ray transition provides a measure of the matrix element of the magnetic dipole moment, $\mathbf{M}$. The experimental data imply

$$20\leqslant|(\mathrm{Li}^7|\mathbf{M}|\mathrm{Li}^{7*})|^2\leqslant 40. \tag{12}$$

Information concerning J^* may now be obtained by investigation of the possibility of finding agreement with both (11) and (12) for each of the J^* values $5/2$, $3/2$, and $1/2$.

For $J^*=5/2$ the set of functions, complete in angular and spin dependence, is

$$\begin{aligned}&\psi_9={}^{22}D[2+1] \quad \psi_{12}={}^{42}P[2+1]\\ &\psi_{10}={}^{24}D[2+1] \quad \psi_{13}={}^{22}F[3].\\ &\psi_{11}={}^{42}D[2+1]\end{aligned} \tag{13}$$

To each of these functions is assigned the same radial dependence as that in the ground state. For the ground state of both Be^7 and Li^7, the wave function given by Eq. (7) is used. By appropriately choosing the coefficients in a linear combination of the functions (13) to describe the excited state,

$$\Psi=\sum_{j=9}^{13}a_j\psi_j,$$

it is found possible to obtain a value of the matrix element (11) in agreement with experiment. No linear combination can be found, however, which gives a sufficiently large value for the matrix element (12). The largest value obtainable is $|\mathbf{M}|^2\approx 10$ and this can be obtained simultaneously with $|\mathbf{I}^*|^2=1.10$ in agreement with (11). The linear combination giving this best agreement consists predominantly of

$$\psi_{11}={}^{42}D[2+1].$$

For the case $J^*=3/2$, the complete set (2) is satisfactory, subject to the restriction that the excited state wave function be orthogonal to that of the ground state [given by Eq. (7)]. The best agreement possible is a value for the γ-lifetime $|\mathbf{M}|^2\approx 14$ and a value for the K-capture partial lifetime $|\mathbf{I}^*|^2\approx 0.60$. The wave function for the excited state which gives the best agreement for $J^*=3/2$ is predominantly $\psi_6={}^{24}D[2+1]$.

[15] S. S. Hanna and D. R. Inglis, Phys. Rev. **75**, 1767 (1949).
[16] See references in Table I.
[17] L. G. Elliott and R. E. Bell, Phys. Rev. **76**, 168 (1949).

For $J^*=1/2$, the complete set of functions is

$$\begin{array}{ll} {}^{22}P[3] & {}^{42}P[2+1] \\ {}^{22}P[2+1] & {}^{42}D[2+1] \\ {}^{24}P[2+1] & {}^{22}S[1+1+1]. \end{array}$$

In this case no good agreement is possible. The best results are obtained with a function predominantly of type ${}^{24}P[2+1]$, which gives $|\mathbf{I}^*|^2\approx 0.16$ (low by a factor of 7) and $|\mathbf{M}|^2\approx 10$. Thus, in the attempt to obtain information concerning J^* from the γ-ray and K-capture lifetimes, all that can be concluded is that $J^*=1/2$ seems to be inconsistent with the K-capture lifetime. It should be emphasized that this conclusion is contingent upon the use of a ground state wave function of the form (7).

This problem was suggested to us by Professor R. G. Sachs, who has contributed valuable advice during the course of the work.

APPENDIX I. THE SET OF GROUND STATE FUNCTIONS

The functions of the set (2) are given here in terms of the functions of the set (1), which can easily be constructed by the standard rules of combining angular momenta.

$$\begin{aligned}
\psi_1&=5^{\frac{1}{2}}/3({}^1S^2p)^2P+2/3({}^1D^2p)^2P \\
\psi_2&=2^{\frac{1}{2}}/3({}^1S^2p)^2P-10^{\frac{1}{2}}/6({}^1D^2p)^2P+1/2^{\frac{1}{2}}({}^3P^2p)^2P \\
\psi_3&=2^{\frac{1}{2}}/3({}^1S^2p)^2P-10^{\frac{1}{2}}/6({}^1D^2p)^2P-1/2^{\frac{1}{2}}({}^3P^2p)^2P \\
\psi_4&=({}^3P^2p)^4P \\
\psi_5&=1/2^{\frac{1}{2}}({}^1D^2p)^2D+1/2^{\frac{1}{2}}({}^3P^2p)^2D \\
\psi_6&=1/2^{\frac{1}{2}}({}^1D^2p)^2D-1/2^{\frac{1}{2}}({}^3P^2p)^2D \\
\psi_7&=({}^3P^2p)^4D \\
\psi_8&=({}^3P^2p)^4S.
\end{aligned}$$

The choice of phases made for the functions of the set (1) is that obtained by a self-consistent use of the tables of Condon and Shortley[18] for the combination of angular momenta. To introduce the isotopic spin formalism, it is only necessary to multiply each ψ by the isotopic spin wave function, $\tau^+(1)\tau^+(2)\tau^-(3)$, representing a state where particles 1 and 2 are neutrons and 3 is a proton, and then to antisymmetrize the entire wave function with respect to permutations of particles.

The relations between the function of the set (2) and the function of the set (9) are given in Table IV.

APPENDIX II. THE GROUND STATE MATRIX ELEMENTS, WITH RESPECT TO THE FUNCTIONS OF SET (2).

TABLE V. Q_{jk} in units of $(1/25)\langle r^2\rangle$.

	1	2	3	4	5	6	7	8
1	-6							
2	$-\sqrt{10}$	0						
3	$-\sqrt{10}$	-5	0					
4	0	0	0	-4				
5	$+\sqrt{2}$	$-2\sqrt{5}$	$+\sqrt{5}$	0	0			
6	$+\sqrt{2}$	$+\sqrt{5}$	$-2\sqrt{5}$	0	7	0		
7	0	0	0	-6	0	0	0	
8	0	0	0	0	0	0	$-2\sqrt{10}$	0

TABLE VI. μ_{jk} in nuclear magnetons $(e\hbar/2M_{\text{proton}}c)$.

	1	2	3	4	5	6	7	8
1	+3.13							
2	+0.53	+0.01						
3	+0.53	+2.98	+0.01					
4	0	−1.98	+1.98	−0.56				
5	+0.14	0	−0.22	0	+0.81			
6	+0.14	−0.22	0	0	−2.19	+0.81		
7	0	0	0	+0.40	−2.66	+2.66	+0.39	
8	0	0	0	+0.63	0	0	0	−1.03

TABLE VII. I_{jk}.

	1	2	3	4	5	6	7	8
1	$+(5/3)^{\frac{1}{2}}$							
2	0	$-(5/27)^{\frac{1}{2}}$						
3	0	$-(20/27)^{\frac{1}{2}}$	$+(20/27)^{\frac{1}{2}}$					
4	0	$-(32/27)^{\frac{1}{2}}$	$-(8/27)^{\frac{1}{2}}$	$-(121/135)^{\frac{1}{2}}$				
5	0	0	0	0	$+(1/15)^{\frac{1}{2}}$			
6	0	0	0	0	$+(4/15)^{\frac{1}{2}}$	$-(4/15)^{\frac{1}{2}}$		
7	0	0	0	0	$-(32/15)^{\frac{1}{2}}$	$-(8/15)^{\frac{1}{2}}$	$-(1/15)^{\frac{1}{2}}$	
8	0	0	0	0	0	0	0	$+(20/3)^{\frac{1}{2}}$

[18] E. U. Condon and G. H. Shortley, *The Theory of Atomic Spectra* (The Macmillan Company, New York, 1935).

The Electric Quadrupole Moment of the Deuteron*

G. F. NEWELL
University of Illinois, Urbana, Illinois
(Received March 2, 1950)

A new electronic wave for the hydrogen molecule is calculated by use of the variation principle. From this the electric field gradient at one of the nuclei is determined and is used in conjunction with the quadrupole interaction energy as given by Kellogg, Rabi, Ramsey, and Zacharias, to find the value of the quadrupole moment of the deuteron. The value obtained is $Q_D=(2.766\pm0.025)\times10^{-27}$ cm². The probable error of 0.9 percent is an improvement over the previous error of 2 percent given for Nordsieck's calculation of $Q_D=2.73\times10^{-27}$ cm² and for Ishiguro's value of $Q_D=2.79\times10^{-27}$ cm².

1. INTRODUCTION

AN electric quadrupole interaction in the molecules HD and D_2 was detected by Kellogg, Rabi, Ramsey, and Zacharias[1] and they were able to measure the energy

$$H'''=-5e^2qQ_D/4\mu_D, \tag{1}$$

where Q_D is the quadrupole moment of the deuteron in cm², μ_D the magnetic moment of the deuteron, and q is a quantity closely related to the electric field gradient at the nucleus due to the charge distribution of the molecule. Since no means have been devised for measuring q directly, it is necessary to calculate it from some appropriate charge density of the molecule using the relations given by Nordsieck.[2]

$$\left.\begin{aligned} q&=-2Jq'/(2J+3),\\ q'&=\left[\frac{1}{R^3}-\frac{1}{2}\int d\tau\rho(R,r,\theta')\frac{3\cos^2\theta'-1}{r^3}\right]_{Nu}\equiv q'(R)_{Nu}.\end{aligned}\right\} \tag{2}$$

R is the internuclear distance, $\rho(R, r, \theta')$ the electron charge density, r the radius vector from the nucleus considered to the charge, θ' the angle r makes with the internuclear line, and J the rotational angular momentum of the molecule. The average is to be taken over the lowest vibration state of the molecule corresponding to the angular momentum J.

The integral over all space is not absolutely convergent and must be evaluated outside a small sphere about $r=0$ after which the limit of the integral is taken as the radius of the sphere shrinks to zero. It is necessary to know ρ quite accurately since the value of the integral is quite sensitive to small changes in ρ.

The most accurate electronic wave function for the ground state of the hydrogen molecule is that given by James and Coolidge.[3] This wave function, however, is in the form of a 13 term power series expansion containing the distance between the two electrons as one of the expansion variables. The labor required to integrate this makes it quite inconvenient, whereas other wave functions available are not sufficiently accurate for this calculation.

It was believed that some wave function of a convenient form could be calculated which, though not as accurate as the James-Coolidge function, would give a charge density sufficiently accurate for the purpose stated above. Two previous attempts have been made along this line,[2,4] but both calculations were estimated to give an error in q of as much as ±2 percent as compared with the experimental error of 0.6 percent in the value of H'''.

2. A NEW ELECTRON WAVE FUNCTION

The wave function for the ground state of the hydrogen molecule can be found by minimizing the integral

$$E=\int d\tau_1 d\tau_2 \psi^* H\psi \tag{3}$$

over the space $d\tau_1 d\tau_2$ of the two electrons. E is the energy of the state, H the (non-relativistic) Hamiltonian, and ψ, ψ^* some normalized wave function and is complex conjugate, respectively.

A trial wave function is assumed of the form

$$\begin{aligned}\psi=(A^3/R^3N)\exp[-\tfrac{1}{2}A(\xi_1+\xi_2)][\cosh\tfrac{1}{2}B(\eta_1-\eta_2)\\ +a\exp[-\tfrac{1}{2}C(\xi_1+\xi_2)]r_1r_2\cos(\varphi_1-\varphi_2)\\ +b\eta_1\eta_2+c(\xi_1-4/A)(\xi_2-4/A)],\end{aligned} \tag{4}$$

ξ_1, ξ_2, η_1, η_2 are the elliptic coordinates of the electrons 1 and 2 with the two nuclei as foci. $(\varphi_1-\varphi_2)$ is the projection of the angle between the two electrons on a plane perpendicular to the internuclear line, N a normalization factor, and $r_1=(\xi_1^2-1)^{\frac{1}{2}}(1-\eta_1^2)^{\frac{1}{2}}$. The parameters A, B, C, a, b, c are chosen to minimize the energy E (Table I).

The reason for choosing this form is as follows. The first term alone is the trial function used by Inui[5] and Nordsieck.[2] It proved to be quite accurate considering its simplicity and it was believed that it could be easily

* This work was begun under the ONR program and finished with the aid of a predoctoral fellowship by the AEC. A preliminary account of this work has been published: Phys. Rev. 77, 141 (1950).
[1] Kellogg, Rabi, Ramsey, and Zacharias, Phys. Rev. 57, 677 (1940).
[2] A. Nordsieck, Phys. Rev. 58, 310 (1940).
[3] H. M. James and A. S. Coolidge, J. Chem. Phys. 1, 825 (1933).
[4] E. Ishiguro, J. Phys. Soc. Japan 3, 129, 133 (1948).
[5] T. Inui, Proc. Phys. Math. Soc. Japan 20, 770 (1938).

TABLE I. Values of the parameters for the new wave function. N, R, and E (including nuclear repulsion term R^{-1}) are in atomic units.

R	1.2	1.3	1.4	1.5
E	1.157,48	1.165,35	1.167,81	1.166,48
A	1.545,7	1.636,6	1.727,0	1.814,6
B	1.255,0	1.344,6	1.435,4	1.524,9
C	0.750	0.800	0.817	0.850
a	−0.269	−0.321	−0.354	−0.399
b	0.1081	0.1350	0.1649	0.1952
c	−0.060,90	−0.069,70	−0.079,78	−0.089,88
N	2.894,82	2.795,66	2.701,00	2.613,90

TABLE II. Values of the binding energy of the hydrogen molecule in ev as calculated by various authors. Trials 1 and 2 refer to intermediate results; see Section 2.

Wang[a]	3.76	New values	
Inui[b]—Nordsieck[c]	4.03	Trial 1	4.22
Ishiguro[d]	4.26	Trial 2	4.31
J-C 5 term[e]	4.51	Final result	4.53
13 term[e]	4.70	(Experimental)	(4.73)

[a] S. C. Wang, Phys. Rev. 31, 579 (1928).
[b] See reference 5.
[c] See reference 2.
[d] See reference 4.
[e] See reference 3.

corrected to give a better wave function by adding some term depending on $(\varphi_1-\varphi_2)$. This would allow the electrons to seek opposite sides of the molecule. An initial attempt was made using only the first two terms of (4) with $C=0$, referred to in Table II as trial 1. From this preliminary calculation it was observed that a significant improvement in E could be made by allowing C to vary independently, referred to in Table II as trial 2. The wave function is then in such a form as to allow for the fact that the interaction between electrons is significant only for small ξ_1 and ξ_2 where the two electrons are on the average close together. One sees from Table II that the energy is appreciably better than the Inui-Nordsieck value, in fact it is better than the Ishiguro[4] value obtained from a six-parameter wave function. A comparison of the charge density $\rho=\int d\tau_1\psi^2$ with an approximate charge density integrated numerically by Nordsieck from the James-Coolidge function showed that the new charge density was worse at the points considered than that obtained using only the first term of (4). Though the error in the wave function itself must be less on the average with each successive correction, this unfortunate coincidence is possible because the change in ψ and in the energy arises mainly from terms linear in a, whereas the charge density contains only terms quadratic in a (ρ does not depend on $\varphi_1-\varphi_2$).

The last two terms of (4) were finally added. The first of these has an appreciable effect on the charge density but little effect on the energy. The last term was added to allow for shielding. If one electron is close to the nuclei, the other is likely to be further away.

It is already apparent from the difficulties encountered here that a substantial improvement in the charge density would require either a tremendous amount of labor or some more fruitful attack than the one attempted here. More convincing evidence is to be found in Section 3. Table I gives the calculated values of the parameters and the energies associated with the wave function (4) for several values of R. In Table II values of the binding energy of the molecule are compared with those of other authors.

3. ERRORS IN THE CHARGE DENSITY

The charge density at $R=1.4$ atomic units obtained by integration from Eq. (4) is compared with the values given in Table I of Nordsieck's paper. He calculated numerically an approximate density from the James-Coolidge function and in the same manner calculated an approximate density from his wave function. The density was also found by exact integration from his wave function. Due to the close agreement between the approximate and exact densities of the Nordsieck wave function, it was believed to be justifiable for further comparisons to assume a value,

$$\rho=\rho'\beta, \tag{5}$$

as the correct charge density at the points considered, where ρ' is the estimated James-Coolidge density, and β the ratio of the exact Nordsieck density to the estimated Nordsieck density. These values are listed in Table III as J-C. The values in the remaining columns are values obtained by exact integration with the corresponding percentage error in parentheses. Figure 1 shows the position of the points $(a, b, \cdots f)$ at which these densities are compared.

If this charge density is to be used in an integral, one must weigh these errors not only according to the magnitude of ρ, but also according to the volume element associated with each point. Since ρ is independent of θ, the charge densities and errors given in Table III are those associated with a volume element of magnitude proportional to the distance from the internuclear line. For most integrals which one might care to evaluate from ρ, including the one of Eq. (2), points such as d and ee' contribute most. The element of volume associated with a, bb', cc' is small, whereas at f the charge density itself is small. For the integral to be considered, the errors must also be weighted according to the value of $(3\cos^2\theta'-1)r^{-3}$.

The error in $q'(R)$ at $R=1.4$ can be estimated in a very crude way by assuming a continuous distribution of errors based on the values of Table III. The errors in the vicinity of a, b' tend to overbalance the errors at other points despite the small volume element assigned to them. One concludes that the new charge density gives a value of $q'(1.4)$ which is almost certain to be larger than the true value. By adjusting the parameters A, B, etc. of Eq. (4), one can obtain a distorted charge density and a second value of $q'(1.4)$ which is even more likely to be too small. The parameters were adjusted to give a charge distribution such that the error at each

of the points a to f was either negligible or contributed to the integral (2) with the same sign. This extreme value of $q'(1.4)$ differs from the first by 1.8 percent. Using either of these charge densities with their assumed error distributions, one can calculate a probable value of $q'(1.4)$. Two such calculations using each of the two charge densities were found to be consistent within ± 0.3 percent, giving a value of $q'(1.4)$ 0.7 percent below the first value and 1.1 percent above the second. That the two calculations were consistent implies only that the continuous distribution of errors assumed in each case gave consistent results. Both error distributions, however, were based on the James-Coolidge values of Table III and were taken to be essentially linear between the given points.

The James-Coolidge wave function should serve as a good standard for comparison of the new function but to evaluate accurately the errors by such a comparison would be a task of comparable difficulty to actually integrating the James-Coolidge function. Though the above procedure is crude, it is felt that it is at least qualitatively correct. A probable error of 0.6 percent is therefore assigned to the new value of $q'(1.4)$ instead of the 0.3 percent mentioned.

4. CALCULATION OF q'

The evaluation of the integral in Eq. (2) presents no serious difficulties and can be done exactly using the wave function (4). The values of $R^3q'(R)$ are given in Table IV for several values of R near the equilibrium position.

Using these values, $R^3q'(R)$ is expanded in a power series about the equilibrium position R_e of the molecule

$$\left.\begin{aligned} R^3q'(R)&=R_e^3q'(R_e)(1+\alpha_1\xi+\alpha_2\xi^2+\alpha_3\xi^3),\\ \xi&=(R-R_e)/R_e. \end{aligned}\right\} \quad (6)$$

Since both $\alpha_2\xi^2$ and $\alpha_3\xi^3$ are small for the range of ξ covered by the zero-point vibration of the molecule, no appreciable error need be assumed for the lack of high terms in the expansion. Due to the large change in R^3 over this range, the average of $q'(R)$ over the zero-point of vibration is quite sensitive to errors in the wave function associated with this vibration.

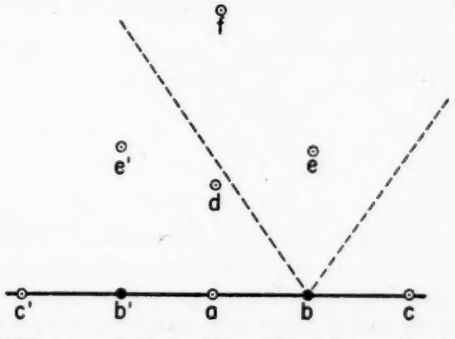

FIG. 1. The circles indicate the positions of the points $(a, b\cdots f)$ relative to the two nuclei bb'. The dashed line separates regions for which $3\cos^2\theta'-1$ has opposite sign.

TABLE III. Values of the charge densities in atomic units with percent error in parentheses for $R=1.4$ atomic units. The positions of the points are shown in Fig. 1.

Point	J-C	Nordsieck[a]		Ishiguro[b]		New values	
a	0.267,3	0.269,9	(+1.0)	0.271,39	(+1.5)	0.264,65	(−1.0)
bb'	0.446,1	0.430,4	(−3.5)	0.434,45	(−2.6)	0.439,76	(−1.4)
cc'	0.067,32	0.068,25	(+1.4)	0.069,34	(+3.0)	0.069,42	(+3.1)
d	0.106,9	0.108,7	(+1.7)	0.106,23	(−0.6)	0.107,22	(+0.3)
ee'	0.047,47	0.048,49	(+2.1)	0.047,28	(−0.4)	0.047,78	(+0.1)
F	0.005,97	0.006,16	(+3.2)	0.005,85	(−2.0)	0.006,16	(+3.2)

[a] See reference 2.
[b] See reference 4.

The shape of the potential well for the molecular vibration can be obtained more accurately from spectroscopic data than from the calculations of Section 2. Using the formulas of Dunham[6] and the experimental data of Jeppeson,[7] the potential can be evaluated in the form

$$V=a_0\xi^2(1+a_1\xi+a_2\xi^2+a_3\xi^3+a_4\xi^4). \quad (7)$$

The values obtained for the Dunham coefficients are given in Table V. The merits of such an expansion are discussed by Coolidge, James, and Vernon.[8] While it may be in serious error for large values of ξ, it should represent the potential quite accurately for the small values of ξ corresponding to the zero-point vibration.

To test the sensitivity of q' to the shape of the potential well, calculations were performed using Morse[9] functions. The two parameters of the Morse potential were assigned in one case to give the correct binding energy and the correct vibration frequency, and in another case to give the correct vibration frequency and the value a_1 of (7) when the Morse potential is expanded in a similar series. The differences between the corresponding values of q' were 1 percent for D_2 and 1.3 percent for HD. The second of these two Morse functions was corrected by means of perturbation theory to conform to the potential of Eq. (7). This last correction gave an additional 0.2 percent change.

It is assumed that no significant error arises from averaging $q'(R)$ over the zero-point vibration. The results for $J=1$ are

$$q'=0.1761 \text{ for } D_2, \quad q'=0.1757 \text{ for HD}. \quad (8)$$

In Section 3, it was argued that the value of $q'(1.4)$ given in Table IV is too large by 0.7 percent. The vibrational wave function has a maximum at about $R=1.4$ and a half-width $\Delta R\sim 0.15$. If one assumes that the error in $q'(R)$ does not change appreciably over the short range of R about 1.4, then the error in q' may also be taken as +0.7 percent. The corrected values of q' are

$$q'=0.1749 \text{ for } D_2, \quad q'=0.1745 \text{ for HD}. \quad (9)$$

5. CONCLUSION

The value of H''' as given by Kellogg *et al.*[1] is 87.2 ± 0.5 gauss. Within experimental error no difference is

[6] J. L. Dunham, Phys. Rev. **41**, 713, 721 (1932).
[7] C. R. Jeppeson, Phys. Rev. **45**, 480 (1934); **49**, 797 (1936).
[8] Coolidge, James, and Vernon, Phys. Rev. **54**, 726 (1938).
[9] P. M. Morse, Phys. Rev. **34**, 57 (1929).

TABLE IV. Calculated values of $R^3q'(R)$ in atomic units.

R	$R^3q'(R)$
1.2	0.603,69
1.3	0.547,18
1.4	0.488,86
1.5	0.430,96

found in the value for HD and D_2. The values of q' given above are consistent with this observation. Taking the average of the two values of q' for HD and D_2, Q_D is found to be 2.766×10^{-27} cm². On the basis of the errors discussed in Section 3, a probable error of 0.6 percent is assigned to q'. Combining this with the error of 0.6 percent in H''' gives $\sqrt{2}(0.6)=0.9$ percent as the probable error in Q_D:

$$Q_D=(2.766\pm0.025)\times10^{-27}\text{ cm}^2. \quad (10)$$

This differs from the value 2.73×10^{-27} cm² ±2 percent obtained by Nordsieck[2] chiefly because the latter performed the average over the zero-point vibration using a Morse function fitted to give the correct binding energy. Though the new value does not differ much from the value 2.79×10^{-27} cm² obtained by Ishiguro, the values of $q'(1.4)$ differ by as much as five percent. On the basis of the James-Coolidge density values of Table III, the errors in Ishiguro's density are very badly distributed in the vicinity of the nucleus. The errors are negative for points *e* and *b*, presumably also for points in between, whereas the errors at *a* and *c* are both definitely positive. The percentage error in $q(R)$ can be considerably larger than the percentage error in ρ due to the cancellation in the integral of the spherically symmetric part of the distribution. Thus one can account for the five percent difference in the values of $q'(1.4)$. That the two values of Q_D are so close is partly due to the 0.7 percent correction of the new value made in Section 4 and partly because Ishiguro used a Morse function for his average over the zero-point vibration, probably the same one used by Nordsieck.

TABLE V. Values of the Dunham[a] coefficients as calculated from spectroscopic data.[b] a_0 is in cm^{-1}.

	HD	D_2
a_0	79,795	79,873
a_1	−1.608,2	−1.589,2
a_2	+1.846,4	+1.750,7
a_3	−1.840	−1.708
a_4	+1.664	+2.07

[a] See reference 6.
[b] See reference 7.

The author wishes to thank Professor A. Nordsieck for suggesting the problem and for helpful advice.

PHYSICAL REVIEW VOLUME 78, NUMBER 6 JUNE 15, 1950

A Hodoscope Study of Penetrating Cosmic-Ray Showers. I. Local Showers*

KURT SITTE
Physics Department, Syracus University, Syracuse, New York
(Received February 1, 1950)

Showers produced locally in a lead absorber were studied with a hodoscope arrangement. It is shown that, in order to record "local penetrating showers," a rigid selection demanding high penetrating power of the secondaries as well as of the primary must be used. If this is done, some of the discrepancies of recent investigations are removed. For showers capable of penetrating at least 200 g/cm² Pb one finds a collision mean free path of (162±10) g/cm², and for showers of at least 100 g/cm² penetration a mean free path of (196±13) g/cm². Besides, "local soft showers" due to electronic or photonic secondaries of ordinary μ-mesons were studied. Their frequency at 3260-m elevation is about 1 in 10^5 traversals of the lead absorber.

I. THE EXPERIMENTAL TECHNIQUE

IN its present stage, work on penetrating showers is particularly strongly affected by the limitations of current experimental methods. Counter arrangements, though suitable for detection and for selection of showers, cannot usually provide a unique answer to questions concerning the nature of the particles involved, or concerning details of their interactions. Cloud chambers, on the other hand, could adequately answer this purpose, but it is troublesome and difficult to stack in them a sufficiently large amount of absorber, and they tend to become slow in operation because of the inevitably long interval between successive expansions of a large chamber, and its equally inevitable unfavorable solid angle of detection. It appeared, therefore, that in this field the use of what one might consider a compromise technique, namely a hodoscope arrangement, is well justified. It offers speedier work than a cloud chamber, as better solid angles and recovery times can be obtained, and it offers more extended evidence than a simple counter arrangement would reveal, though, of course, it is inferior in this respect to the cloud chamber.

* The expense of constructing the equipment and of running the experiment were partly provided by an AEC contract.

In deciding upon the experimental arrangement one might consider still another point. For the purpose of analyzing the shower phenomena in a hodoscope set it would appear desirable to use as large a number of narrow counters as possible, thus approaching the picture recorded in a cloud chamber with a single non-stereoscopic camera. This, however, has obviously two serious drawbacks. The selection of the events under investigation is usually based on a suitable "master pulse" formed by a certain group of counters. Using a large number of narrow hodoscope counters to define the master pulse one might then frequently find it difficult to eliminate undesired secondary effects without rejecting too many showers of the type one wishes to study. Furthermore, it necessitates an unduly complicated electronic circuit, thus again reducing the efficiency of the arrangement because of the inevitable time losses due to faults which these circuits develop during a long period of operation.

For the purpose of the present experiment it was decided, therefore, to use independent "master" and "hodoscope" counters. Groups of larger counters were used to select the showers, and additional narrow counters to indicate the number and the paths of the particles present in the shower. With a large number of counters, this apparent complication actually results in a simplification of the arrangement.

A schematic view of the arrangement is given in Fig. 1. The counter trays A, B, and C contain the "master pulse" counters of dimensions 16×1 in. in A and B, and 24×2 in. in C. Trays a, b, and c operate on the neon lamp system; their diameters are $\frac{1}{2}$ in. in a and b, and 1 in. in c. The thickness of the top absorber, Σ_1, was varied in the different runs of the experiment between 0 and 350 g/cm². The absorber Σ_2 remained at 100 g/cm² throughout the experiment; Σ_3 was 200 g/cm² during the first, and 100 g/cm² during the second series of recordings. An additional thin absorber sheet, either $\frac{1}{2}$ in. of lead or $\frac{3}{4}$ in. of iron, was placed between "master pulse" counters and "hodoscope" counters at all three levels. Heavy shielding by 6 to 7 in. of lead protected the counter trays against side showers.

II. SELECTION OF LOCAL SHOWERS

In several recent papers[1–3] measurements of the collision mean free path of charged particles producing local penetrating showers have been reported. The results, however, were conflicting: thus, while Tinlot and Gregory,[1] working at 4300-m altitude, find an exponential decrease of the shower rate with absorber thickness and a mean free path of 350 g/cm² for lead and 200 g/cm² for iron, Cocconi's[2] experiments indicate a variation of the collision mean free path with absorber thickness. At 3260-m altitude, for instance, he finds in lead between 0 and 500 g/cm² absorber thickness collision mean free paths between 160 and 380 g/cm², and in iron in the same region a variation of the mean free path between 135 and 310 g/cm².

It might be noted here that the evaluation of Cocconi's measurements which led him to these striking results is not quite correct and tends to an overestimate of the variation with absorber thickness of the collision mean free path, if such a variation exists. If the absorption curve is not purely exponential, that is, if the collision probability varies with the amount of absorber traversed, this will affect not only the collisions in the top absorber, but also those in the "production layer," and the simple procedure of calculating the collision mean free path as the reciprocal of derivative of the logarithmical intensity curve is no longer adequate, since it supposes that a constant fraction of the incident single particles will produce showers in the production layer. Even so, a re-evaluation of Cocconi's results would only bring the maximum values for his mean free paths down to about 300 in lead, and 250 g/cm² in iron, thus leaving unexplained the disagreement both in shape and in slope of his absorption curves and those of Tinlot and Gregory.[1]

Both these experiments, however, are open to another more serious criticism. The "penetrating showers" recorded were events in which a single penetrating particle strikes the top counter tray, and two or more particle counters of the lower tray, separated from each other by a few inches of lead and from the top tray by a heavier shield, 4 or 6 in. of lead. The selection thus guarantees the penetrating nature of the primary par-

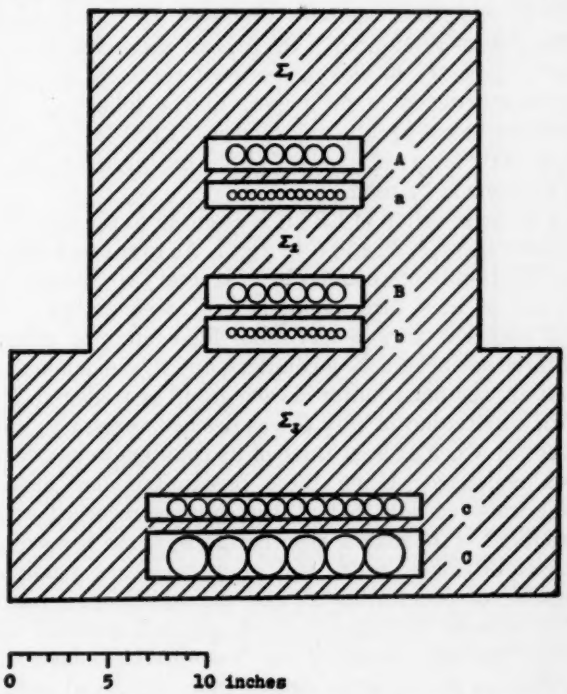

FIG. 1. Schematic diagram of the experimental arrangement. The "master pulse" counters A, B, and C select the events, the "hodoscope" counters a, b, and c operate the neon lamp system.

[1] J. Tinlot and B. Gregory, Phys. Rev. **75**, 519 (1949).
[2] G. Cocconi, Phys. Rev. **75**, 1074 (1949).
[3] W. B. Fretter, Phys. Rev. **76**, 511 (1949).

TABLE I. Rate of local penetrating showers as function of the top absorber thickness Σ_1, taken for two different values of the bottom absorber thickness Σ_3.

Absorber thickness Σ_1	Event	LPS Counts	LPS Time (hr.)	LPS Rate/hr.	LPS+E Counts	LPS+E Time (hr.)	LPS+E Rate/hr.
0	$\Sigma_3=200$	411	107.75	3.82±0.18			
	$\Sigma_3=100$	479	103.25	4.64±0.21	Not recorded		
170	$\Sigma_3=200$	200	149.5	1.34±0.08	2	140.5	0.014
	$\Sigma_3=100$	272	142.5	1.91±0.12	3	140.0	0.021
270	$\Sigma_3=200$	120	164.75	0.73±0.06	1	161.0	0.006
	$\Sigma_3=100$	195	172.25	1.13±0.05	2	163.0	0.012
350	$\Sigma_3=200$	82	189.25	0.43±0.05	0	187.5	0.000
	$\Sigma_3=100$	149	188.75	0.79±0.06	1	185.5	0.005

ticle, but not of the shower particles. It appeared quite possible that at least some of the showers recorded with such an arrangement would not be "penetrating showers" at all, but consist of a penetrating particle with soft secondaries. Therefore, the main purpose of the present experiment was to repeat absorption measurements of local showers under conditions of more rigid control and separation between these events.

Cocconi, continuing his experiments at sea level and underground, has more recently[4] come to a similar conclusion. He concludes that his arrangement recorded an appreciable component of showers, probably of electronic nature, produced by ordinary μ-mesons. At the time when the experiment reported here was prepared these conclusions were not yet known; nevertheless, the separation into "real" penetrating showers and soft showers produced by penetrating primaries, as attempted in the present hodoscope study, can be expected to yield a pertinent check for the corrections deduced in his paper. In the following, the notation "local penetrating shower" (LPS) for the first type, and "local soft shower" (LSS) for the second type of events will be used.

For the selection of LPS it is essential to use all three counter trays A, B, and C in Fig. 1. An event was called an LPS if only one counter in A, at least two counters in B, and at least three counters in C, were struck. For this selection, tray B was subdivided into two groups of three not-neighboring counters, and it was demanded that at least one counter in each group be triggered. No such subdivision of tray C was deemed necessary; any event in which at least three of its counters were struck was registered. Using these precautions one makes practically certain that all the showers recorded were produced in the middle absorber Σ_2, as of the few which might originate in Σ_3 and emit backward particles capable of penetrating Σ_3 and the additional $\frac{1}{2}$ in. of lead between the trays B and b, still only one-half will strike the right group of the B counters. In fact, the hodoscope photographs showed that only about one in 20 of the LPS came from Σ_3, so that it is a good picture to consider Σ_2 as the producing layer, while Σ_3 determines the penetrating power one wishes to demand for the shower particles. As a possible variation of the collision mean free path with absorber thickness would be much more clearly exhibited if a thin producing layer was used, and would disappear for very thick Σ_2, a layer of 100 g/cm² was chosen. In two series of measurements with identical counter geometry and production layer the penetration conditions were then varied by using for Σ_3 absorbers of 200 and 100 g/cm², respectively.

If an LPS was accompanied by an electron shower striking at least three counters of an extension tray E, an additional neon lamp was lit. Tray E consisted of six counters of 2 in. diameter and 24 in. length, and was placed near the "P-set" shown in Fig. 1. These mixed showers will be called "events LPS+E."

In the events selected as LSS only one penetrating particle was required, if it was accompanied by at least two secondaries at either tray B or tray c. The tray of "hodoscope" counters c had to be used in order to arrange identical conditions in both levels. Like tray B, c was subdivided into two groups of not-neighboring counters, and a shower was recorded if all three counters of a subgroup of B, or at least three counters of a subgroup of c, were struck together with one counter in each of the two other levels. As tray c was placed on top of the 2-in. counter tray C directly under the absorber, the LSS were required to extend over at least 3 in. in lead.

All the electronic circuits used were of the conventional type, with crystal diodes applied both in the mixing circuits and in the coincidence sets. The hodoscope was operated by applying the master pulse to the

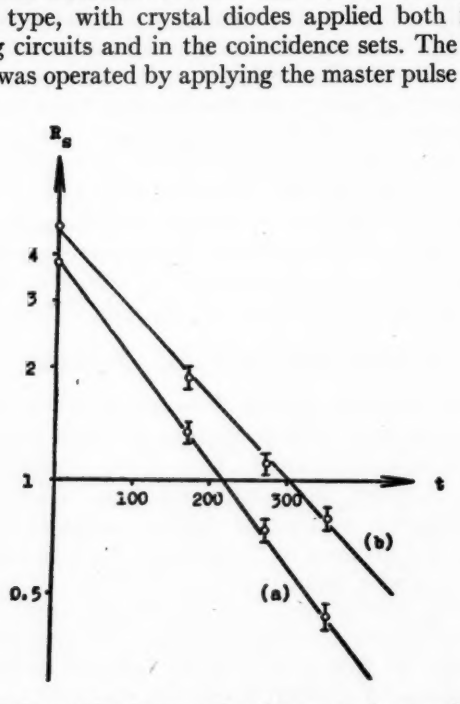

FIG. 2. Rate of local penetrating showers per hour, as function of the absorber thickness t (g/cm² Pb). Curve (a): Minimum penetration 200 g/cm² Pb. Curve (b): Minimum penetration 100 g/cm² Pb.

[4] G. Cocconi, Phys. Rev. **76**, 984 (1949).

suppressor grid, and the pulses from the indicator counters to the control grid of 6SJ7 tubes. The lengthened pulses were then led to the grid of another tube, with a neon lamp connected in parallel across the plate resistance. Tests with artificial pulses proved an efficiency and reliability of the neon lamp system of more than 99 percent. The experiment was carried out at Echo Lake, Colorado, at 3260-m altitude.

III. RESULTS ON LOCAL PENETRATING SHOWERS

It has been shown above that the arrangement recorded mostly showers produced in Σ_2. For the purpose of this experiment, moreover, the knowledge of the exact point of origin is irrelevant; no attempt was thus made to correct for the few events generated in Σ_3. Corrections for threefold knock-on showers with one secondary at B and two at C are small because of the 2-in. separation at C, but not negligible. They have been computed from observations made with the same arrangement on single penetrating particles in air showers.

Another correction which might play an important part in some cases, but proves to be negligibly small in the present experiment, is the difference between the knock-on events in lead and in air. The incident knock-on accompaniment is widely spread out if no lead shield covers the top tray, and only very rarely a penetrating particle will be rejected because one of its knock-on secondaries strikes a top counter. In lead, however, the lateral spread is much reduced and if the counters are not placed directly under the absorber one might lose an appreciable fraction of the penetrating events. With the tight arrangement of Fig. 1, a check on knock-on events observed in the hodoscope pictures reveals that this effect amounted to less than one percent of the number of penetrating particles.

Measurements were performed with four thicknesses of Σ_1: 0, 170, 270, and 350 g/cm². During the first series of the experiment the bottom absorber was 200 g/cm², during the second 100 g/cm². The observed rates, corrected for knock-on showers, are summarized in Table I. To each value of the top absorber thickness in column 1, the upper line refers to the first, the lower line to the second series of measurements.

The LPS-rates are also plotted in the graphs of Fig. 2. Here curve (a) refers to the first series, with a minimum penetration exceeding 200 g/cm², and curve (b) to the second, with $\Sigma_3 = 100$ g/cm². In a logarithmic plot, both can be represented well by a straight line, but with a slightly different slope. From (a) one obtains a collision mean free path

$$\lambda = (162 \pm 10) \text{ g/cm}^2,$$

while (b) leads to

$$\lambda' = (196 \pm 13) \text{ g/cm}^2.$$

It should be noted that even in this second series, though the separation between B and C was in total only $4\frac{1}{2}$ in. of lead, or not much more than the lateral counter separation in Cocconi's experiment, one has good reason to expect no appreciable admixture of LSS of the kind which distorted these earlier experiments. The reason is that here three secondaries were required, against two in the Cocconi experiment.

TABLE II. Rate of local soft showers as function of the top absorber thickness Σ_1, taken for two different values of the bottom absorber thickness Σ_3.

Absorber thickness Σ_1 \ Event		Time (hr.)	Tray B Counts	Tray B Rate/hr.	Tray c Counts	Tray c Rate/hr.
0	$\Sigma_3=200$	107.75	9	0.084±0.028	7	0.068±0.026
	$\Sigma_3=100$	103.0	6	0.058±0.024	8	0.078±0.027
170	$\Sigma_3=200$	140.5	9	0.064±0.021	10	0.071±0.022
	$\Sigma_3=100$	140.0	10	0.071±0.022	10	0.071±0.022
270	$\Sigma_3=200$	161.0	8	0.050±0.018	11	0.068±0.020
	$\Sigma_3=100$	163.0	14	0.086±0.023	9	0.056±0.019
350	$\Sigma_3=200$	187.5	14	0.075±0.020	12	0.065±0.019
	$\Sigma_3=100$	185.5	11	0.059±0.018	11	0.059±0.018

The hodoscope pictures were furthermore used to compare the numbers of recorded particles in the two series. Again one finds a slight but unmistakable difference: The average number of c counters struck in the first series was

$$\langle n_{200} \rangle = 4.18 \pm 0.18,$$

and with the thinner absorber

$$\langle n_{100} \rangle = 4.68 \pm 0.17.$$

This difference, moreover, is apparently not, or not entirely, due to a new group of showers of more particles and smaller penetrating power, but rather to a gradual shift in the distribution curve. One finds in the second series fewer showers with the minimum number of three penetrating particles: 105 in 1042 analyzed showers, against 201 in 751 analyzed showers of more than 200 g/cm² penetration. Thus it must be concluded that in penetrating showers in lead the fraction of particles with ranges between about 150 and 250 g/cm² is by no means negligible.

As to the penetrating showers that are accompanied by air showers, Table I shows that the correlation is only about one percent. This result is in satisfactory agreement with earlier observations of Tinlot and Gregory;[5] it will be discussed in the following analysis of the air shower experiment.

Finally, one can compute the directional intensity of the charged radiation that produces hard showers in lead. Unfortunately, the uncertainty of this estimate is much larger than the statistical error, due to the difficulties encountered in correctly accounting for geometry and zenith angle distribution. The values derived from the data given above are $(1.6 \pm 0.3) \times 10^{-5}$ cm^{-2} sec.$^{-1}$ sterad.$^{-1}$ for the more penetrating, and $(2.2 \pm 0.3) \times 10^{-5}$ cm^{-2} sec.$^{-1}$ sterad.$^{-1}$ for the less penetrating

[5] J. Tinlot and B. Gregory, Phys. Rev. 75, 520 (1949).

showers.† These figures are only slightly higher than those obtained by Hazen, Randall, and Tiffany[6] with a very different experimental method, and agree very well, as far as can be checked, also with the observations of Broadbent and Jánossy,[7] of Cocconi[2,4] and of others.

IV. RESULTS ON LOCAL SOFT SHOWERS

In the study of LSS two striking features became soon apparent: First, the hodoscope records of the *b* tray seemed frequently in disagreement with the selection which demanded at least three counters of the *B* tray struck. Very many photographs showed that only one or two of the *b* counters discharged. (No such effect could be observed at the lower level, where the hodoscope counters *c* were also used to transmit the master pulse of the LSS records.) Second, there was still much less correlation between these LSS and air showers; in fact, during almost 1000 hr. of observations only one such event (LSS+*E*) was recorded.

There could be no doubt that the apparent unreliability of the *b* tray was "selective:" it continued to record reliably everything but the LSS events. It became evident, therefore, that the secondaries produced in the LSS are either very weakly penetrating indeed so that they are partly removed by the ½-in. lead plate between *B* and *b*, or that they are very inefficiently recorded by G-M counters, or, of course, both.

In order to investigate this point, tray *a* was placed during the second series directly under *B*, so that the ½-in. absorber now separated the two hodoscope trays *a* and *b*. For about half the time of each run this absorber was then replaced by a ¾-in. iron plate.

The total numbers of LSS recorded and the counting rates per hour are given in Table II. Again the upper of the two lines to each value of Σ_1 refers to the series with $\Sigma_3=200$ g/cm², and the lower to $\Sigma_3=100$ g/cm².

The most striking feature in these results is the insensitivity of the shower rate to absorber thickness, and that both for the top absorber Σ_1 and for the bottom absorber Σ_3. This, and the absence of a correlation between LSS and air showers, prove that the primaries which generate these local showers must be μ-mesons of very high energies. If one compares the rate of LSS with the total flux of single penetrating particles through the arrangement (about 200/min.) one computes that about one in 10^5 μ-mesons originate either near the *B* tray or near the *c* tray a LSS of the type recorded. Radiation processes and high energy knock-on secondaries may well account for such a rate of soft showers.

During the first run, with $\Sigma_3=200$ g/cm², the pictures of 40 LSS discharging the *B* tray revealed altogether 59 activated counters of the *b* tray, under ½ in. of lead. During the second run, with $\Sigma_3=100$ g/cm², 19 showers originating at *B* were observed with 28 *b* counters discharged when the same ½ in. lead shield was used, and 46 particles in 22 showers when the lead was replaced by ¾ in. of iron. Thus, the number of particles recorded per shower was 1.47 ± 0.16 under ½ in. of lead, and 2.09 ± 0.30 under the iron shield of equivalent mass. Tray *a*, placed above these shields and immediately under *B* during this second run, showed 44 counters discharged in the 19 showers with the lead shield, and 54 in the 22 showers with the iron shield: rates of 2.3 ± 0.35 and 2.45 ± 0.35, respectively. This latter fact, that even with no absorber between the master pulse tray *B* and the hodoscope tray *a* less than the three particles which discharge *B* are registered in the adjacent tray, indicates that the counters are not fully efficient in recording these showers. Together with the strong absorption in lead, and much less strong absorption in iron, this evidence proves that the soft secondaries in these showers are electrons and photons rather than of nucleonic nature.

V. SUMMARY

The results of the present investigation stress the necessity of a more rigid selection of "penetrating" events. If at least three particles capable of penetrating more than 200 g/cm² are demanded, the cross section for shower production is of the order of the geometrical nuclear cross section. These showers contain in average about 4.2 such highly penetrating particles, but also others of a penetration of between 100 and 200 g/cm². This corresponds to a total kinetic energy of all charged shower particles of at least 2 to 3 Bev, with the lower figure valid if most of the particles are mesons, and the higher if they are protons. If only 100 g/cm² penetration is demanded, or in other words a minimum kinetic energy of 1.5 to 2.5 Bev, the cross section is somewhat smaller, and the number of particles recorded about 4.7. It would be interesting to restrict the measurements to that lower energy region and thus to determine the cross section for low energy nuclear interactions; this was, however, not possible from the data of the present experiment.

If the penetration requirements are still more reduced, extra-nuclear interactions of ordinary μ-mesons resulting in the production of a local soft shower of electrons and photons become increasingly important.

In conclusion the author wishes to express his gratitude to the Inter-University High Altitude Laboratories, and in particular to Drs. Cohn and Iona of the University of Denver, for the permission to use the facilities at Echo Lake Laboratory and for their help.

APPENDIX. ON THE ABSORPTION OF THE PARTICLES THAT PRODUCE PENETRATING SHOWERS

In the following an attempt is presented to derive, from a summary of empirical data and from a few plausible general assumptions, a number of characteristics of fast nuclear collisions

† The zenith angle distribution was assumed to follow a $(\cos\theta)^6$ law which was well compatible with observations, and theoretically the most likely correct distribution at a depth of 700 g/cm², or about six absorption mean free paths, under the top of the atmosphere.

[6] Hazen, Randall, and Tiffany, Phys. Rev. **75**, 694 (1949).

[7] D. Broadbent and L. Jánossy, Proc. Roy. Soc. (A)**190**, 497 (1947).

resulting in the production of "penetrating showers." Let it be emphasized that this attempt makes no claim to be a theory of penetrating showers; its aim is only to outline certain general features such a theory would need to embrace, and to deduce certain directives for such a theory.

The mathematical methods which will be used, at this stage, are rather crude. Fluctuations will be neglected, and simplifications, like that of assuming a power law with constant exponent for the energy spectrum of the cosmic-ray primaries, will be made. No further apologies are offered later on whenever such procedures of dubious purity are applied, and no better results can be hoped for than those obtained, for instance, in kinetic gas theory by assuming a uniform velocity of all particles. In a word, it is believed that a more accurate treatment will change many details, but leaves unchanged the basic conclusions.

The essential empirical facts on which any theory must be based are:

(i) The *interaction* cross section for fast nuclear collisions initiating penetrating showers is very nearly equal to the geometrical cross section of the absorber nucleus (e.g., Rossi[8]).‡

(ii) The *absorption* cross section is considerably smaller than the interaction cross section. In air, for instance, an absorption thickness of about 120 g/cm² has been found (e.g., Tinlot[9]), while the interaction mean free path, according to (i), is only about 70 g/cm².

(iii) The ratio of the intensities of neutral and charged shower primaries is nearly unity both at sea level and at mountain altitudes (e.g., Jánossy and Rochester,[10] Walker.[11]

(iv) The total kinetic energy carried by the charged particles of a penetrating shower is in most experiments at least 2 to 3 Bev.

(v) The total intensity of the charged radiation which originates in lead penetrating showers of the energies quoted in (iv) is at sea level about 0.95×10^{-6} cm^{-2} sec.$^{-1}$ sterad.$^{-1}$ (Hazen, Randall, and Tiffany;[6] Section III of this paper).

(vi) At sea level, no noticeable geomagnetic latitude effect is found between equator and moderate latitudes (Appapillai and Mailgavanam[12]).

Let us denote the *collision* mean free path by λ and the *ansorption* mean free path by Λ, and assume that, in the region of large energies which we are to consider, both are constant. Assume further a power law for the integral energy spectrum of the incident primary radiation:

$$S(E)=(E/E_c)^{-\gamma}$$

with E_c=cut-off energy, and $\gamma\sim1.5$. It will be shown later that we have to deal with an energy region in which this value is plausible. However, a change in the value of γ would only affect some of the numerical results found, without invalidating the conclusions drawn from them.

Assume next that on the average each particle in initiating a penetrating shower retains a fraction αE of its initial energy E, and transfers a fraction βE to each of m secondaries that are capable of further shower production ("N component"). The remainder, $(1-\alpha-m\beta)E$, is dissipated in ejection of slow secondaries ("evaporation"), or of particles which cannot reproduce further penetrating showers. In collisions in air, for instance, the energy transferred to π-mesons belongs to the "dissipated" fraction, as for all energies below $\sim10^{11}$ ev their mean free path for decay is much shorter than that for collision. In dense materials π-mesons belong to the "reproducing" N component.

Assume finally that the collision mean free path of the "reproducing" secondaries is the same as that of the primary incident particle; i.e., no distinction can be made between "real" primaries and their descendants which are still capable of originating hard showers.

Let E_s be the minimum energy a particle must have in order to produce showers of penetrating secondaries. If $E_s\gtrsim E_c$ [which, according to (iv), is plausible at least at moderate latitudes], the number of *primary* cosmic-ray particles participating in shower production at depth x from the top of the atmosphere (if measured in units of the collision mean free path this depth will be denoted by $y=x/\lambda$) is

$$N_s^{(0)}=N_0\{(E_s/E_c)^{-\gamma}\cdot e^{-y}+(E_s/\alpha E_c)^{-\gamma}\cdot e^{-y}\cdot y/1! +(E_s/\alpha^2E_c)^{-\gamma}\cdot e^{-y}\cdot y^2/2!+\cdots\} \quad (1)$$

(N_0=primary intensity). The sum gives

$$N_s^{(0)}=N_0\cdot(E_s/E_c)^{-\gamma}\cdot\exp[-(1-\alpha^\gamma)y]. \quad (2)$$

Secondaries emitted in preceding collisions contribute, after n "secondary" generations

$$N_s^{(n)}=m^n\cdot N_0\cdot(E_s/E_c)^{-\gamma}\cdot[(\beta^\gamma y)^n/n!]\cdot\exp[-(1-\alpha^\gamma)y], \quad (3)$$

one-half of which can be assumed charged, and one-half neutral. The total number of shower-producing secondaries is then

$$\sum_{n=1}^{\infty}N_s^{(n)}=N_0(E_s/E_c)^{-\gamma}\cdot\exp[-(1-\alpha^\gamma)y]\cdot\{\exp(m\beta^\gamma y)-1\}, \quad (3a)$$

again divided equally into charged and neutral particles. This gives a total intensity of shower-producing radiation,

$$N_s=N_0+\sum_{n=1}^{\infty}N_s^{(n)}=\sum_{n=0}^{\infty}N_s^{(n)}.$$

$$N_s=N_0(E_s/E_c)^{-\gamma}\cdot\exp[-(1-\alpha^\gamma-m\beta^\gamma)y], \quad (4)$$

and if we divide into charged and neutral components, we obtain for the charged radiation

$$(N_s)^p=\tfrac{1}{2}N_0(E_s/E_c)^{-\gamma}\cdot\exp[-(1-\alpha^\gamma-m\beta^\gamma)y]\cdot\{1+\exp(-m\beta^\gamma y)\} \quad (4a)$$

and for the neutral radiation

$$(N_s)^n=\tfrac{1}{2}N_0(E_s/E_c)^{-\gamma}\cdot\exp[-(1-\alpha^\gamma-m\beta^\gamma)y]\cdot\{1-\exp(-m\beta^\gamma y)\}. \quad (4b)$$

These results permit several important conclusions and estimates:

(a) The absorption mean free paths for both charged and neutral particles are, for not too small depths, very nearly the same:

$$\Lambda\approx\lambda/(1-\alpha^\gamma-m\beta^\gamma). \quad (5)$$

In air, with $\lambda\approx70$ g/cm² and $\Lambda\approx120$ g/cm², we have thus

$$(1-\alpha^\gamma-m\beta^\gamma)\approx0.6. \quad (5a)$$

(b) The ratio of the intensities of neutral and charged shower primaries is

$$(N_s)^n/(N_s)^p=[1-\exp(-m\beta^\gamma y)]/[1+\exp(-m\beta^\gamma y)], \quad (6)$$

and hence approaches unity at sea level ($y\approx15$) or mountain altitudes ($y\approx8-10$) only if an appreciable fraction of the incident energy goes into shower-reproducing secondaries. If we permit a ratio $(N_s)^n/(N_s)^p=0.75$ at mountain altitudes, we have to demand $(m\beta^\gamma)\sim0.20$ to 0.25. Together with (5a) this gives $\alpha^\gamma\sim0.15$ to 0.20, or, with $\gamma=1.5$, $\alpha\sim0.28$ to 0.34. Thus we expect the primary to retain on the average about one-third of its incident energy, and to transfer an about equal amount to shower-producing secondaries, while between one-third and one-fourth of the energy is "dissipated."

---

[8] B. Rossi, M.I.T. Technical Report No. 26 (April 4, 1949).

‡ Professor K. Greisen has kindly informed me that the measurements of the Cornell group give for the collision mean free path in carbon a value which is somewhat larger than that corresponding to the geometrical nuclear cross section of C. This means that light nuclei are apparently not quite opaque. In the following computations no corrections for the partial transparency of air nuclei have been made, but it should be noted that this effect would have very little influence even on the numerical results given later.

[9] J. Tinlot, Phys. Rev. **73**, 1476 (1948); **74**, 1197 (1949).

[10] L. Jánossy and G. D. Rochester, Proc. Roy. Soc. (A)**182**, 180 (1943).

[11] W. D. Walker, Echo Lake Symposium on Cosmic Rays (1949).

[12] V. Appapillai and A. W. Mailgavanam, Nature **162**, 374 (1949).

(c) With these estimates, it is easy to interpret the absence of a geomagnetic effect. Write the number N_s of shower-producing particles from (4) as a sum indicating the number n of collisions the individual particles have suffered:

$$N_s = N_0(E_s/E_c)^{-\gamma} \cdot \exp[-(1-\alpha^\gamma)y] \cdot \sum_{n=0}^{\infty} (m\beta^\gamma y)^n/n!. \quad (4c)$$

As $m\beta^\gamma \sim 0.2$, the maximum contribution to N_s comes from particles that have already suffered about two to three previous collisions, and hence must have started with an energy $\gtrsim(E_s/\alpha^{2.5})$, or about 15 E_s, when incident on the top of the atmosphere. Thus, being descendants of very energetic primaries, the particles that originate penetrating showers will show no appreciable geomagnetic latitude effect at sea level.

(d) The ratio (E_s/E_c) can be estimated if one compares the observed flux of shower-producing particles with the incident primary flux at the top of the atmosphere. Even if the entire contribution of the heavier particles is neglected, and all local penetrating showers are related to the primary proton flux of about 0.1 cm^{-2} sec.$^{-1}$ sterad.$^{-1}$ and their nucleonic secondaries, one gets from (4a) applied to sea-level data ($x/\Lambda \approx 8.75$):

$$(E_s/E_c)^{-\gamma} \approx (2N_s/N_0) \cdot e^{8.75} = (1.9\times 10^{-6}\times 6.3\times 10^{3})/0.1 \approx 0.12,$$

or again with $\gamma = 1.5$,

$$E_s \approx 4E_c,$$

that is, at medium latitudes, about 15 to 20 Bev, and incidentally even more if one believes in a lower value for γ. However, as at lower altitudes at least the bulk of the showers evidently are due to very energetic primaries for which the energy spectrum certainly is not flat, it appears to be justified to approximate it by this particular power law.

This last surprising result merits some further consideration. It may be stated that the following remarks do not depend on any of the special assumptions made above; they are essentially based only on the experimental fact that the flux of shower-producing particles at sea level is less than one-tenth of the flux which one would expect if all primary particles incident at the top of the atmosphere were to contribute to the production of local penetrating showers, and if the absorption at all altitudes did not exceed that observed at sea level or moderate heights.

The following reasons might explain this remarkably small flux: (1) Particles in the lower energy region may be absorbed more readily than those of higher energies. (2) Collisions of low energy particles ($E \lesssim 15$ Bev) will in general not result in the emission of a penetrating shower.

One can easily see that the first is not a very likely explanation. The interaction cross section cannot exceed the geometrical cross section, but attains or approaches this value for high energies. Thus an entirely different mechanism would have to be found to account for an absorption process favoring the low energy region. The simplest would be the assumption that on the average not a constant *fraction* of the incident energy is transferred in a collision, but a constant *amount* of energy. Such a transfer law would lead to a quicker elimination of the slower particles. However, it would also lead to an absorption law which, far from being exponential, resembles the range curves of absorption due to ionization losses. Only with very artificial assumptions could a "selective" absorption of low energy particles be combined with an exponential or near-exponential absorption curve.

Hence the second assumption appears to be the more plausible one. It means that, although for all primaries, and indeed all nucleons and possibly π-mesons of energies $\gtrsim E_c$, the interaction cross section may be equal to the geometrical nuclear cross section, the probability that the energy transfer to several secondaries is large enough so that a penetrating shower results from the collision, is small for small incident energies and increases with the energy. The simplest representation of such a transfer law is by a probability function which depends on the *fractional* transfer U/E only (U is the energy transferred in the collision):

$$p(U, E)dU = p(U/E)d(U/E) \quad (7)$$

and which decreases with increasing fractional transfer. It is well known that one encounters a transfer probability of this kind for instance in radiative collisions. From analogy reasons, a probability function of the type (7) has therefore, been chosen arbitrarily by Heitler and Jánossy[13] in their theory of fast nuclear collisions. From the arguments presented here it appears that there is experimental evidence as well as reasons of analogy to support this rather than other transfer laws.

It should be recalled that, if this interpretation is accepted, α stands for the *average* fractional energy retained by the incident particle. In a similar way, E_s is the *average* energy above which the production of penetrating secondaries in a nuclear collision becomes very likely, while for $E < E_s$ the probability for these processes becomes increasingly small. In this region of lower energies collisions still occur with about equal frequency, but they result in a more star-like "shower" with no or few penetrating secondaries, most likely "knock-on protons," but no mesons.

There is, finally, a simple check on the validity of these estimates and conclusions. If it is so that, on the average, mesons are produced only in high energy collisions, then it must be possible to derive the entire μ-meson component from these collisions. In other words: One can first compute the average number of mesons produced in a single collision by comparing the intensity of the μ-meson component at sea level, corrected for decay while traversing the atmosphere, with the total number of collisions the primary cosmic-ray particles of energy $E \gtrsim E_s$ and their energetic descendants have suffered. One can then re-check by computing the energy each meson would carry off, and comparing it with the observed meson energies. Details of these computations will not be given here; it may suffice to state that not only a very reasonable value for the average multiplicity of the meson production is obtained ($n \approx 4$ to 5), but also a rather satisfactory representation of the altitude dependence of the meson flux.

[13] W. Heitler and L. Jánossy, Proc. Phys. Soc. **A62**, 374 and 669 (1949).

A Hodoscope Study of Penetrating Cosmic-Ray Showers. II. Extensive Showers*

KURT SITTE
Physics Department, Syracuse University, Syracuse, New York
(Received February 1, 1950)

The interactions of penetrating particles in air showers have been studied with a hodoscope arrangement at an altitude of 3260 m. About 90 percent of all charged penetrating particles do not originate local showers of penetrating secondaries, and are absorbed only very slowly. This "non-interacting component," consisting at least predominantly of μ-mesons, has a rather flat range spectrum between 280 and 680 g/cm² Pb. Its zenith angle distribution is approximately proportional to $\cos^4\theta$. The remaining 10 percent constitute a "charged N component"; the total fast N component amounts to about one-fourth of the number of the charged penetrating particles. The collision mean free path of the fast N component was found to be (220±30) g/cm² if a minimum of 100-g/cm² penetration is demanded for the local showers. From the recorded increase of the number of shower particles with absorber thickness it is concluded that further multiplication after the first collision is quite common, and that the mean free path of the secondaries of local showers is not much larger than that of the primary N component.

I. ARRANGEMENT AND SHOWER SELECTION

DURING the last years, much progress has been made in our understanding of the complex phenomena connected with extensive showers. Thus, for instance, important questions like that of the place of the origin of the penetrating particles, or that of the existence of a new light fundamental particle, can be considered as definitely settled. In particular, the work of Cocconi, Tongiorgi, and Greisen[1] on penetrating particles in extensive air showers has clearly established that these particles are mainly μ-mesons which are produced not locally in the absorber surrounding the counter arrangement, but in air, possibly high above the apparatus. On the other hand, the occurrence of local production of groups of penetrating particles has likewise been proven, perhaps most conclusively in the cloud-chamber studies of Ise and Fretter,[2] and of Brown and McKay.[3] However, the relative frequency of such events in the showers, the mean free path of secondary production, and many other details have not yet been completely explored in these investigations. It was the purpose of the present study to obtain additional evidence mainly about the composition of the penetrating component of air showers.

The experimental arrangement was the hodoscope apparatus described in Part I, on local showers.[4] In addition to the "master pulse" trays A, B, and C of the "P-set" shown in Fig. 1 of Part I, extension trays D and E were used to select air showers. Tray D consisted of six counters of 2 in. diameter and 24 in. length, connected in three groups of two counters each, and was placed in about 2½ m distance from the P-set. It was furthermore intended to discriminate between showers of large and small electron density with the help of a similar fifth tray E in about 10 m distance from the P-set, using additional neon lamps to indicate whether or not E was struck. No difference of statistical significance could, however, be established, so that in the following analysis all recorded air showers are included without discrimination as to their densities.

The master pulse used to sensitize the neon indicator lamp system was formed by coincidences ($1A+1B+3D$), that is, at least one particle striking tray A, at least one particle striking tray B, and at least one particle striking each subgroup of the extension trays D or E were required. During the entire air shower experiment tray A was shielded with lead absorbers of not less than 170 g/cm² thickness, while tray D remained unshielded. Thus, the master pulse was formed if a particle capable of penetrating at least 280 g/cm², accompanied by an electron shower, struck the apparatus. It was not required that tray C was also struck; if the penetrating particle reached the bottom tray, an extra neon lamp was discharged to facilitate classification.

In view of the heavy shielding of the trays of the P-set on all sides the probability of cascade particles triggering the trays A and B is negligible. As far as side showers are concerned, the use of separate master counters and hodoscope counters offers an additional check on their contribution. Cascade particles which might penetrate the 6 to 7-in. Pb side absorber, and trigger the master pulse counters, would frequently fail to reach the hodoscope trays, and leave the picture taken with this master pulse blank, or at least one tray apparently not struck. During a total of about 1000 hr. of recording, only 11 such events, that is less than one-half percent of all recorded showers, were found, and they may well have been due to the inefficiency of the trays or of the neon lamp system. While these pictures were disregarded in the analysis, no correction for either high energy cascades or side showers was deemed necessary. The correction for chance coincidences between single penetrating particles (3.4 per sec. in the P-set) and air showers triggering D only (approximately 40 per hr.) was negligibly small because of the short resolving time of the circuits used (about 4 to 5 μsec.).

* The expense of constructing the equipment and of running the experiment were partly provided by an AEC contract.
[1] Cocconi, Tongiorgi, and Greisen, Phys. Rev. **75**, 1063 (1949).
[2] J. Ise and W. B. Fretter, Phys. Rev. **76**, 933 (1949).
[3] W. W. Brown and A. S. McKay, Phys. Rev. **76**, 1034 (1949).
[4] K. Sitte, Phys. Rev. **78**, 714 (1950).

TABLE I. Fraction $F(\theta)$ of non-interacting penetrating particles at zenith angle θ.

Mean zenith angle $\theta°$	0.9	4.0	7.1	10.2	13.3	16.2	19.1	22.0	24.7	27.2	29.7	32.0
Fraction F of showers	0.155	0.149	0.151	0.140	0.146	0.126	0.124	0.111	0.104	0.105	0.083	0.098

In general, the hodoscope pictures permitted a quite unambiguous distinction between the penetrating particles which traversed the apparatus without local production of penetrating secondaries, and those which originated groups of secondaries of considerable penetrating power. The first type of penetrating particles will be called the "non-interacting component," the latter the "interacting component." In order to be ranged among the interacting component, a penetrating particle had to be accompanied by secondaries which were observed at two consecutive levels, a and b, or b and c. Thus a penetrating power of the secondaries in excess of 100 g/cm², and in some cases in excess of 200 g/cm², was demanded, and hence the interacting component should include practically no electronic secondaries. This conclusion is born out in particular by the results of the experiment on local soft showers reported in the preceding paper. Local interactions apparent only at one level were ascribed to electronic secondaries of non-interacting penetrating particles. This interpretation was supported by the fact that they occur with about equal frequency at all three levels. It is possible that a small contribution of local penetrating showers initiated by N particles in the bottom absorber Σ_3 were included, but very few such particles should have escaped collisions in the upper layers Σ_1 and Σ_2.

II. RESULTS ON THE NON-INTERACTING COMPONENT

The pictures and records pertaining to the non-interacting component have been used to re-examine some of the properties of those particles. Evidence concerning the range distribution of the particles was the principal aim, but the zenith angle distribution had first to be studied before the ranges could be properly analyzed.

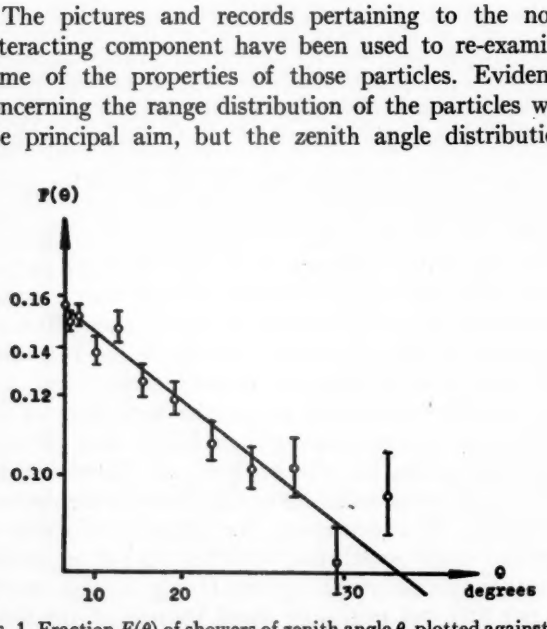

FIG. 1. Fraction $F(\theta)$ of showers of zenith angle θ, plotted against θ. The full line represents a distribution law $F(\theta) \propto \cos^{3.8}\theta$.

The frequency distribution of projected zenith angles θ was obtained from a total of 1592 single penetrating particles not accompanied by secondaries at any level. In evaluating it, correction has to be made for the geometrical bias of the arrangement which favors small zenith angles, and picks out a decreasingly small fraction of inclined particles. With 12 hodoscope counters at each level, one can define 12 zenith angle intervals and finds the distribution shown in Table I. (F is already corrected for the geometrical bias.) Plotting F against θ on a logarithmic scale, one obtains the curve depicted in Fig. 1. Unfortunately, the accuracy is rather low, but a distribution law of the form $N(\theta) \propto \cos^n\theta$ is in reasonable agreement with the experimental results for a value of $n=3.8\pm0.6$. The full curve of the graph represents this function. It is perhaps somewhat steeper than the $\cos^3$ law found by Brown and McKay;[4] the difference, if real, may be due to the fact that their statistics included all penetrating particles, and the present one only the non-interacting component.

The zenith angle distribution was needed to compute a correction that had to be applied in the evaluation of the range measurements, as the lowest tray did not cover the entire solid angle sustained by the master-pulse selecting trays A and B. If one calculates, with the angular distribution given above, the expected ratio of the flux through C to the flux through B in the absence of absorbers, one finds $N_C/N_B=0.74\pm0.03$. This was checked by a short run during which no absorber was placed between trays B and C, and coincidences $(1A+1C+3D)$ were recorded. The result was a ratio $N_C/N_B=0.81\pm0.1$. Therefore, the correction factor adopted was 0.76 ± 0.02.

Measurements were performed with three thicknesses of Σ_1: 170, 270, and 350 g/cm². During the first series of recordings, Σ_3 was 200 g/cm² throughout, and during the second 100 g/cm². The variation of Σ_3 has no influence on the master pulse; the over-all counting rates of the two runs are directly comparable. These are shown in Table II.

The last column gives the ratio of the recorded rates to that at top absorber thickness 170 g/cm² (total absorber thickness 280 g/cm²), which was chosen as reference in all further analyses. The slow variation of R/R_{170} indicates the high penetrating power of the non-interacting component.

More evidence can then be added from the hodoscope records of tray c. These are summarized in Table III. The columns "N_{ab}" give the total number of non-interacting particles which penetrate to at least tray

TABLE II. Rate of extensive penetrating showers as function of the top absorber thickness α_1.

Absorber thickness (g/cm²)	Showers recorded	Recording time (hr.)	Shower rate R (hr.$^{-1}$)	R/R_{170}
170	686	292.5	2.35±0.09	1.0
270	697	327.0	2.13±0.08	0.91±0.07
350	769	388.5	1.98±0.07	0.84±0.07

TABLE III. Number of particles penetrating at least to tray b (N_{ab}) and to tray c (N_{abc}) for different top absorber thicknesses Σ_1.

Absorber thickness (g/cm²)		$\Sigma_1=170$ g/cm²		$\Sigma_1=270$ g/cm²		$\Sigma_1=350$ g/cm²	
		N_{ab}	N_{abc}	N_{ab}	N_{abc}	N_{ab}	N_{abc}
Particles	$\Sigma_2=100$	438	309	452	310	479	316
Recorded	$\Sigma_2=200$	462	295	481	283	530	310

b, and those headed "N_{abc}" the number of particles recorded at c.

In order to use these figures for a determination of the range spectrum of the non-interacting component, the readings at the c tray have to be corrected for losses due to the smaller solid angle sustained by this tray. This was done with the correction factor given.

From the values shown in Table III, a differential range spectrum can be computed over the range intervals (in g/cm²) 280–400 and 280–500, 380–500 and 380–600, 460–580 and 460–680. Using the results of the shorter first interval of each group to subdivide the second, and combining the results of approximately equal range intervals, one can, with a slight adjustment of the interval limits, rearrange the data in four groups: 280–380, 380–480, 480–580, and 580–680 g/cm². The values of Table II furnish additional material, so that all intervals except the last are covered by at least two observations. This procedure, though of questionable correctness, appears to be adequate within the accuracy attainable in the present experiment. The results are presented in the graph of Fig. 2, in which the fraction of non-interacting particles absorbed in range intervals of 100 g/cm² is plotted against the range of the particle. As a second scale the momentum of the particle is shown, taken from the range-momentum curves of E. P. Gross under the assumption that the non-interacting penetrating particles are μ-mesons.

Figure 2 shows that the differential momentum spectrum of the penetrating shower particles in the region between about 450 to 900 Mev/c is rather flat. A very appreciable fraction, probably about 40 percent, of all particles of momentum exceeding the minimum penetration of 280 g/cm²≈450 Mev/c has a momentum of less than 1 Bev/c.

Finally, the frequency distribution of groups of non-interacting penetrating particles was registered. There was no significant variation with the absorber thickness Σ_1, the average over all three runs showing single particles in (75±2) percent of all showers; pairs of particles in (16.6±0.9) percent of all showers; triples in (6.3±0.5) percent of all showers; and larger groups in (2.2±0.3) percent of all showers; with an over-all average of (1.37±0.03) penetrating particles per shower.

III. RESULTS ON THE INTERACTING COMPONENT

A particle was called interacting if it was accompanied by at least one secondary at one hodoscope level a, b, or c, and by at least two secondaries at a neighboring level. Electron cascades would only be recorded as interacting if they contain still at least two charged particles under Σ_1 and Σ_2: an entirely negligible contribution. Triple knock-ons of non-interacting particles would be included, but amount to much less than 0.1 percent of the meson component, and this is less than the accuracy attainable in the present analysis. Therefore, one can be satisfied that practically all the particles classified as "interacting" belong to the N component, and that the "interaction" selected consisted in the ejection of at least one secondary capable of penetrating more than 100 g/cm² Pb (or, in part of the experiment, more than 200 g/cm² for local events originating in Σ_2), together with others of lower penetration.

The summary of the observations on interacting particles is given in Table IV. Local showers are subdivided into "Σ_1-showers"; that is, those originating in the top absorber Σ_1, and "Σ_2-showers" originating in the middle absorber Σ_2. One realizes that the arrangement will record Σ_1-showers initiated by both charged and neutral particles, but discriminates against neutral primaries of Σ_2-showers. Such events will be recorded only if a charged secondary, emitted backward, strikes one of the A counters. In general it is possible to distinguish between the two different events; in the present analysis of 33 Σ_2-showers 23 were clearly recognized as produced by charged N particles, and six as due to neutral particles, with only four classified as uncertain. As these "uncertain" showers cannot be disregarded in the following statistical analysis, they were assigned to the two groups in, as near as possible,

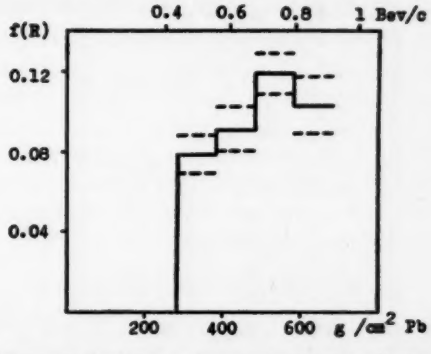

FIG. 2. Fraction f(R) of non-interacting penetrating particles of range between R and (R+100) g/cm² Pb. The dotted lines indicate the probable errors. [*Note added in proof:* Through an unfortunate mistake the dotted lines in Fig. 2 do not show the correct relative errors. The true errors are larger; the values of $f(R)$ in the four intervals are: 7.8±4.8, 9.1±2.4, 11.9±2.3, 10.3±2.0.]

TABLE IV. Rate of local penetrating showers produced by "interacting" penetrating air-shower particles in the top absorber (Σ_1-showers) and in the middle absorber (Σ_2-showers).

Σ_1 (g/cm²)	Time (hr.)	Σ_1-showers Number	Σ_1-showers Rate/hr.	Σ_2-showers Number	Σ_2-showers Rate/hr.
170	280.5	90	0.321±0.033	12(15)	0.043±0.012
270	324.0	139	0.428±0.036	8(11)	0.025±0.018
350	373.0	172	0.462±0.036	6(7)	0.016±0.006

the frequency ratio of the identified showers. This brings the total of neutral primaries to seven against 26 charged particles, and increases the experimental uncertainties somewhat beyond the statistical errors. In column 5 of Table IV, the first figures refer to the number of Σ_2-showers initiated by charged N particles, and those in brackets are the total of all observed Σ_2-showers

It should be noted that the Σ_2-showers of the air shower experiment are related to the events (LPS+E) of the preceding report[4] on local showers. These events are included in the Σ_2-showers; they required at least three penetrating shower particles, while in the selection of Σ_2-showers only two such particles were demanded, plus one of less penetration. Consequently, the rates R_{Σ_2} are considerably higher than those of the events (LPS+E). But even with the less stringent selection the flux of N particles in air showers is obviously much smaller than that of the shower-producing particles not accompanied by an extensive shower. If we exclude primary electrons as the source of air showers, it would then follow that only a small fraction of those primaries which initiate nucleonic showers will simultaneously give origin to electronic showers of the density recorded in this arrangement. The process in which, directly or indirectly, electrons are released in nuclear collisions (including radiation) must either be infrequent for all energies, or be more or less confined to very high primary energies.

The rate R_{Σ_1} of Σ_1-showers can be used immediately for a determination of the flux R_N of N particles in the extensive showers, and of the collision mean free path λ of those particles. It is assumed that the efficiency of the apparatus for recording an interaction with at least one penetrating secondary is practically unity; this assumption is supported strongly by the evidence of the hodoscope records, which show in general too high a multiplicity of the events to make a miss likely. If one then tries to fit the experimental rates to the expression one obtains for the shower rate under the assumption of a uniform collision mean free path:

$$R_{\Sigma_1}=R_N[1-\exp(-\Sigma_1/\lambda)]$$

with the least deviation, one finds $R_N=(0.59\pm0.03)$ hr.$^{-1}$, and $\lambda=(220\pm30)$ g/cm². The results are reproduced in Fig. 3: the observed shower rates by circles and the rates calculated with the values quoted above by the full curve.

In a similar way, one can derive, though rather inaccurately, a value for the flux R_p of charged N particles from the rates of Σ_2-showers. This quantity should be obtained from R_{Σ_2} by using the expression:

$$R_{\Sigma_2}=R_p\exp(-\Sigma_1/\lambda)\cdot[1-\exp(-\Sigma_2/\lambda)].$$

Taking the three values of Table IV, one has an average of $R_p=(0.234\pm0.05)$ hr.$^{-1}$, or very nearly one-half of the value for the entire N component.

The main interest is then in a comparison of these rates with the rate of μ-mesons in extensive showers, measured in the flux of non-interacting particles. Several corrections have to be applied to the data given in the preceding section, in order to avoid a number of possible systematical errors. First of all, the number of "non-interacting" showers is not equal to the number of non-interacting particles, and the same is true for the "interacting" showers. In the former case, we have found about 1.4 penetrating particles per shower. In the latter, a precise analysis of the density distribution of interacting particles is not possible. Whenever several N particles hit the absorber, the resulting shower is so dense that it defies attempts to trace individual particles. An exception is the run with the smallest top absorber thickness, $\Sigma_1=170$ g/cm², where one has a reasonable certainty of distinguishing pairs or groups of incident particles from single primaries. Of the 90 analyzed Σ_1-showers, 62 were clearly recognized as due to events in which only one penetrating particle struck the absorber, while in 10 cases the shower primary was accompanied by another penetrating particle, and 18 showers were too complex for an identification. Thus, it appears that the density distribution of the N particles does not differ very markedly from that of the meson component, and the rates of "interacting" and "non-interacting" showers can be taken as measure of the relative frequency of the two components.†

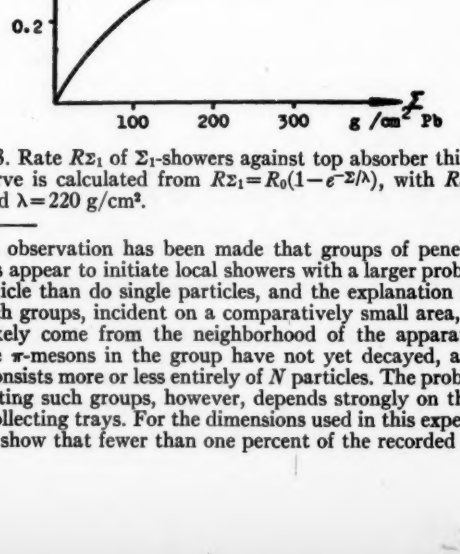

FIG. 3. Rate R_{Σ_1} of Σ_1-showers against top absorber thickness. The curve is calculated from $R_{\Sigma_1}=R_0(1-\epsilon^{-\Sigma/\lambda})$, with $R_0=0.59$ hr.$^{-1}$ and $\lambda=220$ g/cm².

† The observation has been made that groups of penetrating particles appear to initiate local showers with a larger probability per particle than do single particles, and the explanation offered that such groups, incident on a comparatively small area, would most likely come from the neighborhood of the apparatus, so that the π-mesons in the group have not yet decayed, and the group consists more or less entirely of N particles. The probability of detecting such groups, however, depends strongly on the area of the collecting trays. For the dimensions used in this experiment one can show that fewer than one percent of the recorded events

A second correction of the flux of non-interacting particles comes from the fact that some of the N particles will escape collisions in both Σ_1 and Σ_2, and hence be classified as non-interacting. Their contribution can be calculated, with the rates and the collision mean free path given above, and subtracted from the the observed flux. It may be added that the correction is much too small to make the systematical error, introduced in the range distribution of Fig. 2 by the inclusion of these particles, comparable with the statistical errors.

Third, some mesons will arrive in groups containing N particles, and are excluded if the meson flux is computed from the rate of "non-interacting" showers only. Again this correction can be calculated if one assumes the same density distribution of both components; it turns out to be small, but not negligible.

The standard of comparison used in the following discussion is the μ-meson flux under the minimum penetration condition imposed in this experiment, that is under a total of 280 g/cm² or about 10 in. Pb. With all three corrections applied, this flux is 2.23 ± 0.09 hr.$^{-1}$, and from this one obtains for the ratio of the total N component to the μ-meson component:

$$N_N/N_\mu=0.26\pm0.03,$$

and for the ratio of the charged N component to the μ-meson component:

$$N_P/N_\mu=0.105\pm0.022.$$

It is interesting to note that this ratio is more than 10 times larger than that of the primary flux at 700 g/cm², computed from the incident flux with the help of Tinlot's[5] absorption thickness, to the μ-meson flux at the same altitude. Even if a somewhat slower absorption of the N component recorded in this experiment were assumed, as the interactions selected were not very energetic (see Rossi[6]), the difference would remain significant. In other words: If one defines an "average multiplicity of meson production" as the ratio of the total μ-meson flux, that is, the sea-level flux corrected for decay while traversing the atmosphere, to the flux of cosmic-ray primaries, one obtains a value of about 0.1. If one defines, similarily, an average multiplicity of meson production in showers as the ratio of μ-meson flux to the flux of the N component, both re-projected to a producing layer near the top of the atmosphere, he finds a much lower value. This indicates that most collisions of nucleons of moderate energies will result in the ejection of a small number of nucleonic secondaries of moderate penetration, without the production of meson secondaries. Alternatively, one might conclude that the bulk of the showers is produced not near the top of the atmosphere, but at much lower altitudes.

Mention has already been made repeatedly of the frequent complexity of local showers in dense absorbers. This undoubtedly demonstrates the occurrence of "cascades" of nuclear collisions, already well-known from cloud-chamber pictures. While a complete analysis of such entangled events is not possible from a hodoscope picture, some conclusions can be drawn from a statistical analysis based on the records of the numbers of counters struck under a certain absorber thickness. This method faces a serious objection: The number of counters struck is, in a dense shower, certainly not equal to the number of particles present, and this second quantity is the one which should be discussed. Moreover, a method of deducing the latter number from the first cannot be worked out unless the spacial distribution of secondaries in the shower is known. However, the correction will be small if the particle density is not too high, while for very large densities, which in general will occur only if several local events contribute, the resulting distribution cannot be far from random. Hence one can expect that the observed numbers, corrected under the assumption of random distribution of the shower particles, will for all densities deviate very little from the true numbers. Writing $P(m, n, N)$ for the probability that a shower of m particles discharges n out of a tray of N counters, one has then

$$P(m, n, N)=\binom{N}{n}\cdot p^n\cdot(1-p)^{N-n},$$

where p is the probability that one counter is discharged. From this, the average number $\langle n\rangle$ of counters struck can be calculated as a function of m, and by comparison with the experimental values the most probable number $\langle m\rangle$ of particles present can be evaluated. The results are given in Table V. In computing the number of

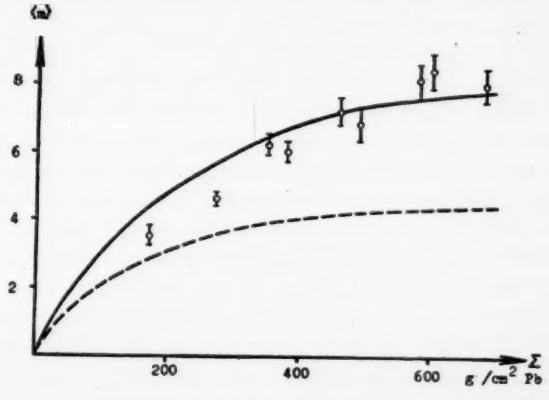

FIG. 4. Average number $\langle m\rangle$ of particles in all Σ-showers against absorber thickness. The full curve represents exponential increase with $\lambda=220$ g/cm², normalized to optimum agreement at large thicknesses. The dotted curve represents the same exponential law, with an asymptotic value $m_0=4.7$.

is due to groups of N particles. This is considerably less than the number of groups of three or more particles of unrelated origin which one would expect in dense showers, or the number of groups due to density fluctuations. It might, though, be that at least some of the disputed "narrow showers" [see J. Wei and C. G. Montgomery, Phys. Rev. **76**, 1488 (1949)] with their peculiar features are indeed such groups of N particles.

[5] J. Tinlot, Phys. Rev. **73**, 1476 (1948); **74**, 1197 (1949).

[6] B. Rossi, M.I.T. Technical Report No. 26 (April 4, 1949).

TABLE V. Average number $\langle m \rangle$ of particles observed in local showers produced by the "interacting" component, as function of the absorber thickness. $\langle m \rangle$ is calculated from the number $\langle n \rangle$ of counters struck under the assumption of random distribution.

Absorber thickness (g/cm²)	170	270	350	380	460	490	580	600	680
Number $\langle m \rangle$ of shower particles	3.5±0.3	4.6±0.2	6.2±0.3	6.0±0.3	7.2±0.4	6.8±0.5	8.1±0.5	8.4±0.5	8.0±0.5

particles hitting the lowest tray, a further correction for the reduced solid angle has been made, using the same efficiency factor as in the range determination of the preceding section.

The results are again represented in the graph of Fig. 4 in which the average number of shower particles ejected in collisions of the interacting component is plotted against the absorber thickness traversed. Evidently, if after the first collision no further "cascade" multiplication occurs, the average number of particles observed under an absorber of thickness Σ is

$$\langle m \rangle = m_0(1-e^{-\Sigma/\lambda})$$

(m_0 = number of particles emitted per collision). The same law holds even if further multiplication does occur, but with a mean free path much larger than that for the first collision. Other, more complex, formulas can be derived if secondary and higher interactions follow the first with a comparable mean free path, and equal or different multiplicities, but it would require a much higher accuracy than that attained in the present experiment for precise quantitative conclusions to be deduced in this way. Only one general feature of such "cascades" should be kept in mind: If absorption is neglected, the number of particles after two steps should approach a saturation value $\langle m \rangle = m_0 \cdot n_0$, if m_0 and n_0 are the multiplicities of the first and second collision.

The full curve in Fig. 4 shows an attempt at representing the measured particle densities by a single exponential increase with the previously determined value of $\lambda = 220$ g/cm², normalized so as to give optimum agreement at larger thicknesses. The dotted curve is calculated with an initial multiplicity $m_0 = 4.7$, the average value observed for unaccompanied local showers of similar penetration. In both cases the disagreement is obvious. The observed numbers increase to values which are extremely unlikely for events of rather low energy, and not at all according to a single exponential law. The conclusion appears inevitable that further multiplication does take place, and with a mean free path of the same order as that of the first step; certainly much smaller than 500 to 600 g/cm², as for still thicker absorbers little, if any, additional shower production occurs. Furthermore, it appears likely that the multiplicity in the later steps is smaller than in the first: $m \cdot n \gtrsim 8$, while probably $m \sim 4$. It may, of course, be that not all of the secondaries are capable of further multiplication; a feature which could also explain the discrepancy between the larger values, about 750 g/cm², of the mean free path of secondaries obtained from cloud-chamber data (e.g., Fretter[7]) and the present estimates. One cannot safely draw more than the qualitative conclusion that whatever "cascade" multiplication of nuclear collisions occurs will be characterized by a collision mean free path which does not vary appreciably throughout the cascade development.

IV. SUMMARY

The hodoscope technique has been found to be a convenient method for distinguishing between "interacting" and "non-interacting" penetrating particles in air showers. The latter component, at least in the bulk μ-mesons, has a rather flat range distribution in the energy interval between 350 and 800 Mev, with about 40 percent of all particles having energies below 1 Bev. The zenith angle distribution of the non-interacting component follows approximately a law of the form $\cos^n\theta$ with $n = 3.8 \pm 0.6$. For those of the "interacting" particles which originate showers of at least three secondaries at two consecutive levels (showers which strike at least five hodoscope counters) a collision mean free path of (220±30) g/cm² is found. Further nuclear collisions occur with apparently not much changed mean free path, but possibly fewer secondaries, if all or most of the particles ejected in the first collision contribute to the developing "cascade" of nuclear events. From the observed flux of non-interacting particles, $R_\mu = (2.23 \pm 0.09)$ hr.$^{-1}$, the flux of all interacting particles, $R_N = (0.59 \pm 0.03)$ hr.$^{-1}$ and the flux of charged interacting particles, $R_p = (0.23 \pm 0.05)$ hr.$^{-1}$, one computes that in air showers, at 3260-m altitude, there are about four μ-mesons present for each N particle, or about 10 μ-mesons per charged N particle. This is considerably less than the ratio of single μ-mesons to shower-producing nucleons at the same altitude, suggesting that N particles of moderate energies would in general still be capable of ejecting "knock-on protons" in nuclear collisions, while no longer producing mesons.

In conclusion the author wishes to thank the Inter-University High Altitude Laboratories, and particularly Drs. Cohn and Iona of the University of Denver, for the permission to use the facilities at Echo Lake Laboratories.

[7] W. B. Fretter, Phys. Rev. **76**, 511 (1949).

The Maximum Range of High Energy Electrons in Aluminum and Copper*

FRANK L. HEREFORD
Rouss Physical Laboratory, University of Virginia, Charlottesville, Virginia
AND
CHARLES P. SWANN
Bartol Research Foundation of the Franklin Institute, Swarthmore, Pennsylvania
(Received January 20, 1950)

The practical maximum range of monoenergetic electrons in aluminum and copper has been measured in the region of energy from 3 to 12 Mev. The magnetically analyzed beta-ray spectrum of B^{12} was employed, range values being determined from absorption curves obtained with a triple coincidence counter train. The values so obtained fall below a semi-empirically computed curve normalized with experimental data in the region of electron energy below 3 Mev. It is shown that the discrepancy can be explained if the influence of multiple scattering effects in the absorber is considered. On this basis the data indicate that the difference between the "absolute maximum range" and the "practical maximum range" increases with electron energy.

INTRODUCTION

THE experimental data concerning the maximum range of electrons in matter have been summarized by various workers in an attempt to establish an accurate empirical relationship between range and energy.[1-3] Until recently the only available measurements were in the region of energy below 3 Mev. The most complete treatment of these data is that of Bleuler and Zünti[2] who determine a semi-empirical curve valid in the low energy region ($E<3$ Mev). With regard to a beam of monoenergetic electrons they distinguish between the *absolute maximum range*, R_0, and the *practical maximum range*, R_p, which is the most conveniently measurable quantity in experiment. The absorption curves of monoenergetic electron beams (Fig. 3) in which thicknesses are measured relative to R_p indicate the significance of this quantity; it is best determined by extrapolation of the linear portion of the absorption curve through zero intensity. The *absolute maximum range*, R_0, lies to the right of this point and represents the maximum thickness penetrated by the few electrons which suffer no scattering or straggling in the absorber. It should be noted that neither of these quantities can be identified immediately with the end-point ranges of beta-spectra where a distribution of energies is involved. Part I of this paper concerns the results of an experimental investigation of R_p in the region of energy above 3 Mev; the results are interpreted in Part II where it is shown that multiple scattering effects can account for the discrepancy between the data and previously computed values of R_p.

PART I

A series of measurements of R_p in aluminum and copper in the region of energy from 3 to 12 Mev was undertaken with monoenergetic electrons and a triple coincidence counter train. The source of electrons employed was the beta-spectrum of B^{12} (produced through the $B^{11}(d,p)B^{12}$ reaction) magnetically analyzed to provide a beam homogeneous in energy. The geometrical arrangement of the counters relative to the 90 degree magnet employed is indicated in Fig. 1. A target of B_2O_3 was placed in the chamber of the Bartlo Van de Graaff machine at approximately the upper focal point of the magnet, the deuteron beam being focused at this point. After traversal of the magnet chamber the analyzed electron beam emerged through a 0.04-g/cm² aluminum window to impinge upon the counters and absorbers.

In order to check the calibration of the magnet the momentum distribution of the B^{12} beta-spectrum was investigated. Comparison of the curve obtained with that of Hornyak, *et al.*[4] is shown in Fig. 2. It is seen that a Kurie plot of the data yields an end point at 27.3 m_0c^2 (13.4 Mev) in good agreement with their value, which fact is gratifying verification of the magnet calibration employed here.

In obtaining the absorption curves of the beam, double coincidences (1, 2) and triple coincidences (1, 2, 3) were recorded simultaneously with two scalers. The beam intensity penetrating each absorber thickness was taken as the triple coincidence rate relative to the

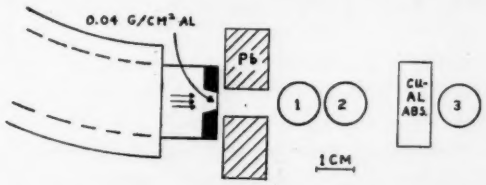

FIG. 1. The arrangement of counters and absorber relative to the magnetic analyzer. The deuteron beam was focused upon a B_2O_3 target at the upper focal point of the magnet (not shown). The analyzed beta-ray beam emerged from the bending chamber as indicated.

* The experiments reported in Part I were carried out at the Bartol Research Foundation under the joint program of the ONR and AEC; the analysis and computation in Part II at the University of Virginia.

[1] N. Feather, Proc. Camb. Phil. Soc. **34**, 599 (1938).
[2] E. Bleuler and W. Zünti, Helv. Phys. Acta **19**, 376 (1946).
[3] L. E. Glendenin, Nucleonics **2**, No. 1, 12 (1948).
[4] Hornyak, Dougherty, and Lauritsen, Phys. Rev. **74**, 1727 (1948).

double, the latter rate monitoring the beam intensity hitting the absorber. By means of this scheme the aluminum absorption curves of Fig. 3 were obtained. In order to avoid confusion, no correlation is indicated between the individual points and the electron energy to which they refer. The high statistical accuracy of the counting rates and the careful determination of the various absorber thicknesses lead to an estimated probable error in each value of R_p of ± 0.1 g/cm^2. The curves shown are corrected for counter wall and window thicknesses. The copper absorption curves which were very similar to those in Fig. 3 are not shown.

The similarity of the shapes of these curves to that predicted through semi-empirical calculation[5] is striking. At first glance the close grouping of the points beyond R_p illustrated in the insert in Fig. 3 seems to indicate that the "tails" of the curves are identical and, hence, that the difference, R_0-R_p, is independent of energy, in agreement with the assumption of Bleuler and Zünti. However, the fact that the statistical inaccuracy of these points is somewhat larger than for those measuring greater intensities lends uncertainty to this conclusion.

Values of R_p have been plotted against the corresponding electron energies in Fig. 4. The dotted curve shown was obtained from the semi-empirical expression for R_p given by Fowler *et al.*[5] This expression was derived through integration of the theoretical energy loss due to ionizing collisions, normalizing the range values so computed with an experimental value at 2.96 Mev. The possible influence of multiple scattering effects on the difference, R_0-R_p, was not considered. The solid lines shown in Fig. 4 were not drawn through the experimental points, but were computed as outlined in Part II. Two striking features of the results are: (1) the discrepancy between the experimental and computed values of R_p for aluminum above the normalization point (2.96 Mev); (2) the fact that the values of R_p for copper lie below those for aluminum. The latter is in disagreement with the relative ranges in copper and aluminum expected on the basis of ionization energy loss alone. Among the immediately evident factors bearing on this point are the increased probabilities of radiative collisions and of Coulomb scattering in copper. The influence of these real effects on the results obtained will be discussed in Part II.

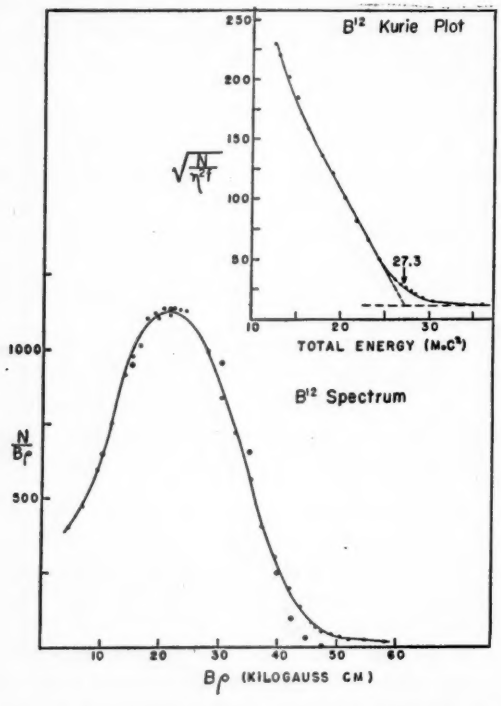

FIG. 2. The momentum distribution of the B^{12} beta-ray spectrum. Open circles are points taken from the curve of Hornyak *et al.* (reference 4). The insert shows a Kurie plot near the end point.

The possible introduction of errors caused by several experimental difficulties, however, requires attention here. First, it is noted that the measured values of R_p are characterized by the background rate present, the counter geometry employed, and various other factors upon which R_p is heavily dependent. In particular at higher energies R_p is determined by a smaller fraction of the incident beam than at lower energies; hence, the influence of the background rate becomes more important. It is difficult to assess the magnitude of this effect. However, within the limits of accuracy of the observed counting rates beyond R_p($\sim\pm 8$ percent), there does not appear to be a sufficient change in the shape of the absorption curves to cause the difference between the computed and measured values of R_p.

Another possible source of experimental error is that arising from the finite resolution or window of the magnet (estimated to be four percent). Beyond the maximum of the momentum distribution (Fig. 2) the steepness of the curve might give rise to an excess of beta-rays of energy below the window midpoint over those of energy above. In the neighborhood of 10 Mev an error of 11 percent in the electron energy would be required to bring the experimental and computed values into agreement, while on the basis of the resolution estimated from geometrical considerations and subsidiary experiments, it does not seem that the average energy could differ from the window midpoint by more than two percent at the most.

It must be emphasized finally that the values of R_p reported herein can only be used in a meaningful way when proper attention is given to the geometry of the detection system. Apparent absorption due to scattering of the particles out of the solid angle subtended by the counters renders R_p sensitive to the separation and size of the counters employed. The range-energy curves given serve only as an experimental definition of R_p for the particular geometry described and for a monoenergetic source of electrons.

[5] Fowler, Lauritsen, and Lauritsen, Rev. Mod. Phys. **20**, 237 (1948).

PART II

In view of the disposal of the possibility of accounting for the discrepancy between the observed and computed values of R_p through the influence of experimental errors, the computation of R_p has been re-examined with regard to possible modes of range reduction in addition to ionization losses. The importance of losses increasing strongly with atomic number is evident from consideration of the relative range values observed in copper and aluminum. Contrary to expectation from ionization loss consideration, the values for copper fall below those for aluminum. Immediately obvious effects which might contribute to this state of affairs are reductions of R_p by radiative collisions and multiple scattering.

It seems very unlikely that radiative collisions could influence appreciably the value of any quantity approximating a maximum range in the region of energy involved here. The energies concerned are considerably less than the critical energies (52 Mev for aluminum, 22.4 Mev for copper), the absorber thicknesses small fractions of the radiation lengths (26.3 g/cm² for aluminum, 13.3 g/cm² for copper). Furthermore, as has been pointed out by various other workers, radiation losses generally appear as large losses by a few particles rather than small losses by many. Hence, the fraction of an incident beam penetrating to a depth approaching the maximum penetration depth should not be effected.

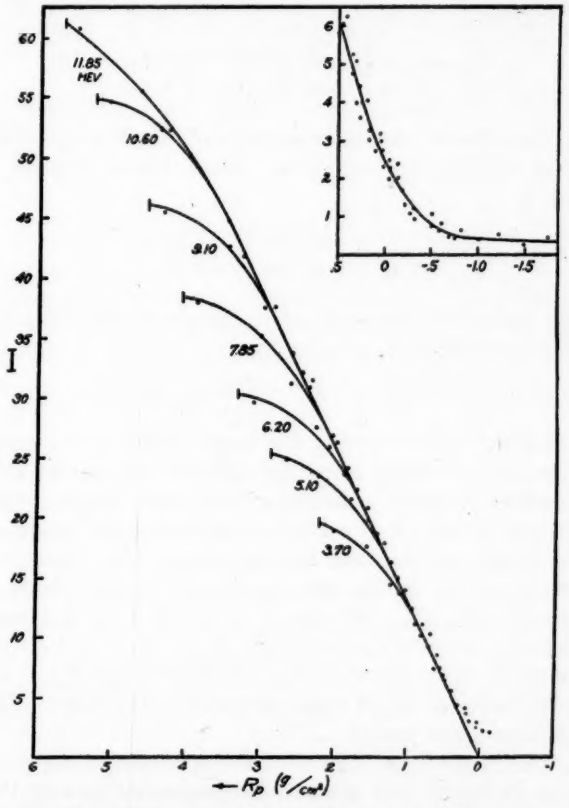

FIG. 3. Aluminum absorption curves for various electron energies. The curves are normalized at the "practical maximum range," R_p. Intensity units are arbitrary. The insert shows the end point region on an expanded scale.

On the other hand, no such arguments are valid as regards multiple scattering. It is normally assumed that R_p as well as the absolute maximum range, R_0, is determined by a small number of the incident electrons which have not experienced scattering in the absorber. Hence, the measured absorber thickness is identified with the trajectories of the electrons reaching both R_p and R_0. In accordance with this, the difference, R_0-R_p, is considered to be a constant characterizing in some way the shape of the absorption curve near the end point. The screening of the nuclear field by the orbital electrons imposes a minimum value on the possible scattering angles in single collisions,[6] a minimum which decreases with increasing energy of the incident electron (decreasing de Broglie wave-length). This fact might be interpreted as allowing the constancy of R_0-R_p. Such is not the case here; we are concerned with the superposition of many such small deviations which can result in any finite angle when averaged over the total path. Thus while the equivalence of trajectory and thickness holds for those few electrons reaching R_0, it cannot hold absolutely for those reaching only R_p. The difference between R_p and the trajectory length, R_0, then will be considered to be due to multiple scattering in the absorber. On this basis it would be expected to increase with increasing absorber thickness and hence with electron energy.

It is possible to take into account the effect of multiple scattering in computation of R_p by means of the semi-empirical method to follow.

We adopt g/cm² as units of range and employ the units and notation of Rossi and Greisen.[7] The absorber thickness, $R_p(E)$, expressing the practical maximum range of an electron of energy E is assumed to be less than the trajectory length, $x(E)$, by an amount characterized by the multiple scattering of those electrons reaching $R_p(E)$. We will compute $R_p(E)$ in terms of a standard value $R_{p0}=R_p(E_0)$ and a standard trajectory length, $x_0=x(E_0)$, as follows:

$$R_p(E)=R_{p0}=\{x(E)-x_0\}\cos\bar{\theta}$$

or, since the deflections are small,

$$R_p(E)-R_{p0}=\{x(E)-x_0\}\{1-\bar{\theta}^2/2\}. \qquad (1)$$

The quantity $\bar{\theta}^2$ is some mean-square angle of scattering suffered by those electrons which reach R_p in traversing the thickness, R_p-R_{p0} (i.e., in traveling the distance along the trajectory given by $x-x_0$). It is assumed that $\bar{\theta}^2$ is proportional to the mean-square angle of scattering of *all* electrons in a beam traversing $x-x_0$,

$$\bar{\theta}^2=\alpha\langle\theta^2\rangle_{Av(x-x_0)}=\alpha\frac{E_s^2}{X_0}\int_{x_0}^{x}\frac{dx}{p^2\beta^2}. \qquad (2)$$

The expression for the mean-square angle of scattering

[6] E. J. Williams, Proc. Roy. Soc. **169**, 531 (1939).

here is that given by Rossi and Greisen.[7] E_s is a constant (21 Mev), X_0 is the radiation length in g/cm², and α is a constant to be determined.

The quantity $x(E)-x_0$ can be computed following Fowler *et al.*[5] by integration of the theoretical energy loss.

$$x(E)-x_0=\int_{E_0}^{E}\frac{dE}{(dE/dx)_{\text{ion}}}. \tag{3}$$

We choose E_0 sufficiently large to render valid the extreme relativistic (E.R.) approximation to $(dE/dx)_{\text{ion}}$ given by Heitler,[8] *viz.*,

$$(dE/dx)_{\text{ion}}=\xi\ln(\gamma M),$$

where, $W=$ total energy in Mev,

$$\xi=6C\mu_e=\begin{cases}0.22\text{ Mev cm}^2/\text{g, for aluminum,}\\ 0.21\text{ Mev cm}^2/\text{g, for copper,}\end{cases}$$

$$\gamma=[2\mu_e I_0^2(Z)]^{-1}=\begin{cases}316\text{ Mev, for aluminum,}\\ 187\text{ Mev, for copper.}\end{cases}$$

We have then for Eq. (3),

$$x(E)-x_0=(1/\xi)\int_{W_0}^{W}dW/\ln(\gamma W). \tag{4}$$

In view of the choice of E_0 and hence of W_0 in the relativistic region, Eq. (2) may be rewritten by a change of variable, using $W^2=p^2+\mu_e^2$, and approximated as,

$$\bar{\theta}^2=\alpha\frac{E_s^2}{X_0}\int_{W_0}^{W}\frac{dW}{\beta^2(W^2-\mu_e^2)(dE/dx)_{\text{ion}}}$$
$$\approx\alpha\frac{E_s^2}{X_0\xi}\int_{W_0}^{W}\frac{dW}{W^2\ln(\gamma W)}. \tag{5}$$

The integrals in Eqs. (4) and (5) can now be evaluated in terms of the exponential integrals of positive and negative argument[9] through introduction of $y=\ln(\gamma W)$ leading to the results

$$x-x_0=(1/\xi\gamma)[Ei(\ln\gamma W)-Ei(\ln\gamma W_0)],$$
$$\bar{\theta}^2=\alpha(E_s^2\gamma/X_0\xi)[Ei(-\ln\gamma W)-Ei(-\ln\gamma W_0)].$$

With reference to Eq. (1) we have,

$$R_p(E)-R_{p0}=(1/\xi\gamma)[Ei(\ln\gamma W)-Ei(\ln\gamma W_0)]$$
$$\times[1-\alpha k\{Ei(-\ln\gamma W)-Ei(-\ln\gamma W_0)\}], \tag{6}$$

where k has been written for $E_s^2\gamma/\xi X_0$.

We now choose two experimental points on the R_p *vs.* E curve, the first as the standard range R_{p0}, the second to allow evaluation of the constant α. Following the summary of Bleuler and Zünti,[2] we take for aluminum,

$$R_{p0}=0.70\text{ g/cm}^2,\text{ for }W=2.04\text{ Mev},$$
$$R_{p1}=0.16\text{ g/cm}^2,\text{ for }W=3.48\text{ Mev}.$$

In the absence of experimental data in the region of lower energies for copper we choose two points from Fig. 4,

$$R_{p0}=1.92\text{ g/cm}^2,\text{ for }W=4.30\text{ Mev},$$
$$R_{p1}=3.12\text{ g/cm}^2,\text{ for }W=6.96\text{ Mev}.$$

The values of the constant α characterizing the particular values of R_{p0} chosen are,

$$\alpha=0.072,\text{ for Al},\quad \alpha=0.26,\text{ for Cu}.$$

It should be noted that the large difference between these values stems from the different choices of the standard range R_{p0} for aluminum and copper. The integral in Eq. (5) is evaluated over a smaller range of energy for copper than for aluminum. The trajectory length, $x-x_0$, is consequently smaller which yields a smaller $\langle\theta^2\rangle_{Av(x-x_0)}$ for copper of which θ^2 is a larger fraction. Introduction of these quantities into Eq. (6) yields $R_p(E)$ in terms of the standard range R_{p0}. The solid curves of Fig. 4 were computed in this fashion for aluminum and copper.

The computation described is empirical to the extent that its importance lies only in demonstration that the dependence of scattering probabilities on electron energy is such as to bring the computed range *vs.* energy curve into agreement with experimental points. The results

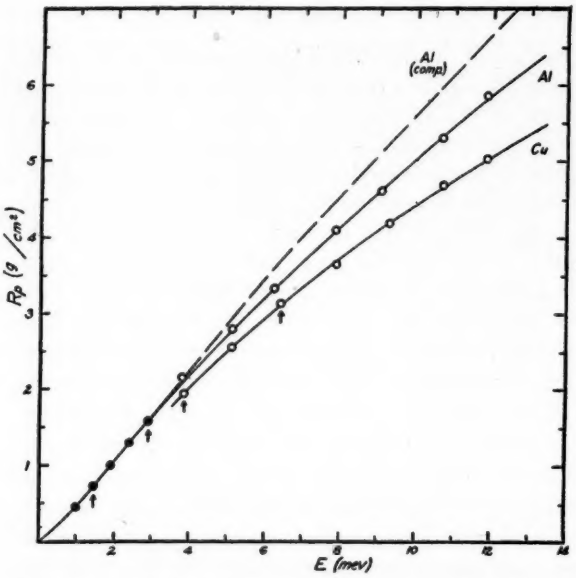

FIG. 4. Values of R_p plotted against corresponding electron energies are represented by open circles. The dotted line was plotted from the calculations of Fowler *et al.* (reference 5). Solid lines were computed by the method described in Part II of this paper. Solid points are from the summary of Bleuler and Zünti (reference 2). The arrows indicate the normalization points, R_{p0} and R_{p1} (see text).

[7] B. Rossi and K. Greisen, Rev. Mod. Phys. **13**, 240 (1941).
[8] W. Heitler, *The Quantum Theory of Radiation* (Oxford University Press, London, 1936), p. 220.
[9] These functions are tabulated in the range of values pertinent here in *Tables of Sine, Cosine, and Exponential Integrals* (Work Projects Administration, New York, 1940), Vol. II.

reported in Part I are thereby seen to be consistent with the theoretical ionization loss in the region of energy involved. It is possible to find a multiplicative correction term of the form, $1-(E-E_0)$, which yields very nearly as satisfactory agreement with data as does Eq. (6). Such a correction, however, would be purely empirical, whereas that of Eq. (6) was obtained through consideration of the actual reduction in R_p expected on the basis of elastic scattering theory. The important point is that the measurement of electron range (and, hence, of energy) by extrapolation of the absorption curve to zero intensity yields approximate values, the error in which increases with electron energy.

The authors are indebted to Dr. W. A. Fowler of the California Institute of Technology for helpful comments regarding possible experimental errors and to Dr. W. F. G. Swann, director of the Bartol Research Foundation, for his interest and frequent advice.

PHYSICAL REVIEW VOLUME 78, NUMBER 6 JUNE 15, 1950

Remarks on the Magnetic Scattering of Neutrons*

H. EKSTEIN
Armour Research Foundation of Illinois Institute of Technology, Chicago, Illinois
(Received January 26, 1950)

The formal calculation of the scattering of neutrons by a magnetized atom leads to a result which is ambiguous in the forward direction. It is shown that, if this singularity is correctly taken into account, apparent discrepancies between macroscopic and atomistic calculations are eliminated.

FOR the calculation of the refractive index of a neutron wave in a ferromagnetic crystal, two different methods have been used with different results.[1-3] The following remarks attempt to explain this discrepancy.

I.

According to Schwinger[4] the amplitude of a neutron beam of spin state χ_0 scattered elastically by an ion of magnetic moment $\mathbf{m}$ is

$$\psi_{sc}\sim\frac{m\exp(ik_0R)}{2\pi\hbar^2R}\cdot 4\pi\mu\mathbf{s}\cdot\left(\frac{\mathbf{q}(\mathbf{q}\cdot\mathbf{m})}{q^2}-\mathbf{m}\right)\chi_0, \quad (1)$$

where $\mathbf{q}=\mathbf{k}_0-\mathbf{k}$ is the difference between the propagation vectors of the incident and scattered waves, and the other symbols have their usual meanings. This expression has a singularity at the point $\mathbf{k}_0-\mathbf{k}=\mathbf{q}=0$. Consider the case where $\mathbf{m}\|\mathbf{q}$. If the point $\mathbf{q}=0$ is approached on a sphere $\mathbf{k}^2=\mathbf{k}_0^2$, the first term in the bracket vanishes. If this point is approached along a line $\mathbf{k}\|\mathbf{k}_0$, ψ_{sc} vanishes, so that the forward scattering is ambiguous in this case.

To find the forward scattering unambiguously, we consider the more general expression for the Born approximation

$$\psi_{sc}=\frac{-\mu m\cdot 4\pi\mathbf{s}}{2\pi\hbar^2}\cdot\int\frac{\exp[ik_0|\mathbf{R}-\mathbf{r}|]}{|\mathbf{R}-\mathbf{r}|}\mathbf{B}(\mathbf{r})\times\exp[i\mathbf{k}_0\cdot\mathbf{r}]\chi_0 d\mathbf{r} \quad (2)$$

valid for finite distances $\mathbf{R}$ from the nucleus. $\mathbf{B}(\mathbf{r})$ is the magnetic field of the ion. In momentum space, Eq. (2) is

$$\psi_{sc}=\frac{-\mu m\cdot 4\pi\mathbf{s}}{2\pi^2\cdot 2\pi\hbar^2}\cdot\lim_{\delta\to 0}\int\frac{\exp(i\mathbf{p}\cdot\mathbf{R})}{p^2-(k_0+i\delta)^2}\mathbf{b}(\mathbf{k}_0-\mathbf{p})d\mathbf{p}\cdot\chi_0, \quad (3)$$

where

$$\mathbf{b}(\mathbf{q})=\int\exp(i\mathbf{q}\cdot\mathbf{r})\mathbf{B}(\mathbf{r})d\mathbf{r}=4\pi\left(\frac{-\mathbf{q}(\mathbf{q}\cdot\mathbf{m})}{q^2}+\mathbf{m}\right). \quad (4)$$

Equation (3) can be verified by substituting Eq. (4) and integrating with respect to $\mathbf{p}$. In evaluating Eq. (3) for large distances $|R|$ ($\mathbf{R}\|\mathbf{k}_0$) care must be used because of the singularity at $\mathbf{p}=\mathbf{k}_0$. The series expansion

$$\int\frac{\exp(i\mathbf{p}\cdot\mathbf{R})}{p^2-(k_0+i\delta)^2}\mathbf{b}(\mathbf{k}_0-\mathbf{p})d\mathbf{p}$$

$$=\int_0^\infty\frac{p^2dp}{p^2-(k_0+i\delta)^2}\int_0^{2\pi}d\phi\int_0^\pi\times\exp(ipR\cos\theta)\mathbf{b}(\mathbf{k}_0-\mathbf{p})\sin\theta d\theta$$

$$=2\pi\int_0^\infty\frac{p^2dp}{p^2-(k_0+i\delta)^2}\left(\frac{\exp(ipR)\mathbf{b}(\mathbf{k}_0-\mathbf{p})}{ipR}\Big|_{\theta=0}^{\theta=\pi}+\frac{\exp(ipR)d/d\theta[\mathbf{b}(\mathbf{k}_0-\mathbf{p})]}{(ipR)^2}\Big|_{\theta=0}^{\theta=\pi}+\cdots\right),$$

is acceptable because $\mathbf{b}$ is continuous on a sphere

* This work was supported by ONR.
[1] Halpern, Hamermesh, and Johnson, Phys. Rev. **59**, 98 (1941).
[2] O. Halpern, Phys. Rev. **76**, 1130 (1949).
[3] H. Ekstein, Phys. Rev. **76**, 1328 (1949).
[4] J. S. Schwinger, Phys. Rev. **51**, 544 (1939).

$|\mathbf{p}|=\text{const}$, even at $|\mathbf{p}|=k_0$. The first term yields

$$\lim_{\substack{\delta\to 0\\ R\to\infty}} \frac{2\pi}{iR}\int_{-\infty}^{+\infty} \frac{z\exp(izR)\mathbf{b}(k_0-z)}{z^2-(k_0+i\delta)^2}dz=\frac{2\pi^2}{R}\mathbf{b}(0)\exp(ik_0R), \tag{5}$$

where $\mathbf{b}(0)$ is approached on the z-axis ($\theta=0$) which is parallel to $\mathbf{k}_0$. Consequently, the forward scattering is zero, and $\psi_{sc}(\mathbf{q}=0)$ should be defined by

$$\psi_{sc}(\mathbf{q}=0)=\lim_{q_z\to 0}\psi_{sc}(q_x=q_y=0;\,q_z)=0.$$

II.

Failure to take into account the singular behavior of the scattering amplitude may lead to erroneous results, as in the following case: consider a thin sheet, infinitely extended in the xy-plane, magnetized in the z-direction. The magnetic field $\mathbf{B}$ is clearly zero everywhere, and there is no scattering of neutrons. If the problem is treated from the atomistic viewpoint, one can proceed as follows:[1] The individual ions scatter according to Eq. (1). If they are "smeared out" on the xy-plane, the total scattering amplitude at point P on the z-axis is

$$\Psi=\int\psi_{sc}dxdy,$$

where R in Eq. (1) is the distance of a point x, y from P, and $\mathbf{k}$ is directed from (x, y) toward P. If L is the z-component of the point P and $\mathbf{k}_0\|z$, the scattered amplitude Ψ is, because of the cylindrical symmetry,

$$\Psi=\int_0^\infty \frac{\exp(ik_0(\rho^2+L^2)^{\frac{1}{2}})}{(\rho^2+L^2)^{\frac{1}{2}}}f(\mathbf{k},\mathbf{k}_0)2\pi\rho d\rho, \tag{6}$$

where the meaning of f is clear by comparison with Eq. (1). Furthermore, formal integration by parts gives

$$\Psi=\frac{2\pi}{ik_0}\int f(\mathbf{k},\mathbf{k}_0)d[\exp(ik_0(\rho^2+L^2)^{\frac{1}{2}})]$$

$$=-\frac{2\pi}{ik_0}\exp(ik_0L)f(\mathbf{k}_0,\mathbf{k}_0)+\cdots, \tag{7}$$

where an oscillatory term and higher orders in $1/L$ have been omitted. This calculation suggests that the point $\mathbf{k}=\mathbf{k}_0$ should be approached on the sphere $\mathbf{k}^2=k_0^2$. Therefore, Halpern, Hamermesh, and Johnson obtain

$$\Psi=\frac{m}{\hbar^2}\frac{\exp(ik_0L)}{ik_0}4\pi\mu\mathbf{s}\cdot\mathbf{m}\chi_0 \tag{8}$$

contrary to the macroscopic result $\Psi=0$. Actually, because of the singular behavior of ψ_{sc}, the integration by parts is not legitimate.

To show that the picture of "smeared-out" ions leads to the same result as the macroscopic theory, we can use Eq. (3) where now $\mathbf{B}_t$, the total magnetic field of all ions, should be substituted for $\mathbf{B}$, the field of a single ion. Thus,

$$\mathbf{B}_t=\int_v\mathbf{B}(\mathbf{r}-\mathbf{r}')d\mathbf{r}', \tag{9}$$

the integration being extended over the volume homogeneously filled by the nuclei. By Eq. (4)

$$\mathbf{b}_t(\mathbf{q})=\int\exp(i\mathbf{q}\cdot\mathbf{r})\mathbf{B}_t(\mathbf{r})d\mathbf{r}$$

$$=\int_\infty d\mathbf{r}\exp(i\mathbf{q}\cdot\mathbf{r})\int_v d\mathbf{r}'\int_\infty \times\exp[-i\mathbf{q}'\cdot(\mathbf{r}-\mathbf{r}')]\mathbf{b}(\mathbf{q}')d\mathbf{q}'\frac{1}{2\pi^3}$$

$$=\mathbf{b}(\mathbf{q})\int_v d\mathbf{r}'\exp(i\mathbf{q}\cdot\mathbf{r}'). \tag{10}$$

If

$$W(\mathbf{q})=\int_v d\mathbf{r}\exp(i\mathbf{q}\cdot\mathbf{r}), \tag{11}$$

Eq. (3) becomes

$$\Psi=\frac{-\mu m\mathbf{s}}{\pi^2\hbar^2}\cdot\lim_{\delta\to 0}\int\frac{\exp(i\mathbf{p}\cdot\mathbf{R})}{p^2-(k_0+i\delta)^2}\mathbf{b}(\mathbf{k}_0-\mathbf{p})W(\mathbf{k}_0-\mathbf{p})d\mathbf{p}\chi_0, \tag{12}$$

If, in particular, the volume is an infinite thin sheet,

$$W(\mathbf{q})=(2\pi)^2\delta(q_z)\delta(q_y) \tag{13}$$

and if $\mathbf{k}_0\|z$, the integration along the z-axis involves only values of $\mathbf{b}(\mathbf{q})$ such that $\mathbf{q}\|\mathbf{m}$ in our case. Since $\mathbf{b}$ vanishes for all such argument values, the scattering Ψ is zero everywhere, in agreement with the macroscopic result.

III.

Occasionally the calculation of scattering by a thin sheet is used to determine the value of the phase velocity in an infinitely extended medium.[1] This determination is based on the assumption that the addition of successive layers does not alter the scattering potential (in our case the magnetic field $\mathbf{B}$) in the existing sheets. However, magnetic forces have such a long range that this assumption is not correct. It is well known that the field in a very large magnet still depends on the shape of the surface. Therefore, this method is impracticable in the case of magnetic scattering.

PHYSICAL REVIEW VOLUME 78, NUMBER 6 JUNE 15, 1950

Deuteron Photo-Effect at High Energies

L. I. SCHIFF
Stanford University, Stanford, California
(Received February 27, 1950)

The cross section for the photoelectric disintegration of the deuteron by gamma-rays with energies in the range 20 to 140 Mev is calculated for various assumptions as to the interaction between neutron and proton. This interaction is taken to be central, half-exchange and half-direct, of approximately Yukawa and exponential forms, and with two effective ranges; experimental data thus far obtained on neutron-proton processes do not provide a firm basis for distinguishing between these assumptions. Only the electric dipole and electric quadrupole cross sections are found, since the magnetic dipole cross section cannot be obtained reliably without explicit reference to a meson theory of nuclear forces. Use is made of a method for approximating to "long-tailed" potentials in such a way that the deuteron wave equation can be solved in simple analytic form. The results show relatively little difference between Yukawa and exponential potentials of the same effective range, either as to total cross section or angular distribution, but an appreciable difference from earlier calculations with a square-well potential, and a dependence on effective range. In the Appendix, it is shown that at very high energies, each photoelectric multipole cross section depends primarily on the coefficient of the lowest odd power of r in the expansion of the deuteron potential about the origin.

I. INTRODUCTION

IT has been shown by Møller and Rosenfeld[1] that the contributions of virtual mesons to the electric dipole and electric quadrupole moment operators of the two-nucleon system are zero through terms of order $\beta_n \equiv v_{\text{nucleon}}/c$. This makes it possible to calculate the cross section for photoelectric disintegration of the deuteron entirely in terms of the interaction potentials between neutron and proton in triplet states of various orbital angular momenta. A similar elimination of the meson field from the magnetic dipole transitions cannot be made, since it is the meson charge density and not the meson current density that is approximately zero. However, the magnetic dipole transitions can be distinguished from the electric dipole and quadrupole transitions by different angular dependences of the emitted protons and neutrons (the former distribution is spherically symmetric and both of the latter vanish in the direction of the gamma-ray beam). It is to be expected, therefore, that corroborative evidence concerning neutron-proton interactions can be obtained by studying the deuteron photo-effect in an energy range where relativistic and free meson effects are unimportant. In the present paper, this energy range is taken to be 20 to 140 Mev; for higher energies other multipoles also become important, and for lower energies the shape of the interaction potential is of less importance than its effective range.[2]

The principles outlined above have already been used in part to calculate the deuteron photo-effect at various energies.[2–5] Thus far, however, the high energy angle distribution (which involves interference between electric dipole and quadrupole transitions) has not been calculated with potentials more realistic than the square well.[6] It seems desirable at this time to attempt to distinguish, on the basis of the photo-effect, between Yukawa and exponential potentials, which when approximately half-exchange and half-direct appear to give about equally good accounts of the neutron-proton scattering.[7] Tensor forces are ignored, since their effect through the deuteron ground state is small,[2,8] and there is no clear evidence for their existence in states of higher angular momenta.[7]

The calculation performed here is expected to be more accurate than is implied by the neglect of terms of order β_n^2. The approximation only involves the neglect of the meson contribution to the electric dipole and quadrupole operators, which can be interpreted as a vanishing of the meson charge density to order β_n. Now the term in the meson charge density of order β_n^2 will be fairly small in comparison with the term in the nuclear charge density of the same order; this is true so long as nuclear forces can be obtained from perturbation theory, since this implies weak coupling and a small probability that virtual mesons are present.[9] Thus the results should be fairly reliable even to order β_n^2.

In Section II, the various choices for the interaction potentials and the ground-state deuteron wave functions are presented. Formulas for the differential photo-effect cross section are given in Section III, and the numerical results presented and discussed in Section IV. The Appendix derives a general result that may prove of interest for very high energy processes.

[1] C. Møller and L. Rosenfeld, Kgl. Danske Vid. Sels. Mat.-Fys. Medd. **20**, No. 12 (1943).
[2] J. F. Marshall and E. Guth, Phys. Rev. **76**, 1879 (1949).
[3] A. Pais, Kgl. Danske Vid. Sels. Mat.-Fys. Medd. **20**, No. 17 (1943).
[4] J. S. Levinger, Phys. Rev. **76**, 699 (1949).
[5] J. F. Marshall and E. Guth, Phys. Rev. **76**, 1880 (1949).
[6] Professor E. Guth has kindly informed the writer of independent calculations that generally confirm the results obtained here; they are reported in an accompanying paper.
[7] R. S. Christian and E. W. Hart, Phys. Rev. **77**, 441 (1950).
[8] M. E. Rose and G. Goertzel, Phys. Rev. **72**, 749 (1947).
[9] The analogous argument does not apply to the magnetic dipole matrix element, since the meson contribution is enhanced by the nucleon-meson mass ratio.

II. INTERACTION POTENTIAL AND DEUTERON WAVE FUNCTION

It is the object of the present paper to compare the Yukawa and exponential interactions without resorting to extensive numerical work. This is accomplished by generalizing the Hulthén potential, which is an excellent approximation to the Yukawa potential, so that it can be made to approximate a large class of "long-tailed" potentials. The ground-state deuteron wave function (energy $-\epsilon$) is assumed to have the form

$$\begin{gathered}\psi_0(r)=[Bu(r)]/r,\\ u(r)=e^{-\gamma r}-e^{-\beta r}(1+ar+br^2+\cdots),\\ \hbar^2\gamma^2=M\epsilon,\quad \beta>\gamma.\end{gathered}\tag{1}$$

Substitution into the wave equation shows that this corresponds to the triplet interaction potential

$$V(r)=-[\hbar^2U(r)]/M,\tag{2}$$

$$U(r)=\gamma^2-\frac{1}{u}\frac{d^2u}{dr^2}$$

$$=\frac{(\beta^2-\gamma^2-2a\beta+2b)+[(\beta^2-\gamma^2)a-4\beta b+\cdots]r+[(\beta^2-\gamma^2)b+\cdots]r^2+\cdots}{e^{(\beta-\gamma)r}-(1+ar+br^2+\cdots)}.$$

The effective range[10,11] computed with the ground-state wave function is about $\frac{1}{2}$ percent less than the zero-energy effective range r_0:

$$r_0=2\int_0^\infty(e^{-2\gamma r}-u^2)dr$$

$$=\frac{4}{\gamma+\beta}-\frac{1}{\beta}+\frac{4a}{(\gamma+\beta)^2}-\frac{a}{\beta^2}+\frac{8b}{(\gamma+\beta)^3}-\frac{a^2+2b}{2\beta^3}-\frac{3ab}{2\beta^4}-\frac{3b^2}{2\beta^5}+\cdots.\tag{3}$$

The normalization constant B is readily expressed in terms of r_0:

$$1/(2\pi B^2)=(1/\gamma)-r_0.\tag{4}$$

The dots in Eqs. (2) and (3) indicate terms that would have to be added if more terms were included in (1); all terms that involve a and b in (1) are included.

All potentials of the type (2) fall off exponentially for large r, at a rate determined primarily by the parameter β. Once β is fixed, the behavior near the origin is determined by the parameters a, b, $\cdots$. Thus, if $\beta^2-\gamma^2-2a\beta+2b\neq 0$, U has a $1/r$ singularity at the origin, and resembles the Yukawa form. If this quantity vanishes, and the ratio of the next two coefficients is not the same as the ratio of the corresponding coefficients in the denominator, both U and dU/dr are finite at the origin, and U resembles the exponential form. Conditions that u have no nodes (so that it corresponds to the lowest eigenvalue of U), and that U be monotonic, are easily formulated. The choice $a=b=\cdots=0$ yields the Hulthén potential.

When this work was started, the best experimental value for the effective range was $r_0=1.56\times10^{-13}$ cm, or $r_0=1.55\times10^{-13}$ cm.[11] The appropriate constants for the Yukawa and exponential potentials were read from the graphs of Blatt and Jackson:[10]

$$U_Y(r)=(1.842/r)e^{-0.785r},\quad U_E(r)=5.511e^{-1.655r}.\tag{5}$$

All lengths are expressed in units of 10^{-13} cm, and U in units of 10^{26} cm^{-2}. It was found that U_Y could best be approximated by the form (2) when a and b were taken equal to zero, and $\beta=1.612$ (Hulthén form). In order to approximate U_E, the following parameters were chosen: $\beta=2.753$, $a=1.593$, $b=0.624$. The original and approximate forms for U_Y agree within 3 percent for $r<1.4(U_Y>0.4)$, and within 0.02 for larger values of r; likewise, the two forms for U_E agree within 2 percent for $r<1.8(U_E>0.2)$, and within 0.01 for larger values of r. It proved impossible to obtain an independent test of the accuracy of these approximations by using (1) to obtain the variational energy of the deuteron with the potential (5), because of the errors involved in getting the parameters of (5) from the graphs of reference 10.

After the calculations based on (5) were completed, a new experimental value for the effective range was reported:[12] $r_0=1.74$, or $r_0=1.73$. Only the Hulthén-

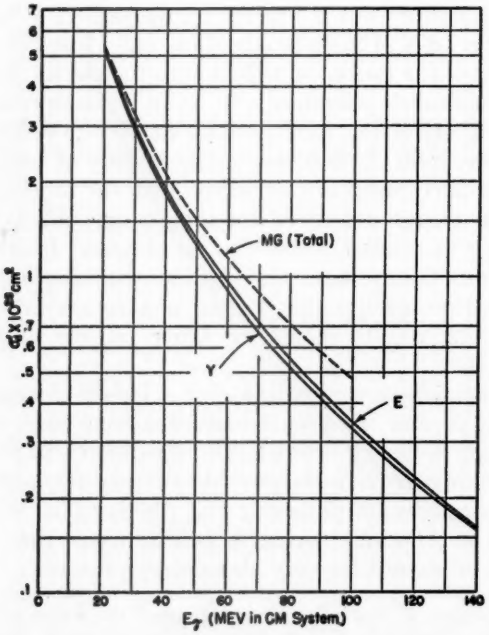

FIG. 1. Solid curves give the total photoelectric dipole cross sections as a function of gamma-ray energy in the CM system for Yukawa and exponential potentials of effective range 1.56×10^{-13} cm. Dashed curve is the total cross section (all multipoles) calculated by Marshall and Guth[5] for a square-well potential of the same effective range.

[10] J. M. Blatt and J. D. Jackson, Phys. Rev. **76**, 18 (1949).
[11] H. A. Bethe, Phys. Rev. **76**, 38 (1949).
[12] Hughes, Burgy, and Ringo, Phys. Rev. **77**, 291 (1950); D. J. Hughes, Phys. Rev. **78**, 315 (1950).

Yukawa case was re-calculated, since the earlier results indicated little difference between the Yukawa and exponential cases in this energy range (see Section IV). With $a=b=0$, the parameter β is determined by (3) to have the value 1.410; an equivalent Yukawa potential was found by making the coefficient of the $1/r$ term the same in the two cases, and making the variational deuteron energy correct when calculated with the Hulthén wave function and the Yukawa potential: $U_Y(r)=(1.641/r)\exp(-0.674r)$.

III. PHOTO-EFFECT CROSS SECTIONS

Owing to the assumption that the neutron-proton interaction is half-exchange and half-direct,[7] the final (^3P) state for an electric dipole transition has no interaction. The differential and total cross sections for dipole transitions alone in the coordinate system in which the center of mass is at rest (CM system) are then:

$$\sigma_d(\theta)=\frac{\pi}{2}\frac{e^2}{\hbar c}\frac{MkE_\gamma}{\hbar^2}I_1^2\sin^2\theta, \tag{6}$$

$$\sigma_d=\frac{4\pi^2}{3}\frac{e^2}{\hbar c}\frac{MkE_\gamma}{\hbar^2}I_1^2, \tag{7}$$

where

$$I_1=\int_0^\infty j_1(kr)\psi_0(r)r^3dr, \quad \hbar^2k^2=M(E_\gamma-\epsilon). \tag{8}$$

For later reference, both the regular and irregular spherical Bessel functions are defined:

$$\begin{aligned} j_l(z)&=[(\pi/(2z)]^{\frac{1}{2}}J_{l+\frac{1}{2}}(z),\\ n_l(z)&=(-)^{l+1}(\pi/2z)^{\frac{1}{2}}J_{-l-\frac{1}{2}}(z). \end{aligned} \tag{9}$$

Here θ is the angle between the direction of the outgoing proton and the incident gamma-ray, and E_γ is the gamma-ray energy, both in the CM system. In terms of the gamma-ray energy $E_{\gamma L}$ in the laboratory system, $E_\gamma=E_{\gamma L}[1+(E_{\gamma L}/Mc^2)]^{-\frac{1}{2}}$, where M is the nucleon mass.

The final (^3D) state for an electric quadrupole transition is affected by the full triplet neutron-proton interaction. It must therefore be taken to be the $l=2$ part of a plane plus outgoing scattered wave; this has the form

$$f(r)=\cos\delta\cdot j_2(kr)-\sin\delta\cdot n_2(kr) \tag{10}$$

outside of the potential, where δ is the scattering phase shift. The differential and total cross sections for quadrupole transitions alone are in the CM system:

$$\sigma_q(\theta)=\frac{\pi}{32}\frac{e^2}{\hbar c}\frac{MkE_\gamma^3}{\hbar^4c^2}I_2^2\sin^2\theta\cos^2\theta, \tag{11}$$

$$\sigma_q=\frac{\pi^2}{60}\frac{e^2}{\hbar c}\frac{MkE_\gamma^3}{\hbar^4c^2}I_2^2, \tag{12}$$

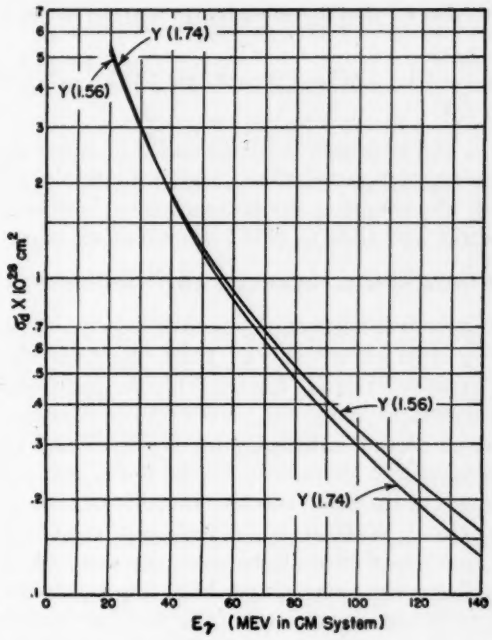

FIG. 2. Total photoelectric dipole cross sections for Yukawa potentials of effective ranges 1.56×10^{-13} cm (same as in Fig. 1) and 1.74×10^{-13} cm.

where

$$I_2=\int_0^\infty f(r)\psi_0(r)r^4dr. \tag{13}$$

Two approximations are now made in calculating I_2 as given by (13). First, it is assumed that $f(r)$ can be represented by the form (10) for all values of r, not just those for which the potential is negligible. This is believed to be a good approximation because ψ_0 extends out well beyond the range of forces, and because the r^4 term in the integrand reduces the contribution from small values of r. Second, it is assumed that the phase shift can be calculated from the Born approximation formula:

$$\sin\delta=k\int_0^\infty j_2^2(kr)U(r)r^2dr. \tag{14}$$

Equation (14) is a good approximation if δ is small; actually, δ does not exceed 12° for the highest energy considered here.

When $\psi_0(r)$ has the form (1), the integrals (8) and (13) can be evaluated in terms of elementary functions. In calculating the phase shift from (14), it is more convenient and is sufficiently accurate to use the true potentials (5) rather than (2), in which case δ can also be expressed in elementary terms. Thus the entire calculation can be placed in simple and compact form for numerical substitution.

The two differential cross sections (6) and (11) actually interfere with each other. The resultant photo-

electric cross section is conveniently written in the form

$$\sigma_e(\theta)=\frac{\sin^2\theta}{8\pi}[3\sigma_d+6(5\sigma_d\sigma_q)^{\frac{1}{2}}\cos\delta\cos\theta+15\sigma_q\cos^2\theta], \quad (15)$$

where σ_d and σ_q are given by (7) and (12), respectively. In the energy range considered, higher multipoles can be ignored. The magnetic dipole cross section is spherically symmetric, and adds to (15) without interference.

IV. NUMERICAL RESULTS AND DISCUSSION

The numerical results are presented in graphical form. The two solid curves in Fig. 1 are the total electric dipole cross sections (7) for the Yukawa and exponential interactions with $r_0=1.56$. For comparison, the total cross section calculated by Marshall and Guth[5] (which is nearly all electric dipole) for a square-well interaction of the same effective range is plotted as the dashed curve. While it would probably be difficult to distinguish experimentally between the two long-tailed potentials of the same range, both are markedly different from the square well. The Yukawa potentials of effective ranges 1.56 and 1.74 are compared in Fig. 2. The difference is quite marked, both as to trend and as to absolute value at the higher energies. The recent experimental value[13] of $(8.5\pm1.2)\times10^{-28}$ cm^2 at 17.6 Mev favors the larger effective range, since all other contributions are negligible in comparison with the electric dipole cross section at this energy.

Figures 3 and 4 show the total electric quadrupole cross section (12); the Yukawa and exponential potentials with $r_0=1.56$ are compared in Fig. 3, and the Yukawa potentials with $r_0=1.56$ and 1.74 in Fig. 4. The contribution of the electric quadrupole transitions to the total cross section is small, ranging from less than $\frac{1}{2}$ percent at 20 Mev to about 4 percent at 140 Mev. It manifests itself mainly in the angular distribution, as shown in Fig. 5. Here the quantity

$$(4/3)\{[\sigma(60°)-\sigma(0°)]/[\sigma(90°)-\sigma(0°)]\},$$

calculated from (15), is plotted against E_γ for the three cases, where $\sigma(\theta)$ is the entire differential cross section in the CM system. This quantity would be unity if only electric and magnetic dipole transitions contributed to the photo-effect; in any event, it is independent of the magnetic dipole contribution. Values greater than unity mean that electric dipole and quadrupole transitions interfere constructively in the forward hemisphere, and hence destructively in the backward hemisphere. The difference between the three curves does not appear to be great enough to be of experimental significance. It is important to note than an experimental determination of the differential cross section at three angles such as 0°, 60° and 90° would also make it possible to determine the magnetic dipole, electric dipole and electric quadrupole cross sections separately, and hence facilitate comparison with theoretical results such as those presented here.

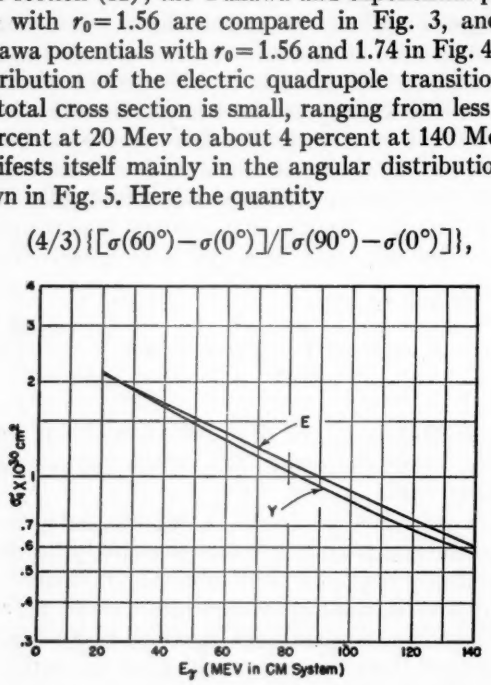

FIG. 3. Total photoelectric quadrupole cross sections for Yukawa and exponential potentials of effective range 1.56×10^{-13} cm.

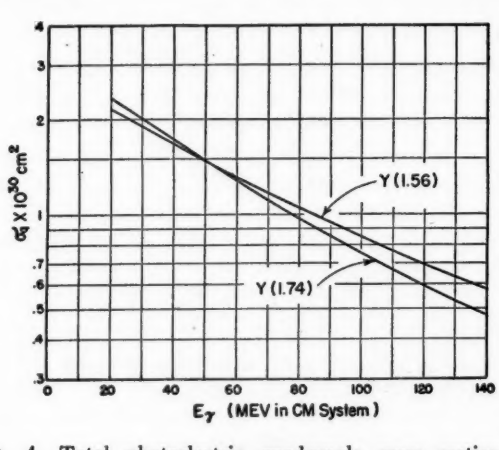

FIG. 4. Total photoelectric quadrupole cross sections for Yukawa potentials of effective ranges 1.56×10^{-13} cm (same as in Fig. 3) and 1.74×10^{-13} cm.

APPENDIX[14]

Suppose that $u(r)$ is continuous and has continuous derivatives of all orders for all positive values of r which fall off as $e^{-\gamma r}$ as r becomes positively infinite, and can be represented by a power series with a finite radius of convergence for small values of r:

$$u(r)=a_1r+a_2r^2+a_3r^3+\cdots, \quad a_1\neq0.$$

Then from the wave equation, the potential is given for small values of r by:

$$\frac{MV(r)}{\hbar^2}=-\gamma^2+\frac{2a_2+6a_3r+12a_4r^2+\cdots}{a_1r+a_2r^2+a_3r^3+\cdots}.$$

It follows from this that the lowest odd power of r in the expansion of $V(r)$ near $r=0$ is determined by the first non-vanishing number in the sequence $a_2, a_4, \cdots$. Thus if $a_2\neq0$, $MV(r)/\hbar^2=2a_2/a_1r+\cdots$; if $a_2=0$, $a_4\neq0$, $MV(r)/\hbar^2=$const. $+12a_4r/a_1+\cdots$; if $a_2=a_4=0$, $a_6\neq0$, $MV(r)/\hbar^2=$const.$+$const.$'r^2+30a_6r^3/a_1+\cdots$; and so on. Conversely, if $V(r)$ can be represented by a power series with a finite radius of convergence for small values of r:

$$[MV(r)]/\hbar^2=A_{-1}r^{-1}+A_0+A_1r+A_2r^2+\cdots,$$

[13] Barnes, Stafford, and Wilkinson, Nature **165**, 69 (1950).

[14] L. I. Schiff, Phys. Rev. **78**, 83 (1950). A closely related but less comprehensive result has recently been obtained by J. S. Levinger and H. A. Bethe (Phys. Rev. **78**, 115 (1950)), from a consideration of sum rules for electric dipole transitions.

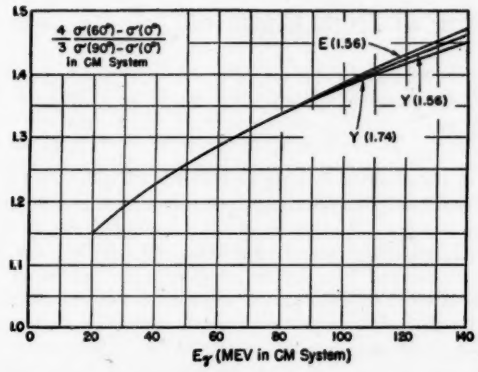

FIG. 5. Angle distribution parameters for Yukawa potentials of effective ranges 1.56 and 1.74×10^{-13} cm, and for exponential potential of the shorter range. This parameter would be unity if only electric and magnetic dipole transitions contributed to the photo-effect.

then the first non-vanishing number in the sequence $a_2, a_4, \cdots$ is given by

$$a_{s+3}=a_1A_s/(s+2)(s+3),$$

where s is the smallest odd number for which $A_s\neq0$.

Now consider the integral

$$\int\psi_0(r)r^lP_l(\cos\theta)e^{ikr\cos\theta}d\tau$$
$$=4\pi Bi^l(\pi/2k)^{\frac{1}{2}}\int_0^\infty u(r)r^{l+\frac{1}{2}}J_{l+\frac{1}{2}}(kr)dr. \quad (16)$$

The matrix element for an electric 2^l-pole transition from the ground state $\psi_0(r)$ of the deuteron to a plane wave can be expressed in terms of this integral. For large gamma-ray energy, the effect of neutron-proton interaction on the final state is small, so that the asymptotic form of (16) for large k determines the transition probability. It can be shown[15] that an asymptotic expansion of the integral on the right side of (16) can be obtained by replacing $u(r)$ in the integrand by $(a_1r+a_2r^2+\cdots)e^{-\alpha r}$, evaluating the integral term by term, and taking the limit of the series as $\alpha\to0$. Each resulting integral can be expressed in terms of a hypergeometric function[16] and its limiting value in terms of gamma-functions.[17] The result for a typical term in the series is

$$\lim_{\alpha\to0}a_n\int_0^\infty e^{-\alpha r}r^{n+l+\frac{1}{2}}J_{l+\frac{1}{2}}(kr)dr$$
$$=\frac{\pi^{\frac{1}{2}}a_n}{2^{l+\frac{1}{2}}k^{n+l+\frac{1}{2}}}\frac{\Gamma(n+2l+2)}{\Gamma\left(\frac{n+2l+3}{2}\right)\Gamma\left(\frac{1-n}{2}\right)}$$
$$=\frac{a_n\Gamma(n+2l+2)\sin\left(\frac{n+1}{2}\pi\right)}{\pi^{\frac{1}{2}}2^{l+\frac{1}{2}}k^{n+l+\frac{1}{2}}\left(\frac{n+1}{2}+l\right)\left(\frac{n+1}{2}+l-1\right)\cdots\left(\frac{n+1}{2}\right)}.$$

Thus the leading term in the asymptotic expansion of (16) is determined by the smallest even value of n for which $a_n\neq0$, and hence by the smallest odd value of s for which $A_s\neq0$. Since $\psi_0(0)=Ba_1$, the result can be written as

$$\int\psi_0(r)r^lP_l(\cos\theta)e^{ikr\cos\theta}d\tau\xrightarrow[k\to\infty]{}\frac{4\pi\psi_0(0)i^{s+l+3}}{2^{l+1}k^{s+l+5}}$$
$$\frac{\Gamma(s+2l+5)\Gamma(\frac{1}{2}s+2)}{(s+2)(s+3)\Gamma(\frac{1}{2}s+l+3)}A_s,$$

where s is the smallest *odd* number for which $A_s\neq0$. Substitution into (7) shows, for example, that the electric dipole cross section falls off as $k^{-2s-9}\sim E_\gamma^{-s-9/2}$ for large E_γ. Thus for the Yukawa potential ($s=-1$), the dipole cross section falls off as $E_\gamma^{-7/2}$, and for the exponential potential ($s=+1$), it falls off as $E_\gamma^{-11/2}$.

This result, while of some formal interest, appears to be of little practical value since in general the leading term of the asymptotic series does not become dominant until E_γ is so large that relativistic and free meson effects are important. For example, it appears from Fig. 1 that the Yukawa potential does not dominate the exponential cross section, as it must for sufficiently high energies, until E_γ is somewhat greater than 140 Mev. It is interesting to note that the zero-range potential (Bethe-Peierls case) corresponds formally to $s=-3$, and the square-well potential (because of its discontinuity) to $s=-1$. The asymptotic expansion of the cross section for an even potential such as the Gauss potential ($s=+\infty$) vanishes; this does not of course mean that the cross section itself vanishes, but only that it falls off faster than any finite power of E_γ. In general, the smoother the potential is (interpreting smoothness at the origin in terms of the way it joins on to its reflection for negative r), the smoother is the wave function, and the smaller are the short wave-length Fourier components of the wave function which determine the cross section at high energy.

[15] The writer is indebted to Professor M. Shiffman for discussion of this point.

[16] G. N. Watson, *Theory of Bessel Functions* (The Macmillan Company, New York, 1945), p. 385.

[17] E. T. Whittaker and G. N. Watson, *Modern Analysis* (The Macmillan Company, New York, 1935), p. 282.

Photo-Disintegration of the Deuteron at High Energies*

J. F. MARSHALL† AND E. GUTH
University of Notre Dame, Notre Dame, Indiana

(Received March 13, 1950)

Total cross sections and angular distributions for the photo-disintegration of the deuteron for energies between 10 and 150 Mev are computed for various types of central neutron-proton interactions. Most of the explicit computations are carried out for the case of 50 percent ordinary and 50 percent exchange interaction. Neutron-proton interactions considered are of the square well, Yukawa, and exponential type with two effective ranges. Theoretical analysis of the experimental data on high energy neutron-proton scattering excludes the square well, but is compatible with both Yukawa and exponential types of potentials. The Yukawa potential is replaced by an equivalent Hulthén potential. For the square-well and exponential potentials explicit analytic solutions were obtained. Our treatment of the case of the exponential potential is rigorous and at the same time almost as simple as that of the Hulthén potential. A qualitative discussion of the photoelectric dipole transition is given on the basis of the *f*-sum rule. This shows how exchange forces greatly increase the cross section at high energies. The discussion can be carried out for any exchange ratio. It is pointed out that only the photoelectric dipole and quadrupole cross sections can be obtained independently of specific meson theories of nuclear forces. The results for photo-disintegration show a pattern similar to those on neutron-proton scattering: very little difference between Yukawa and exponential potentials, somewhat larger difference between these two and the square-well potential. There is a pronounced dependence on effective range. In the Appendix a simple derivation of the dipole cross section for the ordinary square well potential is given, based on a transformation involving the equations of motion.

I. INTRODUCTION

OUR present knowledge of the neutron-proton interaction has been obtained from neutron-proton scattering data and from studies of the ground state of the deuteron. From low energy neutron-proton scattering one can obtain the effective range of the neutron-proton interaction,[1,2] but no information about the shape and exchange character of the potential. The values of the quadrupole and magnetic dipole moments of the deuteron indicate the existence of a tensor force between neutron and proton. High energy n–p scattering should yield, in addition, information concerning the shape of the potential, its exchange character, and further information about the nature of tensor forces. Theoretical interpretation of the data available at present[3] indicates that the potential is of the "long-tailed" type, but it is not possible to distinguish between the Yukawa and exponential potentials. The percentage of charge exchange seems to be somewhat higher than 50 percent but the experimental evidence is not complete enough to assign a definite value. The effect of tensor forces is not negligible at high energies though the present data do not yield conclusive evidence on the strength of the tensor forces.

Similar information can be obtained from a study of the photo-disintegration of the deuteron. At low energies the photo-disintegration is independent of the shape of the potential and depends in a simple way on the effective range of the neutron-proton interaction. At high energies total cross sections and angular distributions depend on the shape of the potential and the percentage of charge exchange, and will be influenced by the type and range of tensor forces assumed.

In the present paper the photo-effect is discussed for three possible potentials: square well, exponential, and Hulthén[4] (which is a good approximation to the Yukawa potential)[5] in the energy range 10 to 150 Mev. In the case of the exponential and Hulthén potentials all calculations are made on the assumption of purely central interaction and an equal mixture of ordinary and charge exchange forces, while for the square well an estimate is made of the influence of different mixtures.

Section II contains the constants for the three n–p potentials used. Section III presents a general discussion of the photoelectric dipole cross section based on the *f*-sum rule generalized for the case of exchange forces. Section IV presents a summary of the calculations in the form of graphs. Section V contains the principal formulas used in the detailed calculations, together with a brief discussion of the limitations of our present theory of the deuteron photo-effect from the point of view of meson theory.

SYMBOLS USED IN THE TEXT

ψ_t: Eigenfunction for the ground state of the system.
u_t: Radial eigenfunction for the ground state.
ψ_l: Eigenfunction for state of angular momentum l.
u_l: Radial eigenfunction for state of angular momentum l.
M: Mean mass of neutron and proton.
μ_n: Magnetic moment of neutron.
μ_p: Magnetic moment of proton.
ϵ: Binding energy of the deuteron.
E_γ: Energy of the incident γ-ray in the center-of-mass system.

* Assisted in part by ONR. Some of our results using a square well have been published. [J. F. Marshall and E. Guth, Phys. Rev. **76**, 1879, 1880 (1949)].

† Part of this work was done while the author was an AEC Predoctoral Fellow.

[1] J. M. Blatt and J. D. Jackson, Phys. Rev. **76**, 18 (1949).

[2] H. A. Bethe, Phys. Rev. **76**, 38 (1949).

[3] R. S. Christian and E. W. Hart, Phys. Rev. **77**, 441 (1950). We are indebted to Drs. Christian and Hart for informing us of their results prior to publication. Hadley, Kelly, Leith, Segrè, Wiegand, and York, Phys. Rev. **75**, 351 (1949).

[4] J. S. Levinger, Phys. Rev. **76**, 699 (1949).

[5] L. I. Schiff has kindly informed us of independent computations, using Hulthén and exponential potentials. His conclusions and ours are in general agreement.

$j_l(x)$: Spherical Bessel function of order l

$$j_l(x)=(\pi/2x)^{\frac{1}{2}}J_{l+\frac{1}{2}}(x).$$

x: Fraction of exchange forces in $n-p$ interaction.
σ_d: Total electric dipole cross section.
σ_q: Total electric quadrupole cross section.
σ_{mq}: Total magnetic quadrupole cross section

$$\alpha^2=(M/\hbar^2)\epsilon, \quad k^2=(M/\hbar^2)(E_\gamma-\epsilon).$$

II. CONSTANTS FOR THE $n-p$ INTERACTION

The constants for Yukawa and exponential potentials were obtained from the graphs of Blatt and Jackson[1] using the latest value of the effective range ($r_0=1.74\times10^{-13}$ cm) of the neutron-proton interaction.[6] The corresponding potentials are then

$$V_Y(r)=Ae^{-\mu r}/r; \quad A=1.53\times10^{13}\ \text{cm}^{-1}, \quad \mu=0.614\times10^{13}\ \text{cm}^{-1}, \quad (1)$$

$$V_E(r)=B^2e^{-2\beta r}; \quad B^2=4.27\times10^{26}\ \text{cm}^{-2}, \quad \beta=0.717\times10^{13}\ \text{cm}^{-1}. \quad (2)$$

The range of the Hulthén potential is chosen to give the same low energy electric dipole cross section as the Yukawa potential (see footnote 21), yielding:

$$V_H(r)=(\beta^2-\alpha^2)\frac{e^{-\beta r}}{e^{-\alpha r}-e^{-\beta r}}; \quad \beta=1.41\times10^{13}\ \text{cm}^{-1}. \quad (3)$$

The binding energy of the deuteron is taken equal to the value used by Blatt and Jackson, $\epsilon=2.208$ Mev.

Calculations for the square well were made at an earlier date and the constants for it correspond to an effective range, $r_0=1.54\times10^{-13}$ cm, and a binding energy, 2.237 Mev.

III. GENERAL DISCUSSION OF DEUTERON PHOTO-EFFECT EMPLOYING SUM RULES

Evaluation of the photo cross sections involves computation of integrals of the type

$$\int_0^\infty \psi_i z^l \psi_l d\tau. \quad (4)$$

For low energies ($E_\gamma<10$ Mev) it is sufficient to take only $l=1$; i.e., consider the dipole cross section only. It is also permissible to use for ψ_1 the wave function of a free nucleon

$$\psi_1 \rightarrow \psi_{1\ \text{free}}. \quad (5)$$

At low energies the main contribution to (4) comes from the region "outside" the $n-p$ interaction. For intermediate and high energies the interactions of the nucleons must be taken into account, and the contribution from the "inside" increases with energy.

For an equal mixture of ordinary and exchange forces (5) is exact and the computation is quite simple. The dipole cross section in this case depends on the range and shape of the $n-p$ interaction only through the ground wave function. For the case of an arbitrary exchange ratio x ($x=0$, ordinary, $x=1$, exchange) it is possible, however, to gain a qualitative understanding of the dependence of the cross section on range, shape, and exchange ratio by application of the f-sum rule. As is well known, the f-sum rule yields a value of the integrated dipole cross section of the deuteron, given by

$$\int^\infty \sigma_d dE=\pi^2e^2\hbar/Mc=\sigma_0. \quad (6)$$

This form implies the assumption of ordinary forces, however. In this case the integrated cross section does not depend on either range or shape of the $n-p$ interaction.

It seems that Fock[7] was the first to point out for atomic problems that the usual form of the f-sum rule needs modification when exchange forces are taken into account. Independently of Fock, Feenberg[8] and Siegert[9] pointed out the same fact in connection with nuclear problems and Way[10] has already applied the modified sum rule to the deuteron photo-effect. For the integrated dipole cross section at exchange ratio x one obtains

$$\sigma_x=\sigma_0\left(1+\frac{2}{3}\frac{M}{\hbar^2}x\int_0^\infty \psi_i^* V r^2 P\psi_i d\tau\right). \quad (7)$$

This formula is in agreement with Way and also with Levinger and Bethe[11] who recently made a detailed application of sum rules to nuclear dipole photo-effects.

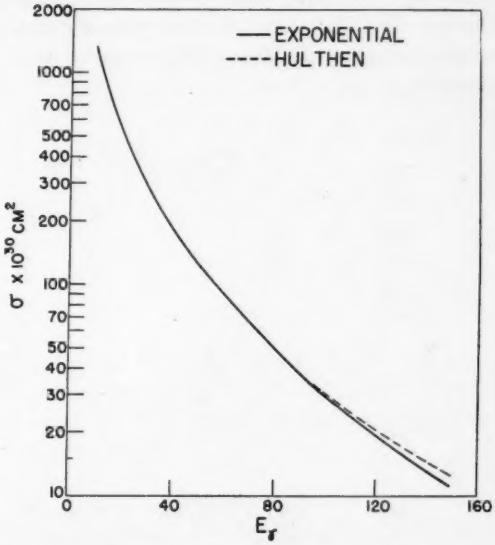

FIG. 1. Total cross sections for $r_0=1.74\times10^{-13}$ cm.

[6] D. J. Hughes, Phys. Rev. **78**, 315 (1950). Hughes, Burgy, and Ringo, Phys. Rev. **77**, 291 (1950).

[7] V. Fock, Zeits. f. Physik **89**, 744 (1934).
[8] E. Feenberg, Phys. Rev. **49**, 328 (1936).
[9] A. J. F. Siegert, Phys. Rev. **52**, 787 (1937).
[10] K. Way, Phys. Rev. **51**, 552 (1937).
[11] J. S. Levinger and H. A. Bethe, Phys. Rev. **78**, 115 (1950). We are indebted to Dr. Levinger and Professor Bethe for communicating their results to us before publication.

Evaluation of (7) for a square, a Hulthén, and an exponential potential leads to the approximate general form

$$\sigma_x=\sigma_0(1+\zeta\alpha r_0 x), \tag{8}$$

where ζ is a shape factor and r_0 the effective range. This form shows clearly that σ_x increases both with x and r. In particular, for $r_0=1.56$ and 1.74 we obtain for a square well

$$\zeta\alpha r_0=\begin{Bmatrix}0.40\\0.44\end{Bmatrix}$$

and for a Hulthén and an exponential potential, which yield about the same value

$$\zeta\alpha r_0=\begin{Bmatrix}0.33\\0.37\end{Bmatrix}.$$

At high energies it seems permissible to conclude that σ_d will also increase with increasing x.[12] An attractive exchange force for the ground (S) state of the deuteron implies a repulsive exchange force for the final (P) state. This repulsion implies, (a) an increase of the energy of a given P state compared to the case $x=0$, when the P state is bound by an attractive ordinary force, and (b) a decrease in the integral (4) for small final energies and an increase in the integral, i.e., in σ_d, for large final energies.

We conclude that at high energies for a given range σ_d for a square well will be larger than that for a Yukawa (Hulthén) or exponential potential, the last two differing but little, and that σ_d increases with increasing x. This last conclusion is certainly not valid for energies less than 30 Mev, as is shown by numerical computations.

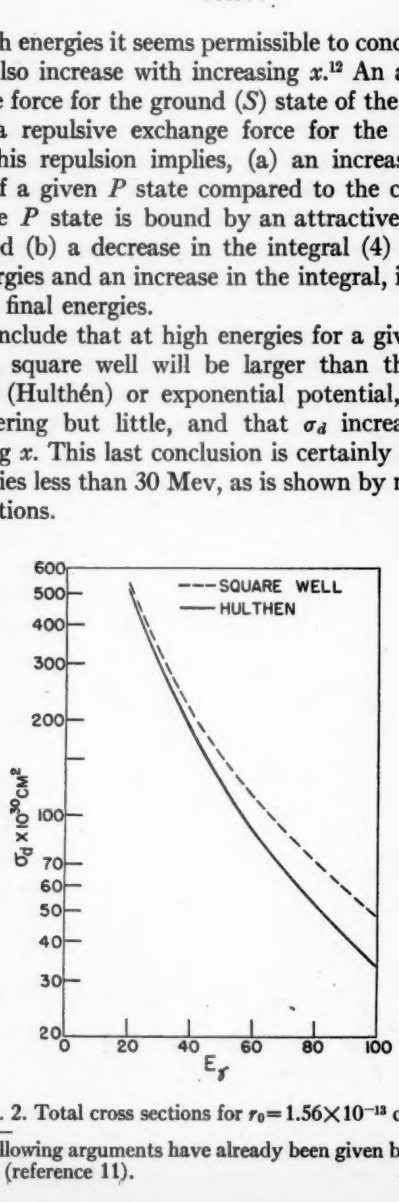

FIG. 2. Total cross sections for $r_0=1.56\times10^{-13}$ cm.

[12] The following arguments have already been given by Levinger and Bethe (reference 11).

For quadrupole (even-even) transitions, in contrast with dipole (even-odd) transitions, exchange forces do not modify the matrix elements or the sum rules.

IV. SUMMARY OF CALCULATIONS

The results of calculations based on the assumption of central forces and 50 percent charge exchange are shown in Figs. 1–4. The energy range 10 to 150 Mev is chosen because below 10 Mev one cannot detect any shape effects, and above 150 Mev relativistic effects and interactions other than photo-disintegration become important (see Section V). Total cross sections for the "long-tailed" potentials, including electric dipole, electric and magnetic quadrupole (the magnetic dipole contribution can be neglected) are shown in Fig. 1 for $r_0=1.74\times10^{-13}$ cm. Throughout most of the energy range the difference between the Hulthén and the exponential cross sections is quite small, but at the higher end they begin to deviate from each other appreciably, the difference amounting to 13 percent at 150 Mev. It is interesting to note that for energies greater than 80 Mev the cross section for the exponential well always lies below that for the Hulthén well. This agrees with Schiff's theorem[13] on the asymptotic energy dependence, according to which the exponential cross section should fall off more rapidly than that for the Hulthén well by a factor $1/E_\gamma$ at high energies.

Total cross sections for the square-well and Hulthén potentials are compared in Fig. 2 for an effective range of 1.56×10^{-13} cm in the energy range 20 to 100 Mev. The difference between the two curves is quite marked, amounting to about 30 percent at 100 Mev. Consequently, while it would be quite difficult to distinguish between the "long-tailed" wells experimentally, a potential of the square-well type should be recognizable.

The electric and magnetic quadrupole cross sections are plotted in Fig. 3 for the two "long-tailed" potentials. [In computing the electric quadrupole cross sections, it was assumed that the outgoing wave could be treated as free (see Section V).] At low energies both can be neglected as far as their influence on the total cross section is concerned, although the electric quadrupole cross section still has an important influence on the angular distribution. At the higher energies their contributions to the total cross section are about the same: electric quadrupole contributing five percent at 150 Mev and magnetic quadrupole eight percent.

Angular distributions in the center-of-mass system are shown for two energies (150 and 17.5 Mev) in Fig. 4. Distributions for other energies can be obtained very readily by use of Figs. 1 and 2 and Eq. (42). In the 17.5-Mev curve[14] the magnetic dipole contribution, which would yield an isotropic term amounting to

[13] L. I. Schiff, Phys. Rev. 78, 83 (1950); see also Levinger and Bethe (reference 11).

[14] Angular distributions in the range 4 to 20 Mev have been measured by Fuller. [E. G. Fuller, Phys. Rev. 76, 576 (1949) and Ph.D. thesis.] We have shown that his forward asymmetry agrees with ours to within the experimental error (see asterisk reference).

about two percent of the 90° cross section, has been subtracted out. The distribution is predominantly of the electric dipole form, but is slightly asymmetric about 90° due to interference between electric dipole and electric quadrupole transitions. At this energy there is no noticeable dependence on shape in the angular distribution, and the angular distribution is given very nearly by the zero-range formula. The distribution normalized to unity at 90° is given by

$$f(\theta)=\sin^2\theta[1+0.264\cos\theta], \text{ at } 17.5 \text{ Mev} \quad (9)$$

which is approximately

$$f(\theta)=\sin^2\theta[1+2((E_\gamma-\epsilon)/Mc^2)^{\frac{1}{2}}\cos\theta]. \quad (10)$$

The coefficient of $\cos\theta$ in (9) is the same for all three potentials and is larger than that for the zero-range distribution (10) by about three percent.

The angular distribution of photo-protons at 150 Mev is plotted in the solid curve of Fig. 4 for the exponential potential, the angular distributions for the other potentials having much the same form. At this energy the angular distribution has the form

$$f(\theta)=\sin^2\theta[1+1.066\cos\theta+0.2839\cos^2\theta]+0.1880\cos^2\theta. \quad (11)$$

The $\sin^2\theta$ term still dominates, but the forward asymmetry is much larger than in the low energy case. Furthermore, since the magnetic quadrupole cross section is appreciable at this energy there is appreciable scattering in the forward direction.

V. DETAILED CALCULATIONS AND DISCUSSION

A. General Considerations[15]

Møller and Rosenfeld[16] have shown that since the charge density of the virtual meson field has an average value of zero, the exchange moment contribution to the electric dipole and electric quadrupole moments is zero to order v_{nucleon}/c. On the assumption of purely central forces corresponding cross sections are then given by:

$$\sigma_d=\frac{\pi}{3}\frac{e^2}{\hbar c}\frac{M}{\hbar^2}kE_\gamma I_1^2; \quad I_1=\int_0^\infty u_1 r u_i dr, \quad (12)$$

$$\sigma_q=\frac{\pi}{240}\frac{e^2}{\hbar c}\frac{M^2}{\hbar^4}\frac{kE_\gamma^3}{Mc^2}I_2^2; \quad I_2=\int_0^\infty u_2 r^2 u_i dr. \quad (13)$$

The situation with respect to magnetic transitions is not quite so simple since exchange effects will depend upon the specific meson theory assumed. It is true that the magnetic exchange moment vanishes for any stationary state of the deuteron, but the exchange moments of H^3 and He^3 amount to about six percent.[17] The exchange currents are likely to contribute to the photomagnetic cross section, as pointed out by Pais.[18] His original estimate of the magnitude of this contribution on the basis of Møller and Rosenfeld's mixed theory was much too large.[19] Still, the magnitude of this contribution is unknown. The same holds *a fortiori* for the magnetic quadrupole transition. Fortunately, the magnetic dipole cross section, assuming zero exchange contribution, is negligible over our energy range. However, the magnetic quadrupole cross section, again assuming zero exchange contribution, is larger than the electric quadrupole cross section above 100 Mev. For the sake of this comparison we retained the magnetic quadrupole transition, though its inclusion, according to our previous discussion, does not have a sound theoretical basis.

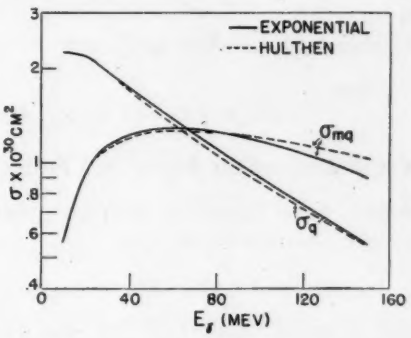

FIG. 3. Electric and magnetic quadrupole cross sections for $r_0=1.74\times10^{-13}$ cm.

Assuming the exchange moment to be negligible, the magnetic quadrupole cross section for transitions to a final triplet state is given by

$$\sigma_{mq}=\frac{\pi}{18}\frac{e^2}{\hbar c}\left(\frac{\hbar^2}{M}\right)^2\frac{k(\alpha^2+k^2)^3}{(Mc^2)^2}(\mu_p-\mu_n)^2 I_1^2 = \frac{(\mu_p-\mu_n)^2}{6}\left(\frac{E_\gamma}{Mc^2}\right)^2\sigma_d. \quad (14)$$

The cross section for transitions to singlet states is about one-fiftieth of this amount and can safely be neglected.

The angular distribution of photo-particles in the center-of-mass system is given by[20]

[15] In these computations it was assumed that the interaction is purely central. The numerical calculations of T-M. Hu and H. S. W. Massey, Proc. Roy. Soc. **A186**, 135 (1949), indicate for $x=\frac{2}{3}$ a 40 percent increase of σ_d by tensor forces at 28.8 Mev. For $x=\frac{1}{2}$ the percentage increase is smaller, but very likely still appreciable.

[16] C. Møller and J. Rosenfeld, Kgl. Danske Vid. Sels. Mat.-Fys. Medd. **20**, No. 12 (1943).

[17] F. Villars, Phys. Rev. **72**, 256 (1947).

[18] A. Pais, Kgl. Danske Vid. Sels. Math-Fys. Medd. **20**, No. 17 (1943).

[19] L. Rosenfeld, *Nuclear Forces* (Interscience Publishers, Inc., New York, 1949), Vol. II, p. 449.

[20] Several authors state that there is no interference between electric dipole and electric quadrupole transitions, as indicated by the above expression, since the final states belong to different isotopic spin states. Were it not for the Pauli principle this would be the case, since cross product terms would vanish on summation over isotopic spins. Since, however, for a given angular momentum and spin one of the two possible isotopic spin states is always

$$\frac{d\sigma}{d\Omega}=\frac{\sin^2\theta}{8\pi}[3\sigma_d+6(5\sigma_q\sigma_d)^{\frac{1}{2}}\cos\delta_1\cos\delta_2\cos\theta$$
$$+15\sigma_q\cos^2\theta]+(3/4\pi)\sigma_{mq}\cos^2\theta. \quad (15)$$

B. Wave Functions for Initial and Final States

The radial wave functions for the ground state satisfy a wave equation of the form

$$u_i''+V(r)u_i-\alpha^2u_i=0. \quad (16)$$

In order to satisfy Eqs. (12)–(14) the function u_i must be normalized to unity,

$$\int u_i^2dr=1. \quad (17)$$

It is more convenient to use a wave function which has the asymptotic form $\exp(-\alpha r)$. Writing

$$u=A\varphi, \quad \text{where} \quad \varphi\underset{r\to\infty}{\longrightarrow}e^{-\alpha r}, \quad (18)$$

we find

$$A^2=2\alpha/(1-\alpha\rho), \quad (19)$$

where

$$2\rho=\int_0^\infty e^{-2\alpha r}-\int_0^\infty\varphi^2dr. \quad (20)$$

It has been shown by Blatt and Jackson that ρ differs from r_0 by about one-half percent, and for all potentials considered here

$$\rho=1.73\times10^{-13} \text{ for } r_0=1.74\times10^{-13},$$
$$\rho=1.55\times10^{-13} \text{ for } r_0=1.56\times10^{-13}.$$

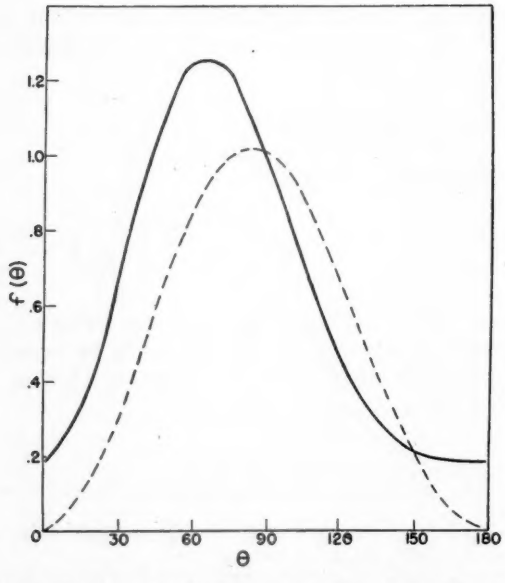

FIG. 4. Angular distributions of photo-protons. The dashed curve is for 17.5-Mev gamma-rays, and the solid curve is for 150-Mev gamma-rays.

forbidden by the Pauli principle, averaging over isotopic spin states is not justified and the cross product terms remain.

The solutions to the wave equation for the three potentials are then:

(a) Hulthén:

$$V(r)=(\beta^2-\alpha^2)\frac{e^{-\beta r}}{e^{-\alpha r}-e^{-\beta r}}, \quad \varphi=e^{-\alpha r}-e^{-\beta r}. \quad (21)$$

(b) Exponential:

$$V(r)=B^2e^{-2\beta r}, \quad \varphi=aJ_p(x) \quad (22)$$

where

$$p=\alpha/\beta; \quad x=(B/\beta)e^{-\beta r}; \quad a=\Gamma(p+1)(B/2\beta)^{-p}. \quad (23)$$

It is found convenient to express (22) in the form of an infinite series

$$\varphi=\sum_0^\infty\frac{(-1)^j(B/2\beta)^{2j}}{j!p_j}e^{-(\alpha+2j\beta)r}, \quad (24)$$

where

$$p_j=(p+1)(p+2)\cdots(p+j).$$

(c) Square well:

$$V(r)=V_0, \quad r<b_i$$
$$V(r)=0, \quad r>b_i$$
$$\varphi=\frac{e^{-\alpha b_i}}{\sin V_0^{\frac{1}{2}}b_i}\sin V_0^{\frac{1}{2}}r, \quad r<b_i, \quad (25)$$
$$\varphi=e^{-\alpha r}, \quad r>b_i. \quad (26)$$

In order to evaluate the integrals I_1 and I_2 we need final state wave functions for the P and D states. On the assumption of $x=0.5$, the nucleons may be treated as free in the P state and the corresponding wave function is simply

$$u_1=rj_1(kr), \quad \delta_1=0. \quad (27)$$

To obtain a general solution of the wave equation for the D state would require a numerical solution for the exponential and Hulthén potentials. A possible approximation would be to assume that in the evaluation of I_2 the important part of the wave function is that outside the range of interaction, and that we can approximate u_2 by

$$u_2=r[\cos\delta_2j_2(kr)-\sin\delta_2n_2(kr)], \quad (28)$$

where δ_2 is given approximately by

$$\sin\delta_2=k\int_0^\infty V(r)j_2^2(kr)r^2dr. \quad (29)$$

It was found that in this approximation the effect of binding in the D state was quite small. Furthermore, the contribution to the integral from inside the well is quite large, and it is not entirely clear that (28) is a much better approximation than the assumption that

the outgoing wave can be treated as free. Consequently, the D wave function for the Hulthén and exponential well was taken to be

$$u_2=rj_2(kr);\quad \delta_2=0. \tag{30}$$

[Use of Eqs. (28) and (29) instead of (30) would change σ_q by about 10 percent. Since the asymmetric term in the angular distribution depends on $(\sigma_q)^{\frac{1}{2}}$, the change there is smaller.]

In the case of the square well, the effect of binding is much more pronounced and exact wave functions were used,

$$\begin{aligned} u_2&=Arj_2(V_0^{\frac{1}{2}}r), && r<b_t, \\ u_2&=r[\cos\delta_2 j_2(kr)-\sin\delta_2 n_2(kr)], && r>b_t. \end{aligned} \tag{31}$$

C. Evaluation of the Cross Sections

1. *Fifty Percent Charge Exchange*

Since over a large part of the energy range considered the cross sections differ very little from the zero-range cross sections, it is convenient to express them in terms of these cross sections. On the assumption of a free outgoing wave in P and D states the expressions for the cross sections take the form

$$\sigma_d=\sigma_B F_1^2/(1-\alpha\rho), \tag{32}$$

where

$$F_1=\frac{(\alpha^2+k^2)^2}{2k}\int_0^\infty \varphi j_1(kr)r^2dr.$$

Also

$$\sigma_B=\frac{8\pi}{3}\frac{e^2}{\hbar c}\frac{\hbar^2}{M}\frac{\epsilon^{\frac{1}{2}}(E_\gamma-\epsilon)^{\frac{3}{2}}}{E_\gamma^3}, \tag{33}$$

$$\sigma_q=\sigma_{Bq}F_2^2/(1-\alpha\rho), \tag{34}$$

where

$$F_2=\frac{(\alpha^2+k^2)^3}{8k^2}\int_0^\infty \varphi j_2(kr)r^3dr.$$

Finally,

$$\sigma_{Bq}=\frac{(E_\gamma-\epsilon)}{5Mc^2}\sigma_B. \tag{35}$$

Substituting (21) and (24) we obtain for F_1 and F_2:
(a) Hulthén potential:[21]

$$F_1=1-[(\alpha^2+k^2)/(\beta^2+k^2)]^2, \tag{36}$$

$$F_2=1-[(\alpha^2+k^2)/(\beta^2+k^2)]^3. \tag{37}$$

[21] At energies below 15 Mev the factor F_1 is very nearly equal to one for all potentials. Consequently, the electric dipole cross section is given by

$$\sigma_d=\sigma_B/(1-\alpha\rho)$$

which is independent of the shape of the potential. Since the constants of the Yukawa potential are chosen to correspond to $\rho=1.73\times10^{-13}$ cm, the constant β in the Hulthén potential must be chosen to correspond to this value of ρ, if the two potentials are to yield the same low energy cross section. From (20) one obtains a relation between ρ and β for the Hulthén case

$$\rho=(3\beta-\alpha)/\beta(\beta+\alpha)$$

which can be solved for β yielding $\beta=1.41\times10^{13}$ cm^{-1}.

(b) Exponential potential:

$$F_1=1-\sum_1^\infty \frac{(-1)^j(B/2\beta)^{2j}}{j!p_j}\frac{(\alpha^2+k^2)^2}{[(p+2j)^2\beta^2+k^2]^2}, \tag{38}$$

$$F_2=1-\sum_1^\infty \frac{(-1)^j(B/2\beta)^{2j}(\alpha^2+k^2)^3}{j!p_j[(p+2j)^2\beta^2+k^2]^3}. \tag{39}$$

Up to 150 Mev, only two terms ($j=1$, $j=2$) are needed for an accuracy of better than one percent in the total cross sections. Putting in values for α, B, β corresponding to an effective range of 1.74×10^{-13} cm, the series can be written

$$F_1=1-1.57\left[\frac{\alpha^2+k^2}{(p+2)^2\beta^2+k^2}\right]^2 +0.146\left[\frac{\alpha^2+k^2}{(p+4)^2\beta^2+k^2}\right]^2, \tag{40}$$

$$F_2=1-1.57\left[\frac{\alpha^2+k^2}{(p+2)^2\beta^2+k^2}\right]^3 +0.146\left[\frac{\alpha^2+k^2}{(p+4)^2\beta^2+k^2}\right]^3. \tag{41}$$

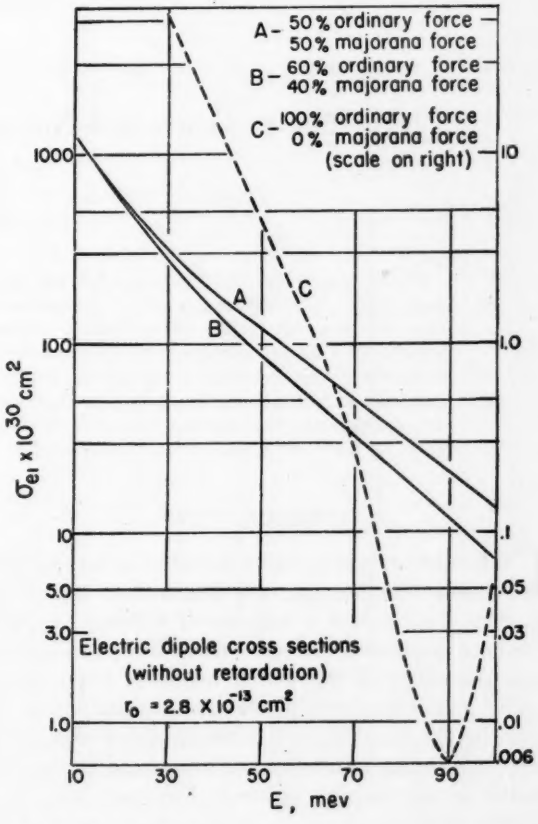

FIG. 5. Electric dipole cross sections for several mixtures.

Taking $\delta_1=\delta_2=0$, we have for the angular distribution

$$d\sigma/d\Omega=(8\pi/3)\sin^2\theta[3\sigma_d+6(5\sigma_d\sigma_q)^{\frac{1}{2}}\cos\theta+15\sigma_q\cos^2\theta]+(3/4\pi)\sigma_{mq}\cos^2\theta. \quad (42)$$

The expressions for the cross sections in the case of the square well are quite a bit more complicated than those for the Hulthén and exponential potentials, and are most simply computed by substitution in recursion formulas.

2. *Effect of Mixture*

Dipole cross sections for several exchange mixtures are plotted in Fig. 5 for a square well of intrinsic range, 2.8×10^{-13} cm. From these curves one can obtain a qualitative idea of how the mixture will affect both total cross sections and angular distributions.

The cross section for $x=0$ (a simple derivation is given in the Appendix) is found to fall off much more rapidly than that for $x=0.5$, and actually goes to zero at 90 Mev. Furthermore, since the quadrupole cross section is unaffected by mixture the angular distributions will be radically different for the two cases. Consequently, it should be very easy to determine experimentally whether the interaction potential has a large percentage of ordinary forces.

The dipole cross section for $x=0.4$, however, is seen to be very nearly equal to that for $x=0.5$ and a rough estimate indicates that all values of x greater than 0.4 yield very nearly the same value of the cross section. Consequently, very careful experiments would have to be made in order to assign an exact value to x.

APPENDIX. DERIVATION OF σ_d FOR ORDINARY FORCES

The matrix element for the dipole transition is proportional to the absolute square of the integral (matrix)

$$x_{01}=\int_0^\infty \psi_i z\psi_1 d\tau. \quad (43)$$

We can transform this integral and evaluate it at once by using the equation of motion

$$M\ddot{x}_{01}=-\left(\frac{\partial V}{\partial x}\right)_{01}, \quad \ddot{x}_{01}=-\frac{(E_1-E_0)^2}{M\hbar^2}x_{01}. \quad (44)$$

inserting (44) in (43) we obtain

$$x_{01}=\frac{M\hbar^2}{(E_1-E_0)^2}\int \psi_i\frac{\partial V}{\partial r}\cos\theta\psi_1 d\tau. \quad (45)$$

But for a square well $\partial V/\partial r=\delta(r-b_i)$, therefore

$$\int_0^\infty \psi_i(\partial V/\partial r)\psi_1 r^2 dr=\psi_i(b_i)\psi_1(b_i)b_i^2 \quad (46)$$

giving σ_d in a rather compact form.

This result agrees with that of Breit and Condon[22] which was obtained on the basis of a more involved computation.

[22] G. Breit and E. U. Condon, Phys. Rev. **49**, 904 (1936).

PHYSICAL REVIEW VOLUME 78, NUMBER 6 JUNE 15, 1950

Hyperfine Structure and Nuclear Spins of Tungsten and Tellurium

G. R. FOWLES*
Department of Physics, University of California, Berkeley, California
(Received March 3, 1950)

By the use of enriched isotopes, hyperfine structure in the optical spectra of Te^{123}, Te^{125}, and W^{183} has been observed. Milligram amounts of the isotopes were used in a modified Schüler hollow-cathode discharge tube. In the visible region, 4000 to 6000A, about a dozen lines of singly ionized tellurium showed hyperfine structure, all of them giving just two components for the odd isotope. Te^{123} and Te^{125} gave identical structures except for a scale factor, the total splitting of the lines of Te^{123} being about 88 percent of that of Te^{125}. In the spectrum of neutral tungsten, all of the lines which show the isotope shift for natural tungsten gave just two components with highly enriched W^{183}. The number of hyperfine-structure components, namely two, gives for Te^{123}, Te^{125}, and W^{183} a nuclear spin of $\frac{1}{2}$. This was also verified by intensity measurements.

I. INTRODUCTION

THE nuclear spins of all the stable isotopes of odd atomic number are now believed to be known, and even the spins of a number of radioactive nuclei have been measured. On the other hand, the spins of about one-third of the stable nuclei of even atomic number and odd atomic weight remain unknown. The reason for the scarcity of data on the spins of even-odd nuclei is in many cases the low abundance of the odd isotopes in the natural element. Enriched isotopes of many elements separated by mass-spectrographic methods have recently become available in milligram amounts through the Atomic Energy Commission. By the use of these enriched isotopes several nuclear spins heretofore not known or not definitely established have been measured recently. Although the spin of any nucleus is a desirable datum, there are some nuclei which are particularly important or interesting from a theoretical point of view. In this investigation the spins of three interesting nuclei—the two odd isotopes of tellurium, Te^{123} and Te^{125}, and the odd isotope of tungsten, W^{183}—are measured by observations on the hyper-

* Now at the University of Utah, Salt Lake City, Utah.

fine structure using enriched isotopes. The result on the spin of Te^{125} was reported earlier by the author.[1] After the work was begun, Mack and Arroe[2] reported a successful measurement on Te^{123}, which was in substantial agreement with the result reported here. The importance of the spins of these nuclei will be discussed in Section III.

II. EXPERIMENTAL

In these investigations of hyperfine structure a silvered Fabry-Perot etalon was used as the instrument of high dispersion and resolving power. To provide the auxiliary dispersion, a large glass spectrograph was used. In order to obtain large linear dispersion only a few fringes near the center of the fringe system were used. This was accomplished by tilting the interferometer so that the desired order of the off-center fringes fell into coincidence with the illuminated portion of the slit.

The etalon plates were of quartz and were figured to a flatness of about 1/30 wave-length of yellow light by W. E. Williams, using the method of localized fringes developed by Rasmussen.[3] The reflecting surfaces of the etalon were evaporated silver of such thickness that the light reflection in the visible amounted to nearly 90 percent. The etalon spacers were invar pins of fixed lengths mounted in brass rings, the lengths varying from 4 to 40 mm.

The spectral source was a Schüler hollow-cathode discharge tube of the type designed by Walcher[4] for the excitation of the spectra of very small amounts of material. Walcher's design was here modified to simplify the removal of the hollow cathode and to allow for a maximum of recovery of the material under investigation. A drawing of the discharge tube is given in Fig. 1. The main feature of the tube is the inner glass cylinder which extends to within about 3 mm of the cathode. This inner cylinder holds the anode at the lower extremity. The anode and the cathode cup are both made of commercially pure aluminum; and they are both easily removable. The whole cathode assembly is removed simply by warming the wax seal and sliding it off the outer glass cylinder. This can be done without disturbing the carrier-gas leads to the vacuum and purifying system. The wax seal is kept at room temperature by means of a water jacket soldered to the upper end of the brass cathode-housing. The cathode assembly is surrounded with water or liquid nitrogen to cool the cathode and reduce line width.

Helium from the inlet tube goes down the inner glass cylinder through the circular opening of the anode and then flows back up in the space between the two glass cylinders to the outlet. This provides a "gas window" to prevent diffusion of the sample out of the hollow cathode. The helium is continuously circulated in a purifying circuit consisting of a liquid-air-cooled charcoal trap and a mercury diffusion pump. The diffusion pump is also used to evacuate the system before admitting the helium. The discharge is run at helium pressures of from 1 to 3 mm.

About 20 mg of the material whose spectrum is to be studied is put into the bottom of the hollow cathode. Using a cathode 6 mm in diameter and 25 mm in length, an excitation current of about 150 milliamperes gave good results. The direct current source was a 1000-volt power supply. A variable series resistor was used to limit the current to the proper value. Tellurium in the form of the powdered element was used for the tellurium spectra. The separated tungsten isotope was furnished in the form of the oxide WO_3. It was found that the unreduced oxide itself gave a good spectrum of atomic tungsten from the Schüler tube after about one-half hour of operation. No special procedures for plating of the cathode or clean-up of the tube were found to be necessary except for a thorough initial pumping out of the system with the diffusion pump.

Under the conditions described, fairly bright spectra were obtained, and good spectrograms could be obtained in from three to five minutes on Eastman 103a-F or 103a-J spectroscopic plates. This short exposure time made it unnecessary to use any temperature control mechanism for the Fabry-Perot etalon. The intensity measurements were made by the standard

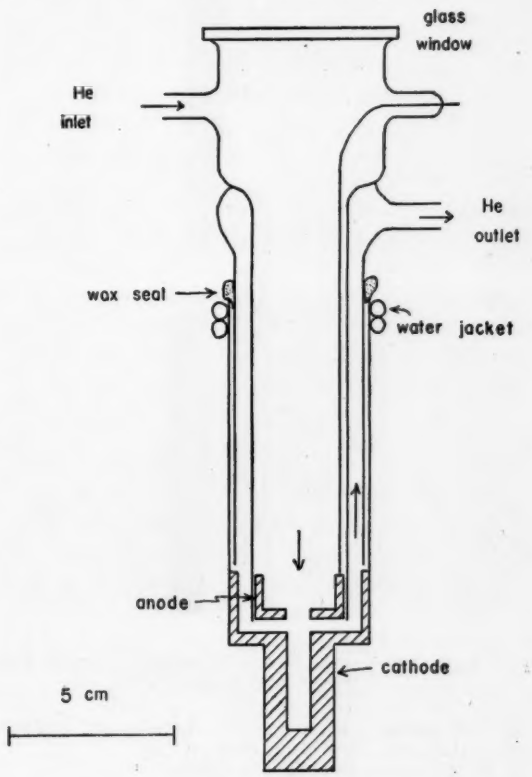

FIG. 1. Modified Schüler tube.

[1] G. R. Fowles, Phys. Rev. **76**, 571 (1949).
[2] J. E. Mack and O. H. Arroe, Phys. Rev. **76**, 1002 (1949).
[3] E. Rasmussen, Physica **12**, 656 (1946).
[4] W. Walcher, Zeits. f. Physik **122**, 62 (1944).

TABLE I. Measurements on the tellurium lines.

Wavelength (Å)	Separations in cm^{-1} Te^{125}	Te^{123}	Ratio $\Delta_{123}/\Delta_{125}$	Intensity ratio $I_{j+\frac{1}{2}}/I_{j-\frac{1}{2}}$	Displacement ratio* $\Delta_{j-\frac{1}{2}}/\Delta_{j+\frac{1}{2}}$
5974	0.169	0.145	0.86	1.5	1.59
5755	0.079				1.5
5708	0.176	0.157	0.89	1.6	1.6
5666	0.115	0.103	0.90	~3	~3
5649	0.205			~3	2.9
5576	0.121	0.108	0.89		1.5
5449	0.226	0.192	0.85	1.4	1.3

* Taken with respect to the central unresolved component of the even isotopes.

method in which the plates are calibrated by the use of a step-slit.[5]

III. RESULTS AND DISCUSSION

Tellurium

The two odd isotopes of tellurium, Te^{123} and Te^{125}, have been observed to have long-lived isomeric states.[6,7] A knowledge of the spins of the ground states of these nuclei would permit one to say something about the angular momentum of the nucleus in the excited state, when the lifetime and energy of the isomeric transition are known.[8] Recent theories[9–11] concerning the shell structure of nuclei indicate that in the region of tellurium (neutron numbers 69 to 79) isomerism should occur. The spin changes which occur in these isomeric transitions have an important bearing on the theories. In addition, Te^{123} has a stable isobar, Sb^{123}, whose spin is known to be 7/2. Only a few odd isobaric pairs exist in the natural elements, and the spins of the members of these pairs are important data.[12]

In natural tellurium the isotopes of mass 123 and 125 occur in the amounts 0.85 and 6.97 percent, respectively. Because of this low abundance of the odd isotopes, hyperfine structure in the spectrum of natural tellurium has never been reported. By the use of the enriched isotopes Te^{125} and Te^{123} in this investigation, it was possible to find hyperfine structure in about a dozen lines of singly ionized tellurium in the visible region, 4000 to 6000A. All of the lines gave only two components for the odd isotope. Tellurium enriched to about 80 percent in Te^{125} in the one case,[13] and to about 45 percent in Te^{123} in the other,[14] showed identical

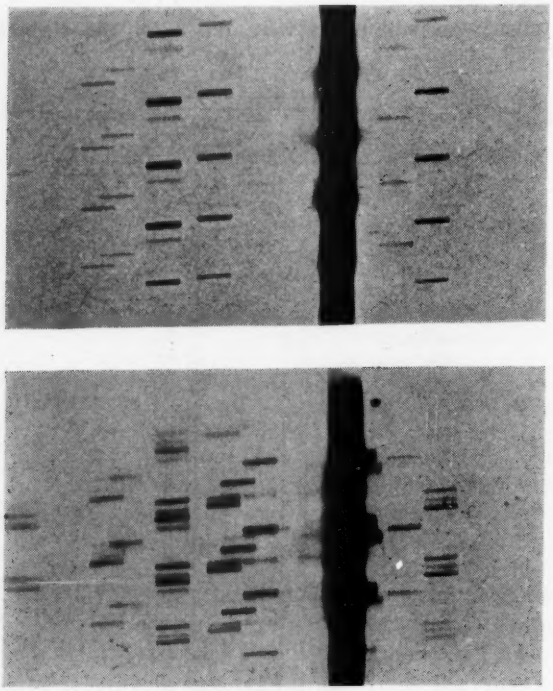

FIG. 2. Fabry-Perot spectrograms of natural tellurium (upper) and Te^{125} (lower). Etalon separation 7 mm.

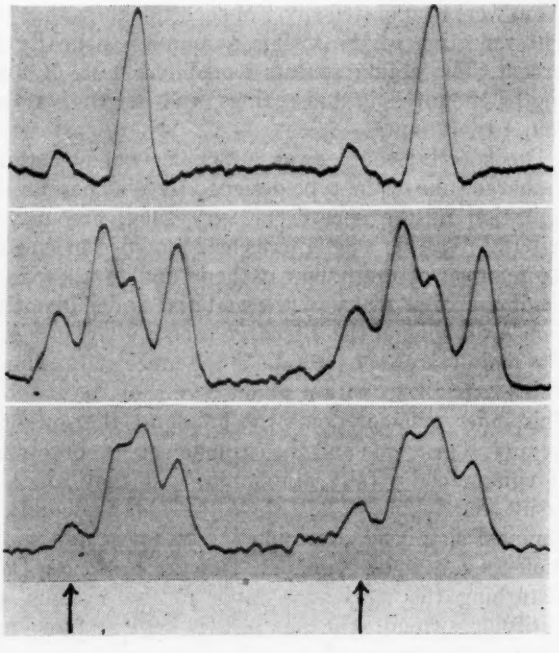

FIG. 3. Microphotometer traces of the line Te II λ5707 taken using natural Te (upper), 80 percent enriched Te^{125} (middle), and 45 percent enriched Te^{123} (lower). The peak indicated by the arrows is not a part of the structure of the line, but is another line appearing in a different order.

[5] See, for example, R. A. Sawyer, *Experimental Spectroscopy* (Prentice Hall, Inc., New York, 1944), p. 259.
[6] R. D. Hill, Phys. Rev. **76**, 333 (1949).
[7] Friedlander, Goldhaber, and Scharff-Goldhaber, Phys. Rev. **74**, 981 (1948).
[8] For an extensive review of this subject, see E. Segrè and A. C. Helmholtz, Rev. Mod. Phys. **21**, 271 (1949).
[9] E. Feenberg and K. C. Hammack, Phys. Rev. **75**, 1877 (1949).
[10] L. Nordheim, Phys. Rev. **75**, 1894 (1949).
[11] M. G. Mayer, Phys. Rev. **75**, 1969 (1949).
[12] H. A. Bethe and R. F. Bacher, Rev. Mod. Phys. **8**, 83 (1936).
[13] Obtained from the Isotopes Division of the Atomic Energy Commission with the assistance of Professors I. Perlman and A. C. Helmholz.
[14] Kindly loaned by Professor J. E. Mack of the University of Wisconsin, as a portion of the material allocated to him by the Isotopes Division of the Atomic Energy Commission.

structures except for magnitude, the splitting of the lines in Te^{123} in each case being about 88 percent that of Te^{125}. Since the splitting is proportional to the magnetic moment of the nucleus, the ratio of magnetic moments in the tellurium isotopes is $\mu_{123}/\mu_{125}=0.88$. A summary of the measurements is given in Table I, and some of the spectrograms are reproduced in Fig. 2. Microphotometer traces of Te II λ5707 are shown in Fig. 3.

In view of the present lack of a term analysis of the Te II spectrum, it is fortunate that the spins of these

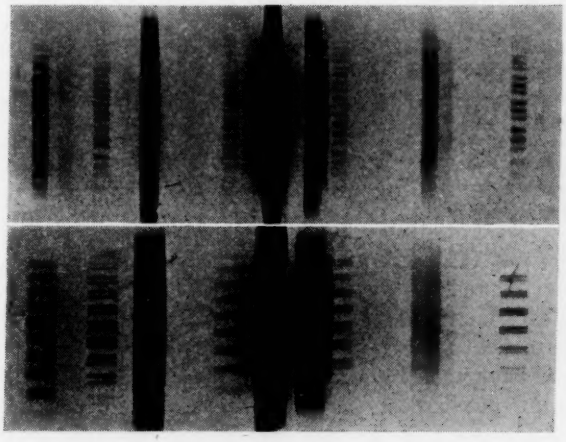

FIG. 4. Fabry-Perot spectrograms taken using natural tungsten (upper) and W^{183} (lower). Etalon separation 19 mm.

isotopes turns out to be $\frac{1}{2}$, since for any higher value it would have been impossible to reach an unambiguous conclusion. As it is, the results are very definite, and should be of considerable interest to the theory of nuclear structure. For example, from Mayer's theory of the shell structure, it would be expected that Te^{123} would have spin $\frac{1}{2}$, but for Te^{125} either $\frac{1}{2}$ or $\frac{3}{2}$ would be possible.

Tungsten

In 1933 Grace, More, and White[15,16] observed isotope structure in the spectrum of neutral tungsten. They found that a number of lines in the visible region consisted of three nearly equidistant components which were attributed to the even isotopes of mass 182, 184, and 186. The abundances of these are 26, 30, and 28 percent, respectively, in natural tungsten. The isotope of mass 180 occurs only in the amount of 0.14 percent, and so its lines did not appear in any of the spectrograms. Tungsten has just one odd isotope, W^{183}, which occurs in the amount 14.4 percent in natural tungsten. Since Grace, More, and White did not observe more than three components in any of the lines, they tentatively suggested that the spin of W^{183} was $\frac{1}{2}$ and that

[15] N. S. Grace and H. E. White, Phys. Rev. 43, 1039 (1933).
[16] N. S. Grace and K. R. More, Phys. Rev. 45, 166 (1935).

TABLE II. Measurements on W^{183}.

Wavelength (Å)	J value	Separation (cm^{-1})	Intensity ratio Meas.	Intensity ratio Theory	Separation of W^{182} and W^{184} (Kopferman and Meyer)
4844	2	0.046	1.4	1.50	0.055
4887	5	0.068	1.1	1.20	0.061
4983	1	0.045			0.059
5053	1	0.050	1.8	2.00	0.052
5069	3	0.057			0.059
5225	2	0.042	1.45	1.50	0.053

the two components due to this isotope practically coincided with two of the three components of the even isotopes. In 1948 Kopferman and Meyer[17] in Germany made some careful measurements on the intensity distribution among the three components in the tungsten spectrum and concluded that the intensities were consistent with the assumption of a spin of $\frac{1}{2}$ for W^{183} and that the two components due to this isotope coincided almost exactly with the components of W^{182} and W^{184} in those lines which show the isotope effect.

In the present investigation photographs taken using tungsten[18] enriched to about 90 percent in W^{183} gave a satisfactory confirmation of Kopferman's conclusions. All of the lines which show the three isotopic components in natural tungsten yield just two components for the enriched odd isotope. The J-values of these lines are known from the classification of Laporte and Mack.[19] Intensity measurements made on some of the lines also verify the fact that the spin is $\frac{1}{2}$. The numerical results are given in Table II. The isotope shift of the components of W^{182} and W^{184} as given by Kopferman and Meyer are included for comparison. A comparison of spectrograms for ordinary tungsten and tungsten 183 is given in Fig. 4.

In conclusion it may be pointed out that although the results reported here merely serve to confirm a conclusion that has been reached by previous investigators, that conclusion was not previously so well substantiated as could be desired. Results based on intensity measurements are notoriously subject to error, and it could well have been that the presence of weak components had been missed. Use of the enriched isotope has, however, put the results on a firm foundation.

The author wishes to express his deep appreciation to Professor F. A. Jenkins under whose very able direction these researches were done. Thanks are due Professor H. E. White for much valuable help. Professor A. C. Helmholz took a stimulating interest in the work for which the author is greatly appreciative.

[17] H. Kopferman and D. Meyer, Zeits. f. Physik 124, 685 (1948).
[18] Obtained from the Isotopes Division of The Atomic Energy Commission with the assistance of Professor I. Perlman.
[19] O. Laporte and J. E. Mack, Phys. Rev. 63, 246 (1943).

The Lorentz Correction in Barium Titanate

J. C. SLATER
*Massachusetts Institute of Technology, Cambridge, Massachusetts**

(Received March 13, 1950)

It is assumed, following Devonshire, that the ferroelectric behavior of $BaTiO_3$ arises because of the Lorentz correction, leading to a vanishing term in the denominator of the expression for dielectric constant. If the polarizability varies slowly with temperature, the temperature variation of dielectric constant follows. This temperature variation is assumed to come from that part of the polarization resulting from the displacement of the Ti ion, in a field whose potential energy has fourth-power as well as second-power terms in the displacement. The main object of this paper is to compute the Lorentz correction exactly, not assuming spherical symmetry, but taking account of the precise crystal structure. When this is done, it is found that the Ti ions, and those oxygen ions which are in the same line with them, the line being parallel to the electric field, exert very strong fields on each other, the resulting local field at the Ti ion being much greater than if computed on the assumption of spherical symmetry. This enhanced field makes it clear that even a relatively small ionic polarizability for the Ti ions will be enough to lead to ferroelectricity. The polarization of the Ti ions is however an essential feature of the theory; if they are not polarized, the Lorentz correction is profoundly modified, leading almost exactly to the value given by the approximate theory assuming spherical symmetry, and not resulting in ferroelectricity. Detailed formulas are given for comparison of the present theory with Devonshire's results, so that the present methods can be incorporated in his treatment of the effect of elastic strain energy on the stability of the various phases below the Curie point.

I. INTRODUCTION

THE ferroelectric properties of barium titanate have aroused much interest in recent years, particularly because its structure is so simple that there is good hope of understanding it fairly completely. Enough progress has been made very recently so that we begin to have a satisfactorily consistent theory of its behavior, but this theory has hardly advanced far enough so that direct numerical comparisons with experiment can be made with complete success. The present paper fills in one missing gap in this theoretical treatment. To explain what this gap is, we give in the present introductory section a discussion of some aspects of the present state of understanding of the problem.

Barium titanate has a ferroelectric Curie point at about 118°C. Above that point, the dielectric constant is of the form $[\text{constant}/(T-T_c)]$, where the constant is very large, of the order of 150,000°K, and where T is the temperature, T_c the Curie temperature.[1] The dielectric constant even of a single crystal does not literally become infinite at the Curie point; the curve is rounded off somewhat, but the Curie law holds to within a very few degrees of the Curie point, so that there are very large dielectric constants. Below the Curie point,[2] there is a permanent polarization and the dielectric constant decreases from the very high values close to the Curie point, but remains high, of the order of several thousand, around room temperature. At about 5°C there is a phase change, and at about −70°C another phase change, the dielectric constant becoming very large near each phase change, and permanent polarization persisting in each phase. The nature of the phase changes is well understood. Above the Curie point at 118°C the crystal is cubic. A unit cell holds a Ba ion at each corner of the cube, an O ion at the center of each face, and a Ti ion at the center of the cube. The permanent polarization in the range between 118° and 5°C is along a 100 direction in the crystal. There is a slight mechanical deformation associated with this polarization: the crystal axis in the direction of the polarization slightly expands, whereas the two axes at right angles to it contract, the amount of mechanical deformation being proportional to the square of the polarization, so that the crystal becomes tetragonal in this range. In the range between 5° and −70°C the polarization is along a 110 direction; here again the crystal stretches along the axis of polarization and shrinks at right angles, producing an orthorhombic symmetry. Below −70°C the polarization is along a 111 direction, again with crystal deformation, resulting now in rhombohedral symmetry. The phase changes from tetragonal to orthorhombic, and from orthorhombic to rhombohedral, are changes of the first order, with latent heats. It is not quite certain experimentally whether the change from cubic to tetragonal is of the first order or is a second-order transition of the lambda-point variety; if it is the latter, however, the increase of polarization just below the transition point occurs much more rapidly than would be expected from elementary theories of lambda-point transitions.

At the various transitions, the free energies of the two phases in equilibrium with each other must be equal. Since these phases correspond to different polarizations, it is clear that it requires a negligible external effect (that is, a negligible electric field) to shift from one phase to the other, or to modify the magnitude or direction of the polarization. This is the qualitative explanation of the very large dielectric constant near the transition temperatures, and it explains as well the directional dependence of dielectric effect. Thus near

* This work was assisted in part by the Signal Corps, the ONR, and the Air Materiel Command.

[1] S. Roberts, Phys. Rev. **75**, 989 (1949); **76**, 1215 (1949).

[2] P. W. Forsbergh, Jr., Phys. Rev. **76**, 1187 (1949) gives an extensive set of references relating to the phase transition.

the transition between tetragonal and orthorhombic form, where the spontaneous polarization is shifting from the 100 to the 110 direction, it is particularly easy to rotate the polarization from the one direction to the other, so that the dielectric constant related to polarizing the crystal at right angles to the existing spontaneous polarization becomes very large, though that associated with changing the magnitude of the polarization, without change of direction, is not unusually large.

With this sketch of some of the observed facts in mind, we naturally ask what is responsible for the abnormally large polarization of the crystal. There are in general two types of possible polarization: electronic polarization, or distortion of the electronic structure of one of the ions, and ionic polarization, arising from the displacement of the ions as a whole. They can be distinguished on the basis of the frequency dependence: in the optical part of the spectrum, where the frequency is too high for whole ions to follow the oscillations, only the electronic polarization remains. The dielectric constant of $BaTiO_3$ as found from the index of refraction in the visible spectrum is no larger than one would expect from the electronic polarizabilities of its constituents, and is[3] in fact about $(2.40)^2=5.76$. Thus it is clear that the abnormality in the low frequency dielectric constant arises from ionic displacement. It is generally considered that it is the Ti ion which is responsible for the effect. The reason is that the Ti ion is surrounded octahedrally by six oxygens; the Ba ions, being rather large, stretch the structure enough so that the hole in the middle of the octahedron occupied by the Ti is slightly too large for that ion, if we compute using conventional ionic radii; and as a result the Ti ion is rather loosely held, with a small restoring force, or large ionic polarizability.[4] This seems to be the qualitative reason for the effect, but it is clear that the ionic polarizability arising in this way is not larger in order of magnitude than that usually found. To explain the enormous effect which this has on the dielectric constant, it is usually to invoke the Lorentz correction in the theory of the Clausius-Mossotti formula. According to the Lorentz correction, we assume that the field acting on a dipole to polarize it is not really $\mathbf{E}$, but is $\mathbf{E}+\mathbf{P}/3\epsilon_0$ (in rationalized m.k.s. units) or $\mathbf{E}+4\pi\mathbf{P}/3$ (in non-rationalized Gaussian units). Let us assume that the dipole moment induced in a volume v is α times the field, where α is the polarizability. We then have $\mathbf{P}=(\alpha/v)(\mathbf{E}+\mathbf{P}/3\epsilon_0)$, so that the dielectric constant is

$$\kappa=1+\frac{P}{\epsilon_0 E}=1+\frac{\alpha/\epsilon_0 v}{1-\alpha/3\epsilon_0 v} \tag{1}$$

in rationalized m.k.s. units; here, as elsewhere throughout the paper, we obtain the corresponding formula in non-rationalized Gaussian units by replacing ϵ_0 wherever it appears by $1/(4\pi)$. From (1) we see that the dielectric constant becomes infinite when $\alpha/3\epsilon_0 v$ (in m.k.s. units) or $4\pi\alpha/3v$ (in Gaussian units) becomes unity. This is the so-called "$4\pi/3$ catastrophe." The ferroelectricity of barium titanate, then, can arise from a quite finite value of the ionic polarizability, and does not demand infinite polarizabilities.

We next ask why the dielectric constant shows the temperature dependence which it does, and why it has a Curie point. We can explain this if we assume that the quantity $\alpha/3\epsilon_0 v$ shows a slow decrease with temperature, being slightly greater than unity at absolute zero, and going through the value unity at a certain temperature T_c, which then must be the Curie temperature. Thus if we have

$$\alpha/3\epsilon_0 v=1-C(T-T_c), \tag{2}$$

where C is a constant, we find at once that

$$\kappa=-2+[3/C(T-T_c)]. \tag{3}$$

This simple hypothesis, then, is enough to result in a Curie law for the dielectric constant; in the region we are interested in, the second term is very large compared to the additive constant, -2, which can be neglected. If, then, the constant in Curie's law is known to be of the order of 150,000°, C is of the order of 2×10^{-5}, indicating a very slow change of the quantity (2) with temperature. What physical mechanism, we may ask, is responsible for this slow decrease of α/v with temperature?

The first suggestion, which has been made by certain writers,[5] is that the change arises from the obvious increase of volume with temperature, coming from the thermal expansion. The volume coefficient of expansion of $BaTiO_3$ is about 3×10^{-5}, so that this alone is more than capable of explaining the whole effect. But this neglects an important fact: as the volume increases, the atoms get farther apart, the repulsive forces between them get smaller, the elastic restoring forces consequently decrease, and the ionic polarizability increases. In fact, there is evidence that α increases faster than v, under these conditions. Thus it is found that either application of pressure,[6] or substitution[4] of smaller ions for Ba, resulting in a decrease of volume at constant temperature, results in a decrease of the Curie temperature. That is, α/v is smaller at a given temperature, for a smaller v, so that we have to go to a lower temperature for the quantity $\alpha/3\epsilon_0 v$ to become equal to unity.

This argument shows that an increase of volume at constant temperature will make α/v increase, rather than decrease. Since we have seen that α/v nevertheless decreases with increasing temperature, there must be an additional influence making α decrease with increasing temperature, at constant volume. Such a possible effect is of course known. The familiar Langevin theory

[3] W. J. Merz, Phys. Rev. **76**, 1221 (1949).
[4] See, for instance, G. H. Jonker and J. H. van Santen, Science **109**, 632 (1949).
[5] For instance, Jonker and van Santen, reference 4.
[6] W. J. Merz, Phys. Rev. **78**, 52 (1950).

of rotating permanent dipoles leads to an average polarization inversely proportional to the absolute temperature. Such a temperature dependence leads to a temperature coefficient C equal to $1/T_c$, very much larger than we are looking for. The rotating dipole is not the only model leading to this temperature dependence. We get it whenever we have an ion which can move in a region of arbitrary shape and size in which the potential energy is constant, surrounded by infinitely high walls; that is, when we have an ion in a potential well. The rotating dipole is the case in which the available region for motion is a thin spherical shell. Other shapes of potential wells which have been discussed are those in which the ion has several alternative locations allowed to it, all with identical energy.[7] Any such model, then, will lead to the same temperature coefficient C, of the order of 100 times as great as the value we are looking for, provided we assume the ordinary Lorentz correction. Such a model is probably approximately correct for rochelle salt,[8] in which C is in fact not far from $1/T_c$; but not for $BaTiO_3$. At the other extreme is an ion held by a linear restoring force; in this case the polarizability α is independent of temperature, so long as the volume, and hence the force constant, remains constant.

Between these two extremes, we should be able to find a model capable of explaining the facts, and in fact we can. If we start with a linear restoring force, but modify the potential by adding a term in the potential energy in the fourth power of the displacement, as well as in the square, we introduce, as Devonshire[9] has shown, a linear decrease of polarizability with temperature whose coefficient C is proportional to the coefficient of the fourth-power term in the potential energy. A reasonable value of this fourth-power term leads to a value of C of the order of magnitude of that observed. It seems highly probable that this is the explanation of the observed temperature variation, and hence of the occurrence of Curie's law. A difficulty arises when we use this model, however. The same fourth-power term in the potential energy of the ion leads not only to a temperature dependence of the polarizability (that is, to a temperature dependence of the coefficient of the term proportional to P^2, where P is the polarization, in the free energy), but leads also to a fourth-power term in the free energy, a term proportional to P^4. Such a term is essential in calculating the spontaneous polarization below the Curie point. If we calculate the spontaneous polarization from this term, however, choosing the coefficient to describe the temperature dependence of polarizability correctly, we find that the polarization increases much more slowly below the Curie point than is observed. This discrepancy between observation and theory is removed, as Devonshire has shown, by including the electromechanical terms in the free energy, the ones which lead to the piezoelectric effect and electrostriction. When the crystal is allowed to distort itself, in the tetragonal phase below the Curie point, the free energy is decreased by a term proportional to the square of the elastic strain. We have already seen that this strain is proportional to the square of the polarization; thus the effect of the electromechanical coupling is to introduce into the free energy a term, with negative coefficient, proportional to P^4. The effect of this term is to make the crystal polarize much more rapidly below the Curie point; in fact, as Devonshire has shown, it is easy for the term to be great enough to lead to a first-order phase change at the Curie point. This mechanical effect does not alter the temperature dependence of the polarizability, however, and hence leaves Curie's law unaffected. Devonshire has shown that, by a complete expansion of the free energy in powers of the polarization and strain, one can arrive at constants for the various coefficients which lead to a rather complete understanding of the successive changes from one type of polarization to another, as the temperature goes down.

This argument seems convincing, and in its broad outlines it is. However, there is a feature missing in it, which we shall supply in the present paper. We have not taken account of the contribution to the polarizability made by the electronic polarization of the various ions of the crystal. The optical value of the dielectric constant shows that the value of $\alpha/3\epsilon_0 v$ arising from the electronic polarization is about 0.61. Thus a further contribution of only about 0.39 must be made to this quantity by the ionic polarizability of the Ti ion, in order to produce ferroelectricity. This fact was entirely neglected in the treatment of Devonshire mentioned above, the most elaborate treatment of the problem to date. Not only this, but our formula (1), on which our discussion has been based, is correct only if the Lorentz correction in its simple form is valid. But it has been pointed out by several writers[4,10] that there are large deviations from the Lorentz formula in the $BaTiO_3$ crystal. If the polarization is along a 100 direction, a third of the oxygens will fall into linear arrays, in the same lines in which the Ti ions are located; these we shall call oxygens of type a. The other two-thirds, which we shall call type b, do not fall in line with the Ti ions. We now find that in the presence of the Ti ions, the type a oxygens are much more strongly polarized than the type b ions. Furthermore, these type a oxygens are very close to the Ti ions, and are oriented in such a way as to be able to polarize the Ti ions with maximum effect. The result is that the Ti ions are really in a field

[7] W. P. Mason and B. T. Matthias, Phys. Rev. **74**, 1622 (1948). These writers explain the temperature variation by use of an artificially low value for the Lorentz correction which, in the light of the present paper, seems to have no physical justification.

[8] W. P. Mason, Phys. Rev. **72**, 854 (1947).

[9] A. F. Devonshire, Phil. Mag. (Series 7) **40**, 1040 (1949). Such calculations regarding the effect of a fourth-power term in the energy were made independently by P. W. Anderson, Phys. Rev. **78**, 341 (1950), and by the present writer, before the work of Devonshire came to their attention.

[10] H. F. Kay and P. Vousden, Phil. Mag. (Series 7) **40**, 1019 (1949).

much greater than the Lorentz value $E+P/3\epsilon_0$. The field is, so to speak, enhanced at the location of the Ti ion by a considerable factor. Thus, in order to result in ferroelectricity, we do not need nearly as great an ionic polarizability on the part of the Ti as we should otherwise suppose. In fact, we shall find that the quantity $\alpha/3\epsilon_0 v$ arising from the ionic polarizability of the Ti need be only 0.06 in order to produce ferroelectricity, rather than the value 0.39 mentioned above. The perovskite structure met in the ferroelectric form of $BaTiO_3$ is thus particularly favorable for the production of ferroelectricity. It has already been pointed out[11] that the other polymorphic forms of $BaTiO_3$, which do not have these rows of alternating Ti and O ions, do not have this favorable predisposition toward ferroelectricity, and in fact they show quite ordinary dielectric behavior.

The main point of the present paper, then, is to work out the Lorentz correction in detail, and to show how it is to be incorporated into calculations of the dielectric constant and the free energy of the type made by Devonshire. As a preliminary to this, we take up in the next section the calculation of the free energy of the crystal, as arising from the displacement of the Ti ion in the field of its neighbors, including a fourth-power term, following to a considerable extent the calculations of Devonshire. We adopt a rather different statistical method, however, which seems more straightforward than his. Then we pass on to the treatment of the Lorentz correction, taking account of the actual crystal structure of $BaTiO_3$.

II. THE FREE ENERGY OF Ti IONS IN A NON-LINEAR FIELD

In our first discussion we shall treat the Ti ions as being independent of each other; later we shall consider their interactions. Let the potential energy of an ion at position (x, y, z) (measured from the position of equilibrium of the ion) in the absence of an external field be $\phi(x, y, z)$. When it is displaced to position x, y, z, let the resulting dipole moment have components (qx, qy, qz), q being the effective charge on the ion. We shall assume ϕ to have cubic symmetry, on account of the symmetry of the field surrounding the Ti ions. In this respect we introduce greater specialization than does Devonshire, who assumes a general potential energy. That assumption is necessary if, for instance, we are interested in the displacement of an oxygen ion, since these are not in positions of cubic symmetry in the lattice, but it is not necessary for the Ti ions, which we assume make the principal contribution to the ionic polarization. Now let there be a local electric field E, of components (E_x, E_y, E_z), acting on the ion. (We postpone until later the question as to how this depends on the external applied field.) Then the additional potential energy of the ions in this local field is $-q(E_x x+E_y y+E_z z)=-q\mathbf{E}\cdot\mathbf{r}$, where $\mathbf{r}$ is the radius vector.

We shall now proceed to treat this system by statistical mechanics. We shall operate entirely with classical statistical mechanics; this should be suitable at the temperatures concerned in the $BaTiO_3$ problem, though our results would need correction at fairly low temperatures. Then the first step in handling the problem statistically is to compute the partition function, Z. If we were dealing with a single polarizable ion, this would be $(2\pi mkT/h^2)^{\frac{3}{2}}w$, where m is the mass of the ion, and

$$w=\int \exp(-\phi+q\mathbf{E}\cdot\mathbf{r})/kT\,dv. \tag{4}$$

If our system contains N identical ions, the whole partition function is the value above, raised to the Nth power, divided by $N!$; or, using the Stirling formula for the factorial, we have

$$Z=[(e/Nh^3)(2\pi mkT)^{\frac{3}{2}}]^N w^N.$$

The free energy A_E is then given by the equation $A_E=-kT\ln Z$. That is,

$$A_E=-NkT\ln[(e/Nh^3)(2\pi mkT)^{\frac{3}{2}}]-NkT\ln w.$$

This free energy is expressed as a function of T and E; it is for this reason that we have denoted it by the subscript E. The entropy is given by $-(\partial A_E/\partial T)_E$, and hence is

$$S=Nk\ln[(e/Nh^3)(2\pi mkT)^{\frac{3}{2}}]+(3/2)Nk+Nk\ln w +NkT(\partial\ln w/\partial T)_E.$$

By differentiation of (4), the last term may be rewritten

$$NkT(\partial\ln w/\partial T)_E=N\langle\phi-q\mathbf{E}\cdot\mathbf{r}\rangle/T,$$

where $\langle\phi-q\mathbf{E}\cdot\mathbf{r}\rangle$ signifies the average value of this quantity over the distribution given by the Boltzmann factor $\exp[(-\phi+q\mathbf{E}\cdot\mathbf{r})/kT]$. The total dipole moment of the distribution is given by $-(\partial A_E/\partial E_x)_T$, etc., so that its x-component is

$$(\text{Moment})_x=NkT(\partial\ln w/\partial E_x)_T=Nqx, \tag{5}$$

where again the last form comes by differentiating (4). The internal energy U is given by $U=A_E+TS$; thus it is

$$U=(3/2)NkT+N\langle\phi-q\mathbf{E}\cdot\mathbf{r}\rangle,$$

the sum of the kinetic energy as given by equipartition, and the mean potential energy of the ions as displaced by the field $\mathbf{E}$. In all these formulas if we are dealing with unit volume of the material, so that N becomes the number of ions per unit volume, our expressions give the values of free energy, entropy, moment, and so on, per unit volume. Thus in particular the moment per unit volume, given by (5), is the polarization vector $\mathbf{P}$. If the volume per ion, or the volume of unit cell, is v, as in the preceding section, we then have the number of atoms per unit volume, or N, equal to $1/v$, so that we can express the quantities properly by replacing N by $1/v$.

[11] R. D. Burbank and H. T. Evans, Jr., Acta Crys. 1, 330 (1948); H. T. Evans, Jr., and R. D. Burbank, J. Chem. Phys. 16, 634 (1948).

If we are dealing with unit volume, we then have $S=-(\partial A_E/\partial T)_E$, $P_z=-(\partial A_E/\partial E_z)_T$. Then we have at once

$$(\partial S/\partial E_z)_T=(\partial P_z/\partial T)_E, \tag{6}$$

analogous to the Maxwell relations of thermodynamics. This shows us that if the polarization depends on temperature, the entropy must depend on the field, or polarization. If, for instance, we assume that the polarizability depends on temperature as in Eq. (2), we then find from (6) that at the Curie point

$$S=S_0-\tfrac{1}{2}\,3\epsilon_0CE^2=S_0-CP^2/6\epsilon_0,$$

where S_0 is the value of entropy when E or P is zero. We therefore see that if C is small, the change of entropy with polarization is also small, so that there is only a small increase of entropy in going from the ferroelectric state at low temperature to the unpolarized state at high temperature.

The free energy A_E which we have computed, like the Helmholtz free energy in ordinary problems of statistical mechanics, is the one which is simplest to find, from the partition function. More convenient for most purposes, however, is a free energy A_P, analogous to the Gibbs free energy, expressed in terms of the polarization and temperature, rather than in terms of the field and temperature. This is defined by the relation

$$A_P=A_E-E_x\left(\frac{\partial A_E}{\partial E_x}\right)_T-E_y\left(\frac{\partial A_E}{\partial E_y}\right)_T-E_z\left(\frac{\partial A_E}{\partial E_z}\right)_T$$

and is to be expressed as a function of P and T. That is, it is $A_P=A_E+\mathbf{E}\cdot\mathbf{P}$, if we are dealing with unit volume of material. When expressed in terms of the proper variables, it has the properties that

$$S=-(\partial A_P/\partial T)_P, \quad E_x=(\partial A_P/\partial P_x)_T. \tag{7}$$

In many ways the most convenient way to approach the problem is to find A_P as a function of P and T; we shall discuss the results later. We note that in the absence of an electric field E, the free energy A_P will have a minimum value as far as changes of polarization are concerned, at constant temperature. Corresponding to this, A_P will be unchanged when there is a change of phase, involving change of polarization, at constant temperature, so that the equality of the values of A_P for the two phases is the condition for equilibrium. It is this free energy A_P which Devonshire considers in his paper, but his method of finding it is less straightforward.

We now have the necessary statistical and thermodynamic background for our calculations of free energy. Following Devonshire, but modifying his results for the special case of cubic symmetry, we shall assume that the potential energy of a displaced ion is

$$\phi(x,y,z)=a(x^2+y^2+z^2)+b_1(x^4+y^4+z^4)+2b_2(y^2z^2+z^2x^2+x^2y^2).$$

For the case of spherical symmetry, b_1 will equal b_2, and ϕ will reduce to ar^2+br^4. We must now insert this expression into (4), and compute the partition function. This cannot be carried out exactly, and we therefore use series expansion methods, treating b_1 and b_2 as small quantities, and disregarding all terms of higher powers than the first in these quantities. We expand the quantity $-\phi+q\mathbf{E}\cdot\mathbf{r}$ appearing in the exponent of (4) in power series in the coordinates about the point where it is a minimum, and it then becomes the sum of a term independent of the b's, and a term linear in the b's. We expand the exponential function of this linear term in power series, retaining only the term in the series linear in the b's. The integration then becomes straightforward, and we find

$$w=(\pi kT/a)^{\frac{3}{2}}\exp(q^2E^2/4akT)\Big\{1-\tfrac{3}{4}(3b_1+2b_2)(kT/a^2)-\frac{q^2(3b_1+2b_2)}{4a^3}(E_x^2+E_y^2+E_z^2)-\frac{q^4}{16a^4kT}[b_1(E_x^4+E_y^4+E_z^4)+2b_2(E_y^2E_z^2+E_z^2E_x^2+E_x^2E_y^2)]\Big\}.$$

This agrees with the result of Devonshire [reference 9, Eq. (10.11)], provided we consider the differences in notation. The free energy A_E is then

$$A_E=-NkT\ln[(e/Nh^3)(\pi kT)^3(2m/a)^{\frac{3}{2}}]-Nq^2E^2/4a+\frac{3N(kT)^2}{4a^2}(3b_1+2b_2)+NkT(3b_1+2b_2)q^2E^2/4a^3+\frac{Nq^4}{16a^4}[b_1(E_x^4+E_y^4+E_z^4)+2b_2(E_y^2E_z^2+E_z^2E_x^2+E_x^2E_y^2)].$$

From this free energy, we can use our general equations to calculate various other quantities. Thus we find

$$S=Nk\ln[(e/Nh^3)(\pi kT)^3(2m/a)^{\frac{3}{2}}]+3Nk-\frac{3}{2}\frac{Nk^2T}{a^2}(3b_1+2b_2)-Nk(3b_1+2b_2)q^2E^2/4a^3, \tag{8}$$

$$P_x=\frac{Nq^2E_x}{2a}\left[1-\frac{kT(3b_1+2b_2)}{a^2}\right]-\frac{Nq^4}{4a^4}E_x[b_1E_x^2+b_2(E_y^2+E_z^2)], \tag{9}$$

$$U=3NkT-Nq^2E^2/4a+\frac{Nq^4}{16a^4}[b_1(E_x^4+E_y^4+E_z^4)+2b_2(E_y^2E_z^2+E_z^2E_x^2+E_x^2E_y^2)],$$

$$A_P = -NkT\ln[(e/Nh^3)(\pi kT)^3(2m/a)^{\frac{1}{2}}]$$
$$+\frac{3N(kT)^2}{4a^2}(3b_1+2b_2)+\frac{aP^2}{Nq^2}\left[1+\frac{kT}{a^2}(3b_1+2b_2)\right]$$
$$+\frac{1}{N^3q^4}[b_1(P_x^4+P_y^4+P_z^4)$$
$$+2b_2(P_y^2P_z^2+P_z^2P_x^2+P_x^2P_y^2)]. \quad (10)$$

At this point our treatment has differed significantly from that of Devonshire (who introduces the Lorentz correction before making these steps), so that (10) does not agree with Devonshire's Eq. (10.13) (which, in addition, contains several misprints).

Let us now call attention to a number of aspects of these results. From (9), giving the polarization as a function of the field, we see, as we mentioned in the preceding section, that the polarization decreases linearly with temperature, for constant local field. It is this decrease of polarizability with temperature which we have seen in Eqs. (2) and (3) to be responsible for the temperature dependence of the dielectric constant in the neighborhood of the Curie point. In order to get a small temperature dependence of polarization, we clearly need only assume a small value of the quantity $(3b_1+2b_2)$, determining the non-linear behavior of the law of force. We shall return later to the necessary value of this quantity, and show that it is reasonable. Associated with this decrease of polarizability with temperature is a decrease of entropy, as given in (8), with electric field; we immediately verify that Eq. (6) is satisfied. It is interesting to look into the physical reason for this change of entropy with polarization, for by (6) this will then tell us why the polarizability decreases with temperature. Let us consider the entropy for a linear oscillator, in which the b's are zero. From (8), we have in this case

$$S = Nk\ln[(e/Nh^3)(\pi kT)^3(2m/a)^{\frac{1}{2}}]+3Nk.$$

Let us particularly observe the dependence on a: S contains a term $-(3/2)Nk\ln a$. This dependence is fundamental, and has a simple explanation. For a large restoring force constant a, the particle at a given energy, or temperature, is confined to a small volume; but we know that the smaller the effective volume available to a particle, the smaller is its entropy. Or alternatively, for a large value of a, the frequency of oscillation of the particle will be large, its stationary states as given by the quantum condition will be far apart, and at a given temperature there will be fewer occupied states than for a smaller value of a; this again leads to small entropy. Now let us return to our case of the non-linear restoring force, where the b's are different from zero, and positive. If we polarize the ion by a local field, so that its position of equilibrium is displaced from the origin of our (x, y, z) coordinates, the fourth-power terms will have the effect of increasing the restoring force constant for this new position of equilibrium, increasing the vibration frequency about that point, and hence decreasing the entropy. It is this effect which results in the term in E^2, in (8). At the same time, as the temperature goes up, the particle spends more time in a region of high amplitude, where the restoring force constant is larger; this results in the decrease of entropy with temperature described by the term $-(Nk^2T/a^2)3(3b_1+2b_2)/2$ in (8). In this way we understand the effect of the fourth-order terms on the entropy, and hence on the polarizability. It is interesting to see that the effect is very simple and elementary, and quite different from any order-disorder explanation of entropy change, such as is invoked in some other phenomena leading to lambda-points.

III. THE NATURE OF THE LORENTZ CORRECTION

In Section II, we assumed that the various Ti ions vibrated quite independently of each other. This assumption is incorrect, since actually they exert forces on each other, rather than having an external force acting on them which depends only on their displacement. This situation is well known from the theory of the specific heat of solids. We know that if we treat the vibrations of the atoms separately, we arrive at a specific heat theory of the Einstein type. On the other hand, if we consider their interactions, we must introduce normal coordinates, describing the various standing waves which can be set up in the crystal, and arrive at a specific heat theory of the Debye type. If there are several types of atoms or ions, then as Born and others have shown, there will be various branches to the vibration spectrum, some being of the so-called acoustical type, and having frequencies extending down to acoustical ranges, while others are of the so-called optical type, with frequencies in the infra-red. These optical vibrations are the ones in which the ions of different type oscillate in opposite directions; they are connected with the residual rays or *Reststrahlen*. In our case, the vibrations of the Ti ions with respect to the rest of the lattice will be of this optical type. And in general it is found that the spectrum of frequencies in an optical branch is not widely spread out, so that the correct theory is not greatly different from an Einstein-type theory, in which all frequencies are assumed to be identical. For this reason, in the present treatment we shall not consider the interactions of the ions, but shall treat them as being independent. The writer has been informed by Dr. P. A. Anderson, of the Bell Telephone Laboratories, that he is working on a more elaborate treatment, in which the normal coordinates are properly introduced.

This simple discussion is correct in some respects; but it neglects a very important aspect of the problem, the Lorentz correction. The ordinary theory of elastic vibrations of the ions deals with short-range forces, only interactions between nearest neighbors ordinarily being considered. When the ions by their displacements

produce electric dipoles throughout the interior of the solid, however, these dipoles produce long-range electric forces acting on each dipole of the system, and these dipole forces must be considered separately. We can make a first approximation to a theory including these Lorentz forces if we proceed in the following way. We introduce as coordinates representing the motion of the Ti ions first the coordinate of the average displacement, or center of gravity, of all the ions; then, as additional coordinates, the displacements of the separate ions from the displaced position which they would take up if the whole Ti lattice were displaced bodily. The displacement of the whole lattice will be equivalent to the polarization produced by the ions, and there will be a term in the energy coming from the Lorentz interaction of the field produced by the resulting dipoles, with the dipoles themselves. There will be further terms in the energy arising from the displacements of the separate ions from this average position, and these will be treated essentially as in the preceding section. This is admittedly only a partially satisfactory way of handling the complete problem of the interactions of the displaced ions, including their electrostatic interactions, but it should give a satisfactory first approximation.

Let us see how it would work out, if the Lorentz assumption of spherical symmetry were correct. In that case, if there were a polarization $\mathbf{P}$, the local field acting on a given ion would be $\mathbf{E}+\mathbf{P}/3\epsilon_0$. If the ions were displaced in such a way as to produce the polarization $\mathbf{P}$, each ion would make a negative contribution to the electrostatic energy, since it is displaced in the direction of the field $\mathbf{P}/3\epsilon_0$. The total electrostatic energy per unit volume arising in this way will be $-P^2/6\epsilon_0$, the factor $\frac{1}{2}$ (leading to $-P^2/6\epsilon_0$ rather than $-P^2/3\epsilon_0$) arising because we are really dealing with interactions of forces between pairs of dipoles, and we must count each pair only once, not twice. We can then take care of the Lorentz correction by supplementing the free energy A_P of (10) by this correction term $-P^2/6\epsilon_0$, where we are dealing specifically with unit volume of material.

We can now take this revised free energy, and inquire what is the polarization as a function of field arising from it, and consequently what effect the Lorentz correction has on the dielectric constant. From (7) we find

$$E_x=\frac{2aP_x}{Nq^2}\left[1+\frac{kT}{a^2}(3b_1+2b_2)\right]-\frac{P_x}{3\epsilon_0}+\frac{4P_x}{N^2q^4}[b_1P_x^2+b_2(P_y^2+P_z^2)]. \quad (11)$$

If we disregard the cubic term, to get the dielectric behavior above the Curie point, in a small field, and solve for P_x, treating the b's as small quantities, we have

$$P_x=\frac{Nq^2}{2a}\left[1-\frac{kT}{a^2}(3b_1+2b_2)\right]\left(E_x+\frac{P_x}{3\epsilon_0}\right).$$

This agrees with the assumption leading to Eq. (1), and when we remember that $N=1/v$, we see that the polarizability α is given by

$$\alpha=\frac{q^2}{2a}\left[1-\frac{kT}{a^2}(3b_1+2b_2)\right], \quad (12)$$

showing a linear decrease with temperature proportional to the b's, qualitatively agreeing with (2). Thus our addition of the correction term $-P^2/6\epsilon_0$ has correctly taken care of the Lorentz correction. We note that the entropy expressed as a function of the P's, by (7), is unaffected by the presence or absence of the Lorentz correction; it is

$$S=Nk\ln[(e/Nh^3)(\pi kT)^3(2m/a)^{\frac{1}{2}}]+3Nk-\frac{3Nk^2T}{2a^2}(3b_1+2b_2)-\frac{P^2k}{Naq^2}(3b_1+2b_2).$$

This shows the quadratic decrease of entropy with polarization, proportional to the b's, which we have already discussed.

We can discuss the spontaneous polarization below the lambda-point from the expression (11). Let the applied field $\mathbf{E}$ be zero. Then we have various possibilities for spontaneous polarization. Let us consider the simple case where P_x is different from zero, P_y and P_z equal to zero. Then we have from (11)

$$\frac{P_x^2}{\epsilon_0}=\frac{N^2q^2a}{2b_1\epsilon_0}\left[\frac{Nq^2}{6\epsilon_0 a}-1-\frac{kT}{a^2}(3b_1+2b_2)\right]. \quad (13)$$

The spontaneous polarization will be zero at the Curie point; hence we have

$$Nq^2/(6\epsilon_0 a)=1+[kT_c(3b_1+2b_2)/a^2]. \quad (14)$$

We may then rewrite (13), correct to linear terms in the b's, in the form

$$(P_x^2)/\epsilon_0=3Nk(3b_1+2b_2)(T_c-T)/b_1. \quad (15)$$

This indicates that P is proportional to $(T_c-T)^{\frac{1}{2}}$ below the Curie point, the usual type of dependence for a lambda-point theory. If the actual transition is a lambda-point transition rather than a phase change of the first order, however, the temperature dependence of polarization given by (15) is much too slow. Thus if we have something not far from spherical symmetry for the Ti ion, so that b_1 and b_2 are comparable in size, and (15) reduces to 15 $Nk(T_c-T)$, comparison with observed curves shows that if the real variation of polarization with temperature is to be fitted to a curve of the form (15), the coefficient must be something like 60 times as large as that given above. This situation, as we indicated in the introductory section, can be corrected by considering elastic distortion of the crystal, as we shall describe in a later section.

IV. THE LORENTZ CORRECTION FOR THE ACTUAL CRYSTAL

In the preceding section, we have considered the way in which the Lorentz correction affects the free energy, and hence the expression for dielectric constant. Now we are ready to ask how this argument is modified if we take account of the polarizability of the other ions in the crystal. In the present section we shall deal only with the polarization above the Curie point, where the polarization is proportional to the field. In the next section we extend the argument to a calculation of the effect of the Lorentz correction on the free energy, so as to treat the problem below the Curie point.

In the $BaTiO_3$ crystal, each unit cell contains five ions. Let us assume that the crystal is polarized along the z axis; symmetry demands that each of the ions be polarized along the z axis. Let us then write the total polarization in the crystal as the sum of five terms: the polarizations arising from each type of ion. When we consider the whole crystal, each of these types of ions will form a simple cubic lattice. We then visualize for each type of ion a simple cubic lattice of equal dipoles, and we wish to find the field of these dipoles at one of the lattice points. It is well known that the field of a simple cubic lattice of dipoles at one of its lattice points is $\mathbf{P}/3\epsilon_0$, where $\mathbf{P}$ is the polarization resulting from this lattice alone. Thus, for instance, if we had only the polarization arising from the displacement of the Ti ions, as we were considering in the preceding section, the Lorentz correction as treated in that section would be correct. However, the field of a simple cubic lattice of dipoles is not equal to $\mathbf{P}/3\epsilon_0$ at most points within the unit cell. Thus for instance the field exerted by the lattice of Ti ions is not equal to $\mathbf{P}/3\epsilon_0$ at the position of one of the oxygen ions, but is quite a different amount. What we must do is to examine the field actually exerted at the position of each ion, by the lattices of the dipoles of all types of ions.

Fortunately the necessary calculations have been performed in papers by McKeehan[12] and by Luttinger and Tisza.[13] Luttinger and Tisza give the field exerted at various points through the lattice by a lattice of dipoles whose polarization is unity, polarized along the z direction. They express their results in the nonrationalized Gaussian units, and the fields which they give are those in addition to the value $4\pi\mathbf{P}/3$. Thus they find that the additional field at a point (ξ, η, ζ) in the unit cell, where ξ, η, ζ are the ratios of the displacement from a lattice point to the lattice spacing, are given by expressions $S_z(\xi, \eta, \zeta)$, where

$$\begin{aligned} &S_z(0,0,0)=S_z(\tfrac{1}{2},\tfrac{1}{2},\tfrac{1}{2})=0 \\ &S_z(0,\tfrac{1}{2},\tfrac{1}{2})=4.334, \quad S_z(\tfrac{1}{2},\tfrac{1}{2},0)=-8.668, \\ &S_z(\tfrac{1}{2},0,0)=-15.040, \quad S_z(0,0,\tfrac{1}{2})=30.080. \end{aligned} \tag{16}$$

Let us see what these mean. The first statements show that the ordinary Lorentz correction $4\pi\mathbf{P}/3$ (in Gaussian units) is correct not only at a lattice point, but at a point in the center of the unit cell. Thus this ordinary correction is valid for the actions of the Ba and Ti ions on themselves and on each other. On the other hand, for interactions between the oxygens and the other ions, the ordinary correction is entirely incorrect. Thus if we ask for the action of the Ti ions on those oxygens which lie along the same line parallel to the polarization (or z axis), which we have previously called oxygens of type a, we find that the Lorentz correction is really $(30.080+4\pi/3)\mathbf{P}$, or approximately 8.2 times the ordinary value $4\pi\mathbf{P}/3$. The action of the oxygens of type a on the Ti ions contains this same greatly enhanced Lorentz factor. It is this fact which we shall find operating to make the field at the position of the Ti ions so much greater than we should get from a simple Lorentz argument, as we mentioned in the introductory section.

Let us now write the polarization of the Ti ions as P_{Ti}, that of the Ba ions as P_{Ba}, that of the oxygens of type a as P_{Oa}, and that associated with the two lattices of oxygens of type b as P_{Ob1} and P_{Ob2}. By symmetry, we shall find that $P_{Ob1}=P_{Ob2}$, but it will simplify our procedure to keep them separate. These polarizations are assumed to arise from electronic polarization, except in the case of P_{Ti}, where we shall sometimes assume that it is the sum of that arising from electronic and ionic polarizations. Then from the relations (16) we can write the effective or local fields acting on each type of ion to polarize it. We shall write these fields in the m.k.s. system; to get the corresponding formulas in the Gaussian system, we replace ϵ_0 by $1/(4\pi)$, as usual. We shall then want to use the quantities $8.668/4\pi$ and $30.080/4\pi$. We shall abbreviate these as

$$8.668/4\pi=0.690=p, \quad 30.080/4\pi=2.394=q. \tag{17}$$

Then we have:

$$\begin{aligned} \text{Field on Ti}&=E+(1/\epsilon_0)[\tfrac{1}{3}P_{\mathrm{Ti}}+\tfrac{1}{3}P_{\mathrm{Ba}} \\ &\quad +(q+\tfrac{1}{3})P_{Oa}+(-\tfrac{1}{2}q+\tfrac{1}{3})(P_{Ob1}+P_{Ob2})]. \\ \text{Field on Ba}&=E+(1/\epsilon_0)[\tfrac{1}{3}P_{\mathrm{Ti}}+\tfrac{1}{3}P_{\mathrm{Ba}} \\ &\quad +(-p+\tfrac{1}{3})P_{Oa}+(\tfrac{1}{2}p+\tfrac{1}{3})(P_{Ob1}+P_{Ob2})]. \\ \text{Field on } Oa&=E+(1/\epsilon_0)[(q+\tfrac{1}{3})P_{\mathrm{Ti}}+(-p+\tfrac{1}{3})P_{\mathrm{Ba}} \\ &\quad +\tfrac{1}{3}P_{Oa}+(\tfrac{1}{2}p+\tfrac{1}{3})(P_{Ob1}+P_{Ob2})]. \\ \text{Field on } O_{b1}&=E+(1/\epsilon_0)[(-\tfrac{1}{2}q+\tfrac{1}{3})P_{\mathrm{Ti}} \\ &\quad +(\tfrac{1}{2}p+\tfrac{1}{3})P_{\mathrm{Ba}}+(\tfrac{1}{2}p+\tfrac{1}{3})P_{Oa}+\tfrac{1}{3}P_{Ob1} \\ &\quad +(-p+\tfrac{1}{3})P_{Ob2}]. \end{aligned} \tag{18}$$

The equation for the field at O_{b2} is like that at O_{b2}, with subscripts 1 and 2 interchanged. We observe, as we pointed out above, the very large factor $q+\frac{1}{3}$ by which the Ti ions and the type a oxygen ions interact on each other.

We can now set up simultaneous equations, stating that the polarization resulting from each type of ion equals the corresponding polarizability per unit volume,

[12] L. W. McKeehan, Phys. Rev. **43**, 913 (1933); **72**, 78 (1947).
[13] J. M. Luttinger and L. Tisza, Phys. Rev. **70**, 954 (1946); **72**, 257 (1947).

multiplied by the appropriate local field.[14] Let the polarizabilities of Ti, Ba, and O be α_{Ti}, α_{Ba}, and α_O, respectively; α_{Ti} will be assumed to be the electronic polarizability, and will be specifically augmented by the ionic polarizability when we are dealing with low frequencies. Then we have

$$\begin{aligned} P_{Ti} &= (\alpha_{Ti}/v)(\text{field on Ti}),\\ P_{Ba} &= (\alpha_{Ba}/v)(\text{field on Ba}),\\ P_{Oa} &= (\alpha_O/v)(\text{field on O}a),\\ P_{Ob1} &= (\alpha_O/v)(\text{field on O}b_1),\\ P_{Ob2} &= (\alpha_O/v)(\text{field on O}b_2), \end{aligned} \tag{19}$$

where the fields are as given in (18). We at once see by inspection that $P_{Ob1}=P_{Ob2}$, so that we have four simultaneous equations for the four unknowns P_{Ti}, P_{Ba}, P_{Oa}, P_{Ob1}. These equations can be solved by determinants for the polarizations, as functions of E. We can also solve for the dielectric constant, which we get from the sum of all the polarizations, divided by the field. In expressing these quantities, we encounter the combinations $\alpha_{Ti}/\epsilon_0 v$, and similar expressions for the other polarizabilities. We abbreviate these as X_{Ti}, etc., so that by definition we have $X_{Ti}=\alpha_{Ti}/\epsilon_0 v$ (in m.k.s. units), or $4\pi\alpha_{Ti}/v$ (in Gaussian units), with similar expressions for X_{Ba}, X_O. In terms of these quantities, the solutions of (19) prove to be

$$\begin{aligned} P_{Ti}/(\epsilon_0 E) &= (X_{Ti}/\Delta)\{1+pX_O\\ &\quad -(3/2)p(p+q)X_{Ba}X_O+\tfrac{1}{2}p(3q-p)X_O^2\}\\ P_{Ba}/(\epsilon_0 E) &= (X_{Ba}/\Delta)\{1+pX_O\\ &\quad -(3/2)q(p+q)X_{Ti}X_O-2p^2X_O^2\}\\ P_{Oa}/(\epsilon_0 E) &= (X_O/\Delta)\{1+2pX_O+qX_{Ti}-pX_{Ba}\\ &\quad -\tfrac{1}{2}q(3q-p)X_{Ti}X_O-2p^2X_{Ba}X_O\}\\ P_{Ob1}/(\epsilon_0 E) &= (X_O/\Delta)\{1+\tfrac{1}{2}pX_O-\tfrac{1}{2}qX_{Ti}+\tfrac{1}{2}pX_{Ba}\\ &\quad -\tfrac{1}{2}q(3q-p)X_{Ti}X_O-2p^2X_{Ba}X_O\}\\ \kappa-1 &= (1/\Delta)\{X_{Ti}+X_{Ba}+3X_O+pX_{Ti}X_O\\ &\quad +pX_{Ba}X_O+3pX_O^2-(3/2)(p+q)^2X_{Ti}X_{Ba}X_O\\ &\quad -\tfrac{1}{2}(3q-p)^2X_{Ti}X_O^2-8p^2X_{Ba}X_O^2\}\\ \Delta &= 1-\tfrac{1}{2}(X_{Ti}+X_{Ba})+(p-1)X_O\\ &\quad -(\tfrac{1}{3}p+(3/2)q^2)X_{Ti}X_O-p(\tfrac{1}{3}+(3/2)p)X_{Ba}X_O\\ &\quad -p(1+\tfrac{1}{2}p)X_O^2+\tfrac{1}{6}(3q-p)^2X_{Ti}X_O^2\\ &\quad +(8/3)p^2X_{Ba}X_O^2+\tfrac{1}{2}(p+q)^2X_{Ti}X_{Ba}X_O. \end{aligned} \tag{20}$$

In Eqs. (20) we have solved our problem of setting up the correct Lorentz factors for the $BaTiO_3$ structure. Let us now examine some of the implications of these formulas. It can be verified that in spite of their complication they reduce to the exact Lorentz expression in two important cases: first, when X_{Ti} is zero, and X_{Ba} equals X_O; second, when X_O is zero. The first case is one in which the oxygen and barium ions, assumed identical for that special case, together form a face-centered cubic lattice; the latter that in which the barium and titanium together form a body-centered cubic lattice. Let us now ask what is the situation with the actual numerical values for $BaTiO_3$, in the optical spectrum, so that we disregard the ionic polarizability of the Ti. As values for the electronic polarizabilities of the various ions, we take the following values:

$$\begin{aligned} &\alpha_{Ti}/\epsilon_0(\text{m.k.s.}) = 4\pi\alpha_{Ti}\ (\text{Gaussian}) = 2.34\times10^{-24}\ \text{cc}\\ &\alpha_{Ba}/\epsilon_0 = 24.42\times10^{-24}\ \text{cc},\quad \alpha_O/\epsilon_0 = 30.0\times10^{-24}\ \text{cc}. \end{aligned} \tag{21}$$

The values for Ti and Ba were supplied by P. W. Anderson and W. Shockley of the Bell Telephone Laboratories; they come from unpublished work involving an intercomparison of the refractivities of a good many crystals.[15] The value for oxygen is chosen to give the correct value for the optical dielectric constant, which except for a small deviation very close to the Curie point is approximately $(2.40)^2=5.76$. This procedure is in accordance with the findings of the group at the Bell Telephone Laboratories, who find that the oxygen ion appears to show different polarizabilities in compounds of different structure.[16] We take the lattice spacing to be 4.00×10^{-8} cm, a value which is correct at a temperature in the required range (we neglect the thermal expansion at this point), so that v is 64×10^{-24} cc. Then we have

$$X_{Ti}=0.0365,\quad X_{Ba}=0.382,\quad X_O=0.470. \tag{22}$$

When we substitute these values, and p and q as given in (17), into Eqs. (20), we find that we get the correct value 5.76 for the dielectric constant. The associated value of $(\kappa-1)/(\kappa+2)$ is 0.613. If the ordinary Lorentz correction were applicable, this would be equal to $\frac{1}{3}(X_{Ti}+X_{Ba})+X_O$, which is 0.609. In other words, in this case of the optical refractivities, the ordinary Lorentz formula gives a very good approximation to the truth. The reason for this is undoubtedly that X_{Ti} is small, X_{Ba} is of the same order of magnitude as X_O, so that we are not very far from the special case $X_{Ti}=0$, $X_{Ba}=X_O$, in which we have pointed out that (20) reduces exactly to the Lorentz case.

It is also interesting to calculate the polarizations of the various types of ions in this high frequency case. When we substitute, we find

$$\begin{aligned} P_{Ti}/(\epsilon_0 E) &= (X_{Ti}/\Delta)(1.262) = 3.30X_{Ti},\\ P_{Ba}/(\epsilon_0 E) &= (X_{Ba}/\Delta)(0.921) = 2.41X_{Ba},\\ P_{Oa}/(\epsilon_0 E) &= (X_O/\Delta)(1.174) = 3.08X_O,\\ P_{Ob1}/(\epsilon_0 E) &= (X_O/\Delta)(0.946) = 2.47X_O. \end{aligned} \tag{23}$$

If the ordinary Lorentz correction were applicable, we should find these numerical coefficients in each case to be equal to $(\kappa+2)/3=2.59$. We notice that they are of the same order of magnitude; but there is a distinct tendency for the Ti and the type a oxygen ions to be polarized more than this value, and for the others to be polarized somewhat less. We shall find in the low frequency case, where the Ti is polarized much more, that this tendency is greatly enhanced.

[14] Similar equations have been set up for this case by J. M. Richardson, formerly of the Bell Telephone Laboratories, in unpublished work, but the results were not carried as far as in the present work. See J. M. Richardson and W. Shockley, Phys. Rev. **70**, 105 (1946). See also J. H. van Santen and W. Opechowski, Physica's Grav. **14**, 545 (1948).

[15] W. Shockley, Phys. Rev. **70**, 105(A) (1946).

[16] W. Shockley, Phys. Rev. **73**, 1273 (1948).

Now let us pass on to the problem of the static dielectric constant, where the Ti ions can polarize by ionic displacement. Let us assume that the total polarizability of the titanium is the sum of the value given in (21), and another quantity α_{Ti}', a function of temperature which is given by (12). Let the corresponding value of X be $X_{Ti}'=\alpha_{Ti}'/\epsilon_0 v$. We shall then have to use $X_{Ti}+X_{Ti}'$ in place of X_{Ti} in Eqs. (20). In that case we see at once from (20) that the dielectric constant can be written in the form

$$\kappa-1=\frac{c_1+c_2X_{Ti}'}{c_3+c_4X_{Ti}'}=\frac{c_2}{c_4}+\frac{(c_1/c_3)-(c_2/c_4)}{1+(c_4/c_3)X_{Ti}'}$$

where

$$c_1=X_{Ti}+X_{Ba}+3X_O+pX_{Ti}X_O+3pX_O^2-(3/2)(p+q)^2X_{Ti}X_{Ba}X_O-\tfrac{1}{2}(3q-p)^2X_{Ti}X_O^2-8p^2X_{Ba}X_O^2$$

$$c_2=1+pX_O-(3/2)(p+q)^2X_{Ba}X_O-\tfrac{1}{2}(3q-p)^2X_O^2$$

$c_3=\Delta$ from Eq. (20),

including terms in X_{Ti} but not in X_{Ti}'

$$c_4=-\tfrac{1}{3}-(\tfrac{1}{3}p+(3/2)q^2)X_O+\tfrac{1}{6}(3q-p)^2X_O^2+\tfrac{1}{2}(p+q)^2X_{Ba}X_O. \quad (24)$$

In case X_{Ti}, X_{Ba}, X_O are all zero, so that the only polarization comes from the ionic displacement, we have $c_1=0$, $c_2=c_3=1$, $c_4=-\frac{1}{3}$, and we have at once the values given in the introductory section,

$$\kappa=1+\frac{X_{Ti}'}{1-\frac{1}{3}X_{Ti}'}=-2+\frac{3}{1-\frac{1}{3}X_{Ti}'} \quad (25)$$

in our present notation. However, when we put in the values of X_{Ti}, etc., from (22), determined from the optical behavior of the material, the situation is entirely different; we find

$$c_1=1.834,\ c_2=-5.892,\ c_3=0.385,\ c_4=-2.076,$$
$$\kappa=3.84+1.93/(1-5.39X_{Ti}'). \quad (26)$$

This important result (26) shows that the effect of the polarization of the other ions is greatly to enhance the effect of the ionic displacement of the Ti ions in producing ferroelectricity. Thus from (25) we see that if these other ions were not helping the polarization, we should get ferroelectricity only when $X_{Ti}'=3$. On the other hand, from (26), we get the same result when $5.39X_{Ti}'=1$, or when $X_{Ti}'=0.186$. This indicates enhancement of the effect of the ionic displacement by a factor of approximately 16. Some such enhancement, of course, would arise from the ordinary Lorentz correction. If this correction were applicable in its simple form, we should get ferroelectricity when

$$\tfrac{1}{3}(X_{Ti}+X_{Ti}'+X_{Ba})+X_O=1.$$

We already know that $\frac{1}{3}(X_{Ti}+X_{Ba})+X_O=0.609$. Thus we should require that $X_{Ti}'=3(1-0.609)=1.173$, as compared with the value 0.186 which we find from our more correct theory. The elementary theory of the Lorentz correction thus is so far wrong that the ionic polarizability of the Ti ion needs to be only 0.186/1.173 $=0.160$ times as great, or about one-sixth as great, as if the elementary theory held. Let us now examine how this very large enhancement of the effect of ionic displacement comes about.

We can understand the situation if we examine the relative polarizations of the various types of ions. We can use (20) to find these, now using $X_{Ti}+X_{Ti}'$ instead of X_{Ti} for the Ti ion. In this case, for ferroelectricity, the determinant Δ', obtained by using $X_{Ti}+X_{Ti}'$ instead of X_{Ti}, is zero, so that at the Curie point the polarization per unit field is infinite. We can still evaluate the brackets in (20), however, and these will still give the relative magnitudes of the polarizations of the various types of ions. We then find

$$P_{Ti}/(\epsilon_0E)=[(X_{Ti}+X_{Ti}')/\Delta'](1.262),$$
$$P_{Ba}/(\epsilon_0E)=(X_{Ba}/\Delta')(-0.047),$$
$$P_{Oa}/(\epsilon_0E)=(X_O/\Delta')(0.939),$$
$$P_{Ob1}/(\epsilon_0E)=(X_O/\Delta')(0.046).$$

These values are strikingly different from those of (23). Only the relative values now have significance; and we see that the polarization is almost entirely contributed by the Ti ions, and the type *a* oxygen ions. The Ba and type *b* oxygen ions are hardly polarized at all. In fact, when we take account of the polarizabilities, we find that the Ti ions contribute about 37 percent of the total polarization (of which about 31 percent comes from ionic displacement, six percent from electronic polarization), the type *a* oxygen ions about 59 percent, the type *b* oxygen ions about six percent, and the Ba ions about two percent in the reverse direction. We thus see the evidence of the effect which we discussed in the introductory section: the Ti ions, by their polarization, polarize the type *a* oxygen ions; these in turn act back on the Ti ions; and the net result is to build up the polarization of both types of ions, resulting in linear chains of dipoles all pointing in the same direction, the positive end of one to the negative end of the other, and producing spontaneous polarization below the Curie point.

Now that we have found the influence of the polarizability of the other ions on the dielectric constant, we can combine Eq. (26) with an assumption similar to (2), to investigate Curie's law. It is clear that, to make the denominator of (26) vanish at the Curie point, we must assume that

$$5.39X_{Ti}'=5.39[\alpha_{Ti}'/(\epsilon_0 v)]=1-C(T-T_c). \quad (27)$$

If we insert this value in (26), we find that

$$\kappa=3.84+1.93/C(T-T_c), \quad (28)$$

as a substitute for (3). It is interesting to find that, in spite of the large change in the general situation produced by the electronic polarizability, still (28) is not

very different from (3), so that the qualitative discussion given in the introductory section regarding the temperature coefficient of the ionic polarizability of the Ti ion is still correct. The constant C, however, is now seen to be about 1.3×10^{-5}, instead of the value 2×10^{-5} given in the introductory section.

We may now compare (27) with (12), the ionic polarizability as determined from our molecular model, and ask whether the constants of (12) have reasonable values. Comparing them, we have approximately

$$5.39q^2/(2a\epsilon_0 v)=1, \quad C=[k(3b_1+2b_2)]/a^2. \tag{29}$$

If we combine these equations, we have

$$(3b_1+2b_2)/a=(5.39Cq^2)/(2\epsilon_0 vk). \tag{30}$$

If we assume that the charge q is n times the electronic charge (where n is 4 if the Ti ion is quadruply charged), and use the value of C given above, and $v=64\times10^{-24}$ cc $=64\times10^{-30}$m^3, the right side of (30) becomes $1.15\times10^{20}n^2$ (m.k.s. units). We can judge whether this value is reasonable or not, by recalling that our expansion of the energy, which in the case of spherical symmetry can be written $ar^2+br^4+\cdots$, is really the beginning of a power series, which is bound to diverge, or have a singularity, when the Ti ion gets very close to one of the oxygen ions of the octahedron. This divergence will arise because all terms of the series have the same order of magnitude. Thus we should expect that at a distance r where we have a divergence, ar^2 and br^4 should be of the same order of magnitude, or $r^2=a/b$, where for this crude calculation we may set $b_1=b_2=b$. Then $b/a=(1.15/5)\times10^{20}n^2=2.30\times10^{19}n^2$, and $r^2=1/2.30\times10^{-19}/n^2$, $r=(2.1/n)\times10^{-10}$m$=2.1/n$ angstroms. This is certainly of the right order of magnitude for interatomic distances, showing that the value of b which we have found necessary to explain the Curie constant is of a reasonable magnitude. Since the actual distance between the Ti ion and its neighboring oxygen ion is just 2A, this crude argument suggests that it might be more likely that n should be approximately unity than 4, which we should have with a quadruply charged ion.

From (29) we can also estimate the value of the constant a. If we assume again that q equals n electronic charges, we find that $a=7.6n^2$ ev/(angstrom)^2. That is to say, the energy of the displaced ion, displaced a distance of 1A from its position of equilibrium, would be $7.6n^2$ volts. This again is of a reasonable order of magnitude, 1A being halfway to the oxygen ion. Here again $n=1$ would be more reasonable than $n=4$, which would lead to an energy of about 120 volts at a distance of 1A. Without more detailed study of the interionic forces, however, it is hardly possible to estimate how great the expected restoring forces should be. It is, of course, not inconsistent with the structure of $BaTiO_3$ to assume a smaller value of n than 4, which would correspond to the strictly ionic compound. Thus if the oxygen ions on the average were singly rather than doubly charged, the Ti ion would have to have a single positive charge. Some evidence as to the charge carried by the Ti ion should eventually become available, when it is known by x-ray measurements exactly how much the Ti ions displace in the spontaneously polarized condition. The magnitude of the spontaneous polarization is known, being equal to about 16×10^{-6} coulomb/cm^2. We have seen that we may expect about 31 percent of this, or 5×10^{-6}, to come from ionic displacement. With a charge of n electronic charges on each Ti ion, this would correspond to a displacement of $0.20/n$ angstroms. There is some x-ray evidence for a displacement of about [17] 0.16A, suggesting $n=1$; but also some evidence for a smaller displacement,[18] suggesting a larger value of n. These questions must await further experimental information.

V. THE LORENTZ CORRECTION AND THE FREE ENERGY

In Section IV we have considered only linear terms in the force acting to polarize the various ions. Now we shall pass to the more general problem, where we include higher power terms as in Section II, but treat the Lorentz correction properly as in Section IV. We shall find it convenient to work backward, starting from the equations for the electric field in terms of the polarization, ending up by integrating these expressions to get a formula for the free energy. First we note that by differentiating (10) with respect to P_x we get the x component of the field polarizing the Ti ion. We have

$$E_x=\frac{2aP_{x\mathrm{Ti}}'}{Nq^2}\left\{1+\frac{kT}{a^2}(3b_1+2b_2)\right\} +\frac{4P_{x\mathrm{Ti}}'}{N^3q^4}[b_1P_{x\mathrm{Ti}}'^2+b_2(P_{y\mathrm{Ti}}'^2+P_{z\mathrm{Ti}}'^2)] \tag{31}$$

where we have now written the polarization arising from ionic displacement of the Ti ion as P_{Ti}'. The field acting here is of course the local field, not the external field; in Section II we were not taking account of the difference between these two fields. But now, using results of Section IV, we know how to find this local field: it is set up in Eq. (18). In interpreting that set of equations, we must now distinguish between that part of the polarization of the Ti ions arising from electronic polarization, and that from ionic displacement. We shall call the first part of the polarization P_{Ti}, the second part P_{Ti}', so that Eqs. (18) are now to be modified by replacing P_{Ti} where it appears by $P_{\mathrm{Ti}}+P_{\mathrm{Ti}}'$. As before, we let X_{Ti} equal $\alpha_{\mathrm{Ti}}/\epsilon_0 v$, where α_{Ti} is the electronic polarizability of the Ti ion. The corresponding relation giving the ionic polarizability must now be given by (31), where we recall that the E_x appearing in that equation is the local field acting on the Ti ion. We may then rewrite Eqs. (18) and (19), modi-

[17] Danielson, Matthias, and Richardson, Phys. Rev. **74**, 986 (1948).

[18] Kay, Wellard, and Vousden, Nature **163**, 636 (1949).

fied to take account of (31), in the form

$$\epsilon_0 E_x+\tfrac{1}{3}(P_{x\mathrm{Ti}}+P_{x\mathrm{Ti}}'+P_{x\mathrm{Ba}})$$
$$+(q+\tfrac{1}{3})P_{x\mathrm{Oa}}+(-\tfrac{1}{2}q+\tfrac{1}{3})(P_{x\mathrm{Ob1}}+P_{x\mathrm{Ob2}})$$
$$=\frac{2a\epsilon_0 P_{x\mathrm{Ti}}'}{Nq^2}\left[1+\frac{kT}{a^2}(3b_1+2b_2)\right]$$
$$+\frac{4\epsilon_0 P_{x\mathrm{Ti}}'}{N^3q^4}[b_1 P_{x\mathrm{Ti}}'^2+b_2(P_{y\mathrm{Ti}}'^2+P_{z\mathrm{Ti}}'^2)],$$

$$\epsilon_0 E_x+\tfrac{1}{3}(P_{x\mathrm{Ti}}+P_{x\mathrm{Ti}}'+P_{x\mathrm{Ba}})+(q+\tfrac{1}{3})P_{x\mathrm{Oa}}$$
$$+(-\tfrac{1}{2}q+\tfrac{1}{3})(P_{x\mathrm{Ob1}}+P_{x\mathrm{Ob2}})=P_{x\mathrm{Ti}}/X_{\mathrm{Ti}},$$

$$\epsilon_0 E_x+\tfrac{1}{3}(P_{x\mathrm{Ti}}+P_{x\mathrm{Ti}}'+P_{x\mathrm{Ba}})+(-p+\tfrac{1}{3})P_{x\mathrm{Oa}}$$
$$+(\tfrac{1}{2}p+\tfrac{1}{3})(P_{x\mathrm{Ob1}}+P_{x\mathrm{Ob2}})=P_{x\mathrm{Ba}}/X_{\mathrm{Ba}},$$

$$\epsilon_0 E_x+(q+\tfrac{1}{3})(P_{x\mathrm{Ti}}+P_{x\mathrm{Ti}}')+(-p+\tfrac{1}{3})P_{x\mathrm{Ba}}$$
$$+\tfrac{1}{3}P_{x\mathrm{Oa}}+(\tfrac{1}{2}p+\tfrac{1}{3})(P_{x\mathrm{Ob1}}+P_{x\mathrm{Ob2}})=P_{x\mathrm{Oa}}/X_{\mathrm{O}},$$

$$\epsilon_0 E_x+(-\tfrac{1}{2}q+\tfrac{1}{3})(P_{x\mathrm{Ti}}+P_{x\mathrm{Ti}}')$$
$$+(\tfrac{1}{2}p+\tfrac{1}{3})P_{x\mathrm{Ba}}+(\tfrac{1}{2}p+\tfrac{1}{3})P_{x\mathrm{Oa}}$$
$$+\tfrac{1}{3}P_{x\mathrm{Ob1}}+(-p+\tfrac{1}{3})P_{x\mathrm{Ob2}}=P_{x\mathrm{Ob1}}/X_{\mathrm{O}}. \quad (32)$$

There is an equation similar to the last one for $P_{x\mathrm{Ob2}}$. We can now solve all equations except the first for $P_{x\mathrm{Ti}}$, $P_{x\mathrm{Ba}}$, $P_{x\mathrm{Oa}}$, $P_{x\mathrm{Ob1}}$, $P_{x\mathrm{Ob2}}$ in terms of $P_{x\mathrm{Ti}}'$ and E_x. We then substitute these values into the first equation of the set (32), and this becomes an equation relating E_x and P_{Ti}', containing now the higher power terms from that equation. When we carry out these steps, which can be simplified by comparison with the similar problem involved in finding the first equation of (20), the resulting equation is

$$E_x=\frac{c_3}{c_5}\left\{\frac{2aP_{x\mathrm{Ti}}'}{Nq^2}\left[1+\frac{kT}{a^2}(3b_1+2b_2)\right]+\frac{4P_{x\mathrm{Ti}}}{N^3q^4}\right.$$
$$\left.\times[b_1 P_{x\mathrm{Ti}}'^2+b_2(P_{y\mathrm{Ti}}'^2+P_{z\mathrm{Ti}}'^2)]\right\}+\frac{c_4}{c_5}\frac{P_{x\mathrm{Ti}}'}{\epsilon_0}, \quad (33)$$

where

$$c_5=1+pX_{\mathrm{O}}-3/2p(p+q)X_{\mathrm{Ba}}X_{\mathrm{O}}+\tfrac{1}{2}p(3q-p)X_{\mathrm{O}}^2,$$

and c_3 and c_4 are as given in (24).

In case the electronic polarizabilities of all the various ions are zero, we have $c_3=c_5=1$, $c_4=-\frac{1}{3}$, and hence the only effect of the Lorentz correction in (33) is to subtract the term $P_{\mathrm{Ti}}'/3\epsilon_0$ from the right-hand side, or to substitute a local field $E+P/3\epsilon_0$ for the field E, as we should expect, and as we saw in Eq. (11). However, when we take account of the electronic polarizability, there are two changes: the Lorentz correction term $P/3\epsilon_0$ is changed from $-\frac{1}{3}$ to c_4/c_5, and the other term is multiplied by a factor c_3/c_5. When we insert the numerical values which we have been using, we find that $c_3/c_5=0.309$, $c_4/c_5=-1.69$. In other words, the Lorentz correction term is $3\times1.69/0.309=16.4$ times as important as would be given by the simple Lorentz theory. This is the same enhancement factor which we have already met in our discussion of Eq. (26), only now expressed in somewhat different language.

In the process of setting up the solution (33), we have had to solve separately for the various polarizations P_{Ba}, etc. We shall not give the separate formulas for these quantities, but we shall give the formula for the total polarization P, in terms of P_{Ti}'. We find that

$$P_x=\frac{c_1}{c_5}\epsilon_0\left\{\frac{2aP_{x\mathrm{Ti}}'}{Nq^2}\left[1+\frac{kT}{a^2}(3b_1+2b_2)\right]+\frac{4P_{x\mathrm{Ti}}'}{N^3q^4}\right.$$
$$\left.\times[b_1 P_{x\mathrm{Ti}}'^2+b_2(P_{y\mathrm{Ti}}'^2+P_{z\mathrm{Ti}}'^2)]\right\}+\frac{c_2}{c_5}P_{x\mathrm{Ti}}'.$$

We are particularly interested in the relation in the case of spontaneous polarization, when $E=0$, but P and P_{Ti}' are not. In that case, we may combine with (33), and find

$$P_x=P_{x\mathrm{Ti}}'[(c_2c_3-c_1c_4)/c_3c_5].$$

But we can prove, by straightforward algebra, that

$$c_2c_3-c_1c_4=c_5^2.$$

Thus the equation above becomes

$$P_x=(c_5/c_3)P_{x\mathrm{Ti}}', \quad (34)$$

under conditions of spontaneous polarization. When we insert numerical values, we find $P_x=P_{x\mathrm{Ti}}'/0.309=3.24P_{x\mathrm{Ti}}'$, as we have mentioned in earlier paragraphs. We readily verify that above the Curie point, where we are interested in the dielectric constant, this same relation still holds to a first order of accuracy, agreeing with the results of Section IV.

We can then use (34) in connection with (33), to express the field in terms of P, rather than P_{Ti}', and find

$$E_x=\frac{c_3}{c_5}\left\{\frac{2a}{Nq^2}\frac{c_3}{c_5}P_x\left[1+\frac{kT}{a^2}(3b_1+2b_2)\right]+\left(\frac{c_3}{c_5}\right)^2\frac{4P_x}{N^3q^4}\right.$$
$$\left.\times[b_1P_x^2+b_2(P_y^2+P_z^2)]\right\}+\frac{c_3c_4}{c_5^2}\frac{P_x}{\epsilon_0}. \quad (35)$$

This expression allows us to integrate Eq. (7), taking account of (10), to get the free energy A_P. We have

$$A_P=-NkT\ln[(e/Nh^3)(\pi kT)^3(2m/a)^{\frac{1}{2}}]$$
$$+[N(kT)^2/a^2]^{\frac{3}{4}}(3b_1+2b_2)$$
$$+\left(\frac{c_3}{c_5}\right)^2\frac{aP^2}{Nq^2}\left[1+\frac{kT}{a^2}(3b_1+2b_2)\right]$$
$$+\left(\frac{c_3}{c_5}\right)^4\frac{1}{N^3q^4}[b_1(P_x^4+P_y^4+P_z^4)$$
$$+2b_2(P_y^2P_z^2+P_z^2P_x^2+P_x^2P_y^2)]+\frac{c_3c_4}{c_5^2}\frac{P^2}{2\epsilon_0}. \quad (36)$$

If we use (34), and express this in terms of P_{Ti}', the expression (with the exception of the last term) reduces to the same value (10) which we found earlier (when we remember that the P appearing in (10) is just the ionic polarization of the Ti ions, which we are now calling P_{Ti}'). The last term, however, is not the same as the Lorentz correction function in Section III. That was $-P_{Ti}'^2/6\epsilon_0$, whereas our term $(c_3c_4/c_5^2)(P^2/2\epsilon_0)$ can be written as $(c_4/c_3)(P_{Ti}'^2/2\epsilon_0)$. We verify from (24) that this reduces to $-P_{Ti}'^2/6\epsilon_0$ for the case where the only polarization is that of the Ti ion, thus verifying our result; but for the actual case, it is 16.4 times as great, in agreement with previous statements concerning the effect of the correct treatment of the Lorentz correction.

Expression (36) is the one which we should use for discussing relations between theory and experiment. We may define the Curie point as the point where the term in P^2 goes to zero. That is,

$$-(c_4/c_3)(Nq^2/2\epsilon_0 a)=1+kT_c(3b_1+2b_2)/a^2, \quad (37)$$

to be compared with (14), the formula derived from the simple Lorentz theory, in which c_4/c_3 is replaced by $-\frac{1}{3}$. If we substitute (37) in (36), we can rewrite the term in P^2 in the form

$$(c_3/c_5)^2(aP^2/Nq^2)(k(T-T_c)/a^2)(3b_1+2b_2).$$

We can also use (37) to rewrite the other terms of (36) in alternative forms; we can disregard the terms of (37) involving the b's in terms which are small of the first order. When we do this, we find the alternative formula in place of (36),

$$\begin{aligned}A_P=&-NkT\ln[(e/N\hbar^3)(\pi kT)^3(2m/a)^{\frac{1}{2}}]\\&+(N(kT)^2/a^2)\tfrac{3}{4}(3b_1+2b_2)\\&+(c_4/\epsilon_0c_5)^2(Nq^2/4a^3)P^2k(T-T_c)(3b_1+2b_2)\\&+(c_4/\epsilon_0c_5)^4(Nq^4/16a^4)[b_1(P_x^4+P_y^4+P_z^4)\\&\qquad+2b_2(P_y^2P_z^2+P_z^2P_x^2+P_x^2P_y^2)]. \quad (38)\end{aligned}$$

This form of the expression is chosen to make comparison easy with Devonshire's formulas. We get agreement with the terms linear in the b's, in Devonshire's Eq. (10.13) (correcting for certain obvious misprints in his equation), if we set his β (Lorentz factor) equal to

$$\begin{aligned}\beta=-c_4/(\epsilon_0c_5)=&-(4\pi c_4)/c_5(\text{Gaussian units})\\&=5.09(4\pi/3). \quad (39)\end{aligned}$$

That is, for these terms, we must use a Lorentz correction 5.09 times as great as given by the elementary theory. On the other hand, in the terms independent of the b's, leading to the value of the Curie temperature, we get agreement with Devonshire's values if we use a value of β equal to

$$\begin{aligned}\beta=-c_4/(\epsilon_0c_3)=&-(4\pi c_4)/c_3(\text{Gaussian units})\\&=16.4(4\pi/3), \quad (40)\end{aligned}$$

thereby bringing about agreement between our Eq. (36) and Devonshire's (10.17). In other words, no single modified Lorentz factor will take care of the whole correct Lorentz treatment, as we have developed it.

VI. FREE ENERGY AND ELASTIC STRAIN

The free energy as we have computed it disregards the elastic energy; it is calculated on the assumption that the crystal does not deform when it polarizes. As we have pointed out earlier, this does not lead to the correct formula for the polarization below the Curie point. If we set $E_x=0$ in (35), solve for P_x (assuming that $P_y=P_z=0$), and use (37), we have

$$\frac{P_x^2}{\epsilon_0}=-\frac{c_5^2}{c_3c_4}Nk\frac{(3b_1+2b_2)}{b_1}(T_c-T), \quad (41)$$

as compared with (15), where we have the factor 3 in place of $-c_5^2/c_3c_4$. We find $-c_5^2/c_3c_4=1.93$; in other words, the relation between polarization and temperature is not very different on the correct treatment from the value given in the elementary theory, so that the disagreement between this function and experiment is as bad as that discussed in Section III.

We have already mentioned that, as pointed out by Devonshire, this disagreement is removed by supplementing A_P, as given in (38), by additional terms in the elastic strains, and terms involving both strains and polarization components, which therefore are responsible for the piezoelectric effect. The partial derivative of this free energy with respect to one of the strain components then gives the related stress component; if we set the stresses equal to zero we get in this way a set of equations from which we can solve for the various strains under conditions of vanishing stress. We substitute these values in the expression for free energy, and have finally a free energy as a function of polarization components, for the condition of vanishing stress. We find that the resulting correction terms are of the fourth-power in the polarization, hence modifying the fourth-power terms in (38), and changing completely the relation (41), and thus the polarization below the Curie point. Since our argument at this point follows exactly that of Devonshire, we merely refer the reader to his paper, particularly his Eq. (9.1), giving the free energy in terms of strains and polarizations. To facilitate comparison with his results, we give formulas, in our notation, for various coefficients appearing in his paper, his Eqs. (10.14), (10.15), (10.16):

$$\begin{aligned}\chi''&=\left(\frac{c_4}{\epsilon_0c_5}\right)^2\frac{Nq^2}{2a^3}k(T-T_c)(3b_1+2b_2),\\\xi_{11}''&=\left(\frac{c_4}{\epsilon_0c_5}\right)^4\frac{Nq^4}{4a^4}b_1,\\\xi_{12}''&=\left(\frac{c_4}{\epsilon_0c_5}\right)^4\frac{Nq^4}{4a^4}b_2. \quad (42)\end{aligned}$$

Devonshire has made some attempt to compare the numerical predictions of the theory with experiment, and it is obvious that the present paper, making very

large changes in some of the coefficients, will invalidate most of that comparison. We shall not attempt at this time, however, to make an alternative comparison with experiment. There are two ways in which this comparison can be made. First, the observed Curie temperature permits an evaluation of q^2/a, and the temperature dependence of the dielectric constant gives us $(3b_1+2b_2)/a^2$. We have already considered the resulting values of these constants, and have shown them to be of reasonable order of magnitude. To check them better we should have to have an elaborate study of the structure of the crystal from the standpoint of atomic theory, in order to be able to compute the interionic forces. Devonshire has given such a theory in a rather elementary way, but the writer believes that a more elaborate treatment would be necessary before the results could have great pretensions to accuracy. On the other hand, the behavior of the polarization below the Curie point gives information about the coefficients of the fourth-power terms (and sixth-power terms, which Devonshire also has to introduce), but modified by the contributions resulting from the elastic strain. If the elastic and piezoelectric constants of single crystals were known accurately enough, we could evaluate these modifications, and then we should be able to find the b's independently from the fourth-order terms, as well as from the second-order terms, and hence have a valuable internal check of the theory. Unfortunately, these elastic and piezoelectric constants are not known sufficiently well. It is to be hoped that future experiments will supply this missing information. In the meantime, it can be said that there does not seem to be anything about the present form of the theory which does not have a good chance of agreeing with experiment, when better experimental data are available.

The writer is greatly indebted to his colleague Professor A. von Hippel for stimulating his interest in the problem, and for useful discussions; and to Drs. W. Shockley and P. W. Anderson of the Bell Telephone Laboratories, for valuable exchange of information regarding the work on the subject of those Laboratories.

PHYSICAL REVIEW VOLUME 78, NUMBER 6 JUNE 15, 1950

Evaporation of Zinc and Zinc Oxide under Electron Bombardment

FRANCIS E. DART*
Cornell University, Ithaca, New York
(Received January 16, 1950)

By use of a mass spectrographic method, the rate of evaporation of zinc and zinc oxide is measured as a function of temperature both with and without electron bombardment of the surface being evaporated. In the case of zinc metal no increase of evaporation could be detected as resulting from bombardment whereas a definite increase was observed in the evaporation of zinc oxide. The enhancement of the evaporation rate of zinc oxide increases slowly at first and then rapidly with increasing temperature.

1. INTRODUCTION

THE experimental investigation of many solid state phenomena would be much simplified if a sensitive method of microanalysis were available for measuring the chemical constitution of solids containing impurities in very small concentration. Especially would this be the case if the method were capable of analyzing the constituents of solid surfaces, for many surface phenomena such as thermionic emission, secondary electron emission, photoelectric emission, etc., are very sensitive to the atomic or molecular constitution of the surface in question. The mass spectrometer is an instrument which would be very well suited to such analysis if means could be found to remove atoms or molecules from the surface and subsequently identify them in the spectrometer.

There is evidence that under electron bombardment atoms or ions may be removed from solids. Baldock[1] found that calcium ions are obtained from calcium metal when it is bombarded with electrons. Jacobs[2] found oxygen compounds to be removed by electron bombardment from anodes coated with thin layers, and Sproule[3] found evidence that electron bombardment of heated triple oxide surfaces removed barium, strontium and calcium atoms. The experiments reported below were undertaken to study this phenomenon in greater detail in order to see whether electrons of themselves can cause dissociation of atoms from a surface or whether this comes about only by virtue of the heating produced by the electrons. A beam of electrons was directed against a target whose temperature could be controlled. The relative number of atoms leaving its surface was detected with a mass spectrometer and compared with the number leaving by thermal evaporation alone.

* Now at University of Oregon, Eugene, Oregon.
[1] R. Baldock, Ph.D. Thesis, Cornell University, Ithaca, New York.
[2] H. Jacobs, Phys. Rev. **69**, 692 (1946).
[3] R. L. Sproule, RCA Laboratories Report.

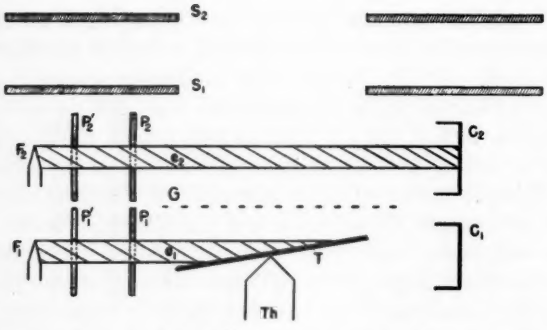

FIG. 1. Cross section of the source end of the spectrometer showing the arrangement of parts. Section taken parallel to the magnetic field.

2. EXPERIMENTAL METHOD

At the source end of the mass spectrometer two electron beams were used, one of which was directly in front of the slit and acted as the ionizing beam while the other was used to bombard the target. The geometrical arrangement of the source end of the spectrometer is shown in Fig. 1. The material to be bombarded was evaporated onto the tantalum strip T mounted so that electrons in the beam e_1 would strike it obliquely. The tantalum strip could be heated by passing a current through it. Its temperature was measured by means of the thermocouple Th made of 0.0025 in. copper and "Advance" wires spot welded to its mid-point. Because of end cooling and the very slight cooling due to the thermocouple wires the temperature of the strip was not uniform, but there was a region of about two thirds of the length of the strip the temperature of which was nearly uniform and could be determined to within about 0.5°C.

Atoms leaving the target passed through the coarse grid G and into the electron beam e_2 where some of them were ionized and subsequently accelerated toward the slits S_1 and S_2 (here shown lengthwise) by electric fields maintained between G and S_1 and S_1 and S_2, respectively. The grid G insures the complete independence of the two beams so that e_1 could be varied at will while the number of electrons per second in e_2 was kept always constant and their energy was adjusted to give maximum ionization cross section. This grid also served to prevent ions originating in e_1 or at the target from reaching the slits.

Since the space between the target and slits is within the magnetic field of the spectrometer, the ions will travel in a curve as they are accelerated toward S_1. Because of this curved path it is uncertain just what direction the accelerating field should have in order that ions will encounter a maximum aperture at S_1 and S_2. Grids on each side of the electron beams and parallel to the plane of Fig. 1 were introduced in order to adjust the direction of the accelerating field and thereby focus ions into the slits. These grids increased the efficiency of ion collection by more than a thousandfold. The mass spectrometer itself was of the conventional Dempster[4] type using a 180° deflection. Ion currents were amplified in a cathode follower circuit similar to that described by Richter[5] and read on a sensitive galvanometer. Currents of the order of 10^{-14} amp. could be detected readily.

3. RESULTS

A. Zinc

With the target strip coated with metallic zinc and the spectrometer set on the Zn^{64} peak, ion currents were recorded as a function of target temperature with only the beam e_2 in operation, no bombarding electrons being present. The results are plotted in Fig. 2 where the solid line represents the mean of six series of measurements and the dashed line is extrapolated from values given in the literature[6,7] for the temperature range 250° to 490° C. These curves are not expected to coincide as absolute measurements were not made here. The data follow a straight line as expected but the slope, 8440, is about 21 percent greater than that given in the literature (the maximum variation among the six sets of measurements was 1.5 percent). This discrepancy might be accounted for by the absence of equilibrium conditions in the present apparatus if it were also assumed that the reflection of zinc atoms from the metal walls is a function of their velocity. The extra-

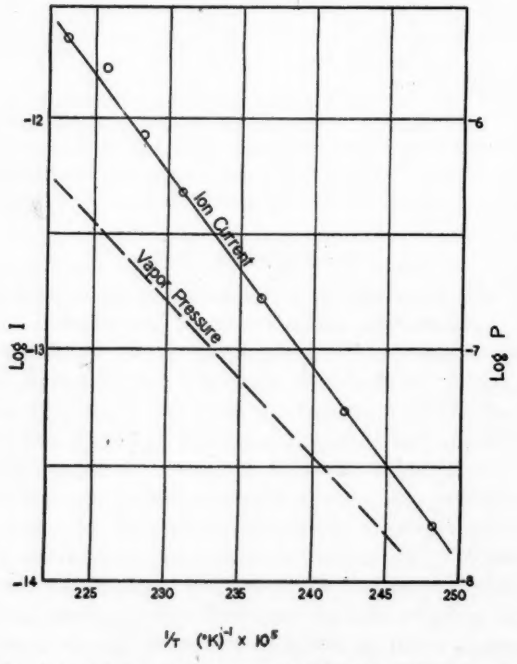

FIG. 2. Logarithms of ion currents (solid line) and vapor pressure (dashed line) plotted against reciprocal absolute temperature. Both curves represent data from metallic zinc.

[4] Dempster, Phys. Rev. **11**, 316 (1918).
[5] W. Richter, Electronics, **16**, No. 11, 112 (1943).
[6] International Critical Tables **3**, 205.
[7] Edgerton, Phil. Mag. **33**, 33 (1917).

polation mentioned above may also be in error, as Edgerton[7] finds evidence for a curved line. It was not possible to extend the measurements into the temperature range covered by Edgerton's results due to the very rapid evaporation of the zinc at higher temperatures.

Data were next taken with the target strip under constant bombardment by 1.2 ma of electrons with energies which were varied in succeeding series of measurements from 200 to 1000 ev. The temperature of the target was controlled during bombardment by varying the current in the tantalum strip. The results are shown in Fig. 3 where the solid curve is an evaporation curve without bombardment and the circles represent data taken with bombardment. In no instance

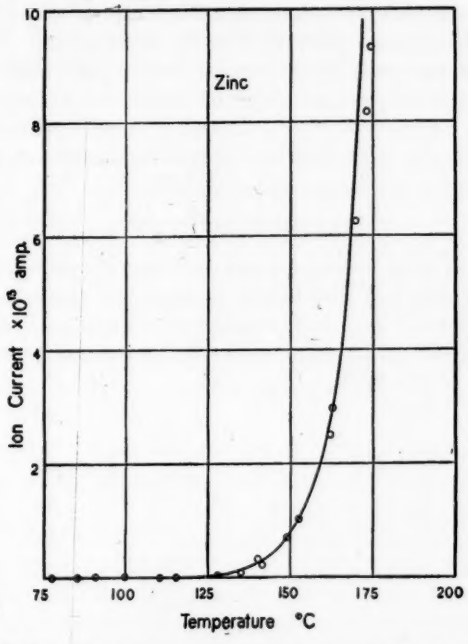

FIG. 3. Ion current *vs.* temperature for a metallic zinc target. The solid line represents data taken without bombardment of the target while the circles represent data taken with bombardment by 1.2 ma of 400 volt electrons.

was any enhancement of the rate of evaporation detected as a result of the electron bombardment.

B. Zinc Oxide

When the target was coated with zinc oxide and heated, ion peaks were detected with the mass spectrometer both at mass 64, corresponding to Zn, and at mass 80, corresponding to ZnO, as was expected. Because the Zn^{64} peak was the larger and in order to avoid any possibility of varying background contamination, the evaporation of the zinc oxide was followed by measuring the Zn^{64} ions produced. The experiments were repeated exactly as with zinc metal both with and without the bombarding beam. In this case the data show a definite increase of evaporation due to bombardment, that is,

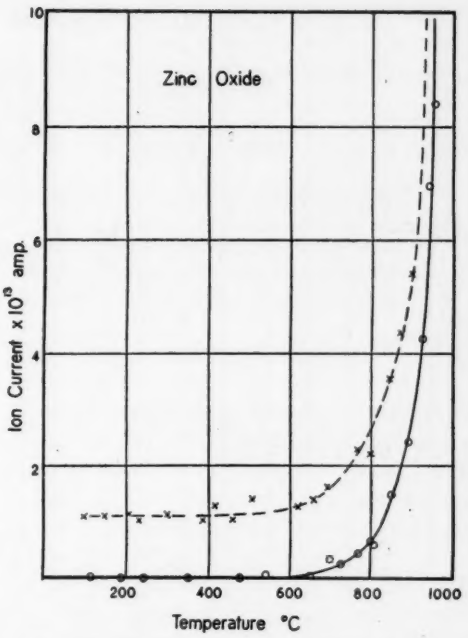

FIG. 4. Ion current *vs.* temperature for a zinc oxide target. The solid curve represents data taken without bombardment while the dashed curve represents data taken with the target bombarded by 400 microamperes of 400 volt electrons.

more atoms of zinc were removed under bombardment than would have evaporated due to temperature alone. Figure 4 shows data taken with a 400 μa beam of electrons with energies of 400 ev striking the target. The solid curve is that taken with no bombardment while the dashed curve was taken with the electron beam striking the zinc oxide. The number of additional atoms removed as a result of electron bombardment increases slowly with increased temperature at low temperatures and almost exponentially at higher temperatures. This is shown in Fig. 5 where the increase of ion current due to bombardment is plotted against target temperature.

4. DISCUSSION

It is difficult to explain the increase in evaporation of ZnO under bombardment as a purely thermal effect. Considerable care was exercised to obtain a uniform distribution of the beam over the central two thirds of the target strip, and the layer of zinc oxide was so thin (about 0.045 mm) that the total power delivered by the beam would be sufficient to maintain average temperature differences across it of less than 2°C. In order to account for the observed data on the basis of local heating in the zinc oxide coating, temperatures 500° C or more above those of the target as a whole would need to be assumed. On the other hand, local heating of 10° or 15° C would have produced a measurable increase in the case of metallic zinc where no increase was observed.

In order that an atom may dissociate from the surface of a solid it must gain enough energy to allow a transition to one of the stable states of a single atom, i.e. of

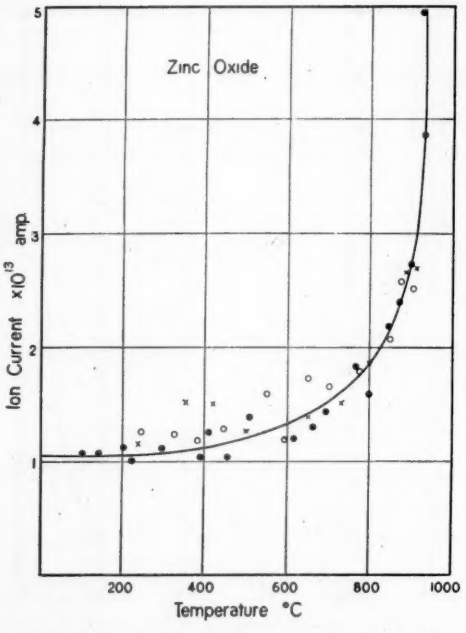

FIG. 5. The increase of Zn^{64} ion current caused by bombarding a zinc oxide target with 400μa of 400 v electrons *vs.* the temperature of the target. The open circles, solid circles, and crosses represent respectively three different sets of data all taken under the same conditions.

an atom of the element in the gaseous phase. The bombarding electrons carried more than enough energy to make such a transition possible. However, there are other processes which may cause the excited atom to lose its energy before it can dissociate. The dissociation time will depend both upon the force of repulsion between the excited atom and its neighbors and upon its vibrational energy, the latter being a function of the temperature. If the de-excitation time due to the transfer of energy to an electron of the solid, or to an exciton state or due to radiative transitions is very much smaller than the dissociation time, then the probability of dissociation will be very small. This appears likely in the case of zinc metal.

It is not unreasonable to suppose, however, that the transfer of energy from an atom of the surface to the lattice or electrons of the solid will take place with more difficulty in the case of an insulator. If the de-excitation time is very much greater than the time for dissociation, almost all excited surface atoms will leave the solid, and the dissociation rate should be independent of the temperature, but if the two processes are strongly competing, a temperature dependence of the sort observed in Fig. 5 might result. The foregoing considerations may then provide a qualitative explanation for the observed behavior of both zinc and zinc oxide.

ACKNOWLEDGMENT

The author wishes to acknowledge his indebtedness to Professor L. P. Smith who proposed this investigation and offered many helpful suggestions and to Professor H. F. Newhall for many valuable discussions during the course of the work.

Stars and Heavy Primaries Recorded during a V-2 Rocket Flight

HERMAN YAGODA, HERVASIO G. DE CARVALHO,* AND NATHAN KAPLAN
Laboratory of Physical Biology, Experimental Biology and Medicine Institute, National Institutes of Health, Bethesda, Maryland

(Received February 23, 1950)

Plates flown to an altitude of 150.7 km in a V-2 rocket exhibit a differential star population of 5000±800 per cc per day and a flux of heavy primaries of about 0.03 per cm² per min. above the stratosphere. The star intensity is about 3.6 times greater than that recorded by plates exposed in the stratosphere, the increment being attributable to secondary star forming radiations created by interaction of cosmic-ray primaries with the massive projectile. The flux of heavy primaries is essentially of the same order of magnitude as reported for elevations of 28 km.

I. INTRODUCTION

A SMALL unit of Kodak NT4 plates were flown to a peak altitude of 150.7 km by a V-2 rocket at White Sands, New Mexico, during a test flight on September 29, 1949. The plate holder was recovered in good condition several hours after the landing. The rocket plates together with a set of monitor plates, which had the same history since manufacture, except for the brief high altitude exposure, were returned to this laboratory and developed three days after the flight. All plates developed satisfactorily and a preliminary microscopic examination at low power revealed several large stars in the rocket plates suggesting that a complete study of all plates might yield significant information on the intensity of the star-producing radiation despite the very brief duration of the high altitude exposure.

The results reported must be considered preliminary, as only a comparatively small number of events were recorded in the 2-cc volume of exposed emulsion and hence the statistical uncertainty in the populations is large. Also, by better timing in the manufacture, shipment and development of the plates it should be possible to reduce the magnitude of the accumulated star population in the control plates.

II. CAMERA AND EXPOSURE

The four plates, coated approximately 200μ thick, were bound together as a rigid unit with black cellulose tape and enclosed in a gas-tight aluminum box packed with sponge rubber and fitted with a thick rubber gasket as described in Fig. 1. The plates were predried over calcium chloride and were infected at selected points with a trace of polonium so as to provide precise registration marks for intercomparison of long tracks recorded through the stack. The camera was assembled and bolted to the tail fin of the rocket shortly before the launching. The gas-tight construction was deemed advisable in order to prevent traces of oxidants originating from the rocket fuel from reaching the emulsion, as these vapors, particularly hydrogen peroxide, cause rapid destruction of the latent image of nuclear particle tracks.[1] The simple inclusion of the sponge rubber seems to be adequate protection against damage from the several mechanical shocks involved in the firing of the rocket, the blow-off of the war-head and the final grounding of the fins.

The rocket reached an altitude of 28 km at 60 sec. after the firing and attained the peak of its trajectory 150.7 km after 223 sec. At 336.5 sec. the war-head was blown off by radio command at an elevation of 90.7 km. From this point, the precise period taken in the grounding of the plates is not known, but neglecting air resistance encountered during free fall in the lower atmosphere a period of 75 sec. is estimated for the last stage of descent. The total period between firing and landing is 6.85 min. and the plates spent approximately 4.78 min. above the stratosphere. For purposes of computing time rates the total period above White Sands (elevation 1.22 km above sea level, $\lambda = 41°N$) has been employed in computing star intensities and the time spent above 28 km for the rate of incidence of heavy primaries.

III. STAR INTENSITY

The entire areas of the monitor and the rocket plates were scanned microscopically using an 8-mm

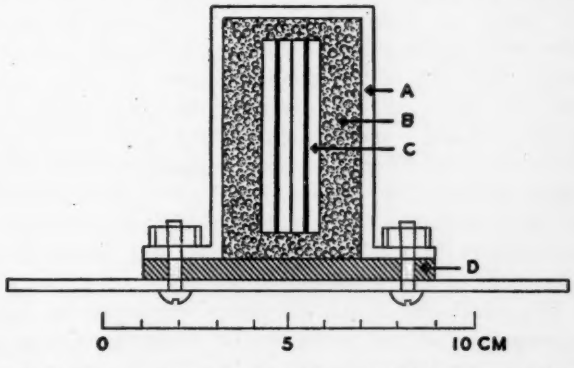

FIG. 1. Cross section of plate holder. A. Aluminum jacket 3 mm thick. B. Sponge rubber packing. C. Plates assembled with emulsion layers adjacent to each other. D. Rubber gasket.

* Public Health Service Research Fellow of The Experimental Biology and Medicine Institute.

[1] H. Yagoda and N. Kaplan, Phys. Rev. **73**, 634 (1948); H. Yagoda *Radioactive Measurements with Nuclear Emulsions* (John Wiley and Sons, Inc., New York, 1949), p. 110.

TABLE I. Star populations in rocket and control plates.

Plate	Star count	Volume, cc	Stars per cc
Rocket a	11	0.391	28.2
A	15	0.480	31.3
b	11	0.359	30.7
B	16	0.470	34.0
Totals	53	1.700	Av. 31.2±4.3
Control c	4	0.341	11.7
C	3	0.344	8.7
Totals	7	0.685	Av. 10.2±3.9

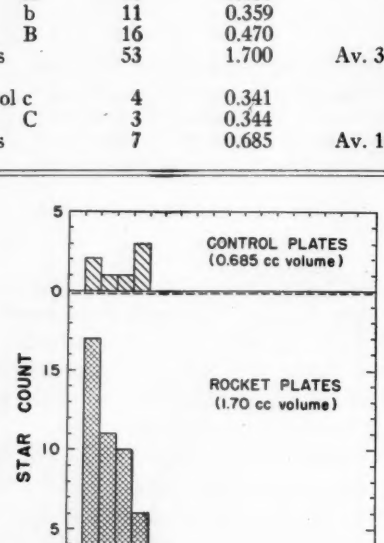

FIG. 2. Histograms of star size distribution in rocket and control plates.

achromatic objective and a pair of 10× wide field oculars, using overlapping fields so that all stars had opportunity for detection. The star counts summarized in Table I show that the plates exposed in the rocket contain a significantly larger population of nuclear evaporations of three or more tracks than the control plates. The size distribution of the events in the rocket plates, shown in Fig. 2, also exhibits the presence of a group of complex stars, characteristic of plates exposed at very high altitudes. In 1.70 cc of emulsion flown in the rocket we observed 53 nuclear evaporations and three stars produced by σ-mesons at the end of their ranges. Scanning of the monitor plates with equal care revealed seven nuclear evaporations, one π-μ-interaction and one σ-meson-induced star in a volume of 0.685 cc. The differential star population, excluding events initiated by mesons, is 21 per cc of emulsion which, if attributed to the 6.85-min. flight of the rocket, corresponds to an average rate of star production equivalent to 5000±800 per cc per day.

The particular batch of plates employed in this experiment did not prove to be sensitive to singly charged particles moving at relativistic velocities. Hence the recorded star spectrum does not include shower particles of fast mesons, or protons with kinetic energies in excess of 60 Mev. Figure 3 depicts one of the more complex evaporations recorded in the rocket plates, which is of interest in exhibiting the tracks of two massive fragments initially ejected with a high charge as indicated by the thin-down of the tracks near the end of their range.

In plates of similar composition, flown in free balloons in Minnesota at altitudes between 27 to 30 km, star populations between 1400 to 2000 per cc per day have been reported in several independent investigations.[2–4] The lower value reported from this laboratory has been corrected for ascent and descent of the balloon and for stars accumulated while the plates remained near sea level, and is therefore selected as a basis for the comparison with the star population recorded in the rocket plates. This basis indicates a rate of star production 3.6 times as large as that observed in the stratosphere. The increment cannot be attributed to the absence of practically all risidual air during the greater part of the rocket flight, but probably has its origin in the formation of energetic secondary particles in the body of the rocket. An intensification factor of 1.5 has been observed by Lord and Schein[5] in the abundance of small stars when plates are exposed in the stratosphere under 15 g/cm^{-2} of lead. Since a large proportion of the stars recorded in the rocket plates are of low multiplicity, the three-and four-branch events constituting 53 percent of the total, the abnormally large value of 5000 per cc per day probably originates in multiplication processes between primary cosmic radiation and the massive rocket body.

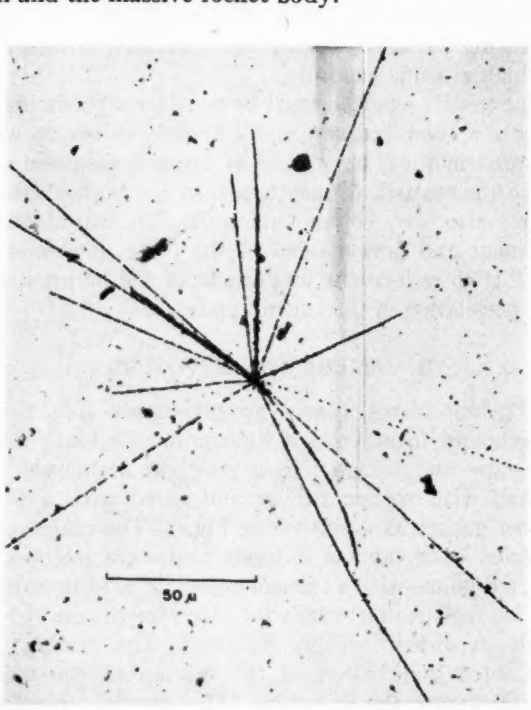

FIG. 3. Nuclear evaporation recorded in one of the rocket plates.

[2] Yagoda, Kaplan, and Conner, Phys. Rev. **76**, 171 (1949).
[3] Salant, Hornbostel, and Dollman, Phys. Rev. **74**, 694 (1948).
[4] M. Addario and S. Tamburino, Phys. Rev. **76**, 983 (1949).
[5] J. J. Lord and M. Schein, Phys. Rev. **75**, 1956 (1949).

IV. HEAVY PRIMARIES

A number of single, densely ionizing tracks were observed, indicative of particles with a charge of two or greater. The positions and orientations of these tracks were noted in an effort to trace the particles through the stack. Only three of the tracks could be followed through the four plates, and on the basis of δ-ray counts (Table II) were identified as particles of charge 14, 8, and 6, respectively. Since the identification of the track as that of a heavy primary was based chiefly on a high δ-ray count along its recorded path, fast He, Li, Be, and B nuclei would escape recognition in a stack of small dimensions. The three tracks thus furnish a rough estimate of the flux of only those heavy primaries of charge $Z \geq 6$. The flux of these particles corresponds to 0.031 ± 0.018 per cm² per min. of flight above the stratosphere. During the flight of a V-2 rocket fired on January 22, 1949, Golian and co-workers[6] observed the trajectory of one heavy primary using a 6-in. cloud chamber in which photographs were taken at 25-sec. intervals.

While the flux of heavy primaries evaluated from the three tracks recorded in the rocket plates is subject to a large statistical uncertainty, it is of interest to compare the magnitude with that derived from the more abundant data obtained in plates exposed at stratosphere levels. The measurements of Bradt and Peters[7] showed the presence of 61 primary tracks in a complete survey of 20.2 cm² of emulsion exposed for 3 hr. at geomagnetic latitude $\lambda = 51°$N. This is equivalent to an incident flux, independent of angle of entry with respect to the zenith, of 0.017 ± 0.002 per cm² per min. of flight, which indicates that our rough estimate for the flux of primaries during the rocket flight is of the correct order of magnitude.

TABLE II. Characteristics of the heavy primary tracks.

Track	R-1	R-2	R-3
Angle with emulsion plane[a]	34.8°	54°	48.5°
Length in top plates[b]	708μ	503μ	533μ
Length in bottom plates	701	493	523
δ-rays in top plates	87	25	16
δ-rays in bottom plates	90	20	14
Average δ-ray count per 100	12.6	4.5	2.7
Probable charge[c]	14±2	8±2	6±2
Range in glass between emulsions	10.5 mm	7.22 mm	7.68 mm
Total range in emulsions and glass	3.2 g/cm²	2.2 g/cm	2.3 g/cm

[a] The orientation of the plates was defined precisely when initially mounted on the rocket. However, since the particles may have been incident either during ascent or descent, the direction of the primaries with respect to the zenith cannot be established.
[b] The plates were assembled with emulsion layers adjacent. After recording in the top plates the particles traversed two glass backings (each 1.5 mm thick) before reaching the lower set of sensitive layers.
[c] Computed from the relationship described by Bradt and Peters (reference 7): $(n\delta)_\beta = (0.060Z^2 + 0.2)$ where $(n\delta)_\beta$ represents the average δ-ray count per 100μ for particles traveling with relativistic velocities.

This exposure has been made possible by the cooperation of the Naval Research Laboratory and the group at the White Sands Proving Ground. We wish to express our appreciation to G. J. Perlow for suggestions on the design of the camera and to C. P. Smith for expediting the return of the plates to the laboratory.

[6] Golian, Johnson, Krause, Kuder, Perlow, and Schroeder, Phys. Rev. **75**, 524 (1949).
[7] H. L. Bradt and B. Peters, Phys. Rev. **77**, 54 (1950).

The Phenomenological Theory of Liquid Helium II*

SADAO NAKAJIMA, KAZUHISA TOMITA, AND TUNEMARU USUI**
Physics Department, Tokyo University, Tokyo, Japan
(Received December 15, 1949)

The purpose of the present paper is to refine the "two-fluid model" as a phenomenological theory of liquid He II. General thermohydrodynamical equations are formulated in Part I, following the treatment of viscous fluids by Eckart and Tolman. The previous phenomenological theories, which have been proposed by Landau, Tisza, F. London and Zilsel, and Gorter, are included in the present general formalism, and their intrinsic relations are discussed from a unified point of view.

The thermodynamic equations of motion are applied in Part II to the stationary flow in He II under the reversible process approximation. Adopting Gorter's type of mutual friction, we can fully describe the fountain pressure (thermomechanical effect) and the anomalous heat transfer (heat-superconductivity). The theoretical predictions concerning the maximum fountain pressure or maximum heat current against temperature, and the critical current appointing the validity limit of H. London's thermostatical relation $dp/dT=\rho s$, are fairly consistent with observed tendencies.

PART I. THE GENERAL THEORY

1. Introduction

As Tisza[1] has insisted, it is very desirable to formulate the phenomenological equations of motion of liquid He II, which correspond to the well-known theory of superconductivity due to F. London and H. London, in order to give a consistent description of various experimental facts and establish a starting point for the considerations from a molecular point of view. Among such phenomenological theories the "two-fluid model" seems to be most promising. This idea was first treated qualitatively by F. London and Tisza, who were guided by the theory of Bose-Einstein condensation, and was then formulated successfully by Landau[2] and Tisza[1] in the case of infinitesimal motions, resulting in the theory of "second sound."

According to their theory, liquid He II is considered as a sort of fluid mixture consisting of the normal and the superfluids. Let the density and the velocity of the normal fluid be ρ_n and $\mathbf{V}_n$, and those of the superfluid ρ_s and $\mathbf{V}_s$. Then the total density

$$\rho=\rho_n+\rho_s$$

and the velocity of the center of gravity

$$\mathbf{V}_1=(\rho_n/\rho)\mathbf{V}_n+(\rho_s/\rho)\mathbf{V}_s$$

have the ordinary hydrodynamical meanings. On the other hand, the velocity of the normal fluid relative to the center of gravity

$$\mathbf{V}_2=\mathbf{V}_n-\mathbf{V}_1$$

is essential to the peculiarity of He II.

Recently F. London and Zilsel[3] have shown that the anomalous heat current in He II can be explained by adding to the Landau-Tisza equation a term which represents the ordinary viscosity of the normal fluid (a term of Navier-Stokes type). On the other hand, Gorter[4] has pointed out that the mutual friction between the normal and the superfluids plays an important role.

The purpose of the present paper is to formulate the idea of "two-fluid model" as generally as possible, and to put in order the various conception which have been discovered by many people, clarifying the intrinsic relations among them. Putting aside premature speculations about the molecular mechanism, we try to refine the two-fluid model as a phenomenological theory. In particular, we adopted Tisza's point of view that in He II, parameters such as the viscosity coefficient, coefficient of thermal conduction, etc., have similar values to those of He I, whereas the differential equations which characterize the motion of He II must be modified. To obtain such fundamental equations, we follow the treatment of a viscous fluid due to Eckart[5] and Tolman.[6] Thus we consider a region τ which is fixed in space and apply the conservation laws of mass and momentum and the first and second laws of thermodynamics to He II in this region. In the following sections, σ is the surface of the region τ, $d\boldsymbol{\sigma}$ the surface element (inward) normal vector to σ, $\mathbf{V}_n\cdot d\boldsymbol{\sigma}$ the scalar product, and $\Pi d\boldsymbol{\sigma}$ a vector which is obtained by operating with a tensor Π on the vector $d\boldsymbol{\sigma}$.

2. Foundations of the Theory

Experiments of Kapitza[7] indicate that no entropy is transferred by the flow of He II through a sufficiently narrow capillary. As F. London[8] has shown, one can define the fraction of the normal part for a given state of He II on the basis of this experimental evidence and without referring to any specific molecular model.

The result is

$$\rho_n/\rho=s/s_\lambda, \tag{2.1}$$

* Read at the Fourth Annual Meeting of the Physical Society of Japan, April 27, 1949.
** Not at the Physics Department, Nagoya University, Nagoya, Japan.
[1] L. Tisza, Phys. Rev. **72**, 838 (1947).
[2] L. Landau, J. Phys. U.S.S.R. **5**, 71 (1941).
[3] F. London and P. R. Zilsel, Phys. Rev. **74**, 1148 (1948).
[4] C. J. Gorter, Phys. Rev. **74**, 1544 (1948).
[5] C. Eckart, Phys. Rev. **58**, 267, 269 (1940).
[6] R. C. Tolman and P. C. Fine, Rev. Mod. Phys. **20**, 67 (1948).
[7] P. Kapitza, J. Phys. U.S.S.R. **5**, 59 (1941).
[8] F. London, Rev. Mod. Phys. **17**, 310 (1945).

where s denotes the entropy per unit mass and s_λ its value at the λ-point $T_\lambda(=2.19°\text{K})$. Experimentally, the entropy proves to be a function of temperature only, under sufficiently low pressures, and is given by[1,8]

$$s=s_\lambda(T/T_\lambda)^r. \tag{2.2}$$

Experiments at Leiden give the values $s_\lambda=0.403$ cal./g-deg. and $r=5.6$, while those of Kapitza give the values $s_\lambda=0.405$ cal./g-deg. and $r=5.5$.

Now, using (2.1), we find the fundamental equation of *thermostatics* for the variation of the internal energy of a fixed volume τ,

$$\delta U=T\delta S+[u-Ts+(p/\rho)]\delta M,$$

is transcribed as

$$\delta U=u\delta M+(Ts_\lambda\delta M_n-Ts\delta M)+(p/\rho)\delta M, \tag{2.3}$$

where M, S, M_n, p, and u are, respectively, the total mass, the total entropy, the mass of the normal fluid, hydrostatic pressure, and the internal energy per unit mass. In order to step into *thermodynamics*, it is necessary to specify the detailed mechanism which governs the change of M and M_n. Especially, it is to be noted that M_n may vary not only by heat conduction (transformation of the superfluid into the normal, see later sections), but also through the flow of the normal fluid which is governed by the different velocity field from that of the total mass flow.

Thus, corresponding to each term of Eq. (2.3), we propose for the energy flow through the surface σ of volume τ to be classified as follows:

(a) Ordinary Convection

$$\int_\sigma u\rho\mathbf{V}_1\cdot d\boldsymbol{\sigma}, \tag{2.4}$$

which corresponds to the first term of (2.3).

(b) Internal Convection

$$\int_\sigma Ts_\lambda\rho_n\mathbf{V}_n\cdot d\boldsymbol{\sigma}-\int_\sigma Ts\rho\mathbf{V}_1\cdot d\boldsymbol{\sigma}=\int_\sigma \rho sT\mathbf{V}_2\cdot d\boldsymbol{\sigma}, \tag{2.5}$$

which corresponds to the third term of (2.3) and the part of the second term due to the flow of the normal fluid. The energy flow appeared in (2.5),

$$\mathbf{q}=\rho sT\mathbf{V}_2 \tag{2.6}$$

is peculiar to He II and responsible for its anomalous thermal properties. To emphasize its important role, we propose to use a special terminology, *internal convection*, which was used already by F. London and Zilsel.[3] In ordinary fluids, where the flow of entropy and that of mass are described by the same velocity field, the internal convection does not appear.†

(c) Heat Conduction

$$\int_\sigma \mathbf{q}_0\cdot d\boldsymbol{\sigma} \tag{2.7}$$

which corresponds to the rest of the second term of (2.3). For $\mathbf{q}_0$, we assume Fourier's expression

$$\mathbf{q}_0=-\kappa\,\mathrm{grad}T, \tag{2.8}$$

where κ is, from our fundamental point of view, expected to be of the same order of magnitude as the heat conductivity of He I ($\sim10^{-5}$ cal./cm deg. sec.).

(d) Work Done by the Hydrostatic Pressure

$$\int_\sigma p\mathbf{V}_1\cdot d\boldsymbol{\sigma}, \tag{2.9a}$$

which corresponds to the last term of (2.3). In the case of motion of finite velocity, we must also take into account work done by the viscous stress,

$$\int_\sigma \mathbf{V}_n\cdot(\Pi' d\boldsymbol{\sigma}), \tag{2.9b}$$

where the viscous stress Π' is assumed to be caused only by the normal fluid and given by

$$\left.\begin{aligned}&\Pi_{xx}'=\tfrac{2}{3}\eta_n\,\mathrm{div}\mathbf{V}_n-2\eta_n(\partial V_{nx}/\partial x),\\&\Pi_{xy}'=-\eta_n[(\partial V_{nx}/\partial y)+(\partial V_{ny}/\partial x)],\quad\cdots.\end{aligned}\right\}\tag{2.10}$$

As Tisza has proposed, and we also support from our general point of view, the temperature dependence of moment of inertia measured by Andronikashvilli[9] and the viscosity measurements by Keesom and Mac Wood[10] indicate the evidence that the viscosity of the normal fluid may be obtained by a suitable extrapolation from that of He I and that the superfluid has no viscosity of this kind.

Finally, we must take account of

(e) Flux of Kinetic Energy

$$\int_\sigma(\tfrac{1}{2}\rho_n\mathbf{V}_n^2)\mathbf{V}_n\cdot d\boldsymbol{\sigma}+\int_\sigma(\tfrac{1}{2}\rho_s\mathbf{V}_s^2)\mathbf{V}_s\cdot d\boldsymbol{\sigma}. \tag{2.11}$$

Summing up the five kinds of energy flow, (2.4), (2.5), (2.7), (2.9), and (2.11), and equating to the rate of change of the total energy contained in the volume τ, one obtains the first law. Similarly, one can formulate the conservation laws of mass and momentum and the second law. These fundamental laws are written as follows:

mass conservation law,

$$\frac{\partial}{\partial t}\int_\tau(\rho_n+\rho_s)d\tau=\int_\sigma(\rho_n\mathbf{V}_n+\rho_s\mathbf{V}_s)\cdot d\boldsymbol{\sigma}; \tag{2.12}$$

† This is incompatible with above-mentioned experiments of Kapitza in the case of He II.

[9] E. Andronikashvilli, J. Phys. U.S.S.R. **10**, 201 (1946).
[10] W. H. Keesom and G. E. Mac Wood, Physica **5**, 737 (1938).

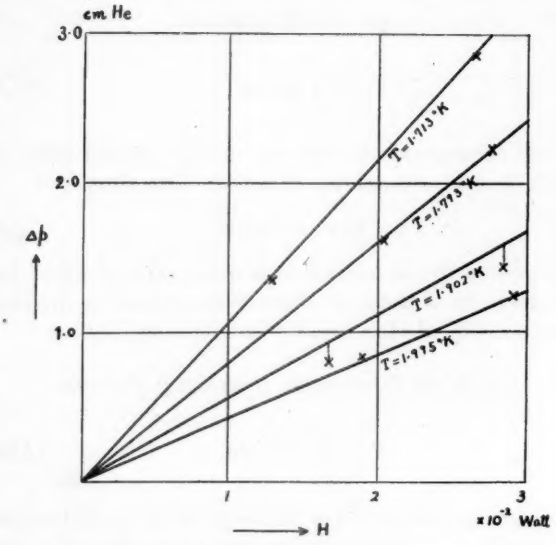

FIG. 1. Fountain effect against heat current, for constant temperature of helium bath. x: observed (KD); ——: calculated $d=19\mu$.

momentum conservation law

$$\frac{\partial}{\partial t}\int_\tau(\rho_n\mathbf{V}_n+\rho_s\mathbf{V}_s)d\tau=\int_\sigma(\rho_n\mathbf{V}_n)\mathbf{V}_n\cdot d\boldsymbol{\sigma}+\int_\sigma(\rho_s\mathbf{V}_s)\mathbf{V}_s\cdot d\boldsymbol{\sigma}+\int_\sigma\Pi d\boldsymbol{\sigma},\quad(2.13)$$

where

$$\Pi_{xx}=p+\Pi_{xx}',\quad \Pi_{xy}=\Pi_{xy}',\quad\cdots;\qquad(2.14)$$

the first law

$$\frac{\partial}{\partial t}\int_\tau(\tfrac{1}{2}\rho_n\mathbf{V}_n^2+\tfrac{1}{2}\rho_s\mathbf{V}_s^2+\rho u)d\tau=\int_\sigma(\tfrac{1}{2}\rho_n\mathbf{V}_n^2)\mathbf{V}_n\cdot d\boldsymbol{\sigma}+\int_\sigma(\tfrac{1}{2}\rho_s\mathbf{V}_s^2)\mathbf{V}_s\cdot d\boldsymbol{\sigma}+\int_\sigma(\rho u\mathbf{V}_1+\rho sT\mathbf{V}_2+\mathbf{q}_0+p\mathbf{V}_1)\cdot d\boldsymbol{\sigma}+\int_\sigma\mathbf{V}_n\cdot(\Pi' d\boldsymbol{\sigma});\quad(2.15)$$

the second law

$$\frac{\partial}{\partial t}\int_\tau\rho s d\tau=\int_\sigma\rho s\mathbf{V}_n\cdot d\boldsymbol{\sigma}+\int_\sigma\frac{\mathbf{q}_0\cdot d\boldsymbol{\sigma}}{T}+\int_\tau\left(\frac{dS}{dt}\right)_{\text{irr}}d\tau,\quad(2.16)$$

where the first term on the right expresses the fact that the entropy is transferred only by the normal fluid; the second is the rate at which the entropy varies through the conduction of heat; the third is the rate of irreversible production of entropy per unit volume. Thus, it is evident that the above formulation of the first and the second laws is consistent with the fundamental equation of thermostatics, (2.3).

3. Thermodynamic Equations of Motion

Now, we transform the laws of integral form in Section 2 into differential equations by means of Gauss' theorem. From Eq. (2.12) we obtain the equation of

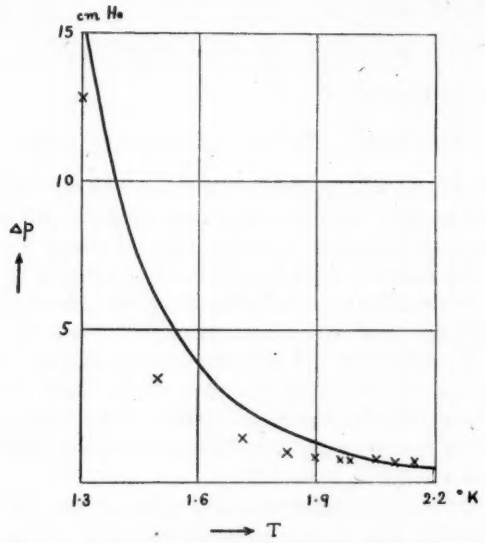

FIG. 2. Fountain effect against temperature. $d=10.5\mu$, $q=0.18$ watt cm^{-2}. x: observed (M); ——: calculated.

continuity

$$(\partial/\partial t)(\rho_n+\rho_s)+\operatorname{div}(\rho_n\mathbf{V}_n+\rho_s\mathbf{V}_s)=0\qquad(3.1)$$

or

$$(\partial\rho/\partial t)+\operatorname{div}(\rho\mathbf{V}_1)=0\qquad(3.2)$$

which may be decomposed into

$$\begin{aligned}(\partial\rho_n/\partial t)+\operatorname{div}(\rho_n\mathbf{V}_n)&=\Gamma,\\(\partial\rho_s/\partial t)+\operatorname{div}(\rho_s\mathbf{V}_s)&=-\Gamma.\end{aligned}\qquad(3.3)$$

Γ is the rate of production of the normal fluid per unit volume which is always accompanied by annihilation of an equal amount of the superfluid, so that it may also be considered as the rate of transformation of the superfluid into the normal fluid. From (2.13), taking account of Eqs. (3.3) (2.10), and (2.14), one obtains

$$\rho_n\left(\frac{\partial}{\partial t}+\mathbf{V}_n\cdot\operatorname{grad}\right)\mathbf{V}_n+\rho_s\left(\frac{\partial}{\partial t}+\mathbf{V}_s\cdot\operatorname{grad}\right)\mathbf{V}_s+\Gamma(\mathbf{V}_n-\mathbf{V}_s)+\operatorname{grad}p+\eta_n\{\operatorname{curl}\operatorname{curl}\mathbf{V}_n-(4/3)\operatorname{grad}\operatorname{div}\mathbf{V}_n\}=0.\quad(3.4)$$

Here it is to be noted that the term $\Gamma(\mathbf{V}_n-\mathbf{V}_s)$ represents that part of the momentum which must be

supplied where the above-mentioned transformation occurs.

Similarly, transforming Eq. (2.15) into a differential form, and using Eqs. (3.3), (3.4), and the thermostatic relation

$$du=(p/\rho^2)d\rho+Tds,$$

and carrying out a somewhat lengthy calculation, one finds that

$$(\mathbf{V}_s-\mathbf{V}_n)\cdot\left[\rho_s\left(\frac{\partial}{\partial t}+\mathbf{V}_s\cdot\text{grad}\right)\mathbf{V}_s+\frac{\rho_s}{\rho}\,\text{grad}p\right.$$
$$\left.-\rho_s s\,\text{grad}T+\frac{\Gamma}{2}(\mathbf{V}_n-\mathbf{V}_s)\right]$$
$$+T\left[\frac{\partial(\rho s)}{\partial t}+\text{div}(\rho s\mathbf{V}_n)\right]+\text{div}\mathbf{q}_0-\epsilon=0, \quad (3.5)$$

where

$$\epsilon=\eta_n[-\tfrac{2}{3}(\text{div}\mathbf{V}_n)^2+(\text{curl}\mathbf{V}_n)^2-2(\mathbf{V}_n\cdot\text{grad div}\mathbf{V}_n)$$
$$-2\,\text{div}(\mathbf{V}_n\times\text{curl}\mathbf{V}_n)+\Delta\mathbf{V}_n^2] \quad (3.6)$$

is Rayleigh's dissipation function, and is essentially positive.

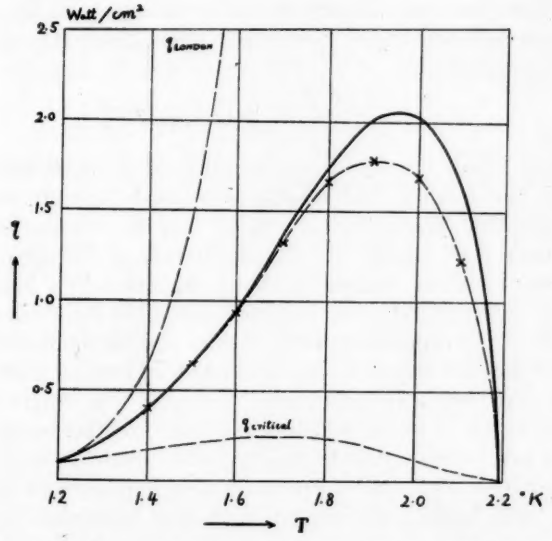

FIG. 3. Heat current density against temperature. $d=19\mu$, $\theta=0.006$ deg. cm^{-1}, x: observed (KD); ——: calculated.

Thus, if the equation of motion of the superfluid takes the form

$$\rho_s\left(\frac{\partial}{\partial t}+\mathbf{V}_s\cdot\text{grad}\right)\mathbf{V}_s=-\frac{\rho_s}{\rho}\,\text{grad}p+\rho_s s\,\text{grad}T$$
$$-\frac{\Gamma}{2}(\mathbf{V}_n-\mathbf{V}_s)+\mathbf{f} \quad (3.7)$$

then Eq. (3.5) reduces to

$$\frac{\partial(\rho s)}{\partial t}+\text{div}(\rho s\mathbf{V}_n)=\frac{1}{T}[-\text{div}\mathbf{q}_0+\epsilon+\mathbf{f}\cdot(\mathbf{V}_n-\mathbf{V}_s)]. \quad (3.5')$$

Meanwhile, the second law (2.16) reduces to the differential form:

$$\frac{\partial}{\partial t}(\rho s)+\text{div}(\rho s\mathbf{V}_n)+\frac{\text{div}\mathbf{q}_0}{T}-\frac{\mathbf{q}_0\cdot\text{grad}T}{T^2}=\left(\frac{dS}{dt}\right)_{\text{irr}}. \quad (3.8)$$

This and (3.5′) lead to

$$\left(\frac{dS}{dt}\right)_{\text{irr}}=-\frac{\mathbf{q}_0\cdot\text{grad}T}{T^2}+\frac{\epsilon}{T}+\frac{\mathbf{f}\cdot(\mathbf{V}_n-\mathbf{V}_s)}{T}. \quad (3.9)$$

The separation parameter $\mathbf{f}$ is, for the time being, undetermined and must be found by considering the physical mechanism of the irreversible production of entropy. At least, however, since the condition $\mathbf{f}\cdot(\mathbf{V}_n-\mathbf{V}_s)>0$ must be always valid, $\mathbf{f}$ may be expected to be $(\mathbf{V}_n-\mathbf{V}_s)$ multiplied by a positive scalar function, which means physically a mutual friction per unit volume existing between the normal and the supercomponent of He II. While we were endeavoring to find out a definite form of this term, Gorter[4] had pointed out that the irreversible production of entropy due to such a mutual friction should play an important role.

If one puts

$$\mathbf{f}=A\rho_n\rho_s(\mathbf{V}_n-\mathbf{V}_s)^2(\mathbf{V}_n-\mathbf{V}_s), \quad (3.10)$$

one can include the Gorter's mutual friction in the present general formalism. Equation (3.10) might be an approximation to the more complicated expression.

To collect the equations obtained, we have

$$\begin{aligned}(\partial\rho_n/\partial t)+\text{div}(\rho_n\mathbf{V}_n)&=\Gamma,\\ (\partial\rho_s/\partial t)+\text{div}(\rho_s\mathbf{V}_s)&=-\Gamma,\end{aligned} \quad (I)$$

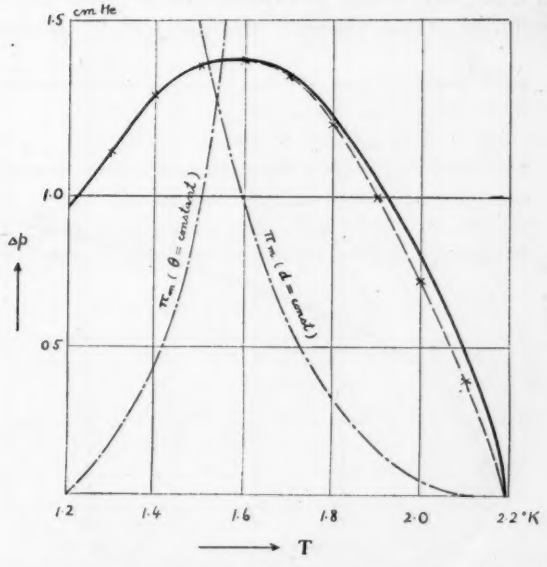

FIG. 4. Fountain pressure against temperature. $d=19\mu$, $\theta=0.006$ deg. cm^{-1}. x: observed (KD); ——: calculated.

$$\rho_n\left(\frac{\partial}{\partial t}+\mathbf{V}_n\cdot\text{grad}\right)\mathbf{V}_n+\rho_s\left(\frac{\partial}{\partial t}+\mathbf{V}_s\cdot\text{grad}\right)\mathbf{V}_s$$
$$+\Gamma(\mathbf{V}_n-\mathbf{V}_s)=-\text{grad}p-\eta_n\{\text{curl curl}\mathbf{V}_n$$
$$-(4/3)\text{ grad div}\mathbf{V}_n\},\quad\text{(II)}$$

$$\rho_s\left(\frac{\partial}{\partial t}+\mathbf{V}_s\cdot\text{grad}\right)\mathbf{V}_s+\frac{\rho_s}{\rho}\text{grad}p-\rho_s s\,\text{grad}T$$
$$+\frac{\Gamma}{2}(\mathbf{V}_n-\mathbf{V}_s)-\mathbf{f}=0,\quad\text{(III)}$$

$$\left.\begin{aligned}&\frac{\partial(\rho s)}{\partial t}+\text{div}(\rho s\mathbf{V}_n)+\text{div}\left(\frac{\mathbf{q}_0}{T}\right)=\left(\frac{dS}{dt}\right)_{\text{irr}},\\&\left(\frac{dS}{dt}\right)_{\text{irr}}=\mathbf{q}_0\cdot\text{grad}\left(\frac{1}{T}\right)+\frac{\epsilon}{T}+\frac{1}{T}\mathbf{f}\cdot(\mathbf{V}_n-\mathbf{V}_s).\end{aligned}\right\}\text{(IV)}$$

When it is necessary, one can obtain the equation of motion for the normal part from (II) and (III):

$$\rho_n\left(\frac{\partial}{\partial t}+\mathbf{V}_n\cdot\text{grad}\right)\mathbf{V}_n+\frac{\rho_n}{\rho}\text{grad}p+\rho_s s\,\text{grad}T$$
$$+(\Gamma/2)(\mathbf{V}_n-\mathbf{V}_s)+\mathbf{f}+\eta_n\{\text{curl curl}\mathbf{V}_n$$
$$-(4/3)\text{ grad div}\mathbf{V}_n\}=0.\quad\text{(III')}$$

4. Discussion

Putting $\Gamma=0$ and $\mathbf{f}=0$, and neglecting at the same time the non-linear terms, $(\mathbf{V}_n\cdot\text{grad})\mathbf{V}_n$ and $(\mathbf{V}_s\cdot\text{grad})\mathbf{V}_s$, and the viscosity term, too, we can obtain the well-known Landau-Tisza equations from Eqs. (I)–(IV). When we take account of the viscosity term, we obtain the fundamental equations of F. London and Zilsel, which may be expected to be useful for the description of the viscosity measurement by Keesom and Mac Wood.[10] Thus, if one assumes that the superfluid moves with the same velocity as that of the normal fluid under uniform pressure and temperature, the calculation of Mac Wood[11] is still valid in the present formalism. On the other hand, if the superfluid is perfectly at rest, we have to put $\mathbf{V}_n$ and η_n/ρ_n in place of $\mathbf{V}$ and η/ρ, respectively, in his calculation. The result is just the same as Tisza has analyzed, i.e., we must multiply the values of Keesom and Mac Wood by the factor ρ/ρ_n. These corrected values of the viscosity coefficient do not agree with the values extrapolated smoothly from those of He I in contradiction to the suggestion of Tisza. Since there exists mutual friction between the normal and the superfluids, it might be unreasonable to assume the superfluid to be perfectly at rest. However, the effect of the mutual friction has been estimated to be negligibly small in this case. The pressure gradient and the temperature gradient neglected in the previous discussion would presumably play an important role. At any rate, the analysis of the viscosity measurement with the oscillating disk seems to be so complicated that one cannot obtain a definite result from it. It is preferable to make use of the fountain pressure measurement. We shall give the detailed description of this method in Part II.

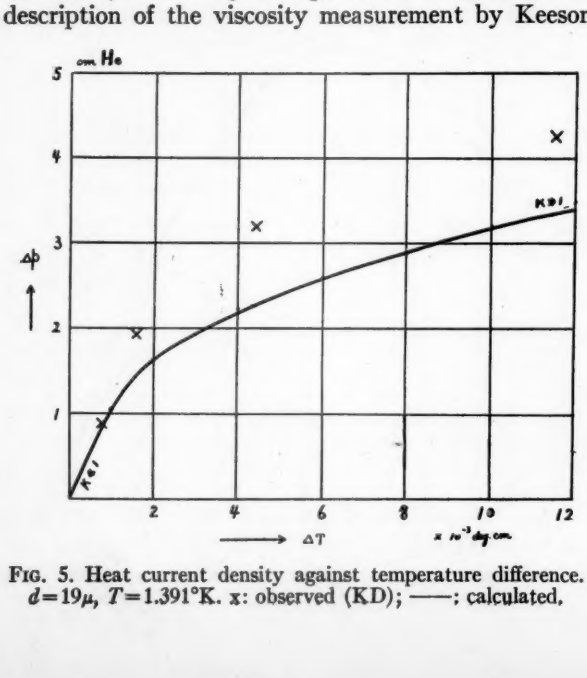

FIG. 5. Heat current density against temperature difference. $d=19\mu$, $T=1.391$°K. x: observed (KD); ——: calculated.

Now, one may assume s_λ to be constant, at least under sufficiently low pressures. Then, from (I) and (IV), one obtains

$$\Gamma=(1/s_\lambda)[(dS/dt)_{\text{irr}}-\text{div}(\mathbf{q}_0/T)],$$

which shows that the transformation of the superfluid into the normal fluid should be caused through the irreversible production of entropy or the conduction of heat. For instance, the transformation, which occurs in the constant volume of He II immersed in a heat bath by quasistatic heating, corresponds to the second term of the expression. Thus, Γ may also be significant near the heat source in the experiment of heat transfer.

Under ordinary conditions, however, the internal convection (2.6) overwhelms the heat conduction $\mathbf{q}_0$, and $\rho s\mathbf{V}_n$ turns out to be much greater than $(dS/dt)_{\text{irr}}$. Therefore, with the exception of singularities such as the heat sources, the reversible process approximation

$$[\partial(\rho s/\partial t]+\text{div}(\rho s\mathbf{V}_n)=0$$

may be valid. All authors have succeeded in describing the essential features of phenomena by means of this approximation.

It might seem rather trivial to have introduced the apparently insignificant term $\mathbf{q}_0$, which, however, appears to us particularly important, for if this term is omitted it follows that the normal fluid flows up the temperature gradient in the case of heat transfer through a slit. The detailed accounts will be given in Part II.

[11] G. E. Mac Wood, Physica 5, 375 (1938).

Finally, we also take up the conventional boundary conditions that

$$\mathbf{V}_n=0 \quad \text{and} \quad \mathbf{V}_{s\perp}=0$$

at the solid wall. F. London and Zilsel have suggested the possibility that the normal fluid also slips along the wall. We shall show, in Part II, that such a modification of the boundary conditions is quite unnecessary.

PART II. HEAT TRANSFER

5. Introduction

As mentioned in Part I, the internal convection $\rho s\mathbf{V}_n$ is much greater than the term $(dS/dt)_{\text{irr}}$ and $\mathbf{q}_0/T$ under ordinary conditions, and therefore the reversible process approximation to Eqs. (IV) of Section 3,

$$(\partial/\partial t)(\rho s)+\text{div}(\rho s\mathbf{V}_n)=0 \text{ (conservation of entropy)},$$

may be considered to be valid. As Γ is explicitly given by the expression

$$\Gamma=(1/s_\lambda)[(dS/dt)_{\text{irr}}-\text{div}(\mathbf{q}_0/T)], \qquad (5.1)$$

we must disregard Γ at the same time in this approximation. All the previous treatments,[1-3] which have used this approximation and succeeded, though only partially, in clarifying some part of the peculiar behavior of He II, prove the validity of this approximation. Therefore, we also assume it and put $\Gamma=0$ in our fundamental equations. Then we have only the $\mathbf{f}$ term left among the newly introduced terms.

According to our general theory, the explicit form of the term is $(\mathbf{V}_n-\mathbf{V}_s)$ multiplied by a positive scalar function α. For more detailed knowledge concerning α we must proceed, by analyzing suitable experimental phenomena.

There are now numerous reports on the many peculiar properties of liquid He II; but many of them are in default of any precise description of the conditions under which the experiments were performed, and few are sufficiently quantitative to be compared with the theory. Among these experiments, those of the Leiden experimenters, Keesom, Saris, and Meyer (K-S-M);[12] Keesom and Duykaerts (K-D);[13] Mellink (M);[14] and Meyer and Mellink (M-M)[15] are so systematic and exhaustive that we can choose their data as source material for investigating the mutual friction.

These investigators measured the stationary heat current and the fountain pressure which were caused by electrically heating liquid He II in one of the two regions separated by a capillary or a slit which is adjustable between two zonal surfaces of a sphere. There the radius of the capillary or the width of the slit is so much smaller than the other dimensions that it may be legitimate to describe it as a two-dimensional case. In the following analysis we take the x axis along the longer side and the y axis along the width. The plane $y=0$ divides the width d equally.

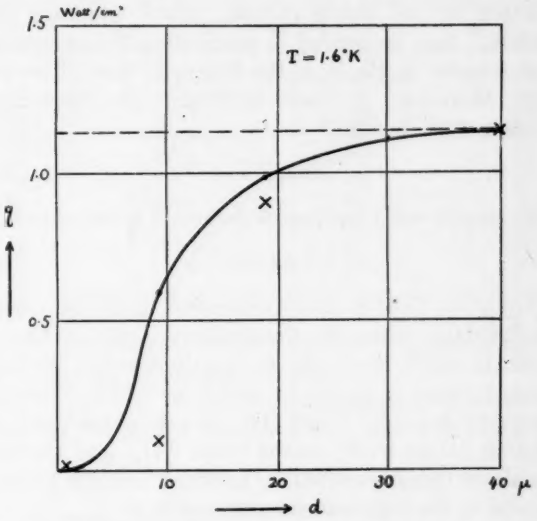

FIG. 6. Heat current against slit width. $\theta=0.006$ deg. cm^{-1}, $T=1.6$°K. x: observed (KD); ——: calculated.

To collect the important results of the Leiden experimenters:

(A) The heat current density $\mathbf{q}$ is exactly proportional to the fountain pressure Δp (Fig. 1).

(B) The fountain pressure decreases with increasing temperature T under constant heat current, but does not vanish at the λ-point T_λ (Fig. 2).

(C) The heat current under constant temperature difference ΔT increases with the temperature, and then, through a maximum, decreases agin, vanishing at the λ-point (Fig. 3). A similar variation is observed for the fountain pressure (Fig. 4).

(D) Under constant temperature, the heat current is proportional to ΔT in the case of a narrow slit or of a small temperature difference. But in the case of wide slit or larger temperature difference it is proportional to $(\Delta T)^{\frac{1}{2}}$ (Fig. 5).

(E) In the case of a capillary under constant temperature difference, the heat current is proportional to the cross section at lower temperatures, but is independent of the cross section at higher temperatures (Fig. 6).

Adding only the viscosity term of the normal fluid to the theory of Landau and Tisza and F. London and Zilsel[3] (abbreviated as L-Z in the following) have tried to explain the Leiden experiments. There appears no Γ in their treatment, and moreover, concerning the velocity fields of two fluids they make the assumption

$$\mathbf{V}_n=(u_n(y),0,0), \quad \mathbf{V}_s=(u_s(y),0,0). \qquad (5.2)$$

The latter assumption includes the existence of two sorts of uniform velocity fields along the length of slit, resulting in a pure *convection* if the thermal energy is carried only by the normal part. In other words, they assumed that irreversible process, e.g., the transformation of super- into normal fluid, are negligibly small compared to the reversible convection, which may be considered as an expression of the above-mentioned approximation.

[12] Keesom, Saris, and Meyer, Physica **7**, 817 (1940).
[13] W. H. Keesom and G. Duykaerts, Physica **13**, 153 (1947).
[14] J. H. Mellink, Physica **13**, 180 (1947).
[15] L. Meyer and J. H. Mellink, Physica **13**, 197 (1947).

Based on the above picture, called "internal convection," they succeeded in attributing the anomalous heat transfer in He II to the Poiseuille flow of normal fluid. Moreover, in their treatment the *thermostatic* relation of H. London[16]

$$dp/dT=\rho s \tag{5.3}$$

still remains valid, and consequently it is expected that

$$q\propto\Delta p\propto\Delta T. \tag{5.4}$$

Equation (5.4) is fairly consistent with the experimental data, when the temperature is low or the slit width is small. However, as already reported by K-D, there appears a region in which $q\propto(\Delta T)^{\frac{1}{2}}$ when the temperature is high [item (D)]. On the other hand, the relation $q\propto\Delta p$ holds always [item (A)], and therefore the above fact shows that H. London's relation becomes invalid in the high temeprature region.

L-Z determined the critical heat current q_c empirically, fixing the region in which a discrepancy appears between experimental data and H. London's formula, and expected that the hydrodynamical description might fail above this current density. But, if so, the "two-fluid model," as discussed by Tisza,[2] would lose its secure basis, even without criticism from the molecular point of view. Of course, avoiding such a hasty conclusion, L-Z proposed several refinements within the scope of the "two-fluid model," but in each case they expected the solution of the problem to come ultimately in refinements and perfection of the fundamental equations of hydrodynamics.

Returning to our thermodynamic equations, we see that they fulfill L-Z's requirement of derivation. However, even under the reversible process approximation, our equations do not coincide with L-Z's in containing the mutual friction term $\mathbf{f}$, and if this plays a role *mechanically* analogous to ordinary viscosity, H. London's formula becomes invalid as is clearly seen from the equation of superfluid motion (III) in Part I, Section 3. Therefore, by giving a suitable form to the mutual friction, we tried to describe the region left unexploted by L-Z and to explain the related phenomena.

On the other hand, Gorter[17] has suggested that in order to explain the empirical formula $q\propto(\Delta T)^{\frac{1}{2}}$ in wide slits, a term of mutual friction of the form

$$A\rho_n\rho_s(V_n-V_s)^3+\cdots$$

per unit volume should be assumed. Of course, we do not know how Gorter has treated the fundamental equations, but, as is readily seen, his form of mutual friction satisfies the requirement of our general theory on the $\mathbf{f}$ term. Therefore, we included his mutual friction as our $\mathbf{f}$,

$$\mathbf{f}=A\rho_n\rho_s(\mathbf{V}_n-\mathbf{V}_s)^2(\mathbf{V}_n-\mathbf{V}_s) \tag{5.5}$$

and examined the resulting conclusion, which will be presented later. Here A is the parameter which characterizes the mutual friction, having dimensions

$$[A]=[M^{-1}LT]=[\eta_n^{-1}].$$

6. Two Velocity Fields in He II

Following the line stated in the preceding section, we also assume $\Gamma=0$ and a stationary solution of laminar flow, (5.2). Then, from (III′) and (III) the velocity fields are governed by the equations

$$(\rho_n/\rho)\,\mathrm{grad}p+\rho_s s\,\mathrm{grad}T+A\rho_n\rho_s(\mathbf{V}_n-\mathbf{V}_s)^2(\mathbf{V}_n-\mathbf{V}_s)=\eta_n\Delta\mathbf{V}_n \tag{III′}$$

and

$$(\rho_s/\rho)\,\mathrm{grad}p-\rho_s s\,\mathrm{grad}T-A\rho_n\rho_s(\mathbf{V}_n-\mathbf{V}_s)^2(\mathbf{V}_n-\mathbf{V}_s)=0. \tag{III}$$

In the reversible process approximation, Eqs. (I) and (IV), expressing only the mass conservation of both fluids, do not give any explicit condition which restricts the phenomena, Note that the $\mathbf{f}$ term should have disappeared, if we neglect the quadratic terms in the velocities as did L-Z. Our approximation is of no such mathematical nature, but a physical one based on the evidence observed in He II.

As is easily seen, these equations should not be confined to the case of heat transfer only, being valid for any stationary laminar flow.

In the first place, eliminating relative motion from these equations, one obtains

$$\mathrm{grad}p=\eta_n\Delta\mathbf{V}_n. \tag{6.1}$$

Thus the velocity field of the normal fluid is directly connected with the pressure gradient, as Gorter[17] has pointed out.

The y-component of (6.1) gives

$$\partial p/\partial y=0,\ \text{i.e.,}\ p=p(x),$$

that is, the pressure is uniform in the plane of a cross section.

Then, the x-component of the same equation gives

$$\frac{dp}{dx}=\eta_n\frac{\partial u^2{}_n}{\partial y^2},$$

which results in the well-known Poiseuille flow, under the ordinary boundary condition that the normal fluid sticks to the wall,

$$u_n=(\pi/2\eta_n)(\tfrac{1}{4}d^2-y^2) \tag{6.2}$$

where

$$\pi\equiv-dp/dx.$$

In the second place, Eq. (III) determines the velocity of the superfluid relative to the normal fluid. Its y-component gives

$$\partial T/\partial y=0,\ \text{i.e.,}\ T=T(x).$$

[16] H. London, Nature 142, 612 (1938).
[17] G. J. Gorter, Phys. Rev. 74, 838 (1947).

Thus, our solution implies that the temperature variation over the cross section does not play an essential role in this phenomena, contrary to the suggestion of L-Z.

The x-component of (III) gives

$$A\rho\rho_s(u_n-u_s)^3=\pi-\rho s\theta,$$

where

$$\theta\equiv -dT/dx.$$

Then, one obtains as the velocity field of superfluid

$$u_s=u_n+\left(\frac{\pi-\rho s\theta}{A\rho\rho_n}\right)^{\frac{1}{3}}. \tag{6.3}$$

While the first term on the right-hand side represents Poiseuille flow, which vanishes on the wall, the second is constant over the cross section and therefore represents a *slip flow*. It is to be noted that the slip flow becomes appreciable only when the fountain effect deviates from H. London's thermostatic relation. Thus, we may expect that the slip flow should play an essential role for the heat current greater than q_c estimated by L-Z. Ordinary heat conduction q_0, which was introduced in our general formalism, is really necessary to secure the existence of slip flow, because omitting q_0, Eq. (IV) leads to a conclusion that $u_s=0$ on the wall under the strict application of second law.

As the temperature T is constant over the cross section, so also ρ_n and ρ_s. Taking account of this fact, one can calculate the mean velocities as

$$\langle V_n\rangle=(d^2/12\eta_n)\pi, \tag{6.4}$$

and

$$\langle V_s\rangle=\langle V_n\rangle+[(\pi-\rho s\theta)/A\rho\rho_n]^{\frac{1}{3}}. \tag{6.5}$$

Finally, the mass flow density is given by the expression

$$\begin{aligned}\langle\rho V_1\rangle&=\langle\rho_n V_n\rangle+\langle\rho_s V_s\rangle\\&=(\rho d^2/12\eta_n)\pi+\rho_s[(\pi-\rho s\theta)/A\rho\rho_n]^{\frac{1}{3}}.\end{aligned} \tag{6.6}$$

7. Heat Transfer in Liquid He II

As discussed in Part I, the convection part of the heat flow is generally given by

$$\langle\rho u V_1\rangle+\langle\rho s T V_2\rangle, \tag{7.1}$$

where $V_2=V_n-V_1$.

If, however, the net mass flow vanishes, i.e.,

$$\langle\rho\mathbf{V}_1\rangle=0, \tag{7.2}$$

as in the case of Leiden measurements, (7.1) reduces to

$$\mathbf{q}=\rho s T\langle\mathbf{V}_n\rangle, \tag{7.3}$$

which was called by L-Z "internal convection."

Substituting for $\langle\mathbf{V}_n\rangle$ by (6.4) of the preceding section, one obtains

$$q=(\rho s T d^2/12\eta_n)\pi. \tag{7.4}$$

As Gorter has pointed out, (7.4) expresses the fact that $q\propto\Delta p$ always, which may be compared with the experimental results (A) and (B).

TABLE I. Relationship of fountain effect, heat current, and temperature in He II.

T°K	$H\times10^4$(watt)	Δp_{calc}(cm He)	Δp_{obs}(cm He)
1.995	189.7	0.806	0.82
1.995	291.1	1.24	1.25
1.902	167.4	0.947	0.80
1.902	283.5	1.60	1.41
1.793	204.1	1.64	1.62
1.793	275.9	2.22	2.22
1.713	264.5	2.80	2.88
1.713	130.0	1.38	1.36

Then, from (7.2) and (6.6) one can obtain the relation of π and θ under the condition of no net mass flow:

$$(\rho d^2/12\eta_n)\pi+\rho_s[(\pi-\rho s\theta)/A\rho\rho_n]^{\frac{1}{3}}=0, \tag{7.5}$$

or with the abbreviations

$$\xi\equiv\rho_n/\rho=s/s_\lambda=(T/T_\lambda)^r \text{ (reduced temperature)}, \tag{7.6}$$

$$\gamma\equiv(\rho/8)(A/\eta_n^3)^{\frac{1}{3}} \text{ (material constant)}. \tag{7.7}$$

Equation (7.5) is rewritten as

$$\pi^3=\frac{27}{\gamma^2}\frac{(1-\xi)^3(\rho s_\lambda\theta\xi-\pi)}{d^6\xi}. \tag{7.8}$$

This equation involves the results of our *thermodynamical* equations of motion under no net mass flow condition, which should substitute H. London's *thermostatic* relation $\pi=\rho s_\lambda\theta\xi$. To obtain a direct comparison, we may solve (7.8) explicitly for π as follows:

$$\begin{aligned}\pi=\rho s_\lambda\theta\xi\cdot(3/2K)\{&[K+(1+K^2)^{\frac{1}{2}}]^{\frac{1}{3}}\\&+[K-(1+K^2)^{\frac{1}{2}}]^{\frac{1}{3}}\},\end{aligned} \tag{7.9}$$

where we have put for the sake of convenience

$$K\equiv(\rho s_\lambda\gamma/2)\cdot\theta d^3[\xi/(1-\xi)]^{\frac{1}{2}} \text{ (dimensionless)}. \tag{7.10}$$

Finally, corresponding to the extreme values of parameters, the expression (7.9) reduces to

$$\pi=\rho s_\lambda\theta\xi, \quad (K\ll1) \tag{7.11}$$

when $K\ll1$, i.e., the temperature gradient θ, the slit width d, or the temperature T are sufficiently small. The result is equivalent to H. London's relation.

For the other extremum $K\gg1$, (7.9) reduces to

$$\pi=3(\rho s_\lambda/\gamma)^{\frac{1}{3}}\cdot\theta^{\frac{1}{3}}d^{-2}(1-\xi). \quad (K\gg1). \tag{7.12}$$

Or, converted into heat current using Eq. (7.4),

$$q=[(\rho s_\lambda)^2/12\eta_n T_\lambda^{2r}]\theta d^2T^{2r+1}, \quad (K\ll1) \tag{7.13}$$

and

$$q=[(\rho s_\lambda)^{4/3}/4\eta_n\gamma^{2/3}T_\lambda^{2r}]\theta^{\frac{1}{3}}T^{r+1}(T_\lambda^r-T^r). \quad (K\gg1). \tag{7.14}$$

These formulas should be compared with the experimental results (C), (D), and (E).

TABLE II. Relationship of γ and T for various slit widths.

$d=19\mu$		$d=10.5\mu$		$d=5\mu$	
T(°K)	$\gamma(10^6$ c.g.s.)	T(°K)	$\gamma(10^6$ c.g.s.)	T(°K)	$\gamma(10^6$ c.g.s.)
1.391	1.34	1.514	2.84	1.328	3.4
1.713	1.82	1.514	2.68	1.716	5.44
1.793	2.24	1.845	3.43	1.725	6.12
1.902	2.69	1.845	4.31	1.902	4.48
1.995	2.35	1.975	3.29	2.036	4.0
2.077	1.39	2.054	2.93	2.119	1.58
2.148	1.30	2.054	2.63	2.120	1.84

Various tendencies in the behavior of thermal current and fountain pressure corresponding to the extreme values of adjustable parameters, given in the above formulas, have been observed by many independent authors experimentally.

K-S-M observed, with capillaries wider than 0.35 mm and in the temperature range $1.6>T>1$°K, that thermal current is not proportional to temperature difference but obeys an empirical formula

$$q=0.623T^5\theta^{\frac{1}{2}} \text{ watt cm}^{-2}.$$

This should correspond to the case $K\gg1$, i.e., Eq. (7.14) (Fig. 5).

K-D performed experiments using thinner capillaries and narrower slits than those of K-S-M. With 9.3μ slit with and $\theta=0.02$ deg. cm^{-1}, they observed the same behavior as K-S-M with temperatures higher than 1.9°K, while at lower temperatures there appeared a region in which q was proportional to ΔT. This means that they have gone through the region $K\sim1$ (Fig. 5).

Then M-M refined the experiments with slits narrower than 1μ and found that q is fairly proportional to ΔT in the entire temperature region. This corresponds to the case $K\ll1$ (Fig. 5). In this case the validity of H. London's formula is secured by Eq. (7.11) for all temperatures, and it is this extreme case only that the theory of L-Z describes. The theory predicts that heat current and conductivity should vary as $T^{2r+\frac{1}{2}}=T^{11.5}$ and $T^{2r-\frac{1}{2}}=T^{10.5}$, respectively, with results which are fairly consistent with the empirical data of K-D and M.

To the detailed comparison with the empirical data, we will contribute Section 8.

8. Comparison with Experiments

In comparing the fountain pressure and heat current, given by Eqs. (7.9) and (7.10), with experimental data, we adopted the following values of equilibrium constants.

Total mass density

$$\rho=0.146 \text{ g cm}^{-3}, \tag{8.1}$$

which was found by Keesom and Keesom[18] to be fairly constant below the λ-point.

The entropy density s varies as a function of temperature according to the empirical formula

$$s=s_\lambda(T/T_\lambda)^r, \tag{8.2}$$

where we adopted Kapitza's values[19]

$$r=5.5 \quad \text{and} \quad s_\lambda=0.405 \text{ cal. deg.}^{-1} \text{ g}^{-1}, \tag{8.3}$$

taking account of the results obtained by M-M who used the values of Keesom and Keesom[18] in the case of extremely narrow slits.

With regards to the *normal viscosity* coefficient there is already the oscillating disk measurement of Keesom and MacWood,[20] which may be reliable at least in the region of He I. But, as we have mentioned in Part I, there remain various difficulties in analyzing the data below the λ-point, possibly because of the mechanocaloric effect. On the contrary, we saw that the analysis of heat transfer in (7.4) is very simple.

We have extrapolated the value of η_n, corresponding to Tisza's opinion,[1] smoothly from the He I region, and obtained as an empirical formula

$$\eta_n=1.45\times10^{-5}T^{\frac{1}{2}} \text{ g cm}^{-1} \text{ sec.}^{-1}. \tag{8.4}$$

From this value of η_n and the observed value of q, we have calculated the fountain pressure Δp according to Eq. (7.4), which is compared in Table I and Fig. 1 with the observed data, showing satisfactory agreement [see item A, Section 5]. It is to be remembered that (7.4) is free from any effect of the mutual friction, and therefore we think that this is the most suitable phenomena for the determination of η_n.

In the case $q=$constant$=0.18$ watt cm^{-2}, the temperature variation of fountain pressure is compared

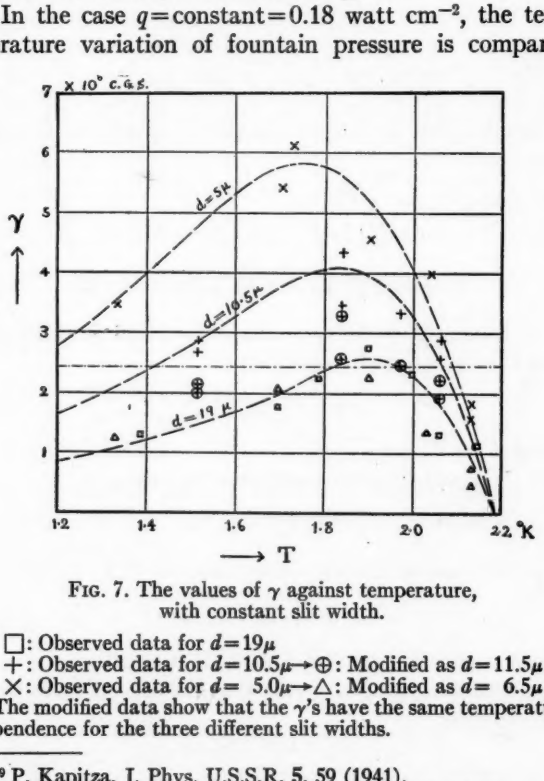

FIG. 7. The values of γ against temperature, with constant slit width.

□: Observed data for $d=19\mu$
+: Observed data for $d=10.5\mu\rightarrow\oplus$: Modified as $d=11.5\mu$
×: Observed data for $d=5.0\mu\rightarrow\triangle$: Modified as $d=6.5\mu$
The modified data show that the γ's have the same temperature dependence for the three different slit widths.

[18] W. H. Keesom and A. P. Keesom, Physica 1, 128 (1934).

[19] P. Kapitza, J. Phys. U.S.S.R. 5, 59 (1941).

[20] W. H. Keesom and MacWood, Physica 5, 737 (1938).

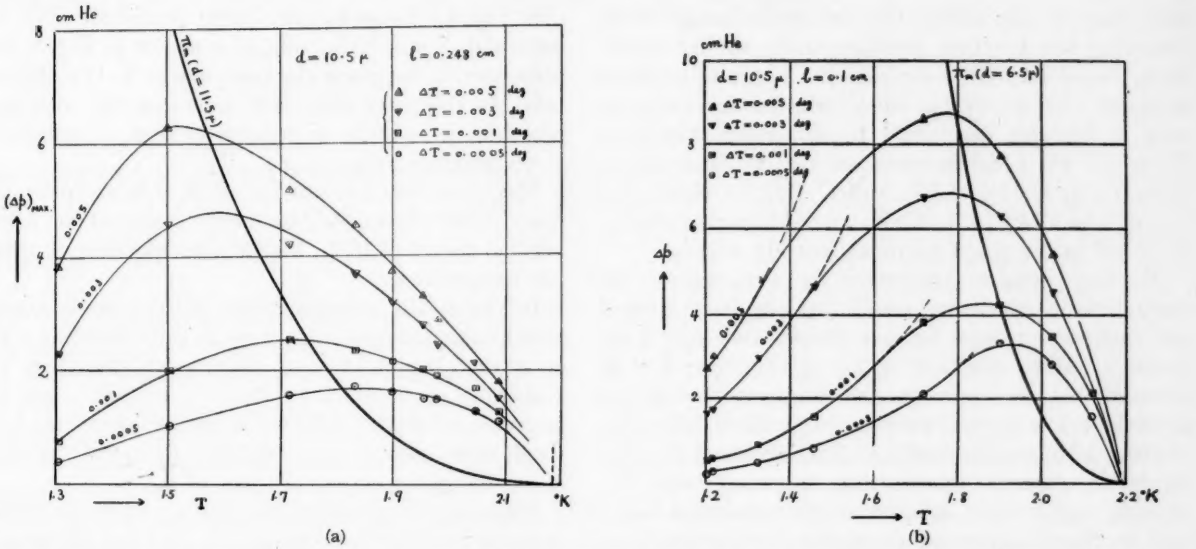

FIG. 8. Maximum fountain pressure against temperature. The numbers attached to the curves give the temperature differences in degrees. Solid curve represents the calculated maximum trace. (a) $d=10.5\mu$, (b) $d+5.0\mu$ (erroneous in the drawing).

with Mellink's data in Fig. 2 [item (B)]. Note that fountain pressure converges to a finite value

$$(\Delta p)_\lambda=(0.248)\pi_\lambda=(0.248)\frac{12\eta_n q}{\rho s_\lambda T_\lambda d^2}=0.54 \text{ cm He}, \quad (8.5)$$

when the temperature approaches to λ-point, just as observed by M.

With this knowledge of η_n we shall be able to determine the parameter A, which characterizes the *mutual friction*, by analyzing the heat current near λ-point.

It is to be noted, however, that A appears in the result only in the form

$$\gamma\equiv(\rho/8)(A/\eta_n)^{\frac{1}{2}} \quad (8.6)$$

as is clear in Eq. (7.8). The dimension of γ is $[M^{-1}L^{-1}T^2]$.

Observing this situation, we put the Leiden data on π, ξ, and d straightforwardly into Eq. (7.8) and determined the value of γ at various temperatures. The result is shown in Table II and in Fig. 7.

While the values of γ show similar tendencies in temperature dependence for various slit width, their absolute magnitudes cannot be said to coincide in each case. But, as the experimenters themselves admit, the width of slit is the most ambiguous among the observed data. Moreover, it appears in our determination of γ as a factor d^3, being magnified in its ambiguity. Therefore, we cannot conclude hastily from these results that γ depends on slit width; in other words, we cannot deny Gorter's idea that the parameter A should be a material constant.

Observing this situation, we have adopted for the present

$$\gamma=2.33\times10^6 \text{ g}^{-1} \text{ cm}^{-1} \text{ sec.}^2, \quad (8.7)$$

and calculated the fountain pressure π and thermal current q in the case of 19μ slit. Calculated results, shown in Figs. 3–6 fairly reproduce the experimental data (C)–(E).

In this case parameter A is estimated as

$$A=50.4\times T^{\frac{1}{2}} \text{ g}^{-1} \text{ cm sec.}, \quad (8.8)$$

which is nearly the same as Gorter's estimation $A=50$, showing a similar tendency in temperature variation. In any case, the investigation of A is a problem for the future, requiring further experimental measurements.

In the case of constant temperature and temperature difference, K-S-M observed that the heat current is proportional to the cross section for a thin capillary, whereas for a wide capillary it becomes independent of the cross section. K-D also observed similar tendencies

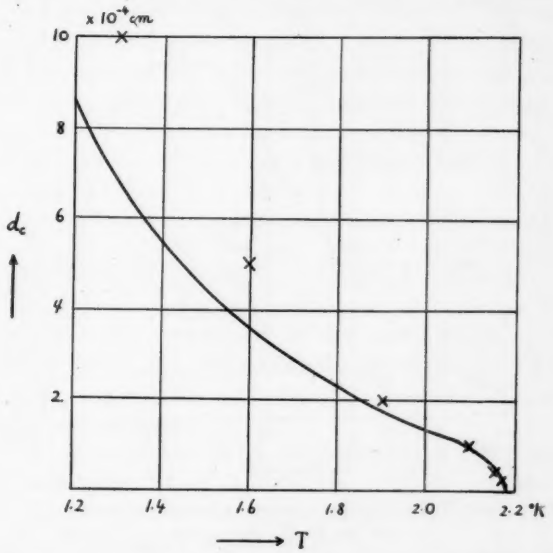

FIG. 9. Critical slit width against temperature. $\theta=7.51\times10^{-3}$ deg. cm^{-1}. x: observed (MM); ——: calculated.

with varying slit width. On the other hand, M-M, observing the fountain pressure under similar conditions, found that for wide slits the fountain pressure increases with decreasing slit width, but for narrower ones it becomes insensitive to slit width variation. These slit width dependences are clearly expressed in Eqs. (7.11), (7.12), (7.14), and (7.15). To obtain the case of a capillary of radius R, we have only to replace d^2 by $\frac{3}{2}R^2$ in the above formulas (see Fig. 6).

We may inquire concerning the behavior of the characteristic maximum shown by the heat current and fountain pressure against temperature (see Figs. 3 and 4). With constant radius of capillary, K-S-M reported that maximum current temperature does not appreciably change with varying temperature difference, whereas Allen and Reekie[21] and K-D observed that the maximum current temperature increases with decreasing temperature difference; the latter also found that the fountain pressure also shows a similar tendency but more strongly, a fact which is clearly expressed in Fig. 8 (due to M).

For the sake of convenience we may first obtain the maximum fountain pressure from (7.8) and $d\pi/d\xi=0$. Then under constant slit width, and varying temperature difference, we obtain

$$\pi_m=-\frac{3\,(1-\xi)^2}{\gamma\quad d^3\xi},\quad (d=\text{constant}),\qquad (8.9)$$

and under constant temperature difference and varying slit width,

$$\pi_m=\rho s_\lambda\theta\frac{3\xi^2}{(1+2\xi)}.\quad (\theta=\text{constant}).\qquad (8.10)$$

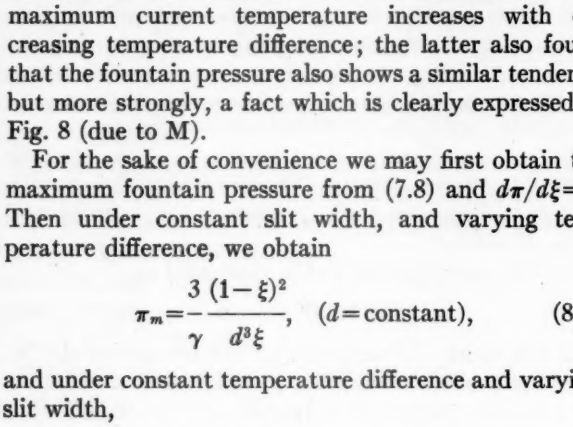

FIG. 9. Critical heat current against temperature. $d=19\mu$, $\theta=0.006$ deg. cm^{-1}.

[21] J. F. Allen and J. Reekie, Proc. Camb. Phil. Soc. **35**, 114 (1939).

(See Fig. 4.) These loci are fairly consistent with M's data with 5 and 10.5μ slits as is shown in Fig. 8, and consequently supports the tendency in K-D's observation. As the ratio of q to π is monotonic with temperature, it is quite reasonable that $q_{\max}$ indicates a same tendency as π_m.

The apparent discrepancy of K-S-M's observation from others means only that they observed the nearly vertical region of (8.9), Fig. 4, corresponding to rather low temperature.

It is especially important that (8.10) does not involve such kinetic parameters as η_n or A, thus affording a way of testing the validity of the theory free from any ambiguity in parameter values. Moreover, these two formulas are analytically much simpler than that for π itself, so we may make a brief estimation of the value of π_m, using the empirical value of π_m.

We have recognized in the above a clear distinction between two different regions, i.e., the fountain pressure is proportional to ΔT in the one region, while in the other it is proportional to $(\Delta T)^{\frac{1}{2}}$. Accordingly, there must be a region in which the characteristics of these two regions alternate. We may call this the *"critical region"* and will investigate the behavior of this region for parameter variation.

Though, of course, there is no unique definition of critical region, we may be allowed to appint it by putting $K=1$. Then we obtain from (7.10) as the critical condition

$$\tfrac{1}{2}\gamma\rho s_\lambda\cdot\theta d^3(\xi/(1-\xi))^{\frac{1}{2}}=1.\qquad (8.11)$$

In this case the fountain pressure is given from (7.9) as

$$\pi_c=c\cdot\rho s_\lambda\theta\xi,\qquad (8.12)$$

where c is a numerical constant

$$c=\tfrac{3}{2}\{(1+\sqrt{2})^{\frac{1}{2}}+(1-\sqrt{2})^{\frac{1}{2}}\}=0.894.\qquad (8.13)$$

Examination of this critical curve may give another possibility of testing the theory.

Keeping the temperature gradient constant M-M observed at each temperature the *critical slit width* d_c at which the fountain pressure becomes insensitive to slit width. Their results are shown in Fig. 9. Correspondingly, from Eq. (8.11) we obtain for d_c

$$d_c=\left(\frac{2}{\gamma\rho s_\lambda\theta}\right)^{\frac{1}{3}}\left(\frac{1-\xi}{\xi}\right)^{\frac{1}{3}},\qquad (8.14)$$

which indicate a tendency quite similar to that of observed data (see Fig. 9). Unfortunately, the specification of temperature gradient is absent in *M*, we took tentatively $\theta=7.5\times10^{-2}$ deg. cm^{-1}.

If we consider a slit of definite width we obtain from (8.11) and (8.12)

$$\pi_c=\frac{2c\,(1-\xi)^{\frac{1}{3}}}{\gamma\quad d^3\xi^{\frac{1}{3}}},\quad (d=\text{constant}),\qquad (8.15)$$

and referring to (6.4)

$$\langle V_n\rangle_c=\frac{c}{6\eta_n\gamma}\frac{(1-\xi)^{\frac{1}{2}}}{d\xi^{\frac{1}{2}}} \tag{8.16}$$

as the *critical flow velocity.*

Consequently, the critical heat flow is given by

$$q_c=\rho sT\langle V_n\rangle_c=\frac{c\rho sT}{6\eta_n\gamma d}\frac{(1-\xi)^{\frac{1}{2}}}{\xi^{\frac{1}{2}}}, \tag{8.17}$$

which is shown in Fig. 10, being the substitute for the curve q_c which was empirically appointed as critical by L-Z. Its maximum current temperature is given by

$$\xi=13/46 \quad \text{or} \quad T=1.74°\text{K},$$

which is independent of slit width and free from any ambiguity in the definition of critical region.

Using no net mass flow condition we obtain further from (8.16)

$$d\langle V_s\rangle_c=-\frac{c}{6\gamma\eta_n}\xi^{\frac{1}{2}}(1-\xi)^{\frac{1}{2}}, \tag{8.18}$$

which secures the remarkable fact that $d\langle V_s\rangle_c$ is independent of the slit width itself, being discovered empirically by L-Z. As they neglect the temperature variation of $d\langle V_s\rangle_c$, it is reasonable that their curve q_c does not coincide with ours (8.17), Fig. 10. In Fig. 11 it is shown that the critical region appointed by (8.18) is in good agreement with the empirical data given by L-Z, where $d\langle V_s\rangle_c$ are, as is expected, expressed as finite segments, not as points.

In this way we could clearly substantiate the empirical facts concerning critical region discovered by L-Z; while we cannot readily agree with their physical interpretation. First, it is already evident that the critical region does not indicate the validity limit of hydrodynamical description. Second, there is but obscure ground in the present stage for their attempt to correlate the critical flow velocity directly to the surface flow. Their relation, if any, may be the remaining problem to be clarified in future by the phenomenological theory.

9. Concluding Remarks

In the above-developed treatments we have seen that the phenomena of stationary heat flow in liquid He II is fully described by the general thermodynamical equations of motion, which we derived in Part I, adopting Gorter's type of mutual friction. This fact proves clearly that the so-called "two-fluid model" is quite satisfactory, at least in the phenomenological part of the theory. Therefore, it is our thought that this model, without being discarded, should be developed from the molecular point of view. For this purpose, the temperature variation of γ, which is clearly expressed in Table II but neglected in our first approximation, should be fully analyzed.

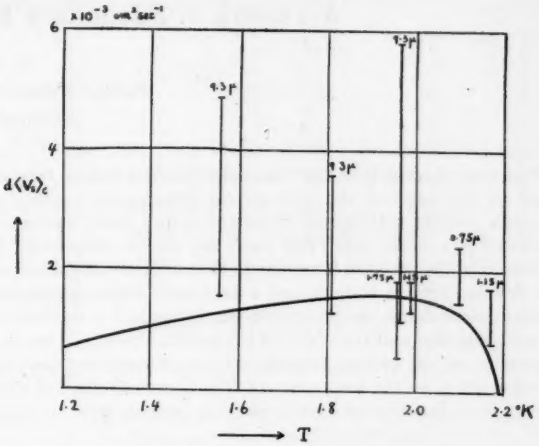

FIG. 11. $d\langle Vs\rangle_c$ against temperature.

In order to investigate the effect of mutual friction, we will take the problem of "capillary flow," having net mass flow, and of "surface flow." As regards the latter phenomenon one may expect the possibility that its description is beyond the present phenomenological treatment. It is to be noted, however, that surface flow can also cause the thermomechanical effect, as was shown first by Daunt and Mendelssohn, [22] and moreover, the ratio of the measured heat flow to that through the slit is just equal to the ratio of film thickness to slit width which was recognized by M-M.

As for the capillary flow, it should be pointed out that the boundary condition is different from that for the internal convection. In the case of capillary flow there is no heat source, but instead the pressure difference is maintained mechanically.

Unfortunately, no special caution was taken about the temperature difference, which is expected to be accompanied by capillary flow and surface flow.

Under stationary conditions our calculation gives the general expression (6.6) for the total mass flow in the reversible process approximation. To check this result, it is necessary to know the empirical relation between π and θ. It should be possible to observe the *mechanocaloric effect* as systematically and exhaustively as in Leiden measurements,[13–15] and is highly desirable from the theoretical point of view.

Our grateful thanks are due Professor M. Kotani who allowed us to undertake our present work in such complete cooperation. We also appreciate the kindness of Professor T. Nagamiya and Associate Professor R. Kubo who were interested in our investigation. Our sincere thanks are due also Mr. M. Mizushima for his valuable suggestions and help in the calculation in Part II of this paper.

We should like to take this opportunity of expressing our deep appreciation to Professor L. Tisza, who was interested in our investigation and afforded assistance in the publication of this paper.

[22] J. G. Daunt and K. Mendelssohn, Nature 143, 719 (1939).

A Theory of Secondary Electron Emission from Metals*

E. M. Baroody
Battelle Memorial Institute, Columbus, Ohio
(Received January 26, 1950)

A theory of secondary electron emission from metals is formulated on the basis of the Sommerfeld free-electron model, momentum transfer between electrons and lattice being included by introducing a finite mean free path for elastic scattering. The approach to the problem is similar to that of Kadyschewitsch, but the development is simpler and comparison with experiment is made in more detail. An understanding is reached of the influence of work function and the width of the conduction band, making it clear why, on the average, metals with large work function might be expected to be the best emitters. The observed effect of changing the work function of a given metal by surface layers of foreign atoms is interpreted, an inverse relationship between emission and work function being obtained which is in qualitative agreement with experiment. The theory also accounts for the velocity distribution of the secondaries, giving the general shape of the curve and determining the approximate position of the maximum, and is consistent with the observed angular distribution of the secondaries. The investigation is not carried far enough to give new theoretical information concerning the variation of secondary emission with primary energy. However, the relation of the present theory to some work of Bruining is indicated, and attention directed to an important empirical relationship.

1. INTRODUCTION

IT is well appreciated that a tremendous clarification of phenomena occurring in metals followed Sommerfeld's application of Fermi-Dirac statistics to the free electrons. The simplicity of the Sommerfeld model gave it lasting value, even in cases where more complicated models were employed with considerable success in later work. It is therefore remarkable that until a few years ago almost no effort was made to provide a simple treatment of secondary electron emission in terms of this model.

The theoretical papers most often quoted in this field are those of Fröhlich[1] and Wooldridge,[2] in which the problem is handled quantum mechanically, the electrons of the metal being described by wave functions of the Bloch type. In a way, this degree of complexity is necessary since, as was emphasized by Fröhlich, momentum transfer between electrons and lattice plays an essential part in secondary emission. In particular, without such transfer no secondaries could leave a surface bombarded by normally incident primaries. When Bloch wave functions are used in the manner of Fröhlich and Wooldridge, this transfer enters automatically, since the conservation of momentum equation for the interaction producing a secondary includes a term representing momentum change of the lattice. This type of treatment also brings to light certain interesting quantum effects associated with the discrete momentum changes which are permitted the lattice.

There would seem to be qualitative value, however, in a much simpler theory in which the primary is considered to interact in a classical manner with a free electron gas, the possibility of momentum transfer to the lattice being introduced by assuming a finite mean free path for elastic collision. Several years ago such a theory was developed by Kadyschewitsch in a series of three papers.[3] In the first of the papers, the author formulates a theory and applies it to metals, giving some attention to most secondary emission phenomena which have been studied experimentally. In the later papers he extends the theory to insulators and semiconductors. The calculations are almost entirely classical and are intended to give insight into the mechanism of emission and to emphasize properly the influence of electron scattering and absorption. Although the use of classical principles greatly simplifies the calculations, the problem remains complex and it is not clear that all the mathematical difficulties have been adequately met. The final results are therefore probably more limited in significance than would have been judged from the starting assumptions. It is partly because of this circumstance, and partly because it is felt that more attention should be given the Sommerfeld model, that the present paper is offered. Here an effort is made to develop an alternative treatment which is less elaborate than that of Kadyschewitsch, but still is capable of giving some results of about the same accuracy. Attention is limited to a few aspects of emission from metals, and certain substantial simplifications are introduced from the beginning. Although the development gives some insight into a variety of secondary emission phenomena, it is most successful in showing how the Sommerfeld model can clarify the role of work function, and account in a qualitative way for the velocity distribution of the secondaries.

2. THE VELOCITIES OF INTERNAL SECONDARIES

Since no attention is to be given to the small temperature dependence of secondary emission from metals, the electrons will be treated as a completely degenerate Fermi-Dirac gas. In momentum space all states lying within a sphere of radius p_0 about the origin are filled, while states of greater momentum are empty. The momentum p_0 corresponds to the maximum Fermi

* This work was supported in part by the Air Materiel Command under Contract No. W33-038 ac 14228, and later by the U. S. Army Signal Corps. under Contract No. W-36-039-sc-38185.

[1] H. Fröhlich, Ann. d. Physik 5, 13, 229 (1932).

[2] D. E. Wooldridge, Phys. Rev. 56, 562 (1939).

[3] A. E. Kadyschewitsch, J. Phys. U.S.S.R. 2, 115 (1940); 4, 341 (1941); 9, 431 (1945).

energy, $E_0=p_0^2/2m$, and is related to the space density of free electrons in the familiar manner.[4]

Primary electrons of about one hundred electron-volts or greater are considered. The collisions of greatest interest are then those in which the fast primary transfers a small part of its energy to an electron of the metal. In calculating the momentum transfer for such a collision one may consider that the primary moves with constant speed along a straight line and interacts with a metal electron whose motion during the collision is negligible. In this approximation, the momentum transferred is perpendicular to the primary path and is given by the integral:

$$\Delta p=\int_{-\infty}^{\infty}\frac{e^2\rho dt}{(\rho^2+V^2t^2)^{\frac{3}{2}}}=\frac{2e^2}{V\rho}. \tag{1}$$

Here, e is the electronic charge, ρ, the distance between the metal electron and the primary path, and V, the velocity of the primary. The time, t, is measured from the instant of closest approach.

Thus, for the metal electrons at distance ρ, the effect of the passing primary is a shift of the center of the occupied momentum-space sphere from the origin by the amount Δp. The number of secondaries *per unit volume* at this distance having momentum greater than μp_0, is the volume of the displaced sphere which lies outside a sphere of radius μp_0 about the origin, multiplied by the density in phase space, $2/h^3$. Denoting this number by G, and calculating for $\mu>1$, which is the only case of interest here, one finds:

$$G(s)=\frac{\pi p_0^3}{6h^3 s}\{3(\mu^2-1)^2-8(\mu^3-1)s+6(\mu^2+1)s^2-s^4\} \tag{2}$$

$$\mu-1\leqslant s\leqslant\mu+1$$

$$G(s)=8\pi p_0^3/3h^3 \quad s\geqslant\mu+1, \tag{3}$$

where h is Planck's constant and $s=\Delta p/p_0$.

By carrying out an integration over ρ, one can now calculate $N(\mu)$, the production of secondaries *per unit primary path length* with momentum exceeding μp_0. According to (1), the element of area is

$$2\pi\rho d\rho=-(8\pi e^4/V^2p_0^2)ds/s^3 \tag{4}$$

and $N(\mu)$ is given by the integral:[5]

$$N(\mu)=(8\pi e^4/V^2p_0^2)\int_{\mu-1}^{mV/p_0}G(s)s^{-3}ds. \tag{5}$$

When the integral is evaluated for high primary velocity, that is $mV\gg(\mu+1)p_0$, one obtains:

$$N(\mu)=\frac{32\pi^2e^4p_0}{3h^3V^2(\mu^2-1)}. \tag{6}$$

The derivative, $-dN/d\mu$, gives the momentum distribution of the internal secondaries, μ being momentum measured in terms of the maximum Fermi gas momentum, p_0. Introducing the maximum Fermi energy, E_0, and the kinetic energy of the primary electron, W, (6) becomes:

$$N(\mu)=BE_0^{\frac{1}{2}}/W(\mu^2-1). \tag{7}$$

When the energies are in electron volts

$$B=\frac{160\pi^2(6)^{\frac{1}{2}}m^{3/2}e^{7/2}}{3h^3}=2.95\times10^8\ \text{ev}^{\frac{1}{2}}-\text{cm}^{-1}. \tag{8}$$

It is of interest to consider whether the calculated rate of production is at all reasonable. If μ_0 is the minimum value of μ needed for escape from the metal, one finds for typical metals, and for $W\sim10^2$ electron volts:

$$N(\mu_0)\sim10^7\ \text{cm}^{-1}.$$

This result does not seem unreasonable. It means that if there were no secondary absorption, so that all secondaries having sufficient energy ultimately escaped, a primary range of about 10A would account for the one secondary per primary ordinarily emitted when the primary energy is several hundred electron volts.

3. THE SECONDARY EMISSION COEFFICIENT

In this paper, attention is limited to perpendicular incidence, and the elastic scattering of the primaries by the metal lattice is neglected. All the secondaries leaving the metal must then have undergone at least one elastic collision. The relative sizes of groups having undergone various numbers of such collisions will depend on the ratio of the mean free path for secondary scattering, l, to that for absorption,[6] λ. In a reasonably complete theory which was to be valid for all values of this ratio, it would be in order to formulate expressions for the contributions to the emission from the various groups, and to obtain the total emission by summing these contributions. The calculations of Kadyschewitsch are organized in this manner. However, in the present discussion, it is not proposed to enter into such relatively complex calculations. Rather, two special calculations will be made. First, the emission of singly scattered secondaries will be considered, which would approximate the total emission only if l were much larger than λ. Then, the total emission will be obtained for the opposite extreme, $l\ll\lambda$. Comparison of results in the two cases will indicate that some fea-

[4] See, for example, the outline of the free electron theory of metals given by F. Seitz, *The Modern Theory of Solids* (McGraw-Hill Book Company, Inc., New York, 1940), Chapter IV.

[5] The upper limit corresponds to a momentum transfer equal to the total momentum of the primary. In this calculation, certain errors are made in the small ρ-range. However, this should not lead to a significant final error, since the collisions in this range are relatively few.

[6] For simplicity, it is pretended that the secondaries can only undergo elastic scattering or absorption; and the energy dependence of secondary free paths is neglected. These two simplifications should partially compensate each other.

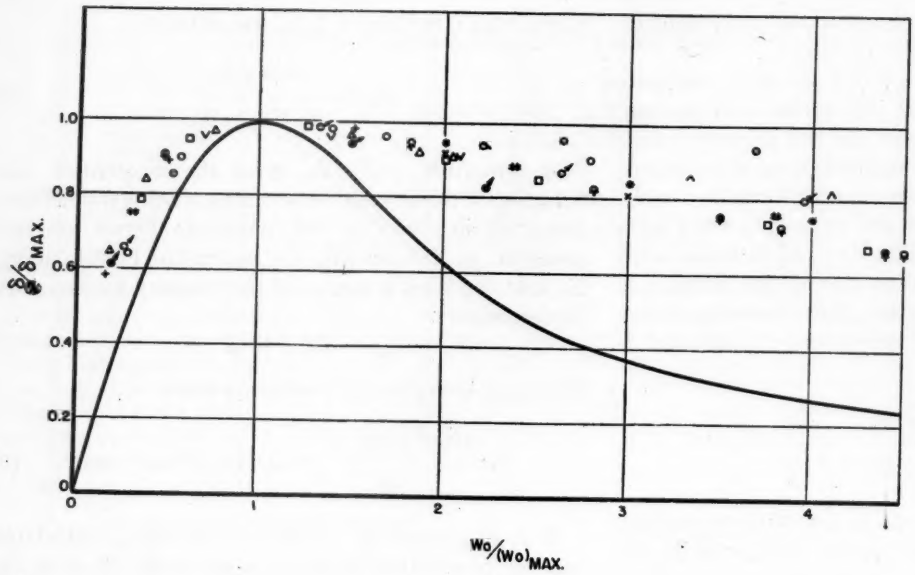

FIG. 1. Variation of secondary emission with primary energy. δ/δ_{max} is the secondary emission coefficient divided by its maximum value, and $W_0/(W_0)_{max}$ is the primary energy divided by the energy for maximum emission. The points show experimental results for various materials, taken from small-scale published curves: + Cu, × Ni, ♀ Li, △ Ti, □ Mo, ○ Pt, ∨ Al, ♂ Mg, # Fe, ♂ Cb, ⊙ Rb, ∧ B, ✳ Ge, ♀ Si. The points approximate a single curve. The curve, based on Eq. (24), is qualitatively similar to the experimental curve.

tures of secondary emission are rather well covered by the calculations, in spite of their simplicity.

Singly Scattered Secondaries

An expression will be obtained for δ_1, the number of secondary electrons which leave the metal surface per incident primary after having undergone a single elastic collision. The probability that this collision takes place at a distance between r and $r+dr$ from the point of interaction with the primary, can be expressed in the form:

$$\exp(-\sigma r)\cdot dr/l, \tag{9}$$

where σ is the inverse mean free path $(l+\lambda)/l\lambda$. Integrating over r, and assuming isotropic scattering, one has for the scattering probability per unit solid angle, $(4\pi\sigma l)^{-1}$. Letting q denote the cosine of the angle with the outwardly directed normal to the surface, the probability of scattering into any range dq is

$$dq/2l\sigma. \tag{10}$$

The typical secondary will be considered to move perpendicularly to the primary path before elastic collision with the lattice, so that a once-scattered secondary, initially produced at depth z and moving in a direction specified by q, must travel a distance z/q to reach the surface. For the numerous weak collisions which account for most of the secondaries from a fast primary, the momentum transferred is, in fact, approximately perpendicular to the primary path. Since the initial velocity distribution of the electrons is isotropic, the behavior taken as typical does correspond in a rough way to the average process.

Letting $n(q, z)$ be the number of secondaries produced per unit path length at depth z with sufficient energy to escape at the angle $\cos^{-1}q$, and taking account of secondary scattering and absorption during traversal of the layer of thickness z, one has:

$$\delta_1=(2l\sigma)^{-1}\int_0^1\int_0^\infty n(q, z)\exp(-\sigma z/q)dzdq. \tag{11}$$

According to Eq. (7) of the previous section

$$n(q, z)=N\left(\frac{\mu_0}{q}, z\right)=\frac{BE_0{}^{\frac{1}{2}}q^2}{W(\mu_0{}^2-q^2)}, \tag{12}$$

where $\mu_0{}^2=(E_0+\Phi)/E_0$, Φ being the work function of the metal. For the typical monovalent metals, to which the present theory should best apply, $\mu_0{}^2$ may be computed from a calculated E_0 and the observed work function. Values obtained in this way range from about 1.5 to 2.0.

The dependence of production on z enters through the slowing down of the primary as it penetrates into the metal. The simplest approximation is that the space rate of energy loss, $-dW/dz$ is inversely proportional to W, which implies:

$$W^2=W_0{}^2-az. \tag{13}$$

Here W_0 is the initial energy of the primary, and a is a constant which is characteristic of the metal. With these assumptions (11) takes the form:

$$\delta_1=\frac{BE_0{}^{\frac{1}{2}}}{2l\sigma}\int_0^1\int_0^{W_0{}^2/a}\frac{q^2\exp(-\sigma z/q)dzdq}{(W_0{}^2-az)^{\frac{1}{2}}(\mu_0{}^2-q^2)}. \tag{14}$$

The integrand in (14) has a singularity at the upper limit of the integration which results from using the expression for the production of secondaries by a *fast* primary to the very end of the primary range. However, the integral converges in spite of the singularity, and, in fact, does not differ significantly from a more carefully calculated value based on a more reasonable variation of productivity in the low energy range.

A simple change of variable[7] makes it possible to express the z-integral in terms of tabulated functions. If, in addition, $\omega=q^{-\frac{1}{2}}$ is introduced, one is led finally to the following expression for δ_1:

$$\delta_1=\frac{2BE_0^{\frac{1}{2}}}{l\sigma^{\frac{1}{2}}a^{\frac{1}{2}}}\int_1^\infty \frac{F(H\omega)d\omega}{(\mu_0^2\omega^4-1)\omega^4}, \tag{15}$$

where

$$F(x)=e^{-x^2}\int_0^x \exp(t^2)dt \tag{16}$$

and

$$H=(W_0^2\sigma/a)^{\frac{1}{2}}. \tag{17}$$

The function $F(H\omega)$ has a maximum at $H\omega=0.92$, and varies slowly in this neighborhood. On the other hand, the remaining factors in the integrand appearing in Eq. (15) are largest at the lower limit $\omega=1$, and decrease rapidly with increasing ω. Thus for H near unity (15) can be approximated by the expression:

$$\delta_1=\frac{2BE_0^{\frac{1}{2}}}{l\sigma^{\frac{1}{2}}a^{\frac{1}{2}}}F(H)\int_1^\infty \frac{d\omega}{(\mu_0^2\omega^4-1)\omega^4}. \tag{18}$$

To this approximation, the variation of δ_1 with primary energy is given simply by $F(H)$. A close examination of (15) with μ_0^2 given the reasonable value 1.6 shows that (18) is, in fact, a very good approximation. The chief difference is that, according to the more exact expression, the maximum of δ_1 occurs at $H=0.82$, instead of $H=0.92$. On the other hand, the value of the maximum is changed only very slightly by the approximation, being increased by about 1 percent.

Multiply Scattered Secondaries

When l is much smaller than λ, most electrons leaving the metal have undergone a large number of elastic collisions and have moved to the surface by a diffusion process. Considering a primary current of unit density (one electron/cm²-sec.), and using Eqs. (7) and (13), we may write for the production of secondaries with μ in the differential range $d\mu$ per unit volume per unit time:

$$\frac{2BE_0^{\frac{1}{2}}\mu d\mu}{(W_0^2-az)^{\frac{1}{2}}(\mu^2-1)^2}. \tag{19}$$

If all secondaries with $\mu>\mu_0$ could freely leave the metal on arrival at the surface, elementary diffusion theory[8] would give for the secondary current density the integral of the following over the primary range and over all $\mu>\mu_0$:

$$\frac{2BE_0^{\frac{1}{2}}\exp(-z/L)\mu d\mu dz}{(W_0^2-az)^{\frac{1}{2}}(\mu^2-1)^2}, \tag{20}$$

where L is the diffusion length $(\lambda l/3)^{\frac{1}{2}}$. Actually an electron approaching the surface with momentum μp_0 will escape only if the cosine of the angle with the normal exceeds μ_0/μ. Expression (20) must accordingly be multiplied by the corresponding fraction of the forward solid angle, $(\mu-\mu_0)/\mu$, before integration. In this way, one obtains:

$$\delta=\frac{2BE_0^{\frac{1}{2}}L^{\frac{1}{2}}}{a^{\frac{1}{2}}}F[(W_0^2/aL)^{\frac{1}{2}}]\int_{\mu_0}^\infty \frac{(\mu-\mu_0)d\mu}{(\mu^2-1)^2}, \tag{21}$$

where $F(x)$ is again the function defined in Eq. (16). The dependence of the emission on the primary energy

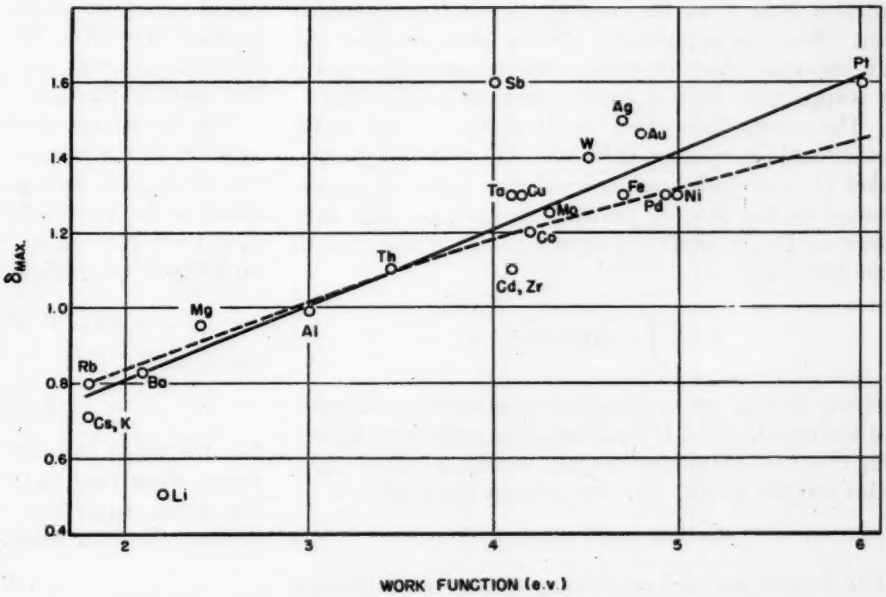

FIG. 2. Correlation between the maximum secondary emission, δ_{max}, and work function, Φ, for various metals. The solid line is drawn to show the trend of the experimental points, while the dashed line is a plot of $\delta_{max}=(0.35\Phi)^{\frac{1}{2}}$. The agreement shows that the influence of work function suggested by expression (26) is in accord with experiment.

[7] H. Bruining, *Die Sekundär-Elektronen-Emission fester Körper* (Verlag Julius Springer, Berlin, 1942; Edwards Brothers, Inc., Ann Arbor, 1944), p. 61.

[8] See, for example, P. R. Wallace, Nucleonics 4, 30 (1949).

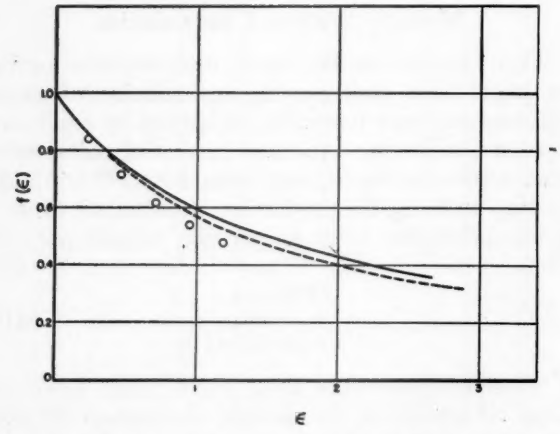

FIG. 3. Normal energy distribution of the secondaries. The ordinate, $f(\epsilon)$, is the fraction of the secondaries emitted with normal energy greater than $e\Phi$, where Φ is the work function. The curves follow from (27) with $\mu_0^2=1.6$ (solid) and 2.0 (dashed). The points are based on experimental data for Mo.

is similar to that found in Eq. (18) but the diffusion length, L, has taken over the position of σ^{-1}. Our principal interest in Eq. (21) lies in the function of μ_0 which appears. It will be seen later that comparison with the corresponding function in Eq. (18) indicates that the dependence of the emission on μ_0 is not sensitive to assumptions concerning multiple scattering.

4. THE VARIATION OF SECONDARY EMISSION WITH PRIMARY ENERGY

Our development of the theory does not go far enough to permit us to draw any new conclusions about the dependence of secondary emission on primary energy. However, we wish to interpolate a few paragraphs on this question in order to indicate the relationship of the present work to earlier considerations given by Bruining.[9] Also, the opportunity will be taken to point out an important fact about the experimental data which has apparently been ignored in previous publications.

The assumptions made by Bruining, as well as by other authors mentioned by him, are that the production of secondaries per unit primary path is proportional to the rate of primary energy loss, and that secondaries are absorbed exponentially. These lead to the following:

$$\delta=K\int(-dW/dz)e^{-\alpha z}dz, \tag{22}$$

where K is a proportionality constant characteristic of the metal, and α is the absorption coefficient. Bruining then uses the energy loss relationship, which we have also adopted in Eq. (13), and obtains the result

$$\delta=K(a/\alpha)^{\frac{1}{2}}F[(W_0^2\alpha/a)^{\frac{1}{2}}]. \tag{23}$$

The dependence of δ on primary energy so deduced is the same as would appear in the present work if we assumed $l\gg\lambda$, so that δ_1, as given by Eq. (18) represented the total emission.

Bruining showed that $F(x)$ has a maximum at $x=0.92$ so that the primary energy for maximum emission is $(W_0)_{\max}=0.92(a/\alpha)^{\frac{1}{2}}$. Also, using values of a and α which he regarded as reasonable, he showed that this leads to optimum energies which are of the correct order of magnitude. However, he does not report a complete comparison of the form of the experimental curve of emission *versus* primary energy with that implied by Eq. (23). This is most simply done by plotting $\delta/\delta_{\max}$ as a function of $W_0/(W_0)_{\max}$. If the emission were given by (23), the equation relating these quantities would be:

$$\delta/\delta_{\max}=1.85F\{0.92W_0/(W_0)_{\max}\}. \tag{24}$$

This relation is plotted in Fig. 1, together with experimental data for a number of materials. The substantial difference between the experimental and theoretical curves is hardly surprising. The interesting thing is the striking degree to which the experimental points approximate a single curve. As far as the writer knows, the existence of such a universal curve has not been pointed out previously, although a related regularity was studied by Copeland[10] and Warnecke.[11]

5. THE INFLUENCE OF WORK FUNCTION ON THE TOTAL NUMBER OF SECONDARIES

There was a natural tendency among early workers to expect that metals with low work function would be characterized by relatively large values of the secondary emission coefficient, but measurements have shown that this is by no means true. The most significant reason for this lack of correlation is the fact that the bulk of the electrons in the conduction band of the metal contribute to the secondary emission. This is in marked contrast to thermionic emission where only the electrons near the top of the band are important and the width of the band is of no significance.

The importance of the width of the conduction band appears in the present investigation when, in each of the alternative treatments, δ is found to be proportional to $E_0^{\frac{1}{2}}$ multiplied by a function of the parameter $\mu_0=(1+\Phi/E_0)^{\frac{1}{2}}$. In each case, this function appears as an integral. On evaluation, one obtains from Eq. (18)

$$(\mu_0^{\frac{1}{2}}/2)(\text{ctnh}^{-1}\mu_0^{\frac{1}{2}}-\text{ctn}^{-1}\mu_0^{\frac{1}{2}})-\tfrac{1}{3},$$

and from Eq. (21)

$$\tfrac{1}{2}(\mu_0\,\text{ctnh}^{-1}\mu_0-1).$$

For the range of interest, there is little difference between these functions, as may be seen by comparing the series expansions appropriate for $\mu_0>1$. Letting $x=\mu_0^{-2}$, these are respectively

$$x/7+x^2/11+x^3/15$$

[9] Reference 7, Chapter VI.

[10] P. L. Copeland, Phys. Rev. **46**, 167 (1934).

[11] R. Warnecke, L'Onde Electr. **16**, 509 (1937).

and

$$x/6+x^2/10+x^3/14+\cdots.$$

The fact that consideration of the two extreme cases leads to very similar functions is a strong indication that these are valid approximations for the actual case.

Since the two functions of μ_0 can be regarded as equally good approximations, the second will be used in examining the implications of the theory, because it is the simpler. The emission is then proportional to

$$E_0^{\frac{1}{2}}(\mu_0 \operatorname{ctnh}^{-1}\mu_0-1). \tag{25}$$

It is often an advantage to express E_0 in terms of the work function, Φ, so that only one parameter appears which is not readily measured. With this change (25) takes the form:

$$[\Phi^{\frac{1}{2}}/(\mu_0^2-1)^{\frac{1}{2}}](\mu_0 \operatorname{ctnh}^{-1}\mu_0-1). \tag{26}$$

If the reasonable assumption is made that the ratio μ_0^2, and such quantities as the secondary mean free paths, do not vary in a systematic way with work function one concludes from (26) that the tendency should be for δ to increase as the square root of the work function. Now McKay, in his recent review article,[12] has plotted δ_{max} against Φ for a large number of metals and has drawn a line among the scattered points which shows the general trend. A similar plot is given in Fig. 2, where the solid line is that drawn by McKay. The dashed line is a plot of $(0.35\Phi)^{\frac{1}{2}}$, where the constant 0.35 has been chosen to give agreement with McKay's line at intermediate work functions. It is seen that the theory is correct in predicting an increase of δ_{max} with Φ, and (over a reasonable range) is about right concerning the rate of increase.

Other experimental data which can be used as a check of the theory are those concerning the effect of surface layers of foreign atoms which leave E_0 unaltered, while changing μ_0 through changes of the work function. Bruining[13] gives such data, originally obtained by Treloar and by Sixtus, for oxygen and thorium on tungsten. Treloar's data, taken at a primary energy of 300 ev (maximum emission around 600 ev) are: for clean tungsten ($\delta=1.31$ $\Phi=4.52$ ev) and for tungsten with oxygen covering ($\delta=1.06$ $\Phi=6.30$ ev).

Expression (25), based on a simple spherical momentum-space distribution, would not be expected to apply too well to a complex metal like tungsten. However, it should give a qualitatively correct result if applied with μ_0 computed from the measured Φ and some arbitrary but reasonable value of E_0. Choosing $E_0=5$ ev, one gets for the ratio of emission coefficients after and before covering

$$\frac{1.50 \operatorname{ctnh}^{-1}1.50-1}{1.38 \operatorname{ctnh}^{-1}1.38-1}=0.78$$

in excellent but partly fortuitous agreement with the observed 0.81.

In the work of Sixtus, the increased emission resulting from decreasing the work function from 4.52 ev, to 3.30 ev and to 2.63 ev, was observed. The primary energy was varied from 100 ev to 1100 ev, which is well past the point of maximum emission. The fractional change of δ was found to be a function of the primary energy, decreasing by about a factor two between 100 ev and 600 ev, and remaining approximately constant thereafter. Constant fractional change is, of course, predicted by the expressions for δ developed in the present paper. Numerical estimates, made in the manner outlined above, lead to a fractional change about twice as large as that observed in the large energy range. It is seen from these comparisons, that the theory leads in a straightforward manner to a work function dependence of about the right magnitude.

6. VELOCITY DISTRIBUTION OF THE EMITTED SECONDARIES

(a) Normal Energy Distribution

Expression (25) may also be used to calculate the fraction of the emitted secondaries for which the "normal energy" (that is, $\frac{1}{2}mv_z^2$) exceeds the value, E. This is just that fraction which could still escape if the work function were greater by the amount E,[14] namely:

$$\frac{\mu_1 \operatorname{ctnh}^{-1}\mu_1-1}{\mu_0 \operatorname{ctnh}^{-1}\mu_0-1}, \tag{27}$$

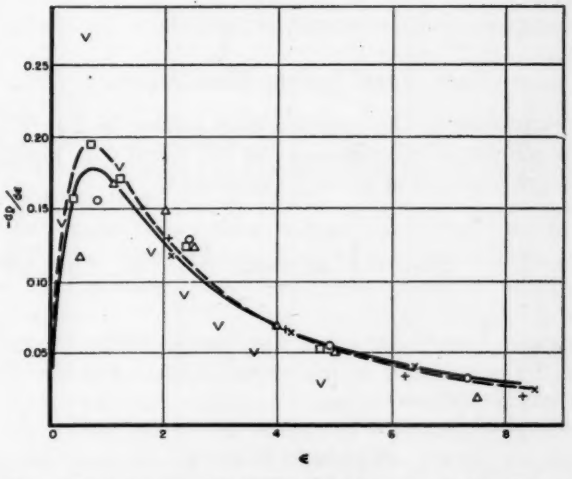

FIG. 4. Total energy distribution of the secondaries. $P(\epsilon)$ denotes the fraction of secondaries emitted with kinetic energy greater than $\epsilon\Phi$. Here $-dP/d\epsilon$, the fraction of secondaries per unit of ϵ, is plotted against ϵ. The curves are from Eq. (30) with $\mu_0^2=1.6$ (solid) and 2.0 (dashed). The points show experimental results for various metals: + Au, × Ag, ○ Cu (Rudberg, 1936); □ Mo, △ Cb (Haworth, 1935 and 1936); ∨ Mo (Kollath, 1941).

[12] K. G. McKay, contribution to *Advances in Electronics* (Academic Press, Inc., New York, 1948), L. Marton, editor, Vol. I.

[13] Reference 7, p. 56.

[14] [L. R. G. Treloar, Proc. Phys. Soc. London **49**, 392 (1937).] The simple relationship between the normal velocity distribution and the effect of work function change has been recognized a long time. Treloar used it in showing that his experimental results on work function change were consistent with observed velocity distributions.

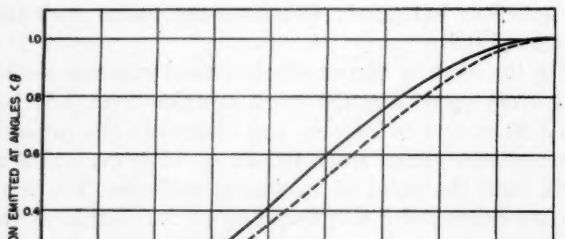

FIG. 5. Angular distribution of the secondaries. The fraction emitted at angles with the normal less than θ is plotted against θ. The solid line, $\sin^2\theta$, is the approximate result of experiment. The dashed line follows from expression (35) with $\mu_0^2=1.6$.

where

$$\mu_1^2=1+(\Phi+E)/E_0=\mu_0^2+(\mu_0^2-1)E/\Phi. \quad (28)$$

The curves in Fig. 3 show the fraction (27) as a function of $\epsilon=E/\Phi$, for $\mu_0^2=1.6$ and 2.0. It appears that the fraction is practically independent of μ_0. The points shown are based on numbers from Treloar's paper,[14] which were computed from experimental data of Haworth on the distribution in total energy of the secondaries from molybdenum ($\Phi=4.2$ ev). In translating from total energy to normal energy, Treloar assumed, in approximate agreement with experiment, that the intensity of emitted secondaries is proportional to the cosine of the angle between the direction of emission and the normal to the surface.

(b) Total Energy Distribution

According to the considerations leading to Eq. (21), the number of electrons leaving the metal with kinetic energy in excess of $\epsilon\Phi$ is proportional to

$$Q(\mu_1)=\int_{\mu_1}^{\infty}(\mu-\mu_0)(\mu^2-1)^{-2}d\mu, \quad (29)$$

where $\mu_1^2=\mu_0^2+(\mu_0^2-1)\epsilon$. The corresponding fraction of the secondaries is $P(\epsilon)=Q(\mu_1)/Q(\mu_0)$, and the differential distribution is:

$$-\frac{dP}{d\epsilon}=\frac{(\mu_0^2-1)(\mu_1-\mu_0)}{2\mu_1(\mu_1^2-1)^2Q(\mu_0)}, \quad (30)$$

In Fig. 4 this function is plotted against ϵ for $\mu_0^2=1.6$ and 2.0. Since these values cover a rather large range of this parameter, one may draw the conclusion that it is actually not of great importance in determining the velocity distribution.

Experimental points for a number of metals are shown in Fig. 4, the data having been taken from small-scale graphs in original papers by Haworth, Kollath, and Rudberg.[15] An adjustment of ordinates was made to make the experimental data correspond roughly to the normalization of the theoretical curves of unit total area. In general, the agreement is actually better than would have been expected. Possibly the data of Kollath, showing more slow secondaries than given by the theory, are more representative of what might reasonably be expected. It may be added that over a reasonable range of μ_0, Eq. (30) gives 0.7 Φ as the energy of the greatest number of secondaries. This agrees well with observation for a number of metals, and seems to be within a factor two of the measured value in essentially all cases.

(c) The Angular Distribution of the Secondaries

It is an almost immediate consequence of the simplifying assumptions made here that the secondary electrons arriving at the metal surface are moving approximately isotropically. It is therefore important to examine explicitly what this implies concerning the angular distribution of the secondaries after leaving the metal. According to the familiar refraction law, an electron incident from the inside at an angle β with the normal, and having momentum μp_0, will emerge at an angle θ given by:

$$\sin\theta=\mu\sin\beta/(\mu^2-\mu_0^2)^{\frac{1}{2}}. \quad (31)$$

For a selected value of β, the electrons emerging at angles less than θ are therefore those for which

$$\mu/(\mu^2-\mu_0^2)^{\frac{1}{2}}<\sin\theta/\sin\beta \quad (32)$$

or

$$\mu^2>\frac{\mu_0^2\sin^2\theta}{\sin^2\theta-\sin^2\beta}. \quad (33)$$

According to Eq. (7), the number of such electrons is proportional to

$$\frac{\sin^2\theta-\sin^2\beta}{(\mu_0^2-1)\sin^2\theta+\sin^2\beta} \quad (34)$$

for $\beta\leqslant\theta$, and zero outside this range. Introducing the assumption that the number of electrons incident in the range $d\beta$ is proportional to the corresponding solid angle, the number of electrons emerging at angles less than θ becomes proportional to the integral:

$$\int_0^{\theta}\frac{(\sin^2\theta-\sin^2\beta)\sin\beta}{(\mu_0^2-1)\sin^2\theta+\sin^2\beta}d\beta. \quad (35)$$

This is readily expressed in terms of elementary functions. The integral, divided by its value at $\theta=\pi/2$, is plotted in Fig. 5 against θ for the typical case, $\mu_0^2=1.6$,

[15] L. J. Haworth, Phys. Rev. **50**, 216 (1936); E. Rudberg, Phys. Rev. **50**, 138 (1936); R. Kollath, Ann. Phys. Lpz. **39**, 59 (1941). Kollath reports that annealing produces substantial changes in the distribution curves. This effect is outside the scope of the present investigation.

thus giving the fraction of secondaries emerging at angles less than θ. Experimental information on the directional distribution is very limited, but indicates that the emission per unit solid angle is approximately proportional to $\cos\theta$, which corresponds to $\sin^2\theta$ for the fraction plotted in the figure. The deviations between our result and $\sin^2\theta$, which appear in the figure, are probably too small to be significant.

The angular dependence implied by the theory is best seen analytically by expanding the integral (35) in powers of $\sin^2\theta$, rather than by considering its exact value. When this is done, one finds that for $\mu_0^2=1.6$, the emission per unit solid angle is proportional to:

$$\cos\theta(1+0.28\sin^2\theta+0.14\sin^4\theta+\cdots) \qquad (36)$$

and that the coefficients vary slowly with μ_0 in the range of interest.

7. CONCLUDING REMARKS

It appears here, as in the earlier work of Kadyschewitsch, that calculations based on the free electron model of Sommerfeld can lead to a considerably improved understanding of secondary electron emission from metals, so that this phenomenon should have its place along with the many others which have been illuminated by this simple picture.

The author wishes to acknowledge the interest and encouragement of colleagues at Battelle, especially Drs. H. R. Nelson and F. C. Todd.

PHYSICAL REVIEW VOLUME 78, NUMBER 6 JUNE 15, 1950

Measurement of the Proton Moment in Absolute Units*

H. A. Thomas, R. L. Driscoll, and J. A. Hipple
National Bureau of Standards, Washington, D. C.

(Received January 23, 1950)

By measuring the absolute value of the magnetic field and the frequency required for nuclear resonance absorption in a water sample, the gyromagnetic ratio of the proton has been determined to be $\gamma_P=(2.67528\pm0.00006)\times10^4$ sec.$^{-1}$ gauss^{-1}. With this value and Planck's constant the value of the magnetic moment of the proton in absolute units becomes $\mu_P=(1.4100\pm0.0002)\times10^{-23}$ dyne cm/gauss.

A combination of our result with recent measurements of the proton moment in Bohr magnetons by Gardner and Purcell results in a value of $e/m=(1.75890\pm0.00005)\times10^7$ e.m.u. gram^{-1}.

I. INTRODUCTION

SINCE the development of molecular beam,[1] nuclear induction,[2] and nuclear resonance absorption[3,4] techniques, considerable work has been done on the determination of nuclear gyromagnetic ratios. From this ratio and the nuclear spin, the magnetic moment of the nucleus can be calculated.

The measurement of a gyromagnetic ratio γ involves the measurement of the frequency ν and magnetic field of induction B_0 required for resonance as indicated by the condition for resonance, $\omega=2\pi\nu=\gamma B_0$. The comparison of either gyromagnetic ratios or magnetic moments requires only frequency determinations and for this reason much of the data on magnetic moments now available is of this type. A few direct measurements of gyromagnetic ratios in absolute units have been made with accuracies of the order of 0.5 percent, which is about the best that can be done with the ordinary techniques of measuring magnetic fields. In the experiment reported here the proton gyromagnetic ratio has been determined with much greater accuracy by using more elaborate methods of measuring the magnetic field and frequency. This precise measurement will allow previous relative determinations to be recalculated in absolute units and will also provide a convenient standard of magnetic field for the measurement of other atomic constants.

The nuclear absorption method of Purcell, Torrey, and Pound[3,4] was used for detecting resonance because the field involved lends itself more readily to precise measurement than that used in the molecular beam method and the apparatus appeared somewhat simpler to construct than that employed by Bloch in the nuclear induction experiment.

The use of one of the Bureau of Standards precision solenoids would provide the most accurately known magnetic field but this possibility was initially discarded because the maximum field available was only of the order of 20 gauss. The nuclear resonance signal-to-noise ratio becomes very low in such a weak field and at the time this experiment was planned no attempt had yet been made to work in this range. The recent success of Brown and Purcell[5] in working in fields as low as 11 gauss now makes the solenoid method more at-

* Further details of this experiment will be published in J. Research Nat. Bur. Stand.

[1] Rabi, Millman, Kusch, and Zacharias, Phys. Rev. **55**, 526 (1939).

[2] F. Bloch, Phys. Rev. **70**, 460 (1946).

[3] Purcell, Torrey, and Pound, Phys. Rev. **69**, 37 (1946).

[4] Bloembergen, Purcell, and Pound, Phys. Rev. **73**, 679 (1948).

[5] L. M. Brown and E. M. Purcell, Phys. Rev. **75**. 1262 (1949).

tractive than when the present work was undertaken; as a means of eliminating systematic errors and possibly improving the accuracy, it is important that the measurements described here be repeated. This is now being done.

In the experiment here described an electromagnet with relatively strong field was used which reduced the signal-to-noise problem but which required auxiliary apparatus for measuring the field. The method of measuring the magnetic field is one similar to that previously described in the literature.[6–8] In this method the magnetic field is determined by measuring the force on a known length of conductor carrying a known current. A long rectangular coil is suspended from an analytical balance with the lower end of the coil in the gap of the magnet. The vertical sides of the coil act as connecting leads to the "force conductors" which are formed by the lower horizontal portion of the coil. The fringing field of the magnet at the upper end of the coil is reduced to a negligible value by means of Helmholtz coils.

Since the force f is measured in the vertical or y direction and the current i is everywhere the same in the circuit the force may be given by

$$f=\int_{\text{coil}} iB(x, y)dx. \tag{1}$$

The integration can be carried out numerically from measurements of the width of the coil at various vertical positions together with determinations of the field at these vertical positions. If we use as a reference point the average value of the field over the bottom wires $\bar{B}$, then the effective width X of this coil when used as described with a particular magnet and Helmholtz coil arrangement may be defined by the relationship

$$X=(1/\bar{B})\int_{\text{coil}} B(x, y)dx. \tag{2}$$

The average field in terms of the observed force f (dynes), X (cm), and I (amp.) in a coil of n turns is

$$\bar{B}=10f/nIX. \tag{3}$$

Since it is the average field over the region occupied by the force conductors that is measured by the force method, it is essential that the field distribution be precisely determined and that the field in this region be reasonably uniform. Then from the value of the average field and the field distribution the value of the field at the proton sample, located just below the coil, may be determined.

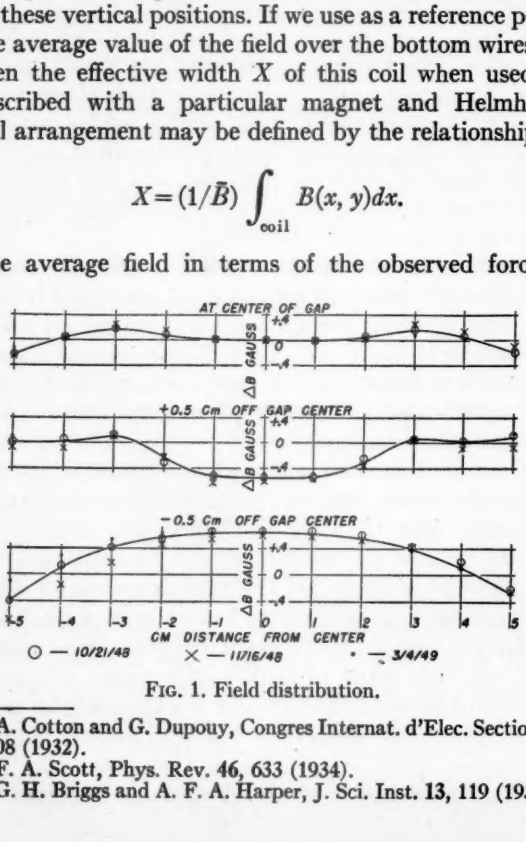

FIG. 1. Field distribution.

II. APPARATUS AND EXPERIMENTAL PROCEDURE

A nuclear resonance detector employing a radio-frequency bridge will show both the absorption and dispersion depending on the amount and kind of unbalance in the bridge.[4] Any dispersion signal present would introduce some error in determining the true center of the resonance line. For this reason and also to eliminate the microphonic problem, an "amplitude bridge" detector was developed[9] which is insensitive to phase changes and hence will not indicate the dispersion signal.

A 0.4-cc sample of water adjusted with a ferric salt was used. The amount of ferric salt added (for adjustment of relaxation time[4] T_1) was just enough to give maximum signal with no appreciable line broadening. Under these conditions the line width, which was determined by the inhomogeneity of the field, was 0.25 gauss at the half-power points. Substitution of an oil sample (Nujol) for the water sample indicated no observable shift in the line due to the susceptibility of the ferric salt. The glass sample holder and r-f coil were mounted in the end of a $\frac{3}{4}$-in. brass tube which served as the coaxial line feeding the coil. Small Helmholtz coils were mounted on either side of the sample for modulating the magnetic field. This whole resonance probe assembly was checked with a magnetometer for magnetic impurities.

The magnetic field of about 5000 gauss was produced by a water-cooled magnet which had auxiliary coils in addition to the main exciting windings. The poles of the magnet were 8.5×12.5 in. and the gap separation was 2 in. The value of the field was adjusted so that the resonance frequency would be 20 Mc which can be heterodyned directly with WWV for the frequency measurement.

The field distribution in the gap was obtained by using two resonance probes: one to plot the field; the other capable of regulating it to two parts per million (ppm) for a change of one percent in the main exciting current by means of a phase detector and a power amplifier supplying the auxiliary coils. The first probe was mounted on a cross feed that would allow accurate positioning in the gap. As the probe is moved, a varia-

[6] A. Cotton and G. Dupouy, Congres Internat. d'Elec. Section 3, 2, 208 (1932).
[7] F. A. Scott, Phys. Rev. 46, 633 (1934).
[8] G. H. Briggs and A. F. A. Harper, J. Sci. Inst. 13, 119 (1936).
[9] H. A. Thomas and R. D. Huntoon, Rev. Sci. Inst. 20, 516 (1949).

TABLE I. Typical results of a series of measurements. Platinum-iridium mass $m=8777.29$ mg; current $=0.1017274$ amp.; sensitivity of the balance $S=1.59$ mg/cm.

Date	Temp. of coil °C	$\delta \cdot s$ (mg)	Temp. corr. (mg)	Corrected mass (mg)	$\bar{B}$ gauss	$(B_0-\bar{B})$ gauss	B_0 gauss	dev. from mean
May 6, 1949	26.9	+0.30	−0.16	8777.43	4697.56	+0.02	4697.58	0.03
May 9, 1949	26.2	−0.08	−0.10	8777.11	4697.38	+0.11	4697.49	0.06
May 12, 1949	26.4	+0.09	−0.12	8777.26	4697.46	+0.07	4697.53	0.02
May 16, 1949	25.6	+0.08	−0.05	8777.32	4697.50	+0.09	4697.59	0.04
							Mean 4697.55	±0.04

Note.—$\nu=20{,}001{,}075\pm20$ cycles per sec. γ_P = gyromagnetic ratio of proton $=2\pi\nu/B_0=2.67523\times10^4$ sec.$^{-1}$ gauss^{-1}.

tion in field is indicated by a shift in the resonance line on the oscilloscope. A second pair of small Helmholtz coils mounted on this probe was used to bring the resonance line back to its original position on the oscilloscope screen. This Helmholtz pair had previously been calibrated by measuring the shift in resonance frequency produced by a given change in current in the coils. To provide reference lines on the oscilloscope, the audiofrequency voltage applied to the field modulating coils was also applied to a peak clipping and differentiating circuit that would produce sharp pulses. With this arrangement, variations in field as a function of position could be plotted with an error of less than 0.02 gauss.

After shimming with thin nickel shims spatial variations in the field were held to a quite low value as indicated by the typical distribution curves shown in Fig. 1. It was not assumed that the field distribution would remain constant and so field distribution data were taken just preceding and following each run of force measurement data. In addition to that shown in Fig. 1 the field distribution up the sides of the coil was taken for the purpose of determining the effective width X of the coil. These data were taken with the resonance probe as far as possible and then with a rotating coil fluxmeter (accuracy 0.2 percent) the remainder of the distance to the top of the coil.

The precision coil for measuring the magnetic field was wound on the edge of a glass plate 10×70 cm and 0.7 cm thick. The coil has nine turns of wire that lie in grooves formed around the edge of the plate.[10] The wires pass around the sides and bottom of the plate parallel to the edge of the glass and cross over to the next groove at the top. Oxygen-free copper wire was drawn through a special die and wound directly on the plate under constant tension.

Measurements on the coil width were made relative to Johannson gage blocks in a temperature controlled cabinet by means of a motor driven micrometer devised by Moon.[11] Measurements of the temperature and resistance of the coil made simultaneously with the width measurements gave a means of correcting later for possible coil expansion. The diameter of the wire was measured by a similar method using samples of wire taken initially from the ends of the coil. After completion of the experiment the turns of the coil were cut from the plate and samples from each side of each turn were measured under proper loading at various vertical positions and angles. By this means an initial uncertainty in the effective width of the coil of 40 ppm was reduced to 10 ppm.

The current through the coil was measured by the conventional method of comparing directly the drop in a standard resistor to the e.m.f. of a standard cell. The errors associated with this measurement are listed later (Table II).

The force produced on the current-carrying coil was evaluated by comparison with the action of gravity on a known mass that was placed on the scale pan of the balance when the current was reversed. In case the comparison was not exact, a small correction was made to the mass in terms of the sensitivity of the balance, s, and the change in its rest point, δ. Remembering the reversal of current and denoting the mass of the removable weight by m, and the acceleration of gravity by g, a working formula for the field $\bar{B}$ is given by

$$\bar{B}=\frac{5(m+\delta\cdot s)g}{nIX[1+a(t-25)]}, \tag{4}$$

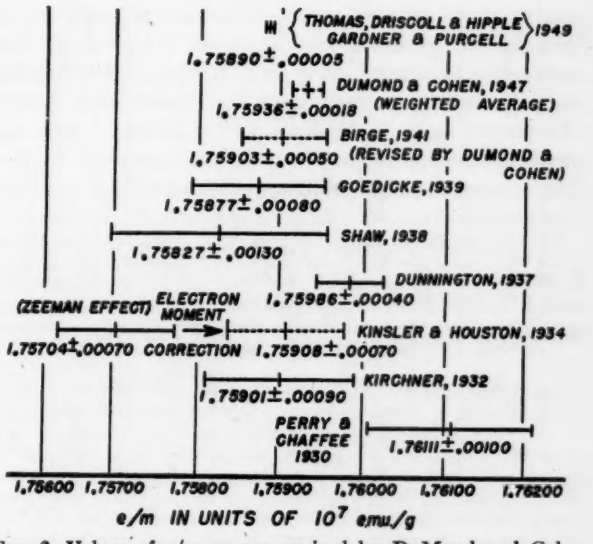

FIG. 2. Values of e/m as summarized by DuMond and Cohen compared with the value reported in this paper.

[10] Curtis, Moon, and Sparks, J. Research Nat. Bur. Stand. **21**, 375 (1938), RP1137.

[11] C. Moon, Bur. Stand. J. Research **10**, 249 (1933), RP528.

TABLE II. Tabulation of errors.

Contributing errors	Parts per million
Platinum-iridium mass—m	1
Precision of balance used in this experiment—$\delta \cdot s$	9
Gravity	3
Electrical standards	10
Comparison of current with standards	3
Width of coil	10
Length standard	5
Field distribution	10
Neutralization of stray field at upper wires	5
Adjustment of resonance pip to reference point on oscilloscope	4
Calibration of Helmholtz coils used for field distribution	4
Resonance frequency	1
Effect of ferric ions in sample	4

where a is the coefficient of thermal expansion for the coil and t its temperature. In practice the current I had some fixed value according to the standards selected and the magnetic field had some value consistent with the frequency required for proton resonance; therefore, the mass m was adjusted by trial to a point where the correction $(\delta \cdot s)$ was so small that the uncertainty in the sensitivity of the balance did not produce more than a tolerable error in the force. The mass was then standardized by the mass section of the Bureau.

III. RESULTS

Two measurements of γ_P were made over a period of about six months with slight improvements in technique being made in the second series. The results of the two series are practically identical. Considering all runs the average deviation is approximately 10 ppm. Typical results of a series of measurements are shown in Table I.

The known contributing errors listed in Table II were estimated conservatively. The square root of the sum of their squares results in an uncertainty of 22 ppm in the gyromagnetic ratio of the proton. The result can be stated as $\gamma_P=(2.67523\pm0.00006)\times10^4$ sec.$^{-1}$ gauss^{-1} uncorrected for the diamagnetic effect. The stated error is thought to be several times the corresponding probable error. If a diamagnetic correction,[12] which was not included in the preliminary result,[13] is applied to the above value one obtains $\gamma_P=(2.67528\pm0.00006)\times10^4$ sec.$^{-1}$ gauss^{-1}.

The magnetic moment of the proton is known less accurately than the gyromagnetic ratio because of the uncertainty in the value of Planck's constant h. Using a value[14] of

$$h=(6.6234\pm0.0011)\times10^{-27} \text{ erg sec.},$$

the magnetic moments of the proton is

$$\mu_P=(1.4100\pm0.0002)\times10^{-23} \text{ dyne cm/gauss}.$$

IV. COMPARISON WITH OTHER MEASUREMENTS

Gardner and Purcell[15] have just completed a measurement of the ratio of the precession frequency of the proton $\omega=\gamma_p B_0$ to the cyclotron frequency $\omega_e=eB_0/m$ of a free electron in the same magnetic field. After making the same diamagnetic correction they give for the ratio $\omega/\omega_e=(1.52100\pm0.00002)\times10^{-3}$. This ratio is the magnetic moment of the proton in Bohr magnetons, and agrees very well with the value $\mu_P=(1.52106\pm0.00007)\times10^{-3}$ obtained by Taub and Kusch.[16] These values of μ_p may be combined with the value of the gyromagnetic ratio of the proton to give a value of e/m. In this calculation it is preferable to use the value of Gardner and Purcell because of its greater accuracy and because the electron moment correction is not involved. The value of e/m becomes $e/m=\gamma_p\omega_e/\omega=(1.75890\pm0.00005)\times10^7$ e.m.u. gram^{-1}. This differs only slightly from the previously published value[17] which was obtained by combining our preliminary value of γ_p with the measurement of Taub and Kusch. A comparison of the measured values of e/m is shown on Fig. 2.

The value of the gyromagnetic ratio of the proton and hence the above value of e/m has recently received further confirmation since it has been used in determining the faraday[18] in which excellent agreement was obtained.

Contributions of other staff members are gratefully acknowledged and in particular the authors wish to thank Dr. Charles Moon for advice on the construction and measurement of the coil and Dr. R. D. Huntoon for his many helpful suggestions.

[12] W. E. Lamb, Jr., Phys. Rev. **60**, 817 (1941). This correction (1.8×10^{-5}) is for the hydrogen atom. N. F. Ramsey [Phys. Rev. **77**, 567 (1950)] has calculated the correction for the H_2 molecule to be 2.7×10^{-5}. If the frequency shift between H_2 and our sample were determined, the result given in this paper would be improved.

[13] Thomas, Driscoll, and Hipple, Phys. Rev. **75**, 902 (1949).

[14] J. W. M. DuMond and E. R. Cohen, Rev. Mod. Phys. **20**, 82 (1948).

[15] J. H. Gardner and E. M. Purcell, Phys. Rev. **76**, 1262 (1949).

[16] H. Taub and P. Kusch, Phys. Rev. **75**, 1481 (1949); P. Kusch and H. Taub, Phys. Rev. **75**, 1477 (1949).

[17] Thomas, Driscoll, and Hipple, Phys. Rev. **75**, 992 (1949).

[18] Hipple, Sommer, and Thomas, Phys. Rev. **76**, 1877 (1949).

Magnetic Field Penetration in Superconducting Lead

M. C. STEELE
Naval Research Laboratory, Washington, D. C.

(Received February 14, 1950)

The magnetic susceptibility of small superconducting lead spheres (radius $\sim 10^{-3}$ cm) has been determined by a self-inductance method. On the basis of relations derived from the London theory for reducing the data, the penetration depth, λ, is calculated for three different lead samples at 4.22°K. Results indicate that λ is $1.3\pm 0.3\times 10^{-5}$ cm at this temperature. In addition, it is found that, within experimental error, λ is not a function of the size of the sphere. It is noted that there is need for using smaller sized particles and accounting for the interaction effects if future colloid investigations designed to test the London theory are to be successful.

1. INTRODUCTION

THE London[1] theory describes the penetration of an applied magnetic field into a superconductor by the equation

$$\nabla^2\mathbf{H}=\mathbf{H}/\lambda^2, \tag{1}$$

where $\mathbf{H}$ is the magnetic field intensity within the superconductor and λ is the penetration depth. The measurement of the parameter λ has been the subject of many investigations[1a] since the advent of the London theory. All these experiments have indicated that $\lambda\sim 10^{-6}$ to 10^{-4} cm.

If the validity of Eq. (1) is assumed, λ can be determined from magnetic susceptibility measurements on superconducting bodies having dimensions of the order of λ. London[2] has shown that for small spheres the relation between susceptibility and λ is given by

$$\chi/\chi_0=1-\frac{3\coth(R/\lambda)}{R/\lambda}+\frac{3}{(R/\lambda)^2}, \tag{2}$$

where χ is the volume susceptibility for a small sphere of radius R, and χ_0 is the susceptibility of a large sphere ($R\gg\lambda$). It follows from the "Meissner-Ochsenfeld Effect"[3] that χ_0 should be $-3/8\pi$. This value has been verified experimentally.[4]

The experiments to be described in this paper were performed to obtain a value for the penetration depth in lead at 4.22°K. The susceptibility of spherical colloidal lead specimens was determined by a self-inductance method. If Eq. (2) is correct, such measurements yield the value of λ directly if R is known.

2. EXPERIMENTAL

(A) Susceptibility Measurement

When a quantity of spherical superconducting particles suspended in a non-magnetic medium is introduced into a coil, the coil suffers a change in self-inductance ΔL given by the relation

$$\Delta L=M\chi KC_i, \tag{3}$$

where M is the mass of superconducting material in the dispersion; K is a constant determined by the coil geometry and specific gravity of the superconducting element, and C_i is a factor correcting for the magnetic interaction between particles. If we define

$$R/\lambda=\rho \tag{4}$$

and

$$\chi/\chi_0=f(\rho) \tag{5}$$

it then follows from (3) that

$$f(\rho)=\Delta L/MK\chi_0C_i. \tag{6}$$

Equation (6) determines λ directly from the inductance change produced by the introduction of the dispersion if R, M, K, and C_i are known.

An earlier investigation[5] has shown that although C_i is a function of the concentration of the metal in the dispersion it is apparently independent of the size of the spheres. Both K and C_i were obtained by calibrating the coil with various concentrations of large lead spheres (so that λ could be neglected, and χ was essentially χ_0).

The experimental procedure consisted of observing the change in self-inductance of the calibrated coil when the dispersion of lead in Vaseline contained in a Pyrex[5a] test tube 5 cm long and 0.6 cm inside diameter, was introduced into the coil. The coil was wound with A.W.G. 40 copper wire on a Bakelite cylinder of 1 cm diameter and 15 cm length. Its self-inductance was 6103.0μh when completely submerged in liquid helium at 4.22°K. Measurements were made with an inductance bridge which was balanced by a null method employing an amplifier and an oscilloscope. Changes of 0.1μh could be observed readily with this arrangement. The

[1] F. London and H. London, Proc. Roy. Soc. **A149**, 71 (1935).
[1a] A summary of methods used to determine λ is given by D. Shoenberg, Intern. Conf. on Fundamental Particles and Low Temperatures, Vol. II (Physical Society), 93 (1947).
[2] F. London, Physica **3**, 450 (1936).
[3] W. Meissner, and R. Ochsenfeld, Naturwiss. **21**, 787 (1933).
[4] D. Shoenberg, Proc. Roy. Soc. **A155**, 712 (1936).
[5] M. C. Steele, Phys. Rev. **76**, 566 (1949). In this earlier paper the correction factor for the interaction effect is designated as χ/χ_0 in place of the C_i used in the present paper.
[5a] In order to account for the possible change in self-inductance due to the Pyrex tube and the Vaseline, a number of runs were made without any lead in the tubes. No change in self-inductance was observed in such cases. Even if there were some small effect, it would be very nearly canceled in determining the susceptibility of the colloids since the calibration and the final runs were made with the same sized Pyrex tubes.

bridge was supplied with 1,000 c.p.s. voltage and the a.c. magnetic field within the measuring coil was calculated to be ~ one oersted.

(B) Specimens

The specimens had to meet a number of critical requirements before any worth while observations could be made. Besides the need for particles having dimensions of the order of λ, it was desirable to have uniformity of size. In additon, they had to be as nearly spherical as possible since Eq. (6) is only applicable for spheres. Finally, there has to be enough metal in the sample to insure a sufficiently accurate determination of the susceptibility.

The technique of preparing colloidal metal particles by the chemical reduction of a suitable salt, as used by Shoenberg[6] in his study of mercury colloids, could not be successfully applied to lead or any of the other superconductors. In fact, a major portion of this investigation was the search for a method of producing small lead spheres. The procedure finally evolved consisted of stirring molten lead in a bath of silicone oil, and then allowing the entire mass to cool below the melting point of the metal. This led to the production of spherical particles having radii $\geqq 10^{-4}$ cm. Figure 1 shows a microphotograph of a typical preparation of lead before any separation into size ranges was attempted.

One advantage of this technique of colloid preparation is that the metal particles can be isolated readily from the silicone oil by using suitable solvents. Therefore an elutriation process can be used to separate the particles into rather narrow size ranges. For this experiment a Roller Air Elutriator was successfully employed[7] to separate particles having from 0 to 40 microns diameter into 5 micron ranges. Figure 2 shows a microphotograph of the 10 to 15 micron fraction after separation. It is noted that the separated particles deviate slightly from spheres when compared with the original material. Unfortunately, this distortion is unavoidable when material as soft as lead is elutriated by air. However, these slight departures from sphericity would probably not have any marked effect upon the results since it is likely that such perturbations would tend to be canceled if there is a random distribution of the particles within the dispersion.[8]

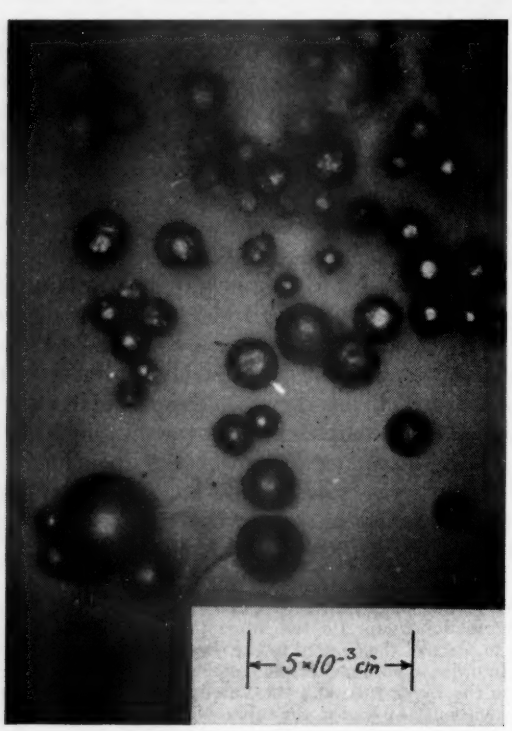

FIG. 1. Lead spheres before separation into size ranges.

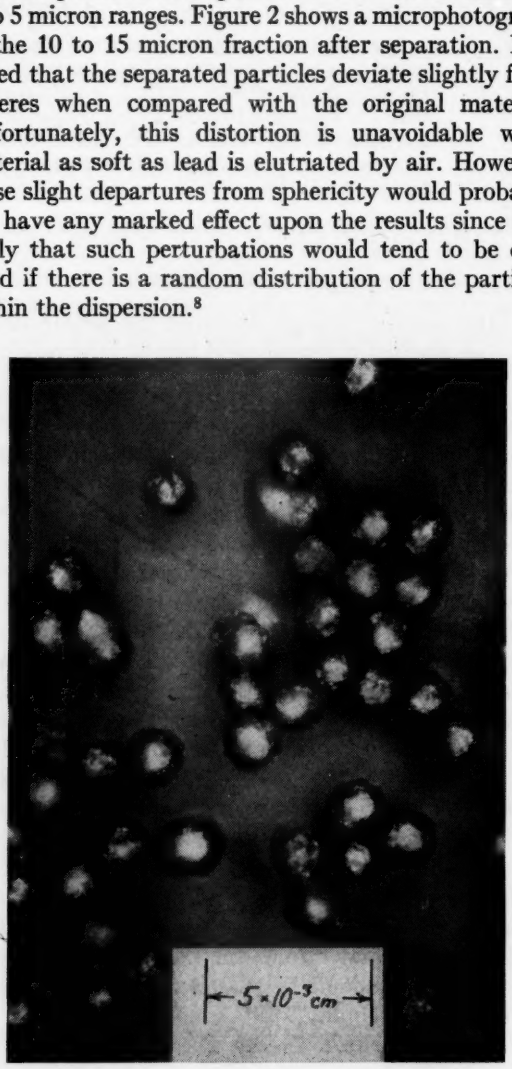

FIG. 2. Lead particles of the 10 to 15 micron fraction obtained by air elutriation.

The final specimens consisted of these separated lead particles dispersed in Vaseline and contained in the Pyrex test tubes described previously. Chemical analysis of the prepared colloidal lead showed that its purity exceeded 99.9 percent.

3. EXPERIMENTAL RESULTS AND DISCUSSION

Data were obtained for three samples of lead having size ranges 10 to 15, 15 to 20, and 30 to 35 microns

[6] D. Shoenberg, Proc. Roy. Soc. A175, 49 (1940).

[7] The separations with the Roller Air Elutriator were carried out by the Metallurgy Division of the National Bureau of Standards, Washington, D. C. The author wishes to express his thanks for their willing assistance.

[8] Shoenberg (reference 6) has presented a similar argument in his paper.

TABLE I. Results for lead at 4.22°K.

$\bar{R}\times10^4$ cm	Mass (grams)	Volume percent in dispersion	$-\Delta L(\mu h)$[a]	C_i	$f(\rho)$	ρ	$\lambda\times10^5$ cm	$\delta\lambda\times10^5$ cm
7.6	0.8607	3.6	15.78	0.987	0.944	53	1.4	±0.2
9.4	2.4108	13.2	43.55	0.954	0.962	78	1.2	±0.4
17.2	2.5557	9.7	47.67	0.966	0.981	157	1.1	±0.4

[a] ΔL as given is the average of five independent observations made over a period of two months.

(diameter) respectively. The average[9] radius ($\bar{R}$) of each specimen was determined from microscopic examination of several hundred particles. Table I gives a summary of the observations and calculated results for these dispersions.

From Table I the weighted mean value of λ is $1.3\pm0.3\times10^{-5}$ cm. This value is, of course, dependent upon the validity of Eq. (2). The only other value of $\lambda_{4.2°K}$ reported for lead has been given by von Laue[10] as 2.09×10^{-5} cm. Von Laue determined this best fitting value from the data of magnetic threshold experiments performed by Pontius[11] on thin lead cylinders.[12]

To date, Eq. (1) has been integrated under the assumption that λ is independent of both the magnetic field strength and the size of the body. Therefore, it is significant to note that within experimental error the results of this investigation are consistent with the latter condition on λ (i.e., λ is independent of size).

The major part of the standard deviation ($\delta\lambda$) is due to the relatively large sizes of the particles. Thus, small uncertainties in the observations are greatly magnified in the calculated value of λ. In fact, if the correction factor C_i had been neglected, the results would not only have been changed by as much as a factor of three, but also there would have been an apparent marked size dependence of λ. Measurements with smaller particles would eliminate most of this difficulty. Finally, there is the error introduced by localized clustering of the particles within the dispersion. No allowance was made for such an effect in the reduction of the data although Fig. 2 shows clearly that particles do cluster in groups. Shoenberg[6] has pointed out that it is difficult to predict the order of magnitude of such a correction.

The results of this study emphasize the need for using smaller particles and for investigating the effect of clustering if the colloid method is to be instrumental in testing the validity of the London theory.

The author wishes to thank Dr. Jules de Launay for his encouragement throughout this investigation, and Mr. J. Babiskin for his most helpful assistance in the preparation of samples.

[9] The use of $\bar{R}$ in place of $[\Sigma_i(R_i)^3]^{\frac{1}{3}}$ does not change the values of λ given in Table I.

[10] M. von Laue, Ann. d. Physik **32**, 71 (1938).

[11] R. B. Pontius, Phil. Mag. **24**, 787 (1937).

[12] Values of $\lambda_{4.2°K}$ calculated from all of Pontius' data actually cover a range from 1.10×10^{-5} to 2.29×10^{-5} cm.

Field and Charge Measurements in Quantum Electrodynamics

N. BOHR
Institute for Theoretical Physics, University, Copenhagen, Denmark

AND

L. ROSENFELD
Department of Theoretical Physics, University, Manchester, England

(Received October 19, 1949)

A survey is given of the problem of measurability in quantum electrodynamics and it is shown that it is possible in principle, by the use of idealized measuring arrangements, to achieve full conformity with the interpretation of the formalism as regards the determination of field and charge quantities.

INTRODUCTION

RECENT important contributions[1] to quantum electrodynamics by Tomonaga, Schwinger and others have shown that the problem of the interaction between charged particles and electromagnetic fields can be treated in a manner satisfying at every step the requirements of relativistic covariance. In this formulation, essential use is made of a representation of the electromagnetic field components on the one hand, and of the quantities specifying the electrified particles on the other, corresponding to a vanishing interaction between field and particles. The account of such interaction is subsequently introduced by an approximation procedure based on an expansion in powers of the non-dimensional constant $e^2/\hbar c$. As regards the interpretation of the formalism, this method has the advantage of a clear emphasis on the dualistic aspect of electrodynamics. In fact, an unambiguous definition of the electromagnetic field quantities rests solely on the consideration of the momentum imparted to appropriate test bodies carrying charges or currents, while the charge-current distributions referring to the presence of particles are ultimately defined by the fields to which these distributions give rise.

Just from this point of view the problem of the measurability of field quantities has been discussed by the authors in a previous paper.[2] A similar investigation of the measurability of electric charge density was then also undertaken, but, owing to various circumstances, its publication has been delayed.[3] When recently the work was resumed, it appeared that by making use of the new development as regards the formulation of quantum electrodynamics a more general and exhaustive treatment could be obtained.[4] As these considerations may be helpful in the current discussions of the situation in atomic physics, we shall here give a brief account of the implications of present electron theory for measurements of charge-current densities. For this purpose, it will be convenient to start with a summary of our earlier treatment of the measurability of field quantities.[5]

1. MEASUREMENTS OF ELECTROMAGNETIC FIELDS

Classical electrodynamics operates with the idealization of field components $f_{\mu\nu}(x)$ defined at every point (x) of space-time. Although in the quantum theory of fields these concepts are formally upheld, it is essential to realize that only averages of such field components over finite space-time regions R, like

$$F_{\mu\nu}(R)=\frac{1}{R}\int_R f_{\mu\nu}(x)d^4x \tag{1}$$

have a well-defined meaning (I, §2). In the initial step of approximation, in which all effects involving $e^2/\hbar c$ are disregarded, these averages obey commutation relations of the general form

$$[F_{\mu\nu}(R), F_{\kappa\lambda}(R')]=i\hbar c[A_{\mu\nu,\kappa\lambda}(R, R')-A_{\kappa\lambda,\mu\nu}(R', R)], \tag{2}$$

where the expressions of the type $A_{\mu\nu,\kappa\lambda}(R, R')$, defined as integrals over the space-time regions R and R' of certain singular functions, have finite values depending on the shapes and relative situation of the regions R and R'.

The measurement of a field average $F_{\mu\nu}(R)$ demands the control of the total momentum transferred within the space-time region R to a system of movable test bodies with an appropriate distribution of charge or current, of density ρ_ν, covering the whole part of space which at any time belongs to the region R. In the case

[1] S. Tomonaga, Prog. Theor. Phys. 1, 27 (1946); Phys. Rev. 74, 224 (1948). J. Schwinger, Phys. Rev. 74, 1439 (1948); 75, 651 (1949); 75, 1912 (1949); 76, 790 (1949). F. Dyson, Phys. Rev. 75, 486 (1949); 75, 1736 (1949). R. Feynman, Phys. Rev. 76, 749 (1949); 76, 769 (1949).

[2] N. Bohr and L. Rosenfeld, Kgl. Danske Vid. Sels., Math.-fys. Medd. 12, No. 8 (1933). This paper will be referred to in the following as I.

[3] An account of the preliminary results of the investigation, which were discussed at several physical conferences in 1938, has recently been included in the monograph by A. Pais, *Developments in the Theory of the Electron* (Princeton University Press, Princeton, New Jersey, 1948).

[4] The bearing of this development on the elucidation of the problem of measurability was brought to the attention of the writers in a stimulating correspondence with Professor Pauli.

[5] A more detailed account of the subject with fuller references to the literature will appear later in the Communications of the Copenhagen Academy.

of an electric field component F_{4l}, we shall take a distribution of charge, with constant density ρ_4, and in the case of a magnetic field component F_{mn}, a uniform distribution of current in a perpendicular direction, with density components ρ_m and ρ_n. The field action of such charge-current distribution, so far as it does not originate from the displacements of the test bodies accompanying the momentum control, can in principle be eliminated by the use of fixed auxiliary bodies carrying a charge-current distribution of opposite sign, and constructed in a way which does not hinder the free motion of the test bodies. In the case of a current distribution, such auxiliary bodies are even indispensable in providing closed circuits for the currents by means of some flexible conducting connection with the test bodies. As a result of this compensation, the field sources of the whole measuring arrangement will thus merely be described by a polarization $P_{\mu\nu}$ arising from the uncontrollable displacements of the test bodies in the course of the field measurements.

If the test bodies are chosen sufficiently heavy, we can throughout disregard any latitude in their velocities, but the control of their momentum will of course imply an essential latitude in their position, to the extent demanded by the indeterminacy relation. Still, it is possible, without violating any requirement of quantum mechanics, not only to keep every test body fixed in its original position except during the time interval within the region R corresponding to this position, but also to secure that, during such time intervals, the displacements of all test bodies in the direction of the momentum transfer to be measured, although uncontrollable, are exactly the same. This common displacement D_μ is described, in the case of the measurement of an electric field, by the component D_l parallel to the field component F_{4l}, and when a magnetic field is measured, by the components D_m and D_n perpendicular to F_{mn}. Without imposing any limit on the accuracy of the field measurement, it is, moreover, possible to keep the displacement D_μ arbitrarily small, if only the charge-current density ρ_ν of the test bodies is chosen sufficiently large. By a further refinement of the composite measuring arrangement described in our earlier paper (I, §3), it is even possible to reduce the measurement of any field average to the momentum control of a single supplementary body, and thus to obtain a still more compendious expression for the ultimate consequences of the general indeterminacy relation.

An essential point in field measurements is, however, the necessity of eliminating so far as possible the uncontrollable contribution to the average field present in R, arising from the displacement of the test bodies in the course of the measurement. In fact, the expectation value of this contribution will vary in inverse proportion to the latitude allowed in the field measurement, since it is proportional to the polarization $P_{\mu\nu}=D_\mu\rho_\nu-D_\nu\rho_\mu$ within the region R. Just this circumstance, however, makes it possible, by a suitable mechanical device, by which a force proportional to their displacement is exerted on the test bodies, to compensate the momentum transferred to these bodies by the uncontrollable field, insofar as the relation of this field to its sources is expressed by classical field theory. With the compensation procedure described, the resulting measurement of $F_{\mu\nu}(R)$ actually fulfils all requirements of the quantum theory of fields as regards the definition of field averages (I, §5). In fact, the incompensable part of the field action of the test bodies due to the essentially statistical character of the elementary processes involving photon emission and absorption, corresponds exactly to the characteristic field fluctuations which in quantum electrodynamics are superposed on all expectation values determined by the field sources.

When the measurement of two field averages $F_{\mu\nu}(R)$ and $F_{\kappa\lambda}(R')$ is considered, it appears (I, §4) that the expectation value of the average field component $\Phi_{\mu\nu,\,\kappa\lambda}(R, R')$ which the displacement of the test bodies operated in the region R produces in the region R' is equal to the product of $\frac{1}{2}RP_{\mu\nu}$ with the quantity $A_{\mu\nu,\,\kappa\lambda}(R, R')$ occurring in the commutation relation (2). Likewise, the expectation value of the average component $\Phi_{\kappa\lambda,\,\mu\nu}(R', R)$ of the field in R due to the test bodies in R' is equal to $\frac{1}{2}R'P_{\kappa\lambda}'A_{\kappa\lambda,\,\mu\nu}(R', R)$. When optimum compensation of the momenta transferred to the test bodies by these fields is established by suitable devices, making use of a correlation by light signals transmitted between points of the two regions R and R', it can be deduced from the reciprocal indeterminacy of position and momentum control that the only limitations of the measurability of the two field averages considered correspond exactly to the consequences of the commutation rule (2) for such averages (I, §6, 7). In this connection, it must be stressed that the field fluctuations which are inseparable from the incompensable parts of the fields created by the operation of the test bodies, do not imply any restriction in the measurability of a field component in two asymptotically coinciding space-time regions. In fact, we have here to do with a complete analog to the reproducibility of the fixation of observables in quantum mechanics by immediately repeated measurements.

2. CHARGE-CURRENT MEASUREMENTS IN INITIAL APPROXIMATION

In the formalism of quantum electrodynamics, charge-current densities, like field quantities, are introduced by components $j_\nu(x)$ at every space-time point, but, even in the initial approximation in which such symbols are formally commutable, well-defined expressions are only given by integrals of the type

$$J_\nu(R)=\frac{1}{R}\int_R j_\nu(x)d^4x, \tag{3}$$

representing the average charge-current density within the finite space-time region R. From the fundamental

equations of electrodynamics it follows quite generally that

$$RJ_\nu(R)=\int_R \frac{\partial f_{\nu\mu}}{\partial x_\mu} d^4x=\int_S f_{\nu\mu} d\sigma_\mu, \tag{4}$$

which expresses the definition of the average charge-current density over the region R in terms of the flux of the electromagnetic field through the boundary S of this region. In this four-dimensional representation, such generalized fluxes comprise, of course, besides the ordinary electric field flux defining the average charge density, other expressions pertaining to the average current densities and representing magnetic field circulations and displacement currents.

In the simple special case in which the region R is defined by a fixed spatial extension V and a constant time interval T, the average charge density, in accordance with (4), will be given, in the ordinary vectorial representation, by

$$J_4(V, T)=\frac{1}{VT}\int_T dt \int_S \mathbf{E}\mathbf{n} d\sigma, \tag{5}$$

where S is the surface limiting the extension V, and $\mathbf{n}$ the unit vector in the outward normal direction on this surface. In such representation, the average current density will be given by

$$\mathbf{J}(V, T)=\frac{1}{VT}\int_T dt \int_S \mathbf{n}\wedge\mathbf{H} d\sigma-\frac{1}{VT}\int_V \mathbf{E} dv \Big|_{t_1}^{t_2}, \tag{6}$$

where the first term on the right-hand side represents the time integral of the tangential component of the magnetic field integrated over the surface S, while the last term expresses the difference of the volume integrals of the electric field at the beginning and at the end of the time interval T.

The determination of an average charge-current density $J_\nu(R)$ thus demands the measurement of a field flux through the boundary S of the space-time region R. The approach to the problem of such measurement must rationally start from the consideration of the average flux over a thin four-dimensional shell situated at the boundary S, and which for simplicity we shall assume to have a constant thickness in space-time. As in the situation met with in the measurement of an average field component $F_{\mu\nu}(R)$, we shall require for this purpose a system of movable test bodies, filling the space which belongs to the shell at any time with an appropriate uniform charge-current distribution, and whose field actions are ordinarily neutralized by a distribution of opposite sign on fixed, penetrable, auxiliary bodies. For the measurement of an average charge density J_4, it suffices to take a set of test bodies with a uniform charge distribution of density ρ_4, while in the measurement of a current component, J_l, we shall have to use, besides such test bodies, another independent set of freely movable test bodies with a uniform current distribution ρ_l parallel to the current component to be measured.

In the measurement of an average charge density, the estimation of the flux over the shell demands the determination of the algebraic sum of the momenta transferred to the test bodies in the direction of the normal to the instantaneous spatial boundary. The evaluation of this sum, however, does not require independent measurements of the momenta transferred to the individual test bodies within the time intervals during which their positions belong to the space-time shell, but can be obtained by a composite measuring process in which the positions of all test bodies are correlated by suitable devices to secure during these intervals a displacement of every test body in the normal direction by the same amount. By choosing the product of the thickness of the shell and the charge density of the test bodies sufficiently large, it is possible to keep the uncontrollable common displacement D of all the test bodies in the normal direction arbitrarily small, and still to obtain unlimited accuracy for the average flux over the shell. Like in the measurement of a simple field average, it is further possible to achieve an automatic compensation of the uncontrollable contribution to this average flux, due to the fields created by the displacement of the test bodies, and proportional to $D\rho_4$. This compensation will even be complete, in the initial approximation considered, because the field fluctuations, owing to their source-free character, do not give any contribution to the flux. Since these considerations hold for any given thickness of the shell, it is in principle possible, in the asymptotic limit of a sharp boundary, to measure accurately the average charge density within a well-defined space-time region.

In measurements of an average current component J_l, we have to take into account the magnetic circulation as well as the electric field in the space-time shell. Thus, in the special case in which R is defined by a spatial extension V and a time interval T, we have to do, according to (6), not only with a contribution from the time average over T of the magnetic circulation around the direction l within a thin spatial shell on the boundary of V, but also with a contribution representing the difference between the volume integrals over V of the electric field component in the direction l, averaged over two short time intervals at the beginning and at the end of the interval T. The evaluation of these contributions requires measuring procedures of a similar kind as those described above in the case of measurements of simple field averages. While the measurement of the latter contribution demands the control of the momentum in the direction l transferred to a set of test bodies with uniform charge density ρ, the evaluation of the former contribution demands the control of the momentum normal to the spatial boundary transferred to another set of test bodies with uniform current density ρ_l.

Just as in the field or charge measurements discussed

above, all these operations can be correlated in such a way that the determination of the algebraic sum of the momenta transferred to each test body within the time interval and in the direction required can be reduced to the momentum control of some supplementary body. In such a correlation, all the test bodies of charge density ρ will be subjected during the appropriate time intervals to the same displacement D_l and all the test bodies of current density ρ_l to the same normal displacement D. The interpretation of the current measurement requires further the establishment of a correlation between these two displacements, satisfying the condition $\rho D_l = \rho_l D$. Under such circumstances, it is possible, by choosing ρ and ρ_l sufficiently large, to achieve that the displacements D_l and D be arbitrarily small without imposing any limitation upon the accuracy of the measurement. Moreover, it is possible, by suitable mechanical devices of the kind already mentioned, to obtain a complete automatic elimination of the uncontrollable contributions from the operation of the test bodies to the average current to be measured.

It need hardly be added that the procedure can be extended to quite general space-time regions R, by using an arrangement in which each test body is displaced just in the time interval during which its position belongs to the space-time shell surrounding the region R. In this connection, it may be noted that a compendious four-dimensional description of all the measuring processes pertaining to charge-current components involves a uniform four-vector current distribution in the shell, parallel to the charge-current component to be measured.

Like in charge measurements, all the considerations concerning current measurements are independent of the thickness of the shell, and in principle it is therefore possible, in the initial approximation considered, to determine with unlimited accuracy any average charge-current component $J_\nu(R)$ within a sharply bounded region R. As regards charge-current measurements over two space-time regions, it can easily be seen that, in the limiting case of sharp boundaries, all field actions accompanying the flux measurements will vanish at any point of space-time which does not belong to the boundaries. In conformity with the formalism, there will therefore, to the approximation concerned, be no mutual influence of measurements of average charge-current densities in different space-time regions.

The situation so far described is of course merely an illustration of the compatibility of a consistent mathematical scheme with a strict application of the definition of the physical concepts to which it refers, and is in particular quite independent of the question of the possibility of actually constructing and manipulating test bodies with the required properties. The disregard of all limitations in this respect, which may originate in the atomic constitution of matter, is, however, entirely justified when dealing with quantum electrodynamics in the initial stage of approximation. In fact, at this stage, the formalism is essentially independent of space-time scale, since it contains only the universal constants c and $\hbar$ which alone do not suffice to define any quantity of the dimensions of a length or time interval.

3. CHARGE-CURRENT MEASUREMENTS IN PAIR THEORY

New aspects of the problem of measurements arise in quantum electrodynamics in the next approximation, in which effects proportional to $e^2/\hbar c$ are taken into consideration, and where we meet with additional features connected with electron pair production induced by the electromagnetic fields. For the commutation rules of the field components, this means in general only a smaller modification expressed by additional terms containing $e^2/\hbar c$. The charge-current quantities, however, will no longer be commutable but will obey commutation relations of the form

$$[J_\nu(R), J_\mu(R')] = i\hbar c[B_{\nu\mu}(R, R') - B_{\mu\nu}(R', R)], \quad (7)$$

where the expressions $B_{\nu\mu}(R, R')$ are integrals of singular functions over the regions R and R'. In contrast to the quantities $A_{\mu\nu,\varkappa\lambda}(R, R')$ occurring in (2), which depend only on simple spatio-temporal characteristics of the problem, the B's will, however, besides such characteristics, also essentially involve the length $\hbar/mc$ and the period $\hbar/mc^2$, related to the electron mass m.

To approach the problem of the measurability of a charge-current quantity $J_\nu(R)$ in this approximation, we must again consider systems of electrified test bodies operated in a space-time shell on the boundary of the region R, but we shall now have to examine the effect of the charge-current density appearing as a consequence of actual or virtual electron pair production by the field action of the displacement of the test bodies during the measuring process. As we shall see, these effects, which are inseparably connected with the measurements, do not in any way limit the possibilities of testing the theory.[6]

In the first place, the average effect of the polarization of the vacuum by virtual and actual pair production in the measuring process can be eliminated by a compensation arrangement like that previously described. It is true that a direct estimate of these polarization effects in quantum electrodynamics involves divergent expressions which can only be given finite values by some renormalization or regularization procedure.[7] By such a procedure the average polarization effects will give rise to a contribution to the charge current density which is proportional to the common displacement of the test bodies. Thus in the limit of

[6] In a paper by Halpern and Johnson, Phys. Rev. **59**, 896 (1941), arguments are brought forward pointing to a far more restrictive limitation of the field and charge measurements. In these arguments, however, no sufficient separation is made between such actions of the charged test bodies as are directly connected with their use in the measuring procedure and those actions which can be eliminated by appropriate neutralization by auxiliary bodies of opposite charge.

[7] Cf. W. Pauli and F. Villars, Rev. Mod. Phys. **21**, 434 (1949).

a sharp boundary of the region R we get, denoting the surface polarization on the boundary by P_ν, the expression $RP_\nu B_{\mu\nu}(R, R)$, where the last factor represents the value of $B_{\mu\nu}(R, R')$ in (7) for coinciding space-time extensions.

Moreover, the statistical effects caused by actual production of electron pairs in the measurement process are inseparably connected with the interpretation of the fluctuations of average charge-current densities in quantum electrodynamics. While the mean square deviation of the field component $F_{\mu\nu}(R)$ over a sharply bounded space-time region R has a finite value, finite mean-square fluctuations of charge-current quantities can only be obtained, however, by further averaging over an ensemble of regions R whose boundaries are allowed a certain latitude around some given surface.[8]

This feature finds its exact counterpart in the estimate of the statistical effects of the real pairs which are produced in measurements of charge-current quantities by the indicated procedure. In fact, the mean square fluctuations of an average flux will increase indefinitely with decreasing thickness of the shell in which the test bodies are operated, in just the same way as, according to the formalism, the mean-square fluctuation of the corresponding charge-current density will vary with the latitude of the ensemble of space-time extensions over which the averaging is performed. The appearance of an infinite mean-square fluctuation in a sharply limited space-time region is in no way connected with the divergencies which appear in vacuum polarization effects but is a direct consequence of the fundamental assumptions of the theory, according to which the electrons are regarded as point charges.

In the case of measurements of charge-current averages over two space-time regions, it can be shown that the polarization effects of the manipulation of the test bodies used for the measurement of $J_\nu(R)$ will give rise, in the limit of sharp boundaries, to a contribution to the average charge-current density component of index μ in the region R', equal to the product of the quantity $B_{\mu\nu}(R', R)$ occurring in formula (7) with RP_ν, where P_ν is the surface polarization created on the boundary of R during the measuring process. Conversely, the measurement of $J_\mu(R')$ will give a contribution $R'P_\mu' B_{\nu\mu}(R, R')$ to the average charge-current density of index ν in R. By similar compensation devices as required for two field measurements, it is therefore possible, as readily seen, to obtain an accuracy of measurements of average charge-current densities in two space-time regions subject only to the reciprocal limitation expressed by the commutation relation (7).

4. CONCLUDING REMARKS

The conformity of the formalism of quantum electrodynamics with the interpretation of idealized field and charge measurements has of course no immediate relation to the question of the scope of the theory and of the actual possibility of measuring the physical quantities with which it deals.

In the present state of atomic physics, the problem of an actual limitation of measurements interpreted by means of the concepts of classical electrodynamics can hardly be fully explored. Still, in view of the great success of quantum electrodynamics in accounting for numerous phenomena, the formal interpretation of which involves space-time coordination of electrons within regions of dimensions far smaller than $\hbar/mc$ and $\hbar/mc^2$, it may be reasonable to assume that measurements within such regions are in principle possible. Indeed, the comparatively heavy and highly charged test bodies of such small dimensions and operated over such short time intervals, which would be required for these measurements, might be conceived to be built up of nuclear particles.

Yet, an ultimate limitation of the consistent application of the formalism is indicated by the necessity of introducing forces of short range in nuclear theory, with no analog in classical electrodynamics, and by the circumstance that the ratio between the electron mass and the rest mass of the quanta of the nuclear field has the same order of magnitude as the fundamental parameter $e^2/\hbar c$ of quantum electrodynamics.[9] The further exploration of such problems may, however, demand a radical revision of the foundation for the application of the basic dual concepts of fields and particles.

[8] Cf. W. Heisenberg, Leipziger Ber. 86, 317 (1934). We are indebted to Drs. Jost and Luttinger for information about their more precise evaluation of charge-current fluctuations, showing that the unlimited increase of the charge-current fluctuations in a space-time region with decreasing latitude in the fixation of its boundary involves only the logarithm of the ratio between the linear dimensions of the region and the width of this latitude. Even a latitude very small compared with $\hbar/mc$ will therefore imply no excessive effect of the charge fluctuations. A situation entirely similar in all such respects to that in electron theory is met with in a quantum electrodynamics dealing with electrical particles of spin zero which obey Bose statistics. We are indebted to Dr. Corinaldesi for the communication of his results regarding the charge-current fluctuations and pair production effects in such a theory.

[9] Cf., e.g., N. Bohr, Report of the Solvay Council (1948).

The Energy Spectrum of Neutrons from a Po—Be Source

B. G. WHITMORE AND W. B. BAKER
Department of Physics, University of Manitoba, Winnipeg, Canada
(Received January 23, 1950)

The energy spectrum of neutrons emitted by a Po—Be source has been determined by the photographic emulsion method. The results agree, on certain assumptions, with the existence of energy levels in the C^{12} nucleus at 2.5, 4.5, and 7.1 Mev. The last two of these are consistently found by other workers, but the existence of the first is sometimes disputed. Possible reasons for the apparent discrepancies in the evidence on this point are discussed.

1. INTRODUCTION

THE energy distribution of the neutrons from a Po—Be source, though studied by various methods by a number of workers, is not known with precision, and a further examination by the photographic emulsion method has been undertaken.

2. EXPERIMENTAL METHOD

Ilford C_2 plates were exposed to neutrons from a pair of Po—Be sources, the plates and sources, 21 cm apart being supported on light wire frameworks in such a way that the nearest scattering material was at a distance of about 150 cm. The sources lay approximately in the plane of the emulsion and on the central axes of the $3''\times1''$ plates, so that the incident neutron directions made angles of not more than 5° with any line in the plate parallel to the axis. Tracks of protons in the emulsion were measured in the usual way, if their initial directions lay within 13° of the plate axis, as determined by cross-hairs in one eyepiece of the binocular microscope used for observations. The measured lengths were converted to energies by use of the calibration curve for Ilford emulsions of Lattes and Cuer,[1] one point on which was checked by neutrons from a deuterons-on-deuterons source, obtained by use of a 300-kev beam of deuterons from the Ottawa high tension generator. The energy distribution obtained was corrected for the varying proton-neutron collision cross section, using the results of Bailey *et al.*,[2] and for the probability of a track leaving the emulsion, to give the final energy distribution.

This final distribution is shown in Fig. 1. It is derived from a total of nearly 7000 observations, made by three different observers on three separate plates. Of these plates, one was placed alone, the other two sandwiched together, to test whether the proximity of extra glass scattering material had any observable effect on the results. No such effect was detected, the curves derived from the three plates separately differing not more than would be expected from experimental error. The internal consistency of the observations was checked further by plotting separately the distribution obtained by each observer, on all plates together.

All these partial distributions showed the same major features namely: (1) a maximum energy of about 11 Mev, (2) pronounced maxima in the distribution at just over 3 Mev and just under 5 Mev, and a fairly well marked smaller maximum at 7.5 to 8 Mev. The small maximum at 1 Mev occurred in most curves. The experimental accuracy was not sufficient to determine whether the small maxima in Fig. 1 at 5.8 and 9.7 Mev are real or spurious, these maxima showing in some but not all of the partial distributions. These results agree with those of Richards[3] and Demers[3] only with regard to the first point, the existence of an upper limit of about 11 Mev, and in the broad fact of the existence of a maximum intensity somewhere in the range 3 to 5 Mev. The statistical errors of these previous determinations, however, would appear to be considerably greater than those of the present work.

We may therefore regard as established by this work intensity maxima at 3.2, 4.8, 7.7 Mev, and probably one at 1.2 Mev, and an upper limit to the energy of 11 Mev; small maxima at 5.8 and 9.7 Mev are doubtfully suggested.

3. ENERGY LEVELS OF THE C^{12} NUCLEUS

We wish to consider the association of this distribution with the energy levels of the C^{12} nucleus. Hornyak and Lauritsen[4] in a review of many experimental papers,

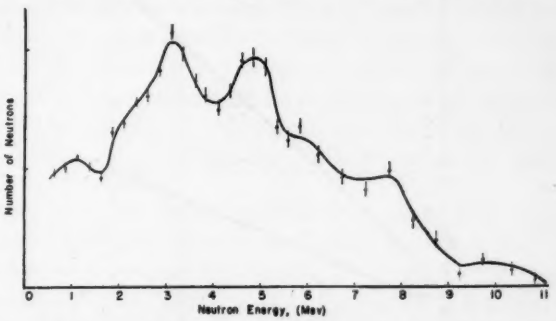

FIG. 1. Energy distribution of neutrons from a Po-Be source, plotted in 0.25 or 0.5 Mev intervals.

[1] C. M. G. Lattes, P. H. Fowler, and P. Cuer, Proc. Phys. Soc. London **59**, 884 (1947).
[2] Bailey, Bennett, Bergstralh, Nuckolls, Richards, and Williams, Phys. Rev. **70**, 583 (1946).
[3] See Anderson, *Neutrons from Alpha-Emitters* (McGraw-Hill Book Company, Inc., New York) Nuclear Science Series, No. 3.
[4] W. F. Hornyak and T. Lauritsen, Rev. Mod. Phys. **20**, 191 (1948).

conclude that the evidence points to the existence of an excited state at 4.3 Mev, another at 7.1±0.4 Mev (as well as higher states), as well as a doubtful level at about 3 Mev. In view of the discussion given below, it is perhaps relevant that all the evidence for this state seems to have been derived from the $Be^9(\alpha,n)C^{12}$ reaction used by us. They give the Q-value for this reaction, ending in the ground state of C^{12}, as 5.75 Mev.

In attempting to correlate our results with these energy levels it is necessary to remember that a reaction of given Q-value will give rise to neutrons of varying energy, owing (a) to the variation in the energy of the incident α-particle and (b) to variation in the direction of emission of the neutron, relative to that of the α-particle. In order to calculate the distribution in energy which one would expect to observe, corresponding to transitions to a single final level in C^{12}, it is necessary to know both the excitation function for this transition, and the distribution in angle of the emitted neutrons.

Considering first this latter point, for α-particles of fixed energy, it is readily seen that a uniform distribution in angle in the center-of-mass system corresponds to a uniform distribution in energy in the laboratory system. For if v_1 be the velocity of center of mass relative to laboratory, v_2 that of neutron relative to the center of mass, and φ the angle between these velocities, then the velocity of the neutron in the laboratory system, V, is given by $V^2=v_1^2+v_2^2+2v_1v_2\cos\varphi$, and its energy E_2 by $E_2=a+b\cos\varphi$. Hence $dE_2=b\sin\varphi d\varphi$. But a uniform distribution in angle gives $dn=k\sin\varphi d\varphi$, hence dn/dE_2 is constant.

The maximum and minimum values of E_2 corresponding to a fixed value of the incident α-energy, E_1, and given Q, are easily calculated from the dyanmics of the collision. They are plotted in Fig. 2 for values of E_1 up to 5.3 Mev, the maximum energy of polonium

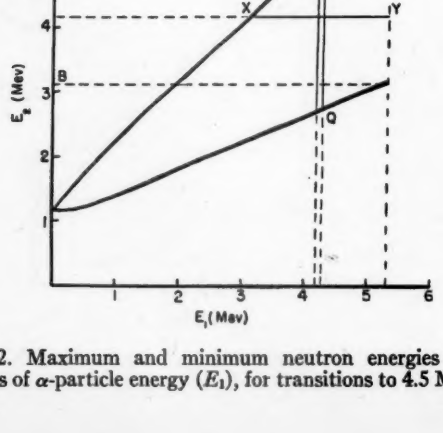

FIG. 2. Maximum and minimum neutron energies (E_2) as functions of α-particle energy (E_1), for transitions to 4.5 Mev level in C^{12}.

α-particles, taking Q as 1.25 Mev, corresponding, on Hornyak and Lauritsen's scheme, to transitions to the 4.5 Mev level in C^{12}.

To determine accurately the effect of varying α-energies we need the excitation function for this transition. Various workers[5] have measured the excitation functions of neutrons and the associated γ-rays for the $Be^9(\alpha,n)C^{12}$ reaction. They use for the detection of the neutrons various methods, which do not all have the same comparative sensitivity for slow and fast neutrons. Their results correspondingly differ considerably in detail, though showing fair agreement in the general form of the function. The results do not, however, refer specifically to transitions to any given final level. As an approximate basis for calculation, the curve given by Halpern was used.

We may first note one general point concerning the results of this calculation, assuming, as discussed above, that α-particles of fixed energy E_1 liberate neutrons with a uniform distribution of energy. If the number of α-particles having energies in any range dE_1 is proportional to dE_1, if each such particle liberates $f(E_1)$ neutrons, and if these neutrons are spread uniformly over a range of energies (PQ in Fig. 2) of $R(E_1)$, then the number of such neutrons having energies between E_2 and (E_2+dE_2) is proportional to $f(E_1)dE_1\cdot dE_2/R(E_1)$. The total number of neutrons of this energy is therefore proportional to

$$dE_2\int_X^Y f(E_1)dE_1/R(E_1)=F(E_2)dE_2.$$

Since the integrand is always positive, $F(E_2)$ will clearly increase steadily as E_2 decreases from A to B; and unless $f(E_1)$ is exceptionally large for low values of E_1 the maximum of $F(E_2)$ almost certainly occurs at $E_2=B$. Exceptionally, it could occur for a lower value of E_2, but not for a higher one.

It is noticeable that in Fig. 2 the value of E_2 at B is 3.1 Mev. This suggests that the prominent maximum in our curve at that value is derived from transitions to the 4.5 Mev level in C^{12}, the emitted neutrons being distributed uniformly in angle in the center-of-mass system.

$F(E_2)$ has therefore been calculated on this basis by graphical integration, using Halpern's curve for $f(E_1)$, taking Q for transitions to the ground state as 5.75 Mev, and assuming transitions to levels at 0, 2.5, 4.5, and 7.1 Mev. The results are shown in Fig. 3. To show that $F(E_2)$ is not very sensitive to the form of $f(E_1)$ the calculations have also been carried out in two cases assuming $f(E_1)=$constant, above a threshold at 1 Mev. These results are shown dotted.

Comparing the curves of Fig. 3 with our distribution of Fig. 1, it will be seen that the upper limit of 11 Mev in Fig. 1 agrees with the calculations, and that the

[5] E. Fünfer, Ann. d. Physik (5) 35, 147 (1939); E. Stuhlinger, Zeits. f. Physik 114, 185 (1939); A. Szalay and J. Zimonyi, Zeits. f. Physik 115, 639 (1940); I. Halpern, Phys. Rev. 74, 1234(A) (1948), or see Anderson.

maxima of the four calculated curves agree with the experimental maxima at 1.2, 3.1, 4.8, 7.7 Mev. Our results, therefore, would seem to agree with the level scheme proposed by Hornyak and Lauritsen, except that the value 2.5 rather than 3.0 fits our results better for their "doubtful" level.

There are, however, difficulties in this interpretation. Evidence for this last level is very conflicting. Various workers (see Bethe and Livingston[6]) with the $Be^9(\alpha,n)C^{12}$ reaction have obtained evidence for it. On the other hand, other reactions involving C^{13} as the intermediate nucleus do not seem to show it. For example Powell,[7] in a photographic emulsion study of the reaction $B^{11}(d,n)C^{12}$ obtained very clear evidence for a 4.5 Mev level in C^{12}, and none at all for any lower one. The $Be^9(\alpha,n)C^{12}$ reaction has also been studied recently by Bradford and Bennett,[8] who used 1.4 Mev α-particles from an accelerator, and photographic emulsion recording at a fixed angle to the beam, thereby eliminating or reducing the causes of our "spread" in neutron energy. They also obtain evidence for a 4.5 Mev level, and no lower ones.

It will be noticed also that, while the maxima of the curves of Fig. 3 agree in position with those of Fig. 1, the experimental maxima are much sharper than the calculated ones. In particular, the pronounced dip in the experimental curve between 3.1 and 4.8 Mev could not be reproduced by combining "calculated" curves in any proportion. Remembering that straggling in the emulsion and varying angles of neutron and proton paths will introduce a broadening into the experimental curves, there seems here to be a definite discrepancy.

We do not feel that we have enough information to account for these apparent discrepancies finally. Certain tentative suggestions may, however, be made. With regard to the 2.5 Mev level, its absence in other experiments might be due to the different excitation of the C^{13} nucleus in those cases. In Powell's experiments, this intermediate nucleus is formed from $B^{11}+d$, in ours from $Be^9+\alpha$. If, as is likely, its life-time is very short, it might remain in fundamentally different states in the two cases such that transitions to the 2.5 Mev level in C^{12}, were forbidden in one case but not in the other. Bradford and Bennett's experiments are more difficult to reconcile with this. But it is noticeable on Halpern's curve that there is a marked resonance for α-energies of about 1.4 Mev. Possibly, therefore, these α-particles enter a fairly clearly marked energy level in C^{13}, from which again transitions to the 2.5 Mev level are forbidden.

The calculated distributions are based on the assumption that neutrons are emitted uniformly in all directions in the center-of-mass system. This appears to be the most plausible assumption. But if, for example, they were emitted predominantly at right angles to the direction of the α-particle, the effect would be to sharpen the maximum of the calculated distribution. It is true that the maximum would also be displaced, perhaps vitiating the whole identification of final levels proposed, but a moderate and symmetrical concentration of directions around the 90° angle might perhaps not displace the maxima greatly.

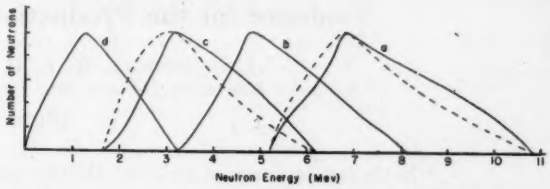

FIG. 3. Calculated neutron distributions for transitions to (a) ground state, (b) 2.5 Mev level, (c) 4.5 Mev level, (d) 7.1 Mev level in C^{12} nucleus.

It is worth noting here that Bradford and Bennett found the ratio of the intensity of their low energy neutron group (transitions to 4.5 Mev level) to that of the high energy group (transitions to ground state) to be 1.3 for observations at 90° and 0.4 in the forward direction. This might be accounted for if the high energy group were uniformly distributed (our high energy group is rather broader than the others) the low one stronger at 90°. Their average ratio also seems to be much lower than in our experiments, where the high energy group is weak, again possibly owing to the different excitations.

It is, of course, clear that the evidence we have is not sufficient to substantiate these suggestions. For example, if the distribution in angle of the emitted neutrons is not uniform, large variations in the calculations can be made by assuming sufficiently asymmetrical angular distributions. If the intensity is assumed to be zero at 90°, and about twice as great in the forward as in the backward direction, it is even possible to obtain, for the single transition to the 4.5 Mev level, a final distribution showing peaks at about 3.1 and 4.8 Mev as observed. The asymmetry necessary is very great, and appears to be in the wrong sense to account for Bradford and Bennett's results, so that this suggestion does not seem to be probable, but it is mentioned to emphasize that without more accurate knowledge the unambiguous interpretation of our results is impossible.

This work was made possible by grants from the National Research Council of Canada to one of us in the form of a Summer Studentship, to the other for the purchase of equipment and payment of assistance. Plates were exposed for us by Mr. A. G. W. Cameron at the Atomic Energy Project at Chalk River, and at the Ottawa High Tension Laboratory of the National Research Council. Constance E. Cox carried out statistical calculations. Our thanks are also due to Dr. B. W. Sargent, of Chalk River, who suggested the problem, for his continual interest and assistance.

[6] M. S. Livingston and H. A. Bethe, Rev. Mod. Phys. **9**, 304 (1937).

[7] C. F. Powell, Proc. Roy. Soc. **A181**, 344 (1943); F. C. Champion and C. F. Powell, Proc. Roy. Soc. **A183**, 64 (1944).

[8] C. E. Bradford and W. E. Bennett, Phys. Rev. **77**, 753(A) (1950).

Evidence for the Production of Neutral Mesons by Photons*

J. STEINBERGER, W. K. H. PANOFSKY, AND J. STELLER
Radiation Laboratory, Department of Physics, University of California, Berkeley, California
(Received April 28, 1950)

In the bombardment of nuclei by 330-Mev x-rays, multiple gamma-rays are emitted. From their angular correlation it is deduced that they are emitted in pairs in the disintegration of neutral particles moving with relativistic velocities and therefore of intermediate mass. The neutral mesons are produced with cross sections similar to those for the charged mesons and with an angular distribution peaked more in the forward direction. The production cross section in hydrogen and the production cross section per nucleon in C and Be are comparable.

I. INTRODUCTION

NEUTRAL mesons which are coupled strongly to nuclei must be expected to be unstable against decay into two or more gamma-rays. The modes of decay, and expected lifetimes, have been discussed extensively.[1] These gamma-rays are then supposed to be responsible for the soft showers which often accompany energetic cosmic-ray nuclear events.[2] The evidence in favor of the existence of the neutral meson has recently been greatly strengthened by the discovery at Berkeley[3] of gamma-rays which behave in all ways as if they were due to the disintegration of a neutral meson. They are produced by proton bombardment of various nuclei and have a production cross section which depends on proton energy much like that of charged mesons. Their energy is approximately 70 Mev on the average, half that of the charged π-meson, and the energy spread is in agreement with the Doppler shift due to the velocity of the parent mesons. The lifetime of the mesons is less than 10^{-13} sec., which is in agreement with the theoretical expectations.

The evidence is therefore already much in favor of the existence of a gamma-unstable neutral meson. However, until now, coincidences between the two gamma-rays have never been observed. We report here the detection of such coincidences, produced by the bombardment of various nuclei in the x-ray beam of the Berkeley synchrotron. This must be regarded as strong additional evidence supporting the existence of the neutral meson.

II. EXPERIMENTAL ARRANGEMENT

The apparatus is sketched in Fig. 1. The synchrotron x-ray beam of 330-Mev maximum energy is collimated in two successive collimators. The second collimator serves only to intercept some of the electrons produced at the edge of the first collimator. The beam then strikes a target, which, for most of the experiment, is a cylinder of beryllium, $1\frac{1}{2}$ inches long and 2 inches in diameter. The particles produced in the target are detected in two telescopes, each consisting of three scintillation counters. A converter, usually $\frac{1}{4}$ inch of lead, is inserted between the two crystals nearest the target in each telescope. An event is recorded if simultaneous (resolving time 10^{-7} sec.) pulses are recorded in the outer four crystals, but none in the two near the target. That is, we require that there be two particles, one in each telescope, neutral at first which are converted into charged particles by the lead, and which penetrate one crystal and enter the next. With a beam intensity of about 10^{11} Mev/min. the counting rate for such coincidences at favorable orientations of the telescopes is about 10 counts/min.

III. NATURE OF THE COINCIDENCES

Let us first describe the experiments which identify the particles as gamma-rays, indicate their energy and show that their origin is the nuclear rather than the Coulomb field. In Table I we list the relative detection

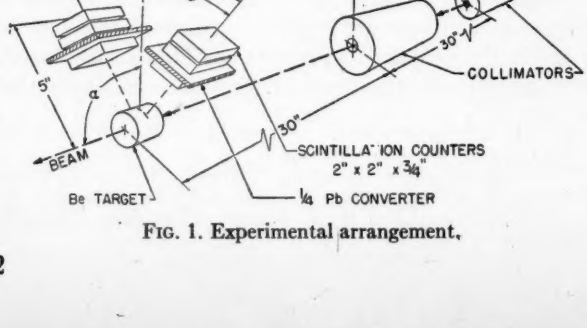

FIG. 1. Experimental arrangement.

* This work was performed under the auspices of the AEC.

[1] Y. Tanikawa, Proc. Phys. Math. Soc. Japan **24**, 610 (1940). R. J. Finkelstein, Phys. Rev. **72**, 414 (1947). H. Fukuda and Y. Miamoto, Prog. Theor. Phys. **4**, 347 (1949). Ozaki, Oneda, and Sasaki, Prog. Theor. Phys. **4**, 524 (1949). J. Steinberger, Phys. Rev. **76**, 1180 (1949). C. N. Yang, Phys. Rev. **77**, 243 (1950).

[2] The implications of the gamma-decay of neutral mesons for the soft component in the cosmic radiation were pointed out by J. R. Oppenheimer (Phys. Rev. **71**, 462 (T) (1947). It was assumed that in high energy nuclear events neutral mesons are emitted with multiplicities similar to those for charged mesons. The neutral mesons decay into photons and account for the early development of extensive showers, as well as the large total amount of soft radiation. These bursts of soft radiation accompanying energetic nuclear events were then actually observed in the cloud chamber by W. Fretter, Phys. Rev. **73**, 41 (1948), **76**, 511 (1949); C. Y. Chao, Phys. Rev. **75**, 581 (1949); Gregory, Rossi, and Tinlot, Phys. Rev. **77**, 299 (1949); and J. Green, Thesis, University of California, 1950. They were found in photographic plates by Kaplan, Peters, and Bradt, Phys. Rev. **76**, 1735 (1949). Both the cloud-chamber pictures and the photographic star show that the showers begin with gamma-rays rather than electrons.

[3] Bjorklund, Crandall, Moyer, and York, Phys. Rev. **77**, 213 (1950).

efficiency for various converter materials and thicknesses. Without converters the counting rate is almost zero, then increases as the converter thickness in each arm is increased to $\frac{1}{4}$ inch of lead, and only slightly from $\frac{1}{4}$ inch to $\frac{1}{2}$ inch. This is as expected from shower theory for about 100-Mev photons. Copper of $\frac{1}{4}$ inch thickness has approximately the same conversion efficiency as has $\frac{1}{16}$ inch of lead, again in agreement with shower theory, since the number of shower units is the same for these thicknesses.

The coincidences are attenuated by a factor of four when $\frac{1}{4}$ inch of lead is inserted between the target and the anticoincidence crystals. This again is as expected for photons. Furthermore, it can be seen from Table I that both telescopes require converters, so that both particles must be photons.

To measure the energy of the conversion electrons, aluminum absorbers were inserted between the last two crystals of one of the telescopes. Unfortunately, at these energies the radiation losses are important, and therefore the straggling large. We have plotted in Fig. 2 the coincidence counting rate as a function of the average energy required to traverse the telescope. Because the photons originate in moving mesons, the average gamma-ray energy is expected to be approximately 100 Mev, and the average electron energy 50 Mev, quite in agreement with the observed attenuation.

The nuclear origin of the photons is demonstrated by the fact that the cross section for these coincidences is only six times as big for a lead nucleus as for beryllium, which is less than the ratio of the nuclear areas. On the other hand, ordinary shower cross sections increase by a factor of 400.

Finally, we have looked for coincidences with the beam energy reduced to about 175 Mev with angles α and β of the telescope both 90°. The cross section per Q (the number Q for a bremsstrahlung beam is equal to the total energy divided by the maximum energy of the spectrum) is at least 50 times smaller here than at 330 Mev. This steep excitation function is also observed for charged meson production.

We believe, therefore, that it is demonstrated that the observed coincidences are caused by gamma-rays of about 100-Mev average energy, of non-Coulombic origin, and with a threshold similar to that for charged mesons.

IV. ANGULAR CORRELATION AND DISTRIBUTION OF THE GAMMA-RAYS

To study further the properties of these coincidences, we have measured their rate as a function of the angle, α, between the beam direction and the plane of the telescopes and of the correlation angle β (see Fig. 1). Consider first the variation with β at a fixed α, say 90°. 180° coincidences are rare. The counting rate increases with decreasing β to a maximum at 90°, and then drops sharply. This behavior must actually be expected of gamma-rays which are the decay products of neutral

TABLE I. Relative detection efficiency as a function of absorber material and thickness.

Converter in telescope 1	Converter in telescope 2	Relative counting rate $\alpha=\beta=90°$
none	none	0.01±0.005
$\frac{1}{32}$-in. Pb	$\frac{1}{32}$-in. Pb	0.17±0.013
$\frac{1}{16}$-in. Pb	$\frac{1}{16}$-in. Pb	0.3 ±0.02
$\frac{1}{8}$-in. Pb	$\frac{1}{8}$-in. Pb	0.67±0.08
$\frac{1}{4}$-in. Pb	$\frac{1}{4}$-in. Pb	1.00±0.06
$\frac{1}{4}$-in. Cu	$\frac{1}{4}$-in. Cu	0.39±0.03
none	$\frac{1}{4}$-in. Pb	0.15±0.05
$\frac{1}{16}$-in. Pb	$\frac{1}{4}$-in. Pb	0.62±0.07
$\frac{1}{2}$-in. Pb	$\frac{1}{4}$-in. Pb	1.07±0.1
$\frac{1}{4}$-in. Pb	$\frac{1}{4}$-in. Pb	0.28±0.05

$\frac{1}{4}$-in. Pb absorbers placed in front of both telescopes.

mesons, because of the motion of the decaying mesons. A meson at rest decaying into two gamma-rays, emits them in opposite direction. But when this is seen from a system in which the meson has a total energy E, then the included angle β varies between π and $2\sin^{-1}(1/E)$ with a probability which favors the small angles tremendously. The median angle is $2\sin^{-1}[2/(3E^2+1)^{\frac{1}{2}}]$. E is the total meson energy in units of its rest energy.

For 70-Mev mesons the minimum angle of β is 84° and the median angle 92°. Since the distribution is so heavily peaked, not much error is introduced if one assumes, as is done in the following, that to an angle β corresponds a unique energy, that of the median angle. Therefore a measurement of the distribution in β is a measure of the distribution in energy of the neutral mesons, although the angular resolution of our telescopes is insufficient to give more than a glimpse of the energy distribution. We have included in Fig. 3 curves in which the observed[4] energy distributions of the π^+-meson made by the same x-rays on hydrogen are transformed into distributions in β and arbitrarily normalized. All corrections due to scattering and angular resolution are omitted. The general shape of the curves is certainly well reproduced by the experiment. It is

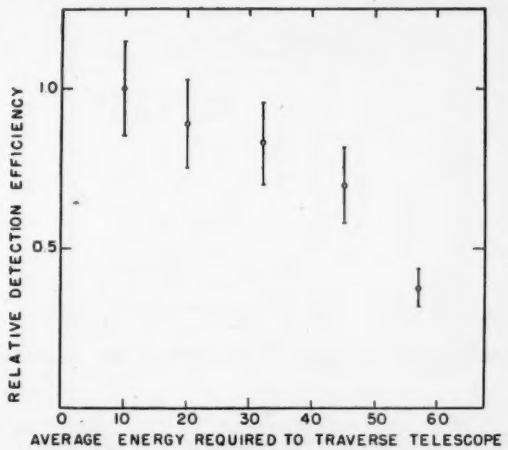

FIG. 2. Absorption of conversion electrons in aluminum. The energy includes the average radiation loss.

[4] Bishop, Cook, and Steinberger (to be published).

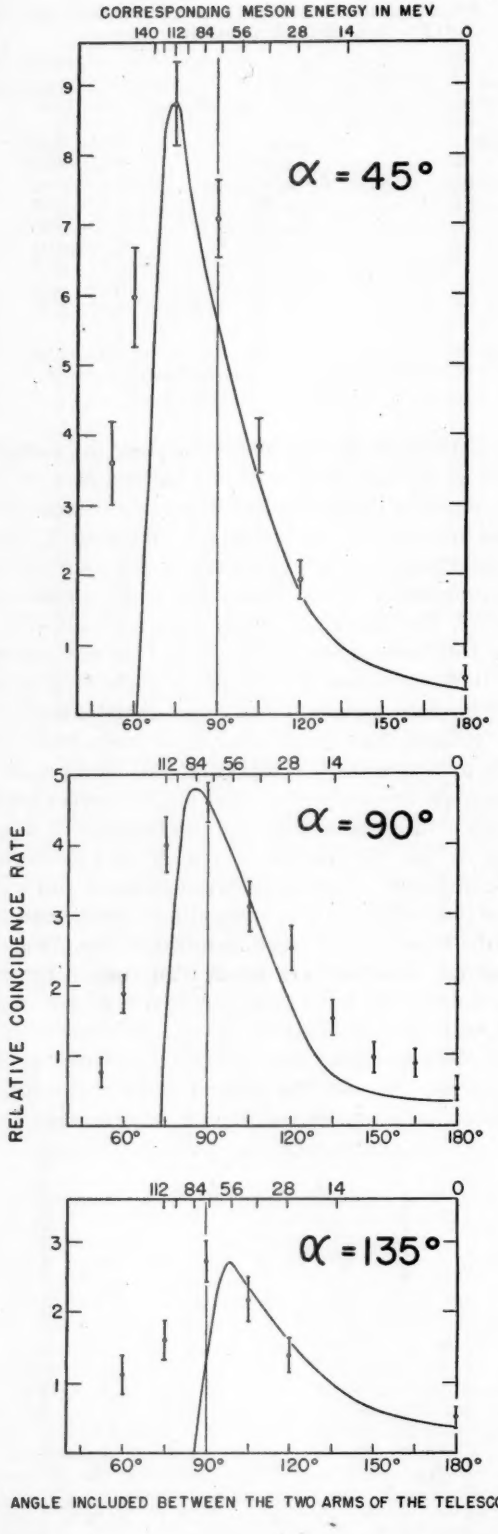
CORRESPONDING MESON ENERGY IN MEV
140 112 84 56 28 14 0
α = 45°
α = 90°
α = 135°
RELATIVE COINCIDENCE RATE
60° 90° 120° 150° 180°
ANGLE INCLUDED BETWEEN THE TWO ARMS OF THE TELESCOPE

FIG. 3. Variation of coincidence rate with the included angle β between the two arms of the telescope. The curves are those expected on the assumption that the gamma-rays are the decay products of a neutral meson, emitted with the same energy distribution as are π^+-mesons from hydrogen. The curves are arbitrarily normalized for each angle α.

therefore clear that if the gamma-rays are the decay product of intermediate particles, these particles must move with velocities of the order of $v/c \simeq 0.8$. Excited nucleons of this velocity cannot be produced by x-rays of 330 Mev; the particles must therefore have an intermediate mass. Furthermore, it is possible to see that the decay must be into only 2 photons, since the expected angular distributions for a decay into more than two photons would not show a valley for small angles β.

The distribution in the angle α of the beam with the plane of the telescope shown in Fig. 4, is interesting chiefly because of the difference between this distribution and the angular distribution of π^+-photo-mesons[5] from either carbon or hydrogen targets. This is not particularly surprising, since various theories also give quite different results for charged and neutral mesons.

V. HYDROGEN CROSS SECTION AND TOTAL CROSS SECTION

At one setting of the telescopic angles, $\alpha=\beta=90°$, we have compared the cross sections of hydrogen and carbon. This was done by comparing the count from a polyethylene (CH_2) block and a perforated carbon block of the same size and carbon content as the CH_2. The result is: $\sigma_{H\pi^0}/\sigma_{C\pi^0}=0.12\pm0.03$. This again differs from the results for positive mesons, where $\sigma_{H\pi^+}/\sigma_{C\pi^+} \simeq 0.55$. The difference is probably in part caused by the fact that both neutrons and protons can contribute to neutral meson production, but only protons to π^+-production. In part, it may also be possible to ascribe this to the same phenomenon which, according to Chew,[6] is responsible for the large hydrogen-carbon ratio for the positive mesons. In the case of π^+-production, the reaction is inhibited by the fact that, when the proton is changed into a neutron, there is an oversupply of neutrons in the immediate neighborhood and the number of states available to it is small because of the Pauli principle. This is not significant in the neutral case because the nucleon's charge does not change.

The curves in Fig. 3 can be integrated to yield a total cross section for beryllium. $\sigma_{Be}=7.5\times10^{-28}$ cm^2 per Q, while for carbon and hydrogen, assuming the same angular distribution, $\sigma_C=10\times10^{-28}$ and $\sigma_H=1.3\times10^{-28}$ cm^2 per Q. The absolute x-ray intensity is known[7] to about 10 percent, but the efficiency of the detecting system only to within a factor of two, so that there is a corresponding error in the above cross sections. The hydrogen cross section is approximately the same as that for π^+-production;[5] those for carbon and beryllium are somewhat higher.[8]

One might assume that the charge of the meson would play an important role in the production of mesons in the electromagnetic field of the photon. This

[5] J. Steinberger and A. S. Bishop, Phys. Rev. **78**, 493 (1950).
[6] G. Chew (private communication).
[7] Blocker, Kenney, and Panofsky (to be published).
[8] McMillan, Peterson, and White, Science **110**, 579 (1949).

is contradicted by the observed angular distribution of π^+-mesons produced by photons in H_2. The angular distribution indicates that the principal process responsible for charged meson production is the interaction of the photon with the spin of the nucleon. If the neutral meson has the same transformation properties as the charged, it then appears plausible that the production cross sections in hydrogen should be comparable, as seems to be the case. However, actual calculations on the basis of pseudoscalar theory, both in the classical and in the perturbation theory approximation, which give a reasonable angular distribution for the π^+-production, give smaller values for neutral meson production. Whether or not this is a new difficulty in a theory which already has several, is not clear. From a less restricted point of view it is not a surprising result.

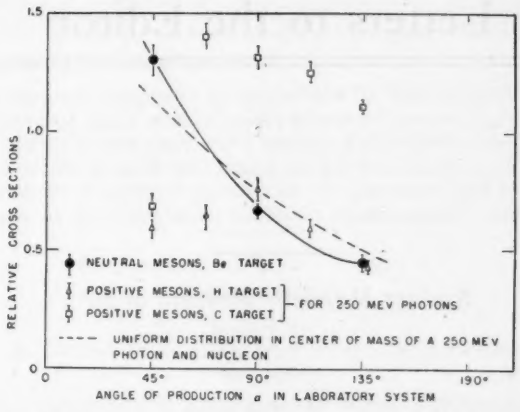

FIG. 4. Variation with the angle α between the plane of the telescope and the beam. Each point represents an integral over the angle β.

VI. SUMMARY

In the bombardment of various nuclei by 330-Mev x-rays, photons with the following properties are emitted:

(1) At least two are emitted in coincidence.
(2) They each have an average energy of about 100 Mev.
(3) The Z dependence of the production indicates that they have their origin in a nuclear interaction, and not in the Coulomb field.
(4) The threshold for their production is at least 150 Mev.
(5) The angular correlation of the photons shows that they are emitted in pairs as the only decay products of particles moving with velocities of the order of $v/c=0.8$, and therefore of intermediate mass.
(6) The total cross section for production from hydrogen is about the same as that for production of π^+-mesons; other light nuclei cross sections are somewhat higher than those for the positive mesons.

It is clear from these properties that the gamma-rays are the decay products of neutral mesons. Since spin $\frac{1}{2}$, and spin 1 mesons are forbidden to decay into two photons,[1] the spin must be zero, excluding the possibility of very high intrinsic angular momenta. It seems reasonable, and it is in good agreement with all observations, to assume that both charged and neutral mesons are of the same type. It then follows from the angular distribution of the x-ray produced π^+-mesons, and the high cross sections for making neutral mesons by x-rays, that the π-meson is a pseudoscalar. This remark applies, of course, only to the character of the meson, and not to any particular field theory for the interaction of mesons with nucleons.

All phases of this experiment have been discussed with Professor Edwin McMillan and his advice has been of great help. The bombardments were carried out by the synchrotron crew under the direction of W. Gibbons.

Letters to the Editor

PUBLICATION of brief reports of important discoveries in physics may be secured by addressing them to this department. The closing data for this department is five weeks prior to the date of issue. No proof will be sent to the authors. The Board of Editors does not hold itself responsible for the opinions expressed by the correspondents. Communications should not exceed 600 words in length.

Nuclear Magnetic Moment of Sc^{45}

D. M. HUNTEN
Radiation Laboratory, McGill University, Montreal, Quebec, Canada
April 24, 1950

RESONANCE in Sc^{45} has been found in a saturated (~0.1 molar) acid solution of $ScCl_3$, and the magnetic moment measured as 4.7560 ± 0.0002 nuclear magnetons. The search was conducted by slow, automatic variation of the magnetic field, which was stabilized to about one part in 100,000. A twin-T bridge with lock-in amplifier and recording meter having a 2-sec. response time was used; the signal-to-noise ratio was about 20.

The proton signal for comparison was produced by a regenerative detector; the two samples were adjacent in the magnetic field, and allowance was made for the small difference between the fields at the two samples, amounting to about 0.006 percent.

The frequency ratio so obtained is $Sc/H = 0.242939 \pm 0.000003$.

Using the value 5.58494 ± 0.00016 of Hipple, Sommer, and Thomas[1] for the gyromagnetic ratio of the proton, and including a diamagnetic correction of 0.151 percent, the gyromagnetic ratio of Sc^{45} is found to be $g(Sc^{45}) = 1.35885 \pm 0.00005$.

Since the spin[2,3] is 7/2, the magnetic moment is as quoted above. The spectroscopic value +4.8 obtained by Kopfermann and Wittke[4] is in very good agreement with this.

The author is indebted to Professor J. S. Foster, for help and encouragement, and to Dr. D. A. Anderson and Mr. M. Bloom for assistance in construction of the apparatus.

Part of the work was aided by a Fellowship from the National Research Council of Canada.

[1] Hipple, Sommer, and Thomas, Phys. Rev. **76**, 1877 (1949).
[2] H. Schüler and T. Schmidt, Naturwiss. **22**, 758 (1934).
[3] H. Kopfermann and E. Rasmussen, Zeits. f. Physik **92**, 82 (1934).
[4] H. Kopfermann and H. Wittke, Zeits. f. Physik **105**, 16 (1937).

Search for Nuclear Energy Levels in C^{13} *

D. W. MILLER
University of Wisconsin, Madison, Wisconsin
April 26, 1950

IN 1935 Paton[1] determined the energies of four groups of protons produced by the bombardment of boron with alpha-particles. Two of these groups were believed to correspond to levels of the residual nucleus in the $B^{10}(\alpha,p)C^{13}$ reaction at 4.9 and 6.0 Mev excitation energies.[2] Investigating the same reaction using enriched B^{10} samples, Creagen[3] reported possible evidence for a level in C^{13} at 5.6 Mev. One might expect that these levels would also appear as resonances in the total cross section of carbon for fast neutrons. Earlier measurements of this cross section[4-6] did not show resonances corresponding to these levels, but there was a possibility that narrow resonances had been missed because of the wide spacing of the experimental points.

In the present investigation the total cross section of carbon for fast neutrons was determined for neutron energies between 20 kev and 1360 kev. By means of a transmission experiment of the type previously described,[7] the cross section was measured with neutrons produced by the $Li^7(p,n)Be^7$ reaction. The neutron energy spread was about 13 kev below 900 kev neutron energy and 20 kev above this energy. Experimental points were taken at intervals of 10 kev below 900 kev and 22 kev above this energy. A smooth monotonic decrease in the total cross section from 4.8 barns at 20 kev neutron energy to 2.4 barns at 1360 kev neutron energy was obtained. Throughout this energy region the standard statistical error in the cross section was less than five percent. The observed total cross section agrees with the results of the Minnesota group[6,8] and of Wattenberg[4] to within three percent, except for one point obtained by Lampi *et al.*,[5] at 1340 kev which is nine percent lower than the present measurement.

If resonances were to be observed corresponding to possible levels in C^{13} listed by Hornyak and Lauritsen[9] at 5.0 and 6.0 Mev excitation energies, they should appear at neutron energies of 130 kev and 1210 kev. On the basis of Breit-Wigner resonance theory, the variation in cross section for such resonances should be at least 24 barns and 2.5 barns respectively. No resonances were observed; the maximum deviation of the experimental points from the smooth curve was about 0.5 barn for neutrons below 400 kev and about 0.2 barn above this energy. On the basis of the resolution used, it may be estimated that the natural width of such levels if they exist is less than five kev.

The author wishes to thank Professor H. T. Richards for suggesting this investigation.

* Work supported by the AEC and the Wisconsin Alumni Research Foundation.

[1] R. F. Paton, Phys. Rev. **47**, 197 (1935).
[2] M. S. Livingston and H. A. Bethe, Rev. Mod. Phys. **9**, 299 (1937).
[3] R. J. Creagen, Phys. Rev. **76**, 1769 (1949).
[4] Fields, Russell, Sachs, and Wattenberg, Phys. Rev. **71**, 508 (1947).
[5] Lampi, Freier, and Williams, Phys. Rev. **76**, 188 (1949).
[6] D. H. Frisch, Phys. Rev. **70**, 589 (1946).
[7] Barschall, Bockelman, Peterson, and Adair, Phys. Rev. **76**, 1146 (1949).
[8] Freier, Fulk, Lampi, and Williams, Phys. Rev. **78**, 508 (1950).
[9] W. F. Hornyak and T. Lauritsen, Rev. Mod. Phys. **20**, 209 (1948).

Detection of Magnetic Resonance by Ion Resonance Absorption

H. SOMMER AND H. A. THOMAS
National Bureau of Standards, Washington, D. C.
April 24, 1950

BY combining the techniques of nuclear resonance absorption[1] and the omegatron,[2] the cyclotron resonance of H_2^+ ions has been observed dynamically with an oscillating detector[3] coupled directly to an oscilloscope.

If an r-f voltage satisfying the cyclotron relationship $\omega = eH/Mc$ is applied to two parallel plates between which ions are produced and trapped as in the omegatron,[2] the ions will absorb energy from the r-f field. If these parallel plates are made part of the capacitance of a parallel resonant circuit, the energy absorbed by the ions can be detected in exactly the same manner as nuclear resonance absorption. Whereas nuclear resonance absorption is detected by the power absorbed in the inductance, the cyclotron resonance here described produces a power loss in the capacitance.

While no effort was made to obtain maximum sensitivity, it can be shown that this method of detection is considerably more sensitive than detection of a resonance directly by collecting the resonant ions. Assuming that the least ion current that can be detected with an electrometer is 10^{-15} amp. and that the H_2^+ ions have a final energy corresponding to 500 v, calculations show that the increase in signal-to-noise ratio using ion resonance absorption should at least be of the order of 50. This could be improved by increasing the size of the tube or the magnetic field intensity.

The sensitivity, simplicity, and speed of response of this method of detection should make it highly desirable for any application where the principle of the omegatron might be used, such as high resolution mass analyzers, analytical mass spectrometers, and mass spectrometer type leak detectors. Furthermore, the ion resonance absorption method of detection makes possible the use of the omegatron for measuring and regulating weak magnetic fields by applying the same techniques used with nuclear resonance absorption.

[1] Bloembergen, Purcell, and Pound, Phys. Rev. **73**, 679 (1948).
[2] Hipple, Sommer, and Thomas, Phys. Rev. **76**, 1877 (1949).
[3] N. J. Hopkins, Rev. Sci. Inst. **20**, 401 (1949).

On the Possibility of Electric Dipole Moments for Elementary Particles and Nuclei

E. M. PURCELL AND N. F. RAMSEY
Department of Physics, Harvard University, Cambridge, Massachusetts
April 27, 1950

IT is generally assumed on the basis of some suggestive theoretical symmetry arguments[1] that nuclei and elementary particles can have no electric dipole moments. It is the purpose of this note to point out that although these theoretical arguments are valid when applied to molecular and atomic moments whose electromagnetic origin is well understood, their extension to nuclei and elementary particles rests on assumptions not yet tested.

One form of the argument against the possibility of an electric dipole moment of a nucleon or similar particle is that the dipole's orientation must be completely specified by the orientation of the angular momentum which, however, is an axial vector specifying a direction of circulation, not a direction of displacement as would be required to obtain an electric dipole moment from electrical charges. On the other hand, if the nucleon should spend part of its time asymmetrically dissociated into opposite magnetic poles of the type that Dirac[2] has shown to be theoretically possible, a circulation of these magnetic poles could give rise to an electric dipole moment. To forestall a possible objection we may remark that this electric dipole would be a polar vector, being the product of the angular momentum (an axial vector) and the magnetic pole strength, which is a pseudoscalar in conformity with the usual convention that electric charge is a simple scalar.

The argument against electric dipoles, in another form, raises directly the question of parity. A nucleon with an electric dipole moment would show an asymmetry between left- and right-handed coordinate systems; in one system the dipole moment would be parallel to the angular momentum and in the other, antiparallel. But there is no compelling reason for excluding this possibility. It would not be the only asymmetry of particles of ordinary experimence, which already exhibit conspicuous asymmetry in respect to electric charge. Although magnetic poles were used above as an illustration of a particular mechanism by which a nuclear electric dipole could arise, this is, of course, not the only possibility.

The question of the possible existence of an electric dipole moment of a nucleus or of an elementary particle in view of the above becomes a purely experimental matter. The evidence from most past experiments on molecules, atoms, nucleons, and elementary particles is not as conclusive as one might suppose. Most past experiments are in fact very insensitive to the effects of a nuclear electric dipole, because of the smallness of the electric field at the position of a charged nucleus or the antisymmetric nature of the electric dipole potential. We have analyzed a number of experiments including conversion of ortho- to parahydrogen, depolarization of neutron beams, ionization by neutrons, relaxation times of nuclei in liquids, nuclear scattering of neutrons, hyperfine structure studies, the Lamb-Retherford experiment, and the experiments on the interaction of electrons and neutrons. Non-scattering experiments on charged nuclei are particularly insensitive to the existence of an electric dipole moment and even the most favorable would not have revealed an electric dipole moment smaller than the charge of the electron multiplied by a distance D less than 10^{-13} cm. The scattering experiments[3,4] to detect an electron-neutron interaction are by far the most sensitive; the results of Havens, Rabi, and Rainwater[3] would correspond to a D of 3×10^{-18} cm if they were due to an electric dipole moment.

We are now undertaking, in collaboration with Mr. James H. Smith, an experiment which should directly measure the electric dipole moment of the neutron if it has a value of D of approximately the above magnitude. The experiment will utilize a neutron beam magnetic resonance[5] apparatus of high resolution[6] to detect a possible shift of the neutron precession frequency upon the application of a strong electric field.

The authors wish to thank Mr. Smith for suggesting an important correction to our original calculation on the neutron-electron interaction experiment.

[1] A typical argument is given by H. A. Bethe, *Elementary Nuclear Theory* (John Wiley and Sons, Inc., New York).
[2] P. A. M. Dirac, Phys. Rev. **74**, 817 (1948).
[3] Havens, Rabi, and Rainwater, Phys. Rev. **72**, 634 (1947).
[4] E. Fermi and L. Marshall, Phys. Rev. **72**, 1139 (1947).
[5] L. W. Alvarez and F. Bloch, Phys. Rev. **57**, 111 (1940).
[6] N. F. Ramsey, Phys. Rev. **76**, 996 (1949).

Supernovae*

L. B. BORST
Brookhaven National Laboratory, Upton, Long Island, New York
April 27, 1950

SUPERNOVAE of type I are characterized by: (a) a high intensity maximum of 20 to 30 days duration; (b) an exponential tail to the light curve of half-life 55 days ($\Delta m=0.0137\pm0.0012$ magnitudes per day;[1] (c) an integrated visual light emission of nearly 10^{49} ergs;[1] (d) a residual gaseous shell of low hydrogen content expanding at a velocity[2] of 1300 km/sec. and radiating 10^{36} ergs/sec. visible light about 900 years later.[3]

These characteristics may be accounted for by the following proposed mechanism. The original star, of mass many times the sun, e.g., $15M_\odot$, undergoes gravitational contraction after burning its hydrogen. As the contraction progresses the central temperature will rise until a new reaction occurs. At a temperature of 2 to 3×10^9 °C a second-order endothermic reaction will occur between alpha-particles

$$2\alpha\rightarrow Be^7+n, \quad Q=-18.6 \text{ Mev}.$$

This reaction absorbs energy at the center of the star, permitting rapid gravitational collapse. The reaction rate can be calculated by methods of simple chemical kinetics since barrier penetration is a negligible correction at an energy of 19 Mev.

$$Z=N^2r^2(4\pi kT/m)^{\frac{1}{2}}e^{-(Q/2kT)},$$

where Z is the number of processes per second cm^3; N is the number of particles per cm^3; r and m are the radius and mass of the alpha-particle (1.6×10^{-13} cm and 6.6×10^{-24} g); Q is the reaction threshold; k is the Boltzman constant and T is the temperature. It may be noted that the reaction velocity per unit volume increases as the square of the helium concentration and exponentially with the temperature. The reaction will therefore accelerate under conditions of gravitational collapse, so that the star may collapse in a time approaching free fall.

The reaction will proceed until there are sufficient concentrations of the reaction products to produce the reverse reaction. The expression at equilibrium may be given

$$K=[Be^7][n]/[He]^2,$$

where the entries denote atomic concentrations per unit volume. Since neutrons will be absorbed rapidly in a system containing

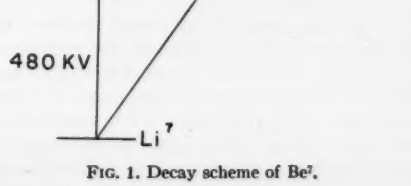

FIG. 1. Decay scheme of Be^7.

heavy elements and heat is removed in the formation of Be^7, the equilibrium will favor the production of Be^7. Even if the system achieves equilibrium, the equilibrium will be displaced toward Be^7 by increased pressure, or temperature.

The reaction may always be rate controlled, however, and may never reach equilibrium during the collapse process.

Neutrons generated will be absorbed by the heavy elements present in the star. Nitrogen in particular has a (n,p) resonance of 0.1×10^{-24} cm² cross section at 550 kev. Since the most probable energy at 3×10^9 °C is 260 kev, and nitrogen may be expected to be present to an extent of 0.1 to 1 percent, nitrogen will be an important absorber.

After collapse the star becomes unstable and explodes, driving off a considerable fraction of its mass as an expanding gas cloud, probably leaving a core in a highly degenerate state. The exact mechanism of this explosion is not understood. Several possible mechanisms are: (a) the formation of a highly degenerate core, driving the outer layers away by radiation pressure;[4] (b) accelerated decay of Be^7 at increased electron density and the regeneration of helium from Li^7 and hydrogen; (c) rotational instability of the star.

The expanding gas envelope carries with it the Be^7 and C^{14} produced by the reaction. As the density drops, the thermal energy is radiated away as the initial maximum of the light curve. Thereafter the energy source is Be^7 ($T=52.9$ days), decaying according to the decay scheme of Fig. 1. The energy source will follow an exponential curve unless, (a) the diffusion of light to the surface of the gas envelope takes a long time compared to the radioactive life or, (b) the gas envelope becomes so tenuous as to permit appreciable loss of the 480-kev gamma-rays. In the case of two well-known supernovae, observed in 1054 A.D. and in 1937 in extragalactic nebula IC 4182, these restrictions were not found to be limiting from 40 days to 600 days past maximum. The quantity of Be^7 required for these stars was 3×10^{32} g.

After the decay of Be^7, the energy source may progress through intermediate periods, representing fortuitous neutron induced activities, but will rapidly approach the period of C^{14} ($T_{\frac{1}{2}}=4700$ years). In the case of the supernova of 1054 A.D. the gaseous envelope, the Crab nebula, is readily observed.[3] Its energy source corresponds to 10^{32} g C^{14}. Assuming an initial mass of 4×10^{34} g, the nebula should contain about 0.2 percent C^{14} and about 0.7 percent Li^7. Spectroscopic data show an unusually low abundance of hydrogen (<5 percent) but show helium, nitrogen and oxygen.[5] The abundances of these elements have not been derived from the spectrum.

Experiments will be initiated to measure the Be^7 yield from the (α,α) reaction. A more extensive discussion will be presented for publication in this Journal.

* This work was done at Brookhaven National Laboratory under the auspices of the AEC.

[1] W. Baade, Astrophys. J. **88**, 285 (1938); Astrophys. J. **102**, 309 (1945); F. L. Whipple, Proc. Am. Phil. Soc. **81**, 253 (1939).
[2] Duyvendak, Mayall, and Oort, Pub. Ast. Soc. Pac. **54**, 91 (1942).
[3] W. Baade, Astrophys. J. **96**, 188 (1942).
[4] J. R. Oppenheimer and H. Snyder, Phys. Rev. **56**, 455 (1939).
[5] R. Minkowski, Astrophys. J. **96**, 199 (1942).

The Chromium Isotope of Mass 55

DANIEL R. MILLER
Department of Chemistry and Laboratory of Nuclear Studies, Cornell University, Ithaca, New York
April 21, 1950

THE isotope of chromium of mass number 55 has been reported by several investigators to be radioactive, with half-lives of 1.3, 1.6, and 2.3 hr.[1] These observations resulted from the bombardment of chromium with deuterons and slow neutrons, and the activity of about two-hour half-life was attributed to Cr^{55} resulting from a (d,p) or (n,γ) reaction. Most of these reports stated that the activity in question was weak. The absence of a chromium activity of about two-hour half-life among the spallation products of copper[2] and arsenic[3] with high energy deuterons has emphasized the need for further investigation of this assignment.

In order to clarify the situation, 6.0 g of manganese dioxide was irradiated for 2.7 hr. with neutrons of maximum energy 16 Mev, produced by bombarding lithium with 56 microampere-hours of 1.4 Mev deuterons. The irradiated MnO_2 was dissolved in a nitric acid-hydrogen peroxide mixture, inactive Cr^{+3} added as carrier, and the chromium fraction chemically separated and purified. The chemical procedure included $Cr(OH)_3$ precipitation, removal of manganese as MnO_2 from concentrated nitric acid, and several extractions of peroxychromic acid from dilute nitric acid into diethyl ether. One-tenth of the purified chromium fraction was mounted and counted with an end-window (*ca.* 3 mg mica/cm²). Geiger-Müller tube at about 10 percent geometric efficiency. The activity observed 2.5 hr. after the end of the bombardment was not appreciably different from the background rate; a maximum of five counts per minute might have been due to radioactivity in the chromium sample. It should be pointed out that the counting system used would not have detected electrons of energy less than about 0.07 Mev. One would certainly expect, however, that a β^--emitter of several hour half-life would emit electrons having an energy appreciably greater than 0.07 Mev. Seren, Friedlander, and Turkel[1] report a mass absorption coefficient of 8.3 cm² per g of aluminum for the electrons of their 1.3-hr. activity, corresponding to an electron energy of one to two Mev.

The only unstable chromium isotope which could have resulted from this irradiation is Cr^{55}, produced by a (n,p) reaction on Mn^{55} (the only stable manganese isotope). The results of this investigation (assuming 100 percent counting efficiency) indicate that, if Cr^{55} has a half-life in the previously reported range (1.3 to 2.3 hr.), the cross section for its formation by $Mn^{55}(n,p)$ is less than 5×10^{-5} barn. Alternatively, if a cross section of greater than 10^{-2} barn is assumed, Cr^{55} would have to possess a half-life of less than 15 min. or greater than 100 days in order to have escaped detection.

Nelson and Pool[4] have recently reported results in agreement with these findings. They found no indication of a two-hour chromium isotope by a (d,p) reaction on Cr^{54}—enriched Cr_2O_3, nor by a (n,α) reaction on Fe^{58}-enriched Fe_2O_3. Present evidence therefore seems to offer no substantiation to the assignment of a one- or two-hour activity to Cr^{55}.

The author wishes to thank Mr. W. B. Dayton for his cooperation in performing the cyclotron bombardment.

[1] Seren, Friedlander, and Turkel, Phys. Rev. **72**, 888 (1947); Amaki, Iimori, and Sugimoto, Phys. Rev. **57**, 751 (1940); Dickson, McDaniel, and Konopinski, Phys. Rev. **57**, 351 (1940).
[2] Miller, Thompson, and Cunningham, Phys. Rev. **74**, 347 (1948).
[3] H. H. Hopkins, Jr., Phys. Rev. **77**, 717 (1950).
[4] M. E. Nelson and M. L. Pool, Phys. Rev. **77**, 682 (1950).

Temperature Dependence of the Energy Gap in Monatomic Semiconductors*

H. Y. FAN
Purdue University, Lafayette, Indiana
April 20, 1950

EXPERIMENTAL evidence indicates that the energy gap in a semiconductor depends upon the temperature. The long wave-length edge of the optical absorption band for both silicon[1] and germanium[2] shifts toward shorter wave-length as the temperature is decreased. The threshold of photoelectric effects in these materials shows corresponding shifts.[3] Furthermore, the variation of intrinsic concentrations of free electrons and holes in silicon, calculated from resistivity and Hall effect data, was found to lead to a temperature dependence of the energy gap.[4]

The volume of the crystal and the excitation of the lattice vibrations change with temperature. Both these effects can produce shifts in the energy levels, thereby changing the energy

TABLE I. Temperature dependence of the energy gap.

	C_c (ev)	C_f (ev)	β (degree^{-1})	$\partial E_G/\partial T$ (ev/degree) Eq. (6)	$\partial E_G/\partial T$ (ev/degree) Eq. (4)+Eq. (6)	$\partial E_G/\partial T$ (ev/degree) experimental
Silicon	9.75	16.9	10×10^{-6}	-1.78×10^{-4}	-5.3×10^{-4}	-4.7×10^{-4}[a] -3.0×10^{-4}[b]
Germanium	2.55	3.6	23×10^{-6}	-0.95×10^{-4}	-1.2×10^{-4}	-4.6×10^{-4}[c]

[a] See reference 1.
[b] See reference 4.
[c] See reference 2.

gap. The effect of volume dilation has been recently considered by Shockley and Bardeen.[5] We shall consider the effect of lattice vibrations, following the method used by Fröhlich and his co-workers[6] for polar crystals. The second-order perturbation gives

$$E(K)=E_0(K)+\sum_q\left[\frac{|H'_{K-q,K}|^2}{E_0(K)-E_0(K-q,n_q+1)}+\frac{|H'_{K+q,K}|^2}{E_0(K)-E_0(K+q,n_q-1)}\right], \quad (1)$$

where K is the electron wave number, n_q is the quantum number of the lattice vibration mode with wave number q, the subscript 0 refers to the unperturbed solution. The matrix elements have the usual expression.

$$H'_{K\pm q,K}=\mp i\frac{1}{N^{\frac{1}{2}}}\frac{2}{3}Cq\left(\frac{\hbar}{2M\omega_q}\right)^{\frac{1}{2}}\begin{cases}(n_q)^{\frac{1}{2}}\\(n_q+1)^{\frac{1}{2}},\end{cases} \quad (2)$$

where N is the total number of unit cells, M is the atomic mass, and C is approximately constant for longitudinal modes and zero for transverse modes. For $kT>\hbar\omega_q$, the longitudinal acoustic waves give

$$E(0)-E_0(0)=-0.175C^2\Omega^{\frac{1}{3}}(mkT/\hbar^2Mc_l^2), \quad (3)$$

where Ω is the volume of the unit cell and c_l is the wave velocity. The value of C can be estimated from the mean free path due to lattice scattering as was done by Lark-Horovitz and Johnson.[7] For the conduction band C_c is to be estimated from electron mobility and m_e is the effective mass of the electrons. For the filled band C_f should be estimated from hole mobility and m_f is the effective mass of the holes with negative sign.

The more general variation method[6] gives an expression similar to (1) except that in the denominators $E_0(K)$ is replaced by $E(K)$. The result reduces (3) by approximately 20 percent. On the other hand, materials with a diamond structure, such as silicon and germanium, have optical branches of vibration. The frequencies of these vibrations are difficult to estimate, but it can be shown that their effect is less than one-third of (3). We shall take (3) as the first approximation. The reduction of the energy gap is then

$$\partial E_G/\partial T=-0.175(\Omega^{\frac{1}{3}}k/\hbar^2Mc_l^2)[m_eC_e^2+|m_f|C_f^2]. \quad (4)$$

The change in energy gap with lattice dilation as given by Shockley and Bardeen[5] is

$$E_{1G}\equiv\partial E_G/\partial(\Delta V/V)=E_{1e}-E_{1f}, \quad (5)$$

where

$$E_{1e}=\tfrac{2}{3}C_e, \quad E_{1f}=\tfrac{2}{3}C_f.$$

This effect alone should give

$$\partial E_G/\partial T=\tfrac{2}{3}(C_e-C_f)\beta; \quad (6)$$

where β is the volume coefficient of expansion. The net result should be the sum of (4) and (6).

The results of the calculations are presented in Table I. To facilitate comparison, the same values for C_e, C_f, β_{Si}, and c_l are adopted as used by Shockley and Bardeen. The value of β_{Ge} is taken from the tables of Landolt and Börnstein. It is seen that for silicon the lattice vibrations have larger effect in producing the temperature variation of the energy gap than the lattice dilation. For germanium it is smaller but not negligible. The calculated value for silicon agrees well with the experimental result of optical measurements. For germanium the calculated value seems to be too low. The optical measurements are now being repeated with greater precision. It must be pointed out that the values of C_e and C_f were calculated by taking the free electron mass for both m_e and m_f. More accurate knowledge of C's and m's is necessary for better estimation of $\partial E_G/\partial T$.

* Work assisted by a Signal Corps contract.
[1] M. Becker and H. Y. Fan, Phys. Rev. 76, 1531 (1949).
[2] Measurement by M. Becker.
[3] M. Becker and H. Y. Fan, Phys. Rev. 78, 301 (1950). Similar results have been reported by F. S. Goucher of Bell Telephone Laboratories.
[4] G. L. Pearson and J. Bardeen, Phys. Rev. 75, 865 (1949).
[5] W. Shockley and J. Bardeen, Phys. Rev. 77, 407 (1950).
[6] Fröhlich, Pelzer, and Zienau, Phil. Mag. 41, 221 (1950). The author is indebted to Professor Fröhlich for discussions.
[7] K. Lark-Horovitz and V. Johnson (private communication).

On the Origin of the Cosmic Radiation from the Sun

K. O. KIEPENHEUER
Yerkes Observatory, University of Chicago, Williams Bay, Wisconsin
March 27, 1950

IT has been shown by Forbush,[1] Ehmert[2] and others that from certain solar flares in suitable heliographic positions there originates cosmic radiation which can be observed on the earth's surface. The intensity is of the order of 1 particle/(cm^2-sec.), the energy of the particles may be as large as 5×10^9 ev. The maximum of cosmic-ray intensity is often reached ½ to 2 hr. after the intensity maximum of the flare itself (H_α).[3] Several explanations have been proposed: Swann[4] thinks that potential differences of the order of 10^9 to 10^{10} volts can be induced by the growth of magnetic fields in sunspots, and Bagge and Biermann[5] think that they can be induced by the observed relative movement of the spots with their fields. But we must not forget that the solar atmosphere in which these fields have to be set up shows an electric conductivity of the order of 10^{15} e.s.u. so that the acceleration path is practically short-circuited. It is generally assumed that the conductivity depends strongly on the presence of a magnetic field. The effect of this field is practically canceled by an electric field which is set up by the movement of charges perpendicular to the magnetic field, as has been pointed out by Schlüter.[6] We shall therefore always use the conductivity in the absence of a magnetic field.

Menzel and Salisbury[7] suggest that a solar flare could be the source of electromagnetic radiation of extremely long wave-length ($\lambda\gtrsim3\times10^{10}$ cm) the field of which is decreasing as $1/r$ at the earth's distance. This field would then be able to accelerate elementary particles to an energy of 10^9 ev or more. But here too it can be said that this radiation would be unable to escape the solar corona, or even to propagate in the interplanetary space with its conductivity of $\sigma\approx10^{12}$ e.s.u. This same objection holds for a proposal of Alfvén[8] which supposes the existence of an electric field inside a solar corpuscular beam producing geomagnetic storms and aurora. His mechanism also cannot explain why the cosmic-ray outburst comes more or less simultaneously with the solar flare.

It seems essential that the acceleration mechanism should affect only a limited number of charged particles. It seems to us that this limitation is merely the result of the high conductivity

of an ionized gas. Every magnetic perturbation produces in its vicinity a shielding system of induction currents which flow, even in a compressible medium, in a layer of the thickness of the order of $c(\tau/\sigma)^{\frac{1}{2}}$ where τ is the period (e.g., in the case of periodic variations) of the field, and σ is the electric conductivity which is practically independent of the density, n, of electrons and ions. Consequently the thickness of the current bearing layer is independent of n, and the number of charged particles forming the shielding current is therefore proportional to n. The accelerations of charges that can be acquired in this way in the chromosphere ($n\approx10^{10}$ cm^{-3}, $\sigma\approx10^{14}$ e.s.u.) and in the corona ($n=10^6$ to 10^8 cm^{-3}, $\sigma\approx5\times10^{15}$ e.s.u.) are negligible but may be of some importance for the interpretation of some deviations from thermodynamic equilibrium observed in these layers. In interplanetary space ($n\approx10^3$ cm^{-3}, $\sigma\approx10^{12}$ e.s.u.), however, very small magnetic field perturbations will be able to accelerate the few effective charges to speeds approaching c. The acquired energies, of course, will never exceed the kinetic energy which a single charge can get when falling through the potential difference which follows from Faraday's law of induction.

After careful consideration of all known phenomena of the solar atmosphere, it seems that the required conditions are best fulfilled in the vicinity of those corpuscular beams which originate from solar flares, and reach the earth 26 hr. later if the heliographic position of the flare is approximately central. The speed of the beam is about 10^8 cm/sec. Measurements based on the absorption of the K line of Ca II or on the absorption of radio waves[9] ($\lambda=4.1$ m) give almost the same value of the density of $n\approx10^5$ electrons and of Ca^+ ions, the latter of which may include an unknown small number of protons. The diameter, D, of the beam may be of the order of 10^{10} cm in the neighborhood of the sun, and its length, L, equal to 4×10^{11} cm; this corresponds to an emission period of one hour. The flares, being observed mostly on the edges of single spots or between spots of opposite polarity, seem to occur in regions where the component of the magnetic field is mostly tangential. Therefore, the beam originating here should be magnetized perpendicular to its movement and should carry an induced current system flowing lengthwise along the beam and should conserve inside it the initial magnetic field.

The lifetime of this current system is practically unlimited because the transformation of electromagnetic energy into Joule heat takes a time of the order of $\sigma a^2/c^2$, where $\sigma\approx10^{13}$ e.s.u. and $a\approx10^{11}$ cm is the dimension of the current system. Only the thermal expansion, which we can ignore near the sun, dilutes the field sensibly on its way to the earth. Let us make the modest assumption that the energy density of the field, $H^2/8\pi$, does not exceed the beam's kinetic energy density, $\rho v^2/2$; which means that $H\lesssim1$ gauss. The beam leaving the solar corona will then be surrounded by an additional thin sheet of shielding current formed by ionized interplanetary matter ($n\approx10^3$ cm^{-3}, $\sigma\approx10^{12}$ e.s.u.). The induced potential difference, Φ, causing this current will be of the order of $10^{-8}LD(dH/dt)=10^{-8}DHv\approx10^{10}$ to 10^{11} volts. The number of electrons and protons contributing to the shielding current is so small as a result of the high conductivity that they can acquire along the beam an energy of nearly $\Phi/2$ ev. Protons and electrons, and also heavier ions, therefore, are ejected along the axis of the beam in both directions, that is, toward the sun and toward the earth. The total kinetic energy of the corpuscular beam, $LD^2\rho v^2/2$ amounts to 10^{29} ergs; the total energy of the current system may be of the same order. The total energy involved in a solar cosmic-ray burst is of the order of 6×10^{32} ergs which corresponds to an additional intensity of 1 particle /(cm^2-sec.) of 5×10^9 ev during 20 min. radiated through a surface of 10^{23} cm^2. It follows that only one out of every 10^7 charges of the induced current system has to become a cosmic-ray particle to fit the observed intensities.

The observed delay between maxima of the flare and cosmic-ray intensities of about one hour is readily explained on this model by the times of formation and traveling of the corpuscular beam from the chromosphere to the outer region of the corona. It is to be understood that charged particles of all masses acquire the same energy by the given acceleration method, hence this appears to provide a satisfactory stellar injection mechanism required in Fermi's[10] theory for interstellar cosmic-ray production.

[1] S. E. Forbush, Phys. Rev. **70**, 771 (1946).
[2] A. Ehmert, Zeits. f. Naturforschung **3a**, 264 (1948).
[3] A. Unsöld, Zeits. f. Astrophys. **26**, 176 (1949).
[4] W. F. G. Swann, Phys. Rev. **43**, 217 (1933).
[5] E. Bagge and L. Biermann, Naturwiss. **35**, 120 (1948).
[6] A. Schlüter, Zeits. f. Naturforschung (to be published).
[7] D. H. Menzel and W. W. Salisbury, Nucleonics **2**, No. 4, 67 (1948).
[8] H. Alfvén, Phys. Rev. **75**, 1732 (1949).
[9] A. Unsöld and S. Chapman, Observatory **69**, 219 (1949).
[10] E. Fermi, Phys. Rev. **75**, 1169 (1949).

Hyperfine Structure of $4^{1,3}F-nG$ of the Spectrum of Al II

S. SUWA
Institute of Science and Technology, Komaba, Meguroku, Tokyo, Japan
February 27, 1950

IN order to clarify the anomalous hyperfine structure (h.f.s.) of atomic spectra, which appears when the mutual distances of terms of a multiplet are comparable with the hyperfine splitting due to the nuclear spin, the h.f.s. of the lines 4^3P-4^3D of Al II was studied.[1] The extreme case, in which the triplet-singlet distance as well as the triplet separation of the upper term vanishes, will present a quite extraordinary h.f.s. As has been pointed out by Paschen[2] and by Goudsmit and Bacher[3] the $4^{1,3}F-nG$ series of Al II is a very typical example of such a case, but these experimental and theoretical investigations seem to require further study.

The spectrum of Al II was excited in a water-cooled aluminum hollow cathode-discharge tube, which was filled with helium. The helium pressure was adjusted until the $4^{1,3}F-nG$ series was emitted with such intensity that it could be photographed through an interferometer of high resolving power. The fine structure was examined by a quartz Lummer-plate (thickness=4.4 mm) and a Fabry-Pérot etalon. The observed structure of $4^{1,3}F-nG$ was found to be identical for $n=6$ and 7 within experimental error, the mean of $n=6$ and 7 being shown in Fig. 1(a).

4^1F-nG consists of two sharp components whose mutual distance could be measured with the accuracy of 0.001 cm^{-1}.

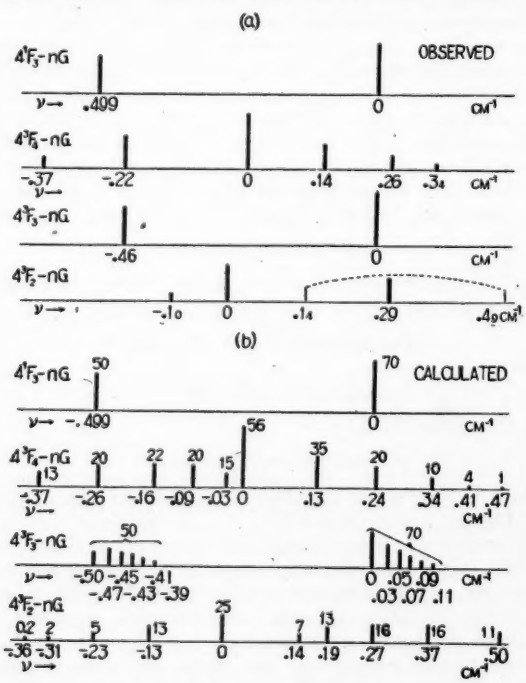

FIG. 1. Hyperfine structure of $4^{1,3}F-nG$ of Al II.
(a) Observed, (b) calculated.

4^3F_4-nG was newly found to have flag patterns on both sides of the central strongest component. 4^3F_3-nG was observed to consist of two components whose further details could not be detected, the accuracy of the measured mutual distance being of the order of 0.02 cm^{-1}. The two components of 4^3F_2-nG were also again found to have a further broadened structure though not well resolved, so that in Fig. 1(a) only the breadth of the component on the short wave-length side is shown.

Since the 4^1F_3 term, like other singlet terms, can be regarded as having no h.f.s., it can be assumed from the observed structure of 4^1F_3-nG that the nG term consists of two levels. This structure of the nG term is obtained when the singlet-triple distance as well as the triplet separation of the nG term is quite negligible compared with the hyperfine splitting due to the interaction between the nuclear spin **I** and the spin **s** of the 3*s*-electron. The nG term thus splits up into two levels depending on whether **I** and **s** are parallel or antiparallel, and the distance of the two levels is given by $3a$, since[4] $I=5/2$ for Al, where a denotes the coupling constant between **I** and **s**.

Based upon this assumption, the transformation matrix for the nG state from the ordinary $L-S$ coupling scheme to the representation of the state, in which the spin **I** is coupled to the spin **s** only, was obtained theoretically,[5] and, together with the general formulas for the multiplet intensity, enabled us to calculate numerically the intensities of all the hyperfine components of $4^{1,3}F-nG$. The structure thus calculated is shown in Fig. 1(b). As for the structure of the terms $4^3F_{4,3,2}$, the h.f.s. constants, A, were determined so as to obtain best agreement between the observed and the calculated structure, and thus the values $A(4^3F_4)=0.021$ cm^{-1}, $A(4^3F_3)=0.007$ cm^{-1} and $A(4^3F_2)=-0.029$ cm^{-1} were obtained. Although the terms 4^3F_J are perturbed by the terms belonging to a configuration other than $3s4f$, the effect of this perturbation upon the hyperfine splittings of 4^3F_J was found to be negligible. As is seen from Fig. 1, agreement between theory and experiment is satisfactory.

In conclusion the writer wishes to express his sincere thanks to Professor K. Murakawa for his cordial and continued guidance throughout this work. Thanks are also due Professor M. Kiuchi who took deep interest in this work.

[1] S. Suwa, Phys. Rev. **76**, 847 (1949).
[2] F. Paschen, Sitz. Preuss. Akad. Wiss. **23**, 502 (1932).
[3] S. Goudsmit and R. F. Bacher, Phys. Rev. **43**, 894 (1933).
[4] M. Heyden and R. Ritschl, Zeits. f. Physik **108**, 739 (1938).
[5] P. Güttinger and W. Pauli, Zeits. f. Physik **67**, 743 (1931).

Electrets

W. F. G. Swann
Bartol Research Foundation of the Franklin Institute, Swarthmore, Pennsylvania
April 25, 1950

THE object of this letter is to trace the consequences of the assumption that an electret consists of (1) a distribution of semipermanent polarization which decays with time, (2) a distribution of surface and volume charge which disappears according to ohmic conductivity having no relation to the decay of the polarization.[1]

The problem will be treated as a one-dimensional one, with a plate A at $x=0$ and a plate B at $x=l$, quantities at these two boundaries being designated by subscripts 1 and 2.

If P_x' is the resulting polarization, P_x the semipermanent polarization at x, K the dielectric constant, D_x the dielectric displacement, E_x the electric field, ρ_x, and ρ_{fx} the real and fictitious volume densities, σ_1, σ_{1f}, σ_2, σ_{2f} the real and fictitious surface densities, we have the following:

$$4\pi\rho_x=\mathrm{div}D_x, \quad (1) \qquad D_x=E_x+4\pi P_x', \quad (4)$$
$$P_x'=P_x+(K-1)E_x/4\pi, \quad (2) \qquad \rho_{xf}=-\mathrm{div}P_x', \quad (5)$$
$$\sigma_{1f}=P_{1n}', \quad (3) \qquad \sigma_{2f}=P_{2n}', \quad (6)$$

where P_{1n}' and P_{2n}' refer to the outwardly directed normal from the medium.

The difference of potential between the plates can easily be seen to be:

$$V=V_1-V_2=-2\pi\int_0^L(\rho_x+\rho_{xf})(2x-L)dx + 2\pi(\sigma_1-\sigma_2)L+2\pi(\sigma_{1f}-\sigma_{2f})L. \quad (7)$$

By use of the relations (1) to (6) and the fact that, for conducting plates, $4\pi\sigma_1=D_1$, (8); $4\pi\sigma_2=-D_2$, (9), we find without much difficulty

$$V=V_1-V_2=2\pi L/K\Big[\sigma_1-\sigma_2-2/L\int_0^L P_x dx + \int_0^L \rho_x dx-2/L\int_0^L x\rho_x dx\Big]. \quad (10)$$

We suppose that the plates of area A are connected by an external resistance R_e, which may be infinite in the limit. For the case of ohmic conductivity, with specific conductivity λ in the dielectric, we have, for the current density i flowing to the plate A from the resistance R_e,

$$i=(d\sigma_1/dt)+\lambda E_1, \quad (11); \quad i=-(d\sigma_2/dt)+\lambda E_2. \quad (12)$$

Using (2), (3), (8) and (9), and observing that the total current I is $-V/R_e$, we find that

$$-2V/AR_e=2I/A=2i =d/dt(\sigma_1-\sigma_2)+(4\pi\lambda/K)(\sigma_1-\sigma_2)-(4\pi\lambda/K)(P_1+P_2). \quad (13)$$

Incorporating $(\sigma_1-\sigma_2)$ as given by (10), and writing $C\equiv AK/4\pi L$, we readily find

$$\frac{dV}{dt}+\left(\frac{1}{R_eC}+\frac{4\pi\lambda}{K}\right)V+\frac{4\pi}{K}\int_0^L\frac{\partial P_x}{\partial t}dx - \frac{2\pi L}{K}\int_0^L\frac{\partial\rho_x}{\partial t}dx+\frac{4\pi}{K}\int_0^L x\frac{\partial\rho}{\partial t}dx + \frac{16\pi^2\lambda}{K^2}\int_0^L P_x dx-\frac{8\pi^2\lambda L}{K^2}(P_1+P_2) - \frac{8\pi^2\lambda L}{K^2}\int_0^L\rho_x dx+\frac{16\pi^2\lambda}{K^2}\int_0^L x\rho_x dx=0. \quad (14)$$

By using the equation of conductivity

$$(\partial\rho_x/\partial t)+\mathrm{div}\lambda E_x=0$$

and also (2) and (3), we find that (14) reduces to

$$(dV/dt)+(V/RC)+(4\pi/K)\int_0^L(\partial P_x/\partial t)dx=0, \quad (20)$$

where

$$1/R=(1/R_e)+(1/R_d)$$

and R_d is the ordinary internal resistance $(L/A\lambda)$ of the dielectric.

The interesting feature of (20) is the fact that it is independent of the initial distribution of volume and surface charges, and is the same as if these charges were zero. If we take the special case where P_x is of the form

$$P_x=P_{0x}e^{-\alpha t}$$

the solution of (20) for the case $V=V_0$ when $t=0$ is

$$V=\frac{4\pi\alpha RC}{(1-RC\alpha)}K[e^{-\alpha t}-e^{-t/RC}]\int_0^L P_{0x}dx+V_0e^{-t/RC}. \quad (21)$$

If the resistance is such as would be determined by ordinary ohmic conductivity in a substance of the normal resistance of a wax and with $K=2.75$, if $\alpha=10^{-8}$, then, starting with $V_0=-2000$ volts, and with an initially produced polarization from A to B, there results the following: V will change from its original value, -2000 volts, to zero in about 1.5 days, then it will rise to a positive maximum V_m in about two weeks, after which it will decay to one-third of this maximum in about three years. In order that V_m shall be 2100 volts, it would only be necessary to have an initial polarization less than one percent of that which would be produced by a complete orientation of the dipole moments of the molecules of the wax in one direction.

[1] While the mathematical analysis is summarized in the present letter, the complete mathematical details, together with extensions of the problem, will appear in a paper to be published by the present writer in the Journal of the Franklin Institute for September, 1950.

Beta-Spectrum of Ne^{23} *

H. Brown and V. Perez-Mendez
Pupin Physics Laboratories, Columbia University, New York, New York
April 24, 1950

Ne^{23} is known to be a negative beta-emitter, of half-life of the order of 40 sec. Pollard and Watson[1] found an end point of about 4.1 Mev for the beta-radiation by absorption in aluminum, and concluded that the spectrum was simple, because no detectable gamma-radiation of the proper half-life was found.

By use of the technique of bombarding gases in a cyclotron and transporting them to a source chamber which fits into a semicircular focusing beta-spectrometer, as previously described,[2] the beta-spectrum and half-life of Ne^{23} have been determined in this laboratory. The Ne^{23} was produced by a (d,n) reaction on Ne^{22} in the Columbia University 36-in. cyclotron. The normal mixture of neon isotopes (90.5 percent Ne^{20}, 0.3 percent Ne^{21}, 9.2 percent Ne^{22}) was used for those measurements not requiring very high intensity, while enriched neon[3] (96 percent Ne^{22}) was used for taking the beta-spectrum.

The half-life of Ne^{23} was obtained from a series of eight decay curves, an example of which is shown in Fig. 1, and found to be 40.2 ± 0.4 sec., in agreement with previous results[4] within their published precisions.

The beta-spectrum was taken with two different thicknesses of Saran window separating the source chamber from the spectrometer, and two different pressures of neon in the chamber, corresponding to total thicknesses of 2.8 and 5.7 mg/cm². The results, a typical sample of which is shown in Fig. 2, indicate that the spectrum is not dependent on the thickness in this range. The spectrum displays an end point (average for several runs, corrected for window absorption) of $\epsilon_{02}=9.24$, giving a maximum kinetic energy for the electrons of 4.21 ± 0.015 Mev. The spectrum is of the allowed shape down to about 1.2 Mev, where it deviates from linearity in the Fermi plot. On subtracting the high energy allowed spectrum, a low energy group of the allowed shape is obtained having an end point (average for several runs) of $\epsilon_{02}=3.3$, corresponding to a maximum kinetic energy of 1.18 ± 0.04 Mev. From the intercepts A_1 and A_2 of the two straight lines on the $\epsilon=1$ axis, one can calculate the relative intensities of the two groups

$$I_1/I_2=(A_1/A_2)^2[(\epsilon_{02}-1)/(\epsilon_{01}-1)]^2[f(Z,\epsilon_{01})/f(Z,\epsilon_{02})],$$

where the symbols have their usual meanings, and subscripts 1 and 2 indicate the components. The data obtained indicates that the low energy group is about seven percent as intense as the high energy group. Since $t_2/t_1=I_1/I_2$ where t_1 and t_2 are the lieftimes for the particular modes of decay, and $1/t=1/t_1+1/t_2$ (t being the observed half-life), we find $t_2=40.2$ sec., $t_1=555$ sec. The ft values are 8.78×10^4 sec. and 6050 sec. for the high and low energy groups, respectively.

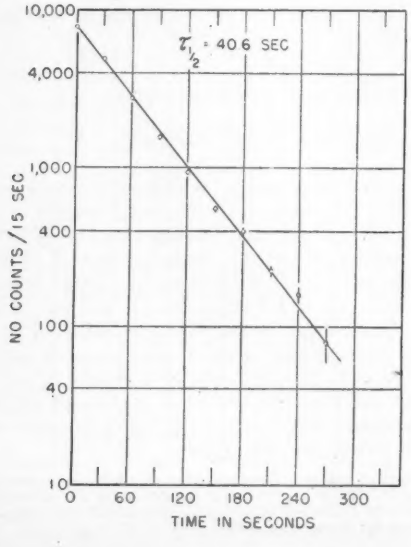

Fig. 1. Decay curve of Ne^{23}.

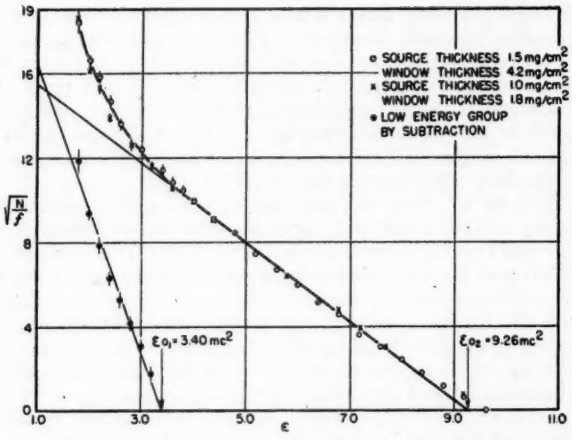

Fig. 2. Kurie plot of the negatrons from Ne^{23}. ϵ is the total energy of the electrons in units of mc^2. N is the number of electrons per unit momentum range, and f the Fermi function $p^2F(Z,\epsilon)$. $(N/f)^{\frac{1}{2}}$ is plotted in arbitrary units. The spectrum of the low energy group was obtained by subtraction and resolution (this is the explanation for the tailing-off at the high energy end).

We should like to thank Mr. P. Lindenfeld for his assistance with this experiment.

* Assisted by the AEC.
[1] E. Pollard and W. W. Watson, Phys. Rev. **58**, 12 (1940).
[2] H. Brown and V. Perez-Mendez, Phys. Rev. **75**, 1276 (1949); V. Perez-Mendez and H. Brown, Phys. Rev. **77**, 404 (1950). A paper describing the instrument in detail is now in print.
[3] Obtained from Yale University through the AEC.
[4] Huber, Lienhard, Scherrer, and Waffler, Helv. Phys. Acta **17**, 195 (1944), obtain (40.7 ± 0.8) sec.

Gamma-Radiation from Ne^{23} *

V. Perez-Mendez and H. Brown
Pupin Physics Laboratories, Columbia University, New York, New York
April 24, 1950

In view of the results obtained from the beta-ray spectrum of Ne^{23}, a search was made for the gamma-ray which should accompany the low energy group of electrons discussed in the previous paper.[1] This gamma-ray would represent a transition between an excited state of Na^{23} and the ground state, and should have an energy of about 3.0 Mev.

The enriched neon was bombarded with deuterons in the cyclotron and pumped into a glass container (source chamber) which was then viewed with a counter shielded by several inches of lead except in the direction of the source chamber. Sufficient lead was placed in front of the counter to stop all beta-radiation (up to 5 Mev at least), and a decay curve was taken of the gamma rays counted. A sample curve is shown in Fig. 1, which indicates that there is a gamma-ray component of about 2 min. half-life, which is attributed to the annihilation radiation from the positrons of 120-sec. O^{15}, produced in a (d,n) reaction from a nitrogen contamination in the neon (arising from incomplete evacuation of the pumping system). There is also a short-lived component, whose lifetime is placed by an average of six such curves at (38 ± 6) sec. and which we identify with Ne^{23}. The O^{15} component would give a large comparative effect even if the contamination is less than one percent because the Ne^{23} gamma-ray would be present in only about seven percent of the Ne^{23} disintegrations and because high energy gamma-rays are detected with less efficiency. This result indicates that there is a gamma-ray associated with the decay of Ne^{23}.

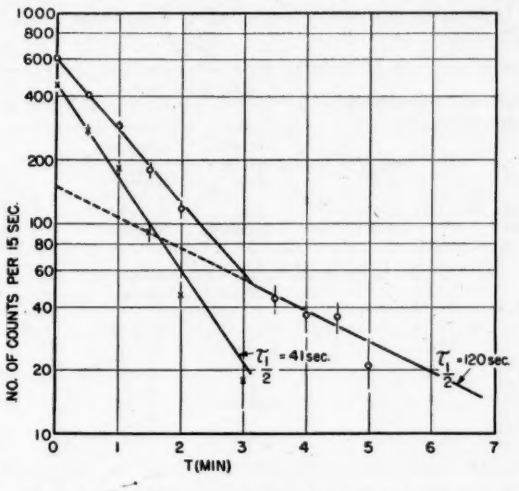

FIG. 1. Decay curve of the gamma-radiation from the neon sample bombarded with deuterons.

To determine whether the Ne^{23} gamma-ray has the energy to be expected on the basis of the beta-spectrum, an experiment was performed to determine the absorption curve for the gamma-radiation. The curve represents the ratio of the counts from the gamma-counter to the counts from a monitor counter attached to the pumping line. The result is shown in Fig. 2. Again, two

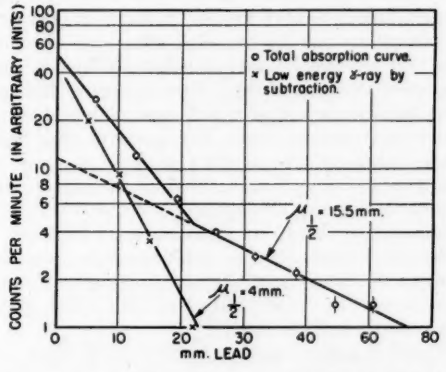
COUNTS PER MINUTE (IN ARBITRARY UNITS)
mm. LEAD
o Total absorption curve.
× Low energy γ-ray by subtraction.
$\mu_{\frac{1}{2}}$ = 15.5 mm.
$\mu_{\frac{1}{2}}$ = 4 mm.

FIG. 2. Absorption curve in lead for the gamma-rays from Ne^{23} (plus O^{15} contamination).

gamma-rays are discernible. The low energy group has a half-thickness of 4 mm of lead, which corresponds to a gamma-ray energy of 500 kev, as would be expected from a positron-emitting contaminant. The high energy group has a half-thickness of 15.5 mm, corresponding to an energy of 2.8 Mev, but the absorption curve is so flat in this region that the energy might lie anywhere

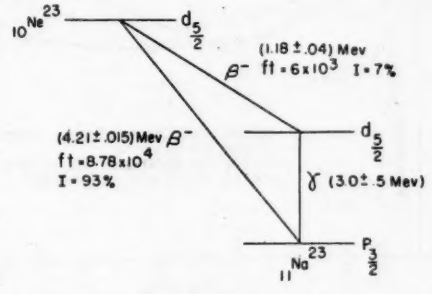

FIG. 3. Decay scheme for Ne^{23}.

from 2.5 to 3.5 Mev. This is the result to be expected if the low energy group of electrons from Ne^{23} represents a transition to an excited state of Na^{23}. The suggested level scheme is shown in Fig. 3.

The state of Ne^{23} is, according to the shell structure models,[2] $3d_{5/2}$. The ground state of Na^{23} should be, on these models, $3d_{5/2}$, but is anomalously found to exhibit a spin of $\frac{3}{2}$. This has been recently discussed by M. Mayer,[3] who suggests that it is due to a failure of pairing, so that three $3d_{5/2}$ protons combine to give a $\frac{3}{2}$ state. On this basis, one would expect that the high energy group, though allowed ($\Delta J = 1$) would have a rather small matrix element, and *ft* value $\sim 10^5$ sec. because an extensive nucleonic rearrangement is involved. The excited state of Na^{23} may have the $d_{5/2}$ configuration predicted for the ground state. In this case the low energy group would involve a $d_{5/2} \rightarrow d_{5/2}$ transition, and its matrix element (and *ft* value) should be comparable to those of the mirror image nuclei, as we find to be the case. To make more certain the assignment of levels, coincidence experiments are planned.

We should like to thank Mr. P. Lindenfeld for his assistance with this experiment.

* Assisted by the AEC.

[1] H. Brown and V. Perez-Mendez, Phys. Rev. **78**, 812 (1950).
[2] M. G. Mayer, Phys. Rev. **74**, 235 (1948); E. Feenberg, Phys. Rev. **77**, 771 (1949).
[3] M. G. Mayer, Phys. Rev. **78**, 16 (1950).

Superconductivity of Isotopes of Mercury*

B. SERIN, C. A. REYNOLDS, AND L. B. NESBITT
Rutgers University, New Brunswick, New Jersey
April 27, 1950

THE critical field measurements on enriched isotopes of mercury reported earlier[1] have been repeated and extended. The alternating field method used for determining the susceptibility has been extensively investigated by Shoenberg.[2] All the new measurements were made at a frequency of 100 c/sec. At this frequency, the ratio of sample radius to a.c. skin depth in the normal conductor is less than 0.6, so that there is a negligible signal from the imaginary part of the susceptibility. Under these conditions, as the external magnetic field is increased through the critical value, the a.c. signal goes through a maximum. The value of the magnetic field at this maximum was taken to be the critical field.

The transition temperatures for the samples obtained by extrapolating the critical field curves are given in Table I.

TABLE I. Transition temperatures for the Hg isotopes.

Av. mass number (M)	Transition temperature (T_0)°K
199.7	4.167
200.7 (natural mercury)	4.154
202.0	4.147
203.4	4.137

The critical field measurements were extended to lower temperatures and higher fields, and it was found that the curves for the isotopes were accurately parallel down to 2.30°K.

Table II shows the product $M^{\frac{1}{2}}T_0$ for the various isotopes. This product is quite constant, and is in fact more constant than any other simple combination of these variables. The constancy

TABLE II. The product $M^{\frac{1}{2}}T_0$ for the Hg isotopes.

Av. mass number (M)	$M^{\frac{1}{2}}T_0$
199.7	58.88
200.7	58.84
202.0	58.93
203.4	58.99

of this product can be interpreted as showing that the ratio of the transition temperature to the Debye temperature of each of the lattices of the different isotopes is a constant, which indicates that the partition function of the lattice is a constant at the transition temperature.

A complete report on these measurements is being prepared.

* This work was supported by the ONR, by the Research Corporation, by the Rutgers University Research Council, and by the Radio Corporation of America.

[1] Reynolds, Serin, Wright, and Nesbitt, Phys. Rev. **78**, 487 (1950).
[2] D. Shoenberg, Proc. Camb. Phil. Soc. **33**, 559 (1937).

Transmutation-Produced Germanium Semiconductors

J. W. CLELAND, K. LARK-HOROVITZ, AND J. C. PIGG
Oak Ridge National Laboratories, Oak Ridge, Tennessee
April 6, 1950

GERMANIUM exposed in a nuclear reactor becomes a *P*-type semiconductor ("hole" or defect conduction).[1] It has been shown that this change is due to (a) lattice displacements produced by fast neutrons and (b) impurity centers produced by the transmutations due to slow neutrons. That this latter defect must exist became apparent when heat treatment at 450°C failed to restore the original conductivity in samples which had been exposed for a long period ($nvt \sim 10^{18}$). The cross sections for activation given in the literature[2] lead to an *N*-type semiconductor and therefore K. Lark-Horovitz suggested a re-determination of the capture cross section on separated germanium isotopes. Such a determination was carried out by H. L. Pomerance,[3] and is shown in Table I.

The capture cross sections obtained by Pomerance predict an excess of *P*-type impurities (Ga) over *N*-type impurities (As).

$$N_e = nvt \times \sigma_e \times N_{Ge} \times P_i, \quad (1)$$

TABLE I. Absolute cross section of separated germanium isotopes.

(L. Seren, Argonne Laboratory)				
Isotope	Abundance	Capture cross section (in barns)		End product
		Isotopic	Atomic	
Ge^{70}	21.2	0.073	0.0155	Ga
Ge^{70}	21.2	0.45	0.093	Ga
Ge^{74}	37.1	0.38	0.14	As
Ge^{76}	6.5	0.085	0.0055	Se

(H. L. Pomerance, Oak Ridge Laboratory)				
Isotope	Abundance	Capture cross section (in barns)		End product
		Isotopic	Atomic	
Ge^{70}	21.2	3.25	0.69	Ga
Ge^{72}	27.3	0.94	0.26	Ge
Ge^{73}	7.9	13.69	1.08	Ge
Ge^{74}	37.6	0.60	0.22	As
Ge^{76}	6.1	0.35	0.02	Se

where N_e is the number of events observed, nvt is the integrated neutron flux, σ_e is the cross section for the event, N_{Ge} is the number of atoms per cc in the material and P_i is the isotopic percentage of the atomic species. Therefore,

$$N_{Ga} - N_{As} = nvt \times 4.4 \times 10^{22}(3.25 \times 21.2 - 0.6 \times 37.6)10^{-26} = 2.05 \times 10^{-2} nvt. \quad (2)$$

The impurity centers are formed at the lattice sites themselves. The semiconductor thus obtained, if one starts with "pure" single crystals of germanium, is therefore a substitutional alloy.

Germanium samples with known type and number of impurity centers (as determined by the Hall effect and the dissociation equation)[4] are exposed for various lengths of time in the reactor, in a region of determined flux. After exposure, Hall effect and resistivity are determined giving *P*-type centers due to (a) displacements (b) transmutations. The sample is then heat treated for various lengths of time at 450°C until further heat treatment no longer produces any changes. Provided the rate of cooling from 450°C does not freeze in any lattice defects, and that all displacements produced by knock-on collisions are completely annealed out at this low temperature, the resulting conductivity is now due to the originally introduced chemical impurities and the newly produced impurities from transmutations. The experimental results are shown in Figs. 1 and 2.

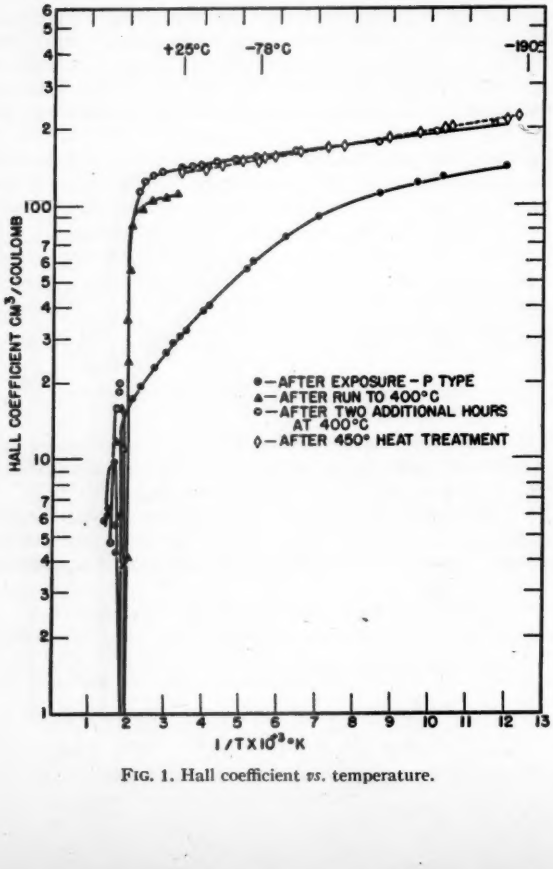

FIG. 1. Hall coefficient *vs.* temperature.

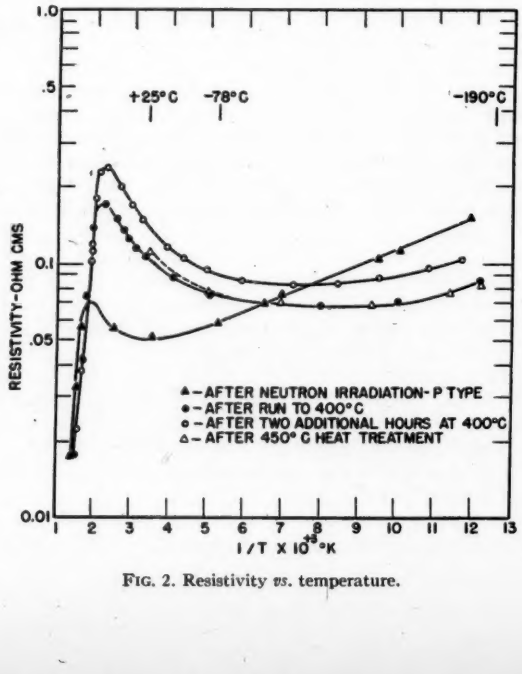

FIG. 2. Resistivity *vs.* temperature.

The Hall curve obtained in a sample containing lattice defects cannot be interpreted by an ordinary dissociation equation, since it shows a curvature which is usually not observed in chemically prepared samples. Quantitatively, Table II shows good agreement

TABLE II. Density of impurity atoms in germanium.

Sample number	Original number of carriers/cm³ n_0	Total flux (nvt)	Final number of carriers/cm³, n_f Calculated from cross sections	Measured by Hall effect	Difference (percent)
1—N-type	-5.25×10^{14}	4.56×10^{17}	$+8.82\times10^{15}$	$+6.16\times10^{15}$	−27
2—N-type	-2.28×10^{16}	2.54×10^{18}	$+2.92\times10^{16}$	$+3.21\times10^{16}$	+9
3—N-type	-5.47×10^{16}	4.37×10^{18}	$+3.48\times10^{16}$	$+5.25\times10^{16}$	+33
4—N-type	-1.17×10^{16}	2.54×10^{18}	$+4.03\times10^{16}$	$+5.20\times10^{16}$	+22
5—N-type	-1.48×10^{14}	2.54×10^{18}	$+5.05\times10^{16}$	$+4.45\times10^{16}$	−13
6—P-type	$+5.02\times10^{14}$	2.54×10^{18}	$+5.15\times10^{16}$	$+4.95\times10^{16}$	−4
7—P-type	$+4.60\times10^{14}$	8.04×10^{17}	$+6.25\times10^{16}$	$+5.22\times10^{16}$	−20
8—N-type	-4.04×10^{14}	1.06×10^{19}	$+2.15\times10^{17}$	$+1.90\times10^{16}$	−13

between the final number of carriers calculated and determined experimentally within the limits of experimental error (20 percent for flux measurements, 20 percent for cross sections, and heat treatment).

Activation cross sections for deuterons measured by E. Bleuler and D. Tendam at Purdue lead to the conclusion that deuteron bombardment should lead to N-type germanium. Similarly α-activation should also lead to N-type germanium. Activation by fast neutrons (Cd shielded samples) should lead to a larger preponderance of P-type centers (Ga) but with a much smaller cross section than slow neutron activation. Preliminary experiments are in agreement with this expectation.

We find, therefore, (a) that there is a balance between donators and acceptors, and that the Hall effect and conductivity are determined by the excess type present, (b) that there is one current carrier released per impurity center produced, (c) agreement between the activation energies of impurity centers produced chemically and by transmutations, indicating that chemical doping is a substitution process.

[1] K. Lark-Horovitz, Electrical Engineering (December, 1949).
[2] Seren, Friedlander, and Turkel, Phys. Rev. **72**, 888 (1947).
[3] H. L. Pomerance, AEC Report, ORNL-577 (1949).
[4] V. A. Johnson and K. Lark-Horovitz, Final Report, NDRC, Purdue (1945).

Fast Neutron Bombardment Effects in Germanium

J. H. CRAWFORD, JR. AND K. LARK-HOROVITZ
Oak Ridge National Laboratories, Oak Ridge, Tennessee
April 6, 1950

NEUTRON bombardment of germanium[1] in a nuclear reactor produces impurities by transmutation (thermal neutron capture[2]) and lattice displacements caused by high energy neutrons. The contribution of transmutation introduced impurities is in general negligibly small compared to the effect of damage by fast neutrons on carrier concentration in Ge.

The initial change in conductivity during neutron bombardment of N-type Ge is $(\sigma=e\mu_e n_e+e\mu_H n_H)$,

$$\frac{d\sigma}{d(nvt)_{\text{fast}}}=e\mu_e\frac{dn_e}{d(nvt)_{\text{fast}}}+en_e\frac{d\mu_e}{d(nvt)_{\text{fast}}}, \tag{1}$$

where e is the electronic charge, n_e is the electron concentration, μ_e is the electronic mobility and $(nvt)_{\text{fast}}$ is the integrated fast neutron flux. The contribution of the added scattering centers will be a negligible portion of the mobility until their concentration becomes comparable to the original impurity concentration. In the initial linear portion of the conductivity *vs.* bombardment curve the finite rate of annealing of neutron produced damage can be neglected, consistent with the fact that the number of acceptors

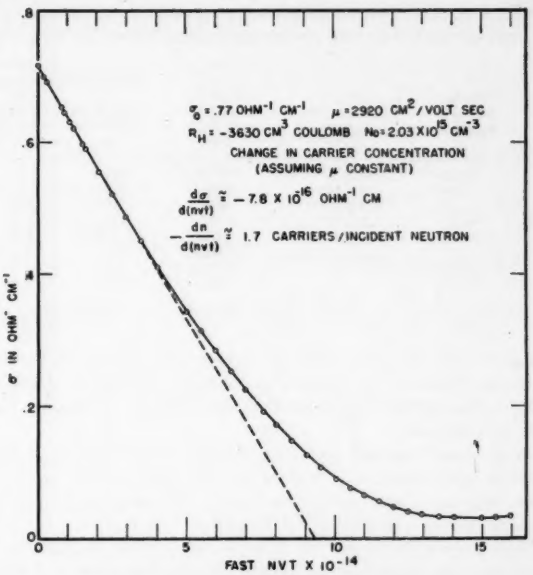

FIG. 1. Conductivity *vs.* bombardment for N-type germanium.

per incident neutron is the same at both dry ice and room temperature. Thus, initially,

$$d\sigma/d(nvt)_{\text{fast}}=-e\mu_e K, \tag{2}$$

where K is the average net number of acceptors produced per incident neutron (K is a weighted average depending on the energy spectrum of the neutron flux in the high energy range) evaluated from the initial slope of the conductivity *vs.* bombardment curve if the initial mobility is known.

Thermal equilibrium between electrons and holes when classical statistics are valid leads to [3]

$$n_e n_h=AT^3\exp(\Delta\epsilon_0/kT)=\kappa(T), \tag{3}$$

where for Ge, $A=5.3\times10^{32}$ and $\Delta\epsilon_0=0.75$ ev. Thus using Eq. (3) and c as the ratio of electron to hole mobility.

$$\sigma=e\mu_h[n_e c+\kappa(T)/n_e]. \tag{4}$$

The electron concentration for minimum conductivity is then

$$n_e=(\kappa(T)/c)^{\frac{1}{2}} \tag{5}$$

and the minimum conductivity is

$$\sigma_{\min}=(2e/c)\mu_e(\kappa c)^{\frac{1}{2}} \tag{6}$$

from which μ_e at the minimum can be calculated. Any photoelectric effects induced by β- and γ-radiation would cause the calculated value to be apparently larger than the expected value. The actual value should be slightly smaller than the original value of the mobility because additional scattering centers are introduced during bombardment.

Figure 1 shows the form of the conductivity *vs.* bombardment curve for 32°C. The curves taken at dry ice temperature are quite similar. Table I summarizes the results of the analysis.

The mean value of K is 3.1 acceptors per incident neutron in agreement with the theoretical value for the number of displaced atoms in Ge obtained by G. E. Evans[4] on the basis of radiation damage theory.

The difference in slope of the bombardment curve after conversion to P-type may be due to (a) the rate of recombination of lattice defects becoming appreciable after a certain concentration is reached and, (b) only those acceptors which can be thermally ionized being effective in increasing the hole concentration. Bombardment data for an initially P-type sample gives 0.77 for the number of conducting holes produced per incident neutron. This

TABLE I. Summary of results.

Sample	Temperature of exposure °C	Initial number of carriers cm^{-3}	Initial mobility cm^2/volt sec.	Mobility at minimum cm^2/volt sec.	Number of acceptors per incident neutron cm^{-3}
1	~32	2.0×10^{15}	2920	2200	1.7
2	30	4.3×10^{14}	2010	2020	1.5
3	20	8.9×10^{14}	2600	2190	3.5
4	~32	2.8×10^{16}	2180	1440	2.6
5	~32	5.5×10^{16}	800	13,700	5.2
6	−79	——	10,000	——	4.3
7	−79	——	6070	——	3.1
8	−79	——	4530	——	3.2

is smaller than the mean value of K given above by a factor of 4. Consequently, since recombination of defects should be negligible initially, one might suspect both of these factors to be important in the general case.

The assumed thermal equilibrium between electrons and holes seems to hold reasonably well in every case but one, sample 5, which has an abnormally low initial mobility indicating an inhomogeneous distribution of impurity centers. An impurity gradient perpendicular to the direction of current would obscure the correct minimum conductivity. Also the presence of a $P-N$ barrier (the gradient parallel to current) would cause a conductivity minimum much higher than the expected value since Lark-Horovitz and co-workers[5] have shown that such a boundary is photo-sensitive to high energy radiations. In either case the calculated value of the mobility at the minimum conductivity would be spurious and high. Thus one is led to the conclusion that photoelectric effects caused by β- and γ-radiation are in general negligible in uniform samples.

[1] Davis, Johnson, Lark-Horovitz, and Siegel, Phys. Rev. **74**, 1255 (1948); W. E. Johnson and K. Lark-Horovitz, Phys. Rev. **76**, 422 (1944). K. Lark-Horovitz and J. C. Pigg (private communication).
[2] Cleland, Lark-Horovitz, and Pigg, Phys. Rev. **78**, 814 (1950).
[3] V. A. Johnson (private communication).
[4] G. E. Evans (unpublished results).
[5] Orman, Fan, Goldsmith, and Lark-Horovitz, Phys. Rev. **78**, 646(A) (1950).

The Photon Yield of Electron-Hole Pairs in Germanium

F. S. GOUCHER
Bell Telephone Laboratories, Murray Hill, New Jersey
April 21, 1950

IT is the purpose of this letter to report that photo-conductivity measurements, made on a single crystal of n-type germanium, indicate a yield of one electron-hole pair per photon absorbed, for wave-lengths less than the long wave limit.

A uniform electric field E is established in a long rectangular specimen of uniform cross section and conductivity, and a portion of one surface is irradiated with I photons per second of monochromatic light of known wave-length, the number being determined by a calibrated thermocouple. The number of photons I_A absorbed in the sample is calculated from the optical constants[1] by subtracting the reflection and transmission losses. Regions at the ends which are long in comparison with the respective mean ranges of positive holes are left unilluminated so that a negligible fraction of these reach the specimen terminals.

The specimen was cut from a single crystal[2] of n-type germanium having a uniform resistivity of about 5 ohm cm. Its approximate dimensions were 0.05 cm×0.05 cm×2.0 cm. When placed in the plane of the image of the exit slit of a monochromator all of the light could be made to fall on one face of the specimen over a length $l=1.5$ cm. The lifetime of holes, τ_p was 67×10^{-6} sec.[3] The field E with one volt across the terminals was such that the mean range of holes was approximately 0.5 mm. The light intensity was such that the field in the illuminated region was not reduced by more than one percent from the dark-current value for the largest photo-currents. Photo-currents were measured by a.c. techniques using pulsed light. The light pulser was synchronized with an auxiliary circuit such that the voltage across the terminals was maintained constant.

If the total number of electron-hole pairs produced per second is Y then the number of holes in the steady state is $Y\tau_p$. Thus the holes increase the conductance of the illuminated region of length l by an amount,[4]

$$\Delta G = Y\tau_p e(\mu_p+\mu_n)/l^2.$$

This segment is in series with the two ends of the filament and the contact resistances of the terminals, the total resistance being R_T. With the voltage V across the terminals, and if the resistance of the segment is R_l, then the change in current is $\Delta i = V\Delta G(R_l/R_T)^2 = V\Delta G(El/V)^2$ which leads to

$$Y = \Delta iV/e\tau_p E^2(\mu_p+\mu_n).$$

Values of Y were calculated using $\mu_p=1700$ and $\mu_n=3600$ cm^2/volt-sec.[5]

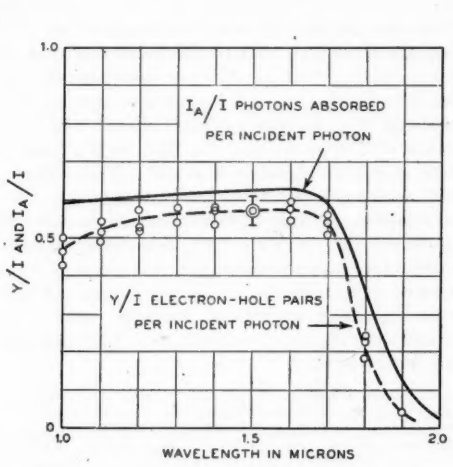

FIG. 1. The ratios I_A/I and Y/I *vs.* wave-length.

The experimental results are summarized in Fig. 1 in which we have plotted I_A/I and Y/I as functions of wave-length from 1.0μ to 2.0μ, the latter being just below the long wave limit of photosensitivity. Within the limits of experimental error, which we cannot claim to be better than 10 percent, and over the major portion of this range of wave-lengths, the two characteristics may be considered coincident.

Thus it appears that each photon absorbed produces one hole-electron pair. The apparent divergence near the long wave limit may reasonably be ascribed to the increase in experimental error with a photo-current which becomes vanishingly small in this region. On the other hand, the divergence for wave-lengths less than 1.2μ may be accounted for by recombination through the concentration of carriers generated in a region which is less than 10^{-4} cm in thickness.

In addition to those already mentioned thanks are due to W. Shockley for suggesting this experiment, to J. Bardeen and W. van Roosbroeck for valuable help in its theoretical aspects, and to H. R. Moore for furnishing the electronic measuring equipment.

[1] Refractive indices and absorption coefficients of Ge by H. B. Briggs, unpublished.
[2] Furnished by G. K. Teal and J. B. Little described in Bull. Am. Phys. Soc. **25**, No. 2, 16 (1950).
[3] Measured by J. R. Haynes.
[4] See Shockley, Pearson and Haynes, Bell Sys. Tech. J. **28**, 344 (1949) for similar calculations.
[5] These are drift mobilities measured by J. R. Haynes.

An Experimental Investigation of the Nuclear Magnetic Moments of D^2 and H^1

GUNNAR LINDSTRÖM
Nobel Institute for Physics, Stockholm, Sweden
April 24, 1950

THE magnetic moment of D^2 was measured against the magnetic moment of H^1 in two different chemical compounds (H_2O and paraffin oil) according to the resonance absorption method introduced by Purcell *et al.* The two samples were placed in different positions in the magnetic field. The h.f. bridge with the H^1 sample was fed by 28 Mc from a frequency standard and the other bridge from a heterodyne frequency meter, which was calibrated during the measurements against a 10-kc signal from the standard. With this arrangement it is possible to measure the frequency fed to the bridge with the D^2 sample with an accuracy of one part in $5 \cdot 10^6$. The two signals were photographed on a double-beam oscillograph. Pictures were taken with slightly different frequencies near the correct value and the measured differences plotted against the frequency according to Fig. 1. The correct value can then be located with very high accuracy. The samples were changed and the measurements repeated.

According to these measurements there seems to be a small effect depending on the different chemical compounds. The results are:

$$\mu_D/\mu_H = 0.30701337 \pm 0.00000050 \text{ for } D_2O \text{ and } H_2O$$

and

$$\mu_D/\mu_H = 0.30701465 \pm 0.00000050 \text{ for } D_2O \text{ and paraffin oil.}$$

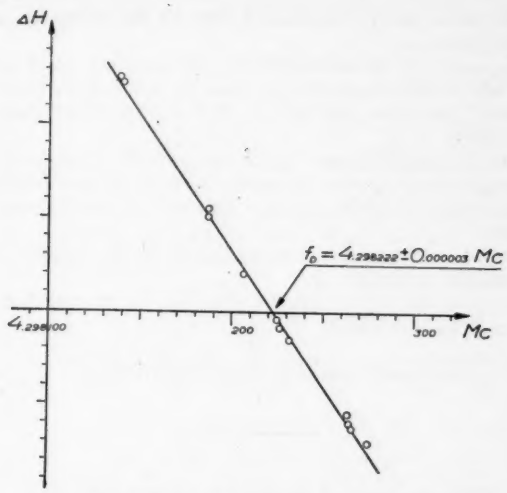

FIG. 1. Signal differences *versus* frequency.

The measured ratio of the magnetic moments for protons in paraffin oil and in H_2O is 1.0000041 ± 0.0000030.

The maximum deviation according to Tables I and II is much less than that given above, but as a conservative estimate the errors given here refer to a tenth of the line width, which gives about 0.00000050.

TABLE I. μ_D/μ_H for D_2O and paraffin oil. Magnetic field about 6580 gauss and modulation amplitude about 0.3 gauss.

Nr.	f_D f_{DI} (Position I)	f_{DII} (Position II)	f_H Position I and II	$2f_D \sim f_{DI} + f_{DII}$	$\mu_D/\mu_H = 2f_D/f_H$	Deviation from mean value
1	4.298225	4.298185	28.000000	8.596410	0.30701464	−0.00000001
2	4.298225	4.298189	28.000000	8.596414	0.30701479	+0.00000014
3	4.298225	4.298187	28.000000	8.596412	0.30701471	+0.00000006
4	4.298224	4.298187	28.000000	8.596411	0.30701468	+0.00000003
5	4.298219	4.298190	28.000000	8.596409	0.30701461	−0.00000004
6	4.298222	4.298190	28.000000	8.596412	0.30701471	+0.00000006
7	4.298222	4.298186	28.000000	8.596408	0.30701457	−0.00000008
8	4.298223	4.298182	28.000000	8.596405	0.30701446	−0.00000019
9	4.298223	4.298188	28.000000	8.596411	0.30701468	+0.00000003
10	4.298221	4.298190	28.000000	8.596411	0.30701468	+0.00000003
11	4.298221	4.298188	28.000000	8.596409	0.30701461	−0.00000004
12	4.298226	4.298188	28.000000	8.596414	0.30701479	+0.00000014
13	4.298226	4.298191	28.000000	8.596407	0.30701454	−0.00000011
				Mean value	0.30701465	±0.00000019 max dev.

TABLE II. μ_D/μ_H for D_2O and H_2O. Magnetic field about 6580 gauss and modulation amplitude about 0.3 gauss.

Nr.	f_D f_{DI} (Position I)	f_{DII} (Position II)	f_H Position I and II	$2f_D \sim f_{DI} + f_{DII}$	$\mu_D/\mu_H = 2f_D/f_H$	Deviation from mean value
1	4.298216	4.298162	28.000000	8.596378	0.30701350	+0.00000013
2	4.298218	4.298162	28.000000	8.596380	0.30701357	+0.00000020
3	4.298218	4.298156	28.000000	8.596374	0.30701336	−0.00000001
4	4.298223	4.298156	28.000000	8.596379	0.30701354	+0.00000017
5	4.298236	4.298146	28.000000	8.596382	0.30701364	+0.00000027
6	4.298236	4.298147	28.000000	8.596383	0.30701368	+0.00000031
7	4.298190	4.298185	28.000000	8.596375	0.30701339	+0.00000002
8	4.298206	4.298161	28.000000	8.596367	0.30701311	−0.00000026
9	4.298215	4.298157	28.000000	8.596372	0.30701329	−0.00000008
10	4.298215	4.298160	28.000000	8.596375	0.30701339	+0.00000002
11	4.298205	4.298160	28.000000	8.596365	0.30701304	−0.00000033
12	4.298205	4.298165	28.000000	8.496370	0.30701321	−0.00000016
13	4.298205	4.298165	28.000000	8.596370	0.30701321	−0.00000016
14	4.298205	4.298165	28.000000	8.596370	0.30701321	−0.00000016
15	4.298210	4.298165	28.000000	8.595375	0.30701339	+0.00000002
				Mean value	0.30701337	±0.00000033 max dev.

The values between horizontal lines in the tables are consecutive values.

$\mu_D/\mu_H = 0.30701337 \pm 0.00000050$ is in extremely good agreement with 0.3070126 ± 0.0000020 given by Bloch, Levinthal, and Packard.[1] The value with paraffin oil is a little higher than the water value.

There is a small decrease in the new paraffin value compared to our previous one,[2] which is mainly due to a more accurate way of determining the field difference between the two positions in the field.

The difference between the water and the paraffin value is being investigated further.

This investigation has been sponsored by the Swedish Natural Science Research Council.

[1] Bloch, Levinthal, and Packard, Phys. Rev. **72**, 1125 (1947).
[2] K. Siegbahn, and G. Lindström, Nature **163**, 211 (1949).

Observation of Second Sound Radiation Pressure by the Thermal Pitot Tube*

JOHN R. PELLAM
Cryogenics Laboratory, National Bureau of Standards, Washington, D. C.
April 24, 1950

THE writer has previously discussed the radiation pressure P_{rad} which should exist for second sound and has expressed[1] this quantity in terms of the square of the temperature fluctuation[1a], τ, in the wave from the ambient absolute temperature T (deg. Kelvin),

$$P_{rad} = \tfrac{1}{2}\rho c_v \tau^2/T. \qquad (1)$$

Entering also in (1) were the density and specific heat of liquid helium ρ(g/cc) and c_v(cal./g.-deg.). This radiation pressure has now been observed directly.

Although proof will be left to a later publication, a completely equivalent formulation of (1) results from the additional fourth term of the generalized Bernoulli equation for pressure, previously employed[2] for analyzing the thermal Rayleigh disk. This form is more realistically suited to the present experiment, as it relates hydrostatic pressure differences directly to heat flow density $\dot{H}$(cal./sec.-cm²) in terms of the properties of the liquid. Thus

$$\tfrac{1}{2}\rho V^2 + \rho g h + p + \tfrac{1}{2}\rho(\rho_n/\rho_s)(\dot{H}/\rho ST)^2 = \text{constant}. \qquad (2)$$

The gross properties of He II appearing in the additional fourth term are the density ρ and the entropy S (cal./cc-deg.); the constituent quantities ρ_n and ρ_s(g/cc) are the density of normal fluid and superfluid, respectively. Employing known thermodynamic expressions for second sound velocity v_2(cm/sec.), an alternative and perhaps more convenient form of (2) may be written

$$\tfrac{1}{2}\rho V^2 + \rho g h + p + \tfrac{1}{2}(1/\rho c_v T)(\dot{H}/v_2)^2 = \text{constant}. \qquad (3)$$

Whereas the thermal Rayleigh disk experiment provides an insight to the hydrodynamics of internal counterflow about an obstacle, this present investigation provides an insight to the one-dimensional aspect of heat flow in liquid He II. Observations of hydrostatic pressure differences between portions of a second sound standing wave system provide a direct measure of the associated radiation pressure.

The simplicity of the apparatus employed is indicated by the diagram of Fig. 1. Second sound generated within the horizontally oriented chamber A by means of the plane electrical heating surface B is tuned to half-wave resonance by varying the driving frequency. The heat flow distribution thus set up (represented by the dotted line of Fig. 1) is maximum at the center, diminishing systematically to zero at either extremity. The junction of the vertical tube C is located at the midpoint of chamber A and therefore at the position of maximum horizontal heat flow density. Tube E, on the other hand, joins A near the end boundary where a heat flow node exists.

On the basis of the mass transport concept of heat flow in liquid He II, the associated internal particle convection is likewise a maximum at the midpoint of A. According to Eqs. (2) and (3) then, this internal streaming of particles horizontally past the orifice of C results in a smaller hydrostatic pressure than at E where no streaming exists, in a manner exactly analogous to the classical operation of the Bernoulli principle. In this situation however, the effect is due to differences in internal mass flow rather than to differences in net mass flow. At resonance the difference is presumably fixed by the value of the heat flow term in Eqs. (2) and (3) (not the classical first term which remains zero throughout).

The arrangement of the tubes constitutes essentially a liquid helium differential manometer system. Actually, a vent D is provided at the midpoint of A (for escape of heat) so that the level within tube C does not change. Thus *at resonance the height of the helium column in E is observed to rise very slightly* (a fraction of a millimeter) above that within C.

In view of the present generalized form of the Bernoulli relationship, it would appear that for the majority of classical hydrodynamical devices (and experiments) there exists the thermal counterpart in liquid He II. Thus the device described herein might be regarded as a form of *thermal pitot tube*. The geometry is modified, but the basic principle of comparing the hydrostatic pressure at a point of no (internal) flow with that in a region of (internal) flow is identical.

So far the observations have been primarily qualitative, but the general results conform to the expected behavior. The response is in the correct sense (i.e., the level in E rises) and second sound velocities deduced from the associated resonance frequencies have proper values. Actual comparison of observed pressure differentials with the heat flow term in Eqs. (2) and (3) awaits more detailed and precise observations. A later paper giving a full description of the experiment will include a complete derivation and discussion of these equations.

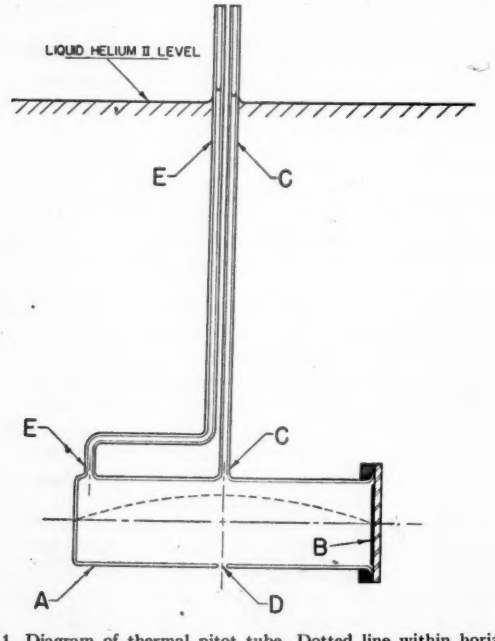

FIG. 1. Diagram of thermal pitot tube. Dotted line within horizontal cavity A represents distribution of heat flow density (and internal particle convection) for condition of resonance. The resulting forced difference in the levels within the vertical tubes (as well as the net elevation due to capillarity) is exaggerated here.

* Supported by the ONR.
[1] J. R. Pellam, Phys. Rev. **76**, 872 (1949).
[1a] The factor $\frac{1}{2}$ appears in (1) because P_{rad} now includes incident plus reflected waves, making τ the *net* temperature fluctuation at a boundary.
[2] J. R. Pellam and P. M. Morse, Phys. Rev. **78**, 474 (1950).

On the Primary Cosmic-Ray Spectrum*

J. A. VAN ALLEN AND S. F. SINGER
Applied Physics Laboratory, Johns Hopkins University, Silver Spring, Maryland
April 21, 1950

ON the basis of a series of high altitude rocket experiments during the past several years, we are now able to report absolute directional intensities of charged particles *above the atmosphere* at geomagnetic latitudes 0°, 41°N, 50°N, and 58°N. Table I summarizes *vertical* intensities obtained with G-M tube coincidence telescopes containing about 3 g/cm² of copper.

In addition there may be noted other results obtained by balloon investigators *near* the top of the atmosphere as shown in Table II.

TABLE I. Vertical intensities obtained in rocket flights.

Geomagnetic latitude λ	Experimental vertical intensity $j(0°)$	Geomagnetic cut-off[a] momentum/charge ratio pc/Ze	Reference
0°	0.028 ±0.004/sec. cm² steradian	15.0 Bev	[b]
41°N	0.073 ±0.006	4.8	[c,d]
50°N	0.18 ±0.02	2.6	[e]
58°N	0.29 ±0.03	1.2	[e]

[a] Derived from the simple Störmer cone. At intermediate latitudes, the effect of the penumbra has been judged to be small from the work of M. S. Vallarta, Phys. Rev. **74**, 1837 (1948). At high latitudes there appears to be no such assurance.
[b] J. A. Van Allen and A. V. Gangnes, Phys. Rev. **78**, 50 (1950).
[c] J. A. Van Allen, Paper No. 53a, p. 195, of Proceedings of the Echo Lake Cosmic Ray Symposium June 23–28, 1949 (ONR, November, 1949).
[d] S. F. Singer, Paper No. 54, p. 206, of Proceedings of the Echo Lake Cosmic Ray Symposium, June 23–28, 1949 (ONR, November 1949); Phys. Rev. **77**, 729 (1950).
[e] Preliminary results of January, 1950 Aerobee flights from the USS Norton Sound, to be reported in full later.

A composite plot of the data of Tables I and II is given in Fig. 1. The plot has been made with momentum-charge ratio (magnetic rigidity) as abscissa because of its generality in relating the intensities of *any* charged component of geomagnetic latitude.

If the atmospheric albedo has a negligible contribution to the experimental vertical intensities, then Fig. 1 exhibits the integral number spectrum (that is, the directional intensity of particles of momentum/charge ratio greater than pc/Ze as a function of pc/Ze) of the primary radiation in absolute units. If the intensity contribution of albedo is in the same proportion to the primary intensity at all latitudes, then Fig. 1 exhibits the *form* but not the absolute value of the integral number primary spectrum.

At any rate, Fig. 1 represents the current status of this type of direct attack, on the determination of the primary spectrum:

(a) Comparing the directly measured intensities with primary intensities deduced from the atmospheric ionization integrals,[1] it is seen that the former are markedly higher at all latitudes.

(b) In the range 2.6 to 15 Bev, our integral number spectrum (see Fig. 1) can best be fitted by $N(>pc/Ze)=0.48(pc/Ze)^{-1.1}$ (sec. cm² steradian)$^{-1}$, corresponding to a differential number spectrum $dN=0.53(pc/Ze)^{-2.1}d(pc/Ze)$. This spectrum is considerably flatter than that hitherto deduced from ionization measurements and other considerations.[2]

TABLE II. Vertical intensities obtained in balloon flights.

Geomagnetic latitude λ	Experimental vertical intensity $j(0°)$	Geomagnetic cut-off momentum/charge ratio pc/Ze	Reference
52°N	0.168 ±0.003/sec. cm² steradian	2.2 Bev	[a]
52°N	0.20	2.2	[b]
56°N	0.22	1.5	[c]
69°N	0.29	0.27	[b]

[a] M. A. Pomerantz, Phys. Rev. **75**, 1721 (1949).
[b] Deduced from, but not explicitly stated by M. A. Pomerantz, Phys. Rev. **77**, 830 (1950), using geometric factors from reference a.
[c] Deduced from, but not explicitly stated by Winckler, Stroud, and Shanley, Phys. Rev. **76**, 1012 (1949).

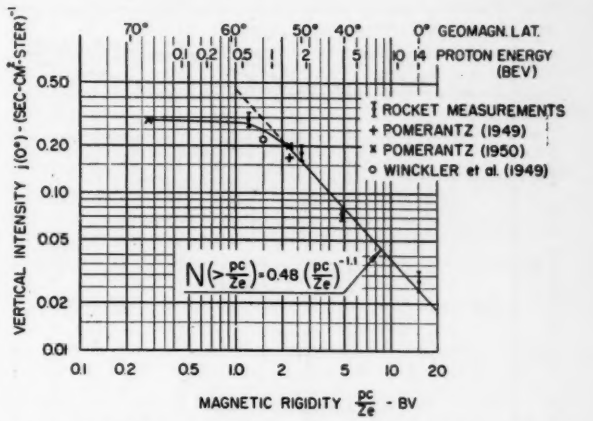

FIG. 1. Vertical intensity of charged particles above and near the "top of the atmosphere" as determined by G-M counter telescopes at various latitudes *vs.* magnetic rigidity for cut-off in the vertical direction as deduced from geomagnetic theory.

(c) A marked flattening of the form of the spectrum appears to occur for rigidities below about 1.5 Bev ($\lambda=56°$). Previously, the Pasadena group[1,3] has been able to show that the latitude effect continues beyond 51°. We feel fairly certain about the change in slope in the vicinity of 56°, but cannot preclude a small rise between 58° and 69°, since atmospheric absorption may have produced an appreciable effect in the balloon measurements at 69°. Clarification of this point can be achieved by a rocket measurement above the atmosphere at high latitude.

Note added in proof.—Dr. Pomerantz informs us in private communication that he interprets his two series of measurements, references a and b of Table II, as in close agreement at 52°, slightly contrary to our deductions from the published curves. His absolute intensity at 69° is thus presumably lowered to about 0.25, a value somewhat less than our intensity 0.29±0.03 above the atmosphere at 58°. Our conclusions remain unchanged.

* Supported by Navy Bureau of Ordnance under Contract NOrd 7386.
[1] H. V. Neher, Paper No. 60, p. 235, of Proceedings of the Echo Lake Cosmic Ray Symposium June 23–28, 1949 (ONR, November, 1949).
[2] L. Janossy, *Cosmic Rays* (Oxford University Press, New York, 1948), pp. 297 ff. D. J. X. Montgomery, *Cosmic Ray Physics* (Princeton University Press, Princeton, 1949), pp. 150 ff.
[3] Biehl, Neher, and Roesch, Phys. Rev. **76**, 914 (1949).

Magnetic Susceptibility of αFe_2O_3 and αFe_2O_3 with Added Titanium

F. J. MORIN
Bell Telephone Laboratories, Murray Hill, New Jersey
April 14, 1950

THE magnetic susceptibility of αFe_2O_3 and αFe_2O_3 with added titanium has been measured at low temperatures and a transition found not previously reported in the literature.

The oxides used were pigment grade αFe_2O_3 analyzing 99.1 percent Fe_2O_3, and rutile TiO_2. The mixed powders were pressed into bars and sintered in oxygen at atmospheric pressure at 1100°C for 16 hours. The bars were ground to a fine powder in a mullite mortar. Structure and lattice constants were determined both above and below the transition point by x-ray diffraction and found to be those given for αFe_2O_3 by Wyckoff.[1] The magnetic susceptibility was measured by the Gouy method. The field strength of the magnet was measured by a rotating coil and voltmeter calibrated against a permanent magnet whose field strength had been measured by the Bureau of Standards. The powdered sample was held in a glass tube (0.181 cm² cross section) extending out of the field above and below and having a thin glass

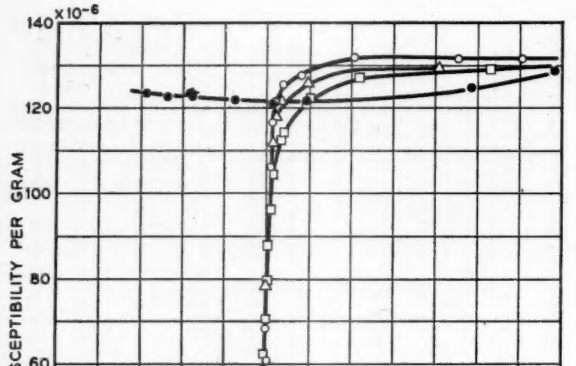

FIG. 1. Magnetic susceptibility per gram as a function of absolute temperature for αFe_2O_3 and αFe_2O_3 with added titanium. The amounts of titanium added are shown as number percent of total metal atoms.

partition at the center. The temperature was measured in the vicinity of the sample with a chromel *P*-alumel thermocouple. The procedure of measurement was to cool the sample to the lowest temperature in zero field and make measurements with increasing temperature, at each temperature point weighing the sample and tube in zero field and in a field of 2000 gauss. A check measurement was also made on αFe_2O_3 while cooling without removing the field. Results were the same as those obtained by the above procedure.

The results are shown in Fig. 1. The presence of ferromagnetism is indicated by the high value and behavior of the susceptibility in the high temperature range. Ferromagnetism was also indicated by permanent magnetization and particle size dependence of susceptibility in the high temperature range. A rough determination of the Curie point of αFe_2O_3 and αFe_2O_3+Ti showed it to be between 660°C and 690°C. Susceptibility above the Curie point was 19×10^{-6}. Reheated the powdered αFe_2O_3 in oxygen at atmospheric pressure for 16 hours at 1100°C and again for 16 hours at 980°C did not significantly decrease the susceptibility. The low temperature susceptibility of samples showing the transition was only slightly field dependent, decreasing from 16.7×10^{-6} to 14.8×10^{-6} for a field increase of from 2000 to 5000 gauss.

No data have been found in the literature for the susceptibility of αFe_2O_3 below 0°C. Above this temperature, a considerable amount of contradictory information is available, which has been reviewed by Selwood.[2] Extensive measurements have been made by Endo,[3] Hayes[4] and Chavalier.[5] Snoek,[6] Hayes[4] and Néel[7,8] have speculated on the cause of ferromagnetism in αFe_2O_3. The Curie point of αFe_2O_3 is about 680°C. Above this point the susceptibility is 19×10^{-6}. The limit of room temperature susceptibility as particle size is decreased is 20×10^{-6}. According to Néel, αFe_2O_3 is essentially antiferromagnetic with a weak ferromagnetism superimposed upon the antiferromagnetism. Néel[8] shows that, from the point of view of structure, a narrow region having magnetite structure could exist in a plane perpendicular to the trigonal axis of αFe_2O_3 and introduce a small amount of ferromagnetism. It has been observed by Smith[9] that a single crystal of αFe_2O_3 was ferromagnetic in a direction perpendicular to its trigonal axis but not in the direction of the trigonal axis.

From the data reported here, it appears that αFe_2O_3 is essentially antiferromagnetic, as suggested by Néel, with weak ferromagnetism superimposed upon antiferromagnetism above 250°K. It seems to be energetically preferable for the spins in the ferromagnetic regions to become antiparallel below 250°K except in the presence of a considerable amount of titanium impurity.

[1] Wyckoff, *The Structure of Crystals* (A.C.S. Monograph 19 and 19A), pp. 254, 36.
[2] P. W. Selwood, *Magnetochemistry* (Interscience Publishers, Inc., New York), pp. 220–226.
[3] K. Endo, Tohoku Imp. Univ. Sci. Rep. **25**, 879 (1937).
[4] E. T. Hayes, Bureau of Mines Report No. 3570.
[5] R. Chavalier and S. Mathiev, Ann. de physique **18**, 258 (1943).
[6] J. L. Snoek, Physica **3**, 463 (1936).
[7] L. Néel, Ann. de physique **3**, 137 (1948).
[8] L. Néel, Ann. de physique **4**, 249 (1949).
[9] Smith, Phys. Rev. **8**, 721 (1916).

Superconductivity of Columbium

D. B. COOK, M. W. ZEMANSKY, AND H. A. BOORSE
Columbia University, New York, New York*
April 17, 1950

IN view of the fact that measurements on the zero field transition of columbium[1–3] have shown widely different values and since $H-T$ data have been obtained only in the liquid helium region,[4] we have investigated the zero field transition, and have measured the $H-T$ curve between 5° and 9°K, of cylindrical specimens of columbium. The material was obtained from Fansteel Metallurgical Corporation with an analysis indicating maximum amounts of titanium, iron, silicon dioxide, and tantalum as respectively 0.002, 0.01, 0.03, and 0.2 percent. The latter maximum figure was dictated by the extreme difficulty of determining the presence of tantalum in columbium when present in amounts less than 0.2 percent. A spectrographic survey of the material by Professor T. I. Taylor of the Chemistry Department of Columbia University indicated traces of iron and molybdenum as the only observable impurities.

In addition, comparison measurements were made on an older sample of columbium which in slow neutron scattering experiments at Columbia[5] had shown evidence of containing 0.4 percent of tantalum. A spectrographic survey in this case indicated tantalum to be present in an amount not greater than 1.0 percent.

The necessary temperatures were obtained by the use of a charcoal desorption cryostat to be described in a forthcoming paper in this journal. Temperatures were measured by means of a helium gas thermometer which was filled to 1 atmos. at 20.4°K. The accuracy of the calculations was checked against observations at the tiple point of hydrogen and at the transition temperature of lead.[6]

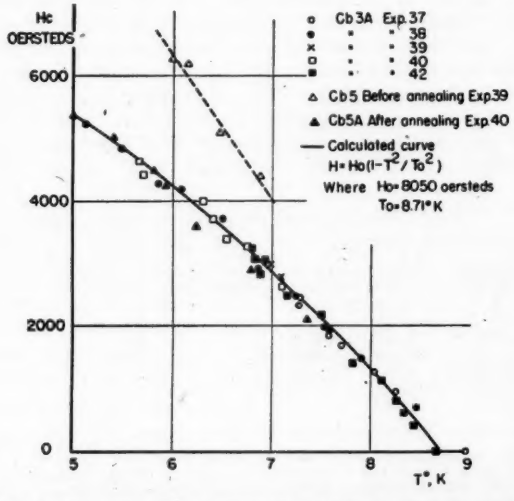

FIG. 1. Magnetic fields at completion of S-N transitions in Cb.

Transitions were observed by an a.c. induction method in which the superconductor was mounted as the core of a secondary coil of a mutual inductance, the primary of which was actuated at 1000 cycles/sec. by a current sufficient to produce an a.c. field at the core of 1.5 oersteds or less. Webber, Reynolds, and McGuire,[7] who described the method in detail, observed that magnetic transitions obtained in this way for a single crystal of tin yielded critical fields in agreement with those obtained by other methods.

The measurements on pure columbium were made on a sample that had been annealed in an induction furnace for five hours at 1000°C in a vacuum of 10^{-6} mm. The results, shown in Fig. 1, were taken in five different experiments extending over a period of several weeks. Comparison measurements on the high tantalum sample yielded higher critical field values before the sample was annealed, but after a three-hour annealing at 1000°C in a vacuum of 10^{-5} mm the values came into agreement with those of the purer material. Two additional samples of the pure material which were less carefully annealed also agreed with the lower curve in Fig. 1.

The zero field transition of the purer columbium occurred at 8.98°K in the first run after annealing, but thereafter the half-normal value was observed repeatedly at 8.55°K with a mean deviation of 0.01°K. The transition was 0.15° wide, the normal state being fully restored at 8.65°K, which was within 0.06° of the zero field transition temperature determined by least squares fit of the curve from magnetic transitions.

The best parabolic fit to the latter curve was given by substituting $H_0=8050$ oersteds and $T_0=8.71$°K into the empirical relation, $H=H_0(1-T^2/T_0^2)$. With the aid of the usual thermodynamic equations, the difference of specific heats in the normal and superconducting states was calculated. The electronic specific heat term in the normal state was found to be 0.0352 T cal./mole-deg., and the Debye Θ in the superconducting state was estimated to be 69°K. The extremely high value of the electronic specific heat is a consequence of the large initial slope of the $H-T$ curve, 1840 oersteds/deg., which is larger than that for any other superconductor so far observed except vanadium,[7] which has an initial slope of 4100 oersteds/deg.

* Assisted by the ONR.
[1] W. Meissner and H. Franz, Zeits. f. Physik **63**, 558 (1930).
[2] Meissner, Franz, and Westerhoff, Ann. d. Physik **17**, 593 (1933).
[3] Bruksch, Ziegler, and Hickman, Phys. Rev. **42**, 554 (1942).
[4] J. G. Daunt and K. Mendelssohn, Proc. Roy. Soc. **160**, 127 (1937).
[5] Wu, Rainwater, and Havens, Phys. Rev. **71**, 174 (1947).
[6] Boorse, Cook, and Zemansky, Phys. Rev. **78**, 635 (1950).
[7] Webber, Reynolds, and McGuire, Phys. Rev. **76**, 293 (1949).

Beta-Gamma-Angular Correlation*

STUART L. RIDGWAY
Princeton University, Princeton, New Jersey
April 27, 1950

IN continuation of the angular correlation work reported earlier,[1] 2.8-day Sb^{122}, and 60-day Sb^{124} have been investigated with a coincidence counting arrangement using scintillation counters and a coincidence circuit of 0.1-μsec. resolution, consisting of blocking oscillator pulse shapers, and a pentode mixing stage. The geometrical arrangement used is shown in Fig. 1, a 30-mil aluminum absorber for the betas (not shown), and a beta-collimator having been added for Sb^{124}. The 1P21 photo-multipliers were dry-ice cooled. The gamma-counter was made insensitive to betas by a $\frac{1}{8}$-in. aluminum absorber. Counts were taken at 90° and 180°, the gamma-counter being moved, and the coincidence rate was normalized by the single counting rate in each channel to compensate for solid angle variation and slight drifts in counter efficiency.

The vacuum chamber was made large and lined with plastic to minimize scattering effects. Sources of the isotope in question with betas shielded at the source by $\frac{1}{8}$-in. brass were counted to evaluate the effects of gamma-scattering from one counter to the other,

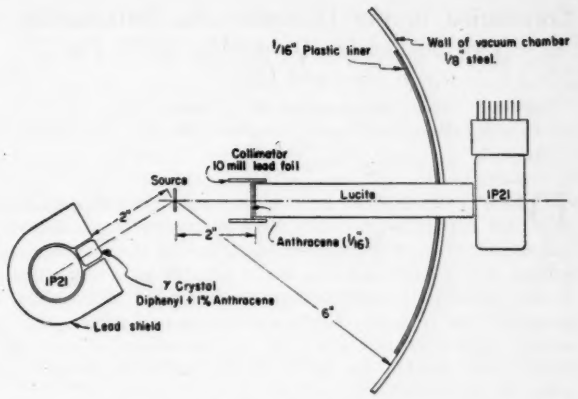

FIG. 1. Geometrical arrangement.

and of any gamma-gamma-correlations for those nuclides that had gamma-rays in coincidence. The gamma-gamma-coincidence rate was largest in Sb^{124}, amounting to 20 percent of the beta-gamma-rate, but showed no angular correlation. Pure beta-emitters Tl^{204} and P^{32} were used to show the absence of beta-scattering from one counter to the other.

The sources were prepared from Oak Ridge irradiated units on 0.1 to 0.2 mg/cm^2 collodion backings. Au^{198} was prepared by the precipitation of a mirror of gold from a chloride solution with oxalic acid, Rb^{86} and Sb^{122} by the evaporation of a solution of a salt to dryness, and Sb^{124} by evaporation of the metal from an electroplated platinum filament in high vacuum. This last method gave a source with no observable irregularities under a 10-power microscope.

Assuming a correlation function $(1+b\cos^2\theta)$, the results are given in Table I. The result for Au^{198} is in agreement with other

TABLE I. Angular correlation function.

Nucleus	Source thickness mg/cm^2	b	Standard deviation
Au^{198}	0.02–0.02	+0.004	0.015
Rb^{86}	1.0	+0.019	0.014
Sb^{122}	0.2	+0.011	0.013
Sb^{124}	<0.2	−0.168	0.025

work,[2,3] that for Rb^{86} agrees with that of Novey,[4] in which the correlation is taken averaged over the whole beta-spectrum as in this work, but is considerably less than the correlations observed by Franckel,[3] and by Deutsch[5] who selected the upper end point of the beta-spectrum. This low result may be due to the chemically deposited source having local thicknesses much greater than the average thickness, which has been experienced with this type of source in beta-spectroscopy. According to the work at Indiana,[6-8] Sb^{124} has five beta-groups, 2.37 (21 percent), 1.62 (8 percent), 1.00 (9 percent), 0.65 (44 percent) and 0.48 (18 percent). It is believed that this correlation should be ascribed to the most energetic transition, and it is consistent with a first- or second-forbidden tensor interaction.[9] A re-analysis of the beta-spectrum data using forbidden shapes might reduce the number of beta-groups necessary to fit the spectrum data, which is not unreasonable in light of the coincidence data not showing the 1.00 and 1.62 groups.[7]

* This work has been supported in part by the joint program of the ONR and AEC.
[1] S. L. Ridgway, Bull. Am. Phys. Soc. **25**, No. 3, 52 (1950).
[2] R. L. Garwin, Phys. Rev. **76**, 1876 (1949).
[3] R. Stump and S. Frankel, Bull. Am. Phys. Soc. **25**, No. 3, 52 (1950).
[4] T. B. Novey, Phys. Rev. **78**, 66 (1950).
[5] D. T. Stevenson and M. Deutsch, Phys. Rev. **78**, 640(A) (1950).
[6] C. S. Cook and L. M. Langer, Phys. Rev. **73**, 1149 (1948).
[7] Kern, Zaffarano, and Mitchell, Phys. Rev. **73**, 1143 (1948).
[8] E. T. Jurney and A. G. C. Mitchell, Phys. Rev. **73**, 1153 (1948).
[9] D. L. Falkoff, Thesis, University of Michigan (1948).

Correlation in the Direction and Polarization of Two Successive Quanta for Rh^{106}, Co^{60}, and Cs^{134}

A. H. WILLIAMS AND M. L. WIEDENBECK
Randall Laboratory of Physics, University of Michigan, Ann Arbor, Michigan
April 21, 1950

DEUTSCH and Metzger[1] have reported their observation of the correlation between the polarization of one quantum and the direction of emission of the other for the two successive gamma-rays of Rh^{106}. We have used a polarimeter of a type similar to that described by Deutsch and have verified their results. In assuming that the two excited states have J-values 020, the angular correlation function $W(\theta)$ can be reasonably well duplicated if one uses half the values of the coefficients α_2 and α_4 as given by Hamilton.[2]

By this same device it is possible also for the data to be in agreement with the theoretical curve in the case of the polarization correlation. Spiers,[3] however, has pointed out that by assuming one of the excited levels to consist of two levels which are close together in energy but which have different spins, then it is possible to account for $W(\theta)$. The expression I_θ/I_ϕ for the polarization correlation, which has been developed by Hamilton[4] can also be accounted for by the assumption of the additional level.

The three spin values ($J_1'=1, 2, 3$) and the two types of transitions (electric dipole and magnetic dipole) suggested by Spiers allow six combinations to be tried for this additional level. Our data, as shown in Fig. 1, indicate that the most likely transitions are $J_1'=3$ (magnetic dipole) or $J_1'=1$ (magnetic dipole or electric dipole). These choices with the resulting parities are shown in Fig. 2.

The experimental curve for Co^{60} is shown in Fig. 1. The directional correlation experiments have shown that both transitions are quadrupole. The polarization correlation experiment indicates that both transitions are electric. The parities of the two excited states are then the same as that of the ground state.

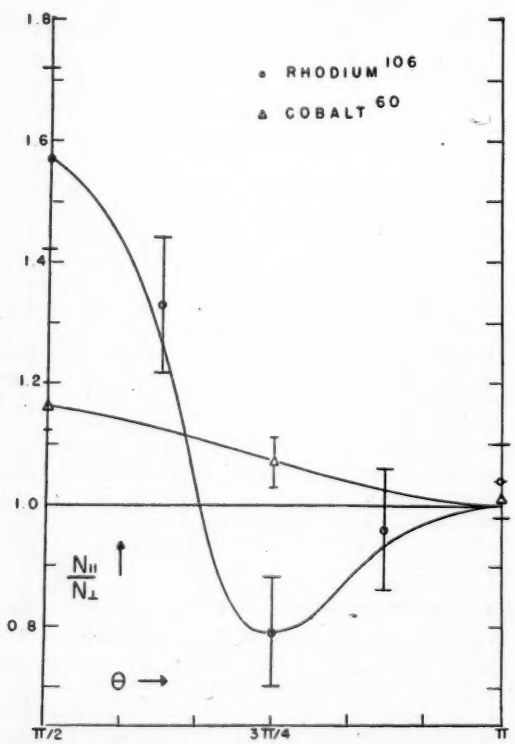

FIG. 1. Polarization of Rh^{106} and Co^{60} gamma-rays.

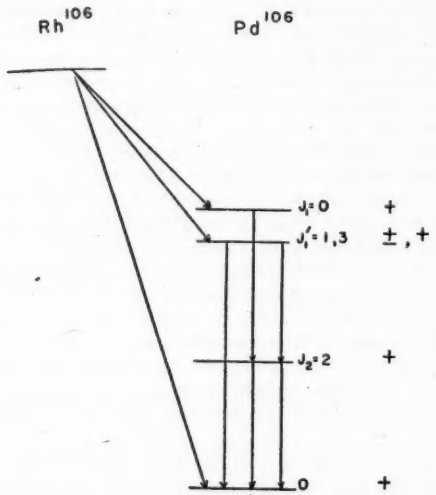

FIG. 2. Energy level scheme for Rh^{106}. The parity for $J'_1=1$ is even or odd, that for $J_1'=3$ is even.

In the case of Cs^{134}, no polarization correlation was observed. According to the theory a correlation should be found for two quadrupole transitions, one of which is magnetic and the other electric, only if the experimental arrangement is such that one can distinguish between which of the two quanta goes to the polarimeter or to the individual counter. In our case this discrimination was not possible. If both transitions are electric or both magnetic, this discrimination is not necessary in order to observe a correlation. If one assumes then that both transitions are quadrupole, the conclusion is that one is electric and the other magnetic.

[1] M. Deutsch and F. Metzger, Phys. Rev. **74**, 1542 (1948).
[2] D. R. Hamilton, Phys. Rev. **58**, 122 (1940).
[3] J. A. Spiers, Phys. Rev. **78**, 75 (1950).
[4] D. R. Hamilton, Phys. Rev. **74**, 782 (1948).

Double Beta-Decay of Te^{130}

MARK G. INGHRAM AND JOHN H. REYNOLDS
University of Chicago and Argonne National Laboratory, Chicago, Illinois
April 27, 1950

IN a previous letter[1] the authors described the preliminary results of a study of the double beta-transition $Te^{130} \rightarrow Xe^{130}$ by the method of isotopic analysis of xenon extracted from geologically old tellurium ores. The ore on which that work was based was blasted from an outcrop at Mångfallberget, Sweden, and it contained 12 percent by weight of the mineral Bi_2Te_3. Although the age of the telluride minerals in Mångfallberget and in Boliden, Sweden is known to be 1500 ± 500 million years, there exists an uncertainty in the "xenon age" of the Mångfallberget material owing to the possibility of comparatively recent crystal alteration by percolating surface waters.

As a result of the generous cooperation of Dr. Erland Grip of the Boliden Mining Company, we have recently obtained some excellent samples of 70 percent rich Bi_2Te_3 from the 240-meter level of the Boliden mine. According to geologists, it is improbable that the crystals of this Bi_2Te_3 have been affected by a recent alteration. A 371-g sample of this material, containing 124 g of tellurium, was broken up to pea size and vacuum roasted at temperatures high enough to decompose the mineral and produce vigorous boiling of the molten bismuth and tellurium. The rare gases evolved were purified as before,[1] and were found to consist of 2.4×10^{-2} cc S.T.P. argon plus 2.6×10^{-7} cc S.T.P. xenon. The results of an isotopic analysis of this xenon are presented in Table I. The percentage composition of the excess or radiogenic

TABLE I. Isotopic composition of xenon extracted from 371 g of a 1.5×10^9 year old mineral containing 70 percent Bi_2Te_3. The total xenon content was 2.6×10^{-7} cc S.T.P.

Mass	Bi_2Te No. 4	Normal	Diff.	Difference normalized
124	<0.004	0.0005	<0.0035	<0.29 —
126	<0.005	0.0005	<0.0045	<0.38 —
128	<0.014	0.011	<0.003	<0.25 —
129	=1.000	0.1525	0.8475	71.66±0.7
130	0.0652	0.0236	0.0416	3.52±0.17
131	0.4088	0.1235	0.2853	24.12±0.3
132	0.1566	=0.1566	=0.0000	=0.00 —
134	0.0651	0.0611	0.0040	0.34±0.25
136	0.0562	0.0519	0.0043	0.36±0.16

xenon has been given in the last row of the table. These percentages were calculated by assuming that all of the Xe^{132} present was normal (atmospheric), and by subtracting corresponding amounts at the other mass positions. It is evident from the table that, aside from the somewhat questionable excess xenon at mass 134 and 136 (possibly due to uranium fission), the excess xenon is distributed among the isotopes Xe^{129}, Xe^{130}, and Xe^{131}.

The excess Xe^{129} and Xe^{131} is probably caused by (n,γ) reactions on Te^{128} and Te^{130}. To account for the neutron "flux" required to produce this much xenon in 1.5×10^9 years, it is necessary to assume that there was considerable uranium in the immediate neighborhood of the tellurium mineral. Dr. Grip informs us that unusually large amounts of the uranium mineral thucholite have been found in the stope from which the Bi_2Te_3 was taken. Thus we ascribe the excess Xe^{129} and Xe^{131} to the proximity of such a deposit.

An interesting discrepancy appears in the ratio of Xe^{129} to Xe^{131} found in the sample. The present measurements show this to be 3.0, whereas one would expect a ratio of 0.6 from Seren's values[2] for the tellurium cross sections. One possible explanation is that Xe^{129} was also produced by the decay of small amounts of $I^{129}(\sim3\times10^7$ yr.) present in the mineral. This nuclide, as yet undetected in nature, may have been formed originally in amounts comparable to that of I^{127}.

The excess Xe^{130} is attributed to double beta-decay of Te^{130}. There appears to be no other explanation for its formation. Assuming an age of 1.5×10^9 years for the Bi_2Te_3, the excess Xe^{130} present corresponds to double beta-decay of Te^{130} with a half-life of 1.4×10^{21} years. This result is to be compared with theoretical half-lives of 6×10^{14} years and 10^{24} years, the former computed from the Majorana theory of the neutrino, and the latter from the Dirac theory. Both calculations are for allowed transitions with 1.6 Mev of available energy.

[1] M. G. Inghram and J. H. Reynolds, Phys. Rev. **76**, 1265 (1949).
[2] Seren, Friedlander, and Turkel, Phys. Rev. **72**, 888 (1947).

The Effect of the Compressibility of the Earth on Its Magnetic Field

C. TRUESDELL
Applied Mathematics Branch, Mechanics Division, Naval Research Laboratory, Washington, D. C.
April 25, 1950

IN his recent review of geomagnetism associated with the earth's interior Elsasser[1] has noted that the equation for the magnetic induction **B** in a fluid moving with velocity **v** reduces to

$$D\mathbf{B}/Dt=\mathbf{B}\cdot\mathbf{grad}\mathbf{v}-\mathbf{B}\,\mathrm{div}\mathbf{v}, \tag{1}$$

provided displacement currents and decay may be neglected. He remarks that "we may safely drop the last term, considering the fluid as incompressible," so that (1) reduces to a form "analogous to the well-known Helmholtz equations for the conservation of vorticity . . . ," whence results analogous to the Helmholtz theorems follow.

While the neglect of volume changes is doubtless justified for motions at uniform depth, the great pressure gradients conjectured to exist in the earth's interior make it rather unlikely that Elsasser's approximation is justified if there be any considerable vertical motion. In some of the models suggested by Bullard[2] a part of the flow is nearly vertical. The neglect of compressibility effects is quite unnecessary, however, to obtain the conservation theorems. Equation (1) as it stands is a youthful discovery of Lagrange,[3] and Nanson[4] observed that by using Euler's continuity equation

$$\mathrm{div}\mathbf{v}=-D\log\rho/Dt, \tag{2}$$

where ρ is the density, one can reduce it to the form

$$D(\mathbf{B}/\rho)/Dt=(\mathbf{B}/\rho)\cdot\mathbf{grad}\mathbf{v}. \tag{3}$$

Hence the analogs of the Helmholtz theorems for the present instance may be stated in the following form: (a) the lines of induction are material lines, (b) the flux of induction,[5] $\int_S\mathbf{B}\cdot d\mathbf{S}$, is constant in time for a material surface S.

Among the finest proofs of these results are those of Kirchhoff,[6] who derived them directly from Cauchy's formula[7]

$$\mathbf{B}/\rho=\mathbf{B}_0/\rho_0\cdot\mathbf{GRAD}\,\mathbf{r}, \tag{4}$$

where $\mathbf{B}_0$ and ρ_0 are the values of **B** and ρ at some arbitrary initial instant $t=0$, and **GRAD r** is the gradient of the present position field **r** with respect to the initial position field **R**. It is easy to see that (4) is the general solution of (3).

In fact, however, Zorawski[8] showed directly that a condition of the form (a) is both necessary and sufficient for the validity of theorems of the Helmholtzian type for the field **B**, irrespective of its physical significance.

Equivalent to (b) is the conservation of the circulation of the magnetic vector potential around a material circuit.

For motions in the earth's interior the case when the flow is rotationally symmetric and the field **B** is perpendicular to the axial planes might be relevant for part of the motion. Equation (4) then reduces to a result analogous to the vorticity convection theorem of Svanberg:[9]

$$B/r\rho=\mathrm{const.} \tag{5}$$

for each particle, r being the distance from the axis of symmetry. In motions of this type the effect of density changes appears in a particularly lucid way, tending to counteract the increase in B incident upon approaching the axis of symmetry.

[1] W. M. Elsasser, Rev. Mod. Phys. **22**, 1 (1950). See p. 30.
[2] E. C. Bullard, Proc. Roy. Soc. **A197**, 433 (1949). See Section 8.
[3] J. L. Lagrange, Misc. Taur. **2**[3] (1760–1761), 196–298 (1762) =Oeuvres I, 365–468. See Chapter XLII.
[4] E. J. Nanson, Mess. Math. **3**, 120–121 (1874).
[5] This result was discovered by Cowling. See W. M. Elsasser, Phys. Rev. **72**, 821 (1947), see p. 827.
[6] G. Kirchhoff, *Vorlesungen über mathematische Physik: Mechanik* (Leipzig, 1876); second edition (1877); third edition (1883). See Vorlesung 15, §3.
[7] A.-L. Cauchy, *Théorie de la propagation des ondes à la surface d'un fluide pesant d'une profondeur indéfinie* (1815). Mem. Divers Savants (2) **1** (1816), 3–312 =Oeuvres (1) **1**, 5–318. See part I, Section 1, §4.
[8] K. Zorawski, Bull. Acad. Sci. Cracovie, Comptes Rendus 335–342 (1900). See R. Prim and C. Truesdell, Proc. Am. Math. Soc. **1**, 32–34 (1950).
[9] A. F. Svanberg, *On fluides rörelse*, K. Vetenskaps-Acad. Handlingar (1839), pp. 139–154 (1841)—trans. "Sur le mouvement des fluides," J. Reine Angew. Math. **24**, 153–163 (1842).

The Production of π^+-Mesons by Protons on Protons in the Direction of the Beam*

W. F. CARTWRIGHT, C. RICHMAN, M. N. WHITEHEAD, AND H. A. WILCOX
Radiation Laboratory, Department of Physics, University of California, Berkeley, California
April 26, 1950

A SIMPLE method[1] has recently been developed for measuring the differential production cross sections of positive and negative π-mesons when various nuclei are struck by high energy charged particles from the 184-in. synchrocyclotron. In this

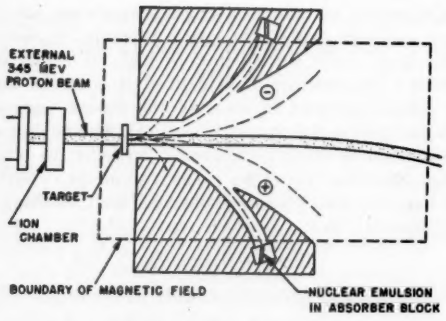

FIG. 1. Experimental arrangement for observing mesons produced in direction of proton beam.

method mesons and other particles leave a target and lodge in suitably arranged absorber blocks. Nuclear emulsions are embedded in these blocks to sample the population of stopped positive and negative π-mesons of all energies. The method is not very desirable for extreme forward angles, however, because the number of scattered beam particles relative to the number of mesons leaving the target rises very rapidly in the forward direction.

We have developed the following technique for making easy and reliable observations in the extreme forward directions. A magnetic field is produced in the region about the target (Fig. 1). The external beam from the cyclotron traverses this target after being integrated by a calibrated ionization chamber. Positive and negative π-mesons leaving the target in the forward direction circle out and away from the beam on opposite sides, as is indicated by the dotted trajectories in the diagram. Broad channels are cut symmetrically in massive Cu shielding blocks as shown in Fig. 1. Positive and negative mesons possessing appropriate momenta are able to traverse these channels and to lodge in the absorber blocks. Nuclear emulsions are embedded in these blocks, as in our previous method. Some protons and other heavy charged particles also are able to traverse the channel on the positive side, but those which do so must necessarily possess roughly the same momenta as do the mesons. Hence their ranges will be much smaller than the meson ranges, and a complete separation is obtained between the positive π-mesons and the "background" of heavy charged particles coming from the target. On the negative side no trouble is to be expected from electrons because they do not ionize sufficiently heavily to leave background tracks in the nuclear emulsions employed.

This technique for measuring meson production cross sections can easily be adapted for use over the entire meson energy and angular spectrum.

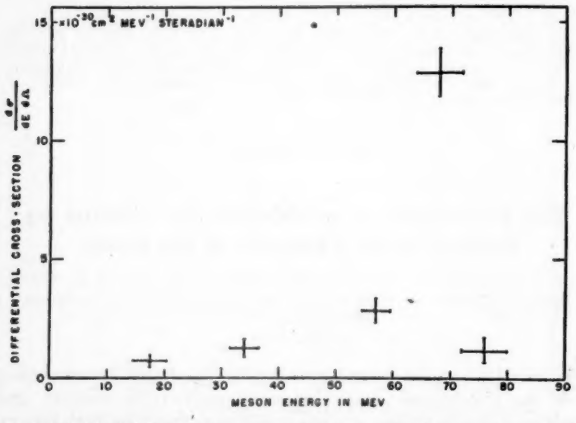

FIG. 2. Absolute differential cross section for production of π^+-mesons by 345-Mev protons on protons in the direction of proton beam.

In our first application of this method we have used the 345-Mev external proton beam from the cyclotron. Two different targets were used, of which one was pure carbon and the other was $(CH_2)_n$ (polyethylene). The angle of observation was $0°\pm5°$. By subtracting the carbon production cross section from that of the CH_2 molecule, we obtain the production from the two "free" protons. The preliminary results on the $p-p$ differential production cross section are presented in Fig. 2. These results are based on 231 π^+-mesons from the CH_2, and 176 π^+-mesons from the C. The errors indicated are statistical probable errors, and are valid for the relative values. The absolute scale is uncertain by ±15 percent.

The main features of this curve are the cut-off around 75 Mev and the high peak near this cut-off. From energy and momentum considerations no mesons should be formed with energies above 70 Mev if a free neutron and proton are the resulting heavy particles. However, at this meson energy, the heavy particles are ejected with the same momenta. G. F. Chew has suggested to us that the peak may be due to the attractive $n-p$ resonance interaction in the final states. If a deuteron is formed the cut-off would be around 74 Mev. We are now investigating, with improved energy resolution, the exact cut-off energy and possible fine structure in the peak.

We wish to thank Professor E. O. Lawrence for his interest and encouragement. We wish also to thank Mr. J. Vale and the cyclotron crew for making the bombardments.

* This work was sponsored by the AEC.

[1] C. Richman and H. A. Wilcox, Phys. Rev. **78**, 496 (1950).

On the Positive and Negative Excess of the Penetrating Component of Cosmic Radiation at 3500 m above Sea Level

I. F. QUERCIA, B. RISPOLI, AND S. SCIUTI
Istituto di Fisica dell'Università di Roma,
Centro di Fisica Nucleare del C.N.R., Roma, Italy

April 18, 1950

WITH a device similar to that of Bernardini *et al.*[1] (Fig. 1), measurements on the "charge effect" of the hard component of cosmic radiation were made at the Laboratio della Testa Grigia, 3500 m above sea level, 45° 50′ north geographical latitude. We recorded the coincidences (AB) per minute between counters A and B, those (BC) between counters B and C, and the threefold coincidences (ABC) the cut-off energy of each lens is about 230 Mev for mesons. The crossed counters worked in anticoincidence. The axis of the telescope was inclined at 0° to the vertical, 60° east and 60° west of the vertical. The "charge effect" is the ratio

$$\delta=[2(N_{cc}-N_{dd})/(N_{cc}+N_{dd})]\times100$$

where N_{cc} and N_{dd} refer, respectively, to the measurements taken with the magnetic lenses converging the positive or negative particles. Our present results, agreeing well with previous ones obtained at different altitudes, are summarized in Tables I and II. Lacking definite information on the meson spectrum at high altitudes, from Table I we can conclude only that the "positive

TABLE I. Charge effect in vertical direction.

Altitude above sea level (m)	δ_{AB}	δ_{BC}	δ_{ABC}
88	2.8±1.3	2.5±1.1	7.3±1.3
3500	2.5±0.7	7.2±0.7	12.3±0.4
5100	9.4±1.4	11.4±1.0	12.8±3.0
7300	13.6±1.2	5.0±1.2	11.7±3.5

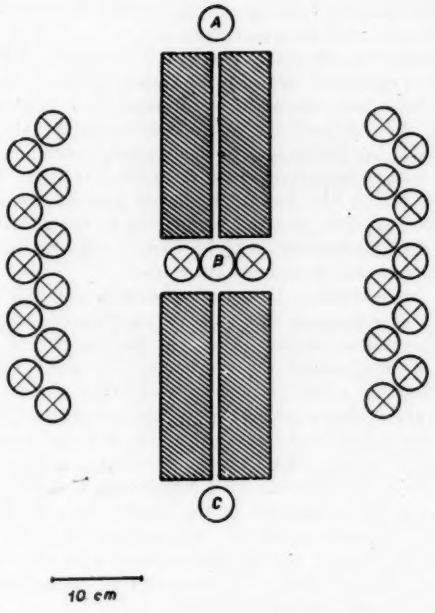

FIG. 1. Schematic diagram of the apparatus.

excess" in the vertical direction shows very little if any increase above 3500 m. *The data given in Table II show that at 3500 m the "charge effect," δ, decreases from positive values in the western direction to negative in the eastern, the observed decrease being monotonic with the change in zenith angle from west to east.*[2] It can be observed that the average values, δ', of δ for the east and west directions at 3500 m agree very well, as expected, with the corresponding values of δ for the vertical direction at sea level. Further, the intensities of the penetrating component of cosmic radiation, i.e., the sums of N_{ee} and N_{dd}, agree very closely with the relative intensities deduced by Rossi's estimates.[3] Obviously one might first be tempted to explain the observed behavior of the values of δ by assuming that the primary radiation responsible for the hard component contains some negative particles, but more probably the observed east-west asymmetry of δ is due to the deflection of the meson trajectories by the earth's magnetic field.[4]

TABLE II. Charge effect at 3500 m.

Zenith angle	δ_{AB}	δ_{BC}	δ_{ABC}
0°	+2.5±0.7	+7.2±0.7	+12.3±0.4
60°E	−5.3±0.7	−4.9±0.8	−7.4±1.0
60°W	+11.2±0.6	+10.9±0.7	+22.2±1.1
$\delta'=\frac{1}{2}(\delta_E+\delta_W)$	δ_{AB}' +2.9±0.9	δ_{BC}' +3.0±1.1	δ_{ABC}' +7.4±1.5

For information on this point some measurements on the energy of the particles that cause the "charge effect" are in progress.

We wish to thank Professor G. Bernardini who suggested this experiment, and Mr. Johannes Buschmann[5] who helped construct and operate the apparatus.

[1] Bernardini, Conversi, Pancini, Scrocco, and Wick, Phys. Rev. **68**, 109 (1945).
[2] After completing the above experiments we learned that Professor Brode had performed similar ones; our results seem to agree fairly well with those he reported at the New York meeting (January, 1950).
[3] B. Rossi, Rev. Mod. Phys. **20**, 537 (1948).
[4] This argument was suggested by Dr. T. H. Johnson at the New York meeting, and was also pointed out to us by Dr. G. Bernardini.
[5] Max Planck Institut für Physik at Göttingen; now at Centro di Fisica Nucleare del C.N.R. at Rome.

The Gamma-Ray Spectrum from the Absorption of π^--Mesons in Hydrogen*

WOLFGANG K. H. PANOFSKY, LEE AAMODT, AND HERBERT F. YORK
Radiation Laboragory, Department of Physics, University of California, Berkeley, California
April 28, 1950

THE gamma-ray spectrum resulting from the absorption of π^--mesons in high pressure hydrogen has been analyzed by means of a pair spectrometer. The results reported here are preliminary and of low accuracy; some of the implications of the experiment are of sufficient certainty at present, however, to warrant giving the results here.

The experimental arrangement is shown in Fig. 1. Protons having energy of 330 Mev circulate in the internal beam of the 184-in. cyclotron and strike a ½-in. deep, 0.040 in., thin tungsten target. The tungsten target is located 2½-in. from the centerline of a hydrogen pressure vessel of 600 cc volume. The hydrogen vessel is surrounded by a very thin-walled liquid nitrogen jacket. Total thickness to be penetrated by the mesons, including the liquid N_2 and two stainless steel walls, is 4.0 g/cm². The vessel is operated at a pressure of 2700 p.s.i.; at liquid nitrogen temperature this gives a density[1] of 0.048. Interference from gamma-rays originating outside the hydrogen volume is reduced by two lead collimators. The gamma-rays are analyzed by use of a pair spectrometer similar to the one used by Bjorklund, Crandall, Moyer, and York.[2] The detectors placed in the pair spectrometer are proportional counters divided by a central bead on the counting wires into two counting volumes. It is thus possible to make observations simultaneously in three energy channels. Various tantalum converters were used to keep multiple scattering losses near 60 percent.

The results from the first series of runs are shown in Fig. 2. The results are principally limited by a low counting rate (of the order of 1 c/min.) and consequently low resolving power and statistics. The total counting rate is in qualitative agreement with the assumption that all the π^--mesons stopped in the H_2 lead to gamma-ray emission. The cross sections as measured by Weissbluth[3] were used in this computation. This fact is in agreement with the conclusion of Wightman[4] that $\pi-\mu$-decay branching is small.

It is certain that the gamma-rays observed are not formed by direct $p-p$ collisions due to protons scattered in the cyclotron

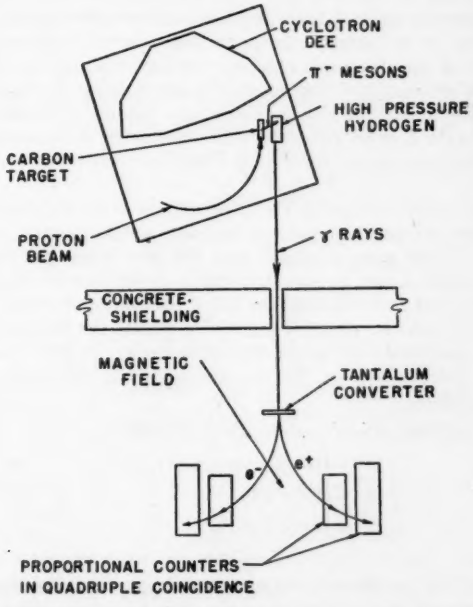

FIG. 1. Geometrical arrangement of cyclotron target, hydrogen pressure vessel, gamma-ray collimators and pair spectrometer.

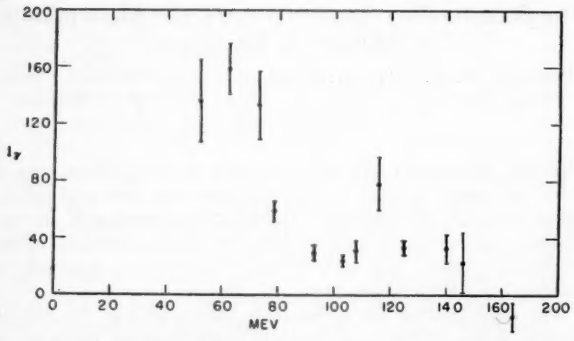

FIG. 2. Gamma-ray intensity as a function of energy. Resolving power "window" is triangular, of 45 percent total base width. One-half its area is contained within ±7.5 percent of peak.

target. If there were sufficient scattered proton flux hitting the hydrogen vessel, then the background count would be much higher. It is known from the experiments of Crandall, Moyer, and York[5] that the cross section for gamma-ray production in H_2 is less than 0.02 of that in carbon; since there is more weight of steel than of H_2 "seen" by the pair spectrometer, and since the background is always less than one-half the total count, the H_2 counts cannot be due to direct production.

Several experiments were made using materials other than H_2. Null results were obtained in helium, carbon, polyethylene (CH_2) and lithium hydride. The fact that null results were obtained in hydrogeneous materials like CH_2 and LiH is a matter of particular interest. It indicates that the probability of final capture in a K-orbit in H_2 in a hydrogeneous compound is small (in fact is less than 1×10^{-3} in CH_2 and less than 3×10^{-3} in LiH). The physical reason is presumably that although a fairly large fraction of π^--mesons is initially captured into high Bohr orbits in hydrogen, the neutral π^-−H system will then diffuse through the lattice and make collisions with C or Li atoms, respectively. During the collisions the π^- in the high Bohr orbit has a large probability of being captured by a Li or C nucleus, with consequent production of a nuclear star rather than a gamma-ray.

The case of absorption of π^--mesons in H_2 as compared with absorption in other materials is a singular one, since the reaction $\pi^-+H^+\rightarrow n$ is possible only in the presence of other nucleons; for absorption by the free proton an additional particle of integral spin must be emitted. Such an additional particle might be a single photon, or, if energetically permitted, a neutral π^0-meson. The details of the absorption process have been discussed by Marshak and Wightman[6] and Wightman.[4] In particular, it has been shown that the sum of the slowing down time, capture time, and arrival time in the K-orbit, caused by collisions leading to Auger electrons, is sufficiently short to compete effectively with the $\pi-\mu$-decay time.[7]

The results plotted in Fig. 2 permit us to state definitely that (1) the emitted gamma-rays are not monochromatic near 130 Mev; (2) the group of points near 130 Mev is not just the tail of a distribution near 70 Mev; the points are significantly higher than the amount inferred from the finite resolving power and a peak near 70 Mev. In terms of number of counts the intensity at 130 Mev approximately equals the intensity at 70 Mev; the curve (Fig. 2) results from the conversion factors pertaining to the spectrometer.

Accordingly let us consider three processes:

$$\pi^-+H\rightarrow n(9\text{ Mev})+\gamma(132\text{ Mev}), \quad (1)$$

$$\pi^-+H\rightarrow n+2\gamma, \quad (2)$$

$$\pi^-+H\rightarrow n+\pi^0+Q, \quad \pi^0\rightarrow 2\gamma \quad (3)$$

Process (2) can almost certainy be ruled out. First, the distribution function seems to be incompatible with any reasonable distribution from a two gamma-process. Second, it is very difficult to see how a selection rule favoring a two gamma-process over a one gamma-process could be constructed.

Accordingly we are led to interpret the results of Fig. 2 in terms of competition between processes (1) and (3). These processes have been discussed by Marshak and Wightman;[6] in particular they derived the lieftimes of processes (1) and (3) under various assumptions as to the character of the meson. The evidence concerning gamma-rays from the cyclotron target[2] in combination with the recent results on gamma-gamma-coincidences obtained from material bombarded in the 330-Mev x-ray beam of the synchrotron[8] is highly convincing that a π^0-meson exists and also that it cannot have spin 1.

If the interpretation that both processes (1) and (3) exist is inferred from the data, then some important approximate quantitative conclusions can be drawn. The first conclusion relates to the mass of the π^0-meson. The width of the "π^0-peak" is defined by the Doppler shift of the gamma-ray emitted by the decay of the π^0-meson and is thus a measure of the reaction energy Q of process (2). If δ is the fractional half-width of the π^0-peak, we can easily show that $\delta=p/M_{\pi^0}$, where p is the momentum of the π^0 and the neutron. From the data we can conclude that $\delta<0.21$, and hence we obtain a direct measure of the upper limits on the kinetic energies of the neutron and π^0. Accordingly the mass difference ΔM between the π^-- and π^0-mesons must obey the inequality: 1.3 Mev $<\Delta M<$4.7 Mev. It is expected that further experiments will narrow these limits considerably.

Since the π^- is principally captured from an orbit of zero angular momentum, and since the kinetic energy of the π^0 is so small that it can be emitted as an S wave only, one can conclude that the π^-- and π^0-mesons have equal parity. Direct calculations[6] based on the various forms of meson theories using the relative magnitudes of π^0- and gamma-yields have been made and yield estimates of the coupling constants involved.[9]

It should be pointed out that the above calculations are significant only if the qualitative arguments for process (3) can be justified.

The authors are indebted to Mr. Hugh Smith for mechanical design and to the operating crew of the 184-in. cyclotron for bombardments. The authors have benefited greatly by discussion of this problem with Drs. Wick and Marshak.

* This work was performed under the auspices of the AEC.
[1] Johnston, Bezman, Rubin, Rifkin, Swanson, and Corak, MDDC-850.
[2] Bjorklund, Crandall, Moyer and York, Phys. Rev. **77**, 213 (1950).
[3] M. Weissbluth, Phys. Rev. **78**, 86(A), (1950).
[4] A. S. Wightman, Thesis, Princeton University (June, 1949), and Phys. Rev. **77**, 521 (1950).
[5] Crandall, Moyer and York (private communication).
[6] R. Marshak and A. Wightman, Phys. Rev. **76**, 114 (1949).
[7] J. R. Richardson, Phys. Rev. **74**, 1720 (1948). E. A. Martinelli and W. K. H. Panofsky, Phys. Rev. **77**, 465 (1950).
[8] Steinberger, Panofsky and Steller (private communication).
[9] R. Marshak and A. Wightman, Bull. Am. Phys. Soc. **25**, No. 3, 29 (1950).

An Oscillographic Method for Observing Magnetic Resonance Spectra

R. MALVANO AND M. PANETTI
Centro Studi per l'Elettrofisica del C.N.R., Physical Institute of the University of Turin, Turin, Italy.
December 19, 1949

A NUMBER of paramagnetic salts, especially those containing ions of the iron group, under the influence of a high frequency magnetic field H and of a steady magnetic field H_0, normal to the former, show one or more peaks of energy absorption for different values[1] of H_0 according to the formula:

$$hc/\lambda=g\beta H_0,$$

where g is Landé's constant, β is Bohr's magneton, and the other symbols have their usual meanings.

This resonance absorption has been investigated by several authors, at least qualitatively, by means of a resonant cavity, enclosing a single crystal or powder of the substance placed in the

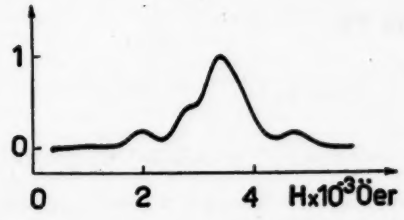

FIG. 1. Oscillogram of the spectrum for potassium chrome alum.

maximum of the magnetic field H and therefore in a node of the electric field, in order to reduce the electric losses. At the same time the substance is subjected to a static magnetic field, the intensity of which is checked with great accuracy. The energy absorption is recorded through the measure of the loaded Q-factor of the cavity. The investigations are carried out with a static method, being the absorption diagram determined point-by-point by many successive measurements.

In the present dynamical method the absorption spectrum is obtained on a cathode-ray oscillograph. On the X-axis the deflection of the cathode beam is proportional to the magnetic field $H_0(t)=H_{01}+H_{02}\sin 2\pi\nu t$ ($\nu=50$ c.p.s.). An integrating circuit is connected with two coils linked with the magnetic field and situated just above and below the absorption cavity. Through a phase shifter, the phase difference between the magnetic field inside and outside the cavity is corrected; the output voltage is applied to the X-axis of the oscillograph.

The Klystron oscillator, which supplies the high frequency power with a wave-length $\lambda\sim 3.16$ cm, is modulated at a frequency of 5×10^4 c.p.s. Such a frequency modulation is transformed into an amplitude modulation determined by the resonance curve of the cavity. A microwave receiver, with a silicon crystal rectifier, placed in a small resonant cavity, is coupled with the measuring cavity. The voltage at the terminal of the crystal is brought to a selective amplifier, tuned to the second harmonic of the modulation frequency (10^5 c.p.s.). At the output of the amplifier the voltage amplitude is a function of the Q of the cavity and hence of the energy absorption. Small variations of Q, and there are always such, are proportional to the variations of the voltage. These are amplified and applied to the input terminals of the Y-axis of the oscillograph, that records directly the oscillogram of the spectrum under examination.

In the discussion of the theory[2] the crystal is assumed to be a square-law detector, since the energy is quite low in the receiver. The fractional deflection on the Y-axis depends linearly (with good approximation) on $\Delta Q/Q$, the term of second-order being ~ 3 percent of the term of first order up to $\Delta Q/Q<5$ percent, assuming for the parameters of the system generator-cavity-detector the following values: $Q\sim$some hundreds; the ratio between mean frequency of the Klystron and the resonance frequency of the cavity $\sim 1:10^{-4}$; the alternating repeller voltage being of the amplitude of ~ 6 volt and of the stated frequency (5×10^4 c.p.s.); $\lambda\sim 3.16$ cm as stated above, and taking into account also the Klystron characteristic parameters. The deflection of the cathode beam does not depend on the variations of the real part of the magnetic permeability, which necessarily accompany the variations of the imaginary part.

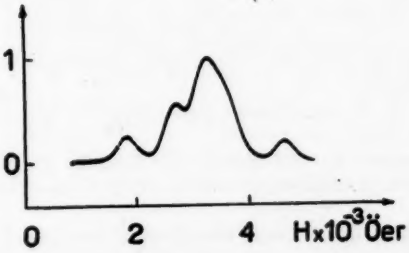

FIG. 2. Oscillogram of the spectrum for ammonium chrome alum.

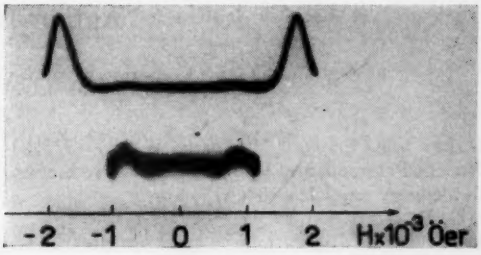

FIG. 3. Oscillogram of the spectrum for ammonium chrome alum, for low values of the magnetic field. The lower curve, traced with the greater amplification, shows the presence of the peak for $H=900$ oersted.

With this method two chrome alums, (potassium chrome alum and ammonium chrome alum) have been examined. In Figs. 1 and 2 the spectra of these salts are shown for the orientation (111). It is worth noting the presence of a small peak of absorption not observed previously, with $H=900$ oersted; this fact is shown on Fig. 3, referring to the spectrum of ammonium chrome alum, which has been obtained with $H_{01}=0$, $H_{02}\sim 2200$ oersted. The splitting determined by the electric field owing to the presence of water molecules of crystallization, is $\delta=0.12_2$ for potassium chrome alum and $\delta=0.13_4$ for ammonium chrome alum.

The authors wish to acknowledge the assistance of Professor Daglio and Dr. Garelli.

[1] B. Bleaney, R. P. Penrose, Proc. Phys. Soc. London **60**, 395 (1948). Whitmer, Weidner, Hsiang, and Weiss, Phys. Rev. **74**, 1478 (1948). D. Halliday and J. Wheatley, Phys. Rev. **74**, 1712 (1948). P. R. Weiss, Phys. Rev. **73**, 470 (1948). R. Malvano and M. Panetti, Nuovo Cimento **7**, 28 (950).

[2] R. Malvano and M. Panetti, Alta Frequenza (to be published).

Erratum: On the Role of the Subsidiary Condition in Quantum Electrodynamics

[Phys. Rev. **78**, 149 (1950)]

F. COESTER AND J. M. JAUCH
Department of Physics, State University of Iowa, Iowa City, Iowa

IN Section III, pp. 151 and 152, the transverse field $\mathfrak{A}_\mu(x)$ defined by Eq. (46), a field $\mathcal{A}_\mu(x)$ defined by Eq. (32),

$$\mathcal{A}_\mu(x)=A_\mu(x)+\partial_\mu B(x),$$

and the ordinary vector potential $A_\mu(x)$ have been confused by a series of typographical errors. $\mathfrak{A}$ should be replaced by $\mathcal{A}$ everywhere on p. 151. A should be replaced by $\mathcal{A}$ in Eq. (34) and on the left-hand side of (48). The last sentence of Section III should read: We may therefore replace $\mathcal{A}_\mu$ by the transverse field $\mathfrak{A}_\mu$ in this case.

The following note was to have been added in proof but was omitted through error. In a recent Letter to the Editor (Phys. Rev. **77**, 420 (1950)) F. J. Dyson discusses the role of the longitudinal photons in Schwinger's theory. Dyson's result is essentially contained in his Eq. (7), which is an immediate consequence of our Eq. (81) as it should be since the definition of the vacuum state is the same as in the present paper.

Author Index to Volume 78

References with (A) are to abstracts of papers presented at meetings of the American Physical Society, and those with (T) designate title only. References with (L) are to Letters to the Editor.

Aamodt, Lee (see Panofsky, Wolfgang, K. H.)—825(L)
——, **Vincent Peterson, and Robert Phillips.** Production of C^{11} by high energy particles—87(A)
Adams, G. D. (see Kerst, D. W.)—297(L)
Adelman, Frank L. Observations on tracks in electron sensitive emulsions—86(A)
Alburger, David E. Beta-ray spectrum of K^{40}—629(L)
—— (see Sunyar, A. W.)—326(A)
——, **D. J. Hughes, and C. Eggler.** β-spectrum of Be^{10}—318(A)
Alfrey, T. (see Mark, H.)—315(T)
Alfvén, H. and N. Herlofson. Cosmic radiation and radio stars—616(L)
Allen, R. C. and Waldo Rall. Energy levels of the F^{20} nucleus from the $F^{19}(d,p)F^{20}$ reaction—337(A)
Allison, H. W. and George E. Moore. Use of radioactive Sr in some thermionic experiments on thin films—354(A)
Alpert, D. (see McCoubrey, A. O.)—315(T)
Anderson, C. D. (see Seriff, A. J.)—290
Anderson, C. E. (see Manning, Thurston E.)—417
—— (see Watson, W. W.)—343(A)
Anderson, P. W. Simple model for ferroelectricity—341(A)
—— Theory of antiferromagnetism—638(T)
Andrews, C. L. Diffraction pattern in the plane of a circular aperture—344(A)
Andrews, F. A., D. A. Spohr, and R. T. Webber. Thermal conductivity of copper and tin at liquid helium temperatures—342(A)
Andrews, R. D., F. H. Holmes, and A. V. Tobolsky. Elastoviscous properties of polyisobutylene. III. Relaxation of stress in whole and fractionated polymers; effect of carbon black—357(T)
Apker, Leroy. Photoelectric techniques in the study of ionic semiconductors—352(T)
Arfken, G. B. (see Breit, G.)—390
Argo, H. V., H. T. Gittings, A. Hemmendinger, G. A. Jarvis, and R. F. Taschek. Properties of the $T^3(p,\gamma)He^4$ reaction—691
Arons, A. B. Pressure at which a rarefaction wave initiates cavitation in sea water—333(A)
Autler, S. H. and C. H. Townes. Resonant modulation, a new technique in radio spectroscopy—340(A)
Averbach, B. L. and B. E. Warren. Cold work and particle size broadening in x-ray diffraction lines—644(A)
Avery, R. (see Blanchard, C. H.)—292(L)
—— **and C. H. Blanchard.** Low states of Li^7—704
Axel, Peter. Isomeric transitions in nuclei—638(T)

Baez, Albert V. and Paul Kirkpatrick. Design and construction of an x-ray microscope—83(A)
Bailey, V. A. Growth of circularly polarized waves in the sun's atmosphere and their escape into space—428
Bailin, Louis L. (see Saxon, David S.)—327(A)
Baker, W. B. (see Whitmore, B. G.)—799
Baker, W. R. (see Kerns, Q. A.)—85(A)
Baldwin, G. C. and F. R. Elder. Neutron production in various substances by 50-Mev x-rays—76(L)
Bandel, H. W. Point-to-plane corona studies in dried air—91(A)
Baños, Alfredo, Jr. (see Saxon, David S.)—327(A)
—— **and William B. McLean.** Theory of the no load characteristics of saturable reactors with hysteresis, I—92(A)
Barber, W. C. Coincidence studies on the decay of Hf^{181}—82(A)
—— Excited state of Ta^{181} with 1.1×10^{-8}-second lifetime—641(A)
Barbour, Ian. Magnetic deflection of cosmic-ray mesons using nuclear plates—319(A), 518
Bardeen, J. Energy bands and electron mobilities in non-polar crystals—315(T)
Barkas, Walter H. Non-equilibrium cyclotron orbits—90(A)
—— (see Smith, F. M.)—86(A)
Baron, M. L. and A. de Bretteville, Jr. Combination two-circle goniometer and x-ray spectrometer—344(A)
Baroody, E. M. Theory of secondary electron emission from metals—780
Barrett, C. S. and D. F. Clifton. Transformation characteristics of a lithium-magnesium alloy—639(A)
Bartholomew, G. A. (see Kinsey, B. B.)—77(L), 481(L)
Bartnoff, Shepard, Charles R. Mingins, and Joseph F. Clayton. Vibrations of a circular crystalline plate—316(A)
Bates, D. R. Dissociative recombination—492(L)
Bateson, W. O. Proton groups from the deuteron bombardment of boron—337(A)
Beams, J. W. Magnetic suspension balance—471(L)
Becker, M. (see Fan, H. Y.)—178(L), 335(A)
—— (see Lark-Horovitz, K.)—334(A)
—— **and H. Y. Fan.** Photovoltaic effect of *P-N* junctions in germanium—301(L)
Bederson, B. (see Fisher, L. H.)—331(A)
—— **and L. H. Fisher.** Interpretation of formative time lags of spark breakdown in air at low overvoltages—331(A)
Beeman, W. W. (see Kaesberg, Paul)—336(A)
——, **Paul Kaesberg, and H. N. Ritland.** Shapes and hydrations of several protein molecules in solution—336(A)
Beenakker, J. J. M. (see Taconis, K. W.)—171(L)
Belinfante, Frederik J. Quantum-electrodynamics—642(A)
——**and J. S. Lomont.** Quantization of Wheeler-Feynman's electrodynamics—346(A)
Bell, P. R. Measurement of forbidden beta-spectra with the scintillation spectrometer—638(T)
Bell, R. E. and R. L. Graham. Measurement of a second half-life in Yb^{170}—490(L)
Béné, G. J., P. M. Denis, and R. C. Extermann. Nuclear magnetic moments of the gallium isotopes—66(L)
Benfield, A. E. Temperature in an accreting planet—334(A)
Bennett, W. E. (see Bradford, C. E.)—302(L)
Bennett, Willard H. Non-magnetic radiofrequency mass spectrometer—332(A)
Bergmann, Peter G. (see Heller, Jack)—329(A)
——, **Robert Penfield, Ralph Schiller, and Henry Zatzkis.** Hamiltonian of Einstein's theory of gravitation with electromagnetic field—329(A)
Beringer, Robert and J. G. Castle, Jr. Magnetic resonance absorption in nitric oxide—567
—— **and J. G. Castle, Jr.** Microwave magnetic resonance spectra of NO—340(A)
Berlin, T. H. and L. Madansky. On the detection of γ-ray polarization by pair production—623(L)
Bernardini, G. Neutron evaporations produced by cosmic rays—314(T)
Bernstein, R. B. and Daniel Cubicciotti. Hydrogen permeability of zirconium—639(A)
Berry, Chester R. and Robert L. Griffith. Structure and growth mechanism of photolytic silver in silver bromide—317(A)
Berry, Clifford E. Effects of initial energies on mass spectra—597
Bethe, H. A. (see Levinger, J. S.)—115

Bickford, L. R., Jr. Ferromagnetic resonance absorption in magnetite single crystals—449
—— Magnetic resonance abosrption in magnetite at low temperatures—342(A)
Biedenharn, L. and J. M. Blatt. Some calculations concerning neutron-proton scattering with tensor forces—322(A)
Biehl, A. T. and H. V. Neher. Latitude and longitude effects in cosmic rays over the United States and Canada at 30,000 feet—172(L)
Binder, Daniel. Delayed coincidence measurement of $Hg^{203,205}$—325(A)
Bishop, A. S. (see Smith, F. M.)—86(A)
—— (see Steinberger, J.)—319(A), 493(L), 494(L)
Blair, K. W. (see Burson, S. B.)—89(A)
Blanchard, C. H. (see Avery, R.)—704
——, **R. Avery, and R. G. Sachs.** Velocity dependent nuclear interactions—292(L)
Blatt, J. M. (see Biedenharn, L.)—322(A)
Blau, Marietta (see Rudin, Robert)—319(A)
——, **John Nafe, and Herbert Bramson.** Dependence of high altitude star and meson production rates on absorbers—320(A)
Bleakney, Walker (see Fletcher, C. H.)—634(L)
Bleaney, B. Nuclear specific heats in paramagnetic salts—214
Bloch, F. and R. K. Wangsness. Differential equations of nuclear induction—82(A)
Blocker, Wade and Robert W. Kenney. Showers initiated by 335-Mev bremsstrahlung—87(A)
Bloembergen, N. Nuclear relaxation in solids—638(T)
—— On the ferromagnetic resonance in nickel and supermalloy—578
Boehmer, Howard W. (see Broxon, James W.)—411
Bogle, R. W. Noise spectra from vacuum tubes at ultra low frequencies—354(A)
Bohm, D., M. Weinstein, and H. Kouts. Covariant description of extended charges—346(A)
Bohr, N. and L. Rosenfeld. Field and charge measurements in quantum electrodynamics—794
Bolef, D. (see Zeiger, H.)—340(A)
Bond, W. L. Technique of cutting germanium filaments—646(A)
——, **W. P. Mason, H. J. McSkimin, K. M. Olsen, and G. K. Teal.** Elastic constants of germanium single crystals—176(L)
Bondelid, R. O. (see Mather, K. B.)—292(L)
Boorse, H. A. (see Cook, D. B.)—343(A), 820(L)
——, **D. B. Cook, and M. W. Zemansky.** Superconductivity of lead—635(L)
Borowitz, S., W. Kohn, and J. Schwinger. On the self-stress of the electron—345(A)
Borst, L. B. Supernovae—807(L)
Bostick, W. H. Effective reduction of scattering of electron beams in tissue by means of a magnetic field—327(A)
Bowker, J. Kent. Observations on grain counting and the photographic emulsion—87(A)
Bowles, J. S. Crystallographic mechanism of the martensite transformation in iron-carbon alloys—639(A)
Boyer, Keith. Energy spectrum of protons from (d,p) reactions—345(A)
—— (see Livingston, M. S.)—344(A)
Boyer, R. F. Random noise in dielectric materials—357(T)
Bradford, C. E. and W. E. Bennett. Neutron groups from $Be^{9}(\alpha,n)C^{12}$—302(L)
Bradner, Hugh (see Smith, F. M.)—86(A)
—— **and S. B. Jones.** Ratio of positive to negative π-meson yields from various targets bombarded by 345 Mev protons—90(A)
Bradt, H. L. (see Kaplon, M. F.)—68(L), 680
Brady, E. L. and M. Deutsch. Angular correlation of successive gamma rays—558
Bragg, J. K. (see Goldstein, J. H.)—347(A)
Bramson, Herbert (see Blau, Marietta)—320(A)
Branscomb, Lewis M. Abnormally low molecular rotation and upper atmosphere temperatures—333(A)
Branyan, C. E. (see Cork, J. M.)—299(L), 304(L)
Brattain, W. H. and G. L. Pearson. Changes in conductivity of germanium induced by alpha-particle bombardment—646(A)
Breckenridge, Robert G. (see Cook, Richard K.)—315(A)
—— **and A. L. Ward.** Anelastic effects in ionic crystals—315(A)
Breit, G. Schmidt model and odd-even staggering of the isotopic shift—470(L)
——, **G. B. Arfken, and W. W. Clendenin.** Spectroscopic isotope shift and nuclear polarization—390
—— **and R. D. Hatcher.** Analysis of proton-proton scattering by means of the f-function—110
Briggs, Thomas H. Determination of oxide cathode performance in diode tubes through figures of merit—356(A)
Brillouin, L. Can the rectifier become a thermodynamical demon?—627(L)
Brobeck, W. M. (see Lofgren, E. J.)—85(A)
—— (see Sewell, D. C.)—85(A)
Brode, R. B. Ratio of positive to negative particles in the cosmic radiation at 3650 meters elevation—92(A)
—— (see Merkle, T. C., Jr.)—92(A)
Brophy, James J. Secondary emission of electrons at oblique angles of incidence—643(A)
Brown, A. B., C. Y. Chao, W. A. Fowler, and C. C. Lauritsen. Excited states of the mirror nuclei Be^{7} and Li^{7}—88(A)
Brown, Frederick C. and J. C. Street. Investigation of cosmic-ray stars and slow protons with a silver chloride crystal—320(A)
Brown, Harold (see Perez-Mendez, Victor)—317(A), 812(L)
—— **and Victor Perez-Mendez.** Beta-spectra of gaseous A^{41} and O^{15}—649
—— **and V. Perez-Mendez.** Beta-spectrum of Ne^{23}—812(L)
Brown, L. J. (see Ogle, W. E.)—63(L)
Brown, Richard M. Nuclear magnetic resonance in weak fields—530
Brown, W. W. and A. S. McKay. Erratum: a cloud-chamber study of cosmic-ray nuclear interactions at 3260 meters elevation—67(L)
Browning, George V. (see Ferry, John D.)—359(A)
Broxon, James W. and Howard W. Boehmer. Cosmic-ray intensity following a solar flare—411
Brueckner, Keith A. Production of mesons by x-rays, part III: theory—84(A)
—— **and K. M. Watson.** Proton-proton scattering in charged scalar theory—495(L)
Bube, Richard H. Trapping in zinc-sulfide-type phosphors—349(A)
Buchdahl, Rolf (see Nielsen, Lawrence E.)—359(A)
——, **L. E. Nielsen, and R. E. Pollard.** Transition phenomenon of polymeric substances—359(A)
Buckingham, R. A. and H. N. V. Temperley. Viscosity of liquid He^{3}—482(L)
Buechner, W. W. (see Malm, R.)—337(A)
—— (see Strait, E. N.)—337(A)
Bullock, M. Loren (see McMinn, William O.)—296(L)
Burg, Anton B. (see Gordy, Walter)—512
Burns, G. Preston. Efficiency of the thermoelectric process—327(A)
Burson, S. B. and K. W. Blair. Proposed decay scheme for $_{72}Hf^{181}$ (46 day, 5.7 hour)—89(A)
Burstein, E. and John J. Oberly. Infra-red properties of diamond, silicon, and germanium—642(A)
—— **and J. J. Oberly.** Optical band width of F centers at liquid helium temperatures—349(A)

Burte, Harris M. Non-destructive mechanical test for wool fibers and some preliminary results—357(A)
Burton, J. A., H. E. Kern, and R. T. Lynch. Thermionic properties of dense oxide cathodes—355(A)
Busala, A. (see Talbott, F. L.)—336(A)
Bushkovitch, A. V. (see Rouse, A. G.)—347(A)
Butler, J. W. (see Whaling, Ward)—72(L)

Caldwell, Richard L. Internal conversion electrons of several short-lived neutron indiced radioactivities—407
Cameron, A. G. W. (see Millar, C. H.)—78(L)
—— **and C. H. Miller.** Evidence for the reactions $N^{14}(\gamma,\alpha)B^{10}$ and $O^{16}(\gamma,\alpha)C^{12}$—337(A)
Campbell, Edward C. and Max Goodrich. Scintillation spectra of short-life activities—640(A)
Carlson, R. O. (see Lee, C. A.)—340(A)
Carr, E. F. and C. Kikuchi. Angular dependence of crystalline nuclear resonance absorption—470(L)
Carson, A. N. (see Ogle, W. E.)—63(L)
Cartwright, W. F., C. Richman, M. N. Whitehead, and H. A. Wilcox. Production of π^+ mesons by protons on protons in the direction of the beam—823(L)
Caspari, M. E. Electro-mechanical coupling of $BaTiO^3$ single-domain crystals—341(A)
Castle, J. G., Jr. (see Beringer, Robert)—340(A), 567
Chamberlain, O. (see Wiegand, C.)—326(A)
Chambers, William H. (see Sheriff, Robert E.)—476(L)
——, **Robert E. Sheriff, and Dudley Williams.** Gyromagnetic ratios of vanadium^{51} and manganese^{55}—640(A)
——, **Robert E. Sheriff, and Dudley Williams.** Nuclear magnetic moment of praseodymium^{141}—482(L)
Chang, Chia-hua (see Cook, C. Sharp)—171(L)
Chang, T. S. Quantum mechanics of localizable dynamical systems—592
Chao, C. Y. (see Brown, A. B.)—88(A)
——, **A. V. Tollestrup, W. A. Fowler, and C. C. Lauritsen.** Low energy α-particles from $F^{19}(p\alpha)O^{16}$—88(A)
Chapman, Robert M. (see Shaw, J. H.)—497(L)
—— **and J. H. Shaw.** Fine structure of HDO near 3.7μ in the solar spectrum—71(L)
——, **John H. Shaw, and Dudley Williams.** High dispersion studies of the solar spectrum—333(A)
Charpie, R. A. (see Sun, Kuan-Han)—338(A)
Cheng, Lin-Sheng and J. D. Kurbatov. Disintegration of cesium 131 and metastable state of xenon 131—319(A)
Cheston, W. B. and L. J. B. Goldfarb. Disintegration of nuclei by π^--mesons—320(A), 683
Chew, Geoffrey F. (see Taylor, T. B.)—86(A)
—— **and Jack L. Steinberger.** Positive-negative ratio for π-mesons produced in complex nuclei—86(A)
—— **and Jack L. Steinberger.** Positive-negative ratio of π-mesons produced singly in collisions of nucleons with complex nuclei—497(L)
Chodorow, Marvin. Stanford University microwave laboratory—82(T)
Christian, Richard S. High energy scattering—theoretical—89(A)
Clarke, Edward N. (see Kelly, Edward)—316(A)
Clayton, Joseph F. (see Bartnoff, Shepard)—316(A)
Cleland, J. W., K. Lark-Horovitz, and J. C. Pigg. Germanium semiconductor alloys produced by transmutation—645(A)
——, **K. Lark-Horovitz, and J. C. Pigg.** Transmutation-produced permanium semiconductors—814(L)
Clendenin, W. W. (see Breit, G.)—390
Clifton, D. F. (see Barrett, C. S.)—639(A)
Coester, F. and J. M. Jauch. On the role of the subsidiary condition in quantum electrodynamics—149; Erratum—828(L)
Cohen, B. L., C. E. Falk, and S. K. Kao. Neutron energy spectra—639(A)
Cohen, E. Richard and M. A. Greenfield. Two group equations for the diffusion of neutrons in a multiplying medium—639(A)
Cohn, Ruth A. and J. D. Kurbatov. Disintegration of zinc 65 by positron emission—318(A)
Coleman, J. S. (see Lindner, M.)—67(L)
Coleman, R. P. Random-circuit theory of resistance and noise in a composition resistor—644(A)
Collins, C. B. (see Macnamara, J.)—129
Conant, F. S., G. L. Hall, and W. James Lyons. Equivalent effects of time and temperature in the shear creep and recovery of elastomers—357(A)
Conrad, Carl M. (see Segal, Leon)—358(A)
Cook, C. Sharp (see Owen, George E.)—686
—— **and Chia-hua Chang.** On the determination of the relative positron activity of Cu^{64} in a source of Cu^{61}—171(L)
Cook, D. B. (see Boorse, H. A.)—635(L)
——, **H. A. Boorse, and M. W. Zemansky.** Superconducting temperature of lead—343(A)
——, **M. W. Zemansky, and H. A. Boorse.** Superconductivity of columbium—820(L)
Cook, Richard K. and Robert G. Breckenridge. Anelasticity of quartz crystals—315(A)
Copeland, Paul L. (see Eggenberger, Delbert N.)—643(A)
Corak, W. S. (see Wexler, Aaron)—260
Corben, H. C. Accelerated and rotating coordinate systems—329(A)
Corey, Victor B. (see Green, James H., Jr.)—328(A)
Cork, J. M., C. E. Branyan, W. C. Rutledge, A. E. Stoddard, and J. M. LeBlanc. Gamma-rays from terbium 160—304(L)
——, **H. B. Keller, W. C. Rutledge, and A. E. Stoddard.** Reinterpretation of the electron spectra of radioactive ytterbium and tantalum—95
——, **A. E. Stoddard, W. C. Rutledge, C. E. Branyan, and J. LeBlanc.** Radioactivity in hafnium—299(L)
Cowan, E. W. (see Seriff, A. J.)—290
Crandall, W. E., B. J. Moyer, and H. F. York. High energy photons from proton nucleon collision—89(A)
Crawford, J. H., Jr. and K. Lark-Horovitz. Fast neutron bombardment effects in germanium—645(A), 815(L)
Crawford, M. F. (see Hume, J. N. P.)—343(A)
Creely, Joseph J. (see Segal, Leon)—358(A)
Creutz, E. (see Foss, M. H.)—641(A)
Crittenden, E. C., Jr. (see Hoffman, R. W.)—349(A)
—— **and R. W. Hoffman.** Relation of stress and rupture in evaporated metal films to distortion decay—349(A)
Croning, Leo J. Notes on thoria and other refractory materials—352(A)
Cross, W. G. Causes of abnormal efficiencies in scintillation counters—185(L)
Crossley, Walter (see Jacobs, Harold)—356(A)
Crowell, Albert D. and H. E. Farnsworth. Measurements of gas adsorption on metals using a radioactive tracer method—351(A)
Cubicciotti, Daniel (see Bernstein, R. B.)—639(A)
Curtis, C. W. First spark spectrum of manganese—343(A)
Curtiss, L. F. (see Feister, I.)—179(L)

Dailey, B. P. (see Minden, H. T.)—347(A)
—— (see Shulman, R. G.)—145
—— (see Townes, C. H.)—346(A)
Dale, E. B., E. L. Zimmerman, D. G. Thomas, and J. D. Kurbatov. Gamma-spectrum of barium 131—640(A)
Dancoff, S. M. Non-adiabatic meson theory of nuclear forces—382
Dandurand, P. and R. B. Holt. Electron density and spectroscopic measurements in metal vapor afterglows—331(A)

Danforth, W. E. Thoria as a cathode emitter—352(T)
—— **and F. H. Morgan.** Electrical conductivity of sintered thoria—353(A)
Dannis, M. L. Fundamental studies of plasticization of PVC—358(A).
Dart, Francis E. Evaporation of zinc and zinc oxide under electron bombardment—761
Daunt, J. G. and C. V. Heer. Lambda-points of solutions of He^3 in He^4 below 1°K—342(A)
Davis, Leverett, Jr. Polarization of starlight—84(A)
Davis, R. E. (see Lark-Horovitz, K.)—334(A)
De Benedetti, S. (see McGowan, F. K.)—638(T)
de Bretteville, A., Jr. (see Baron, M. L.)—344(A)
—— **and G. Katz.** Preliminary results with macrocrystals of ferroelectric barium titanate—340(A)
de Carvalho, Hervasio G. Range of α-particles in water and ice—330(A)
—— (see Yagoda, Herman)—765
de Hoffmann, Frederic. Neutron-deuteron scattering at high energies—216
Dekker, A. J. and A. H. Morrish. Investigation of color centers by a single-photon counting method—301(L)
de Klerk, D., M. J. Steenland, and C. J. Gorter. Thermodynamic temperature of 1.5 millidegrees absolute—476(L)
de Launay, Jules (see Dolecek, R. L.)—58
Demers, Pierre. Cosmic-ray phenomena in extremely thick emulsions—320(A)
Denis, P. M. (see Béné, G. J.)—66(L)
der Mateosian, E. (see Scharff-Goldhaber, Gertrude)—325(A)
—— **and M. Goldhaber.** Photo-neutron production—326(A)
Deutsch, Martin (see Brady, E. L.)—558
—— (see Livingston, M. S.)—344(A)
—— (see Metzger, Franz)—551
—— (see Stevenson, Donald T.)—640(A)
DeWitt, J. H., Jr. and C. K. Seyfert. Notes on the 1P21 photomultiplier tube when used for astronomical photometry—643(A)
Dibeler, Vernon H. (see Reese, Robert M.)—332(A)
Dickey, J. E. (see Taft, E. A.)—625(L)
Dickinson, W. C. Factors influencing the positions of nuclear magnetic resonances—339(A)
di Francia, G. Toraldo. Variational principle for the computation of reflection coefficients—298(L)
Dodd, Edward E. Short method for evaluation of the Townsend integral for electron avalanche formation—620(L)
—— (see Loeb, L. B.)—91(A)
Dokoupil, Z. (see Taconis, K. W.)—171(L)
Dolecek, R. L. and Jules de Launay. Conservation of flux by a superconducting torus—58
Domenicali, C. A. Magnetic and electric properties of natural and synthetic single crystals of magnetite—458
Donovan, Russell A. (see McMath, Robert R.)—65(L)
Driscoll, R. L. (see Thomas, H. A.)—787
——, **H. A. Thomas, and J. A. Hipple.** Absolute value of the gyromagnetic ratio of the proton—339(A)
Duckworth, Henry E. and Howard A. Johnson. Masses of Cr^{50}, Cr^{52}, and Fe^{54}—179(L)
—— **and Howard A. Johnson.** Packing fractions of Fe^{56}, Ni^{58}, and Ni^{60}—330(A)
——, **Howard A. Johnson, Richard S. Preston, and Richard F. Woodcock.** Some new mass comparisons involving Si, Fe, Ni, Cu, Zn, W, and Pt—386
——, **Karl S. Woodcock, and Richard S. Preston.** Masses of Pd^{104}, Pd^{108}, Pt^{195}, and Cu^{65}—479(L)
DuMond, J. W. M. (see Lind, D. A.)—474(L)
Dunlap, W. C., Jr. (see Jacobi, G. T.)—349(A)
du Pré, F. K. Suggestion regarding the spectral density of flicker noise—615(L)
——, **R. A. Hutner, and E. S. Rittner.** On the interpretation of conduction and thermionic emission of (Ba-Sr)O cathodes—355(A), 573
du Toit, Stefaan J. (see Slätis, Hilding)—498(L)
Dwight, Kirby. Solar magnetic moment and diurnal variation in intensity of cosmic radiation—40
—— (see Stix, T.)—324(A)
—— (see Winckler, J. R.)—324(A)
——, **R. Sabin, T. Stix, and J. R. Winckler.** Directional and latitude survey of cosmic rays at 95,000 feet. II. Interpretation of vertical flux data—324(A)

Edmonds, Frank N., Jr. On the diffusion of imprisoned resonance radiation—424
Eggenberger, Delbert N. and Paul L. Copeland. Transit time of electrons in simple diodes as a function of current density—643(A)
Eggler, C. (see Alburger, D. E.)—318(A)
Eggleston, R. R. and G. L. Weissler. Sensitivity of a positive ion space charge detector—91(A)
Eirich, F. R. (see Schoenberg, M. D.)—359(A)
Eisenstein, A. Oxide-cathode research at the University of Missouri—352(T)
Ekstein, H. Remarks on the magnetic scattering of neutrons—731
Elder, F. R. (see Baldwin, G. C.)—76(L)
Elion, Herbert A. Experimental and theoretical transient heat propagation in a one-dimensional composite material—350(A)
Elliot, J. O. (see Hofstadter, R.)—81(L)
—— (see Liebson, S. H.)—65(L)
Elliott, Norman. Interaction between paramagnetic ions in crystals—341(A)
Elsasser, W. M. Zero-point equation of state at extreme pressures—351(A)
—— (see Swift, C. J.)—64(L)
Elvey, C. T. Progress in upper air research at N.O.T.S.—82(T)
Emmerich, Werner S. and J. D. Kurbatov. Beta-spectrum of prometheum 147—187(A)
Engel, Olive G. (see Rice, O. K.)—183(L)
—— **and O. K. Rice.** Lambda-temperatures of solutions of He^3 in He^4—55
England, R. E. (see Ogle, W. E.)—63(L)
English, W. N. (see Loeb, L. B.)—91(A)
Ertel, A. Effect of impurities on thermionic emission from platinum—352(T), 353(A)
Espersen, George A. (see Levi, Roberto)—231
Estermann, I. Semiconductors as low temperature thermometers—83(A)
Evvard, J. C. Development of supersonic airfoil theory—315(T)
Ewald, A. W. (see Gildart, Lee)—645(A)
Extermann, R. C. (see Béné, G. J.)—66(L)
Eyges, L. Transition curves in lead of x-rays causing nuclear reactions. II. Theoretical—85(A)

Fabricand, B. P. (see Lee, C. A.)—340(A)
Falk, C. E. (see Cohen, B. L.)—639(A)
Fan, H. Y. Temperature dependence of the energy gap in monatomic semiconductors—808(L)
—— (see Becker, M.)—301(L)
—— (see Lark-Horovitz, K.)—334(A)
—— (see Odell, N. H.)—334(A)
—— (see Orman, C.)—646(A)
—— (see Taylor, W. E.)—335(A)
—— **and M. Becker.** Infra-red absorption of silicon—178(L)
—— **and M. Becker.** Temperature dependence of photovoltaic effects on P-N barriers in germanium—335(A)

Faris, F. E. (see Wright, Byron T.)—89(A)
Farly, G. M. (see Kerns, Q. A.)—85(A)
Farnsworth, H. E. (see Crowell, Albert D.)—351(A)
—— (see Kelly, Edward)—316(A)
—— (see Landeen, Stanley A.)—351(A)
—— (see Schlier, Robert E.)—316(A)
Faul, Henry (see Goodman, Clark)—640(A)
Faust, William R. Specific activity of potassium—624(L)
Feenberg, E. (see Present, R. D.)—328(A)
Feister, I. Numerical evaluation of the Fermi beta-distribution function—375
—— **and L. F. Curtiss.** On the disintegration scheme of I^{131}—179(L)
Feld, B. T. (see Osborne, L. S.)—324(A)
——, **I. L. Lebow, and L. S. Osborne.** Relativistic showers in nuclear emulsions (II)—324(A)
Feldman, L. and C. S. Wu. Beta-spectrum of Be^{10}—318(A)
Ferry, John D., W. M. Sawyer, George V. Browning, and Arthur H. Groth, Jr. Dispersion of dynamic rigidity and viscosity in concentrated polyvinyl acetate solutions—359(A)
Feshbach, Herman (see Pease, Robert L.)—322(A)
Feuer, Paula and Hubert M. James. Effect of surface states on the Fermi level of a semiconductor—645(A)
Feynman, R. P. Physical viewpoints in quantum electrodynamics—314(T)
Fierz, M. Non-local fields—184(L)
Fireman, E. L. Double beta-decay—638(T)
Fisher, L. H. (see Bederson, B.)—331(A)
—— **and B. Bederson.** Further measurements of formative time lags of spark breakdown in air—331(A)
Fletcher, C. H., D. K. Weimer, and Walker Bleakney. Pressure behind a shock wave diffracted through a small angle—634(L)
Fluke, Donald J. Apparatus for ultraviolet irradiation of viruses at the temperature of liquid hydrogen—335(A)
—— (see Setlow, R. B.)—335(A)
Foldy, Leslie L. Lower bound on the range of the triplet neutron-proton interactions—636(L)
—— (see Osborn, R. K.)—322(A)
—— **and Siegfried A. Wouthuysen.** On the Dirac theory of spin ½ particles and its non-relativistic limit—29, 345(A)
Forbush, Scott E., Thomas B. Stinchcomb, and Marcel Schein. On the extraordinary increase of cosmic-ray intensity on November 19, 1949—323(A)
Forman, Guy. Study of color centers produced in quartz by x-rays—644(A)
Forman, Ralph and Glenn F. Rouse. Investigation of magnesium as an additive to the nickel base of an oxide cathode—355(A)
Forro, F., Jr. (see Pollard, Ernest)—335(A)
Forster, Harriet H. Cosmic-ray induced nuclear disintegrations at 11,000 meters—247
—— Photographic evidence for the existance of a meson of more than 450 electron masses—92(A)
—— (see Sun, H.)—86(A)
Foss, Martyn H. Steady high magnetic fields—641(A)
——, **J. G. Fox, R. B. Sutton, and E. Creutz.** Synchro-cyclotron magnet—641(A)
Fowler, E. C. (see Fowler, W. B.)—323(A)
——, **J. C. Street, W. B. Fowler, and R. D. Sard.** Cosmic-ray showers observed in a cloud chamber triggered by neutron coincidences—323(A)
Fowler, W. A. (see Brown, A. B.)—88(A)
—— (see Chao, C. Y.)—88(A)
—— (see Tollestrup, A.)—372
Fowler, W. B. (see Fowler, E. C.)—323(A)
——, **R. D. Sard, E. C. Fowler, and J. C. Street.** Stopped cosmic-ray particles observed in a cloud chamber triggered by neutron coincidences—323(A)
Fowles, G. R. Hyperfine structure and nuclear spins of tungsten and tellurium—744
Fox, Francis E. and Karl F. Herzfeld. On the forces producing the ultrasonic wind—156
Fox, J. G. (see Foss, M. H.)—641(A)
Franklin, A. D. "Heterocharge" of Carnauba wax electrets—342(A)
Freier, G., M. Fulk, E. E. Lampi, and J. H. Williams. Total cross section of C, O, Mg, Si, and S for fast neutrons—508
Freistadt, Hans. Approximate solutions of the field equations in Einstein's generalized theory of gravitation—329(A)
Frerichs, R. New optical glasses transparent in the infra-red up to 12μ—643(A)
Fretter, W. B. (see Green, John R.)—92(A)
—— **and John Ise, Jr.** Extensive showers under water—92(A)
Friedlander, G. (see Sunyar, A. W.)—326(A)
Froehlich, H. Shape of absorption lines in dielectrics—315(T)
Fulk, M. (see Freier, G.)—508
Fuoss, R. M. Conduction in liquids and plastics—315(T)

Gaerttner, E. R. and M. L. Yeater. Pair production in the field of the electron by x-rays from a 100-Mev betatron—621(L)
Gammel, J. L. Phase shifts in *p-d* scattering and exchange forces—321(A)
Gangnes, A. V. (see Van Allen, J. A.)—50
Gardner, Eugene (see Smith, F. M.)—86(A)
Garren, A. A. (see Smith, Lloyd)—85(A)
George, Waller (see Kauffman, John)—357(A)
—— **and John Kauffman.** Load-induced x-ray line broadening in nylon filaments—358(A)
Gerjuoy, E. and Harold Gruen. Iteration procedure in the Rayleigh-Ritz principle—90(A)
Germain, Lawrence S. Auger effect in the decay of At^{211}—90(A)
Geschwind, S., H. Minden, and C. H. Townes. Microwave measurements on the stable selenium isotopes in OCSe—174(L)
Ghiorso, A. (see Thompson, S. G.)—298(L)
——, **R. A. James, L. O. Morgan, and G. T. Seaborg.** Preparation of transplutonium isotopes by neutron irradiation—472(L)
Gildart, Lee and A. W. Ewald. Electron mobilities in conducting phosphors—645(A)
Gilliam, O. R., Charles M. Johnson, and Walter Gordy. Microwave spectroscopy in the region from two to three millimeters—140
Gilmore, G. D. (see Spencer, R. S.)—358(A), 358(A)
Gittings, H. T. (see Argo, H. V.)—691
Glendenin, L. E. (see Steinberg, E. P.)—624(L)
Gold, Louis. Analysis of multiple echo effect arising from the release of a stored wave train—332(A)
Goldberg, Leo (see McMath, Robert R.)—65(L)
——, **Orren C. Mohler, A. Keith Pierce, and Robert R. McMath.** $3\nu_3$-band of telluric CO^2 in the solar spectrum—74(L)
Goldfarb, L. J. B. (see Cheston, W. B.)—320(A), 683
Goldhaber, M. (see der Mateosian, E.)—326(A)
—— (see Katz, Robert)—9
—— (see Sunyar, A. W.)—326(A)
Goldsmith, G. J. (see Orman, C.)—646(A)
Goldstein, J. H. and J. K. Bragg. Determination of double-bond character from the microwave spectrum of planar asymmetric top molecules with a quadrupolar nucleus—347(A)
Goldstein, Louis. On the specific heat of liquid-vapor mixtures—351(A)
Goldstein, Martin and Ralph S. Halford. Infra-red spectra of some fibrous protein in polarized radiation—336(A)
Goldwasser, E. L. (see Merkle, T. C., Jr.)—92(A)

Goldwater, D. L. and R. E. Haddad. Certain refractory compounds as thermionic emitters—353(A)
Goodman, Clark, Charles W. Tittle, and Henry Faul. Nuclear radiations in well logging—640(A)
Goodrich, Max (see Campbell, Edward C.)—640(A)
Gordon, Gary D. Theory of thickness-shear resonance of piezoelectric resonators—642(A)
Gordon, W. E. Pressures in hydrogen-oxygen detonations—351(A)
Gordy, Walter (see Gilliam, O. R.)—140
——, **Harold Ring, and Anton B. Burg.** Microwave determination of the structure of borine carbonyl and of nuclear moments of the stable boron isotopes—512
Gorter, C. J. (see de Klerk, D.)—476(L)
Goucher, F. S. Photon yield of electron-hole pairs in germanium—816(L)
—— Quantum yield of electron-hole pairs in germanium—646(A)
Gove, Harry E. Angular distributions of protons emitted in reactions induced by 14-Mev deuterons—345(A)
—— (see Livingston, M. S.)—344(A)
Graham, R. L. (see Bell, R. E.)—490(L)
Graves, J. D. Effect of magnetic fields on the response of gamma-scintillation counters—309(L)
Green, Alex E. S. Experimental and theoretical mesons—187(A)
—— Formalistic *vs.* realistic theories—187(A)
—— Meson mass spectrum—642(A)
Green, James H., Jr. and Victor B. Corey. Analog solution of simultaneous partial differential equations by means of passive and active electrical networks—328(A)
Green, John R. and W. B. Fretter. Production of penetrating showers in carbon—92(A)
Green, L. C. and N. E. Weber. Oscillator strength for the 4*s*-4*p* transition in Ca II—343(A)
Green, Thomas A. Quantum electrodynamics—second-order corrections to the current operator—297(L)
Greene, Richard F. and Sol E. Harrison. Microwave conductivity of semiconductors—348(A)
Greenfield, M. A. (see Cohen, E. Richard)—639(A)
Gregory, Christopher. Commutator equations for fields derived from a variation principle—67(L)
—— General operator field equations derived from a variation principle. Construction of "divergence-less" four-vector operator—479(L)
Greisen, Kenneth. Interpretation of underground cosmic-ray data—65(L)
Griffith, Robert L. (see Berry, Chester R.)—317(A)
Gross, Leonard and Donald R. Hamilton. Beta-spectrum of S^{35}—318(A)
Groth, Arthur H., Jr. (see Ferry, John D.)—359(A)
Gruen, Harold (see Gerjuoy, E.)—90(A)
Grunlund, Jean M., B. G. Harvey, N. Moss, and L. Yaffe. Determination of the maximum energy of the β-rays from 16-hour Am^{242}—69(L)
Guth, E. (see Marshall, J. F.)—738

Haddad, R. E. (see Goldwater, D. L.)—353(A)
Hahn, E. E. (see Miller, P. H., Jr.)—349(A)
—— **and P. H. Miller, Jr.** Conductivity and Hall coefficient of zinc oxide semiconductor—348(A)
Halford, Ralph S. (see Goldstein, Martin)—336(A)
—— (see Savitzky, Abraham)—344(A)
—— **and Roger Newman.** Infra-red spectra for single crystals of ammonium nitrate and thallous nitrate in polarized radiation—348(A)
Hall, G. L. (see Conant, F. S.)—357(A)
Hall, H. (see Halpern, O.)—320(A)
Hall, R. N. Recrystallization purification of germanium—645(A)
Halpern, Otto. On the ratio of positive and negative photomesons—69(L)
—— **and H. Hall.** Statistical considerations concerning the mass of the μ-meson—320(A)
—— **and Charles B. Shaw, Jr.** Further remarks on neutron optics—88(A)
Hamermesh, Bernard and Virginia Hummel. Neutron groups from the reaction $Li^7(p,n)Be^7$—73(L)
Hamermesh, M. and C. O. Muehlhause. Resonance and thermal neutron scattering in V^{51}—175(L)
Hamilton, Donald R. (see Gross, Leonard)—318(A)
Hanna, G. C., B. G. Harvey, and N. Moss. Half-life of Cm^{242}—617(L)
Harkins, William D. Equivalence of protons and neutrons in nuclei—634(L)
Harrison, F. B. (see Reynolds, George T.)—488(L)
Harrison, Sol E. (see Greene, Richard F.)—348(A)
Hart, R. J., K. Russell, and R. M. Steffen. Efficiency of γ-counters—334(A)
Hartz, T. R. and A. van der Ziel. Square-wave modulation method for microwave spectra—473(L)
Harvey, B. G. (see Grunlund, Jean M.)—69(L)
—— (see Hanna, G. C.)—617(L)
Harvey, J. A. (see Livingston, M. S.)—344(A). Neutron binding energies from (d,p) reactions—345(A)
Hatcher, R. D. (see Breit, G.)—110
Haynes, J. R. (see Pearson, G. L.)—295(L)
Haynes, S. K. and J. W. Wedding. Use of three long narrow coils for neutralization of the earth's magnetic field in a beta-ray spectrometer—641(A)
Hayward, Raymond W. Beta-spectra of Zn^{62} and Cu^{62}—87(A)
Hazen, W. E. On the nuclear collision path length for π-mesons—320(A)
Heer, C. V. (see Daunt, J. G.)—342(A)
Hees, George (see Jacobs, Harold)—356(A)
Heller, Jack and Peter G. Bergmann. Covariant spinor theory—329(A)
Heller, Robert (see McGannon, J.)—317(A)
—— (see Sturcken, Edward)—327(A)
Helmholz, A. C. and K. Strauch. Nuclear cross sections for x-rays from the Berkeley synchrotron—86(A)
Helstrom, C. W. Production and annihilation of antiprotons—88(A)
Hemmendinger, A. (see Argo, H. V.)—691
Henri, V. P. (see Kraushaar, W. L.)—486(L)
Henrich, L. R. (see Smith, Lloyd)—85(A)
Henry, Allan (see Margenau, Henry)—587
Hereford, Frank L. Multiple scattering effects in the measurement of maximum electron ranges—327(A)
—— **and Charles P. Swann.** Maximum range of high energy electrons in aluminum and copper—727
Herlofson, N. (see Alfvén, H.)—616(L)
Herring, Conyers. Review of some facts on temperature variation of activation energies—352(T)
Herzfeld, Karl F. (see Fox, Francis E.)—156
Heydenburg, N. P. (see Whitehead, W. D.)—338(A)
Hill, David L. Asymmetry of nuclear fission—320(A)
Hill, R. D. (see Katz, Robert)—9
Hiltner, W. A. On polarization of radiation by interstellar medium—170(L)
Hipple, J. A. (see Driscoll, R. L.)—339(A)
—— (see Thomas, H. A.)—787
——, **H. Sommer, and H. A. Thomas.** Omegatron—332(A)
Hoffman, R. W. (see Crittenden, E. C., Jr.)—349(A)
—— **and E. C. Crittenden, Jr.** Determination of stresses in evaporated metal films—349(A)
Hofstadter, Robert (see McIntyre, John A.)—617(L)
——, **S. H. Liebson, and J. O. Elliot.** Terphenyl and dibenzyl scintillation counters—81(L)
—— **and John A. McIntyre.** Measurement of gamma-ray energies with two crystals in coincidence—619(L)

—— **and John A. McIntyre.** Simultaneity in the Compton effect—24
Hogan, C. L. and R. B. Sawyer. Measurement of thermal conductivity of metals at high temperature—350(A)
Holden, R. B., W. J. Taylor, and H. L. Johnston. Variable thickness low temperature infra-red absorption cell—344(A)
Holmes, F. H. (see Andrews, R. D.)—357(T)
Holstein, T. (see McCoubrey, A. O.)—315(T)
Holt, R. B. (see Dandurand, P.)—331(A)
Homer, H. H. (see Lowry, E. F.)—355(A)
Hopkins, John I. Response of the anthracene scintillation counter to monoenergetic electrons—643(A)
Hornig, D. F. and F. P. Reding. Infra-red spectra of crystalline ammonia and deutero-ammonia—348(A)
Horton, C. W., F. C. Karal, and C. M. McKinney. On the radiation patterns of dielectric rods of circular cross section—327(A)
Howard, Louis N. (see McGuire, T. R.)—342(A)
Hsiao, C. (see Seriff, A. J.)—290
Hsiao, C. C. and J. A. Sauer. On crazing of linear high polymers—358(A)
Hsu, Kung-Ngou (see Hu, Tsi-Ming)—633(L)
Hu, Tsi-Ming and Kung-Ngou Hsu. Binding energy of the triton—633(L)
Hudson, Alvin M. (see Rosen, Louis)—533
Hudspeth, Emmett L. and Charles P. Swann. Deuteron bombardment of C^{14}—337(A)
Huggins, M. L. Plasticity and elasticity: some fundamental concepts—336(A)
Hughes, D. J. Neutron mirrors—315(T)
—— (see Alburger, D. E.)—318(A)
—— **and D. Sherman.** Fast neutron cross sections and nuclear shells—632(L)
Hume, J. N. P. and M. F. Crawford. Configuration interactions in the Pb III spectrum—343(A)
Hummel, Virginia (see Hamermesh, Bernard)—73(L)
Hung, C. S. and V. A. Johnson. Resistivity of semiconductors containing both acceptor and donator impurity levels—335(A)
Hunten, D. M. Nuclear magnetic moment of Sc^{45}—806(L)
Hurst, G. S. Measurement of fast neutron dosage to tissue with a proportional counter—640(A)
Hutner, R. A. (see du Pré, F. K.)—355(A), 573

Inghram, Mark G. and John H. Reynolds. Double beta-decay of Te^{130}—822(L)
Inglis, D. R. Doublets of N^{15} and O^{16}—616(L)
—— Scarcity of states of Li^7, from magnetic observation of $Be^9(d,\alpha)Li^7$—104
Ise, John, Jr. (see Fretter, W. B.)—92(A)
Ivey, H. F. and C. L. Shackelford. Convenient methods for thermionic emission calculations—356(A)

Jacobi, G. T. and W. C. Dunlap, Jr. Low temperature instability of germanium—349(A)
Jacobs, Harold, George Hees, and Walter Crossley. Effects of controlled impurities in nickel core metal on thermionic emission from oxide-coated cathodes—356(A)
—— **and Jack Martin.** Role of cathode temperature in a glow discharge—331(A)
James, Hubert M. (see Feuer, Paula)—645(A)
James, R. A. (see Ghiorso, A.)—472(L)
Jarvis, G. A. (see Argo, H. V.)—691(A)
Jauch, J. M. (see Coester, F.)—149, 828(L)
Jeffries, C. D. Magnetic moment of the proton in units of the nuclear magneton—83(A)
Jen, C. K. Nuclear magnetic moment of S^{33}—339(A)
Jeppesen, C. R. and Paul E. Pflueger. New bands in the $3p^1\Pi$-$ls^1\Sigma$ system of the hydrogen molecule—91(A)
Jepsen, Robert L. Thermionic and secondary emission properties of magnetron cathodes and their influence on magnetron operation—354(A)
Jesse, William P. and John Sadauskis. Range-energy curves for alpha-particles and protons—1
Johnson, Charles M. (see Gilliam, O. R.)—140
Johnson, Gerald W. Oriented overgrowth of alkali halides on Ag, Bi, Sb, and Fe—316(A)
Johnson, Howard A. (see Duckworth, Henry E.)—179(L), 330(A), 386
Johnson, M. H. and B. A. Lippmann. Relativistic Kepler problem—329(A)
Johnson, V. A. (see Hung, C. S.)—335(A)
Johnston, H. L. (see Holden, R. B.)—344(A)
—— (see Taylor, W. J.)—343(A)
Jones, L. C. (see Rouse, A. G.)—347(A)
Jones, R. J. (see Livingston, R. S.)—329(A)
Jones, Stanley B. (see Bradner, H.)—90(A)
—— **and R. Stephen White.** Relative yield functions for π^--mesons from carbon—12
Jones, W. B., H. R. Kratz, J. L. Lawson, G. L. Ragan, and H. G. Voorhies. New method for particle injection into accelerators—60

Kaesberg, Paul (see Beeman, W. W.)—336(A)
——, **W. W. Beeman, and H. N. Ritland.** Double crystal and slit methods in small angle x-ray scattering—336(A)
Kallmann, Hartmut. Scintillation counting with solutions—621(L)
Kao, S. K. (see Cohen, B. L.)—639(A)
Kaplan, Joseph. Heat of dissociation of nitrogen—93(A)
—— Infra-red spectra of the night sky, aurora and afterglows—82(A)
Kaplan, Nathan (see Yagoda, Herman)—765
Kaplon, M. F., H. Bradt, and B. Peters. Erratum: evidence for multiple meson and γ-ray production in cosmic-ray stars—68(L)
——, **B. Peters, and H. L. Bradt.** Energy transfer to nucleons in cosmic-ray stars at 95,000 feet—680
Karal, F. C. (see Horton, C. W.)—327(A)
Karash, W. J. (see Kenty, C.)—625(L)
Karr, H. J. (see Mather, K. B.)—292(L)
Katz, G. (see de Bretteville, A., Jr.)—340 (A)
Katz, Robert, R. D. Hill, and M. Goldhaber. Disintegration of Te^{121} and Te^{123} isomers—9
Katzenstein, J. Radiative collisions of positrons and electrons—161
Kauffman, John (see George, Waller)—358(A)
—— **and Waller George.** Incubation of plastic shocks in certain polymeric films—357(A)
Kaufman, Raymond. Ionization potentials of some molecules commonly used in counters—332(A)
Kauzmann, W. (see Slifkin, L.)—631(L)
Kê, T'ing-Śui. Anomalous internal friction associated with the precipitation of copper in cold worked Al-Cu alloys—420
Keepin, G. R., Jr. and J. H. Roberts. Fast neutron spectrometer employing Li^6 impregnated emulsions—87(A)
Keilholtz, G. W. (see Southern, A. L.)—639(A)
Keller, H. B. (see Cork, J. M.)—95
Keller, J. W., Jr. (see Liebson, S. H.)—305(L)
Kelly, Edward, H. E. Farnsworth, and Edward N. Clarke. Photoelectric work function of a silver film on the (100) face of a silver crystal—316(A)
Kenney, Robert W. (see Blocker, Wade)—87(A)
Kenty, Carl. Temperature of the mercury arc—626(L)
—— **and W. J. Karash.** X-ray determination of Hg arc temperature—625(L)
Kern, H. E. (see Burton, J. A.)—355(A)
—— **and R. T. Lynch.** Diode studies of oxide-coated cathodes—355(A)

Kerns, Q. A., W. R. Baker, G. M. Farly, and J. Riedel. Bevatron model radiofrequency system—85(A)
Kerst, D. W., G. D. Adams, H. W. Koch, and C. S. Robinson. Operation of a 300-Mev betatron—297(L)
Kiepenheuer, K. O. On the origin of cosmic radiation from the sun—809(L)
Kies, J. A. and A. M. Sullivan. Fracture markings in plastics—357(A)
Kikuchi, C. (see Carr, E. F.)—470(L)
King, Gilbert W. Effect of excluded volume on the configurations of long chain molecules—359(T)
—— Monte-Carlo method in quantum mechanics—328(A)
Kinsey, B. B., G. A. Bartholomew, and W. H. Walker. Neutron binding energies in Pb^{207}, Pb^{208}, and in Bi^{210}—77(L)
——, **G. A. Bartholomew, and W. H. Walker.** Transitions to the ground states in nuclei excited by slow neutron capture—481(L)
Kirkpatrick, Paul (see Baez, Albert V.)—83(A)
Kisliuk, P. and C. H. Townes. Rotational spectrum and molecular structure of PCl_3—347(A)
Kittel, C. (see Shockley, W.)—341(A)
Klein, J. A. (see Loubser, J. H. N.)—348(A)
Klick, Clifford C. Luminescence of color centers in lithium fluoride—644(A)
Koch, G. P. (see Taylor, W. J.)—343(A)
Koch, H. W. (see Kerst, D. W.)—297(L)
Koehler, W. C., E. O. Wollan, and C. G. Shull. Studies of neutron diffraction by some nuclei with zero spin—640(A)
Kohn, W. (see Borowitz, S.)—345(A)
Konopinski, E. J. Theory of forbidden beta-ray transitions—638(T)
Kouts, H. (see Bohm, D.)—346(A)
Kowarski, Lew. Magic numbers and elements with no stable isotopes—477(L)
Kratz, H. R. (see Jones, W. B.)—60
Kraushaar, W. L., J. E. Thomas, Jr., and V. P. Henri. Detection of the π-μ-decay with a scintillation crystal—486(L)
Kruger, P. G. (see Leiter, H. A.)—663
—— (see Rodgers, F. A.)—656
Kundu, D. N. and M. L. Pool. Copper 61 and 67—488(L)
—— **and M. L. Pool.** Dependence of Fermi $|M|^2 f$ on Z for certain isotopic numbers—328(A)
Kunkel, W. B. Electrical charges on dust particles—91(A)
Kunstadter, John W. Correction to be applied to the activity neutron-activated cadmium-covered indium foils—484(L)
Kurbatov, J. D. (see Cheng, Lin-Sheng)—319(A)
—— (see Cohn, Ruth A.)—318(A)
—— (see Dale, E. B.)—640(A)
—— (see Emmerich, Werner S.)—187(A)
Kusch, P. Nuclear magnetic moments of the gallium isotopes—615(L)
—— (see Ochs, S. A.)—184(L)

Lamb, Willis E., Jr. and Miriam Skinner. Fine structure of singly ionized helium—539
Lampi, E. E. (see Freier, G.)—508
Landé, Alfred. Interaction between elementary particles—346(A)
Landeen, Stanley A., H. E. Farnsworth, and Russell K. Sherburne. Application of a mass spectrometer to the study of surface reactions at low pressures—351(A)
Landon, H. H. Proton-gamma-ray coincidence study of the energy level scheme of Si30—338(A)
Langer, Lawrence M. and R. Douglas Moffat. Precise determination of the energy of the Cs^{137} gamma-radiation—74(L)
Lark-Horovitz, K. Nucleon bombardment of semiconductors—638(T)
—— (see Cleland, J. W.)—645(A), 814(L)
—— (see Crawford, J. H., Jr.)—645(A), 815(L)
——(see Orman, C.)—646(A)
——, **M. Becker, R. E. Davis, and H. Y. Fan.** Nucleon-bombarded silicon—334(A)
Lauer, James L. Optical alignment of a recording near infrared spectrophotometer—344(A)
Lauritsen, C. C. (see Brown, A. B.)—88(A)
—— (see Chao, C. Y.)—88(A)
—— (see Tollestrup, A.)—372
Lauritsen, T. (see Thomas, R. G.)—88(A)
—— **and R. G. Thomas.** Gamma-radiation from an excited state of Be^7—88(A)
Lawrance, Richard B. Centrifugal distortion in the formal dehyde molecule—347(A)
—— (see Weiss, M. T.)—202
Lawrence, E. O. (see Lofgren, E. J.)—85(A)
—— (see Sewell, D. C.)—85(A)
Lawson, A. W. Thermal expansion in silver halides—185(L)
Lawson, J. L. (see Jones, W. B.)—60
Lax, Melvin. On k well-known cross-section theorem—306(L)
—— Variational method for non-conservative collisions—306(L)
—— Variational methods and cross-section theorem for non-conservative collisions—322(A)
Leaderman, H. Structure and physical properties of crystalline polymers—315(T)
LeBlanc, J. M. (see Cork, J. M.)—299(L), 304(L)
Lebow, I. L. (see Feld, B. T.)—324(A)
—— (see Osborne, L. S.)—324(A)
Lee, C. A., R. O. Carlson, B. P. Fabricand, and I. I. Rabi. Radiofrequency spectrum of $TlCl^{35}$—340(A)
Lehovec, K. Recovery of selenium rectifiers after passing of short current pulses—348(A)
Leighton, R. B. (see Seriff, A. J.)—290
Leiter, H. A. (see Rodgers, F. A.)—656
——, **F. A. Rodgers, and P. G. Kruger.** Angular distribution of protons from the D-D reaction at 10 Mev—663
Leith, C. E. Multiple scattering deflector for the 184-inch cyclotron—89(A)
Leser, W. H. (see Weir, C. E.)—357(A)
Levi, Roberto and George A. Espersen. Preparation of rhenium emitters and measurements of their thermionic properties—231
Levinger, J. S. and H. A. Bethe. Dipole transitions in the nuclear photo-effect—115
Levinstein, Henry (see Wyrick, Ralph)—304(L)
Levinthal, C. (see Silverman, A.)—87(A)
——, **E. A. Martinelli, and A. Silverman.** Inelastic scattering of protons by aluminum and carbon—199
Levinthal, E. C. Relative nuclear moments of H^1 and H^2—204
Levitas, Alfred. Analysis of acoustic scattering by variational methods—333(A)
Lewis, H. W. Multiple scattering in an infinite medium—321(A), 526
Lewis, Harold W. Cosmic-ray bursts in ionization chambers of different materials—483(L)
Lidofsky, L. J. (see Macklin, P. A.)—318(A)
——, **P. A. Macklin, and C. S. Wu.** Bromine 80 and its isomers—318(A)
Liebson, S. H. (see Hofstadter, R.)—81(L)
—— **and J. O. Elliot.** Temperature variation of decay times of scintillation phosphors—65(L)
—— **and J. W. Keller, Jr.** Temperature dependence of organic scintillation counters—305(L)
Lin, C. C. Stability theory of viscous flows—315(T)
Lind, D. A., W. J. West, and J. W. M. DuMond. Erratum: x-ray and gamma-ray reflection properties from 500 x-units to 9 x-units of unstressed and of bent quartz plates—474(L)
Lindenbaum, Seymour (see Rudin, Robert)—319(A)

Lindner, M. and J. S. Coleman. New beta-emitting isotopes in region of tungsten—67(L)
—— **and I. Perlman.** Spallation products of antimony irradiated with high energy particles—499
Lindström, Gunnar. Experimental investigation of the nuclear magnetic moments of D^2 and H^1—817(L)
Lippmann, B. A. (see Johnson, M. H.)—329(A)
Little, J. B. (see Teal, G. K.)—647(A)
Livingston, M. S., K. Boyer, H. E. Gove, J. A. Harvey, and M. Deutsch. Studies of disintegrations by 14-Mev deuterons—344(A)
Livingston, R. S., R. J. Jones, and R. E. Wright. High intensity ion source for cyclotrons—329(A)
Loeb, Arthur L. Interionic attraction theory for regions of solutions near high potential surfaces—350(A)
Loeb, L. B., J. H. Parker, E. E. Dodd, and W. N. English. Choice of gap forms for corona breakdown studies and the electrostatic field in a point-to-plane gap—91(A)
Lofgren, E. J. (see Sewell, D. C.)—85(A)
——, **W. M. Brobeck, E. O. Lawrence, and D. C. Sewell.** Bevatron model operating results—85(A)
Logan, R. A. (see Ochs, S. A.)—184(L)
Lomont, J. S. (see Belinfante, F. J.)—346(A)
Loomis, C. C. (see Weiss, M. T.)—202
Loomis, F. W. Can physics serve two masters?—315(T)
Lopes, J. Leite. Nucleon magnetic moment in meson pair theories—36
Lord, J. J. and Marcel Schein. Fluctuation of the nuclear disintegration rate in photographic emulsions exposed in the stratosphere following a solar flare—321(A)
—— **and Marcel Schein.** Intensity of primary heavy nuclei in the stratosphere at night—484(L)
Loubser, J. H. N. and J. A. Klein. Absorption of millimeter waves in ND^3—348(A)
Lowry, E. F., E. L. Mager, and H. H. Homer. Study of cathode behavior in fluorescent lamps—355(A)
Luyet, B. On the heat of devitrification of aqueous solutions—641(A)
Lynch, R. T. (see Burton, J. A.)—355(A)
—— (see Kern, H. E.)—355(A)
Lyons, W. James. Some theoretical considerations of dynamic-property data on textile specimens—357(A)
—— (see Conant, F. S.)—357(A)

Mackenzie, Alexander (see Murray, R. T. K.)—350(A)
Macklin, P. A. (see Lidofsky, L. J.)—318(A)
——, **L. J. Lidofsky, and C. S. Wu.** Beta-spectrum of Na^{22}—318(A)
Macnamara, J., C. B. Collins, and H. G. Thode. Fission yield of Xe^{133} and fine structure in the mass yield curve—129
—— **and H. G. Thode.** Comparison of the isotopic constitution of terrestrial and meteoritic sulfur—307(L)
Madansky, L. (see Berlin, T. H.)—623(L)
Mager, E. L. (see Lowry, E. F.)—355(A)
Magnusson, L. B., S. G. Thompson, and G. T. Seaborg. New isotopes of neptunium—363
Malm, R. and W. W. Buechner. Energy levels in N^{15}—337(A)
Malvano, R. and M. Panetti. Oscillographic method for observing magnetic resonance spectra—826(L)
Mandeville, C. E. Some characteristics of the 11-day neodymium—319(A)
—— (see Shapiro, E.)—319(A)
—— (see Swann, C. P.)—338(A)
—— (see Whitehead, W. D.)—337(A)
Manning, Thurston E., C. E. Anderson, and W. W. Watson. Isotope shift in the spectrum of neutral lead—417
Margenau, Henry and Allan Henry. Theory of magnetic resonance in nitric oxide—587
Mark, H. and T. Alfrey. Modern plastics—315(T)
Marquez, Luis and I. Perlman. Neutron deficient isotopes of iodine—189
Marshak, R. E. Isobaric state of nucleon—346(A)
Marshall, J. F. and E. Guth. Photo-disintegration of the deuteron at high energies—738
Martin, Jack (see Jacobs, Harold)—331(A)
Martinelli, E. A. (see Levinthal, C.)—199
Mason, W. P. (see Bond, W. L.)—176(L)
Massey, H. S. W. and B. L. Moiseiwitsch. Scattering of electrons by hydrogen atoms—180(L)
Mather, K. B., H. J. Karr, and R. O. Bondelid. Deuteron-proton scattering at 10 Mev—292(L)
Matheson, R. M. and L. S. Nergaard. Decay and recovery of the pulsed emission of oxide-coated cathodes—355(A)
Maxwell, Emanuel. Isotope effect in the superconductivity of mercury—477(L)
Mayer, Maria Goeppert. Nuclear configurations in the spin-orbit coupling model. I. Empirical evidence—16
—— Nuclear configurations in the spin-orbit coupling model. II. Theoretical considerations—22
Mays, J. M. (see Minden, H. T.)—347 (A)
McAfee, K. B., Jr. Magnetic electron spin—nuclear spin interaction in the rotational spectrum of NO^2—340(A)
McCord, R. V. (see Snell, Arthur H.)—310(L), 317(A)
McCoubrey, A. O., D. Alpert, and T. Holstein. Imprisonment of resonance radiation in mercury vapor—315(T)
McElhinney, J. and W. E. Ogle. Cu^{63} photo-neutron threshold—63(L)
McGannon, J., R. Heller, and A. H. Weber. Lattice constants of zinc oxide—317(A)
McGowan, F. K. Radiation from $Au^{197*}(7\times10^{-9}$ sec.)—325(A)
—— **and S. De Benedetti.** Measurement of short-lived isomeric states—630(T)
McGuire, T. R. and Louis N. Howard. Specific heat determination on non-metallic ferrites—342(A)
McIntyre, John A. (see Hofstadter, Robert)—24, 619(L)
—— **and Robert Hofstadter.** Measurement of gamma-ray energies with one crystal—617(L)
McKay, A. S. (see Brown, W. W.)—67(L)
McKeown, M. (see Scharff-Goldhaber, Gertrude)—325(A)
McKinney, C. M. (see Horton, C. W.)—327(A)
McLean, William B. (see Baños, Alfredo, Jr.)—92(A)
McMath, Robert R. (see Goldberg, Leo)—74(L)
——, **A. Keith Pierce, Orren C. Mohler, Leo Goldberg, and Russell A. Donovan.** N^2O bands in the solar spectrum—65(L)
McMillan, Edwin M. (see Peterson, Jack M.)—84(A)
—— (see White, R. Stephen)—84(A)
McMinn, William O., M. B. Sampson, and M. Loren Bullock. Proton groups from the alpha-particles bombardment of beryllium—296(L)
McNally, J. O. Life tests of oxide-coated cathodes—an engineering report—356(A)
McSkimin, H. J. (see Bond, W. L.)—176(L)
Meacham, L. A. and S. E. Michaels. Observations of the rapid withdrawal of stored holes from germanium transistors and varistors—175(L)
Meagher, R. E. Proton-proton scattering at 5 Mev—667
Meinel, A. B. Near-infra-red spectrum of the night sky and aurora—82(T)
Meinke, W. W. and G. T. Seaborg. Extension of alpha- and beta-decay systematics of protactinium isotopes—475(L)
Merkle, T. C., Jr., E. L. Goldwasser, and R. B. Brode. Mass measurements of cosmic-ray particles—92(A)
Merz, W. J. Behavior of $BaTiO^3$ crystals under hydrostatic pressure—341(A)
—— Dependence of the piezoelectric effect of $BaTiO^3$ single crystals on temperature up to 160°C—642(A)
—— Effect of hydrostatic pressure on the Curie point of barium titanate single crystals—52

Metzger, Franz and Martin Deutsch. Study of the polarization-direction correlation of successive gamma-ray quanta—551
Michaels, S. E. (see Meacham, L. A.)—175(L)
Millar, C. H. (see Cameron, A. G. W.)—337(A)
—— **and A. G. W. Cameron.** Photo-alpha-reactions in oxygen and nitrogen—78(L)
Miller, D. W. Search for nuclear energy levels in C^{13}—806(L)
Miller, Daniel R. Chromium isotope of mass 55—808(L)
Miller, P. H., Jr. (see Hahn, E. E.)—348(A)
—— (see Russell, B. R.)—645(A)
—— **and E. E. Hahn.** Some electrical properties of zinc oxide semiconductor—349(A)
—— **and B. J. Rothlein.** Preliminary study of the work function of contaminated metal surfaces—354(A)
Minden, H. T. (see Geschwind, S.)—174(L)
——, **J. M. Mays, and B. P. Dailey.** Microwave spectrum of CH_3SiF_3—347(A)
Mingins, Charles R. (see Bartnoff, Shepard)—316(A)
Moffat, R. Douglas (see Langer, Lawrence M.)—74(L)
Mohler, Fred L. Total ionization of hydrocarbons from mass spectral data—332(A)
—— (see Reese, Robert M.)—332(A)
Mohler, Orren C. (see Goldberg, Leo)—74(L)
—— (see McMath, Robert R.)—65(L)
Moiseiwitsch, B. L. (see Massey, H. S. W.)—180(L)
Molnar, J. P. Conduction phenomena in gases—315(T)
Montgomery, H. C. and W. Shockley. Noise in germanium related to fluctuations in hole concentration—646(A)
Moon, M. L. (see Waggoner, M. A.)—295(L)
Moore, Donald C. (see Neissel, John P.)—643(A)
Moore, George E. (see Allison, H. W.)—354(A)
Morgan, F. H. Refractory thermocouples and emissivity determinations—353(A)
—— (see Danforth, W. E.)—353(A)
Morgan, H. W. (see Southern, A. L.)—639(A)
Morgan, L. O. (see Ghiorso, A.)—472(L)
Morin, F. J. Magnetic susceptibility of αFe_2O_3 and αFe_2O_3 with added titanium—819(L)
Morrish, A. H. (see Dekker, A. J.)—301(L)
Morrison, P. On the history of the noble gases—334(A)
Morse, Philip M. (see Pellam, John R.)—474(L)
Morton, G. A. Scintillation counters and photo-multipliers—315(T)
Moseley, H. M. and Nathan Rosen. Are mesons elementary particles?—67(L)
Moses, H. E. and Ta-You Wu. Distribution of atomic and molecular oxygen in the upper atmosphere—333(A)
Moss, N. (see Grunlund, Jean M.)—69(L)
—— (see Hanna, G. C.)—617(L)
Moyer, B. J. (see Crandall, W. E.)—89(A)
Mrozowski, S. Semiconductivity of polycrystalline graphite—644(A)
Muehlhause, C. O. (see Hamermesh, M.)—175(L)
Mueller, D. W. (see Seitz, Frederick)—605
Murakawa, K. Revision of the hyperfine structure of the spectrum of mercury—480(L)
Murray, R. T. K. and Alexander Mackenzie. Field electron emission from dielectrics—350(A)
Myers, Vernon. Intermolecular forces in benzene—348(A)

Nafe, John (see Blau, Marietta)—320(A)
Nakajima, Sadao, Kazuhisa Tomita, and Tunemaru Usui. Phenomenological theory of liquid helium II—768
Nechaj, J. F. (see Sun, Kuan-Han)—338(A)
Neher, H. V. Correlation of geomagnetic cosmic-ray effects—674
—— (see Biehl, A. T.)—172(L)
Neissel, John P. and Donald C. Moore. Scintillation counters as detectors of soft x-rays—643(A)
Nelson, Herbert. Base-metal effects in thoria-coated filaments—353(A)
Nergaard, L. S. (see Matheson, R. M.)—355(A)
Nesbitt, E. A. Magnetostriction of permanent magnet alloys—638(A)
Nesbitt, L. B. (see Reynolds, C. A.)—487(L)
—— (see Serin, B.)—813(L)
Neumann, H. M. and I. Perlman. Isotopic assignments of bismuth isotopes produced with high energy particles—191
Newell, G. F. Crystal statistics of a two-dimensional Ising lattice—444
—— Electric quadrupole moment of the deuteron—711
Newman, Roger (see Halford, Ralph S.)—348(A)
—— **and Edward M. Purcell.** Nuclear spin relaxation in KH_2PO_4, KH_2AsO_4, $NH_4H_2PO_4$, and $NH_4H_2AsO_4$—339(A)
Newton, T. D. Decay constants from coincidence experiments—490(L)
Nichols, M. H. Average thermionic constants of polycrystalline tungsten wires—158
Nielsen, Harald H. *l*-type doubling in OCS and HCN—296(L)
—— Note on the centrifugal stretching in axially symmetric molecules—415
Nielsen, John P. Interfacial energies *vs.* tensions in polycrystalline matter—350(A)
Nielsen, Lawrence E. (see Buchdahl, R.)—359(A)
—— **and Rolf Buchdahl.** Mechanical properties of oriented polystyrene films—359(A)
Nordheim, L. W. β-decay and the nuclear shell model—294(L)
Nottingham, W. B. Experimental techniques involved in thermionic studies of clean metals—352(T)
Novey, Theodore B. Beta-gamma-angular correlation—66(L)
Noyes, H. P. Phenomenological interpretation of *p-p* scattering at 32 Mev—90(A)

Oberly, John J. (see Burstein, E.)—349(A), 642(A)
Ochs, S. A., R. A. Logan, and P. Kusch. H.f.s. anomaly of the potassium isotopes—184(L)
Odell, N. H. and H. Y. Fan. Impedance characteristics of grain boundaries in high resistivity *N*-type germanium—334(A)
Oetjen, R. A. (see Shaffer, W. H.)—187(A)
Ogle, W. E. (see McElhinney, J.)—63(L)
——, **L. J. Brown, and A. N. Carson.** Thresholds for the photo-disintegration of Zr^{90}, Pr^{141}, As^{75}, I^{127}, and Ni^{58}—63(L)
—— **and R. E. England.** Photo-neutron thresholds of titanium^{46} and chromium^{50}—63(L)
Olsen, K. M. (see Bond, W. L.)—176(L)
Orman, C., H. Y. Fan, G. J. Goldsmith, and K. Lark-Horovitz. Germanium *P-N* barriers as counters—646(A)
Osborn, R. K. and L. L. Foldy. On the phenomenological theory of exchange moments—322(A)
Osborne, L. S. (see Feld, B. T.)—324(A)
——, **B. T. Feld, and I. L. Lebow.** Relativistic showers in nuclear emulsions (I)—324(A)
Ostroski, A. S. and R. B. Stambaugh. Emulsion polymerization with ultrasonic vibration—358(A)
Owen, George E., C. Sharp Cook, and Paul H. Owen. Disintegration of Cu^{61}—686
Owen, Paul H. (see Owen, George E.)—686
Oxholm, M. L. (see Shaw, J. H.)—497(L)
Oxley, C. L. (see Towler, O. A., Jr.)—326(A)

Packard, M. E. Nuclear induction apparatus for observing signals in gases—83(A)
Palumbo, T. R. Ceramic heaters and cathodes for electron tubes—356(A)
Panetti, M. (see Malvano, R.)—826(L)
Panofsky, Wolfgang, K. H. (see Steinberger, J.)—802

——, **Lee Aamodt, and Herbert F. York.** Gamma-ray spectrum from the absorption of π^--mesons in hydrogen—825(L)
—— **and H. F. York.** Absorption of π^--mesons in hydrogenous materials—89(A)
Parker, J. H. (see Loeb, L. B.)—91(A)
Parkins, W. E. (see Rasor, N. S.)—638(A)
Pauli, W., Jr. Recent developments of quanticized field theories—315(T)
Pearson, G. L. Magneto-resistance effect in oriented single crystals of germanium—646(A)
—— (see Brattain, W. H.)—646(A)
——, **J. R. Haynes, and W. Shockley.** Comment on mobility anomalies in germanium—295(L)
Pease, Robert L. and Herman Feshbach. Range of tensor forces and the theory of H^3—322(A)
Pecjak, F. A. (see Sun, Kuan-Han)—338(A)
Peck, R. A., Jr. Spectrum of neutrons from Ta(*dn*)—338(A)
Pellam, John R. Observation of second sound radiation pressure by the thermal pitot tube—818(L)
—— **and Philip M. Morse.** Thermal Rayleigh disk in liquid He II—474(L)
Penfield, Robert (see Bergmann, Peter G.)—329(A)
Penndorf, R. On the origin of the sodium *D*-lines during twilight—66(L)
Perez Mendez, Victor (see Brown, Harold)—649, 812(L)
—— **and Harold Brown.** Beta-spectrum of He^6—317(A)
—— **and H. Brown.** Gamma-radiation from Ne^{23}—812(L)
Perlman, I. (see Lindner, M.)—499
—— (see Marquez, Luis)—189
—— (see Neumann, H. M.)—191
Peters, B. (see Kaplon, M. F.)—68(L), 680
Peterson, Jack M. (see White, R. Stephen)—84(A)
——, **Edwin M. McMillan, and R. Stephen White.** Production of mesons by x-rays, part II: experimental results—84(A)
Peterson, John W. Influence of the piezo-electric effect on tribo-electrification—91(A)
Peterson, Vincent (see Aamodt, Lee)—87(A)
Petropoulos, G. M. Avalanche transformation during breakdown in uniform fields—250
Pflueger, Paul E. (see Jeppesen, C. R.)—91(A)
Phillips, Robert (see Aamodt, Lee)—87(A)
Piccioni, Oreste. Interaction of pi-mesons—78(L)
Pierce, A. Keith (see Goldberg, Leo)—74(L)
—— (see McMath, Robert R.)—65(L)
Pietenpol, W. J., J. D. Rogers, and Dudley Williams. Microwave spectra of asymmetric top molecules—480(L)
Pigg, J. C. (see Cleland, J. W.)—645(A), 814(L)
Piore, E. R. Government support and thermionics—352(T)
Pirani, F. A. E. (see Schild, A.)—329(A)
Plass, Gilbert N. and John Strong. Radiation equilibrium in the stratosphere—334(A)
Pleasonton, Frances (see Snell, Arthur H.)—310(L), 317(A)
Plumlee, R. H. Mass spectrometric studies of oxide cathode sublimation phenomena—90(A)
Podolsky, Boris. Heat conduction problem—187(A)
Pollard, Ernest and F. Forro, Jr. Cyclotron bombardment of enzymes and viruses—335(A)
Pollard, R. E. (see Buchdahl, R.)—359(A)
Pomerantz, Martin A. Increase in the primary cosmic-ray intensity at high latitudes, and the non-existence of a detectable permanent solar magnetic field—325(A)
Pool, M. L. (see Kundu, D. N.)—328(A), 488(L)
—— (see Robertson, B. E.)—318(A)
Post, R. F. Preliminary results—operation of a high power electron linear accelerator—92(A)
—— **and N. S. Shiren.** Characteristics of scintillation counters using pulsed photo-multipliers—644(A)
—— **and N. S. Shiren.** Decay time of stilbene scintillations as a function of temperature—80(L)
—— **and N. S. Shiren.** Performance of pulsed photo-multiplier scintillation counters—81(L)
Potter, C. A. (see Rouse, A. G.)—347(A)
Present, R. D. and E. Feenberg. On the nuclear quadrupole moment of Li^7—328(A)
Preston, Richard S. (see Duckworth, Henry E.)—386, 479(L)
Price, William J. Thermionic emission, conductivity, and contact potential difference measurements—354(A)
Pringle, R. W., K. I. Roulston, and S. Standil. Gamma-rays from $Be^9(\alpha,n)$—627(L)
——, **S. Standil, and K. I. Roulston.** Natural activity of lanthanum—303(L)
Pringsheim, Peter. Fluorescence and phosphorescence—315(T)
—— **and Philip Yuster.** Absorption bands and luminescence of LiF irradiated at low temperature—293(L)
Pritchard, Benjamin S. (see Sharbaugh, A. Harry)—64(L)
Proctor, W. G. and F. C. Yu. Nuclear induction radiofrequency spectrometer—83(A)
—— **and F. C. Yu.** On the magnetic moments of Xe^{129}, Bi^{209}, Sc^{45}, Sb^{121}, and Sb^{123}—471(L)
Purcell, Edward M. Recent work on the ratio of the magnetic moments of electron and proton, and related atomic constants—315(T)
—— (see Newman, Roger)—339(A)
—— **and N. F. Ramsey.** On the possibility of electric dipole moments for elementary particles and nuclei—807(L)

Quercia, I. F., B. Rispoli, and S. Sciuti. On the positive and negative excess of the penetrating component of cosmic radiation at 3500 m above sea level—824(L)

Rabi, I. I. (see Lee, C. A.)—340(A)
—— (see Zeiger, H.)—340(A)
Racah, Giulio. Nuclear coupling and shell model—622(L)
Ragan, G. L. (see Jones, W. B.)—60
Rall, Waldo (see Allen, R. C.)—337(A)
Ramsey, Norman F. Internal diamagnetic field correction in precision measurements of the proton magnetic moment—339(A)
—— Magnetic shielding of nuclei in molecules—699
—— Molecular beam resonance method with separated oscillating fields—695
—— Quadrupole moment of the electron distribution in hydrogen molecules—221
—— (see Purcell, E. M.)—807(L)
Randall, C. A. Properties of cosmic rays under 1100 ft. of earth—320(A)
Rasmussen, V. K. (see Rubin, S.)—83(A)
Rasor, N. S. and W. E. Parkins. Pulse-annealing method for the study of changes in physical properties resulting from heat treatment—638(A)
Raymond, Richard C. Entropy of non-equilibrium systems—351(A)
Read, W. T. Quantitative prediction of grain boundary energies by anisotropic dislocation theory—350(A)
—— **and W. Shockley.** Dislocation models of crystal grain boundaries—275
Reardon, Gerald V. (see Wiederhorn, Norman M.)—359(A)
Reding, F. P. (see Hornig, D. G.)—348(A)
Reekie, James (see Rutter, J. W.—70(L)
Reese, Robert M., Vernon H. Dibeler, and Fred L. Mohler. Temperature variation of mass spectra of hydrocarbons—332(A)
Reynolds, C. A. (see Serin, B.)—813(L)
——, **B. Serin, W. H. Wright, and L. B. Nesbitt.** Superconductivity of isotopes of mercury—487(L)
Reynolds, George, T., F. B. Harrison, and G. Salvini. Liquid scintillation counters—488(L)
Reynolds, John H. (see Inghram, Mark G.)—822(L)

Reynolds, S. E. (see Workman, E. J.)—254
Rhodin, T. N., Jr. Low temperature oxidation of copper—638(A)
Rice, O. K. Partial molal entropy of superfluid in pure He^4 below the λ-point—182(L)
—— (see Engel, Olive G.)—55
—— **and Olive G. Engel.** Thermodynamics of He^3-He^4 solutions—183(L)
Richard, C. D., Jr. "Figure of merit" and a "quality ratio" for d.c. emission from oxide-coated cathodes—356(A)
Richman, C. (see Cartwright, W. F.)—823(L)
—— (see Wilcox, H. A.)—85(A)
—— **and H. Wilcox.** Measurement of the production of positive and negative π-mesons by 345-Mev protons on carbon—85(A)
—— **and H. A. Wilcox.** Production cross sections for π^+- and π^--mesons by 345-Mev protons on carbon at 90° to the beam—496(L)
Ridgway, Stuart L. Beta-gamma-angular correlation—821(L)
Riedel, J. (see Kerns, Q. A.)—85(A)
Ring, Harold (see Gordy, Walter)—512
Riseman, Jacob and Robert Ullman. Concentration dependence of viscosity of solutions of macromolecules—359(A)
Rispoli, B. (see Quercia, I. F.)—824(L)
Ritland, H. N. (see Beeman, W. W.)—336(A)
—— (see Kaesberg, Paul)—336(A)
Rittner, E. S. (see du Pré, F. K.)—355(A), 573
Roberts, A. (see Waggoner, M. A.)—295(L)
Roberts, J. H. (see Keepin, G. R., Jr.)—87(A)
Robertson, B. E., W. E. Scott, and M. L. Pool. Radioactive Y^{87} and Sr^{87}—318(A)
Robinson, C. S. (see Kerst, D. W.)—297(L)
Robson, J. M. Radioactive decay of the neutron—311(L)
Rodgers, F. A. (see Leiter, H. A.)—663
——, **H. A. Leiter, and P. G. Kruger.** Deuteron-proton scattering using photographic techniques—656
Rogers, J. D. (see Pietenpol, W. J.)—480(L)
Rogers, T. H. (see Yanagisawa, S. T.)—353(A)
Rogosa, George L. and Guenter Schwarz. Electronic excitation of L_{III} states—343(A)
Rohrlich, F. On the electromagnetic interaction of mesons of zero spin—346(A)
Rose, B. and A. R. W. Wilson. Angular correlation in the reaction $B^{10}(n,\alpha)Li^{7*}(\gamma)Li^7$—68(L)
Rose, D. C. On the sudden increase in cosmic-ray intensity on November 19, 1949—181(L)
Rose, M. E. Erratum: internal pair formation—184(L)
Rosen, Louis and Alvin M. Hudson. Symmetrical tripartition of U^{235} by thermal neutrons—533
Rosen, Nathan (see Moseley, H. M.)—67(L)
Rosenbaum, B. Nuclear recoil momentum in pair production—628(L)
Rosenbluth, M. N. and L. I. Schiff. High energy electron-proton scattering—326(A)
Rosenfeld, L. (see Bohr, N.)—794
Rothlein, B. J. (see Miller, P. H., Jr.)—354(A)
Rothstein, Jerome. Holes and retrograde arc spot motion in a magnetic field—331(A)
Roulston, K. I. (see Pringle, R. W.)—303(L), 627(L)
Rouse, A. G., A. V. Bushkovitch, L. C. Jones, C. A. Potter, and W. F. Sullivan. Pressure shift and broadening in microwave spectra—347(A)
Rouse, Glenn F. (see Forman, Ralph)—355(A)
Rubin, S. and V. K. Rasmussen. Chemical analysis by proton scattering—83(A)
Ruderman, I. W. Neutron diffraction study of vitreous silica—317(A)
Rudin, Robert, Marietta Blau, and Seymour Lindenbaum. Semi-automatic device for analyzing events in nuclear emulsions—319(A)
Russell, B. R., P. H. Miller, Jr. and C. F. Wahlig. A. c. circuit for rapid determination of Hall coefficients of semiconductors—645(A)
Russell, K. (see Hart, R. J.)—334(A)
Rutledge, W. C. (see Cork, J. M.)—95, 299(L), 304(L)
Rutter, J. W. and James Reekie. Effect of cold working on the electrical resistivity of copper and aluminum—70(L)

Sabin, R. (see Dwight, K.)—324(A)
—— (see Stix, T.)—324(A)
—— (see Winckler, J. R.)—324(A)
Sachs, R. G. (see Blanchard, C. H.)—292(L)
Sadauskis, John (see Jesse, William P.)—1
Salvini, G. (see Reynolds, George T.)—488(L)
Sampson, M. B. (see McMinn, William O.)—296(L)
Sard, R. D. (see Fowler, E. C.)—323(A)
—— (see Fowler, W. B.)—323(A)
Sauer, J. A. (see Hsiao, C. C.)—358(A)
Savitzky, Abraham and Ralph S. Halford. Ratio-recording double beam infra-red spectrophotometer using phase discrimination and a single detector—344(A)
Sawyer, R. B. (see Hogan, C. L.)—350(A)
Sawyer, W. M. (see Ferry, John D.)—359(A)
Saxon, David S., Alfredo Baños, Jr., and Louis L. Bailin. Radiation characteristics of a turnstile antenna in a cylindrical shield—327(A)
Scharff-Goldhaber, Gertrude (see Sunyar, A. W.)—326(A)
——, **E. der Mateosian, M. McKeown, and A. W. Sunyar.** Low energy photons from radioactive nuclei—325(A)
Schein, Marcel (see Forbush, Scott E.)—323(A)
—— (see Lord, J. J.)—321(A), 484(L)
—— (see Vidale, M. L.)—325(A)
Schiff, L. I. Deuteron photo-effect at high energies—321(A), 733
—— High energy deuteron break-up—83(A)
—— (see Rosenbluth, M. N.)—326(A)
Schild, A. and F. A. E. Pirani. On the quantization of Einstein's gravitational field equations—329(A)
Schiller, Ralph (see Bergmann, Peter G.)—329(A)
Schlier, Robert E. and H. E. Farnsworth. Studies of gas adsorption on the (100) face of a copper crystal by low speed electron diffraction—316(A)
Schoenberg, M. D. and F. R. Eirich. Molecular weights from flow birefringence and intrinsic viscosities—359(A)
Schulz, L. G. Growth of alkali halides onto single crystal substrates—638(A)
—— Intense multiple reflection of electrons—316(A)
Schwarz, Guenter (see Rogosa, George L.)—343(A)
Schweber, S. Note on commutators in quantized field theories—613
Schwinger, Julian. On the charge independence of nuclear forces—135
—— (see Borowitz, S.)—345(A)
Sciuti, S. (see Quercia, I. F.)—824(L)
Scott, Robert L. Crystal strain energy in solid solutions—317(A)
Scott, W. E. (see Robertson, B. E.)—318(A)
Scott, W. T. On a difference-equation method for solving diffusion equations in cosmic-ray shower theory and similar problems—323(A)
—— **and H. S. Snyder.** On scattering induced curvature for fast charged particles—223
Seaborg, G. T. (see Ghiorso, A.)—472(L)
—— (see Magnusson, L. B.)—363
—— (see Meinke, W. W.)—475(L)
—— (see Thompson, S. G.)—298(L)
Sears, W. R. Transonic flow—315(T)
Segal, Leon, Joseph J. Creely, and Carl M. Conrad. Rotating specimen mount for use with x-ray spectrometer in measuring crystalite orientation of cellulosic and other textile fibers—358(A)

Seitz, Frederick. Mechanism of plastic flow in single crystals—315(T)
—— Physicists in the cold war—315(T)
—— Statistics of luminescent crystal counters—638(T)
—— **and D. W. Mueller.** On the statistics of luminescent counter systems—605
Seliger, H. H. Saturation backscattering of positive electrons—491(L)
Senatore, Samuel J. Microwave absorption spectra of POF_3—293(L)
Senitzky, I. R. "High vacuum" cold cathode gaseous discharge. I—331(A)
Seriff, A. J., R. B. Leighton, C. Hsiao, E. W. Cowan, and C. D. Anderson. Cloud-chamber observations of the new unstable cosmic-ray particles—290
Serin, B. (see Reynolds, C. A.)—487(L)
——, **C. A. Reynolds, and L. B. Nesbitt.** Superconductivity of isotopes of mercury—813(L)
Setlow, R. B. and D. J. Fluke. Large water-prism monochromator—335(A)
Sette, D. On the structural absorption of ultrasonic waves in ethyl alcohol—476(L)
Sewell, D. C. (see Lofgren, E. J.)—85(A)
——, **W. M. Brobeck, E. O. Lawrence, and E. J. Lofgren.** Design of the bevatron quarter scale operating model—85(A)
Seyfert, C. K. (see DeWitt, J. H., Jr.)—643(A)
Shackelford, C. L. (see Ivey, H. F.)—356(A)
Shaffer, W. H. and R. A. Oetjen. Multi-layer optical interference filters—187(A)
Shapiro, E. Rate of disappearance of thoria from coated filaments—352(A)
—— **and C. E. Mandeville.** Radiations from the 33-hour cerium (143)—319(A)
Sharbaugh, A. Harry, Virginia G. Thomas, and Benjamin S. Pritchard. Determination of the dipole moment and molecular structure of fluorosilane—64(L)
Shaw, Charles B., Jr. (see Halpern, Otto)—88(A)
Shaw, John H. (see Chapman, Robert M.)—71(L), 333(A)
——, **M. L. Oxholm, and R. M. Chapman.** Fine structure of N_2O near 4.06μ in the solar spectrum—497(L)
Sherburne, Russell K. (see Landeen, Stanley A.)—351(A)
Sheriff, Robert E. (see Chambers, William H.)—640(A), 482(L)
——, **William H. Chambers, and Dudley Williams.** Nuclear magnetic moment of niobium^{93}—476(L)
Sherman, D. (see Hughes, D. J.)—632(L)
Shiren, N. S. (see Post, R. F.)—80(L), 81(L), 644(A)
Shockley, W. Energy band structures in semiconductors—173(L)
—— Germanium filament experiments—637(T)
—— Theories of high values of alpha for collector contacts on germanium—294(L)
—— (see Montgomery, H. C.)—646(A)
—— (see Pearson, G. L.)—295(L)
—— (see Read, W. T.)—275
—— (see Williams, H. J.)—341(A)
——, **H. J. Williams, and C. Kittel.** Dynamic experiments with a simple domain boundary in a ferromagnetic crystal—341(A)
Shull, C. G. Neutron diffraction studies of ferromagnetic and antiferromagnetic substances—638(T)
—— (see Koehler, W. C.)—640(A)
Shulman, R. G. and C. H. Townes. Microwave transitions between *l*-type doublets of HCN—347(A)
——, **C. H. Townes, and B. P. Dailey.** Molecular dipole moments and Stark effects. III. Dipole moment determinations—145
Siegbahn, Kai (see Slätis, Hilding)—498(L)
Siegert, A. J. F. On the probability distribution of recurrence times—328(A)
Silverman, A. (see Levinthal, C.)—199
—— **and C. Levinthal.** Measurement of protons produced in the synchrotron beam—87(A)
Simon, Albert. "Bremsstrahlung" in high energy nucleon-collisions—321(A)
Singer, S. F. (see Van Allen, J. A.)—819(L)
Sitte, Kurt. Hodoscope study of local cosmic-ray showers—323(A)
—— Hodoscope study of penetrating cosmic-ray showers I. Local showers—714
—— Hodoscope study of penetrating cosmic-ray showers II. Extensive showers—721
Skinner, Miriam. Fine structure of singly ionized helium—82(T)
—— (see Lamb, Willis E., Jr.)—539
Slater, J. C. Lorentz correction in barium titanate—748
—— Structure and polarization of atoms and molecules—315(T)
—— Theory of ferroelectricity—638(T)
Slätis, Hilding, Stefaan J. du Toit, and Kai Siegbahn. Disintegration scheme of In^{116}—498(L)
Slifkin, L. and W. Kauzmann. Unusual effect in the creep of zinc single crystals—631(L)
Smith, F. M., Walter H. Barkas, A. S. Bishop, Hugh Bradner, and Eugene Gardner. Meson mass measurements—86(A)
Smith, L. P. Principal processes in thermionic emission and electrical conductivity of BaO—352(T)
Smith, Lloyd, A. A. Garren, and L. R. Henrich. Theoretical discussion of the performance of the model bevatron—85(A)
Smith, W. V. (see Southern, A. L.)—639(A)
Smoluchowski, R. Behavior and properties of grain boundaries—315(T)
—— Recent work on diffusion—638(T)
—— Statistical theory of magnetic saturation in alloys—638(A)
—— (see Wu, T. L.)—468
Smyth, C. P. Relaxation phenomena in liquids and solids—315(T)
Snell, Arthur H., Frances Pleasonton, and R. V. McCord. Radioactive decay of the neutron—310(L), 317(A)
Snow, George. Cross section of $(n,2n)$ reactions near the threshold—322(A)
Snowdon, S. C. Excitation curve of protons in the reaction $F^{19}(d,p)F^{20}$—299(L), 337(A)
Snyder, Hartland S. Quantum electrodynamics: the self energy problem—98
—— Self-energies of electrons and photons—346(A)
—— (see Scott, W. T.)—223
Sommer, H. (see Hipple, J. A.)—332(A)
—— **and H. A. Thomas.** Detection of magnetic resonance by ion resonance absorption—806(L)
Southern, A. L., H. W. Morgan, G. W. Keilholtz, and W. V. Smith. Isotopic analysis of nitrogen by means of a microwave mass spectrograph—639(A)
Spencer, R. S. and G. D. Gilmore. Equation of state for high polymers—358(A)
——, **G. D. Gilmore, and R. M. Wiley.** Behavior of granulated polymers under pressure—358(A)
Spiers, J. A. On the γ—γ-angular correlation in Pd^{106}—75(L)
Spohr, D. A. (see Andrews, F. A.)—342(A)
Sproull, Robert L. Optical absorption in strontium oxide films—630(L)
Spruch, L. Space exchange magnetic moments in light nuclei—328(A)
Stambaugh, R. B. (see Ostroski, A. S.)—358(A)
Stammreich, H. Raman spectrum of bromine—79(L)
Standil, S. (see Pringle, R. W.)—303(L), 627(L)
Steele, M. C. Magnetic field penetration in superconducting lead—342(A), 791

—— Thermoelectromotive force of superconducting versus normal junctions of the same metal—308(L)
Steenland, M. J. (see de Klerk, D.)—476(L)
Steffen, R. M. (see Hart, R. J.)—334(A)
Steinberg, E. P. and L. E. Glendenin. Long-lived zirconium activity in fission—624(L)
Steinberger, Jack L. (see Chew, Geoffrey F.)—86(A), 497(L)
—— **and A. S. Bishop.** Detection of artificially produced photo-mesons with counters—493(L)
—— **and A. S. Bishop.** Detection of photo-mesons and the relative cross section of carbon and hydrogen for their production—319(A)
—— **and A. S. Bishop.** Preliminary results on the production of mesons by photons on carbon and hydrogen—494(L)
——, **W. K. H. Panofsky, and J. Steller.** Evidence for the production of neutral mesons by photons—802
Steller, J. (see Steinberger, J.)—802
Sternheimer, R. On the compressibility of metallic cesium—235
Stevenson, Donald T. and Martin Deutsch. Beta-gamma-angular correlations—640(A)
Stinchcomb, Thomas B. Large cosmic-ray bursts under thick absorbers at 11,500 feet elevation—321(A)
——.(see Forbush, Scott E.)—323(A)
Stix, T. (see Dwight, K.)—324(A)
—— (see Winckler, J. R.)—324(A)
——, **K. Dwight, R. Sabin, and J. R. Winckler.** Directional and latitude survey of cosmic rays at 95,000 feet. I. Experimental procedure—324(A)
Stoddard, A. E. (see Cork, J. M.)—95, 299(L), 304(L)
Strait, E. N., D. M. Van Patter, and W. W. Buechner. Alpha-particles from $F^{19}(p,\alpha)O^{16}$—337(A)
Strandberg, M. W. P. (see Weiss, M. T.)—202
Strauch, K. Transition curves in lead of x-rays, causing nuclear reactions. I. Experimental—84(A)
—— (see Helmholz, A. C.)—86(A)
Street, J. C. (see Brown, Frederick C.)—320(A)
—— (see Fowler, E. C.)—323(A)
—— (see Fowler, W. B.)—323(A)
Street, K., Jr. (see Thompson, S. G.)—298(L)
Strick, E. and D. ter Haar. Production of π-mesons by high energy electrons—68(L)
Strong, John (see Plass, Gilbert N.)—334(A)
Sturcken, Edward, Robert Heller, and Alfred H. Weber. Percent beta-ray transmission through thin windows—327(A)
Suhl, H. Measurements of magneto-resistance of germanium in very intense magnetic fields—646(A)
Sullivan, A. M. (see Kies, J. A.)—357(A)
Sullivan, W. F. (see Rouse, A. G.)—347(A)
Sun, H. and Harriet H. Forster. Nuclear disintegration under different absorbers—86(A)
Sun, Kuan-Han, F. A. Pecjak, R. A. Charpie, and J. F. Nechaj. Excitation function of $Ta^{181}(d,p)Ta^{182}$—338(A)
Sunyar, A. W. (see Scharff-Goldhaber, Gertrude)—325(A)
——, **D. E. Alburger, G. Friedlander, M. Goldhaber, and G. Scharff-Goldhaber.** Isomerism in Pb^{204} and radiations of Bi^{204} and Bi^{206}—326(A)
Sutton, R. B. (see Foss, M. H.)—641(A)
Suwa, S. Hyperfine structure of $4^1,^3F$-nG of the spectrum of Al II—810(L)
Swann, Charles P. (see Hereford, Frank L.)—727
——.(see Hudspeth, Emmett, L.)—337(A)
——, **C. E. Mandeville, and W. D. Whitehead.** Neutrons from deuterons on magnesium (25)—338(A)
Swann, W. F. G. Electrets—811(L)
—— Magnetic deviation of cosmic-ray particles in the atmosphere—243
—— Matters pertaining to the magnetic deviation of cosmic-ray particles in the atmosphere—324(A)
Swift, C. J. and W. M. Elsasser. True magnitude of the geomagnetic secular variation—64(L)
Taconis, K. W., J. J. M. Beenakker, and Z. Dokoupil. Measurements of the influence on the fountain effect of He^3 dissolved in He^4—171(L)
Taft, E. A. and J. E. Dickey. Optical absorption edge for BaO as determined by the method of Ives and Briggs—625(L)
Talbott, F. L. and A. Busala. Angular distribution of the alpha-particles from the $Li^7(p,\alpha)\alpha$ reaction—336(A)
Taschek, R. F. (see Argo, H. V.)—691
Taylor, T. B. and G. F. Chew. Energy and angular distribution of π-mesons produced by 350-Mev protons—86(A)
Taylor, W. E. and H. Y. Fan. D.c. characteristics of high resistance barriers at crystal boundaries in germanium—335(A)
Taylor, W. J. (see Holden, R. B.)—344(A)
——, **G. P. Koch, and H. L. Johnston.** Improved Wadsworth mounting for a concave grating spectrometer—343(A)
Tchen, Chan-Mou. Statistical theory of volume effect in a long chain molecule—336(A)
Teal, G. K. (see Bond, W. L.)—176(L)
—— **and J. B. Little.** Growth of germanium single crystals—647(A)
Teller, Edward. Application of magneto-hydrodynamics to cosmic-ray physics and geomagnetism—82(T)
Temperley, H. N. V. (see Buckingham, R. A.)—482(L)
Templeton, D. H. Half-life of Po^{208}—312(L)
ter Haar, D. (see Strick, E.)—68(L)
Thode, H. G. (see Macnamara, J.)—129, 307(L)
Thomas, D. G. (see Dale, E. B.)—640(A)
Thomas, H. A. Regulation of large electromagnets using proton resonance—339(A)
—— (see Driscoll, R. L.)—339(A)
—— (see Hipple, J. A.)—332(A)
—— (see Sommer, H.)—806(L)
——, **R. L. Driscoll, and J. A. Hipple.** Measurement of the proton moment in absolute units—787
Thomas, J. E., Jr. (see Kraushaar, W. L.)—486(L)
Thomas, R. G. (see Lauritsen, T.)—88(A)
—— **and T. Lauritsen.** Gamma-radiation from C^{13} d—88(A)
Thomas, Virginia G. (see Sharbaugh, A. Harry)—64(L)
Thompson, S. G. (see Magnusson, L. B.)—363
——, **K. Street, Jr., A. Ghiorso, and G. T. Seaborg.** Element 98—298(L)
Thorndike, A. M. and A. W. Wotring. Stars and showers at balloon altitudes—473(L)
Tisza, L. Theory of superconductivity—342(A)
Tittle, Charles W. (see Goodman, Clark)—640(A)
Tobolsky, A. V. Static and dynamic viscosities of amorphous polymers—315(T)
—— (see Andrews, R. D.)—357(T)
Tollestrup, A. V. (see Chao, C. Y.)—88(A)
——, **W. A. Fowler, and C. C. Lauritsen.** Nuclear mass determinations from nuclear Q-values—372
Tomita, Kazuhisa (see Nakajima, Sadao)—768
Towler, O. A., Jr. and C. L. Oxley. Magnetic deflection method for observing proton-proton scattering at 250 Mev—326(A)
Townes, C. H. (see Autler, S. H.)—340(A)
—— (see Geschwind, S.)—174(L)
—— (see Kisliuk, P.)—347(A)
—— (see Shulman, R. G.)—145, 347(A)
—— **and B. P. Dailey.** Nuclear quadrupole coupling and ionic character of molecules—346(A)
Truesdell, C. Effect of the compressibility of the earth on its magnetic field—823(L)
Twersky, Victor. On the non-specular reflection of sound—332(A)

Tyler, Winfield W. Photo-conductivity and optical absorption in BaO crystals—315(T)

Ullman, Robert (see Riseman, Jacob)—359(A)
Usui, Tunemaru (see Nakajima, Sadao)—768

Valente, Frank A. Possible existence of a constant third-order difference among the nuclear magic numbers—77(L)
Van Allen, J. A. and A. V. Gangnes. Cosmic-ray intensity above the atmosphere at the geomagnetic equator—50
—— **and S. F. Singer.** On the primary cosmic-ray spectrum—819(L)
van der Ziel, A. (see Hartz, T. R.)—473(L)
Van Dyke, Karl S. Motional capacitance of AT-cut quartz resonators—642(A)
—— Status of the measurement of the properties of some piezoelectric crystals—315(A)
Van Patter, D. M. (see Strait, E. N.)—337(A)
Van Vleck, J. H. Concerning the theory of ferromagnetic resonance absorption—266
Vedam, K. Elastic and photoelastic constants of fused quartz—472(L)
Vidale, M. L. and Marcel Schein. Measurement of the cosmic-ray intensity as a function of altitude at a geomagnetic latitude of 28 degrees—325(A)
von Hippel, A. Dielectrics in electrical engineering—315(T)
—— Research on ferroelectricity—638(T)
Von Weiszaecker, C. F. Turbulence and the evolution of spiral nebulae—315(T)
Voorhies, H. G. (see Jones, W. B.)—60

Wachtell, G. P. Refraction effect in interferometry of boundary layer of supersonic flow along flat plate—333(A)
Waggoner, M. A., M. L. Moon, and A. Roberts. Internal conversion coefficients for Co^{60}—295(L)
Wahlig, C. F. (see Russell, B. R.)—645(A)
Walker, W. H. (see Kinsey, B. B.)—77(L), 481(L)
Wangsness, Roald K. Nuclear magnetic moments and shell structure—620(L)
—— (see Bloch, F.)—82(A)
Wannier, G. H. On the triangular Ising net—341(A)
Wantuch, E. Scattering of 4.5 and 5.5 Mev neutrons by deuterons—326(A)
Warburton, F. W. Constant-mass electron in uniform fields—93(A)
Ward, A. L. (see Breckenridge, R. G.)—315(A)
Ward, J. C. Identity in quantum electrodynamics—182(L)
Warren, B. E. Order and disorder in alloys—638(T)
—— (see Averbach, B. L.)—644(A)
Watson, K. M. (see Brueckner, K. A.)—495(L)
Watson, W. W. (see Manning, Thurston, E.)—417
—— (see Zucker, A.)—14, 338(A)
—— **and C. E. Anderson.** Isotope shift in the lines of Pb I—343(A)
Webber, R. T. (see Andrews, F. A.)—342(A)
Weber, Alfred H. (see McGannon, J.)—317(A)
—— (see Sturcken, Edward)—327(A)
Weber, N. E. (see Green, L. C.)—343(A)
Wedding, J. W. (see Haynes, S. K.)—641(A)
Weimer, D. K. (see Fletcher, C. H.)—634(L)
Weinberg, A. M. Role of physics in current atomic energy development—648(T)
Weinreich, O. A. Thermal emissivity changes of thoria-coated tungsten filaments—337(A)
Weinstein, M. (see Bohm, D.)—346(A)
Weir, C. E., W. H. Leser, and L. A. Wood. Crystallization and second-order transitions in silicon rubbers—357(A)
Weiss, M. T., M. W. P. Strandberg, R. B. Lawrence, and C. C. Loomis. On the nuclear spin of B^{10}—202
Weissbluth, Mitchel. Measurement of production of positive and negative π-mesons in lead by 345-Mev protons—86(A)
Weissler, G. L. (see Eggleston, R. R.)—91(A)
Wert, Charles. Diffusion of C in α-iron—639(A)
West, W. J. (see Lind, D. A.)—474(L)
Wexler, Aaron and W. S. Corak. Magnetic properties of a rotating superconductor—260
Weyl, W. A. Rheological properties of glass—315(T)
Whaling, Ward and J. W. Butler. Neutrons from the bombardment of Li^6 by deuterons—72(L)
White, Gladys R. Co-60 γ-ray penetration through large masses of water—330(A)
White, R. Stephen (see Jones, Stanley B.)—12
—— (see Peterson, Jack M.)—84(A)
——, **Edwin M. McMillan, and Jack M. Peterson.** Production of mesons by x-rays, part I: experimental method—84(A)
White, William C. (see Yagoda, Herman)—330(A)
Whitehead, M. N. (see Cartwright, W. F.)—823(L)
Whitehead, W. D. (see Swann, C. P.)—338(A)
—— **and N. P. Heydenburg.** Proton groups from the deuteron bombardment of aluminum, sodium, and manganese—338(A)
—— **and C. E. Mandeville.** Neutrons from the disintegration of beryllium by deuterons—337(A)
Whitmore, B. G. and W. B. Baker. Energy spectrum of neutrons from a Po-Be source—799
Whyte, G. N. Cosmic-ray bursts at high altitudes—321(A)
—— Evidence from cosmic-ray bursts for a nuclear cascade process—630(L)
Wiedenbeck, M. L. (see Williams, A. H.)—822(L)
Wiederhorn, Norman M. and Gerald V. Reardon. Stress-strain behavior of thermally shortened collagen tendons—359(A)
Wiegand, C. and O. Chamberlain. Proton-proton scattering at 340 Mev—326(A)
Wilcox, H. A. (see Cartwright, W. F.)—823(L)
—— (see Richman, C.)—85(A), 496(L)
—— **and C. Richman.** Experiment for measuring heavy meson production by high energy particles—85(A)
Wiley, R. M. (see Spencer, R. S.)—358(A)
Williams, A. H. and M. L. Wiedenbeck. Correlation in the direction and polarization of two successive quanta for Rh^{106}, Co^{60}, and Cs^{134}—822(L)
Williams, Dudley (see Chambers, William H.)—482(L), 640(A)
—— (see Chapman, Robert M.)—333(A)
—— (see Pietenpol, W. J.)—480(L)
—— (see Sheriff, Robert E.)—476(L)
Williams, H. J. Recent experiments on ferromagnetic domains and domain walls—638(T)
—— (see Shockley, W.)—341(A)
—— **and W. Shockley.** Memory in simple ferromagnetic domain crystal—341(A)
Williams, J. H. (see Freier, G.)—508
Williams, Paul D. Investigation of contaminants in vacuum tubes—353(A)
Wilson, A. R. W. (see Rose, B.)—68(L)
Winckler, J. R. (see Dwight, K.)—324(L)
—— (see Stix, T.)—324(A)
——, **K. Dwight, R. Sabin, and T. Stix.** Directional and latitude survey of cosmic rays at 95,000 feet. III. Interpretation of azimuthal and zenithal data—324(A)
Winston, Harvey. Explanation for "extra levels" in rare earth crystal spectra—316(A)
Witmer, Enos E. Integral expressions for nuclear magnetic moments—352(A)
—— Integral relationships between atomic and nuclear quantities—330(A)
—— Integral relationships between nuclear masses and the electron mass—641(A)

Wolfenstein, L. Statistical theory and the angular distribution of nuclear reactions—322(A)
Wolfson, J. L. Energies of some gamma-rays from ThC″, RaC, and Na^{24}—176(L)
Wollan, E. O. (see Koehler, W. C.)—640(A)
Wood, L. A. (see Weir, C. E.)—357(A)
Woodcock, Karl S. (see Duckworth, Henry E.)—479(L)
Woodcock, Richard F. (see Duckworth, Henry E.)—386
Workman, E. J. and S. E. Reynolds. Electrical phenomena occurring during the freezing of dilute aqueous solutions and their possible relationship to thunderstorm electricity—254
Worth, Donald C. Recoil coincidence-absorption measurement of neutron spectra from the reactions $A^{40}(d,n)$ and $N^{15}(d,n)$—378
Wotring, A. W. (see Thorndike, A. M.)—473(L)
Wouthuysen, Siegfried A. (see Foldy, Leslie L.)—29, 345(A)
Wright, Byron T. and F. E. Faris. Proton-proton scattering at 12.4 Mev.—89(A)
Wright, D. A. Electrical conductivity of oxide cathode coatings—355(A)
Wright, R. E. (see Livingston, R. S.)—329(A)
Wright, W. H. (see Reynolds, C. A.)—487(L)
Wu, C. S. Recent investigations on the shapes of beta-ray spectra—315(T)
—— (see Feldman, L.)—318(A)
—— (see Lidofsky, L. J.)—318(A)
—— (see Macklin, P. A.)—318(A)
Wu, T. L. and R. Smoluchowski. New criterion for the occurrence of slip in thin single crystals—468
Wu, Ta-You (see Moses, H. E.)—333(A)
Wyrick, Ralph and Henry Levinstein. Thermoelectric voltage in lead telluride—304(L)
Yaffe, L. (see Grunlund, Jean M.)—69(L)
Yagoda, Herman, Hervasio G. de Carvalho, and Nathan Kaplan. Stars and heavy primaries recorded during a V-2 rocket flight—765
—— **and William C. White.** Ratio of N^{15}/N^{14} in gases occluded in radioactive minerals—330(A)
Yanagisawa, S. T. and T. H. Rogers. Experimental use of thoria cathodes in high voltage rectifier tubes—353(A)
Yeater, M. L. (see Gaerttner, E. R.)—621(L)
Yevick, G. J. Relativistic model of a finite-sized electron—345(A)
York, Herbert F. (see Crandall, W. E.)—89(A)
—— (see Panofsky, Wolfgang K. H.)—89(A), 825(L)
Yu, F. C. (see Proctor, W. G.)—83(A), 471(L)
Yuan, Luke C. L. Measurements on the latitude effect of the neutron component of cosmic radiation at high altitudes—325(A)
Yuster, Philip (see Pringsheim, Peter)—293(L)

Zatzkis, Henry (see Bergmann, Peter G.)—329(A)
Zeiger, H., D. Bolef, and I. I. Rabi. Molecular beam spectrum of $TlCl^{35}$ and $TlCl^{37}$ at zero fields—340(A)
Zemansky, M. W. (see Boorse, H. A.)—635(A)
—— (see Cook, D. B.)—343(A), 820(L)
Zener, C. Internal friction in solids—315(T)
—— Ring diffusion in metals—638(T)
Zimm, Bruno H. Study of high polymer molecules by light scattering—82(T)
Zimmerman, E. L. (see Dale, E. B.)—640(A)
Zucker, A. and W. W. Watson. *d-p* reactions with separated neon isotopes—338(A)
—— **and W. W. Watson.** Protons from the deuteron bombardment of separated neon isotopes—14

Analytic Subject Index to Volume 78

References with (A) are to abstracts of papers presented at meetings of the American Physical Society, References with (L) are to Letters to the Editor.

Absorption coefficient
Of Si, infra-red, H. Y. Fan and M. Becker—178(L)
Absorption and reflection of radiation (see also **Spectra, absorption**)
Of LiF at low temperature, Peter Pringsheim and Philip Yuster—293(L)
Reflection coefficients from variational principle, G. Toraldo di Francia—298(L)
Acoustics
Absorption of ultrasonic waves in ethyl alcohol, D. Sette—476(L)
Echo effect from release of stored wave train, Louis Gold—332(A)
Non-specular reflection, Victor Twersky—332(A)
Scattering analysis by variational methods, Alfred Levitas—333(A)
Ultrasonic wind, Francis E. Fox and Karl F. Herzfeld—156
Adsorption
In Cu, study by electron diffraction, Robert E. Schlier and H. E. Farnsworth—316(A)
On metals, radioactive tracer method, Albert D. Crowell and H. E. Farnsworth—351(A)
Alloys (see **Crystalline state**)
Astrophysics
Absorption bands of N_2O in solar spectrum, J. H. Shaw, M. L. Oxholm, and R. M. Chapman—497(L)
Polarized waves in sun's atmosphere, escape into space, V. A. Bailey—428
Na *D*-lines during twilight, origin, R. Penndorf—66(L)
Supernovae, mechanism of, L. B. Borst—807(L)
Temperature in accreting planet, A. E. Benfield—334(A)
Atomic and molecular beams
Molecular beam resonance method, separated oscillating fields, Norman F. Ramsey—695
Atomic mass (see **Isotopes**)
Atomic structure (see also **Energy states of atoms; Spectra**)
Configuration interactions in Pb III, J. N. P. Hume and M. F. Crawford—343(A)

Biophysics
d and α—bombardment of enzymes and viruses, Ernest Pollard and F. Forro, Jr.—335(A)
Electron scattering in tissue, reduction, W. H. Bostick—327(A)
Infra-red spectra of fibrous protein, Martin Goldstein and Ralph S. Halford—336(A)
Neutron dosage given to tissue, G. S. Hurst—640(A)
Range of α-particles in water and ice, H. G. de Carvalho—330(A)
Shapes and hydrations of protein molecules, W. W. Beeman, Paul Kaesberg, and H. N. Ritland—336(A)
Ultraviolet irradiation of viruses, Donald J. Fluke—335(A)
Water-prism monochromator, R. B. Setlow and D. J. Fluke—335(A)
Bremsstrahlung
Nucleon-nucleon collisions, Albert Simon—321(A)

Chemical reactions
Surface reactions at low pressures, Stanley A. Landeen, H. E. Farnsworth, and Russell K. Sherburne—351(A)
Colloids (see also **Polymerization, properties of polymers**)
Interionic forces near high potential surfaces, Arthur L. Loeb—350(A)
Compressibility
Of Ce, volume discontinuity, R. Sternheimer—235
Compton effect (see **Scattering of radiation**)
Conductivity, electrical (see **Electrical conductivity; Discharge of electricity in gases**)
Constants, physical standards
Integer constants, Enos E. Witmer—330(A)
Cosmic radiation
Altitude effect, latitude effect of hard component, M. L. Vidale and Marcel Schein—325(A)
Bursts at high altitudes, G. N. Whyte—321(A)
Bursts in chambers of different materials, Harold W. Lewis—483(L)
Bursts under absorbers at 11,500 feet, Thomas B. Stinchcomb—321(A)
Cascade process, G. N. White—630(L)
Directional and latitude survey of cosmic rays at 95,000 ft.—method, T. Stix, K. Dwight, R. Sabin, and J. R. Winckler—324(A); Vertical flux data, K. Dwight, R. Sabin, T. Stix, and J. R. Winckler—324(A); Azimuthal and zenithal data, J. R. Winckler, K. Dwight, R. Sabin, and T. Stix—324(A)
Disintegrations at 11,000 meters, H. H. Forster—247
Diurnal variation and solar magnetic moment, Kirby Dwight—40
Energy transfer to nucleons, M. F. Kaplon, B. Peters, and H. L. Bradt—680
Extensive showers under water, W. B. Fretter and John Ise, Jr.—92(A)
Geomagnetic effects, H. V. Neher—674
Heavy nuclei in stratosphere at night, J. J. Lord and Marcel Schein—484(L)
Intensity above atmosphere at equator, J. A. Van Allen and A. V. Gangnes—50
Intensity following a solar flare, James W. Broxon and Howard W. Boehmer—411
Intensity increase on 11/19/49, D. C. Rose—181(L); Scott E. Forbush, Thomas B. Stinchcomb, and Marcel Schein—323(A)
Latitude and longitude effects in U.S. and Canada at 30,000 ft., A. T. Biehl and H. V. Neher—172(L)
Latitude effect of the neutron component, high altitudes, Luke C. L. Yuan—325(A)
Local penetrating showers, Kurt Sitte—714
Magnetic deflection of mesons, nuclear plates, Ian Barbour—319(A), 518
Magnetic deviation in the atmosphere, W. F. G. Swann—243, 324(A)
Mass measurements, analysis, T. C. Merkle, Jr., E. L. Goldwasser, and R. B. Brode—92(A)
Non-existence of permanent solar magnetic field, Martin A. Pomerantz—325(A)
Penetrating extensive showers, Kurt Sitte—721
Penetrating showers in C, production, John R. Green and W. B. Fretter—92(A)
Phenomena in thick emulsions, Pierre Demers—320(A)
Positive and negative excess of penetrating component, I. F. Quercia, B. Rispoli, and S. Sciuti—824(L)
Primary spectrum above atmosphere, J. A. Van Allen and S. F. Singer—819(L)
Radio stars as source, H. Alfvén and N. Herlofson—616(L)
Ratio of positive to negative particles at 3650 meters, R. B. Brode—92(A)
Shower energy as function of collision cross section, K. Sitte—323(A)

Shower theory diffusion equations, W. T. Scott—323(A)
Showers in cloud chamber, E. C. Fowler, J. C. Street, W. B. Fowler, and R. D. Sard—323(A)
Showers in emulsions—data, L. S. Osborne, B. T. Feld, and I. L. Lebow—324(A); Theory of meson production, B. T. Feld, I. L. Lebow, and L. S. Osborne—323(A)
Star and meson production rates, dependence on absorbers, Marietta Blau, John Nafe, and Herbert Bramson—320(A)
Star production rate, solar flare, J. J. Lord and Marcel Schein—321(A)
Stars and heavy primaries, rocket flight, Herman Yagoda, Hervasio G. de Carvalho, and Nathan Kaplan—765
Stars and showers at balloon altitudes, A. M. Thorndike and A. W. Wotring—473(L)
Stars, slow protons studied with AgCl crystal, Frederick C. Brown and J. C. Street—320(A)
Stopped particles in cloud chamber, W. B. Fowler, R. D. Sard, E. C. Fowler, and J. C. Street—323(A)
Sun as origin, K. O. Kiepenheuer—809(L)
Underground data, Kenneth Greisen—65(L); C. A. Randall—320(A)
Unstable particles, cloud-chamber observations, A. J. Seriff, R. B. Leighton, C. Hsiao, E. W. Cowan, and C. D. Anderson—290

Cross section, measurements, theory (see also **Scattering of electrons, mesons, protons, neutrons, and ions**)
Of C, O, Mg, Si, and S for fast neutrons, G. Freier, M. Fulk, E. E. Lampi, and J. H. Williams—508
Of $C^{12}(p,pn)C^{11}$ reaction, Lee Aamodt, Vincent Peterson, and Robert Phillips—87(A)
For (γ,n) reactions, A. C. Helmholz and K. Strauch—86(A)
Neutron cross sections and nuclear shells, D. J. Hughes and D. Sherman—632(L)
$(n,2n)$ reactions near threshold, George Snow—322(A)
Nuclear photo-effect, dipole transitions, J. S. Levinger and H. A. Bethe—115
For photons for p-nucleon collision, W. E. Crandall, B. J. Moyer, and H. F. York—89(A)

Crystal structure
Anisotropy of Fe_3O_4, L. R. Bickford, Jr.—342(A)
Of barium titanate, A. de Bretteville, Jr. and G. Katz—340(A)
Crystallization, second-order transitions in Si rubbers, C. E. Weir, W. H. Leser, and L. A. Wood—357(A)
Growth of alkali halides, L. G. Schulz—638(A)
Lattice defects due to neutron bombardment, J. H. Crawford, Jr. and K. Lark-Horovitz—645(A)
Martensite transformation in iron-carbon alloys, J. S. Bowles—639(A)
Oriented overgrowth of alkali halides, Gerald W. Johnson—316(A)
Transformation in Li-Mg alloys, C. S. Barrett and D. F. Clifton—639(A)
Of ZnO, lattice constants, J. McGannon, R. Heller, and A. H. Weber—317(A)

Crystalline state
Adsorption in Cu crystal, Robert E. Schlier and H. E. Farnsworth—316(A)
Anelastic effects in ionic crystals, R. G. Breckenridge and A. L. Ward—315(A)
Anelastic effects in quartz crystals, Richard K. Cook and Robert G. Breckenridge—315(A)
Anisotropy and g-factor of magnetite, L. R. Bickford, Jr.—449
$BaTiO^3$ under hydrostatic pressure, W. J. Merz—52, 341(A)
Color centers in quartz due to x-rays, Guy Forman—644(A)
Creep of Zn crystals, L. Slifkin and W. Kauzmann—631(L)
Decay times of scintillation phosphors, S. H. Liebson and J. O. Elliot—65(L)
Diffusion of C in α-iron, Charles Wert—639(A)
Domain wall velocity, W. Shockley, H. J. Williams, and C. Kittel—341(A)
Electrical effects of freezing of dilute solutions, E. J. Workman and S. E. Reynolds—254
Energy band structures in semiconductors, W. Shockley—173(L)
"Extra levels" in rare earth spectra, Harvey Winston—316(A)
Ferroelectric behavior, theoretical model, P. W. Anderson—341(A)
Ferromagnetic resonance absorption, theory, J. H. Van Vleck—266
Ge alloys produced by transmutation, J. Cleland, K. Lark-Horovitz, and J. C. Pigg—645(A)
Ge filament cuts, W. L. Bond—646(A)
Ge P-N barriers as counters, C. Orman, H. Y. Fan, G. J. Goldsmith, and K. Lark-Horovitz—646(A)
Grain boundary dynamics, dislocation models, W. T. Read and W. Shockley—275
Grain boundary energies from anisotropic dislocation theory, W. T. Read—350(A)
Growth of Ge crystals, G. K. Teal and J. B. Little—647(A)
Impedance of grain boundaries in Ge, N. H. Odell and H. Y. Fan—334(A)
Interaction between paramagnetic ions, Norman Elliott—341(A)
Interfacial energies *vs.* tensions, John P. Nielsen—350(A)
Internal friction in cold worked Al-Cu alloys, T'ing-Sui Kê—420
Magnetic and electric properties of magnetite, C. A. Domenicali—458
Memory in ferromagnetic domain crystal, H. J. Williams and W. Shockley—341(A)
Multiple reflection of electrons, L. G. Schulz—316(A)
Noise in Ge due to hole fluctuations, H. C. Montgomery and W. Shockley—646(A)
Optical band width of F centers at low temperature, E. Burstein and J. J. Oberly—349(A)
Optical glasses in infra-red, R. Frerichs—643(A)
Oxidation of copper, T. N. Rhodin, Jr.—638(A)
Partition function of a two-dimensional Ising lattice, G. F. Newell—444
Permeation of H through Zr, R. B. Bernstein and Daniel Cubicciotti—639(A)
Photoelectric work function of Ag film, Edward Kelly, H. E. Farnsworth, and Edward N. Clarke—316(A)
Of photolytic Ag in AgBr, growth mechanism, Chester R. Berry and Robert L. Griffith—317(A)
Piezoelectric coefficient of $BaTiO_3$, M. E. Caspari—341(A)
Piezoelectric constants, Karl S. Van Dyke—315(A)
Pulse-annealing method for changes in properties on heat treatment, N. S. Rasor and W. E. Parkins—638(A)
Recrystallization purification of germanium, R. N. Hall—645(A)
Slip in thin single crystals, T. L. Wu and R. Smoluchowski—468
Specific heat of non-metallic ferrites, T. R. McGuire and Louis N. Howard—342(A)
Specific heats in paramagnetic salts at low T, B. Bleaney—214
Stilbene and anthracene scintillations, decay time, R. F. Post and N. S. Shiren—80(L)
Strain energy in solid solutions, Robert L. Scott—317(A)
Stress in evaporated metal films and distortion decay, E. C. Crittenden, Jr. and R. W. Hoffmann—349(A)
Stresses in evaporated metal films, R. W. Hoffman and E. C. Crittenden, Jr.—349(A)
Surface states, effect on Fermi level of semiconductor, Paula Feuer and Hubert M. James—645(A)
Temperature instability of Ge, G. T. Jacobi and W. C. Dunlap, Jr.—349(A)

Crystalline state (continued)
Trapping in ZnS-type phosphors, Richard H. Bube—349(A)
Triangular net applied to antiferromagnetism, G. H. Wannier—341(A)
Vibrations of structure of diamond, Si, and Ge, E. Burstein and John J. Oberly—642(A)
Volume discontinuity of Ce, R. Sternheimer—235

Diffraction of radiation
Patterns in the planes of circular apertures, C. L. Andrews—344(A)

Diffusion (see also **Thermal diffusion**)
Of C in α-iron, Charles Wert—639(A)
Of imprisoned resonance radiation, Frank N. Edmonds, Jr.—424
Permeation of H through Zr, R. B. Bernstein and Daniel Cubicciotti—639(A)

Discharge of electricity in gases
Avalanche transformation during breakdown, G. M. Petropoulos—250
Cathode temperature in glow discharge, Harold Jacobs and Jack Martin—331(A)
Cold cathode low pressure discharge, I. R. Senitzky—331(A)
Corona discharge, gap forms, electrostatic field in gap, L. B. Loeb, J. H. Parker, E. E. Dodd, and W. N. English—91(A)
Corona in dried air, point-to-plane, H. W. Bandel—91(A)
Electrical charge on dust particles, W. B. Kunkel—91(A)
Electron avalanche formation, Edward E. Dodd—620(L)
Electron density, emission spectrum in metal vapor afterglows, P. Dandurand and R. B. Holt—331(A)
Formative time lags of spark breakdown in air, B. Bederson and L. H. Fisher—331(A); L. H. Fisher and B. Bederson—331(A)
Holes and retrograde arc spot motion, Jerome Rothstein—331(A)
Hg arc temperature, Carl Kenty—626(L)
Hg arc temperature by x-rays, C. Kenty and W. J. Karash—625(L)

Disintegration and excitation of nucleus (see also **Photo-disintegration; Radioactivity**)
Absorption of π^--mesons in hydrogen, gamma-rays, Wolfgang K. H. Panofsky, Lee Aamodt, and Herbert F. York—825(L)
Of Al, Na, Mg, proton groups, W. D. Whitehead and N. P. Heydenburg—338(A)
Of Al^{27} by α, proton groups, H. H. Landon—338(A)
Angular correlation in $B^{10}(n,\alpha)Li^{7*}(\gamma)Li^7$, B. Rose and A. R. W. Wilson—68(L)
Angular distribution of α-rays from $Li^7(p,\alpha)\alpha$, F. L. Talbott and A. Pusala—336(A)
Angular distribution, momentum conservation requirements, L. Wolfenstein—322(A)
Of Be by d, levels of B^{10}, W. D. Whitehead and C. E. Mandeville—337(A)
Of C by high energy particles, Lee Aamodt, Vincent Peterson, and Robert Phillips—87(A)
Of C and Al by p, C. Levinthal, E. A. Martinelli, and A. Silverman—199
Of C^{14} by d, Emmett L. Hudspeth and Charles P. Swann—337(A)
Of Ce^{131}, metastable Xe^{131}, Lin-Sheng Cheng and J. D. Kurbatov—319(A)
Cosmic-ray reactions at 11,000 meters, H. H. Forster—247
Of deuteron at high energy, L. I. Schiff—83(A)
d induced reactions, M. S. Livingston, K. Boyer, H. E. Gove, J. A. Harvey, and M. Deutsch—344(A)
(d,p) reactions, angular distributions of protons, Harry E. Gove—345(A)
(d,p) reactions, neutron binding energies from Q-values, J. A. Harvey—345(A)
(d,p) reactions, p energy spectrum, Keith Boyer—345(A)
d-p reactions with separated Ne isotopes, A. Zucker and W. W. Watson—338(A)
Energy of neutrons from $Be^9(\alpha,n)C^{12}$, C. E. Bradford and W. E. Bennett—302(L)
Excited states of Li^7, D. R. Inglis—104
Of F^{19} by d, excitation curve for protons, S. C. Snowdon—337(A)
Of F^{19} by p, α-groups, E. N. Strait, D. M. Van Patter, and W. W. Buechner—337(A)
Of F^{19}, Q-value of α-particles, C. Y. Chao, A. V. Tollestrup, W. A. Fowler, and C. C. Lauritsen—88(A)
Gamma-rays, angular correlation, E. L. Brady and M. Deutsch—558
Gamma-rays from $Be^9(\alpha,n)$, R. W. Pringle, K. I. Roulston, and S. Standil—627(L)
γ-rays from meson absorption, W. K. H. Panofsky and H. F. York—89(A)
Isomeric transition energies, Richard L. Caldwell—407
Of Li by α-particles, proton groups, William O. McMinn, M. B. Sampson, and M. Loren Bullock—296(L)
Of Li^6 by d, neutron energies, Ward Whaling and J. W. Butler—72(L)
Of Li^7 by p, neutron energy, Bernard Hamermesh and Virginia Hummel—73(L)
Of Mg^{25} by d, neutron groups, C. P. Swann, C. E. Mandeville, and W. D. Whitehead—338(A)
Masses from Q-values, A. Tollestrup, W. A. Fowler, and C. C. Lauritsen—372
Neon isotopes bombarded by deuteron, masses of isotopes, A. Zucker and W. W. Watson—14
Neutron production by 50-Mev x-rays, G. C. Baldwin and F. R. Elder—76(L)
Neutron spectra from reactions $A^{40}(d,n)$ and $N^{15}(d,n)$, Donald C. Worth—378
Of nuclei by π^--mesons, W. Cheston and L. Goldfarb—320(A)
Photo-neutron production, E. der Mateosian and M. Goldhaber—326(A)
Photons, from p-nucleon collision, yield, energy, W. E. Crandall, B. J. Moyer, and H. F. York—89(A)
By π^--mesons, W. B. Cheston and L. J. B. Goldfarb—683
Polarization-direction correlation of successive gamma-rays, Franz Metzger and Martin Deutsch—551
Protons from D-D reaction at 10 Mev, angular distribution, H. A. Leiter, F. A. Rodgers, and P. G. Kruger—663
Protons from $F^{19}(d,p)F^{20}$, S. C. Snowdon—299(L)
Spallation of Sb, M. Lindner and I. Perlman—499
Of Sr^{87}, Y^{87} isomers, B. E. Robertson, W. E. Scott, and M. L. Pool—418(A)
Of Ta by d, neutron spectrum, R. A. Peck, Jr.—338(A)
Of Ta^{181}, excitation function, yields, Kuan-Han Sun, F. A. Pecjak, R. A. Charpie, and J. F. Nechaj—338(A)
Transitions to ground states, slow neutron capture, B. B. Kinsey, G. A. Bartholomew, and W. H. Walker—481(L)
$T^3(p,\gamma)He^4$ reaction, H. V. Argo, H. T. Gittings, A. Hemmendinger, G. A. Jarvis, and R. F. Taschek—691

Elasticity
Of Ce, volume discontinuity, R. Sternheimer—235
Constants of fused quartz, K. Vedam—472(L)
Creep of Zn crystals, L. Slifkin and W. Kauzmann—631(L)
Of Ge crystals, W. L. Bond, W. P. Mason, H. J. McSkimin, K. M. Olsen, and G. K. Teal—176(L)
Stress in evaporated metal films and distortion decay, E. C. Crittenden, Jr. and R. W. Hoffman—349(A)
Stresses in evaporated metal films, R. W. Hoffman and E. C. Crittenden, Jr.—349(A)

Transition to plasticity, M. L. Huggins—336(A)
Vibrations of crystalline plate, Shepard Bartnoff, Charles R. Mingins, and Joseph F. Clayton—316(A)

Electrets
"Heterocharge" of wax, A. D. Franklin—342(A)
Ohmic conductivity, W. F. G. Swann—811(L)

Electrical conductivity and resistance
Of (Ba-Sr)O cathodes, F. K. du Pré, R. A. Hutner, and E. S. Rittner—355(A), 573
Of barriers at boundaries in Ge, W. E. Taylor and H. Y. Fan—335(A)
Ceramic heaters and cathodes, T. R. Palumbo—356(A)
Collector contacts on Ge, values of α, W. Shockley—294(L)
Of Cb, superconductivity, D. B. Cook, M. W. Zemansky, and H. A. Boorse—820(L)
Of Cu and Al, cold-working effect, J. W. Rutter and James Reekie—70(L)
Energy gap in semiconductors, temperature dependence, H. Y. Fan—808(L)
Fast neutron bombardment effects in Ge, J. H. Crawford, Jr. and K. Lark-Horovitz—815(L)
Flux in a superconducting torus, R. L. Dolecek and Jules de Launay—58
Of Ge, changes due to α-particle bombardment, W. H. Brattain and G. L. Pearson—646(A)
Of Ge, transmutation-produced, J. W. Cleland, K. Lark-Horovitz, and J. C. Pigg—814(L)
Hall coefficients of semiconductors, rapid determination, B. R. Russell, P. H. Miller, Jr., and C. F. Wahlig—645(A)
Impedance of grain boundaries in Ge, N. H. Odell and H. Y. Fan—334(A)
Magneto-resistance of Ge, G. L. Pearson—646(A); H. Suhl—646(A)
Mobility anomalies in Ge, G. L. Pearson, J. R. Haynes, and W. Shockley—295(L)
Nucleon-bombarded silicon, K. Lark-Horovitz, M. Becker, R. E. Davis, and H. Y. Fan—334(A)
Of oxide cathode coatings, D. A. Wright—355(A)
Of polycrystalline graphite, dependence on temperature, S. Mrozowski—644(A)
Random-circuit theory of resistance and noise, R. P. Coleman—644(A)
Rectifier as a thermodynamical demon, L. Brillouin—627(L)
Of rotating and stationary superconductors, equivalent magnetic properties, Aaron Wexler and W. S. Corak—260
Of semiconductors with acceptor and donator impurity levels, C. S. Hung and V. A. Johnson—335(A)
Of sintered thoria, W. E. Danforth and F. H. Morgan—353(A)
Superconducting lead, field penetration, M. C. Steele—791
Superconductivity of lead, H. A. Boorse, D. B. Cook, and M. W. Zemansky—635(L)
Superconductivity of isotopes of Hg, B. Serin, C. A. Reynolds, and L. B. Nesbitt—813(L); C. A. Reynolds, B. Serin, W. H. Wright, and L. B. Nesbitt—487(L)
Superconductivity of mercury, Emanuel Maxwell—477(L)
Superconductivity theory, L. Tisza—342(A)
Temperature instability of Ge, G. T. Jacobi and W. C. Dunlap, Jr.—349(A)
Thermionic emission, contact potential difference, William J. Price—354(A)
Of ZnO, E. E. Hahn and P. H. Miller, Jr.—348(A); P. H. Miller, Jr. and E. E. Hahn—349(A)

Electromagnetic theory (see also **Quantum electrodynamics**)
Constant-mass electron in uniform fields, F. W. Warburton—93(A)
Polarized waves in sun's atmosphere, escape into space, V. A. Bailey—428

Electron diffraction
Multiple reflection, L. G. Schulz—316(A)

Electronic tubes (see also **Methods and instruments**)
Ceramic heaters and cathodes, T. R. Palumbo—356(A)
Diode studies of oxide-coated cathodes, H. E. Kern and R. T. Lynch—355(A)
Photo-multiplier tube in photometry, J. H. DeWitt, Jr. and C. K. Seyfert—643(A)
Transit time of electrons in diodes, Delbert N. Eggenberger and Paul L. Copeland—643(A)
Investigation of contaminants, Paul D. Williams—353(A)
Life tests of oxide-coated cathodes, J. O. McNally—356(A)
Noise spectra at ultra low frequencies, R. W. Bogle—354(A)
Oxide cathode in diodes, Thomas H. Briggs—356(A)
Stored holes, withdrawal from Ge transistors and varistors, L. A. Meacham and S. E. Michaels—175(L)
For study of cathode materials, William J. Price—354(A)
Sublimation characteristics of cathode, emission processes, R. H. Plumlee—90(A)
Thoria cathodes in high voltage rectifiers, S. T. Yanagisawa and T. H. Rogers—353(A)
Thoria, use in secondary emission tube, chemistry, Leo J. Croning—352(A)

Electrons (see also **Positrons**)
Emission from dielectrics, R. T. K. Murray and Alexander Mackenzie—350(A)
Ranges, scattering effects, Frank L. Hereford—327(A)
Transmission through thin films, Edward Sturcken, Robert Heller, and Alfred H. Weber—327(A)

Electrons, secondary
Emission at oblique angles of incidence, James J. Brophy—643(A)
From magnetron cathodes, magnetron operation, Robert L. Jepsen—354(A)
From metals, theory, E. M. Baroody—780
From thoria and refractory materials, Leo J. Croning—352(A)

Electrostatics
Piezo-electric, tribo-electrification contribution to charge, John W. Peterson—91(A)

Elements
Element 98, S. G. Thompson, K. Street, Jr., A. Ghiorso, and G. T. Seaborg—298(L)

Energy states of nucleus (see **Disintegration and excitation of nucleus; Nuclear structure**)

Equations of state
At high pressures, W. M. Elsasser—351(A)

Errata
Cloud-chamber study of cosmic-ray nuclear interactions at 3260 meters, W. W. Brown and A. S. McKay—67(L)
Evidence for multiple meson and γ-ray production in cosmic-ray stars, M. F. Kaplon, H. Bradt, and B. Peters—68(L)
Internal pair formation, M. E. Rose—184(L)
On the role of the subsidiary condition in quantum electrodynamics, F. Coester and J. M. Jauch—828(L)
X-ray and gamma-ray reflection properties from 500 x-units to 9 x-units of unstressed and of bent quartz plates, D. A. Lind, W. J. West, and J. W. M. DuMond—474(L)

Excitation of nuclei (see **Disintegration and excitation of nucleus; Nuclear structure**)

Explosion phenomena (see also **Shock waves**)
Hydrogen-oxygen detonation pressures, W. E. Gordon—351(A)

Ferroelectric phenomena
Curie point of $BaTiO^3$, effect of pressure, W. J. Merz—52, 341(A)

Ferromagnetism (see **Magnetic properties**)

Field theory (see also **Quantum electrodynamics**)
Electromagnetic interaction of mesons of zero spin, F. Rohrlich—346(A)
Experimental and theoretical mesons, Alex E. S. Green—187(A)
Formalistic *vs.* realistic theories, Alex E. S. Green—187(A)
Interaction between elementary particles, Alfred Landé—346(A)
Isobaric state of nucleon, R. E. Marshak—346(A)
Non-adiabatic meson theory of nuclear forces, S. M. Dancoff—382
Non-local fields, M. Fierz—184(L)
Films, properties of
Optical absorption and photoelectric effect, E. A. Taft and J. E. Dickey—625(L)
Fission of nucleus (see also **Disintegration and excitation of nucleus**)
Tripartition of U^{235}, Louis Rosen and Alvin M. Hudson—533
Unequal mass division due to asymmetric oscillations, David L. Hill—320(A)
Yield of Xe^{133}, fine structure in curve, J. Macnamara, C. B. Collins, and H. G. Thode—129

Geophysics
Geomagnetic secular variation, C. J. Swift and W. M. Elsasser—64(L)

Hall effect
In ZnO, E. E. Hahn and P. H. Miller, Jr.—348(A); P. H. Miller, Jr. and E. E. Hahn—349(A)
Heat of dissociation (see **Molecular structure and constants**)
Helium, liquid
Entropy of superfluid in pure He^4 below λ-point, O. K. Rice—182(L)
Fountain effect of He^3 dissolved in He^4, K. W. Taconis, J. J. M. Beenakker, and Z. Dokoupil—171(L)
λ-points of He^3 in He^4 for superfluidity, J. G. Daunt and C. V. Heer—342(A)
λ-temperatures of He^3 in He^4, Olive G. Engel and O. K. Rice—55
Rayleigh disk in liquid He II, John R. Pellam and Philip M. Morse—474(L)
Second sound radiation pressure, John R. Pellam—818(L)
Theory of liquid He II, Sadao Nakajima, Kazuhisa Tomita, and Tunemaru Usui—768
Thermodynamics of He^3-He^4 solutions, O. K. Rice and Olive G. Engel—183(L)
Viscosity of He^3, R. A. Buckingham and H. N. V. Temperley—482(L)
Hydrodynamics
Pressure for cavitation due to rarefaction wave, A. B. Arons—333(A)
Ultrasonic wind, Francis E. Fox and Karl F. Herzfeld—156
Viscosity of solutions of macromolecules, concentration dependence, Jacob Riseman and Robert Ullman—359(A)
Hyperfine structure (see also **Nuclear moments and spin**)
Of Al II, S. Suwa—810(L)
Anomaly of K isotopes, S. A. Ochs, R. A. Logan, and P. Kusch—184(L)
Isotope shift and nuclear polarization, G. Breit, G. B. Arfken, and W. W. Clendenin—390
Isotope shift in Pb spectrum, Thurston E. Manning, C. E. Anderson, and W. W. Watson—417
Of Hg spectrum, K. Murakawa—480(L)

Ionization
Waves in ionized medium, V. A. Bailey—428
Ionization potentials
Of molecules by electron bombardment, Raymond Kaufman—332(A)

Isomers, nuclear (see also **Nuclear structure; Radioactivity**)
Of Te^{121} and Te^{123}, Robert Katz, R. D. Hill, and M. Goldhaber—9
Isotopes
Mass of Ne isotopes, A. Zucker and W. W. Watson—14
Masses of Cr^{50}, Cr^{52}, and Fe^{54}, Henry E. Duckworth and Howard A. Johnson—179(L)
Masses of Pd^{104}, Pd^{108}, Pt^{195}, and Cu^{65}, Henry E. Duckworth, Karl S. Woodcock, and Richard S. Preston—479(L)
Of Np, L. B. Magnusson, S. G. Thompson, and G. T. Seaborg—363
Of N, microwave techniques, A. L. Southern, H. W. Morgan, G. W. Keilholtz, and W. V. Smith—639(A)
Ratio of N^{15}/N^{14} in occluded gases, Herman Yagoda and William C. White—330(A)
Of Se in OCSe, masses, S. Geschwind, H. Minden, and C. H. Townes—174(L)
Terrestrial and meteoritic sulfur, J. Macnamara and H. G. Thode—307(L)
Transplutonium isotopes by neutron irradiation, A. Ghiorso, R. A. James, L. O. Morgan, and G. T. Seaborg—472(L)

Liquids (see also **Helium, liquid; Hydrodynamics**)
Heat of devitrification, B. Luyet—641(A)
Structural arrangements of ethyl alcohol, D. Sette—476(L)
Low temperature phenomena (see also **Helium, liquid**)
Magnetic susceptibility of Pb, M. C. Steele—342(A)
Nuclear specific heats in paramagnetic salts, B. Bleaney—214
Optical band width of *F* centers, E. Burstein and J. J. Oberly—349(A)
Oxidation of copper, T. N. Rhodin, Jr.—638(A)
Superconducting temperature of Pb, D. B. Cook, H. A. Boorse, and M. W. Zemansky—343(A)
Superconductivity theory, L. Tisza—342(A)
Thermal conductivity of Cu and Sn, F. A. Andrews, D. A. Spohr, and R. T. Webber—342(A)
Thermodynamic temperature of 1.5 millidegrees, D. de Klerk, M. J. Steenland, and C. J. Gorter—476(L)
Luminescence
Of LiF, Peter Pringsheim and Philip Yuster—293(L)
In lithium fluoride, color centers, Clifford C. Klick—644(A)

Magnetic fields
Lorentz correction in $BaTiO^3$, J. C. Slater—748
Shielding of nuclei in molecules, Norman F. Ramsey—699
Steady high fields, Martyn H. Foss—641(A)
Magnetic properties (see also **Crystal structure; Nuclear moments and spin**)
Of αFe^2O^3 and αFe^2O^3 with added titanium, F. J. Morin—819(L)
Flux in a superconducting torus, R. L. Dolecek and Jules de Launay—58
Gyromagnetic ratio of the proton, R. L. Driscoll, H. A. Thomas, and J. A. Hipple—339(A)
Gyromagnetic ratios of Va^{51} and Mn^{55}, William H. Chambers, Robert E. Sheriff, and Dudley Williams—640(A)
Magneto-resistance of Ge, G. L. Pearson—646(A); H. Suhl—646(A)
Magnetostriction of alloys, E. A. Nesbitt—638(A)
Memory in ferromagnetic domain crystal, H. J. Williams and W. Shockley—341(A)
No load characteristics of saturable reactors with hysteresis, Alfredo Baños, Jr. and William B. McLean—92(A)
Nuclear spin relaxation in PO_4, AsO_4 compounds, Roger Newman and Edward M. Purcell—339(A)
Saturation in alloys, statistical theory, R. Smoluchowski—638(A)
Superconducting lead, field penetration, M. C. Steele—791

Of superconductive Pb, Aaron Wexler and W. S. Corak—260
Susceptibility of Pb, M. C. Steele—342(A)
Magnetic resonance absorption (see also **Nuclear moments and spin**)
Angular dependence, E. F. Carr and C. Kikuchi—470(L)
Detection by ion resonance absorption, H. Sommer and H. A. Thomas—806(L)
Ferromagnetic materials, theory, J. H. Van Vleck—266
In nickel and supermalloy, N. Bloembergen—578
In NO, Robert Beringer and J. G. Castle, Jr.—567; Henry Margenau and Allan Henry—587
Oscillographic method for observing, R. Malvano and M. Panetti—826(L)
Protons in weak fields, Richard M. Brown—530
Shift of nuclear resonances, W. C. Dickinson—339(A)
Mass ratios (see **Isotopes**)
Mass spectroscopy
Initial energies of ions, Clifford E. Berry—597
Ionization of hydrocarbons, Fred L. Mohler—332(A)
Non-magnetic radiofrequency spectrometer, Willard H. Bennett—332(A)
Omegatron, J. A. Hipple, H. Sommer, and H. A. Thomas——332(A)
Temperature variation of mass spectra of hydrocarbons, Robert M. Reese, Vernon H. Dibeler, and Fred L. Mohler—332(A)
Mean or half-life (see **Radioactivity**)
Mechanics, quantum—atomic structure and spectra
Relativistic Kepler problem, M. H. Johnson and B. A. Lippmann—329(A)
Mechanics, quantum—general
Commutator equations for fields from variation principle, Christopher Gregory—67(L)
Commutators in quantized field theories, S. Schweber—613
Covariant spinor theory, Jack Heller and Peter G. Bergmann—329(A)
Cross-section theorem, Melvin Lax—306(L)
Dirac theory for spin $\frac{1}{2}$ particles, Leslie L. Foldy and Siegfried A. Wouthuysen—29
Field equations from variation principle, four-vector operator, Christopher Gregory—479(L)
Hamiltonian of gravitation with electromagnetic field, Peter G. Bergmann, Robert Penfield, Ralph Schiller, and Henry Zatzkis—329(A)
Iteration procedure in the Rayleigh-Ritz principle, E. Gerjuoy and Harold Gruen—90(A)
Of localizable dynamical systems, T. S. Chang—592
Quantization of gravitational field equations, A. Schild and F. A. E. Pirani—329(A)
Stationary states by solution of diffusion equation, Gilbert W. King—328(A)
Variational method for non-conservative collisions, Melvin Lax—306(L)
Mechanics, quantum—nuclear
Analysis of proton-proton scattering, G. Breit and R. D. Hatcher—110
Binding of H^3, range of tensor forces, Robert L. Pease and Herman Feshbach—322(A)
Cross-section theorem extended for capture, Melvin Lax——322(A)
Dependence of Fermi $|M|^2 f$ on Z, D. N. Kundu and M. L. Pool—328(A)
Deuteron break-up at high energy, L. I. Schiff—83(A)
Deuteron photo-effect, n-p interaction, L. I. Schiff—321(A)
Differential equations of nuclear induction, F. Bloch and R. K. Wangsness—82(A)
$(n,2n)$ reaction cross section near threshold, George Snow—322(A)
Nuclear forces from p-p scattering data, H. P. Noyes—90(A)
Production and annihilation of antiprotons, C. W. Helstrom——88(A)
Quadrupole moment of Li^7, R. D. Present and E. Feenberg——328(A)
Space exchange moments in light nuclei, L. Spruch—328(A)
Mechanics, quantum—of solid bodies
Energy band structures in semiconductors, W. Shockley—173(L)
Mechanics, statistical
Differential equations of nuclear induction, F. Bloch and R. K. Wangsness—82(A)
Mesons (see also **Cosmic radiation**)
Absorption in hydrogenous materials, W. K. H. Panofsky and H. F. York—89(A)
Absorption of π^--mesons in hydrogen, gamma-rays, W. K. H. Panofsky, Lee Aamodt, and Herbert F. York—825(L)
Collision path length for π-mesons, W. E. Hazen—320(A)
Detection of photo-mesons, J. Steinberger and A. S. Bishop——493(L)
Elementary particle nature, H. M. Moseley and Nathan Rosen—67(L)
Evidence for heavy meson, more than 450 electron masses, Harriet H. Forster—92(A)
Interaction of π-mesons, Oreste Piccioni—78(L)
Magnetic deflection, Ian Barbour—319(A), 518
Mass determination from momentum in cyclotron, Walter H. Barkas—90(A)
Mass from grain counts, J. Kent Bowker—87(A)
Mass measurements, F. M. Smith, Walter H. Barkas, A. S. Bishop, Hugh Bradner, and Eugene Gardner—86(A)
Mass of μ-meson, statistical considerations, O. Halpern and H. Hall—320(A)
Mass spectrum, Alex E. S. Green—642(A)
Neutral mesons by photons, J. Steinberger, W. K. H. Panofsky, and J. Steller—802
Nuclear forces, S. M. Dancoff—382
Nucleon magnetic moment in meson pair theories, J. Leite Lopes—36
π-μ-decay, W. L. Kraushaar, J. E. Thomas, Jr., and V. P. Henri—486(L)
Positive-negative ratio of π-mesons, Geoffrey F. Chew and Jack L. Steinberger—497(L)
Production by cascade process, B. T. Feld, I. L. Lebow, and L. S. Osborne—324(A)
Production by high energy particles—method, H. A. Wilcox and C. Richman—85(A); Energy and angular distribution, T. B. Taylor and G. F. Chew—86(A); Protons on C, C. Richman and H. Wilcox—85(A); Protons on Pb, Mitchel Weissbluth—86(A)
Production by photons, J. Steinberger and A. S. Bishop——493(L)
Production by x-rays, R. Stephen White, Edwin M. McMillan, and Jack M. Peterson—84(A); Jack M. Peterson, Edwin M. McMillan, and R. Stephen White—84(A); Keith A. Brueckner—84(A)
Production cross sections for π^+- and π^--mesons, C. Richman and H. A. Wilcox—496(L)
Production, detection, J. Steinberger and A. S. Bishop——319(A)
Production of π^+-mesons, W. F. Cartwright, C. Richman, M. N. Whitehead, and H. A. Wilcox—823(L)
Production of π-mesons by electrons, E. Strick and D. ter Haar—68(L)
Production, + to − π-meson yield ratio, Geoffrey F. Chew and Jack L. Steinberger—86(A); H. Bradner and S. B. Jones—90(A)
Production rates, dependence on absorbers, Marietta Blau, John Nafe, and Herbert Bramson—320(A)
Proton tracks in emulsions by π^--mesons, W. Cheston and L. Goldfarb—320(A)

Mesons (continued)
Ratio of + and − photo-mesons, Otto Halpern—69(L)
Yield functions for π^--mesons from *C*, Stanley B. Jones and R. Stephen White—12
Meteorology
Atomic and molecular O^2 in upper atmosphere, H. E. Moses and Ta-You Wu—333(A)
History of the noble gases, P. Morrison—334(A)
Low molecular rotation and upper atmosphere temperatures, Lewis M. Branscomb—333(A)
Radiation in the stratosphere, heat balance, Gilbert N. Plass and John Strong—334(A)
Thunderstorms, formation process, E. J. Workman and S. E. Reynolds—254
Methods and instruments (see also **Electronic tubes**)
Absorption cell, infra-red, R. B. Holden, W. J. Taylor, and H. L. Johnston—344(A)
A.c. circuit for rapid determination of Hall coefficient, B. R. Russell, P. H. Miller, Jr., and C. F. Wahlig—645(A)
Analog solution of equations by means of electrical networks, James H. Green, Jr. and Victor B. Corey—328(A)
Antenna radiation characteristics, David S. Saxon, Alfredo Baños, Jr., and Louis L. Bailin—327(A)
Attenuation of radiation under Pb, paraffin in emulsions, H. Sun and Harriet H. Forster—86(A)
Bevatron model, design, D. C. Sewell, W. M. Brobeck, E. O. Lawrence, and E. J. Lofgren—85(A)
Bevatron model, operating results, E. J. Lofgren, W. M. Brobeck, E. O. Lawrence, and D. C. Sewell—85(A)
Bevatron model radiofrequency system, Q. A. Kerns, W. R. Baker, G. M. Farly, and J. Riedel—85(A)
Bevatron model, theory of performance, Lloyd Smith, A. A. Garren, and L. R. Henrich—85(A)
Chemical analysis by proton scattering, S. Rubin and V. K. Rasmussen—83(A)
Coils for neutralization of earth's field in beta-ray spectrometer, S. K. Haynes and J. W. Wedding—641(A)
Counter method for neutron spectra, Donald C. Worth—378
Crystalite orientation of textile fibers, use of x-ray spectrometer, Leon Segal, Joseph J. Creely, and Carl M. Conrad—358(A)
Cyclotron orbits, non-equilibrium, meson mass determination, Walter H. Barkas—90(A)
Decay constants from coincidence experiments, T. D. Newton—490(L)
d and *α*, bombardment of enzymes and viruses, Ernest Pollard and F. Forro, Jr.—335(A)
Dielectric rods, patterns, C. W. Horton, F. C. Karal, and C. M. McKinney—327(A)
Diffusion equations, solution, W. T. Scott—323(A)
Directional and latitude survey of cosmic rays at 95,000 ft., T. Stix, K. Dwight, R. Sabin, and J. R. Winckler—324(A)
Double-crystal spectrometer, modifications, Paul Kaesberg, W. W. Beeman, and H. N. Ritland—336(A)
Efficiency of γ-counters, R. J. Hart, K. Russell, and R. M. Steffen—334(A)
Electron linear accelerator, operation, R. F. Post—92(A)
Electron sensitive emulsions, track observations, Frank L. Adelman—86(A)
Electroplating Rh on W wire, Roberto Levi and George A. Espersen—231
Emulsion for cosmic-ray studies, Pierre Demers—320(A)
Evaporation of zinc under electron bombardment, Francis E. Dart—761
Gamma-ray energies measured with one crystal, John A. McIntyre and Robert Hofstadter—617(L)
Gamma-ray energies measured with two crystals in coincidence, Robert Hofstadter and John A. McIntyre—619(L)
Ge filament cuts, W. L. Bond—646(A)
Goniometer and x-ray spectrometer, M. L. Baron and A. de Bretteville, Jr.—344(A)
Grain count variations in emulsions, J. Kent Bowker—87(A)
Initial energies of ions in mass spectrometer, Clifford E. Berry—597
Ion source for cyclotrons, R. S. Livingston, R. J. Jones, and R. E. Wright—329(A)
Line width determination in microwave spectra, Robert Beringer and J. G. Castle, Jr.—340(A)
Liquid scintillation counters, George T. Reynolds, F. B. Harrison, and G. Salvini—488(L)
Magnetic deflection method for *p-p* scattering, O. A. Towler, Jr. and C. L. Oxley—326(A)
Magnetic deflection of mesons, nuclear plates, Ian Barbour—319(A), 518
Magnetic suspension balance, J. W. Beams—471(L)
Mass spectrometer for studying surface reactions at low pressures, Stanley A. Landeen, H. E. Farnsworth, and Russell K. Sherburne—351(A)
Hg arc temperature by x-rays, C. Kenty and W. J. Karash—625(L)
Meson production by high energy particles, H. A. Wilcox and C. Richman—85(A)
Microwave apparatus for dielectric constants and conductivity, Richard F. Greene and Sol E. Harrison—348(A)
For microwave spectroscopy, O. R. Gilliam, Charles M. Johnson, and Walter Gordy—140
Mounting for a concave grating spectrometer, W. J. Taylor, G. P. Koch, and H. L. Johnston—343(A)
Multiple scattering deflector for cyclotron, C. E. Leith—89(A)
Neutron activated cadmium covered indium foils, John W. Kunstadter—484(L)
Neutron spectrometer employing emulsions, G. R. Keepin, Jr. and J. H. Roberts—87(A)
Nuclear emulsion events, device for analysis, Robert Rudin, Marietta Blau, and Seymour Lindenbaum—319(A)
Nuclear induction apparatus for signals in gases, M. E. Packard—83(A)
Nuclear induction radiofrequency spectrometer, W. G. Proctor and F. C. Yu—83(A)
Omegatron for e/m ratio of ions, J. A. Hipple, H. Sommer, and H. A. Thomas—332(A)
Optical interference filters, multi-layer, W. H. Shaffer and R. A. Oetjen—187(A)
Particle injection into accelerators, W. B. Jones, H. R. Kratz, J. L. Lawson, G. L. Ragan, and H. G. Voorhies—60
Photo-mesons by delayed coincidence, J. Steinberger and A. S. Bishop—319(A)
Photo-multiplier tube photometry, J. H. DeWitt, Jr. and C. K. Seyfert—643(A)
Piezoelectric constants, static and resonator methods, Karl S. Van Dyke—315(A)
Positive ion space-charge detector, sensitivity, R. R. Eggleston and G. L. Weissler—91(A)
Probability distribution of recurrence times, A. J. F. Siegert—328(A)
Protons from synchrotron beam, A. Silverman and C. Levinthal—87(A)
Pulse-annealing method for changes in properties on heat treatment, N. S. Rasor and W. E. Parkins—638(A)
Pulsed photo-multiplier scintillation counters, R. F. Post and N. S. Shiren—81(L)
Random-circuit theory of resistance and noise, R. P. Coleman—644(A)
Rayleigh disk in liquid He II, John R. Pellam and Philip M. Morse—474(L)

Recrystallization purification of germanium, R. N. Hall—645(A)
Regulation of electromagnets using proton resonance, H. A. Thomas—339(A)
Resonance by ion resonance absorption, H. Sommer and H. A. Thomas—806(L)
Resonant modulation for microwave spectroscopy, S. H. Autler and C. H. Townes—340(A)
Scintillation counter characteristics using pulsed photomultipliers, R. F. Post and N. S. Shiren—644(A)
Scintillation counters, abnormal efficiencies, W. G. Cross—185(L)
Scintillation counters as detectors of x-rays, John P. Neissel and Donald C. Moore—643(A)
Scintillation counter response to electrons, John I. Hopkins—643(A)
Scintillation counters, effect of magnetic fields, J. D. Graves—309(L)
Scintillation counters, temperature dependence, S. H. Liebson and J. W. Keller, Jr.—305(L)
Scintillation counting with solutions, Hartmut Kallmann—621(L)
Scintillation spectra of short-life activities, Edward C. Campbell and Max Goodrich—640(A)
Se rectifiers, recovery time, K. Lehovec—348(A)
Single-photon counting, A. J. Dekker and A. H. Moorish—301(L)
Spectrophotometer, alignment, James L. Lauer—344(A)
Spectrophotometer, ratio-recording, double beam, Abraham Savitzky and Ralph S. Halford—344(A)
Statistics of luminescent counter systems, Frederick Seitz and D. W. Mueller—605
Synchro-cyclotron magnet, M. H. Foss, J. G. Fox, R. B. Sutton, and E. Creutz—641(A)
Terphenyl and dibenzyl scintillation counters, R. Hofstadter, S. H. Liebson, and J. O. Elliot—81(L)
Thermionic emission calculations, H. F. Ivey and C. L. Shackelford—356(A)
Thermometers for low temperatures, use of semiconductors, I. Estermann—83(A)
300-Mev betatron at Illinois, D. W. Kerst, G. D. Adams, H. W. Koch, and C. S. Robinson—297(L)
Ultraviolet irradiation of viruses, Donald J. Fluke—335(A)
Water-prism monochromator, R. B. Setlow and D. J. Fluke—335(A)

Mobility of electrons
In conducting phosphors, Lee Gildart and A. W. Ewald—645(A)

Molecular structure and constants (see also **Raman spectra; Spectra, molecular**)
Of borine carbonyl, Walter Gordy, Harold Ring, and Anton B. Burg—512
Of CO, O. R. Gilliam, Charles M. Johnson, and Walter Gordy—140
Centrifugal distortion in excited vibration states, Harald H. Nielsen—415
Centrifugal distortion in formaldehyde, Richard B. Lawrance—347(A)
Dipole moments, R. G. Shulman, C. H. Townes, and B. P. Dailey—145
Double-bond character from microwave spectrum, J. H. Goldstein and J. K. Bragg—347(A)
Of fluorosilane, dipole moment, A. Harry Sharbaugh, Virginia G. Thomas, and Benjamin S. Pritchard—64(L)
Heat of dissociation of N, Joseph Kaplan—93(A)
Intermolecular forces in benzene, Vernon Myers—348(A)
Nuclear quadrupole coupling and ionic character of Cl^{35}, C. H. Townes and B. P. Dailey—346(A)
Of PCl^3, microwave spectrum, P. Kisliuk and C. H. Townes—347(A)
Quadrupole moment of the electron distribution in H, Norman F. Ramsey—221
Weights from flow birefringence and viscosities, M. D. Schoenberg and F. R. Eirich—359(A)

Moments, of particles (see **Nuclear moments and spin**)

Neutrons
Binding energies in Pb^{207}, Pb^{208}, Bi^{210}, B. B. Kinsey, G. A. Bartholomew, and W. H. Walker—77(L)
Decay, A. H. Snell, F. Pleasonton, and R. V. McCord—310(L), 317(A); J. M. Robson—311(L)
Diffusion in multiplying medium, E. Richard Cohen and M. A. Greenfield—639(A)
Energy and direction measurement, G. R. Keepin, Jr. and J. H. Roberts—87(A)
Energy of neutrons from $Be^9(\alpha,n)C^{12}$, C. E. Bradford and W. E. Bennett—302(L)
Magnetic scattering, H. Ekstein—731
Neutron activated cadmium-covered indium foils, John W. Kunstadter—484(L)
From Po-Be energy spectrum, B. G. Whitmore and W. B. Baker—799
Production by 50-Mev x-rays, G. C. Baldwin and F. R. Elder—76(L)
Refraction theory extended to capture and scattering, Otto Halpern and Charles B. Shaw, Jr.—88(A)

Neutron diffraction
By nuclei with zero spin, W. C. Koehler, E. O. Wollan, and C. G. Shull—640(A)
Of vitreous silica, I. W. Ruderman—317(A)

Nuclear moments and spin (see also **Hyperfine structure**)
Of boron, Walter Gordy, Harold Ring, and Anton B. Burg—512
Of D^2 and H^1, effect of chemical compound, Gunnar Lindström—817(L)
Electric dipole moments of elementary particles and nuclei, E. M. Purcell and N. F. Ramsey—807(L)
Electron spin from microwave spectra of NO^2, K. B. McAfee, Jr.—340(A)
Exchange moments in H^3 and He^3, R. K. Osborn and L. L. Foldy—322(A)
Gyromagnetic ratio of the proton, R. L. Driscoll, H. A. Thomas, and J. A. Hipple—339(A)
Integral expressions for moments, Enos E. Witmer—352(A)
Of Li^7, R. Avery and C. H. Blanchard—704
Magnetic moment of Nb^{93}, Robert E. Sheriff, William H. Chambers, and Dudley Williams—476(L)
Magnetic moment of Pr^{141}, William H. Chambers, Robert E. Sheriff, and Dudley Williams—482(L)
Magnetic moments and shell structure, Roald K. Wangsness—620(L)
Magnetic moments of Ga isotopes, G. J. Béné, P. M. Denis, and R. C. Extermann—66(L); P. Kusch—615(L)
Magnetic moments of Xe^{129}, Bi^{209}, Sc^{45}, Sb^{121}, and Sb^{123}, W. G. Proctor and F. C. Yu—471(L)
Moments of p and d, E. C. Levinthal—204
Nucleon magnetic moment in meson pair theories, J. Leite Lopes—36
Of proton in absolute units, H. A. Thomas, R. L. Driscoll, and J. A. Hipple—787
Proton magnetic moment, diamagnetic field corrections, Norman F. Ramsey—339(A)
Proton magnetic moment in units of nuclear magnetron, C. D. Jeffries—83(A)
Quadrupole interactions due to Cl^{35} and Cl^{37}, H. Zeiger, D. Bolef, and I. I. Rabi—340(A)
Quadrupole interactions due to Cl^{35}, electric resonance method, C. A. Lee, R. O. Carlson, B. P. Fabricand, and I. I. Rabi—340(A)
Quadrupole moment of deuteron, G. F. Newell—711

Nuclear moments and spin (continued)
Quadrupole moment of Li^7, theory, R. D. Present and E. Feenberg—328(A)
Of Sc^{45}, D. M. Hunten—806(L)
Space exchange moments in light nuclei, L. Spruch—328(A)
Spin of B^{10}, M. T. Weiss, M. W. P. Strandberg, R. B. Lawrance, and C. C. Loomis—202
Spin relaxation in PO_4, AsO_4 compounds, Roger Newman and Edward M. Purcell—339(A)
Of S^{33} from Zeeman effect, C. K. Jen—339(A)
Of Te and W, G. R. Fowles—744
Nuclear spectra (see also **Disintegration and excitation of nucleus**)
Beta-gamma-angular correlations, Donald T. Stevenson and Martin Deutsch—640(A)
β-spectrum of Be^{10}, D. E. Alburger, D. J. Hughes, and C. Eggler—318(A); L. Feldman and C. S. Wu—318(A)
β-spectrum of He^6, Victor Perez-Mendez and Harold Brown—317(A)
β-spectrum of prometheum 147, Werner S. Emmerich and J. D. Kurbatov—187(A)
β-spectrum of Na^{22}, P. A. Macklin, L. J. Lidofsky, and C. S. Wu—318(A)
β-spectrum of S^{35}, Leonard Gross and Donald R. Hamilton—318(A)
Gamma-ray energies from ThC″, RaC, Na^{24}, J. L. Wolfson—176(L)
γ-rays from Be^7, T. Lauritsen and R. G. Thomas—88(A)
γ-rays from Bi, A. W. Sunyar, D. E. Alburger, G. Friedlander, M. Goldhaber, and G. Scharff-Goldhaber—326(A)
γ-rays from $C^{13}+d$, R. G. Thomas and T. Lauritsen—88(A)
γ-rays of Ba^{131}, E. B. Dale, E. L. Zimmerman, D. G. Thomas, and J. D. Kurbatov—640(A)
Internal conversion electrons, Richard L. Caldwell—407
Neutron energy spectra, B. L. Cohen, C. E. Falk, and S. K. Kao—639(A)
Photons of low energy, Gertrude Scharff-Goldhaber, E. der Mateosian, M. McKeown, and A. W. Sunyar—325(A)
Positron activity of Cu^{64} in a source of Cu^{61}, C. Sharp Cook and Chia-hua Chang—171(L)
Of Zn^{62} and Cu^{62}, β-rays, Raymond W. Hayward—87(A)
Nuclear structure (see also **Disintegration and excitation of nucleus; Radioactivity; Nuclear spectra**)
Of Al^{26}, energy levels, C. P. Swann, C. E. Mandeville, and W. D. Whitehead—338(A)
Of Be^7 and Li^7, excited states, A. B. Brown, C. Y. Chao, W. A. Fowler, and C. C. Lauritsen—88(A)
Binding energy of triton, Tsi-Ming Hu and Kung-Ngou Hsu—633(L)
Binding of H^3, range of tensor forces, Robert L. Pease and Herman Feshbach—322(A)
Of B^{10}, excitation levels, W. D. Whitehead and C. E. mandeville—337(A)
Of C^{13}, search for levels, D. W. Miller—806(L)
Charge independence of nuclear forces, Julian Schwinger—135
Configurations in spin-orbit coupling model, empirical evidence, Maria Goeppert Mayer—16
Coupling and shell model, Giulio Racah—622(L)
Deuteron photo-effect, n-p interaction, L. I. Schiff—321(A)
Doublets of N^{15} and O^{16}, D. R. Inglis—616(L)
Energy levels of C^{14}, C^{13}, C. Levinthal, E. A. Martinelli, and A. Silverman—199
Equivalence of protons and neutrons, William D. Harkins—634(L)
Of F^{20}, energy levels, R. C. Allen and Waldo Rall—337(A)
Integers in mass ratios, Enos E. Witmer—641(A)
Low states of Li^7, R. Avery and C. H. Blanchard—704
Magic numbers, possible third-order difference, Frank A. Valente—77(L)
Magic numbers, stable isotopes, Lew Kowarski—427(L)
Magnetic moments and shell structure, Roald K. Wangsness—620(L)
n-p scattering, tensor forces, L. Biedenharn and J. M. Blatt—322(A)
Of N^{15}, energy levels, R. Malm and W. W. Buechner—337(A)
Nuclear configurations in spin-orbit coupling model, theoretical, Maria Goeppert Mayer—22
Nuclear forces, meson theory, S. M. Dancoff—382
Polarization of nucleus, isotope shift, G. Breit, G. B. Arfken, and W. W. Clendenin—390
p-d scattering phase shifts, exchange forces, J. L. Gammel—321(A)
Schmidt model, staggering of isotopic shift, G. Breit—470(L)
Shell model, β-decay, L. W. Nordheim—294(L)
Of Si^{30}, energy level scheme, H. H. Landon—338(A)
Of Ta^{181}, excited state, W. C. Barber—641(A)

Optical constants and properties
Of films of SrO, Robert L. Sproull—630(L)
Of films on BaO, E. A. Taft and J. E. Dickey—625(L)

Packing fraction (see also **Isotopes**)
For doublets from mass comparisons, Henry E. Duckworth, Howard A. Johnson, Richard S. Preston, and Richard F. Woodcock—386
Of Fe^{56}, Ni^{58}, and Ni^{60}, Henry E. Duckworth and Howard A. Johnson—330(A)
Pair production
Nuclear recoil momentum, B. Rosenbaum—628(L)
X-rays from 100-Mev betatron, E. R. Gaerttner and M. L. Yeater—621(L)
Phosphorescence
Color centers by single-photon counting, A. J. Dekker and A. H. Morrish—301(L)
Photoconductivity
Photon yield of electron-hole pairs in Ge, F. S. Goucher—816(L)
Photo-disintegration
Of Cu^{63}, threshold for n, J. McElhinney and W. E. Ogle—63(L)
Cross section for (γ,n) reactions, A. C. Helmholz and K. Strauch—86(A)
Of deuteron at high energies, J. F. Marshall and E. Guth—738; L. I. Schiff—733
Of deuteron, n-p interaction, L. I. Schiff—321(A)
Dipole transitions, cross section, J. S. Levinger and H. A. Bethe—115
Of N^{14} and O^{16}, evidence for, A. G. W. Cameron and C. H. Millar—337(A)
Of O^{16} and N^{14}, α-tracks, C. H. Millar and A. G. W. Cameron—78(L)
Of Ti^{46}, Cr^{50}, thresholds for n, W. E. Ogle and R. E. England—63(L)
Transition curves in Pb, K. Strauch—84(A); L. Eyges—85(A)
Of Zr^{90}, Pr^{141}, As^{75}, I^{127}, and Ni^{58}, thresholds for n, W. E. Ogle, L. J. Brown, and A. N. Carson—63(L)
Photoelectric effect and properties; cells
Of metal films on BaO, E. A. Taft and J. E. Dickey—625(L)
Quantum yield of electron-hole pairs in Ge, F. S. Goucher—646(A)
Work function of Ag film, Edward Kelly, H. E. Farnsworth, and Edward N. Clarke—316(A)
Photovoltaic effect
Of P-N junctions in Ge, M. Becker and H. Y. Fan—301(L)
Temperature dependence of P-N barriers in Ge, H. Y. Fan and M. Becker—335(A)

Piezoelectric effect
Of $BaTiO_3$, dependence on temperature, W. J. Merz—642(A)
Of $BaTiO_3$ single-domain crystals, M. E. Caspari—341(A)
Capacitance of AT-cut quartz resonators, Karl S. Van Dyke—642(A)
Measurement methods, Karl S. Van Dyke—315(A)
On tribo-electrification, John W. Peterson—91(A)
Thickness-shear resonance of resonators, Gary D. Gordon—642(A)
Plasticity
Fracture markings, J. A. Kies and A. M. Sullivan—357(A)
Shocks in polymeric films, John Kauffman and Waller George—357(A)
Transition to elasticity, M. L. Huggins—336(A)
Polarization of radiation
Gamma-rays by pair production, T. H. Berlin and L. Madansky—623(L)
By interstellar medium, W. A. Hiltner—170(L)
Of starlight, Leverett Davis, Jr.—84(A)
Polymerization, properties of polymers
Collagen tendons, stress-strain behavior, Norman M. Wiederhorn and Gerald V. Reardon—359(A)
Crazing of linear polymers, C. C. Hsiao and J. A. Sauer—358(A)
Crystallite orientation of textile fibers, Leon Segal, Joseph J. Creely, and Carl M. Conrad—358(A)
Crystallization, second-order transitions in Si rubbers, C. E. Weir, W. H. Leser, and L. A. Wood—357(A)
Dynamic-property data on textile specimens, W. James Lyons—357(A)
Emulsion polymerization with ultrasonic vibration, A. S. Ostroski and R. B. Stambaugh—358(A)
Equation of state, R. S. Spencer and G. D. Gilmore—358(A)
Granulated polymers under pressure, R. S. Spencer, G. D. Gilmore, and R. M. Wiley—358(A)
Oriented polystyrene films, mechanical properties, Lawrence E. Nielsen and Rolf Buchdahl—359(A)
Plasticization of PVC, M. L. Dannis—358(A)
Polyvinyl acetate solutions, dynamic properties, John D. Ferry, W. M. Sawyer, George V. Browning, and Arthur H. Groth, Jr.—359(A)
Shear creep and recovery of elastomers, F. S. Conant, G. L. Hall, and W. James Lyons—357(A)
Transition phenomenon, R. Buchdahl, L. E. Nielsen, and R. E. Pollard—359(A)
Wool fibers, Harris M. Burte—357(A)
X-ray line broadening in nylon filaments, Waller George and John Kauffman—358(A)
Probability
Distribution of recurrence times, A. J. F. Siegert—328(A)
Volume effect, long chain molecules, Chan-Mou Tchen—336(A)
Proceedings of the American Physical Society
Stanford Meeting, Stanford University, California, December 29–30, 1949—82
Division of Electron Physics, New York University, New York, January 31 and February 1, 1950—352
Division of High-Polymer Physics, Polytechnic Institute of Brooklyn, New York, February 1 and 3, 1950—357
Annual Meeting, New York City, February 2–4, 1950—313
Ohio Section, Cincinnati, Ohio, March 4, 1950—187
Oak Ridge Meeting, Oak Ridge, Tennessee, March 16–18, 1950—637
Ohio Section, Columbus, Ohio, April 29, 1950—648

Quantum electrodynamics (see also **Field theory**)
Collisions of positrons and electrons, J. Katzenstein—161
Corrections to current operator, Thomas A. Green—297(L)
Covariant description of extended charges, D. Bohm, M. Weinstein, and H. Kouts—346(A)
Dirac theory of spin ½ particles, non-relativistic limit, L. L. Foldy and S. A. Wouthuysen—345(A)
Electromagnetic interaction of mesons of zero spin, F. Rohrlich—346(A)
e-p scattering, M. N. Rosenbluth and L. I. Schiff—326(A)
Electron self-energy, Frederik J. Belinfante—642(A)
Field and charge measurements, N. Bohr and L. Rosenfeld—794
Identity, J. C. Ward, 182(L)
Interaction between elementary particles, Alfred Landé—346(A)
Quantization of Wheeler-Feynman's electrodynamics, F. J. Belinfante and J. S. Lomont—346(A)
Relativistic model of a finite-sized electron, G. J. Yevick—345(A)
Self-energies of electrons and photons, Hartland S. Snyder—346(A)
Self-energy problem, Hartland S. Snyder—98
Self-stress of the electron, S. Borowitz, W. Kohn, and J. Schwinger—345(A)
Subsidiary condition, role of, F. Coester and J. M. Jauch—149; 828(L)

Radiation (see also **Thermal radiation**)
Antenna characteristics, David S. Saxon, Alfredo Baños, Jr., and Louis L. Bailin—327(A)
Bremsstrahlung in nucleon-nucleon collisions, Albert Simon—321(A)
Dielectric rod patterns, C. W. Horton, F. C. Karal, and C. M. McKinney—327(A)
Diffusion of imprisoned resonance radiation, Frank N. Edmonds, Jr.—424
Showers from 335-Mev bremsstrahlung, Wade Blocker and Robert W. Kenney—87(A)
Radioactivity (see also **Disintegration and excitation of nucleus; Spectra, nuclear**)
Of Am^{242}, maximum energy of β-rays, Jean M. Grunlund, B. G. Harvey, N. Moss, and L. Yaffe—69(L)
Of Sb, beta-gamma-angular correlation, Stuart L. Ridgway—821(L)
Of A^{41} and O^{15}, beta-spectra, Harold Brown and Victor Perez-Mendez—649
Of At^{211}, Auger effect, Lawrence S. Germain—90(A)
β-emitting isotopes in W region, M. Lindner and J. S. Coleman—67(L)
β-γ-angular correlation, Theodore B. Novey—66(L); Donald T. Stevenson and Martin Deutsch—640(A)
Of Bi isotopes, H. M. Neumann and I. Perlman—191
Of Br^{80}, isomers, L. J. Lidofsky, P. A. Macklin, and C. S. Wu—318(A)
Of Ce^{143}, E. Shapiro and C. E. Mandeville—319(A)
Of Cs^{137}, γ-ray energy, Lawrence M. Langer and R. Douglas Moffat—74(L)
Of Cr^{55}, Daniel R. Miller—808(L)
Of Co^{60}, passage γ-rays through water, Gladys R. White—330(A)
Of Cu^{61} and Cu^{67}, D. N. Kundu and M. L. Pool—488(L)
Of Cu^{61}, positrons, George E. Owen, C. Sharp Cook, and Paul H. Owen—686
Of Cm^{242}, half-life, G. C. Hanna, B. G. Harvey, and N. Moss—617(L)
Decay scheme for $_{72}Hf^{181}$, S. B. Burson and K. W. Blair—89(A)
Dependence of Fermi $|M|^2 f$ on Z, D. N. Kundu and M. L. Pool—328(A)
Of element 98, S. G. Thompson, K. Street, Jr., A. Ghiorso, and G. T. Seaborg—298(L)
Fermi β-distribution function, I. Feister—375
Gamma-ray energies from ThC″, RaC, Na^{24}, J. L. Wolfson—176(L)
Of Au^{197*}, F. K. McGowan—325(A)

Radioactivity (continued)
Of Hf, J. M. Cork, A. E. Stoddard, W. C. Rutledge, C. E. Branyan, and J. LeBlanc—299(L)
Of Hf^{181}, coincidence studies, W. C. Barber—82(A)
Of In^{116}, disintegration scheme, Hilding Slätis, Stefaan J. du Toit, and Kai Siegbahn—498(L)
Internal conversion coefficients for Co^{60}, M. A. Waggoner, M. L. Moon, and A. Roberts—295(L)
Internal conversion electrons, transition energies, Richard L. Caldwell—407
Of $I^{123, 122, 121, 120}$, Luis Marquez and I. Perlman—189
Of I^{131}, decay scheme, I. Feister and L. F. Curtiss—179(L)
Of La, R. W. Pringle, S. Standil, and K. I. Roulston—303(L)
Of Pb^{204}, Bi^{204}, Bi^{206}, A. W. Sunyar, D. E. Alburger, G. Friedlander, M. Goldhaber, and G. Scharff-Goldhaber—326(A)
Of long-lived zirconium from fission, E. P. Steinberg and L. E. Glendenin—624(L)
$Hg^{203, 205}$, half-life of γ-ray level, Daniel Binder—325(A)
Of Nd^{147}, C. E. Mandeville—319(A)
Of Ne^{23}, beta-spectrum, H. Brown and V. Perez-Mendez—812(L)
Of Ne^{23}, gamma-radiation, V. Perez-Mendez and H. Brown—812(L)
Of Np, new isotopes, L. B. Magnusson, S. G. Thompson, and G. T. Seaborg—363
Of neutron, half-life, A. H. Snell, F. Pleasonton, and R. V. McCord—310(L), 317(A); J. M. Robson—311(L)
Of Pd^{106}, γ—γ-angular correlation, J. A. Spiers—75(L)
Photons of low energy, Gertrude Scharff-Goldhaber, E. der Mateosian, M. McKeown, and A. W. Sunyar—325(A)
Polarization-direction correlation of successive gamma-rays, Franz Metzger and Martin Deutsch—551
Of Po^{208}, half-life, D. H. Templeton—312(L)
Positron activity of Cu^{64} in a source of Cu^{61}, C. Sharp Cook and Chia-hua Chang—171(L)
Of K, specific activity, William R. Faust—624(L)
Of K^{40}, beta-ray spectrum, David E. Alburger—629(L)
Of protactinium isotopes, W. W. Meinke and G. T. Seaborg—475(L)
Of Rh^{106}, Co^{60}, and Cs^{134}, correlation of successive quanta, A. H. Williams and M. L. Wiedenbeck—822(L)
Of Ag^{110} by scintillation method, Edward C. Campbell and Max Goodrich—640(A)
Of Te^{130}, double beta-decay, Mark G. Inghram and John H. Reynolds—822(L)
Of Tb^{160}, γ-rays, J. M. Cork, C. E. Branyan, W. C. Rutledge, A. E. Stoddard, and J. M. LeBlanc—304(L)
Tracers for film properties, H. W. Allison and George E. Moore—354(A)
In well logging, Clark Goodman, Charles W. Tittle, and Henry Faul—640(A)
Of Yb and Ta, β-spectra, J. M. Cork, H. B. Keller, W. C. Rutledge, and A. E. Stoddard—95
Of Yb^{170}, half-life, R. E. Bell and R. L. Graham—490(L)
Of Y^{87} and Sr^{87}, B. E. Robertson, W. E. Scott, and M. L. Pool—318(A)
Of Zn^{62} and Cu^{62}, analysis of spectrum, Raymond W. Hayward—87(A)
Of Zn^{65}, Ruth A. Cohn and J. D. Kurbatov—318(A)
Raman spectra
Of Br_2, H. Stammreich—79(L)
Range of particles
Of α-particles in water and ice, H. G. de Carvalho—330(A)
Of high energy electrons in Al and Cu, Frank L. Hereford and Charles P. Swann—727
Of p from $B(d,p)$ reaction, W. O. Bateson—337(A)
Range-energy curves for α and p, William P. Jesse and John Sadauskis—1
Recombination
Dissociative recombination of ions, D. R. Bates—492(L)
Relativity
Accelerated and rotating coordinate systems, H. C. Corben—329(A)
Gravitational field equations, Hans Freistadt—329(A)
Hamiltonian of gravitation with electromagnetic field, Peter G. Bergmann, Robert Penfield, Ralph Schiller, and Henry Zatzkis—329(A)
Quantization of gravitational field equations, A. Schild and F. A. E. Pirani—329(A)

Scattering of electrons, ions, mesons, neutrons, and protons (see also **Cross section, measurements, theory; Electron diffraction**)
Analysis of proton-proton scattering, G. Breit and R. D. Hatcher—110
Backscattering of positive electrons, H. H. Seliger—491(L)
Charge independence of nuclear forces, Julian Schwinger—135
Curvature for fast charged particles, W. T. Scott and H. S. Snyder—223
Deuteron-proton, photographic techniques, F. A. Rodgers, H. A. Leiter, and P. G. Kruger—656
Deuteron-proton scattering at 10 Mev, K. B. Mather, H. J. Karr, and R. O. Bondelid—292(L)
e-p scattering, M. N. Rosenbluth and L. I. Schiff—326(A)
Electron scattering by H atoms, H. S. W. Massey and B. L. Moiseiwitsch—180(L)
Electron scattering in tissue, reduction by magnetic field, W. H. Bostick—327(A)
Lower bound, range of n-p interaction, Leslie L. Foldy—636(L)
Magnetic scattering of neutrons, H. Ekstein—731
Multiple scattering in infinite medium, H. W. Lewis—321(A), 526
n-d cross section at high energies, Frederic de Hoffmann—216
n-d scattering, E. Wantuch—326(A)
n-p, p-p, high energy scattering, theory, Richard S. Christian—89(A)
n-p scattering, tensor forces, L. Biedenharn and J. M. Blatt—322(A)
Neutron scattering in V^{51}, resonance and thermal cross section, M. Hamermesh and C. O. Muehlhause—175(L)
Of neutrons, extension of refraction theory, Otto Halpern and Charles B. Shaw, Jr.—88(A)
Non-conservative collisions, Melvin Lax—322(A)
p-d scattering phase shifts, exchange forces, J. L. Gammel—321(A)
Proton-proton at 5 Mev, R. E. Meagher—667
Proton-proton in charged scalar theory, K. A. Brueckner and K. M. Watson—495(L)
p-p scattering at 12.4 Mev, Byron T. Wright and F. E. Faris—89(A)
p-p scattering at 250 Mev, magnetic deflection method, O. A. Towler, Jr. and C. L. Oxley—326(A)
p-p scattering at 340 Mev, C. Wiegand and O. Chamberlain—326(A)
p-scattering by Al and C, C. Levinthal, E. A. Martinelli, and A. Silverman—199
Scattering effects in electron range measurements, Frank L. Hereford—327(A)
Velocity-dependent interactions, C. H. Blanchard, R. Avery, and R. G. Sachs—292(L)
Scattering of radiation (see also **Raman spectra**)
Simultaneity in Compton effect, Robert Hofstadter and John A. McIntyre—24

Secondary electrons (see **Electrons, secondary**)
Semiconductors (see **Electrical conductivity and resistance**)
Shock waves (see also **Explosion phenomena**)
Decay, hydrogen-oxygen detonation pressures, W. E. Gordon—351(A)
Pressure behind diffracted wave, C. H. Fletcher, D. K. Weimer, and Walker Bleakney—634(L)
Solid state (see **Crystalline state**)
Spallation(see **Disintegration and excitation of nucleus**)
Specific heat
In paramagnetic salts at low T, B. Bleaney—214
Spectra, absorption (see also **Absorption of radiation**)
Of HDO near 3.7μ in solar spectrum, R. M. Chapman and J. H. Shaw—71(L)
Of H_2, bands in the $3p^1\Pi$-$1s^1\Sigma$ system, C. R. Jeppesen and Paul E. Pflueger—91(A)
Of N_2O near 4.06μ in solar spectrum, J. H. Shaw, M. L. Oxholm, and R. M. Chapman—497(L)
Of Si, infra-red, H. Y. Fan and M. Becker—178(L)
Spectra, atomic
Of Ca II, $4s$-$4p$ transition, L. C. Green and N. E. Weber—343(A)
Fine structure of He^+, Willis E. Lamb, Jr. and Miriam Skinner—539
Isotope shift in Pb I lines, W. W. Watson and C. E. Anderson—343(A)
Of Pb I, isotope shift, Thurston E. Manning, C. E. Anderson, and W. W. Watson—417
Of Pb III, configuration interactions, J. N. P. Hume and M. F. Crawford—343(A)
Of L_{III}, electronic excitation, George L. Rogosa and Guenter Schwarz—343(A)
Of Mn II, C. W. Curtis—343(A)
Spectra, general
Of the night sky, aurora and afterglows, Joseph Kaplan—82(A)
Solar spectrum, high dispersion studies, Robert M. Chapman, John H. Shaw, and Dudley Williams—333(A)
Spectra, microwave
Of asymmetric top molecules, W. J. Pietenpol, J. D. Rogers, and Dudley Williams—480(L)
Of Ch_3SiF_3, H. T. Minden, J. M. Mays, and B. P. Dailey—347(A)
Double-bond character of molecules, J. H. Goldstein and J. K. Bragg—347(A)
Fine structure of He^+, Willis E. Lamb, Jr. and Miriam Skinner—539
Of HCN, transitions between l-type doublets, R. G. Shulman and C. H. Townes—347(A)
Of ND_3, absorption of millimeter waves, J. H. N. Loubser and J. A. Klein—348(A)
Of NO, line width determination, Robert Beringer and J. G. Castle, Jr.—340(A)
Of NO_2, electron spin, K. B. McAfee, Jr.—340(A)
Of POF_3, Samuel J. Senatore—293(L)
Of PCl_3, molecular structure, P. Kisliuk and C. H. Townes—347(A)
Pressure shift and broadening, A. G. Rouse, A. V. Bushkovitch, L. C. Jones, C. A. Potter, and W. F. Sullivan—347(A)
In region two to three mm, O. R. Gilliam, Charles M. Johnson, and Walter Gordy—140
Spectra, molecular (see also **Molecular structure and constants**)
Of ammonium nitrate and thallous nitrate, infra-red, Ralph S. Halford and Roger Newman—348(A)
Of Br_2, Raman, H. Stammreich—79(L)
Of HDO near 3.7μ in solar spectrum, R. M. Chapman and J. H. Shaw—71(L)
l-type doubling in OCS and HCN, H. H. Nielsen—296(L)
Of NH_3 and ND_3, infra-red, D. F. Hornig and F. P. Reding—348(A)
Of NO, theory of magnetic resonance, Henry Margenau and Allan Henry—587
N_2O bands in solar spectrum, Robert R. McMath, A. Keith Pierce, Orren C. Mohler, Leo Goldberg, and Russell A. Donovan—65(L)
Of telluric CO_2, $3\nu_3$-band in solar spectrum, Leo Goldberg, Orren C. Mohler, A. Keith Pierce, and Robert R. McMath—74(L)
Spectra, nuclear (see **Nuclear spectra**)
Superconductivity (see **Electrical conductivity and resistance**)
Supersonics (see also **Shock waves**)
Refraction effect along boundary layer of flat plate, G. P. Wachtell—333(A)

Terrestrial magnetism
Effect of compressibility of the earth, C. Truesdell—823(L)
Thermal conductivity
Of Cu and Sn at low temperature, F. A. Andrews, D. A. Spohr, and R. T. Webber—342(A)
Of metals at high temperature, C. L. Hogan and R. B. Sawyer—350(A)
Temperature distribution, moving medium, Boris Podolsky—187(A)
Transient heat propagation in composite material, Herbert A. Elion—350(A)
Thermal expansion
In Ag halides, A. W. Lawson—185(L)
Thermionic emission; Emitting surfaces
Of (Ba-Sr)O cathodes, conduction and emission, F. K. du Pré, R. A. Hutner, and E. S. Rittner—355(A), 573
Base-metal effects in thoria-coated filaments, Herbert Nelson—353(A)
Cathode behavior in fluorescent lamps, E. F. Lowry, E. L. Mager, and H. H. Homer—355(A)
Ceramic heaters and cathodes, T. R. Palumbo—356(A)
Conductivity and contact potential difference, William J. Price—354(A)
Diode studies of oxide-coated cathodes, H. E. Kern and R. T. Lynch—355(A)
Disappearance of thoria from coated filaments, E. Shapiro—352(A)
Emissivity changes of thoria-coated W filaments, O. A. Weinreich—337(A)
Of Mg-Ni base of an oxide cathode, Ralph Forman and Glenn F. Rouse—355(A)
From magnetron cathodes, magnetron operation, Robert L. Jepsen—354(A)
Methods for calculations, H. F. Ivey and C. L. Shackelford—356(A)
From oxide cathodes, J. A. Burton, H. E. Kern, and R. T. Lynch—355(A)
From oxide cathodes, performance, Thomas H. Briggs—356(A)
From oxide-coated cathodes, decay and recovery of pulsed emission, R. M. Matheson and L. S. Nergaard—355(A); "Figure of merit" and "quality ratio," C. D. Richard, Jr.—356(A); Impurities in Ni core metal, Harold Jacobs, George Hees, and Walter Crossley—356(A); Life tests, J. O. McNally—356(A)
From Pt, effect of impurities, A. Ertel—353(A)
Polycrystalline tungsten wires, M. H. Nichols—158
Refractory compounds as sources of electrons, D. L. Goldwater and R. E. Haddad—353(A)
Of rhenium, Roberto Levi and George A. Espersen—231
Spectral density of flicker noise, F. K. du Pré—615(L)
Thermoelectric power and emissivity of refractory materials, F. H. Morgan—353(A)

Thermionic emission; Emitting surfaces (continued)
Thoria cathodes in high voltage rectifier, S. T. Yanagisawa and T. H. Rogers—353(A)
Tracers for film properties, H. W. Allison and George E. Moore—354(A)
Work function of contaminated metal surfaces, P. H. Miller, Jr. and B. J. Rothlein—354(A)
Thermodynamics
Entropy of non-equilibrium systems, Richard C. Raymond —351(A)
Entropy of superfluid in pure He^4 below the λ-point, O. K. Rice—182(L)
Of He^3-He^4 solutions, O. K. Rice and Olive G. Engel—183(L)
λ-temperatures, He^3 in He^4, Olive G. Engel and O. K. Rice—55
Rectifier as a thermodynamical demon, L. Brillouin—627(L)
Specific heat discontinuity in liquid-vapor mixtures, Louis Goldstein—351(A)
Thermoelectric effects
Efficiency of couple, G. Preston Burns—327(A)
In lead telluride, Ralph Wyrick and Henry Levinstein—304(L)
Refractory thermocouples, emissivity determinations, F. H. Morgan—353(A)
Superconducting *versus* normal junctions, M. C. Steele—308(L)
Viscosity
Of liquid He^3, R. A. Buckingham and H. N. V. Temperley—482(L)
X-rays, absorption, diffraction, scattering, reflection, refraction, and polarization
Cold work and particle size broadening in diffraction lines, B. L. Averbach and B. E. Warren—644(A)
Reflection properties of bent quartz plates, erratum, D. A. Lind, W. J. West, and J. W. M. DuMond—474(L)
X-rays, emission (see also **X-rays, spectra and spectroscopy,** etc.)
Energy distribution from 19.5-Mev electrons, H. W. Koch and R. E. Carter—165
X-rays, spectra and spectroscopy, wave-length measurements (see also **X-rays, emission**)
Microscope, design and construction, Albert V. Baez and Paul Kirkpatrick—83(A)
Zeeman effect
In NO, magnetic resonance, Robert Beringer and J. G. Castle, Jr.—567; Henry Margenau and Allan Henry—587

P

A journal of experim

Amerdcan Institute of Physic
for the

PHYSICAL SOCIET

Officers

President

E. L. Hahn
Columbia University
New York, New York

Vice-President

C. G[illegible]
California Institute of Technolog
Pasadena, California

Secretary

K. K[illegible] Darrow
Bell Telephone Laboratories
[illegible]
Columbia University
New York 27, New York

Treasurer

G. B. Beyram
Columbia University
New York 27, New York

Local Secretary
for the Pacific Coast

J. Kaplan
University of California at Lo
Angeles
Los Angeles, California

Managing Editor

John T. Tate
University of Minnesota
Minneapolis, Minnesota

The Physical Review is
Entered as second-class matter Mar
Authorized for mailing at special rate of pos